Report No. FAA-RD-70-19

AIRCRAFT DYNAMIC WHEEL LOAD EFFECTS ON AIRPORT PAVEMENTS

J. E. Wignot
P. C. Durup
G. Wittlin
R. B. Scott
M. A. Gamon

Lockheed-California Company
P. O. Box 551
Burbank, California 91503

MAY 1970

FINAL REPORT

Prepared for

FEDERAL AVIATION ADMINISTRATION
Systems Research and Development Service
Washington, D.C. 20590

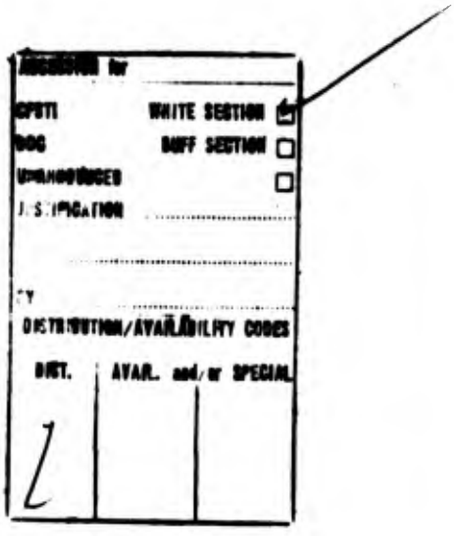

The contents of this report reflect the views of the Lockheed-California Company which is responsible for the facts and the accuracy of the data presented herein. The contents do not necessarily reflect the official views or policy of the Department of Transportation. This report does not constitute a standard, specification or regulation.

TECHNICAL REPORT STANDARD TITLE PAGE

1. Report No.	2. Government Accession No.	3. Recipient's Catalog No.
FAA-RD-70-19		

4. Title and Subtitle	5. Report Date
AIRCRAFT DYNAMIC WHEEL LOAD EFFECTS ON AIRPORT PAVEMENTS	May 1970
	6. Performing Organization Code

7. Author(s)	8. Performing Organization Report No.
J. E. Wignot, P. C. Durup, G. Wittlin R. B. Scott, M. A. Gamon	LR 23307

9. Performing Organization Name and Address	10. Work Unit No.
Lockheed-California Company P. O. Box 551 Burbank, California 91503	450-702-02E
	11. Contract or Grant No. DOT-FA69WA-2143
	13. Type of Report and Period Covered Final Report May 1969 - May 1970
12. Sponsoring Agency Name and Address Systems Research and Development Service Federal Aviation Administration Department of Transportation Washington, D. C. 20590	14. Sponsoring Agency Code

15. Supplementary Notes

16. Abstract

A study has been performed which concludes that airplane dynamic wheel loads have significant effects on portions of airport pavements. The program included scaled pavement tests, analyses to determine airplane imposed loads on pavement and pavement response, correlation between empirical data and analyses and a literature review.

The results of the investigation indicate that the two distinguishable effects that influence the stress the pavement experiences are (1) airplane induced loads and (2) moving load phenomenon. For a given level of runway unevenness the loads that will be imposed on the pavement can be accurately defined for various ground operations performed. However, the pavement response to a moving load can vary substantially depending upon the kinds of materials and types of construction used. To obtain proper assessment of moving load effects, full scale pavement tests are considered necessary to provide needed data.

Two test plans are presented. One approach involves "Operational Statistical Tests" and depends upon a heavy statistical sample of data. The alternate approach involves "Moving Load Track Tests" and provides data for point-by-point correlation using analytical data under carefully controlled conditions and configurations.

17. Key Words	18. Distribution Statement
dynamic loads, pavement response, flexible and rigid pavements, viscoelastic, elastic, material characterization, speed effects, wave length and runway uneveness	Availability is unlimited. Document may be released to the Clearinghouse for Federal Scientific and Technical Information, Springfield, Virginia 22151, for sale to the public.

19. Security Classif. (of this report)	20. Security Classif. (of this page)	21. No. of Pages	22. Price
Unclassified	Unclassified	429	$3.00

Form DOT F 1700.7 (8-69)

Preface

This Final Technical Report covers the work performed under contract DOT-FA69WA-2143 from May 1969 to May 1970.

The program, performed by the Lockheed-California Company, Burbank, California was initiated by the Systems Research and Development Service, Federal Aviation Administration.

The Lockheed-California Company acknowledges the valuable contributions to the success of the program provided by G. K. Williams and M. B. Crenshaw of the Lockheed-Georgia Company in performing the scaled pavement tests and B. Vallerga and Dr. K. Nair of the Materials Research and Development, Inc. in providing laboratory tests and expertise in pavement construction and response contained in Appendixes C, H and I. The supporting efforts of R. C. Schnitzer of Lockheed-California Company are also appreciated.

TABLE OF CONTENTS

TABLE OF CONTENTS (Continued)

LIST OF ILLUSTRATIONS

LIST OF ILLUSTRATIONS (Continued)

LIST OF ILLUSTRATIONS (Continued)

LIST OF ILLUSTRATIONS (Continued)

LIST OF TABLES

LIST OF ABBREVIATIONS AND SYMBOLS

TABLE OF CONTENTS

1. DEFINITION OF TERMS

Pavement - The entire load support structure constructed on the virgin soil, including subbase, base and surface course

Rigid Pavement - A pavement whose surface course is Portland cement concrete or similar material

Flexible Pavement - A pavement whose surface course is asphaltic-concrete or similar material

Surface Course - Top layer of a pavement which serves as a wearing surface or a load-spreading device

Foundation - Includes all layers below surface course (base, subbase, subgrade)

Base - A layer of compacted granular material lying beneath the pavement surface course

Subbase - A layer of compacted granular material resting underneath the base

Subgrade - The layer of compacted virgin soil upon which the pavement is laid

Cohesive Soil - A soil with clay-like cohesive properties

Cohesionless Soil - A sand-like soil which has no tensile strength

Elastic Material - A material which responds instantaneously to applied loads and which returns to the undeformed state when the applied loads are removed

Viscoelastic Material - A time-dependent material which responds slowly to applied loads, but still returns to the undeformed shape when applied loads are removed

Plastic Material - A time-dependent material which responds slowly to applied loads and retains permanent deformation after the applied loads are removed

Stress - The local pressure in a material

Strain - The local curvature [or spacewise rate of change of deflection] in a material

Static - Stationary, independent of time

Dynamic - Moving, dependent on time

Runway - Landing and takeoff pavement area of airport

Taxiway - Maneuvering and taxi pavement area of airport

Dynamic Pavement Loading - All loads, imposed on pavement by moving aircraft

Dynamic Pavement Response - All response [deflection, stress, strain, etc.] of a pavement caused by dynamic loading

Total Load Factor - Total load divided by static load

Incremental Load Factor - The value of load factor above or below the static 1 g value

Reduced Frequency - Ratio of the radian frequency in radians per second to the airplane velocity in feet per second

Taxi Segment - A segment of the taxi operation that can be readily defined, such as velocities, airplane weight, landing rollout, or takeoff run

Limit Design - The maximum design value expected in service

Normal Roughness - Average or typical roughness level

Wave Length - The length of an actual runway bump or the length corresponding to a certain component of runway roughness

Power Spectral Density - A statistical measure of runway roughness at a certain wavelength, averaged over the entire length of the runway

Air Load-Stroke Curve - The relationship between vertical strut load and strut compression (stroke) generally, nonlinear

2. NOTATIONS (PAVEMENT RESPONSE)

(A) Primary

x, y, z = spatial coordinates

h = plate thickness

q = plate normal loading

D_t = time-dependent plate bending stiffness operator

∇^4, ∇^2 = Laplacian operators

w = plate deflection

ϕ = harmonic stress function for foundation

I_i, J_i = integrands

α, β, s = transform parameters

$\nu^*(s)$, $\ell^*(s)$, $G^*(s)$, $D^*(s)$ = parameterized material constants

$\bar{q}^*$ = Laplace and double Fourier transform of loading

ρ, θ = dummy integration variables

X, Y, Z = nondimensional spatial coordinates

ℓ = system characteristic length

Z', z' = vertical coordinates for foundation

P = magnitude of normal load

v = velocity of load

t = time

T = nondimensional time

$\delta(x)$ = Dirac delta function

λ = $\rho(X \cos \theta + Y \sin \theta)$

$^{-1}[\ ]$ = inverse of Laplace transform

P_z = vertical foundation stress

ε_x, ε_y = longitudinal and lateral plate strains

σ_x, σ_y = longitudinal and lateral plate stresses

M_x, M_y = longitudinal and lateral plate bending moments

E_p = plate primary stiffness

F_p = plate secondary stiffness

η_p = plate damping

D_1 = plate primary bending stiffness

D_2 = plate secondary bending stiffness

CBR = California Bearing Ratio

C = plate bending damping

ν_p = plate Poisson's ratio

r_p = plate local radius of curvature

M = plate bending moment

μ_p = ratio of dynamic to static plate stiffnesses

τ = plate material relaxation time

σ_{ij} = foundation stress tensor

ε_{ij} = foundation strain tensor

σ'_{ij}, ε'_{ij} = foundation stress and strain deviators

E_f = foundation primary stiffness

F_f = foundation secondary stiffness

η_f = foundation damping

K = foundation bulk modulus

τ_σ, τ_ε = foundation material relaxation times

δ_{ij} = kronecker delta

Q = characteristic Laplace transform, horizontal load

a_o, a_1 = deflection terms

a'_o, a'_1 = pressure terms

a''_o, a''_1 = stress terms

ζ = ratio of plate to foundation relaxation time

μ_f = ratio of dynamic to static foundation stiffnesses

V = nondimensional velocity

$\delta, \Omega, \Gamma_1, \Gamma_2, G, F$ = characteristics terms of system

k_w = deflection coefficient

k_p = pressure coefficient

k_ϵ = strain coefficient

k_σ = stress coefficient

p = tire pressure

r = load radius

$X, Y, R, \theta, \Delta, \phi$ = dummy geometric variables

K_1, K_2 = constants

J_o, J_1 = Bessel functions

C_r = distributed load correction factor

A = tire area

$C_\omega, C_\rho, C_\epsilon, C_\sigma$ = nondimensional correction factors

R = ratio of plate to foundation stiffness

a = tire footprint radius

k = subgrade modulus

γ_d = dry density

σ_3 = confining pressure (radial) in a triaxial test

σ_1 = axial stress

σ_d = deviator stress $(\sigma_1 - \sigma_3)$

η_s = exponent of confining pressure in formula for M_s for sand

η_g = exponent of confining pressure in formula for M_g for gravel

MC = moisture content

M_R, M_r = modulus of resilience

M_s, M_g = resilient modulus for sand, gravel

ξ = ratio of relative stiffness μ_p/μ_f

μ = coefficient of friction

(B) Subscripts

o : V = o

∞ : V = ∞

w : deflection

p : pressure

ϵ : strain

σ : stress

3. NOTATIONS (Airplane Imposed Loads)

(A) Primary

A = equalizer piston area

C_L = lift aerodynamic coefficient

C_M = pitching moment coefficient

C, C', C'' = constants proportional to level of runway roughness

D = dynamic load factor $(F_p - F_o)/(F_s - F_o)$, diameter of interconnecting line (5 gear model)

E, E_{max} = elevator force, maximum elevator force

F_N, F_{ng} = vertical force nose gear

F_M = vertical force main gear

F_o = initial vertical gear load

F_P = peak vertical gear load

F_S = steady state vertical gear load

F_{ST} = static vertical gear load

$F_{C_{ST}}$ = static vertical load on center main gear

F_{ST_M} = maximum static vertical gear load

F_{TOT} = total vertical gear load due to combined turning and roughness

$F_{TOT(V)}$ = total vertical gear load during taxi

I = airplane pitching moment of inertia

K_T = linear tire stiffness combining all tires on one gear in parallel

K_{G_o} = linear gear stiffness @ V = 0, slope of air load stroke curve at static position

$K_e(V)$ = effective main gear stiffness at velocity

K_{e_o} = effective main gear stiffness at V = 0

L = wave length

L_A = aerodynamic lift

$\bar{L}_A$ = aerodynamic lift/airplane weight

$L_{A_{100}}, \bar{L}_{100}$ = $\dfrac{\text{total airplane aerodynamic lift at V = 100 knots}}{\text{maximum takeoff gross weight}}$

L_T = lift due to thrust

$\bar{L}_T$ = lift due to thrust/airplane weight

M, M_A = aerodynamic pitching moment

$\dot{M}$ = pitching moment due to thrust

$\bar{M}_A$ = aerodynamic pitching moment/airplane weight

S = surface area

T = thrust

V = airplane velocity, equalizer fluid flow velocity

V_{sink} = sink speed

W = airplane weight

$\bar{c}$ = mean aerodynamic chord

e = lateral distance between main gear

f = $\frac{\text{effective main gear stiffness}}{\text{static effective main gear stiffness}}$

f_{n1} = airplane plunge mode natural frequency

f_{n_o} = airplane plunge mode natural frequency @ V=0

g = gravity

h = airplane c.g. height above ground

K_{ng}, k_m = equivalent gear and tire spring rate

ℓ = wheelbase

m = mass of equalizer

p = piston pressure

q = dynamic pressure

r = distance from c.g. to main gear

r_{max} = maximum value of r

s = distance from nose gear to airplane c.g.

t = time

Δt = increment of time

x = gear load equalizer piston displacement

y = vertical displacement at top of gear + downward

z = airplane plunge motion

θ = airplane pitching motion

α = angle of attack

$\Delta\eta_g$ = gear incremental load factor

$\Delta\eta_{bump}$ = incremental load factor, $(F-F_{ST})/F_{ST}$ that would be produced by the chosen bump when the main gear is in static position

$\Delta\eta_{g_a}(V)$ = gear incremental load factor on smooth runway due to aerodynamics and thrust

$\Delta\eta_g(V)$ = gear incremental load factor due to runway uneveness

μ = braking coefficient of friction

Ω = $2\pi/L$, reduced frequency

Φ = power spectral density

$\Delta\eta_{turn}$ = gear incremental centrifugal turning acceleration

k = pressure loss coefficient in equalizer tube

ℓ_{ng} = distance from airplane c.g. to nose gear, + aft

ℓ_e = distance from airplane c.g. to horizontal, + aft

ℓ_n = distance from airplane c.g. to wing gear, + aft

ℓ_b = distance from airplane c.g. to body gear, + aft

C_{L_α} = lift curve slope

C_{L_o} = value of lift coefficient at $\alpha = o$

C_{M_α} = pitching moment curve slope

C_{M_o} = value of pitching moment coefficient at $\alpha = o$

(B) NONDIMENSIONAL

$\bar{r}_m = r_{max}/\ell$

$\bar{r} = r/\ell$

$\bar{h} = h/\ell$

$\bar{m} = m/\ell$

$\bar{c} = \bar{c}/\ell$

(C) SUBSCRIPT (5 GEAR MODEL)

ng = nose gear

w = wing gear (forward main gear)

b = body gear (aft main gear)

INTRODUCTION

BACKGROUND

Unabated changes in the nature of modern commercial aviation have brought increasing pressure on a fundamental link in the air transportation system. the airport. Although hazards resulting from increased traffic are undoubtedly the primary concern, the recent rapid progress in commercial aviation has magnified many problems, and the one which is becoming paramount is the adequacy of available and projected runways and taxiways.

The three major reasons for the impending pavement strength problems are shown on Figure 1. Aircraft gross weight has made an exponential rise over the years and the trend will certainly not reverse. Aircraft taxi speeds have shown a similar rise and, in addition, the daily use of runways has drastically increased. The net effect of these trends is to amplify the need for re-evaluation of current airfield pavement design procedures.

Both major national and international airports, as well as suburban or feeder-type airports, are affected by the problem. While there is a large increase in the rate of traffic in the national and international airports, which could account for potential runway problems, the large increase in airplane gross weight is the greatest source of difficulty to the pavement of feeder-type airports.

The problem of pavement and airplane compatibility is not unlike many of the other airplane compatibility problems for which compromise solutions have to be reached so that neither of the opposing elements are required to take a substantially greater burden. To insist that the landing gear flotation be increased to protect all runways in existence would place an undue economic burden on the airplane which, in the extreme, would greatly hamper the growth of commercial aviation. It would, on the other hand, be unrealistic to require a unilateral rework of runway/taxiways to meet the requirements of new airplanes. Accordingly, an understanding of the details of the problems involved is needed before a meaningful compromise can be made.

The determination of realistic design loads to account for the effect of runway and taxiway roughness has been a continuous concern ever since the late 1940's and early 1950's, when wing-tip fuel tanks were incorporated in the design of airplanes. As outer wing and wing-tip weights increased, the effect has been a decrease in the net flight loads on the wing, but an increase in the bending loads experienced during taxi operations.

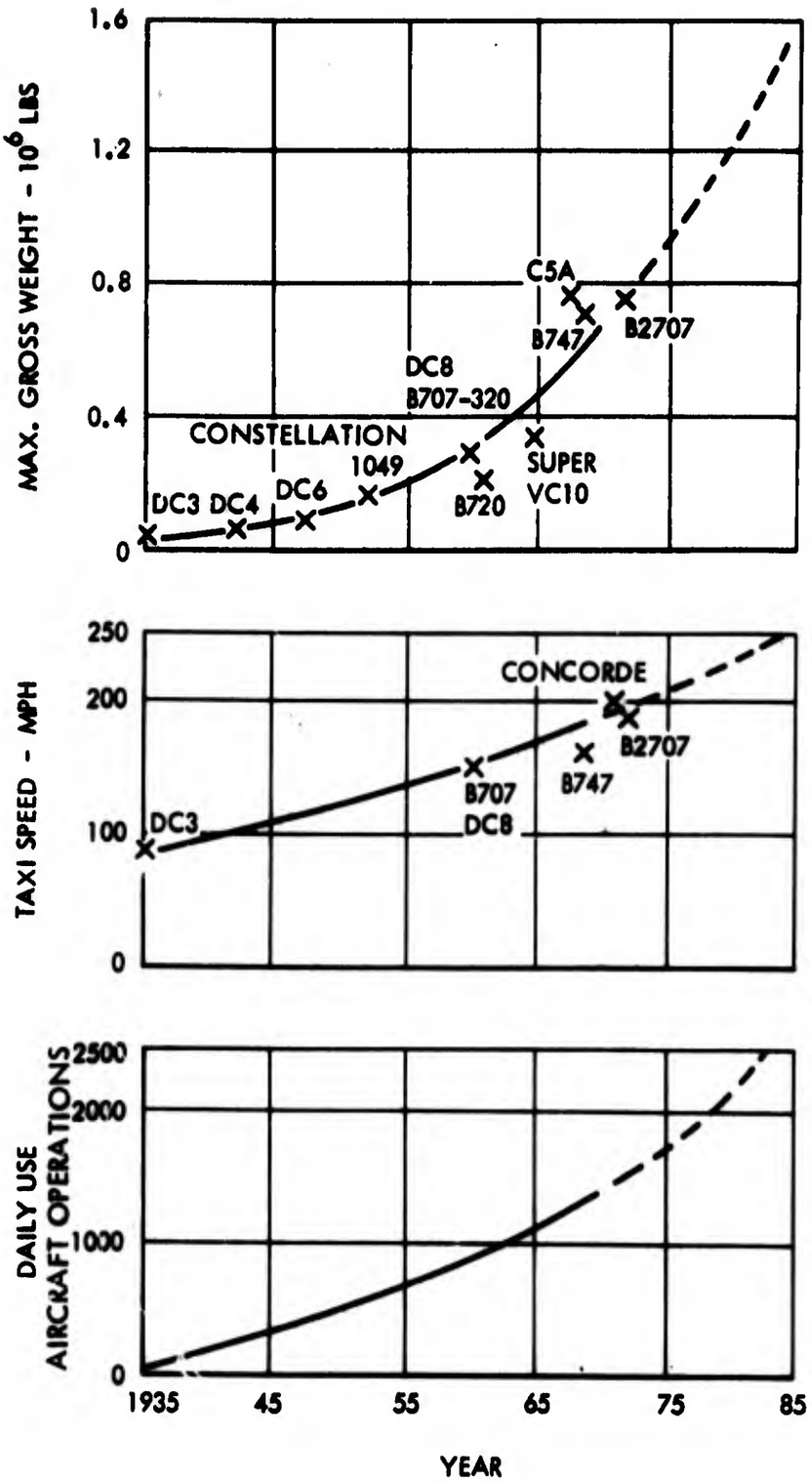

FIGURE 1 - Trends in Airport Use

During the studies of Lockheed's SST (L-2000) in late 1966, it became apparent that in addition to the dynamic loads imposed on the airplane during taxi operations, the runway was experiencing higher than static loads during takeoff and rotation for lift-off. As a result, an investigation was initiated to provide a method of analyzing the response of a runway to a moving load and to obtain measured data on the phenomenon.

The analyses performed assumed that the primary parameters which describe the characteristics of the runway are the thickness of the pavement, the elastic and time-dependent coefficients of the subgrade, the modulus of elasticity of the concrete pavement, and the elastic and time-dependent coefficients of the asphalt-concrete pavement.

Analyses of the rigid pavement indicated that the inertia effects of the slab and soil are negligible at all speeds and at high forward speeds the "rate of load build-up" effects are of secondary importance. The dominant dynamic effect is due to interaction between the viscoelastic (time-dependent) characteristics of the soil and the flexural and shear rigidity of the slab. The essence of the simplest theoretical model is shown in Figure 2. The top sketch shows the slab and viscoelastic subgrade with no load. The middle sketch illustrates the reaction of the slab and subgrade to the load wherein the elastic effects dominate. The bottom sketch portrays the same load moving across the theoretical runway and shows the effect of the dominance of the viscous reaction due to the dynamic loading.

A two-dimensional viscoelastic analysis of the dynamic equilibrium condition of the pavement includes the interaction between the bending rigidity of the pavement in extending the area supporting the load and the elastic as well as the time dependent characteristics of the supporting soil. The results of this analysis are shown in Figure 3 as the ratios of dynamic quantities to static quantities for various values of the velocity parameter for the pavement deflection under the load, bending moment under the load, shear force behind the load, and shear force ahead of the load. For comparison purposes the deflection curve derived from the AASHO Road Test formula is included in Figure 3.

To obtain a greater understanding of dynamic loads imposed on pavements by moving loads, a study entitled Runway Taxi Strength was initiated in 1968, and is reported in Reference 1. This work differed from the earlier study in that a slab on a Voight type subgrade was used. In the analysis, the plate was assumed rectangular and simply supported on all four edges. Expression for the deflections and bending moments normalized to the static values, are given in the Reference 1.

The results obtained from the 1968 study were compared with measured data. The largest and most comprehensive series of tests to study the performance of pavements under moving loads was conducted between 1958 and 1961, by the Highway Research Board of the National Academy of Sciences, under sponsorship of the American Association of State Highway Officials (AASHO). Part of the investigation dealt with rigid and flexible pavement deflections (Reference 2).

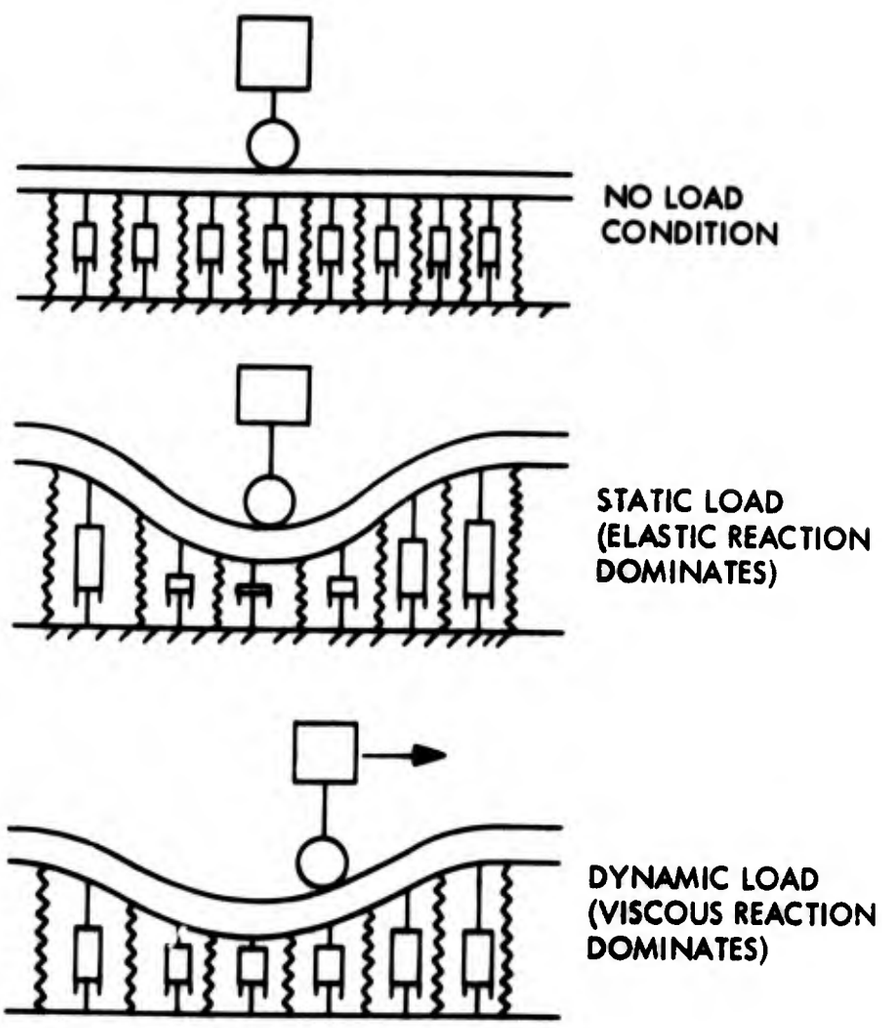

FIGURE 2 - Theoretical Model of Pavement Voight Type Subgrade

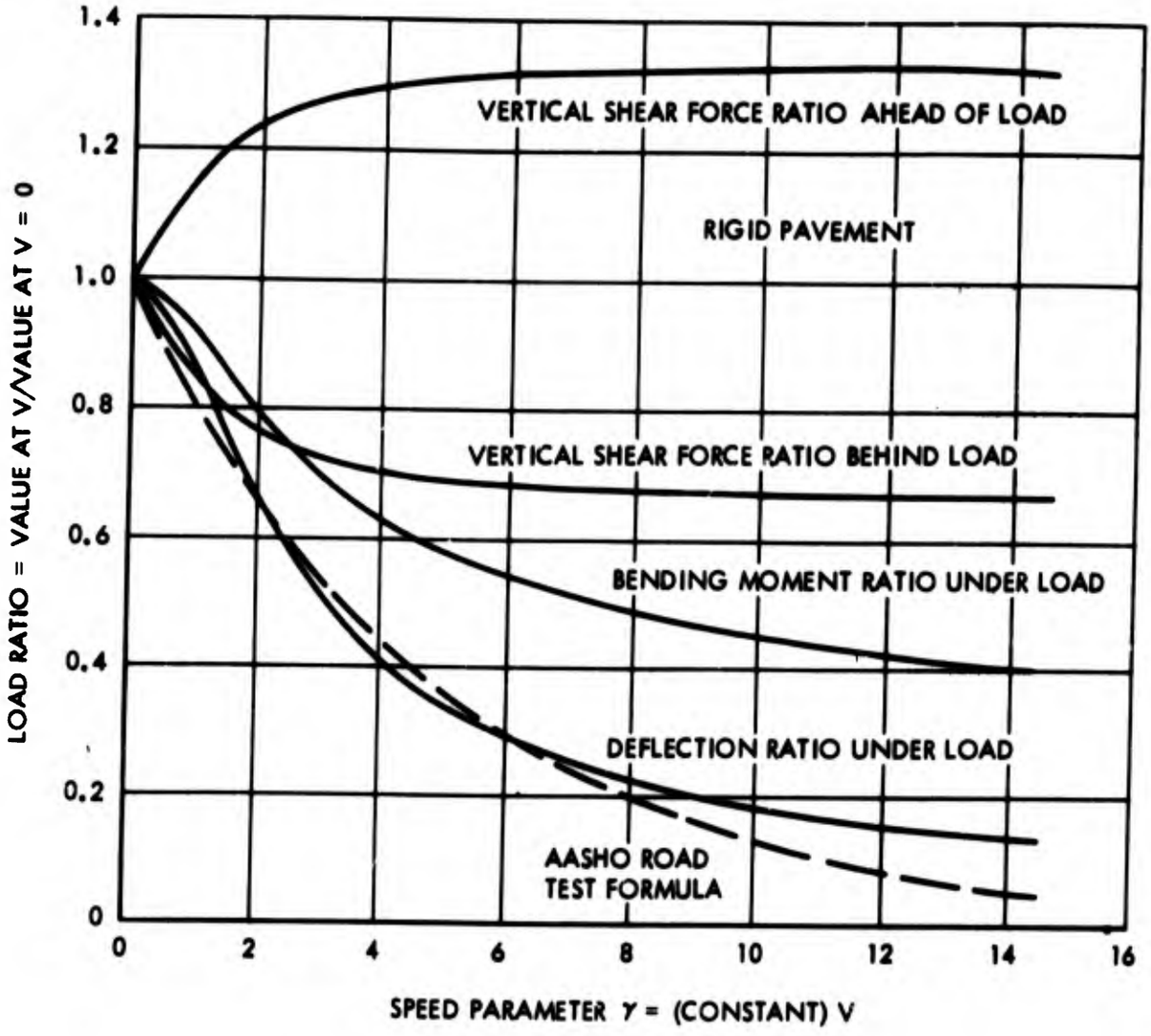

FIGURE 3 - Speed Effects on Pavement Deflection and Stresses Under a Moving Load

The comparison between this study and the empirical expression was limited for the following significant reasons:

- The test data was obtained at speeds limited to 60 miles per hour, which is well below the speeds encountered in airplane operations.
- The measurements were obtained along the edge of the pavement and, therefore, do not accurately reflect the deflections that would be obtained in the center of the runway.
- Airport pavements differ a great deal from highway pavements with regard to loading, geometry and construction techniques. Therefore, the extrapolation of the data for application to airplane dynamic loading effects, although representing the only data of this type available, is questionable.

Review of past developments show a definite need to study the response of flexible airport pavements subject to aircraft operations. Such a study, to be meaningful, must provide a theoretical representation capable of predicting the material behavior in the actual system under a moving load. The development of such a model must also be evaluated in terms of its usefulness to designers.

DEFINITION OF DYNAMIC EFFECTS

Dynamic effects include all effects which are not static. Figure 4 is a schematic of aircraft/pavement interaction. It shows that the two form a system and indicates the feedback relationship that exist between them. The pavement acts on the airplane because it is not perfectly smooth and the airplane acts on the pavement by causing it to fail, locally or widespread, and thus increases its roughness. During periods in which runways are free from vehicle operation they are acted upon by time and weather, which also increases the roughness. Thus, Figure 4 defines the system to be analyzed and pinpoints a closed-loop cycle. Compatibility of design between vehicles and support structures has been widely recognized by airframe manufacturers, who spend considerable time in optimizing vehicle suspension systems to accommodate both dynamic loads imposed on the airframes and flotation requirements imposed by pavement strength. However, the pavement strength considerations are only devoted to static capabilities and do not account for airplane dynamic loads and/or pavement behavior under these loads. The program reported herein is concerned with determination of the significance of these dynamic effects on the present FAA design criteria, set forth in FAA document AC150/5320-6A, Reference 3. For ease in defining the dynamic effects, the contributions of the airplane due to its characteristics and the response of the pavement will be considered separately.

(A) Airplane Imposed Dynamic Loads - The contribution of the airplane to the dynamic effects is of two types: (1) the response of the airplane to the pavement environment, and (2) the response of the airplane to the air environment and operational conditions such as braking and turning. Figure 5 is a

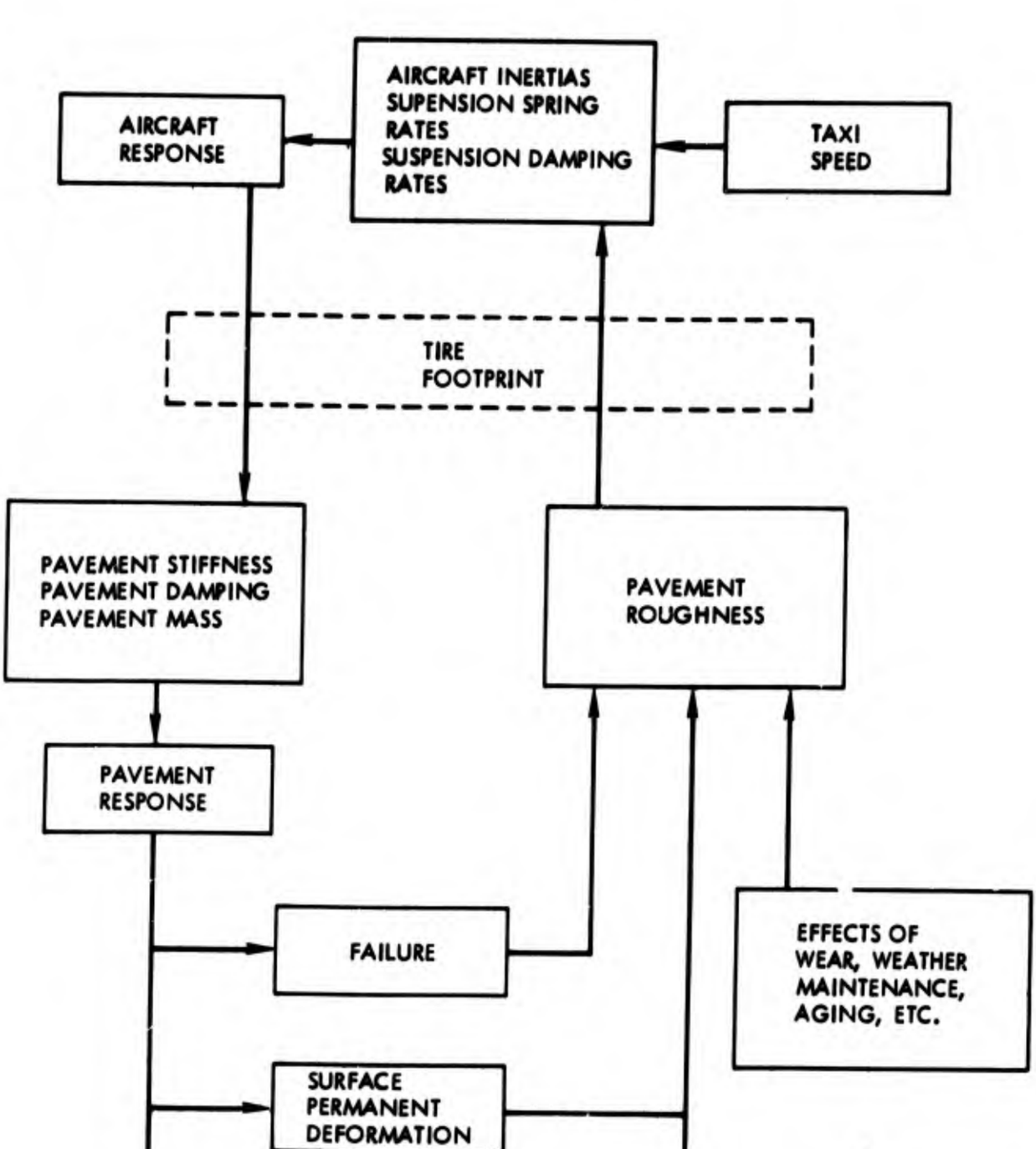

FIGURE 4 - Airplane/Pavement Interaction

schematic of a typical airport operational cycle indicating the velocities, braking, turning, takeoff and landing activities that are associated with the various parts of the ground taxi operations. Specifically these operations are:

Departure	Arrival
Static (parked)	Landing impact
Low speed taxi	High speed braking
Turning	Decelerated roll-out
Low speed braking	Low speed braking
Accelerated takeoff roll	Turning
Aborted takeoff roll (emergency, very infrequent)	Low speed taxi
Takeoff rotation	Static (parked)

The types and magnitudes of the loads that airplanes impose on airport pavements during the various operations are functions of airplane characteristics and the runway surface characteristics. Among the more salient airplane characteristics which influence airplane gear load responses are: weight, c.g., location, inertia, aerodynamic lift, landing gear design, tire sizes, pressures, and spacing. The airplane is subject to surface unevenness, i.e., vertical deviations from a flat plane, to a greater degree than any other individual influencing factor. The load amplitudes that result from the constant exposure to surface roughness depends on the airplane pitch and plunge frequencies and their compatibility with the wavelengths of the surface contours.

Since the slope of the main gear load stroke curve increases approximately proportionally to the aircraft weight in the static range, the plunge frequency does not vary much with weight. The frequency range of interest for both gears is between 0.5 to 1.5 cps. Therefore, the response to runway roughness increases as the taxi speed increases and the airplane is exposed to longer wavelengths. During taxi operations at the higher velocities, there is also an effect on the dynamic loads introduced due to the airplane lift characteristics. Negative lift has been shown to cause increased main gear loads during takeoff runs. In addition to the vertical loads imposed on the pavement as the airplane traverses the runway, horizontal shear loads are also induced. These loads are a result of such operations as braking, turning, and landing impact spin-up. The magnitudes and rates of loading are related to the speed regime at which they occur. The operations as depicted in Figure 5 indicate at what point a particular dynamic vertical and/or horizontal load will be imposed on the pavement by the airplane. The operations are discussed in detail in the subparagraph entitled, Loadings Imposed on Airport Pavements, starting on page 74. All operations shown in Figure 5 are dynamic, with the exception of parking and run-up. Runways, as opposed to taxiways and apron, primarily experience dynamic loadings, and a good portion of both runways and taxiways are subjected to horizontal shear loads as well as static loads.

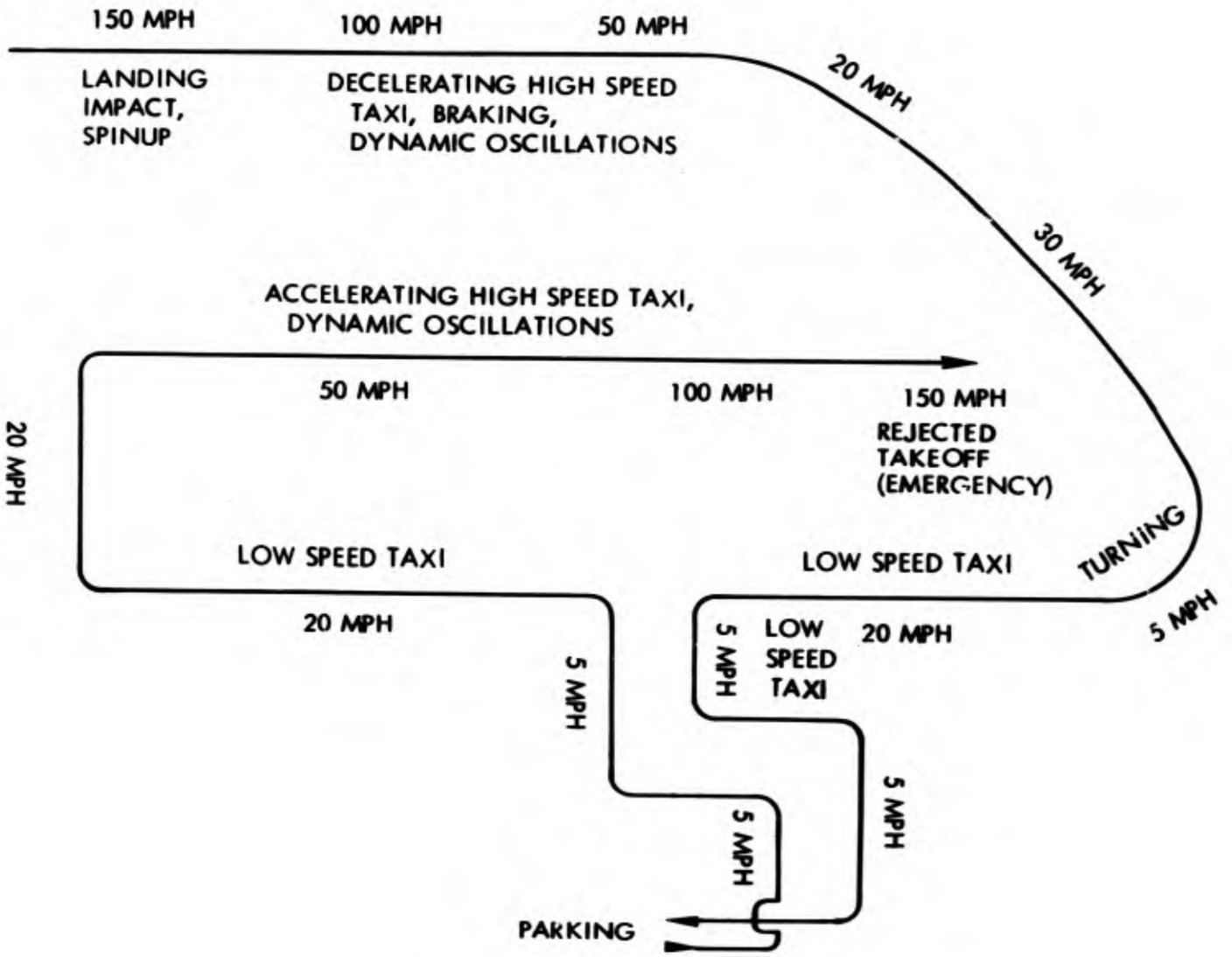

FIGURE 5 - Airport Operational Cycle

(B) Airplane/Pavement Interface - The immediate interface between airplane and pavement is the tire footprint. The footprint is the area of contact between tire and surface and can vary in size and shape depending on tire load, pressure, type and the airplane operation. The loads distributed over this area, which are equal and opposite on pavement and tire at each area, may be normal to the pavement, horizontal shear or twisting. The latter, which may result from a ground maneuver such as pivoting, is generally considered negligible because the frequency of occurrence is small and it is not executed on the same spot on the pavement. The normal loads are associated with the airplane taxi operations, while the horizontal shear loads are generated by such operations as braking and turning. Both the normal and horizontal shear loads are nearly always uniformly distributed over the footprint. Since no horizontal shear loads are present in the static condition, no existing design procedure based on static considerations will account for them. These loads may, therefore, be regarded as strictly a dynamic effect.

The normal applied stresses are determined by the tire pressure requirement. Tire pressures have been shown to vary very little as a function of airplane operation. Although the load imposed on the pavement due to the airplane operations involved varies with time, the area under the load adjusts to maintain a nearly constant applied stress. The horizontal shearing stresses on the other hand do vary with time, depending strictly on the operation which the airplane is undergoing. The horizontal shear stress is related to the normal load by use of coefficient of friction and can be shown by the expression.

$$Q(t) = \mu(t) P \qquad A(t)\,\mu(t)p$$

where

Q	=	horizontal load	(lb)
P	=	normal load	(lb)
A	=	tire area	(in^2)
p	=	tire pressure	(lb/in^2)
μ	=	coefficient of friction	
t	=	time	

Thus, the loading on a pavement may be regarded as two parts, a vertical load and a horizontal load.

(C) Pavement Dynamic Effects - Pavements in contrast to aircraft are constructed of earth materials, primarily soils, gravels, and cemented aggregate. These materials vary in characteristics, are somewhat erratic in behavior and are environmentally sensitive; and hence are difficult to properly represent analytically. Their properties are known with less precision than aircraft metals, rubbers, and plastics; so pavement analysis is, in general, less accurate then structural analysis of aircraft components.

The type of dynamic effect that a pavement undergoes, is a function of both the type loading and its material properties. The latter influence is summarized in Table 1 which presents various pavement materials and their material properties.

TABLE 1 - PAVEMENT MATERIALS AND PROPERTIES

Pavement Layer	Material	Linearity	Elasticity	Moisture Effect	Temperature Dependent	Stress Level Dependent
Surface	Portland-Cement Concrete	L	E	No	No	No
	Bituminous Concrete	N	V.E.-$\bar{P}$	No	Yes	Yes
Base and Subbase	Lime and Cement Treated Materials	N	E	Yes	-	Yes
	Gravel	N	E	No	No	Yes
	Gravel-Sand	N	V.E.-$\bar{P}$	Yes	No	Yes
Subgrade Compacted	Sand	N	V.E.-$\bar{P}$	Yes	No	Yes
	Clay and Silt	N	V.E.-$\bar{P}$	Yes	No	Yes
	Peat and Saturated Clay	N	V.E.-$\bar{P}$ Fluid	No	No	Yes

L = Linear

N = Nonlinear

E = Elastic

V.E.= Viscoelastic

$\bar{P}$ = Plastic

The dynamic effects on the two types of materials which are time-rate sensitive, (1) plastic and (2) viscoelastic, are described as follows:

(1) Plastic Effect - Dynamic loads effect plastic materials by causing permanent set in the materials. Fortunately, most of the deformation occurs during construction loading while the remaining deformation occurs gradually under static and dynamic loading conditions. During long period parking, which is a static condition, continuous vertical nonrecoverable deformation takes place. Evidence of this effect is wheel sinkage in asphalt during long term parking. Dynamic loadings contribute to permanent set through cumulative vertical nonrecoverable deformation due to repetitive loading during taxi. The loads vary in magnitude and point of application depending on the operating speed and airplane plunge frequency. In addition, cumulative horizontal longitudinal and lateral nonrecoverable deformation, due to repetitive loadings during braking and turning, also occurs. The consequence of this loading condition is warped, rutted, or grooved asphalt runways resulting in wavy shapes.

(2) Viscoelastic Effects - The characteristic of a viscoelastic material is that it is time dependent and responds slowly to applied loads but returns to its undeformed shape after the load is relieved. Both elastic and viscous properties are present. The elastic properties act as a spring in the system while the viscous properties provide damping.

The significance of the viscoelastic response is that it alters the immediate deformation pattern and, thereby, changes the stresses, strains, pressures, and deflections which occur over and over again during innumerable dynamic loadings. If the effect is to lessen the response, relative to the static case, then dynamic loading would be alleviated by the viscoelastic effects. But, if the effect is to increase the response, relative to static response, dynamic loading would be increased by the viscoelastic effects.

(3) Mass Effects - The term, "mass or inertia effects" refers to the inclusion of the pavement mass in the analysis of pavement response. With consideration for the pavement mass the system degenerates to a spring and dashpot representation as discussed under viscoelastic effects.

Mass effects (or effects of pavement inertias) have generally been disregarded in pavement design, since each particle must be given sufficient acceleration to alter the response and this does not occur statically or at low speed (quasi-statically). There are, however, two possible types of dynamic loading which might excite pavement dynamic mass effects, (1) high speed loads or (2) high frequency loads.

(4) Other Pavement Dynamic Effects - Other pavement dynamic effects, as briefly discussed below, may be significant under specialized loadings.

(a) Thixotropic Effects - Under high frequency loads, clays, sands and some other soils show a reduction in stiffness that is neither attributable to mass or damping effects. It is the so-called stirring effect, which causes the particles to act like fluid particles and lose their resistance to loading. This effect is similar to placing an object (stone) in sand and then shaking the sand. The object will gradually descend toward the bottom.

(b) Wave Effects - Wave propagation velocities have been determined for various paving soils and subgrade materials, primarily as a means of measuring elastic properties of materials insitu. Layered systems can propagate waves which have lower velocity than the waves in the pure soil. The wave propagation effects could have significance depending on the relative closeness between the properties of the material and the loading rate.

(c) Transient Effects - Short lived conditions such as sudden starting loads and irregular time history loads may produce unusual dynamic effects in the pavement. The degree to which the response of the pavement is affected by these loads requires an insight into the material behavior under such loads.

(d) Adverse Environmental Effects - The behavior of material is to some extent a function of the environment to which it is exposed. Adverse conditions such as frost, precipitation, and intense heat have been known to alter the properties of materials. These alterations, combined with dynamic loading conditions can have deleterious effects.

COMPARISON BETWEEN AIRPORT PAVEMENTS AND HIGHWAY PAVEMENTS

Modern pavements for both airports and highways are similar to the extent that they are essentially layered systems designed to support imposed traffic and to withstand the detrimental effects of environment factors within acceptable limits. However, there exist significant differences between airport and highway pavement structural design with regards to loading characteristics and geometrical configurations. Present methods of highway design do not rely on ideas developed specifically for airport pavements and disregard the following basic differences between the two systems. Some of the basic differences between airport and highway pavements presented below are discussed in Appendix H.

- Airport pavements are subjected to high normal loadings (approx. 40,000 pound loads at 200 psi tire pressure) compared to highway pavements which take low normal loadings (approx 10,000 pound loads at 50 psi tire pressure).
- Airport traffic volume is substantially lower than highway traffic volume.
- Airport pavements are not uniformly loaded (i.e., there are many seldom stressed areas of the runways) whereas highway pavements are more uniformly loaded.

- Airport pavements are traversed by loads moving at higher maximum speeds (up to 240 mph) than are highway pavements (maximum 75 mph).

- Airport pavements are subjected to large horizontal shear loads during each aircraft landing (up to 20,000 pounds) whereas shear loads are less severe on highway pavements.

- Load patterns on airport pavements are variable, ranging from simple dual wheels, to multiple, interconnected gears.

- Airport pavements are subjected to dynamic load oscillations of a significantly different character than those that act on highway pavements, due to the differences in vehicles and vehicle suspension systems over the two pavement types.

In brief, loading on airport pavements is a combination of vertical and horizontal loads which are oscillatory, low volume, high intensity, and high speed as compared to highway loading which is primarily vertical loads which are oscillatory, high volume, low intensity, and low speed.

Secondly, there is a difference in construction in airport pavements.

- Airport pavements sections are wider and longer than highway sections.

- Airport pavements are thicker than highway pavements.

- Airport pavements are flatter than highway pavements.

- Airport pavements are constructed with lower tolerance levels on roughness material variability, etc., than are highway pavements.

Analysis methods must be altered to account for difference in airfield and highway characteristics. In particular:

- High loads, high speeds, and roughness/vehicle response interactions means that dynamic effects must be considered in any comprehensive airfield pavement analysis.

- The geometry of airfield pavements justifies neglecting edge effects in the analysis of airport pavements.

- Few load repetitions diminish the effect of pumping, joint problems, and elaborate fatigue considerations.

- Shear loads should be considered in any complete airfield pavement analysis.

- Environmental factors, other than loading, must be weighted differently during design considerations for airports.

Specifically, (1) low gradients increase the drainage problems on runways and taxiways, (2) runways and taxiways must be protected from deterioration due to fuel spillage, and (3) frost is a less important factor at airports, because of greater runway/taxiing thickness, than on highways.

OBJECTIVES OF THE PROGRAM

The objectives of the program are:

- Determine the significance of dynamic loads on pavement stresses in comparison with static loads.
- If dynamic loads are significant, describe the manner in which they can be best accounted for.
- Determine the necessity for full scale pavement testings.
- If a test program is required, describe what the test program should consist of.

REPORT FORMAT

The table of contents conveys the general plan of the report. The main body of the report contains the discussions of the program details and results which lead to the conclusions. The appendixes present the supporting analyses, data and related analytical techniques.

The background information is presented initially to provide a proper perspective in relation to the objectives of the program. The discussion proper presents both the general scope as well as the specifics of the program. The program details then show how the analyses, test data and literature survey are combined to determine the validity of the program results. Included in the discussion on program details is a correlation study of experimental data versus theoretical data. These studies are essential to the development of a pavement model which is capable of representing material behavior under dynamic operations.

The information and data included in the appendixes provide detailed information which supports the appropriate discussions and is best presented as a separate entity. Included as an appendix is a comprehensive computer program which determines pavement responses and subsoil pressures. One appendix contains the detailed description of the scaled test program. Also included are a categorized bibliography by subject matter for easy access, a simplified five gear model and supplementary analyses.

DISCUSSION

GENERAL

The primary elements of the program and the manner in which they are related are shown in Figure 6. The study proceeded along several concurrent paths, which ultimately tied together to provide a means of determining the significance of dynamic effects on airport pavements. Particular emphasis was placed on: (1) empirical aspects through scaled pavement tests, (2) analyses through the development of flexible pavement models, (3) correlation between theory and measured results, (4) accumulation of pertinent works in the field through a thorough literature survey, and (5) the analysis of dynamic loading conditions. The scaled pavement tests were conducted at the Lockheed-Georgia Facility under the direction of Lockheed-California personnel. Materials Research and Development Inc. (MRD) provided supplementary studies which included a critique of materials and construction in existing pavement design, translation of dynamic loads into equivalent static loads, and an evaluation of subgrade soil from the actual pavement test sections. MRD efforts are reported in Appendixes C, H, and I.

As is indicated in the primary element chart,(Figure 6), the problem of pavement and airplane compatibility requires the mating of two engineering disciplines: civil and aeronautical. The interaction compatibility problem can be considered to consist of two parts, (1) the imposed aircraft loads and (2) the response of various types of runways. Under most conditions the airplanes produce the loads to which the runway responds. However, in the case of runway unevenness, the airplane responds dynamically to the surface contours and the resulting airplane motions are fed back to the runway in the form of oscillatory loads. The runway in turn responds to the aircraft load in a manner, depending on its materials characteristics, to deflect unevenly which in turn produces still further runway unevenness of small amplitude.

In pursuance of the basic objectives of the program it was recognized that the investigation, in addition to being directed toward current goals, would be most beneficial if designed with future endeavors in mind.

Specifically the approach is to:

- Review available literature with regards to material characterization, construction techniques, test data, analytical techniques, design procedures and criteria.

- Develop a testing program including instrumentation, installation, procedures, and the techniques which would provide the data necessary to evaluate pavement response. The program would determine what if any problems and limitations are associated with scaled testing and provide the experience and knowledge to conduct meaningful future test programs, if required.

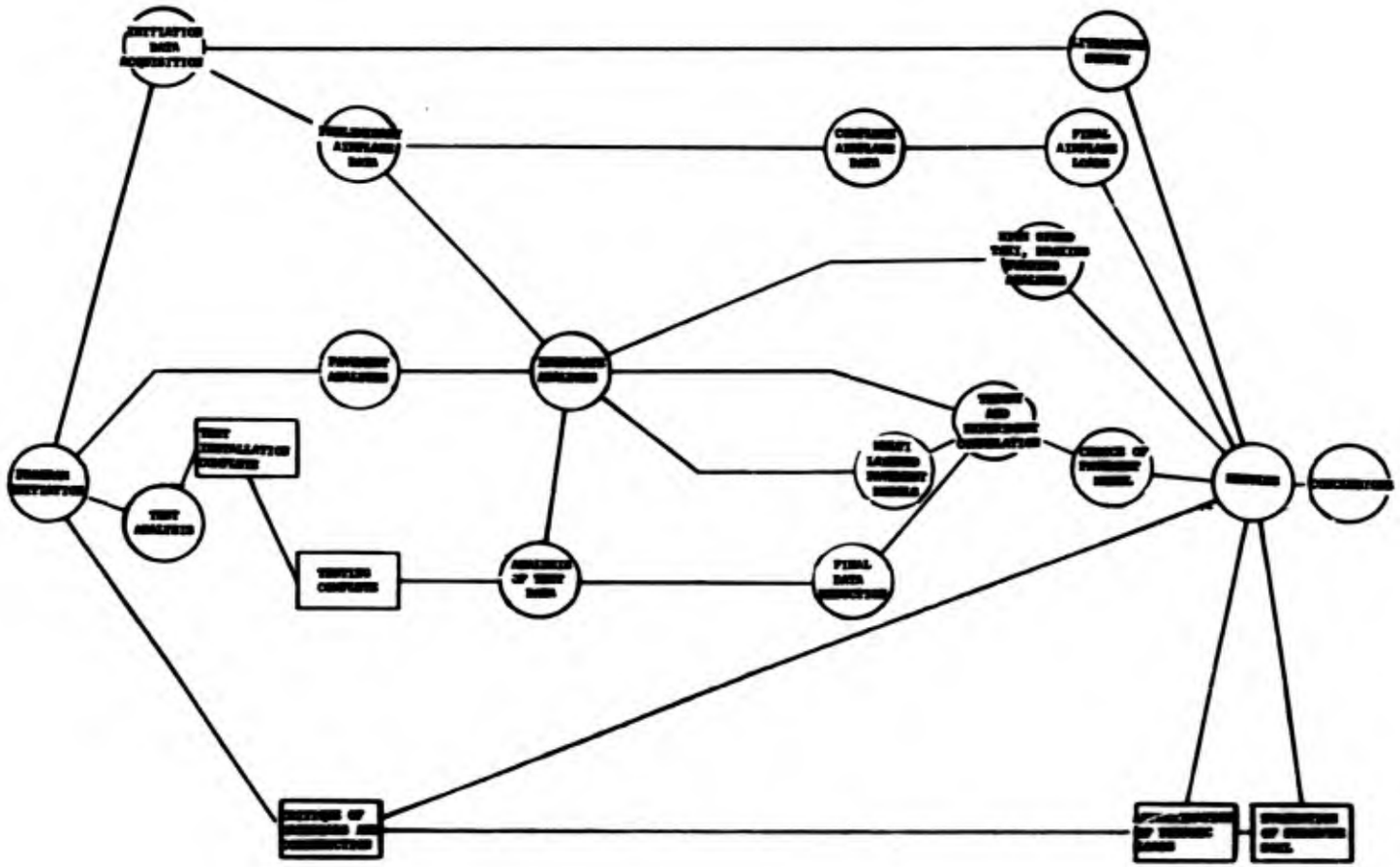

FIGURE 6 - Primary Element of the Program

- Define the inputs to the pavement system from operating airplanes. The airplanes are to be representative of the various high gross weight airplanes either currently in operation or expected to be operative within the next several years. The operating conditions are to be consistent with the spectrum of loads that could be expected from low speed taxi takeoff to return landing and taxi. The analyses in this area are to utilize existing digital computer programs and techniques.

- Develop an analytical representation of the pavement system, modified as dictated by empirical results, which is capable of predictive studies on typical airport pavement systems.

- The program developed will be used as a basis for future investigation into design procedures, if necessitated.

- Investigate the practical aspects of construction technique, materials characterization and evaluate related requirements for future programs.

PROGRAM DETAILS

The program consisted of a literature survey and review, scaled pavement tests, analyses to determine both the airplane loads imposed on airport pavements and the response of the pavement to such loads and correlation between predicted and measured strains and pressures. A detailed discussion of each aspect of the program follows.

(A) Literature Survey and Review - The published information relating to pavements is voluminous, and a complete listing and review of the total field has not been published. This report presents: (a) a categorized bibliography of a typical comprehensive cross-section of literature relating to dynamic wheel load effects, (b) an indexing of this literature by specific subject matter, and (c) a brief review of the major literature categories as they pertain to this report. The bibliography and the index are presented in Appendix A. The review is presented in this section.

The literature pertaining to dynamic wheel load effects can be divided into four major categories (I) Airport Pavement Loading, (II) Airport Pavement Response, (III) Materials Characterization, and (IV) Pavement Testing. The discussion in this section refers to the index numbers shown in Appendix A.

(I) Airport Pavement Loading

- Airport Pavement Loading - The response of the aircraft during ground operations, which constitutes the loading of the pavement beneath the vehicle, has been extensively dealt with in the literature. The best comprehensive report in this area is item (1) in the bibliography, which also contains a thorough summary of the other reports available on the subject. Report (2) discusses, primarily, heat and blast loading on pavements. All reports in the general field of airport pavements must of course make some reference to loading, but usually this is done very superficially concentrating primarily on static loading as in (3) and (4). Yang (5) and (6) examines dynamic loading in considerable detail and does the best job of relating it to pavement response.

(II) Airport Pavement Response

- Static Analyses - Static analyses of pavement structures and layered systems have been a subject of interest since the 1880's, and numerous approaches have been used. Beginning with Burmister (7), vertical loading of pavements using elastic theory has been thoroughly pursued (8, 9, 10). There has been a dichotomy between

so-called rigid and so-called flexible pavements and many methods have been more empirically than analytically oriented. Report (11) gives a summary of the static analyses methods in use throughout the world. Vertical loading from multiple gears has been examined (12) and (13) and a tensionless foundation is analyzed in (14). Nonvertical loading caused by braking is examined in (15), (16), (17) and (18).

- Dynamic Analyses - Dynamic analysis of pavement structures is a more recent subject than static analyses, but considerable material is available and this literature review is most complete in this area. Text books which delve into the subject (as well as static analyses) are (19), (20), and (21). Papers which deal with the general subject of viscoelastic analysis are (22) and (23). Item (23) is particularly interesting in that it discusses the effect of differing assumptions regarding viscoelastic material properties in two-layer systems. The problems of a moving load on viscoelastic substances (which is probably the central feature of dynamic wheel load effects on airport pavements) is dealt with in items (24), (25), (26), (27), (28), (29), (30), (31), (32), (33), (34) and (35). This report relies heavily on the system developed in (25), (26) and (27), but an equally comprehensive analysis is presented in (28). Item (29) is applicable to plastic and steel combinations, (30) deals with highways, and (31) analyzes ground rather than pavement systems. Several reports, (32), (33), (34), (35), (36) and (37), incorporate inertia effects in their analyses and a couple, (36) and (38), look at vibratory loads. Very high speed loads are examined in (32). Item (39) is brief but comprehensive and lays the groundwork for a inclusive dynamic design procedure.

- Design Procedures - Most design methods are statically oriented; one (40) is in general used for flexible pavements and one (41) is in general used for rigid pavements. Item (42) is a computerization of the method presented in (41). Alternative and extended methods are found elsewhere (43), (44), (45) and (46). Dynamic design is discussed in depth in (47) and the systems approach is presented in (48) and (49).

(III) Material Characterization

- Surface Course Materials - The properties of Portland cement concrete are well presented in (41). The properties of asphaltic-concrete are less well known, but are adequately covered in (50), (51), (52), (53), (54), (55) and (56). These reports deal primarily with the viscoelastic and plastic properties of asphaltic-concrete, but (57) covers the characteristics of asphalt broadly and completely. A general review of pavement properties in total including surface course and foundation is presented in (58).

- Foundation Materials - Foundation materials are of several types: granular bases, cohesive soils, and noncohesive soils. The rheology of these materials is discussed in (59), (60), (61), (62) and (63) and the more general properties are discussed in (47), (58), (49) and (21). Analyses of vibratory loads applied to soils is presented in (64).

(IV) Pavement Testing

- Pavement Testing - Most of the testing has been static (65), (66), (67) and (68) and in some cases slowly rolling loads have been treated as static. Dynamic testing, with moving load response, is available in (69), (70), (71) and (72). The effect of vibrations is examined experimentally in (73) and a full scale highway test is discussed in (74). The properties of airport pavements worldwide is examined in (75).

(B) Scaled Pavement Test - The scaled pavement test was conducted at the Lockheed-Georgia facility in accordance with a coordinated effort by both Lockheed-Georgia and Lockheed-California personnel. Primary purposes of the test program were:

- To develop and evaluate instrumentation for use in multilayer runway/taxiway tests to determine stresses in the pavement due to a moving load.
- To perform tests at scaled speeds corresponding to airplane takeoff velocities and weights compatible with scaled runway strength on two simulated layered runways.
- To develop techniques and procedures which could be used if full scale tests are required.
- To obtain empirical data to relate to analytical procedures for evaluating pavement responses to moving loads.

(1) Test Analyses - Supporting analyses for the tests were performed to provide a means of determining the scaled properties of the test runways, the significant parameters to be evaluated, the collection of necessary data and the literature associated with the work. The investigation included a study of:

Required soil characteristics
Concrete slab characteristics
Asphaltic-concrete slab characteristics
Loading device design
Pavement and soil instrumentation selection
Data requirements

The pavement sections chosen are shown in Figure B-7 Appendix B. The concrete pavement is a type I portland cement with a 28 day curing time. The asphalt pavement is asphaltic concrete whose properties are shown in Appendix B, Figure B-6.

The analysis of the test program included predictions of the expected pavement deflection and subsoil pressures, and the theoretical interaction of the test parameters was investigated to determine the maximum lateral and vertical influence of the moving gear and to determine the parameter values necessary to achieve optimum scale speeds.

The theoretical response depends upon an expression relating vehicle velocity to nondimensional velocity.

$$V \quad \frac{v\tau}{l}$$

$\tau = \eta/F$ = Material relaxation time (sec)

where:

ℓ = characteristic length (inches)

v = vehicle velocity (in/sec)

F = material stiffness (lbs/in)

η = subgrade damping coefficient ($lb\text{-}sec/in^2$)

$$\ell = \sqrt[3]{\frac{E_p h^3}{12(1-\nu_p^2)\, E_f}}$$

E_f = Subgrade stiffness (lb/in^2)

E_p Young's modulus of slab (lb/in^2)

ν_p Poisson's ratio of slab

The ratio of scaled and actual velocities can then be obtained for known slab and subgrade properties. Expressions for both concrete and asphalt are given in Appendix B.

Since the scale thickness was dictated by a need to obtain the maximum deflection consistent with pavement strength for the test weight used, the velocity ratio of scale to actual then becomes more a function of the properties of the subgrade. The two subgrade moisture contents chosen so that two varied damping properties existed were:

Dry soil (CBR 10)
Wet soil (CBR 2)

(2) Test Program - The detailed test plan is shown in Appendix B. The testing was covered over a period of several days and was designed to encompass the following types of tests:

Velocity (moving load)
Impact
Static
Soil and pavement
Weight and dimension measurement

(a) Moving Load Tests - The velocity tests were conducted in several stages; each stage consisting of a series of speed runs ranging from 0 to 45 mph, with the load cart, over a given combination of gages. The recorded combinations were changed for each new series of speed runs over the test bed. This system of recording data used was necessary because of the limited number of channels that were available on the recording equipment. In all, over 50 moving load tests were performed.

The original instrumentation diagram (Appendix B) called for 124 strain gages and 20 pressure gages. The development of a crack in pavement Section B (concrete over CBR 2 material), prior to the start of testing, reduced the strain gage requirements to approximately 90. Since pressure gages were already installed under the cracked pavement some strain gages were installed to note any differences in response.

The following event sequence comprised a single speed test:

1) The load cart was connected to the truck and the cart hydraulic accumulator was charged.

2) The truck and cart were positioned on the test bed access road and the gages balanced.

3) Both recording oscillographs were turned on and the zero point and calibration switches were momentarily activated.

4) The cart hydraulic system was used to impose the desired test load on the load wheel.

5) The truck was accelerated to the test speed.

6) The truck and cart entered the test bed, tripping a micro-switch which placed event markers on both oscillograph traces. These event markers served to synchronize the traces (one in the truck to record vertical load and speed and the other to record pavement strains and pressures).

7) Data was recorded and a second switch was activated to signal the end of the test.

Notes taken at the time of each test included run number, approximate speed and load, active gage readings, time and temperature.

The maximum speed possible with the truck and cart arrangement was slightly in excess of 40 mph. However, higher speeds were attained with the truck alone. Still higher speeds were achieved with an MGB roadster. Vehicle load time histories were not obtained in the tests performed with these latter two vehicles. However, the mean tire loads were known and were used as a first approximation to relate to strain data.

(b) Impact Tests - Upon completion of the vehicle tests, the load wheel and hydraulic system were removed from the load cart and mounted on a stationary drop-test rig. This device was then used to perform a series of impact tests on Section A (concrete on CBR 10 material). The weight used in the impact tests was constant at 1250 pounds, and the tire pressure varied from 50 psi to approximately 100 psi. The relationship between drop height, weight and tire spring rate is shown in Appendix B.

The purpose of the impact tests is to verify the results of the speed tests by varying the period of the impact load instead of speed. The period of the impact load is considered to vary inversely with the speed.

An analysis, which shows the relationship between period of impact and speed, is shown in Appendix B. These tests were also intended to determine if supposition of a moving load could be obtained from a series of impacts.

Time histories of strain, load and pressure were taken during the impact tests, and they were recorded in a manner analogous to that used for the speed test. A total of nine impact tests were performed.

(c) Static Tests - The static tests were incorporated into the test program to establish a reference to which the moving load responses could be compared. In addition, static values provided a means of developing a composite of the pavement strain and/or soil pressure comparable to the airplane operational speed range including the parking condition. Measurements of strain and pressure were taken in each section by applying a load of approximately 1000 pounds and maintaining a constant level for several seconds and then increasing the load to approximately 7000 pounds and once again maintaining the new load level for several seconds. A total of eight static tests on the four sections was performed.

(d) Soil and Pavement Measurements - The pavements were cut into sections at the conclusion of the tests for examination to determine if any variations in thickness or construction resulted from the tests, or if any soil characteristics changed due to the loading conditions.

Specimens of the soil were transported to Materials Research and Development where additional tests were run. Appendix C "Laboratory Tests" describes the test procedures and results. The samples tested there had the following characteristics:

Sample 1: Moisture content 20 percent; dry density 107.9 lbs/ft^3 corresponding to CBR 10

Sample 2: Moisture content 30 percent; dry density 91.2 lbs/ft^3 corresponding to CBR 2

Repeated load tests for the determination of modulus of resilience (dynamic stiffness) were conducted at three stress levels and three frequencies, for the CBR 10 specimen and one stress level for the CBR 2 specimen. The frequencies were designed to cover the range of test values obtained. After the repeated load tests had been completed, the sample was subjected to a conventional unconfined compression test with loading and unloading to determine the 'static' stress-strain curve and the area of the hysteresis loop. The purpose of the tests was to obtain practical values of soil stiffness and damping to support the correlation studies.

(e) Weight and Dimension Measurements - In addition to the basic strain, load and pressure time histories, it was also necessary to obtain supplementary data pertaining to loads on the truck and tow cart tires, in order to examine their contribution to the measurements. Therefore, complete geometric data was taken on all vehicles including the sports car. The load distribution (front to rear) was also determined for the load cart. Table 2 shows the pertinent geometry and weight data.

TABLE 2 - GEOMETRY AND WEIGHT DATA

Vehicle	Weight	Geometry
Truck	Weight = 5460 lbs Front Axle = 2480 lbs Rear Axle = 2980 lbs	Wheelbase = 10 ft 6 in. Width = 5 ft 2 in.
Tow Cart	Weight = 4240 lbs (Includes Load Wheel 2200 lbs)	Wheelbase = 10 ft Width = 5 ft 2 in.
Sports Car	Weight = 2275 lbs	Wheelbase = 7 ft 7 in. Width = 4 ft 1 in.

(3) Test Data Reduction - Time histories of strain, pressure and load were obtained for the moving load and impact tests. Velocities were determined from time measurement between known distance markers. Since instrumentation was not used to record vehicle wheel loads, the load time histories for the load wheel were used. In addition to pressure, strain and velocity, such data as temperature, load variation and location, and speed variation were recorded. A summary of the number of data points that were obtained from the scaled pavement testing is shown in Table 3. The summary includes all data obtained with the truck load cart and sports car as well as the load wheel. The actual number of data points considered valid for correlation was less than that shown. Questionable load values, load identification, calibration and response characteristics limited the use of the measured data. A complete summary of the data points for the strains and pressures due to the load wheel is presented in Appendix B. The summary data include: data point identification, test trace number, test date, load speed, mean load, variation from mean, tracking error, data point relative to load, pavement section, ambient temperature, response and comments pertinent to the interpretation of the data. The choice of data for presentation, as best representative of the tests results for further reduction, was determined from this summary.

TABLE 3 - TEST DATA SUMMARY

Number of Data Points Obtained						
Concrete CBR 10	Static	Moving Load △	Moving Load □	Moving Load ○		Impact
Strain	4	19	23	-	2*	45
Pressure	1	35	82	38	4*	30
Concrete CBR 7**						
Strain	-	-	-	-		-
Pressure	-	8	18	18		-
Asphalt CBR 2						
Strain	3	37	65	71		-
Pressure	-	12	32	26		-
Asphalt CBR 10						
Strain	6	60	56	35		-
Pressure	-	14	8	8		-

△ Load Wheel

□ Truck Wheel Load

○ Cart Wheel Load

*Sports Car Wheel Load

**Crack Noted in Pavement Prior to Test

(a) Moving Load Time Histories - Time histories of the load trace were recorded on one oscillograph while the response strains and pressures were recorded on another oscillograph. For convenience all the traces are plotted together on Figure 7. The sequence of load events are identified on the trace in the figure as follows:

(1) Truck front axle
(2) Truck rear axle
(3) Load cart front axle
(4) Load wheel
(5) Load cart rear axle

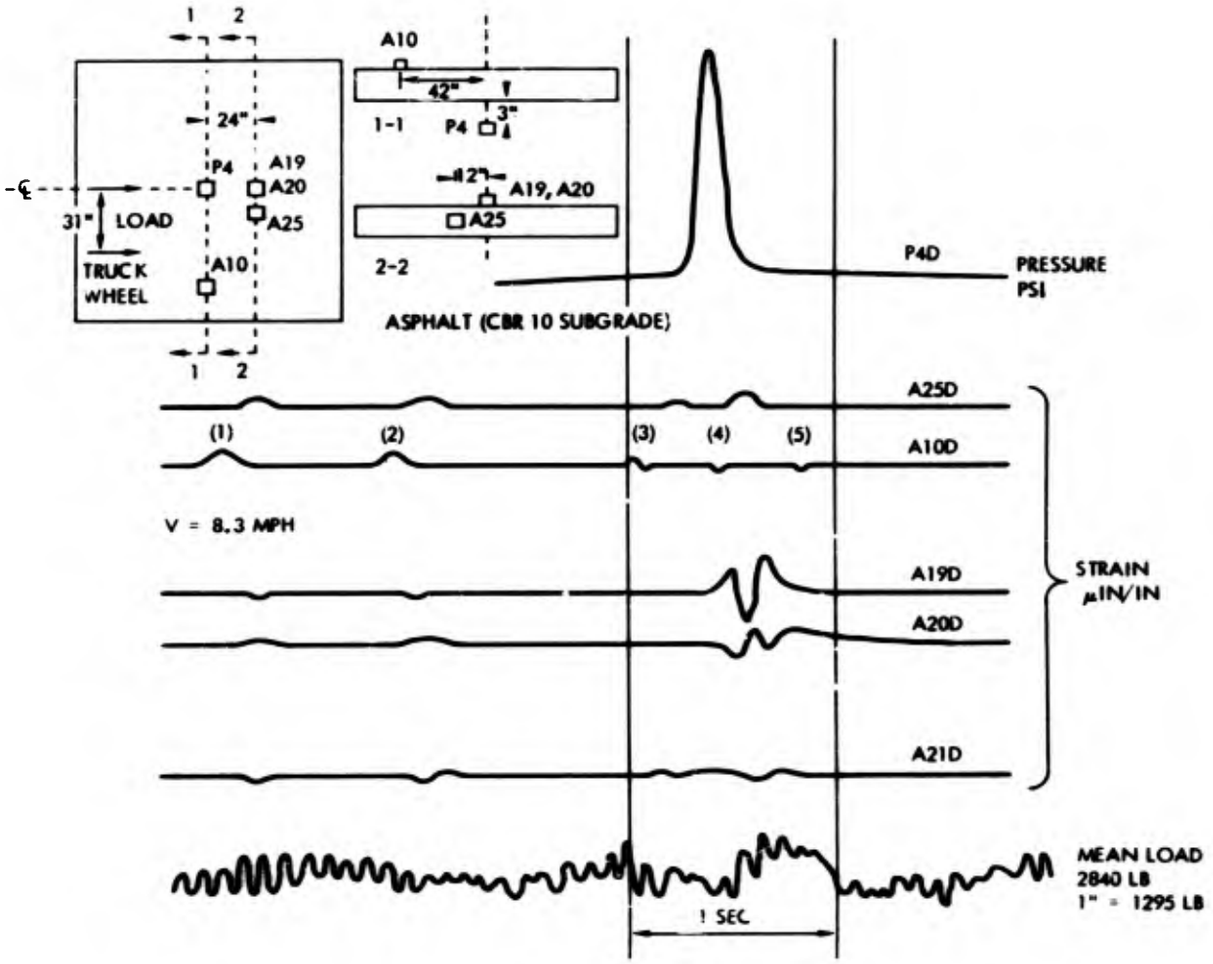

FIGURE 7 - Raw Data Moving Load Time History

All the response data representing the various loading events shows good separation. This particular trace shows strain gages located in the asphalt pavement and pressure gages in the subgrade (CBR 10).

The section is the second asphalt section which is denoted by the "D" (P4D, A25D, etc.). The figure depicts the time-wise character of the response in relation to the load. The pressures and strains have different calibration factors (See Appendix B), and therefore, the absolute values cannot be determined by relative trace heights measurements. Although the pressures, strains, and loads are plotted together on the same trace for convenience, the load trace used is taken from a different oscillograph recording.

(b) Moving Load Data - The raw data was plotted for the measured average mean load. To present a consistent picture for comparative purposes, since the mean load varied for the different speeds, the data was initially modified to a normalized 2200 pound mean load. However, due to the nonlinear relationship between pavement response and moving load, determined from subsequent analysis, this particular reduction technique was not extensively employed in the correlation between analysis and test data. Figures 8 and 9 show strain and pressure responses prior to and after the load normalization process for the asphalt pavement with CBR 10 subgrade and CBR 2 subgrade, respectively. The raw data and normalized data show good agreement i.e. the trend does not appear to be affected by the adjustment to the load. Figure 10 is a curve for the concrete pavement on CBR 10 subgrade. The unnormalized raw data is shown for strain gage I11A and Pressure gage P2A. Both gage locations are noted on the figure. Figure 11 shows unnormalized strains on the C pavement section. The gage locations are noted on the figure. The relative response magnitude reflect relationship of the gage locations with regard to the point of load application.

(c) Impact Tests - The impact test data was reduced to show the maximum tire load versus strain and pressure used in the testing. Figure 12 shows a time history of the load pressure and strain responses at 3 inches and 10 inches below the pavement. The drop height used was 3.5 inches and the tire pressure used was 100 psi. The load trace gives a good indication of when the load separates from the ground after impact. After 3 or 4 impacts the mean load starts deviating from zero, showing a tendency to maintain contact with the ground and for decreased drop heights the number of clean impacts decreases. The measured load pulse frequencies vary between 3.6 and 4.3 Hz, a frequency range which is equivalent to a test speed range of approximately 31 to 37 mph. The frequencies and loads measured are in good agreement with that determined by analytical expressions described in Appendix B. The strain designations in the time history reflect changes from the oscillograph recording and check of the data indicates that the designations between I8 and I11 were reversed. The relative values of strain now shown in Figure 12 reflect the practical relationship for the geometry and test conditions. Figures 13 and 14 show the soil pressures below the pavement at 3 inches (P4A) and 10 inches (P5A), respectively. In the region where the load leaves the ground, the P4A gage shows higher responses. The slopes of the two curves differ and below approximately 1.25 psi the P5A gage shows

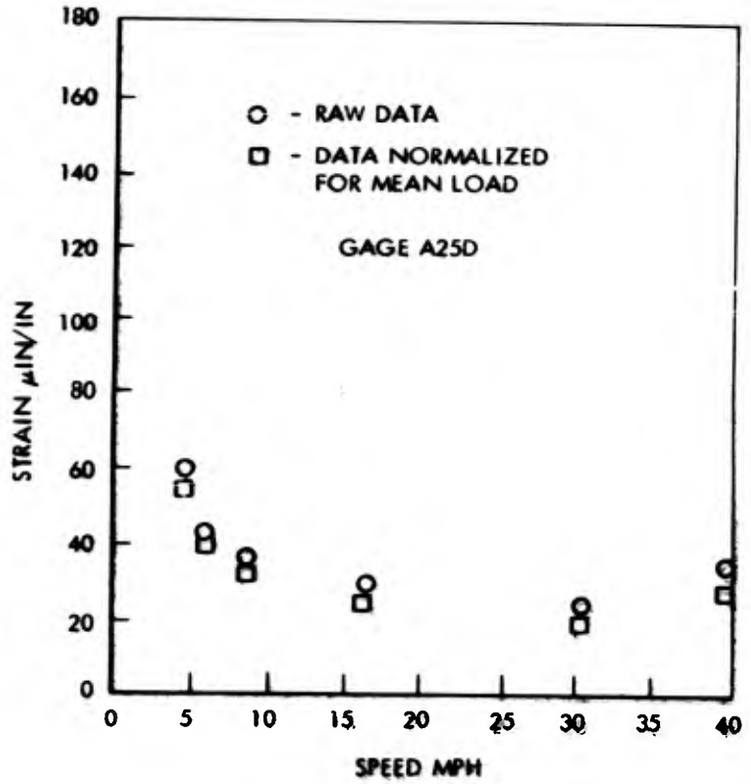

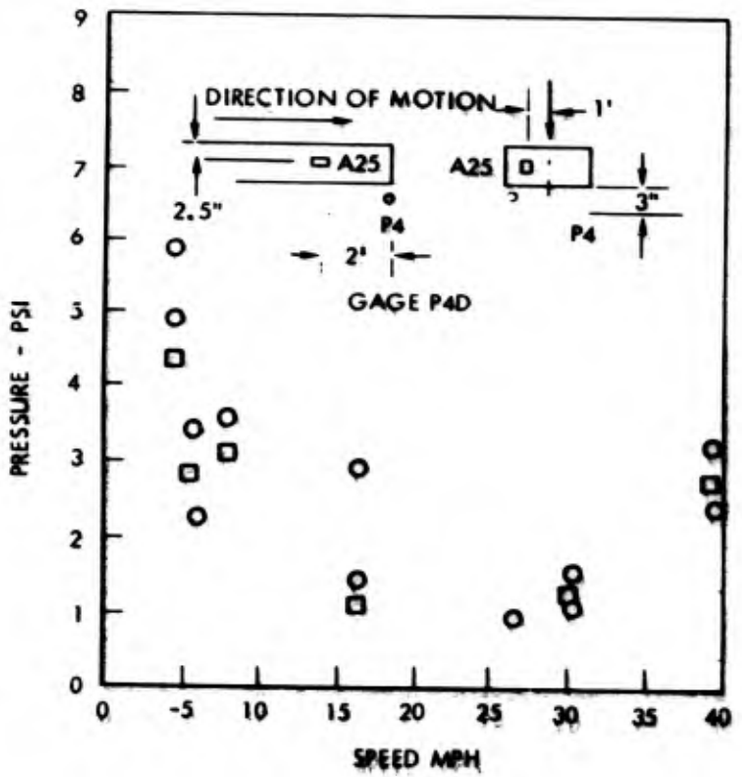

FIGURE 8 - Moving Load Data - Asphalt, CBR 10 Gages A25D, P4D

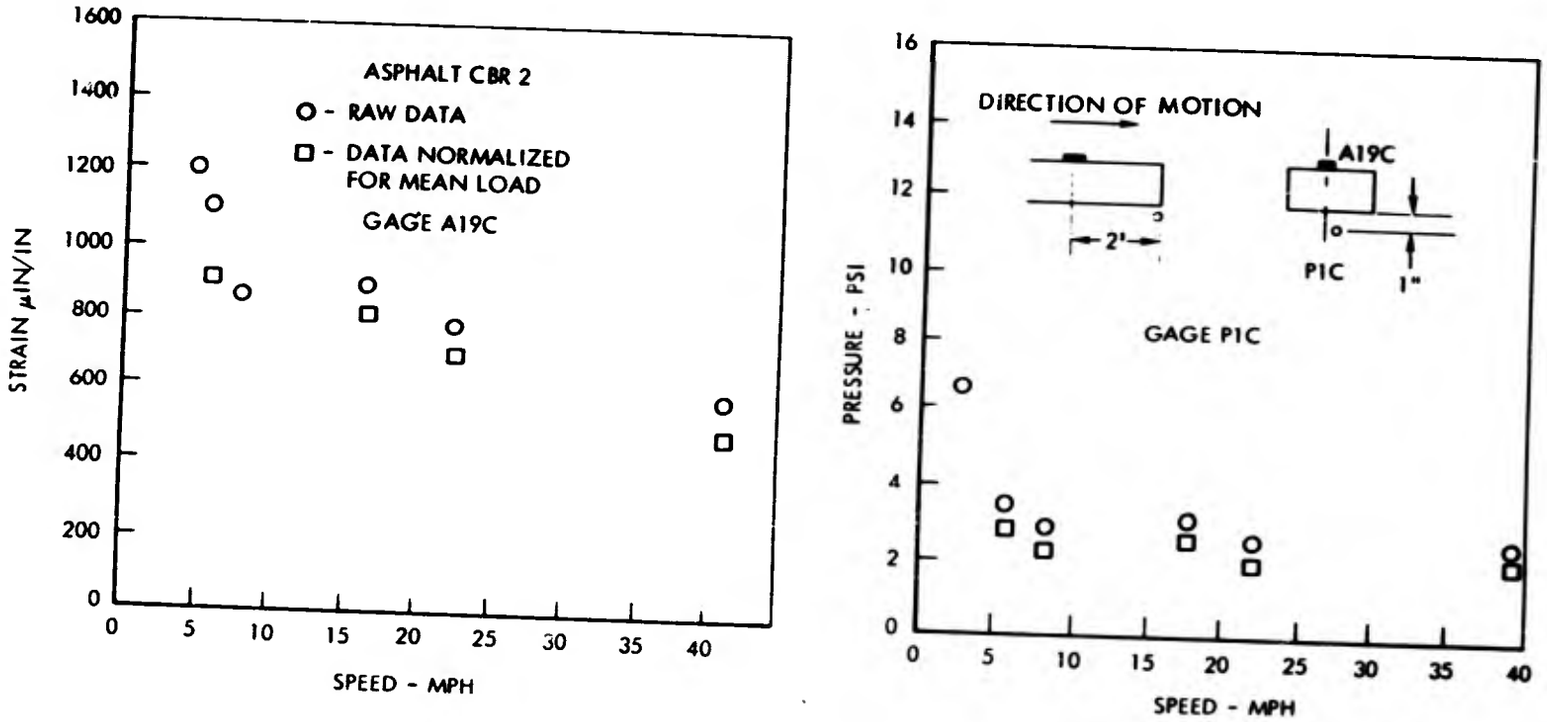

FIGURE 9 - Moving Load Data - Asphalt, CBR 2 A19C, P1C

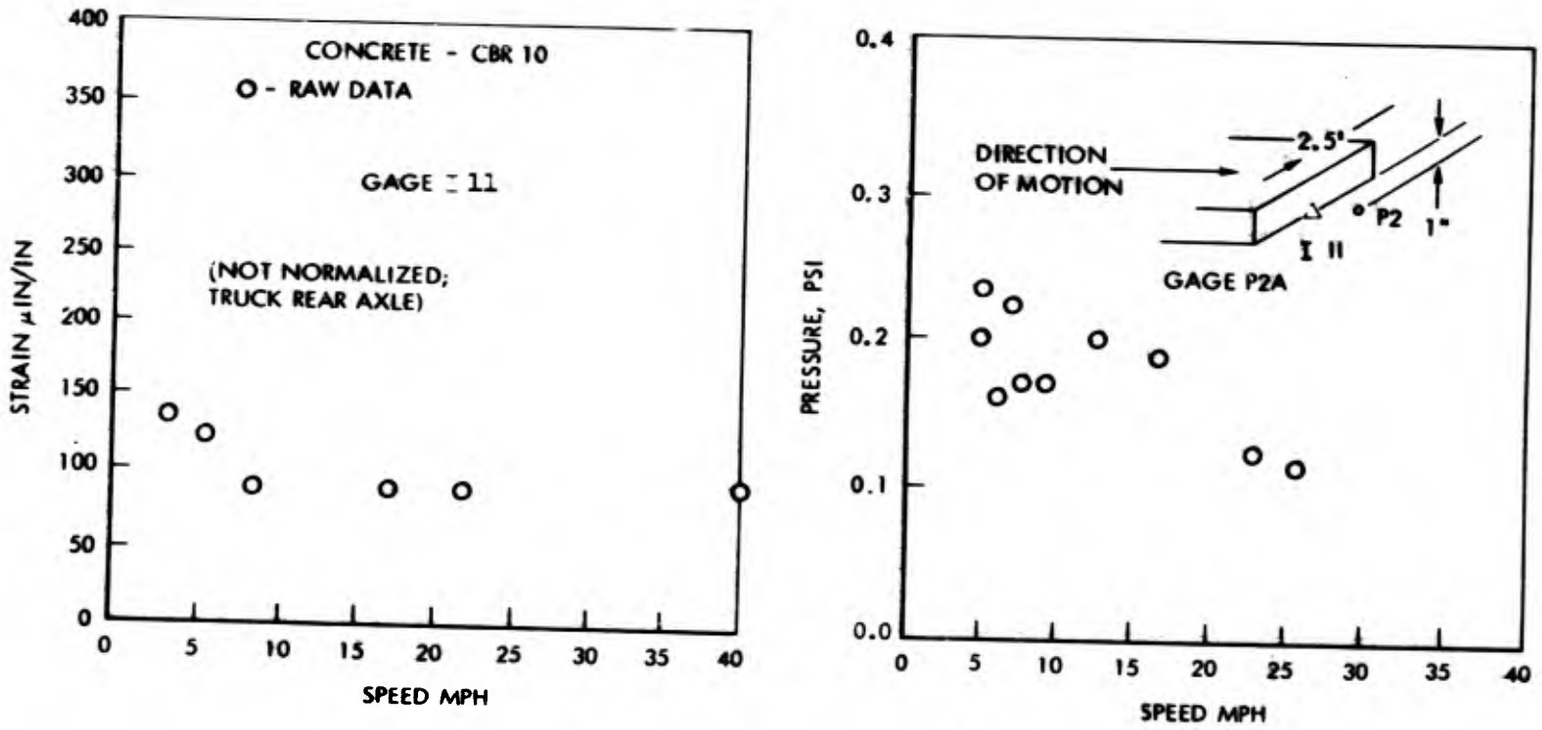

FIGURE 10 - Moving Load Data - Concrete, CBR 10 I11, P2A

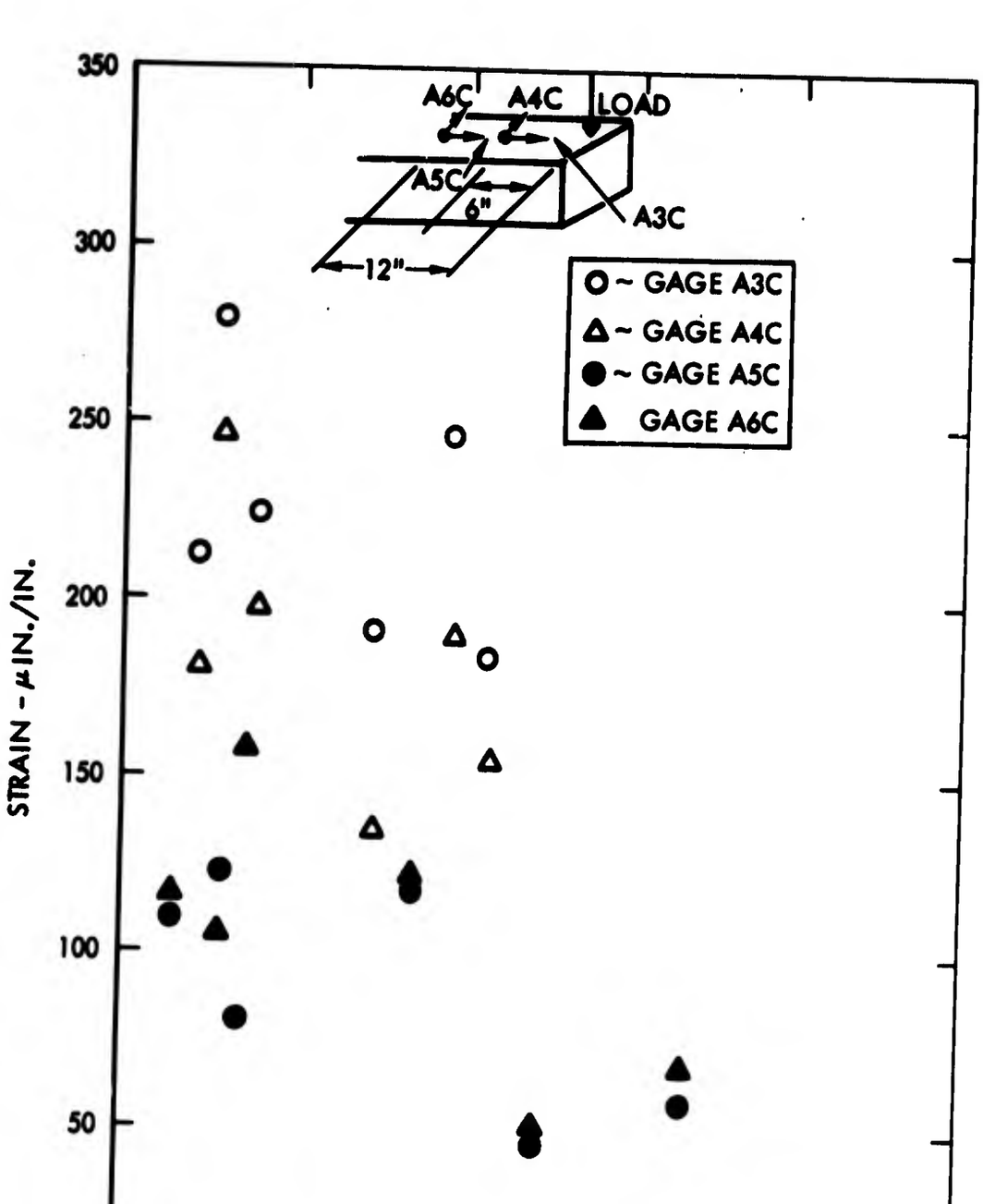

FIGURE 11 - Moving Load Data - Asphalt, CBR 2 - A3C, A4C, A5C, A6C

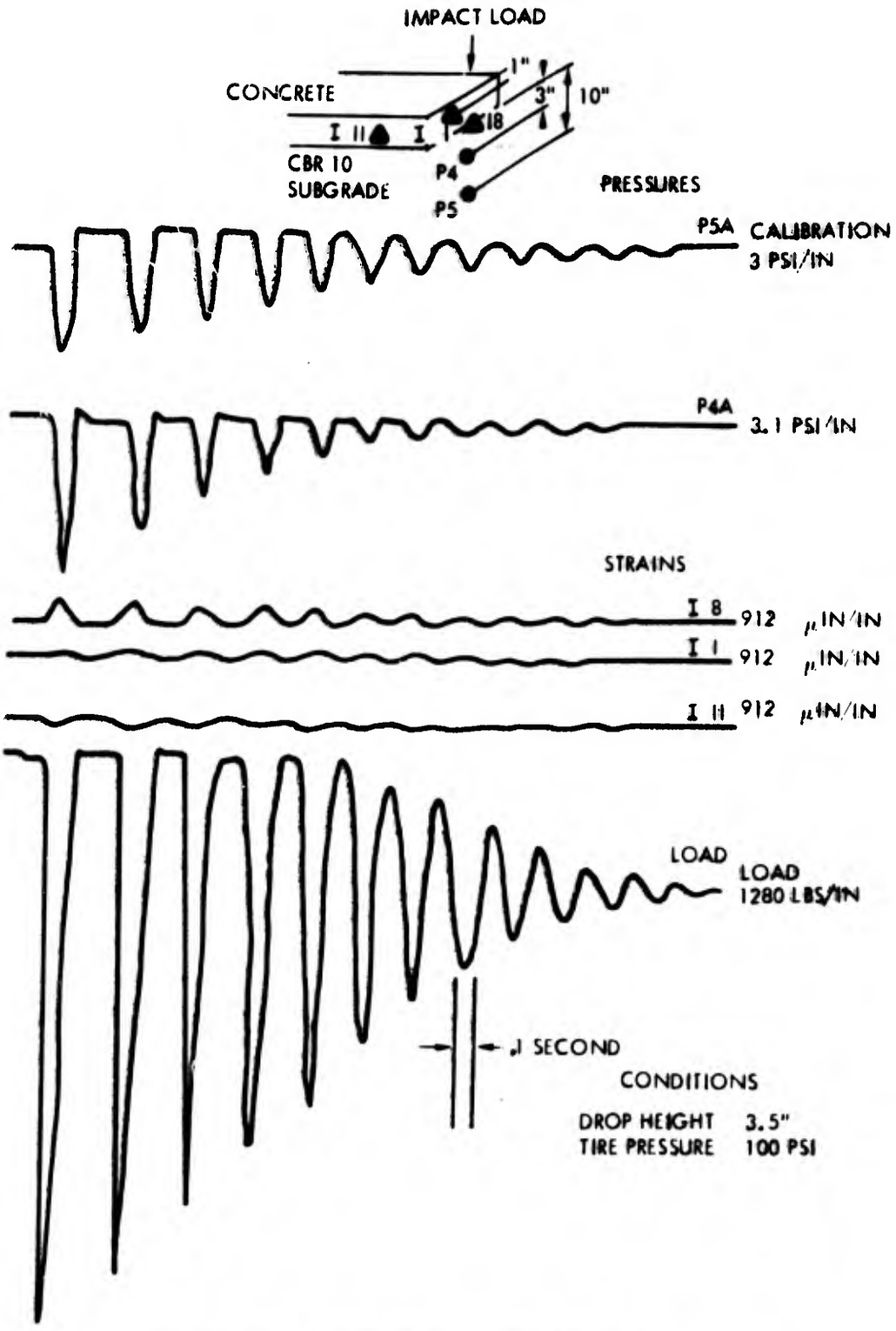

FIGURE 12 - Impact Tests - Time History Data

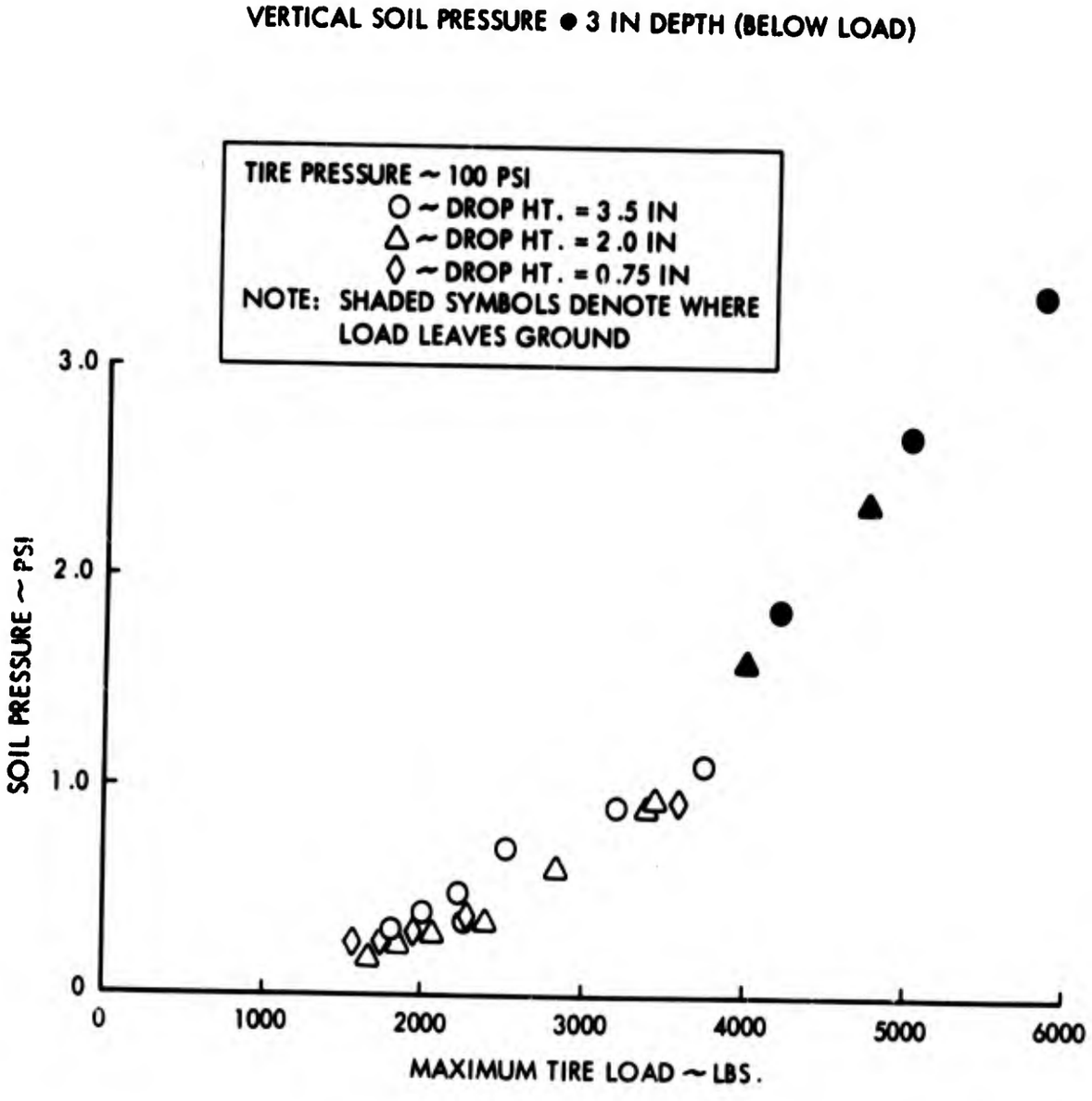

FIGURE 13 - Impact Tests on Concrete, CBR 10 - Soil Pressure versus Load, 100 psi Tire Pressure

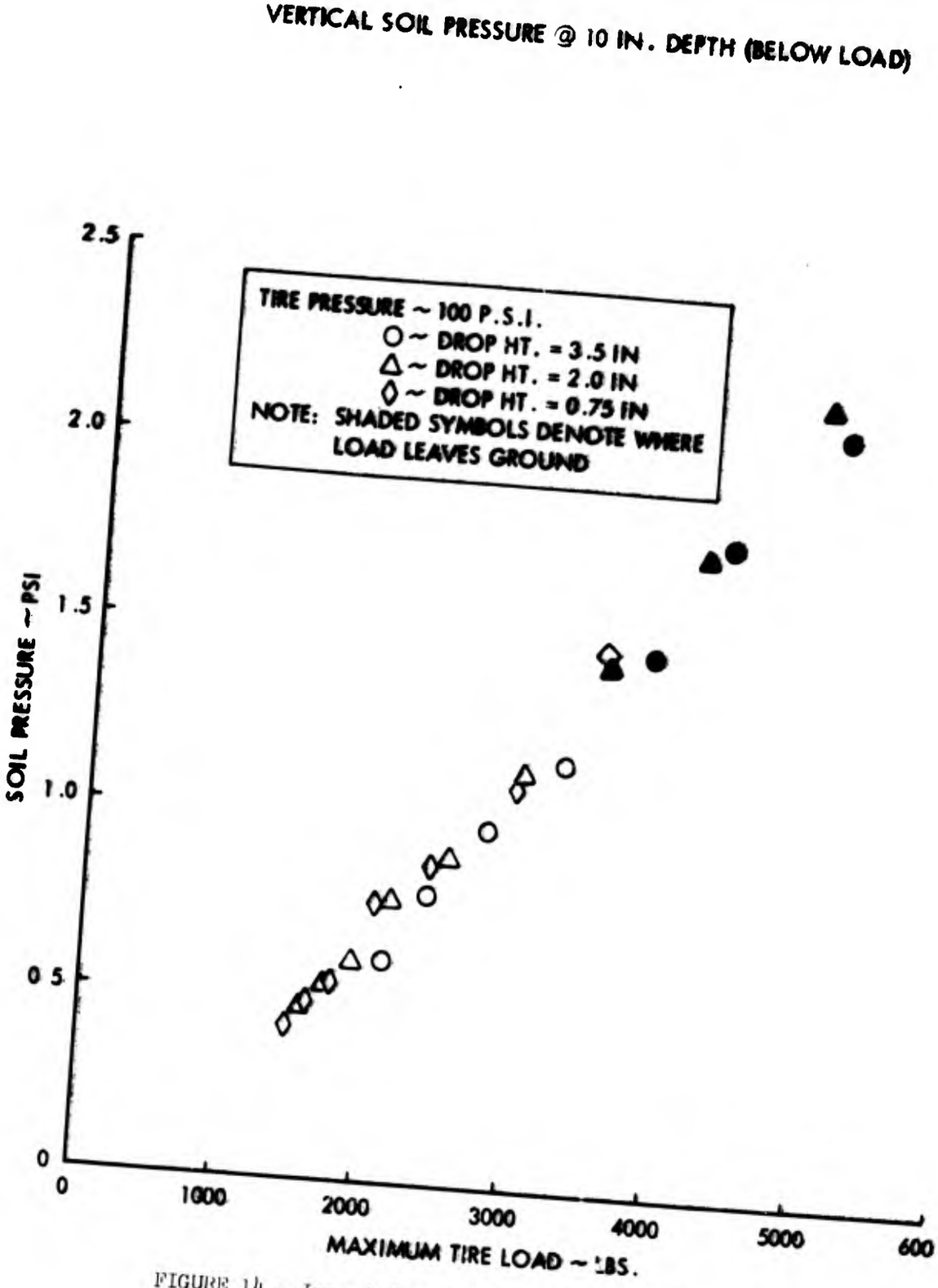

FIGURE 14 - Impact Tests on Concrete, CBR 10 - Soil Pressure versus Load, 100 psi Tire Pressure

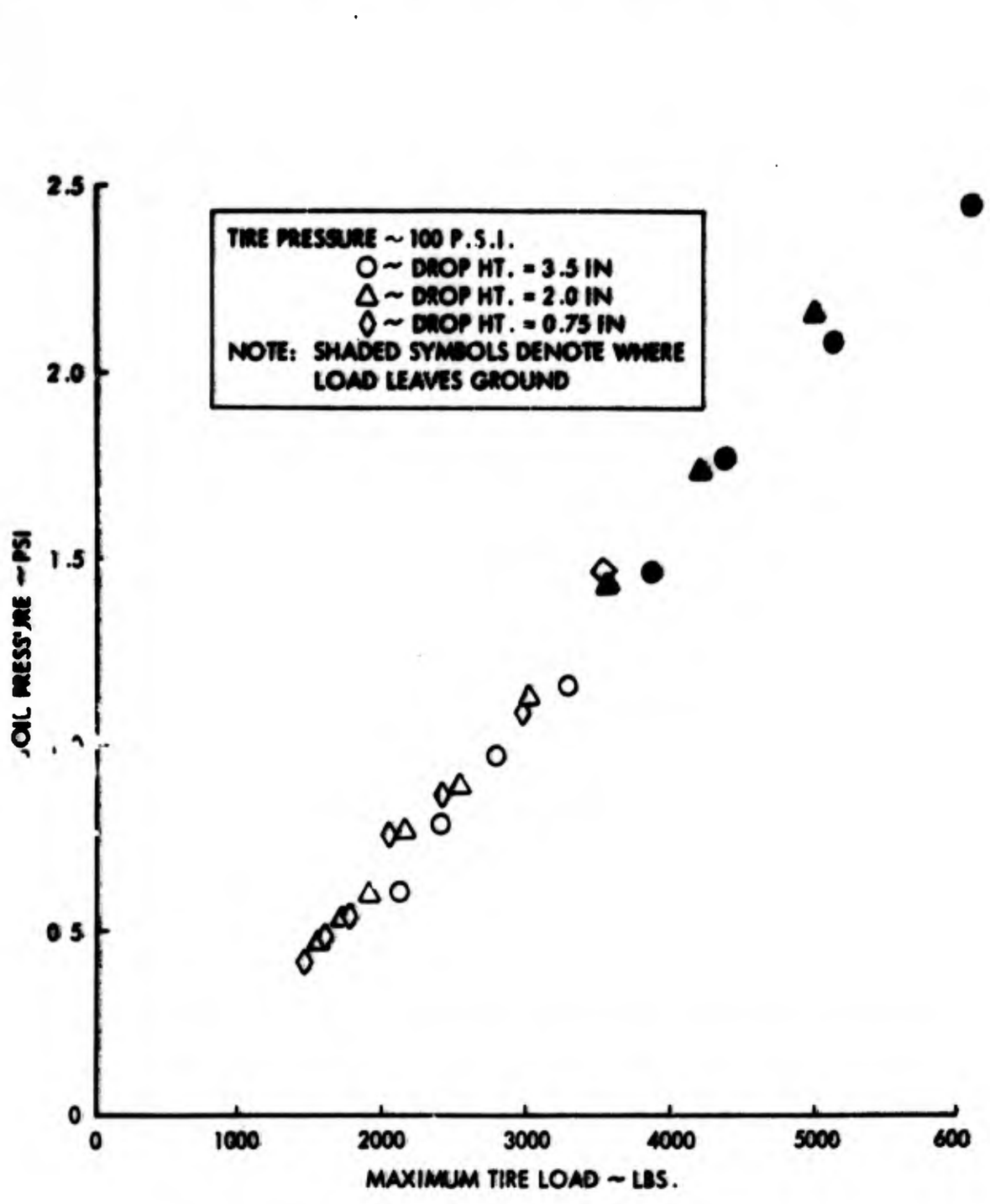

FIGURE 14 - Impact Tests on Concrete, CBR 10 - Soil Pressure versus Load, 100 psi Tire Pressure

higher values. The load where the crossover takes place is approximately 3500 pounds. This data indicates a sensitivity of the pressure gages below certain limiting values.

Figure 15 shows the PHA pressures for a tire pressure of 54 psi and the data in this curve approximates the results obtained from the higher pressures.

Figures 16 to 18 show the pavement strain below the load versus load applied for the three test tire pressures of 100, 72 and 54 psi, respectively. The plots show a linear relationship of strain with load. The range between 72 psi and 100 psi is very narrow and doesn't show much difference between the data although the lower strain curve does show a slightly lower slope.

(d) Static Test - Table 3 indicates that limited static test data was obtained. The prime difficulty appeared to be the inability to properly define the load trace and the conversion factors. Those strains that were used in the analysis are shown in Figure 19.

(e) Composite Data - The test data summary on Table 3 shows that only for the concrete section on subgrade CBR 10 is there sufficient information to construct a composite for all the tests. However, in order to develop such a curve, it was necessary to use load data from the truck wheels and the sports car wheel. As stated previously, these loads are estimates based on the geometry and weight data given in Table 2. Figure 20 shows the pressure measurements at a depth of 1 inch below the pavement for static and moving loads. The truck and sports car wheels have been normalized to 2200 pounds and the load wheel at 14 mph has been adjusted for dynamic load variation at that speed. The pressure gage was located off center from the load wheel. Data from the impact test is shown for a gage placed 3 inches below the pavement, subjected to an estimated impact load of 2200 pounds at a tire pressure and drop weight which simulates a load moving at 37 mph. The general trend is consistent with the majority of the data, although the curve is flatter than from most other data.

(f) Load Variation - The moving load time history trace shown in Figure 7 illustrates the oscillations of the moving load. The severity of the oscillations at the time the pavement experiences the load can influence the measured responses, and the degree of oscillation differs for each pavement section and for the speed at which the individual runs were made. During the test data reduction phase of the program, the percent deviations from the mean load were recorded for each gage. Figure 21 shows a typical plot of percent deviation from mean load versus speed for strain gages in the asphalt pavement supported by the CBR 10 subgrade. The curve shows a tendency for the percentage deviations to increase with speeds. The variation in load appears more severe for the asphalt pavement on CBR 10 subgrade than for the asphalt pavement on CBR 2. Unfortunately, the load variation measurements are based on maximum values in the vicinity of the responses and are not correlated exactly. The loads and responses are not recorded on the same oscillograph and the time correlating lines were always not accurate enough for this requirement. The discrepancy in timing correlation between oscillographs was attributed to a malfunction in either the paper speed control or timing mechanism.

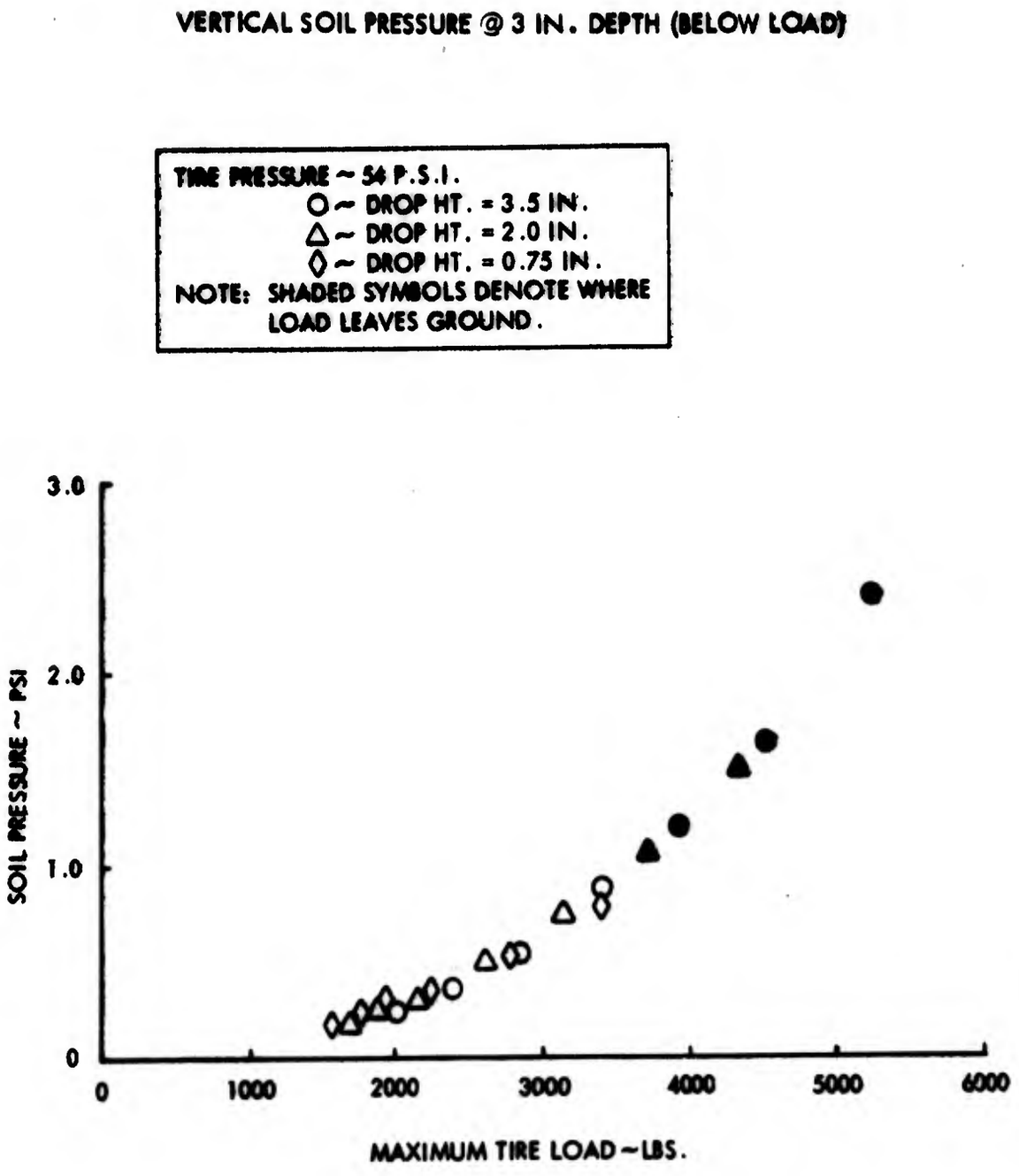

FIGURE 15 - Impact Tests on Concrete, CBR 10 - Soil Pressure versus Load, 54 psi Tire Pressure

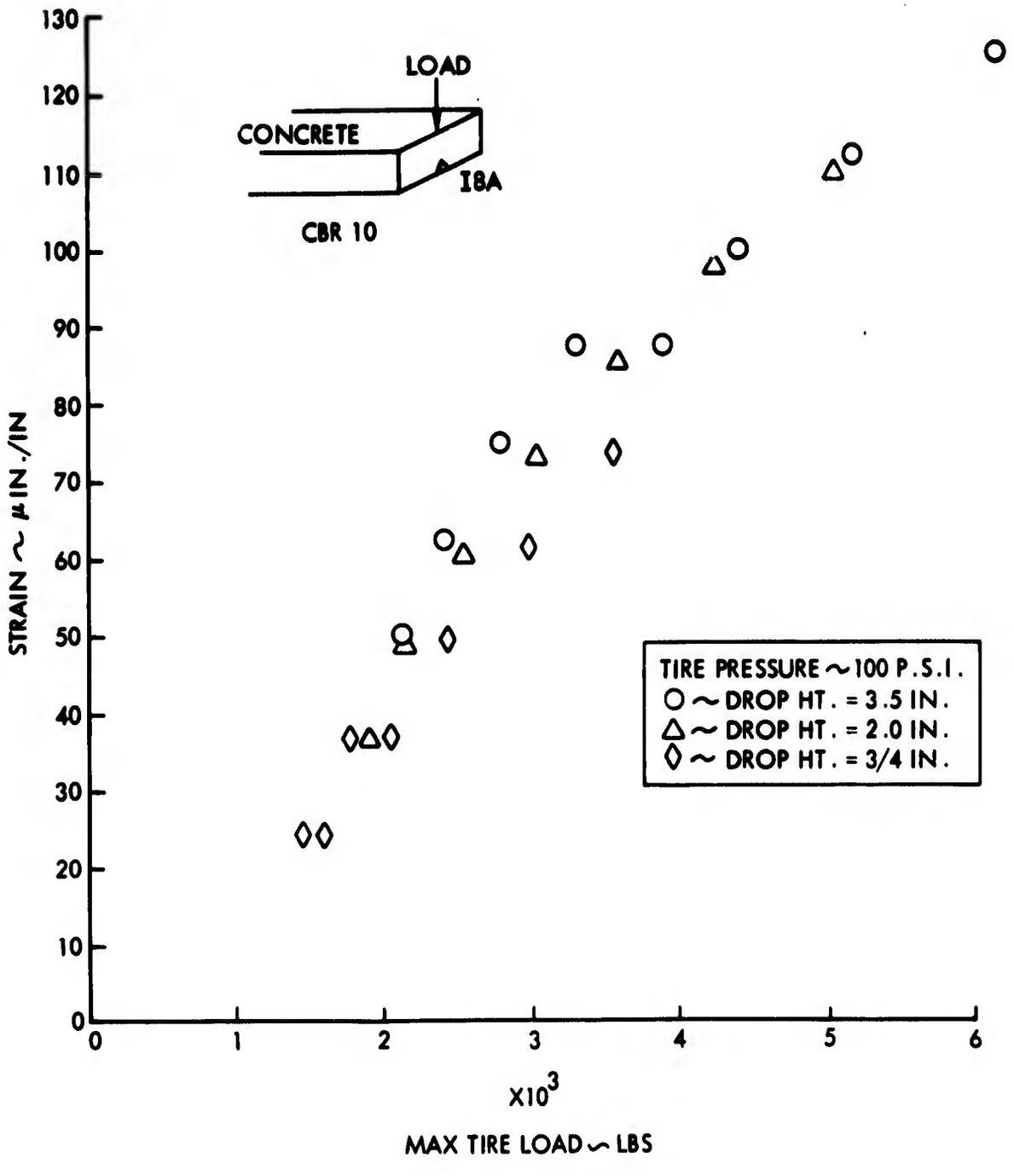

FIGURE 16 - Impact Tests - Concrete, CBR 10 - Soil
Pavement Strain versus Load 100 psi Tire Pressure

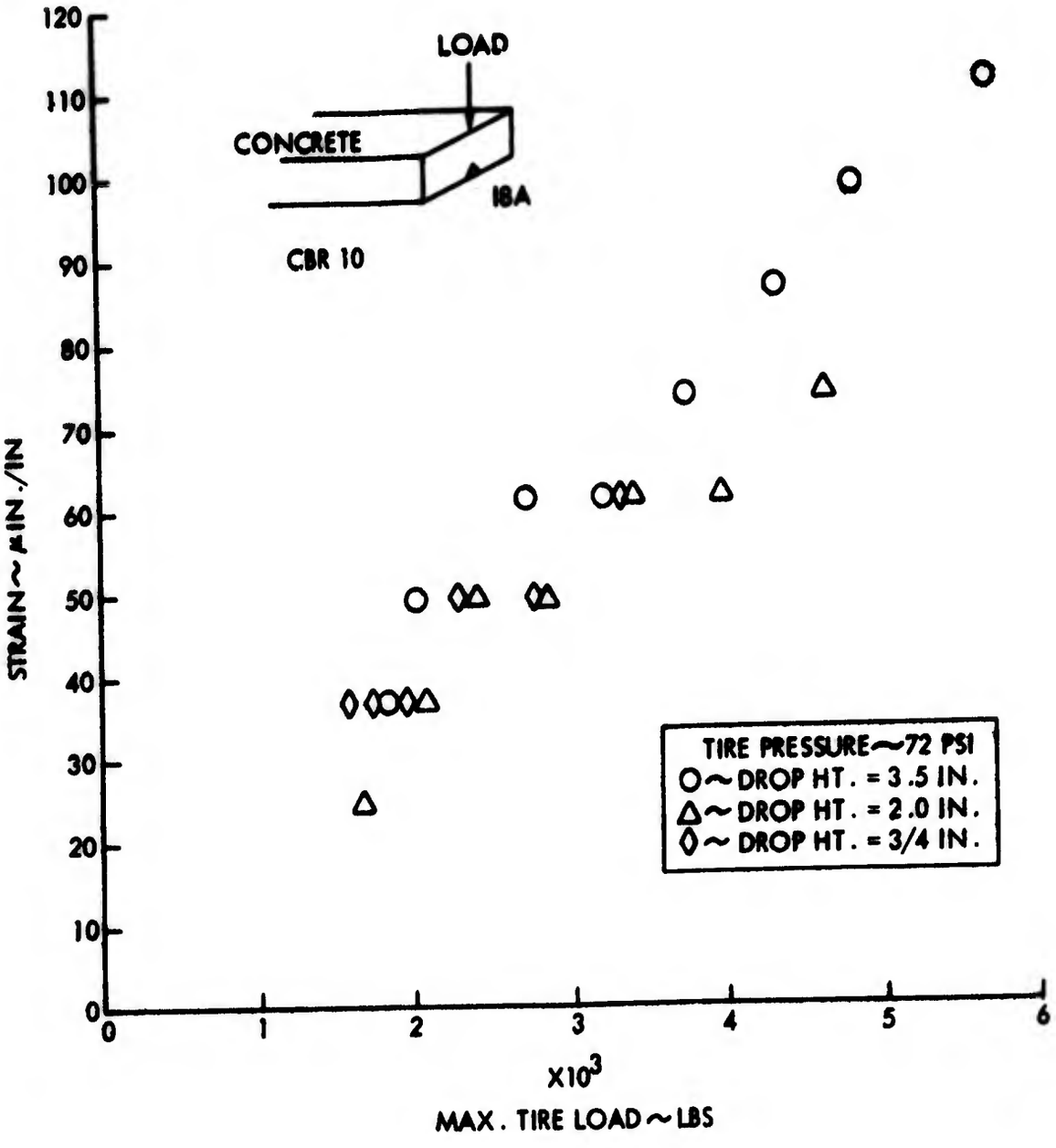

FIGURE 17 - Impact Test - Concrete, CBR 10 - Soil
Pavement Strain versus Load 72 psi Tire Pressure

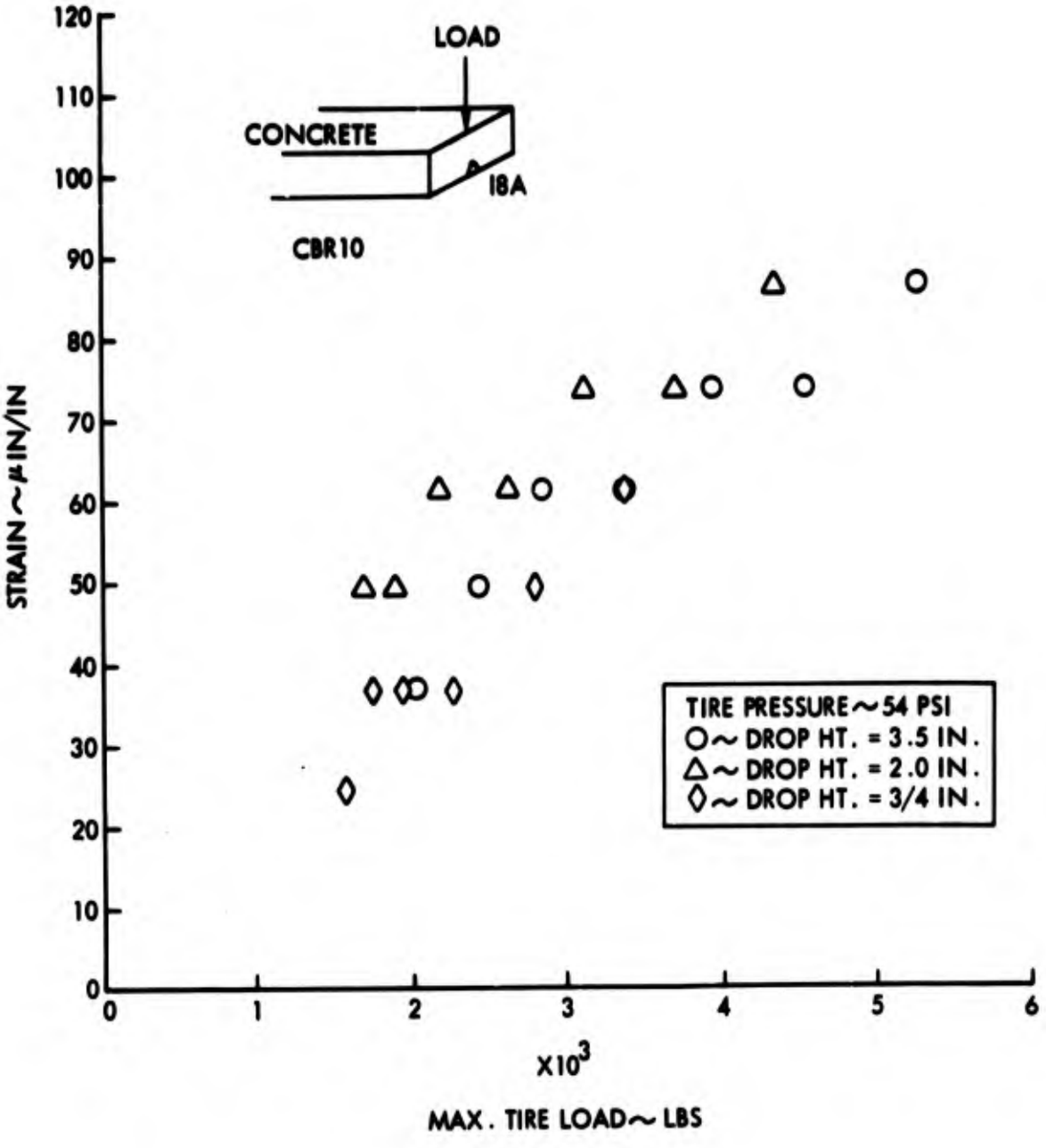

FIGURE 18 - Impact Test - Concrete, CBR 10 - Soil
Pavement Strain versus Load 54 psi Tire Pressure

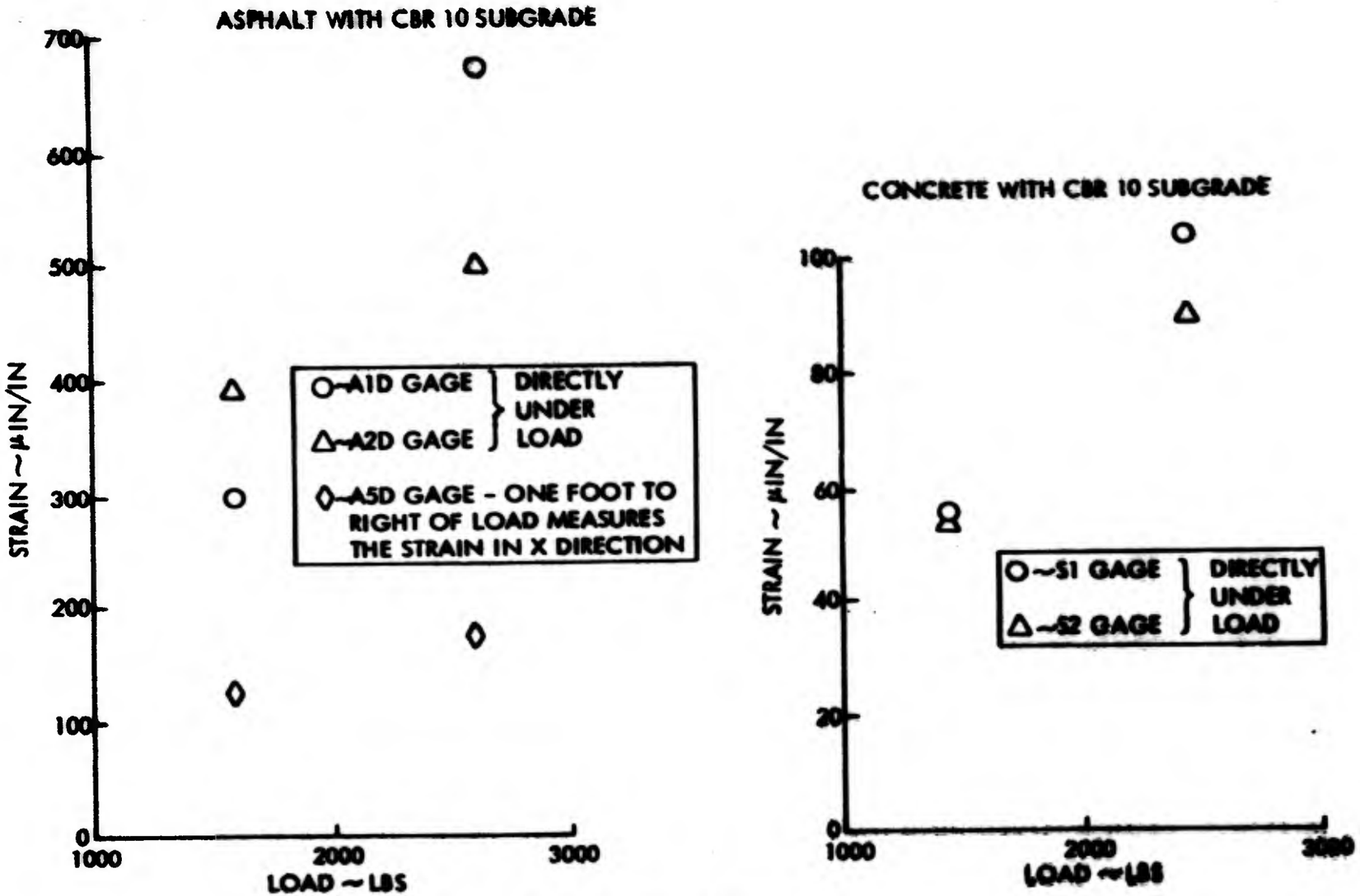

FIGURE 19 - Static Test Data

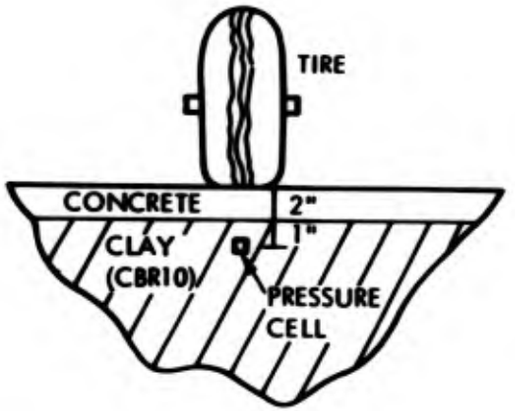

◊~LOAD WHEEL (GAGE PIA)
*18" x 7" P = 54 PSI

□~LOAD CART (LEFT FRONT AND LEFT REAR TIRES)
15" x 8" P = 40 PSI

O~TRUCK (LEFT FRONT AND LEFT REAR TIRES)
15" x 8" P = 40 PSI

O~SPORTS CAR (LEFT FRONT AND LEFT REAR TIRES)
16" x 5" P = 30 PSI

X~IMPACT DATA

*TIRE DIAM x TIRE WIDTH

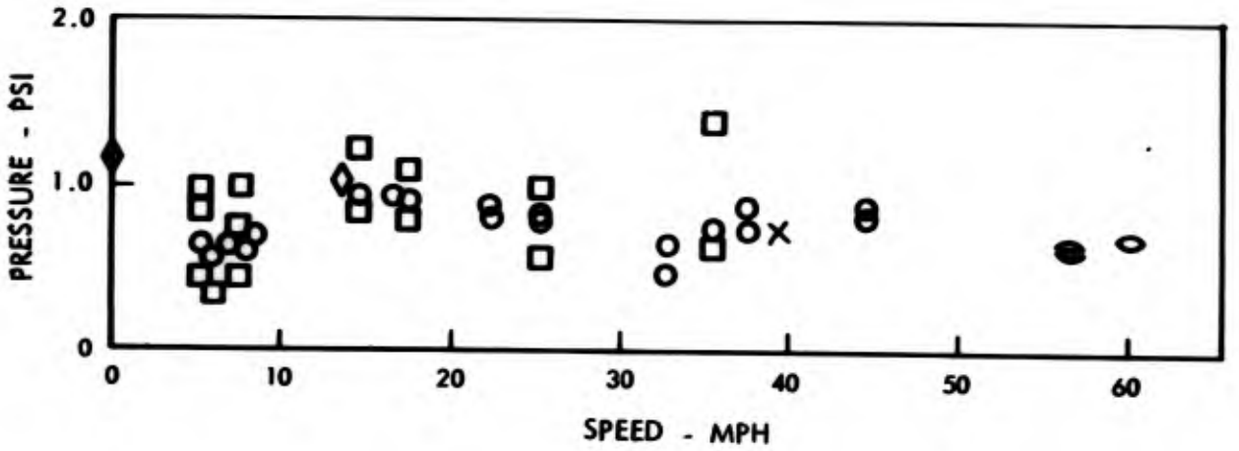

FIGURE 20 - Composite Data

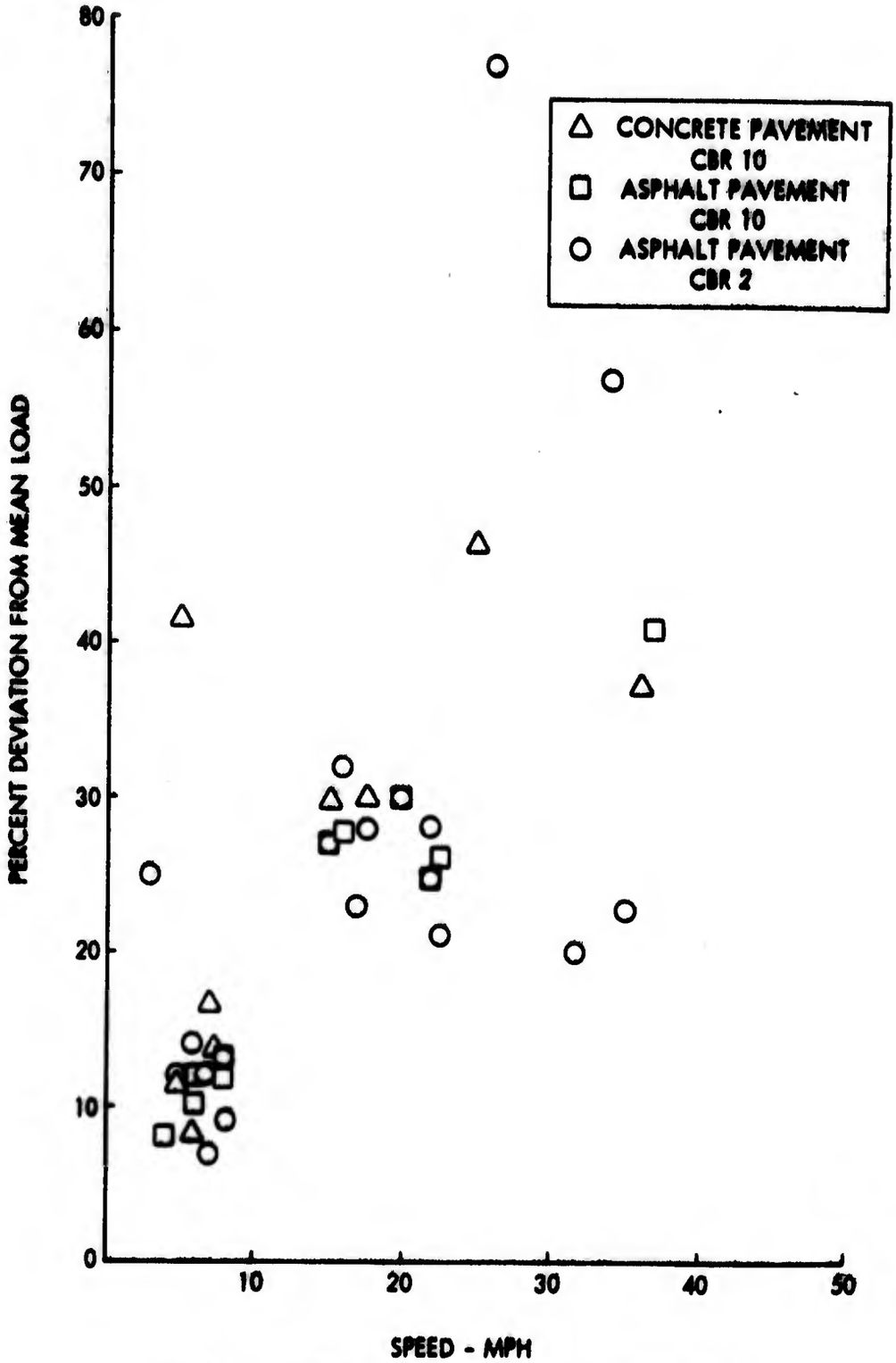

FIGURE 21 - Mean Load Variations versus Speed

(g) Integrated Pressure Values - Since the accuracy of the load measurements were consided important in performing correlation studies, a sampling of pressure time histories was integrated and compared with the measured load values. The integration scheme assumes a symmetrical radius of load. This procedure, illustrated in Figure 22, showed varied results. Although the particular case shown indicates a good agreement between the integrated and measured load values, other integrations showed wide disagreement between the two. The integrated values were also used in correlating between the test and analysis.

(h) Soil and Pavement Measurements - Upon completion of the tests, the pavements were cut into sections and removed. The thickness was found to vary no more than 1/8 inch for the two inch concrete slab and no more than 1/4 inch for the five inch asphalt slab. It was observed that the asphalt slab could easily be parted at its mid-plane (constructed in two 2-1/2 inch thickness layers so that instrumentation could be installed between layers). This shows possible weakness in horizontal shear. The CBR tests indicated that the soils held their respective 2 and 10 ratings throughout the tests.

Materials Research and Development laboratory test results are described in Appendix C. The measured modulus of resilience, which is a measure of dynamic stiffness, for the two soils used in the scaled pavement testing, was obtained for a range of frequencies of compression stresses applicable to the test conditions. The static modulii, dynamic modulii and the rates of damping values obtained from the tests were used in the correlation studies and are discussed further in later sections of the report.

(4) Scaled Runway Test Conclusions - The scaled test program helped establish some very essential requirements for future test work. When the tests were originally planned, it was recognized that scaling effects could present some difficulties in evaluating the results. However, many of the problems that were encountered were due to factors which can easily be improved upon in the future. Some of the significant conclusions that can be drawn from the scaled test results are:

- Material Property Evaluation - Soil measurements should be made on site. These measurements should consist of static and dynamic modulii, damping, moisture content, CBR rating and compaction.

  The material characteristics should be determined, as much as feasible, under various rates of loads.

  Both pre- and post-tests should be performed to determine the nature of any geometrical or material property changes that have taken place in either the pavement or the subsoil.

  To minimize the effect of construction techniques on the test results, standardized methods should be employed. The test bed ideally should

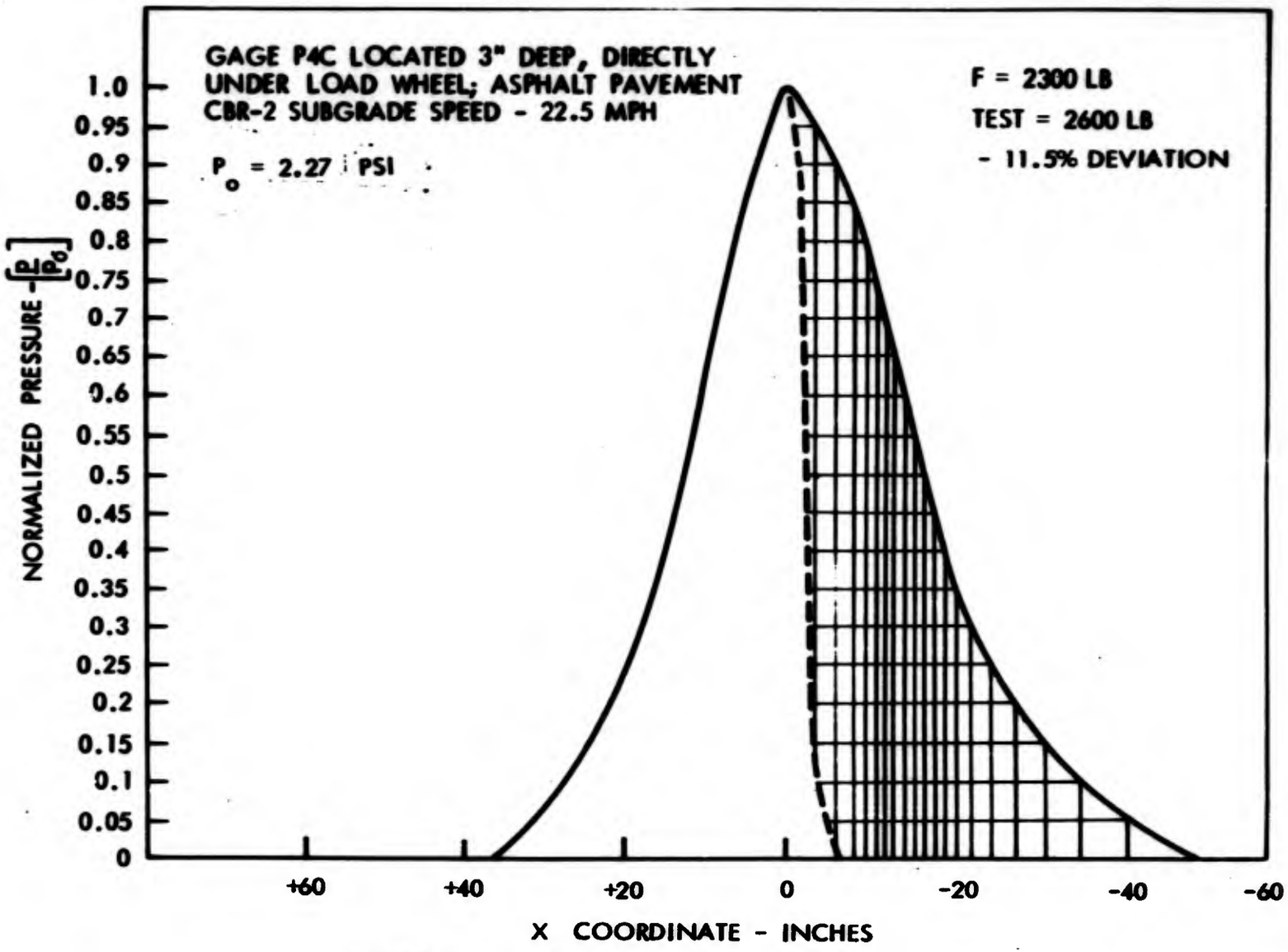

FIGURE 22 - Pressure Integration Scheme

be identical to that used in airport pavements. Compaction techniques, for example, could influence the material properties and consequently their responses.

- Test Design - Load oscillations must be minimized. The tests showed variations of up to 80 percent of the mean load. The design of the loading device should attempt to limit these oscillations to less than 10 percent. The oscillation levels should be tested at all speeds prior to the actual test.

  There must be a positive means of determining the tracking error. A load several inches off the intended track can have a significant effect on the measured response since the radius of influence is less than three feet. Furthermore, the tracking error could vary during the course of the run and, consequently, result in an inconsistent evaluation of the results.

  The variation in load velocity should be controlled, particularly at low speeds (0-10 mph) where the pavement response is very sensitive.

  The loading scheme should be designed such that any loading effect from other than the load wheel should be eliminated or minimized. At the very least, any such affects should be accounted for by analysis prior to the test. All loads that can influence the responses should be recorded such that the timing is fully correlated with all other data.

  A complete set of data should be planned for and include static, moving and impact loads, for all combinations of pavement and subgrade test sections; fragmentary data makes comparative analysis extremely difficult.

  Impact tests should be designed to cover a wide range of tire pressures, loads and drop heights. The results of impact testing are significant for evaluating response over a wide frequency range and for ascertaining whether superposition of loads can be achieved to represent a moving load.

  Tests should be performed at more than one mean load and one tire pressure. The relationship of response to load magnitude and distribution is important data.

  Static tests should be conducted with different load levels and with different rates of loading. These measurements are important as references on which to evaluate moving load effects. The importance of varying the load rate is to obtain a duration of loading which will not produce plastic deformation.

- Test Procedure - The load must have accurate time correlation with both the pressure and strain gages. A prime consideration in the recording procedure is to obtain an accurate assessment of the output-input relationship in the system at all times.

  The moving load tests should be planned so that each measurement is obtained several times. The data obtained on this program showed a wide scatter range. Without the benefit of redundant tests, it is difficult to ascertain whether the variation in data measurement is due to instrumentation, load conditions, environmental conditions, test equipment and/or techniques.

  Preliminary spot checks of the oscillograph data should be performed to determine the validity of the data. Such checks will assist in determining what, if any, problems exist in the instrumentation or test equipment and will provide information for possible modifications in the test plan.

  Environmental conditions should be continually recorded. Thermocouples installed in the material will provide data to evaluate material properties.

  Care must be taken to make sure that basic test procedures are adhered to including proper identification of recording channels and calibration notations. The calibrations must be performed before each test to ensure consistent conversion factors.

  A thorough check of the instrumentation prior to and during the test program is necessary. Spare gages should be available for replacement of malfunctioning instrumentation and used where there is accessibility.

- Instrumentation - Strain gages should not be imbedded in a pavement section. The major portion of these gages were inoperative throughout the test program.

  Particular care must be taken in evaluating strain and pressure readings when the signal is extremely low. In this test the reliability of pressures below 1 psi and strain values less than 50 μin./in. are questionable. Unless the calibration values of the instrumentation are such that response parameters are easily read, large percentage errors result even though only small absolute values are involved. However, for the purpose of these tests, trends may be evaluated on this basis of the data obtained.

The placement of metal plates above the strain gage is questioned. Distortion in the output of the gage due to the influence of the plate acting on the gage is suspected in several instances.

The measurement of pavement surface deflection would provide valuable data in evaluating pavement response and correlating it with theory. An optical system, if used in the future, should be mounted in such a manner that the system is isolated from excitations resulting from the test.

- Scaled Effects - The requirements of scale testing nondimensionalizing parameters limit the applicability of the test data to speeds below the actual runway speeds.

The consequence of inertia effects is difficult to determine on scale testing since the wave propagation speed of materials is much greater than that of the maximum scaled test moving load speed.

Scaled testing, to be descriptive of all aspects of actual parameters, requires an extensive development program in itself, prior to the performance of any tests. The extension of scaled tests in total to the actual system is questionable when considering the many variables associated with each portion of the total system, including pavement, subgrade construction techniques, geometry, stress distribution, load requirement, inertia effects, and speed.

The construction of the scaled pavement introduces artificial effects which are not necessarily associated with existing airport pavements. Among these differences are:

Partitioning of sections
Preparation of surface
Installation of instrumentation at section midplane

The combination of partitioning of the sections and preparations of the surface apparently created a situation where each section developed a distinct surface contour which influenced the load induced into the pavements. The wide variation in loads associated with the asphalt on CBR 2 subgrade gives evidence of this effect.

The separation of the pavement at the mid-plane had an effect on the strength capability of the section which, as a result of reducing pavement stiffness, may have produced higher loads than originally anticipated.

The pavement surfaces, having been designed for short term testing, are inadequate representations of surface finishes on actual pavements. This is indicated from observations of surface deterioration after a few test runs.

(C) Analyses - The problem of pavement/airplane compatibility consists of two parts: (1) the imposed airplane loads and (2) the response of the runway to the induced loads. The analyses performed in this program simplified the problem to some extent by considering each part independently. This treatment is considered reasonable since the pavement under most operating conditions responds to the load. An exception to this occurs during operations where runway unevenness is encountered and the airplane is responsive to the ground contours and as a result produces oscillatory loads which act upon the runway and possibly create additional unevenness. The analyses in the following sections for both the airplane induced loads and pavement response to such loads describe the significant factors which effect the magnitudes of each.

(1) Loading Imposed on Airport Pavements - The airplanes that have been selected for analysis have been categorized primarily according to their maximum takeoff gross weight and assigned certain code designations as indicated in Table 4 below. Current and future jet transports have been chosen so that the analyses will be consistent with the intended application of the study results.

TABLE 4 - AIRPLANE IDENTIFICATIONS

Code	General Description	Max. Gross Wt. - Kips	Landing Gear Configuration
A-1, A-2,....	Current Jet Transports	200 - 350	3-Gear Conventional
B-1, B-2,....	"Airbuses"	400 - 600	3-Gear Conventional 3 Main Gear
C-1, C-2,....	"Jumbo Jets"	>600	5-Gear
D-1, D-2,....	Large Supersonic Aircraft	>500	3-Gear 5-Gear

The airplanes were analyzed for those operations which cover the spectra of operating loads that are anticipated. These operations were stated in the introduction and are reiterated again in Table 5.

TABLE 5 - AIRPLANE OPERATIONS

	Operation
Departure	1. Parking (static) 2. Low speed taxi 3. Turning 4. Low speed braking 5. Accelerated takeoff roll 6. Aborted takeoff - high speed braking 7. Takeoff rotation
Arrival	8. Landing impact 9. High speed braking 10. Decelerated landing roll out 11. Low speed braking 12. Turning 13. Low speed taxi 14. Parking (static)

The loads that airplanes impose on airport pavements are a function of three primary variables:

Airplane Characteristics

Runway Surface Characteristics

Airplane Operation

The significant airplane characteristics include the following:

Weight, c.g. location, inertia

Aerodynamics

Landing gear characteristics - number of gears

Tire characteristics - size, pressure, number per gear, spacing

The loads imposed on airport pavements during each of the operations listed in Table 5 will be discussed in turn. The significant factors for the respective operations will be discussed in detail and parametric variations will be presented to illustrate the effect of airplane and runway characteristics on dynamic loads.

(a) Static Loads - The maximum static loads obviously occur at zero velocity and at maximum ramp weight. Table 6 below lists maximum static loads for those airplanes for which data is available. Maximum main gear static loads correspond to an aft c.g., maximum nose gear static loads occur with a forward c.g.

TABLE 6 - MAXIMUM STATIC LOADS

Airplane	Max. Gross Wt.	Max. Main Gear Static Load	Max. Nose Gear Static Load	Number of Main Gear Tires	Number of Nose Gear Tires
A-1	310,000	146,940	32,830	4	2
A-2	310,000	145,740	34,360	4	2
B-1	411,000	195,700	39,890	4	2
B-2	413,000	193,280	46,030	4	2
B-3	510,000	193,280	46,030	4 & 2	2
C-1	713,000	166,500	71,300	4	2
C-2	861,500	202,000	93,100	4	4
D-1	595,000	273,330	59,090	6	2

Also shown in Table 6 are the number of tires on each main and nose gear. Since the main gear and nose gear tire pressures are roughly equal for a given airplane, the load per tire gives an indication of the relative severity of pavement loading between main gear and nose gear. For all the airplanes shown, the main gear loads the pavement more severely than the nose gear, although for airplane C-1 this is barely true. This does not account for interaction loading effects between closely spaced tires on a gear.

For airplanes with more than three independent gears, the static loads are statically indeterminate, and runway crown effects can become significant due to a distribution of loads. For airplane B-3, with a centerline main gear, variations in runway crown from 0 to 1.5 percent result in static centerline gear loads varying from 85 to 103 percent of nominal.

For those airplanes with data available, the extreme forward and aft c.g. limits were quite similar from plane to plane. With an aft c.g., the main gears (2, 3 or 4) carried from 92 to 95 percent of the airplane weight. With a forward c.g., the nose gear carried between 9.7 and 11.2 percent of the airplane weight.

(b) Low-Speed Taxi - Low-speed taxi (< 30 knots) can yield vertical gear loads which are in excess of static load, due to taxiway roughness. The airplane is still at essentially its maximum ramp weight, since very little fuel has been burned. The airplane velocity is too low to achieve any significant aerodynamic lift. Hence, even without any braking or turning, discussed separately below, the airplane will impose greater than static vertical loads on taxiway surfaces.

From the data available, it appears that taxiways can be considerably rougher than runways. For example, Figure 23 shows the power spectral density

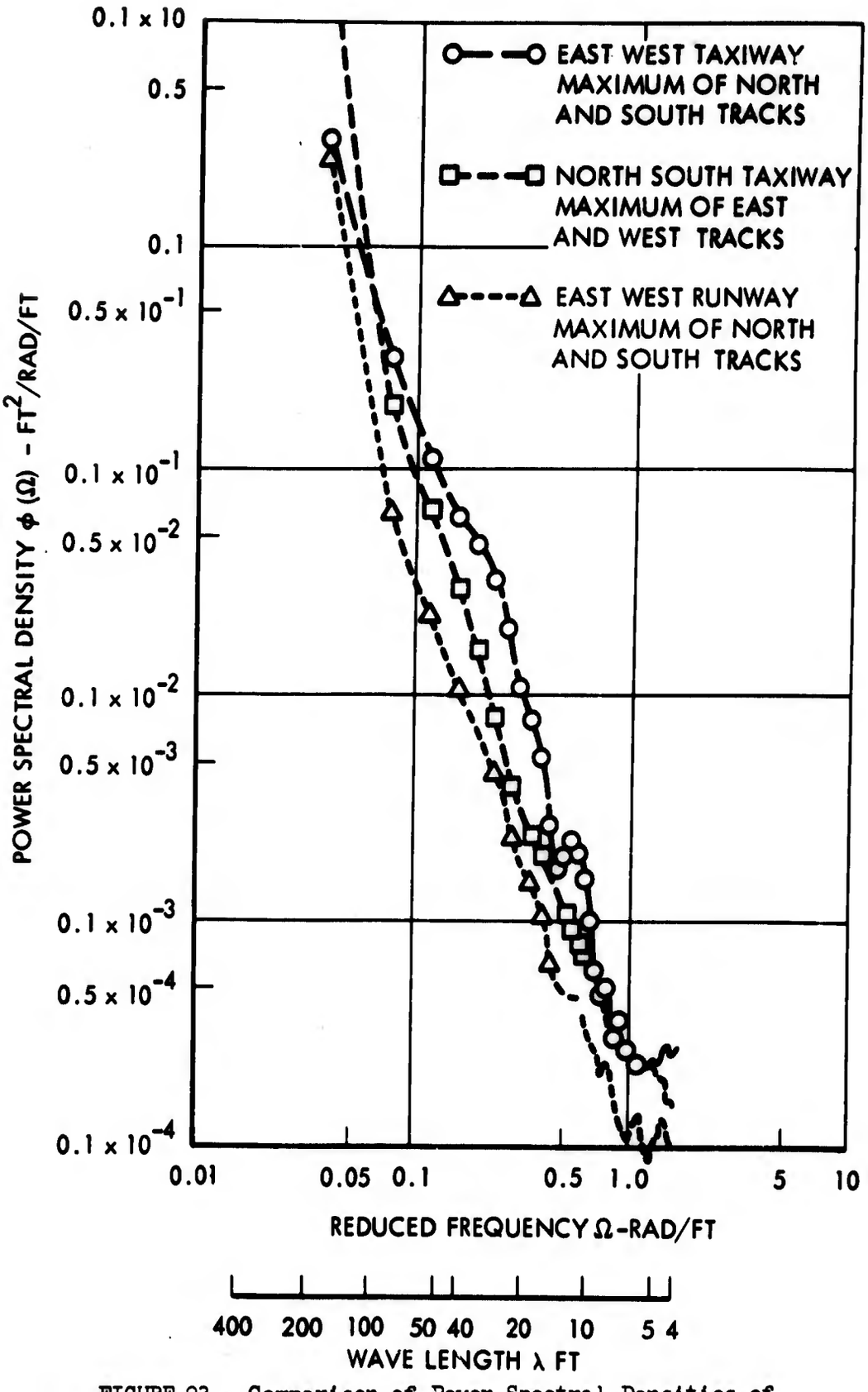

FIGURE 23 - Comparison of Power Spectral Densities of Lockheed Air Terminal Runway and Taxiways

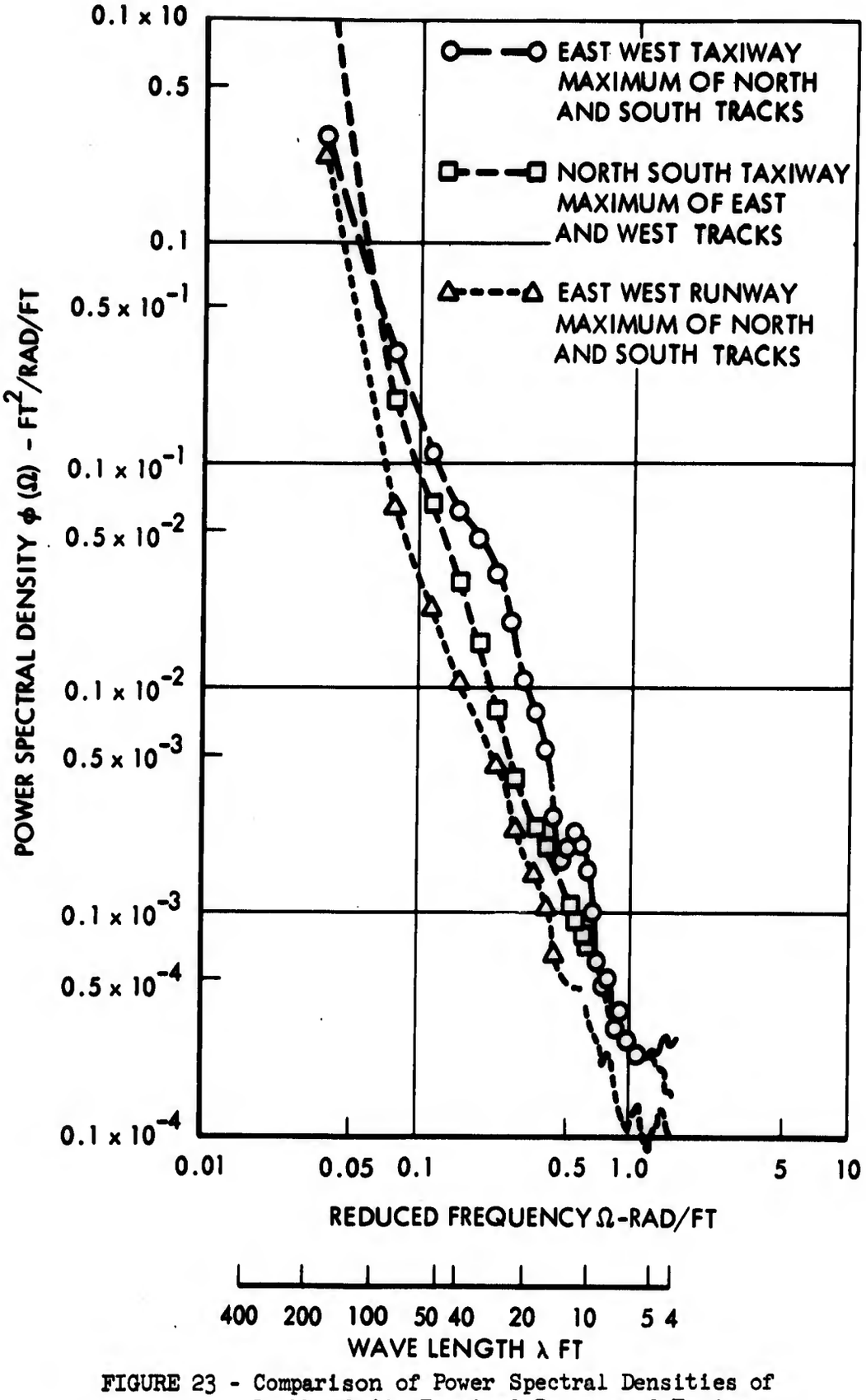

FIGURE 23 - Comparison of Power Spectral Densities of Lockheed Air Terminal Runway and Taxiways

The quantities (ℓ/s), (h/e), $(1 + Fc_{ST}/2F_{ST})$ and their product are shown in Table 7 for various airplanes. The s value shown corresponds to an aft c.g.

TABLE 7 - STEADY STATE TURNING PARAMETERS

Airplane	ℓ	s	h	e	(ℓ/s)	$(\frac{h}{e})$	$1+\frac{Fc_{ST}}{2F_{ST}}$	$\frac{\Delta n}{\Delta n_g}$
A-1	708	671.17	119	132.6	1.0549	0.8974	1	0.9467
A-2	690	648.76	119 ▷1	125	1.0636	0.952	1	1.0125
B-1	840	799.93	170	216	1.0501	0.787	1	0.8264
B-2	868.6	813	170 ▷1	210	1.0684	0.8095	1	0.8649
B-3	868.6	813	170 ▷1	210	1.0684	0.8095	1.225	1.0595
C-1	1008	941.62	250 ▷1	146.1	1.0705	1.7112	1	1.8318
C-2	873.91	819.95	258	155.25	1.0658	1.6618	1	1.7711
D-1	1224	1124.55	230 ▷1	146	1.0884	1.5753	1	1.7146

▷1 Estimated

The last column of the above table is a measure of how severe the vertical load shift is from inside to outside gear for a given turning acceleration. For example, for a 0.10 g turn, airplane A-2 would have a $\Delta n_g = 0.101$. Thus the outside main gear vertical load would increase to 1.101 times static.

Since (ℓ/s) is virtually constant for all airplanes (at the same c.g.), the ratio (h/e) clearly controls how severely the outside main gear loads up in a turn. Combinations of high c.g. and narrow track width result in high weight transfer to the outside main gear, an intuitively obvious result. It is interesting to note the significant differences among the various airplane classes. The current jet transports have $\Delta n_g/\Delta n$ ratios of around 1.0. The airbuses have grown more in track width than in c.g. height, so that the ratio of $\Delta n_g/\Delta n$ is around 0.85. Airplane B-3 is an exception to this since it has three main gears, so that the outboard gear loads up more on an incremental load factor basis. On the other hand, the jumbo jets have track widths about the same as the current jets, and about twice the c.g. height, so that their $\Delta n_g/\Delta n$ ratios are around 1.8. The same is true for the supersonic transport shown.

Typical Δn values for a normal turn are in the order of 0.15, with perhaps 0.3 for a severe turn and 0.5 for a limit design criterion. In the following Table 8 typical total vertical gear load factors ($1 + \Delta n_g$) are computed for the various airplane classes and degrees of turn severity.

TABLE 8 - STEADY STATE TURNING VERTICAL MAIN GEAR LOAD FACTORS

		$(1 + \Delta n_g)$ for:		
Airplane Class	Typical $\Delta n_g/\Delta n$	Normal Turn $\Delta n = .15$	Severe Turn $\Delta n = .30$	Limit Design Turn $\Delta n = .50$
A	1.00	1.150	1.300	1.500
B	0.85	1.128	1.255	1.425
C	1.80	1.270	1.540	1.900
D	1.70	1.255	1.510	1.850

From the above table it is self-evident that significant vertical gear load factors occur during turning, especially for class C and D airplanes.

In addition to increasing the vertical load on the outside main gear, the gear stiffness is increased, since the gear compresses to a steeper portion of the air load-stroke curve. The extent of this effect can be seen in Figure 24, which shows the effective main landing gear stiffness (air curve and tire spring in series), normalized to the static value, plotted against main gear vertical load, also normalized to the static value for various airplanes. The majority of the airplanes fall within a relatively narrow band, with the stiffness increasing roughly in direct proportion to vertical load increase (dashed line). Hence, a vertical gear load factor of 1.5 based on static would result in a gear stiffness of about 1.5 times the static value. In marked contrast to this is airplane C-2, which has a dual chamber oleo. At load levels slightly above static, the air curve flattens out, resulting in the considerably reduced gear stiffness shown in Figure 24. For this airplane, the gear stiffness never becomes more than 1.2 times the static stiffness for the load range shown.

It could be expected that the increased gear stiffness resulting from increased vertical load during a turn will produce an increased dynamic response to runway/taxiway roughness that is approximately proportional to the increase in stiffness. For example, if a given runway bump produced an incremental (not total) gear load factor Δn_g of 0.3, then the same bump would produce a Δn_g of about 1.5 (0.3) = 0.45 if the outside main gear were loaded up to 1.5 times static in a turn (resulting in an increase in stiffness of 1.5). The total peak vertical load transmitted to the pavement would then be

$$F_{TOT} = 1.5\ F_{ST} + 0.45\ F_{ST} = 1.95\ F_{ST}$$

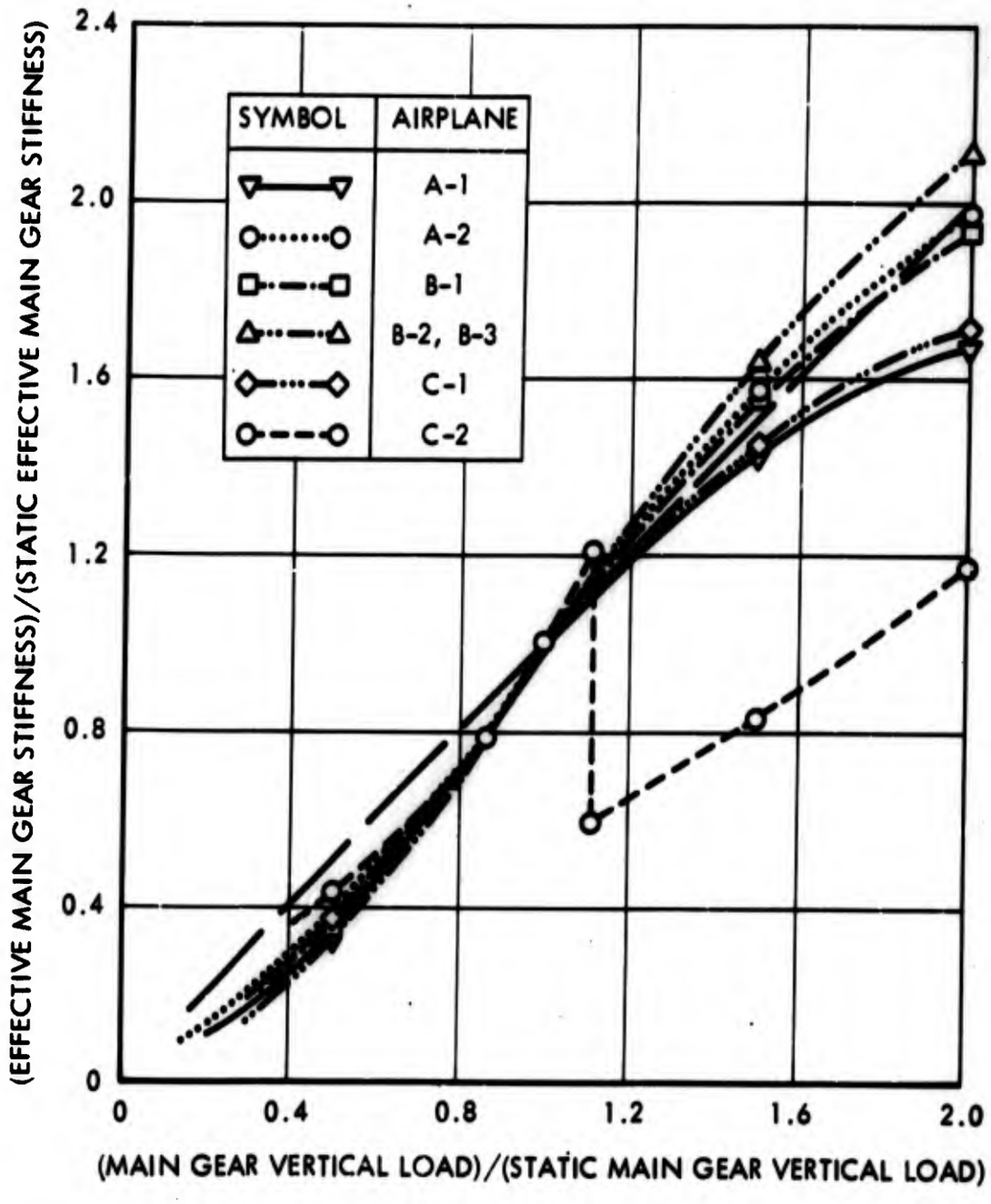

FIGURE 24 - Variation of Effective Main Gear Stiffness with Vertical Load

The first term is due to steady turning on a smooth runway, the second term is due to runway roughness that would produce a Δn_g of 0.3 with the gear in the static position.

However, this is obviously a rather extreme condition, requiring, simultaneously, a turn severe enough to yield a 1.5 total main gear load factor and a runway/taxiway bump rough enough to produce a Δn_g of 0.3 under static conditions. From Table 8 we see that either a "severe" turn or a "limit design" turn is required to yield a 1.5 total main gear load factor, depending upon the class of airplane. Also, as mentioned above in the discussion of low speed taxi loads, the pilot would tend to restrict the speed of the airplane to preclude exorbitantly high gear loads. On the other hand, he would be more sensitive to oscillatory loads from runway roughness than to the steady state load buildup due to a turn. Therefore, the pilot could conceiveably load up the outside gear in a turn while on relatively smooth pavement, and then hit a rough section of pavement which would produce large dynamic loads because of the roughness, before he could slow down sufficiently to reduce the loads.

Clearly then, the actual loads imposed on the pavement depend strongly on pilot technique and are therefore difficult to assess. It appears that in theory the loads could reach as high as twice static, but this would be rather infrequent. Collecting the above results, the total gear force due to combined turning and runway roughness is given by

$$\frac{F_{TOT}}{F_{ST}} = 1 + \left[\left(\frac{\Delta n_g}{\Delta n} \right)_{turn} \Delta n_{turn} \right] + \left[(\Delta n_{g_{bump}})(f) \right] \qquad (2)$$

where

F_{TOT} = total vertical gear load due to combined turning and roughness

F_{ST} = static vertical gear load

$\left(\frac{\Delta n_g}{\Delta n} \right)_{turn}$ = gear turn loading factor = $\frac{t}{s} \frac{h}{e} \left(1 + \frac{Fc_{ST}}{2F_{ST}} \right)$, last column of Table 7

$\Delta n_{g_{bump}}$ = incremental gear load factor, $(F-F_{ST})/ F_{ST}$), that would be produced by the chosen bump when the main gear is in the static position

f = ordinate of Figure 24, which accounts for the change in effective gear stiffness during turning

For a given airplane, $\left(\frac{\Delta n_g}{\Delta n}\right)_{turn}$ and f are known, and the independent variables in Equation (2) are Δn_{turn} and $\Delta n_{g_{bump}}$. How high these are chosen, in combination, determines how high F_{TOT}/F_{ST} will be. Extreme values are computed below:

$$\left(\frac{\Delta n_g}{\Delta n}_{turn}\right)\left(\Delta n_{turn}\right) + \left(\Delta n_{g_{bump}}\right) \quad (f)$$

$$\frac{F_{TOT}}{F_{ST}} = 1 + \begin{matrix}(0.947) & (0.15) \\ (1.832) & (0.5)\end{matrix} + \begin{matrix}(0.1) & (0.6) \\ (0.3) & (2.1)\end{matrix} \quad \begin{matrix}\text{Min.} \\ \text{Max.}\end{matrix}$$

$$\frac{F_{TOT}}{F_{ST}} = 1 + \begin{matrix}(0.142) \\ (0.916)\end{matrix} + \begin{matrix}(0.060) \\ (0.630)\end{matrix} \quad \begin{matrix}\text{Min.} \\ \text{Max.}\end{matrix}$$

$$\frac{F_{TOT}}{F_{ST}} = \begin{matrix}1.202 \text{ Min.} \\ 2.546 \text{ Max.}\end{matrix}$$

From considerations of pilot technique, it is felt that an appropriate range for F_{TOT}/F_{ST}, due to combined turning and runway/taxiway roughness, would be from 1.2 to 2, with the higher value corresponding to limit design conditions. For a given Δn_{turn} and $\Delta n_{g_{bump}}$, F_{TOT}/F_{ST} is most sensitive to the ratio (h/e) and to whether or not a dual chamber oleo is used.

For airplanes with single chamber oleos, f in Equation (2) can be shown to be

$$f = \left(1 + \Delta n_{g_{turn}}\right)^2 \left[\frac{1 + K_T/K_G}{\left(1 + \Delta n_{g_{turn}}\right)^2 + K_T/K_{G_o}}\right] \quad (3)$$

where

$$\Delta n_{g_{turn}} = \left(\frac{\Delta n_g}{\Delta n_{turn}}\right) \Delta n_{turn}, \; 2^{ND} \text{ term in Equation (2)}$$

K_T = linear tire stiffness, combining all tires on one gear in parallel

K_{G_o} = linear gear stiffness in static position, slope of air load-stroke curve

Equation (2) can therefore be rewritten in terms of more basic parameters as

$$\frac{F_{TOT}}{F_{ST}} = 1 + C\frac{\ell}{s}\frac{h}{e}\Delta n_{turn} + \Delta n_{g_{bump}}\left(1 + C\frac{\ell}{s}\frac{h}{e}\Delta n_{turn}\right)^2 \frac{1 + K_T/K_{GO}}{\left(1 + C\frac{\ell}{s}\frac{h}{e}\Delta n_{turn}\right)^2 + \frac{K_T}{K_{G_o}}} \qquad (4)$$

where

$$C = 1 + \frac{Fc_{ST}}{2F_{ST}}$$

In Equation (4), the basic airplane parameters are C, ℓ/s, h/e, and K_T/K_{G_o}. The independent variables are Δn_{turn} and $\Delta n_{g_{bump}}$.

The other significant aspect of turning loads is that lateral forces parallel to the ground are transmitted to the pavement. These forces can quite frequently reach their friction limited values, about 0.6 to 0.8 of the vertical load, on both main and nose gears of certain airplanes. The limiting value is readily attained on bogie type main gears during pivot turns (using differential braking and unsymmetrical thrust, or towing). This would occur most frequently at the loading ramps. Likewise, the nose gears of the airplanes studied have sufficient steering rate capabilities, together with high airplane yaw inertia, to allow nose gear skidding during abrupt turns. This is not a common occurrence. More frequent, however, is the pivot turn using differential braking and unsymmetrical thrust during

which the nose gear is forced to follow a tighter path than its maximum steering angle allows, resulting in nose gear sliding. Hence, the pivot turn maneuver results in both main and nose gear sliding, with side loads applied to the ground in the order of 0.6 to 0.8 times the vertical loads. Repeated performance of this maneuver occurring at approximately the same ramp location could lead to concentrated local pavement damage.

(d) Low-Speed Braking - Low-speed (< 30 knots) braking that occurs primarily on ramps and taxiways is generally rather mild. Typical braking friction coefficients generated are in the order of 0.3 or less. However, even this moderate braking, if rapidly applied, can lead to significantly increased nose gear vertical loads. A full treatment of dynamic and steady state braking is given under paragraph (f) - Aborted Takeoff - High Speed Braking starting on page 99.

(e) Accelerated Takeoff Roll - The loads imposed on the pavement during the accelerated takeoff roll are strongly dependent on the following:

1) Airplane characteristics

   a) Characteristics determining static loads

      Weight
      c.g.
      Number of gears

   b) Characteristics determining loads on a smooth runway during takeoff roll

      Aerodynamics
      Thrust

   c) Characteristics determining dynamic increment in loads due to runway roughness

      Effective gear stiffness (tires and oleo in series)
      Airplane mass

2) Runway roughness

The significance of these various items is discussed in great detail in Reference 4. A typical time history of main gear vertical load during a takeoff roll is shown in Figure 25. The example shown is for airplane A-1 at maximum takeoff gross weight, aft c.g., on a typical runway profile from Reference (4). The velocity varies from 30 to 140 knots during the run. The load that would have been obtained over a smooth runway is shown as a dashed line. The maximum load at t = 18.76 seconds and V = 107 knots is broken down into components in Table 9.

TABLE 9 - COMPONENTS OF MAXIMUM LOAD DURING TAKEOFF ROLL

Component	Magnitude	Magnitude/max. static load
1. Max. static load	146,940	1.000
2. Δ due to thrust	0	0
3. Δ due to aerodynamics	-35,740	-0.243
4. Δ due to runway roughness	+66,800	+0.455
5. Resultant load	178,000	1.212

Although the increment due to thrust is zero in this case, this factor may be significant for other configurations. The results of Table 9 are typical of the airplanes in classes A, B and C; namely, there is a reduction in load due to aerodynamic lift and an increase in load due to runway roughness. Typically, the roughness increment will be predominant, so that the resultant load is greater than static.

The class D airplanes for which data is available indicate a tendency to develop negative lift during the takeoff roll. For these aircraft, the aerodynamic increment and the runway roughness increment are both positive, resulting in total loads well above static. Figure 26 which is actual test data, shows a time history of the main gear vertical load during an accelerated takeoff roll for airplane D-2. We see that the mean load prior to rotation has increased to about 1.25 times the static load, due to negative aerodynamic lift. Also, the oscillations due to runway roughness tend to increase slightly in magnitude up until rotation. This is due in part to the increasing gear effective stiffness as the gear is compressed during the run. Also, as the airplane's velocity increases, it is in resonance at the plunge natural frequency (1 cps) with progressively longer wave length components of the runway roughness; the longer the wave length, the greater is the magnitude of runway roughness, as seen from analytical power spectrum of runway roughness presented in Figure 23 (reduced frequency Ω is inversely proportional to wave length).

Hence, from the nature of runway roughness, an airplane's dynamic taxi response can be expected to increase with velocity, ignoring aerodynamic effects. For class A, B, and C airplanes, this is offset by the decrease in gear stiffness due to aerodynamic lift. In Figure 25, the local roughness variations along the runway somewhat shadow the tendency for the dynamic increment, due to roughness, to increase monotonically with velocity. However, Table 10 below shows the components of the maximum peak main gear load during an accelerated takeoff run over a typical runway profile from Reference (4) for airplanes A-2 and B-1 in addition to A-1 (Table 9).

TABLE 10 - COMPONENTS OF MAXIMUM LOAD DURING TAKEOFF ROLL NORMALIZED TO MAXIMUM STATIC LOAD

Component	A-1	A-2	B-1
1. Max. static load	1.000	1.000	1.000
2. Δ due to thrust	0	0	-0.020
3. Δ due to aerodynamics	-0.243	-0.108	-0.040
4. Δ due to runway roughness	+0.455	+0.405	+0.246
5. Resultant load factors	1.212	1.297	1.186
Velocity at peak load, knots	107	76	63

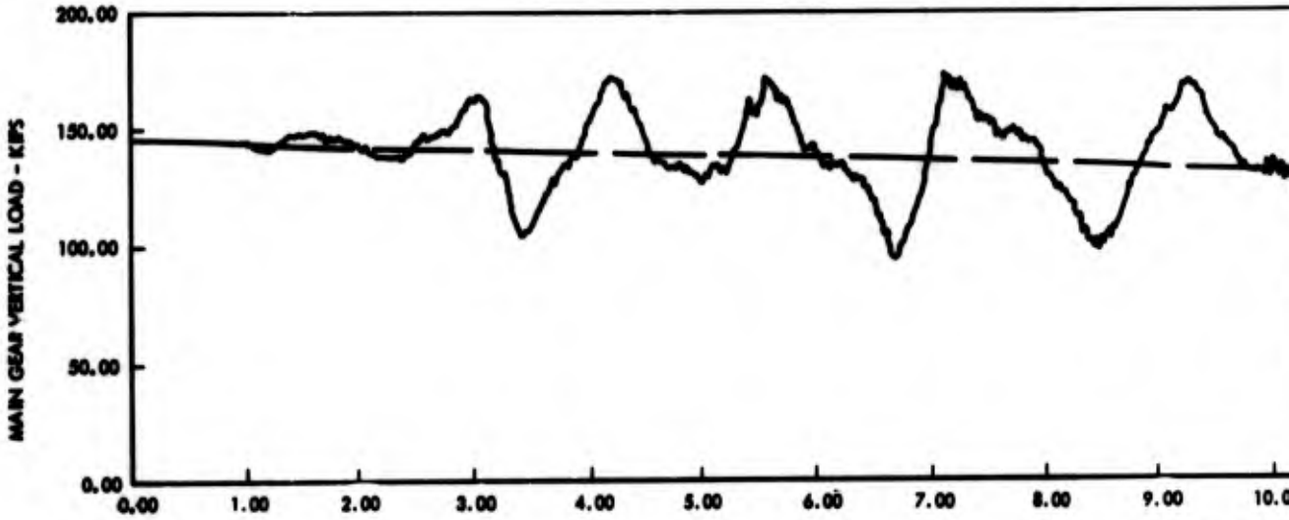
200.00
150.00
100.00
50.00
0.00
MAIN GEAR VERTICAL LOAD - KIPS
0.00
1.00
2.00
3.00
4.00
5.00
6.00
7.00
8.00
9.00
TIME - SE

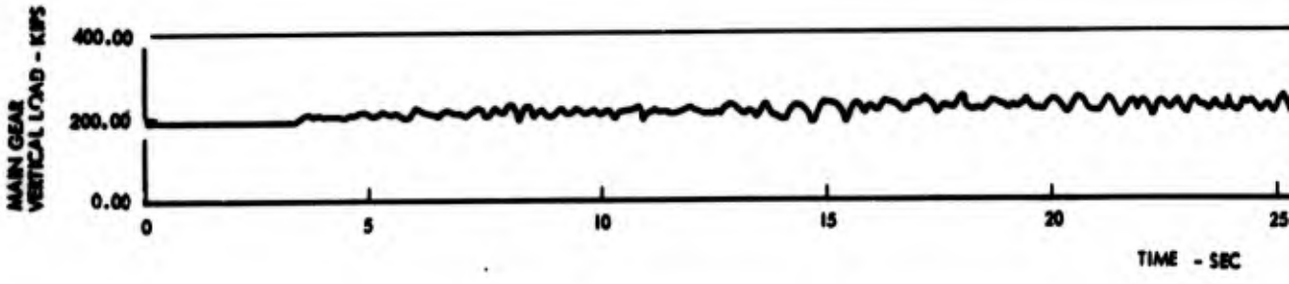
400.00
200.00
0.00
MAIN GEAR
VERTICAL LOAD - KIPS
0
5
10
15
20
25
TIME - SEC

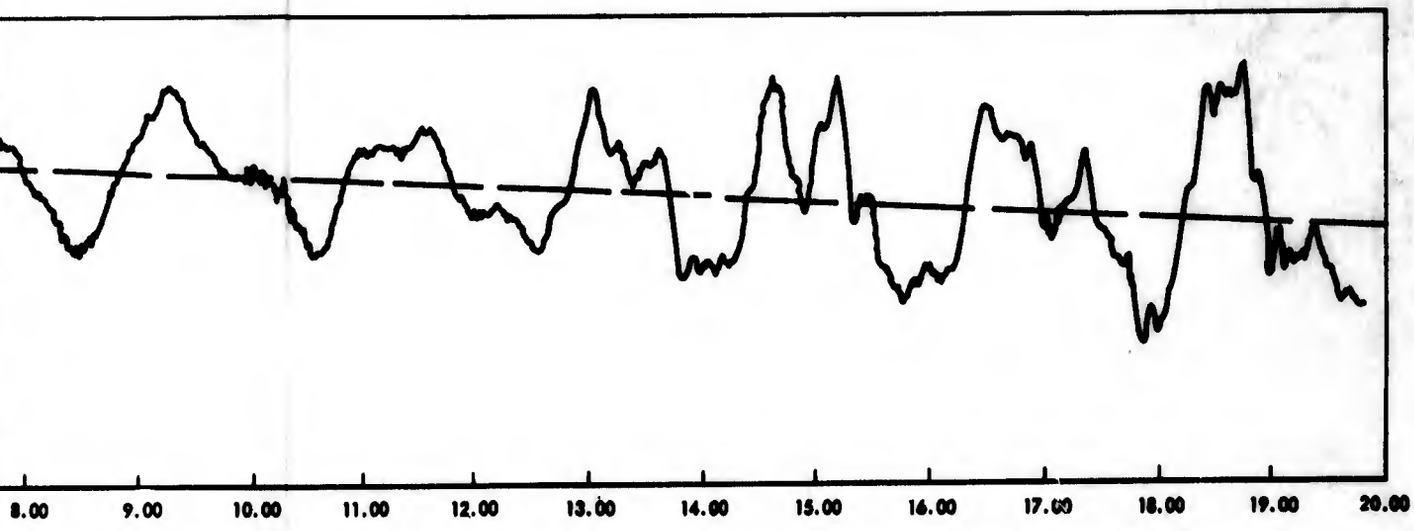

FIGURE 25 - Takeoff Roll Main Gear Vertical Load Time History, Airplane A-1

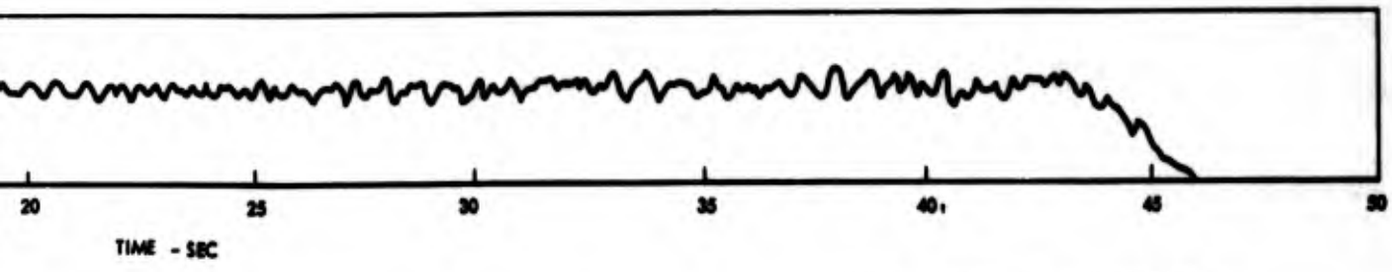

FIGURE 26 - Takeoff Roll Main Gear Vertical Load Time History, Airplane D-2

B

BLANK PAGE

Note that the peak loads all occur at different velocities, and at different points on the runway. Comparisons between airplanes are difficult to make due to these velocity and location variations; however, the resultant load factor does not vary greatly among the airplanes shown. Airplane B-1, using a softer gear than the other airplanes shown, has a considerably reduced dynamic increment due to runway roughness.

A rough prediction of the dynamic taxi loads can be obtained from

$$F_{TOT}(V)/F_{ST} = 1 + \Delta n_{g_a}(V) + \Delta n_{g}(V)_{\text{roughness}} \qquad (5)$$

where

$F_{TOT}(V)$ = Peak total vertical gear load

$\Delta n_{g_a}(V)$ = Incremental gear load factor on smooth runway due to aerodynamics and thrust

$\Delta n_{g}(V)$ = Incremental gear load factor due to runway roughness

Note that all quantities are a function of velocity. For a given airplane $\Delta n_{g_a}(V)$ can readily be calculated once the basic lift and thrust characteristics during takeoff are known.

An expression which gives an analytical prediction of the expected dynamic taxi loads is developed in Appendix D, and presented below

$$\frac{F_{TOT}}{F_{ST}} = \left[1-\bar{L}_{100}\left(\frac{V}{100}\right)^2\right]\left\{1+C''\,Vf_{n_o}\left[\frac{1+K_T/K_{G_o}}{\left(1-L_{100}\left(\frac{V}{100}\right)^2\right)^2+\frac{K_T}{K_{G_o}}}\right]^{1/2}\right\} \qquad (6)$$

where

V = airplane velocity, knots (1 knot = .866 mph)

L_{100} = $\frac{\text{total airplane aerodynamic lift at V = 100 knots}}{\text{maximum take-off gross weight}}$

C'' = constant proportional to level of runway roughness

f_{n_o} = airplane plunge mode natural frequency at V = 0

K_T = linear tire stiffness combining all tires on one gear in parallel

K_{G_o} = linear gear stiffness, at V = 0, slope of air load stroke curve at static position

Equation (6) accounts for the following significant effects:

- Airplane characteristics

  Aerodynamics

  Landing gear effective stiffness/airplane weight ratio

  Effect of aerodynamics in modifying effective gear stiffness

- Runway Roughness - variation of roughness with wave length

For a given airplane, the only independent variable in Equation (6) is the airplane velocity V. The constant "C" is linearly proportional to the degree of runway roughness. A value of C" corresponding to a limit dynamic taxi design roughness level is chosen based on the results of runs of airplane B-1 on a typical runway from Reference (4), multiplied by the factor 2.17. This runway corresponds to a limit design roughness level, as presented in Reference (4). A value of C" = 0.00746 corresponds to this limit design roughness level. Therefore, a "typical" roughness level would correspond to 0.00746/2.17 = 0.0034, on the assumption that this runway represents "typical" roughness.

Figure 27 shows analytically predicted dynamic taxi load levels, using Equation (6), for airplane B-1. Also shown are the loads imposed on a smooth runway. Since the C" values were chosen based on analyses of this airplane over the amplified runway, the limit design level curve exactly duplicates the peak F_{TOT}/F_{ST} of 1.54 obtained from an accelerated take-off run on this amplified runway with airplane B-1. The normal roughness level, corresponding to the same runway with an amplification of 1.0, shows a peak level of 1.17, compared to 1.186 shown in Table 10 from the time history analysis.

Figures 28,29,30 show plots of F/F_{ST} versus V from Equation (6), varying the parameters L_{100}, f_{n_o}, and K_T/K_{G_o}, respectively. Notice that all three figures

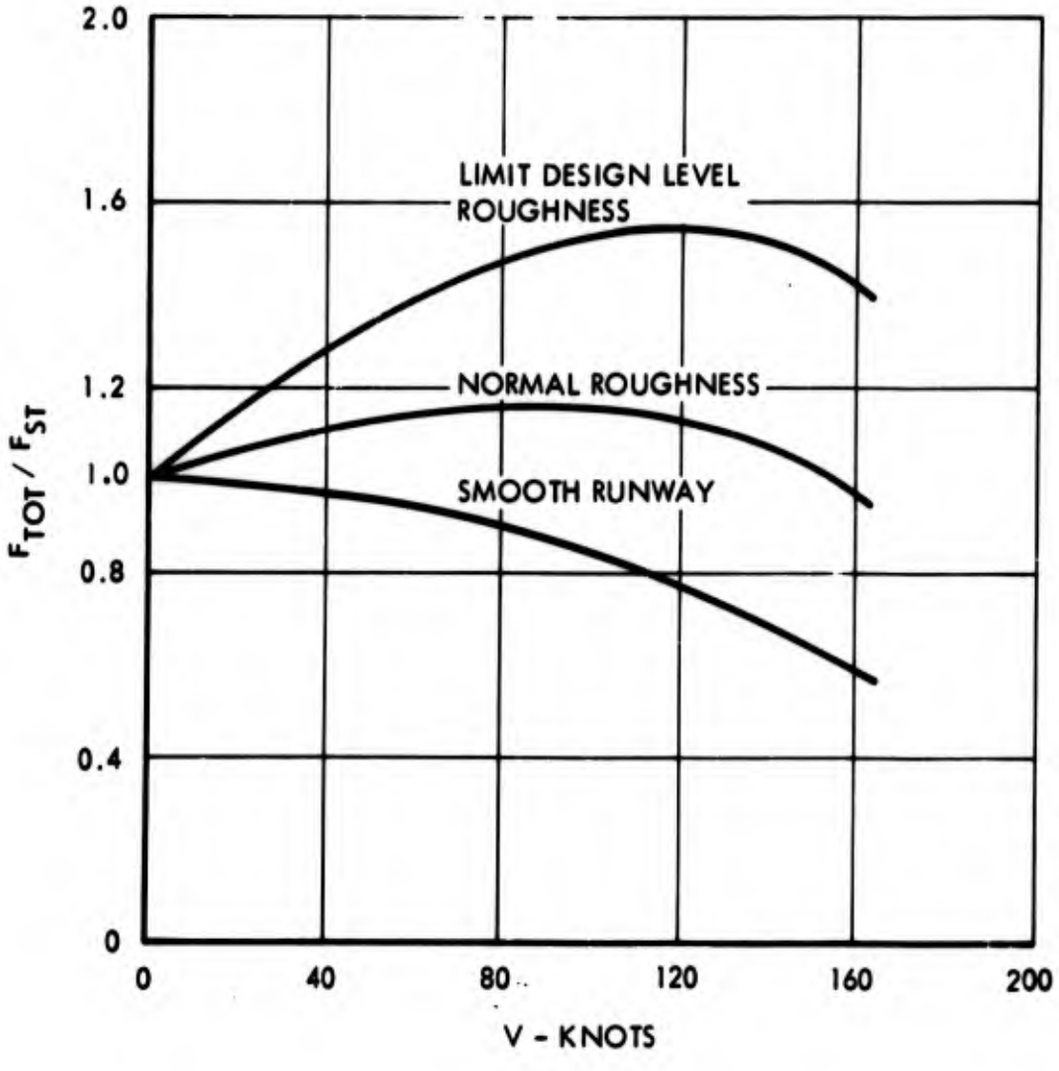

FIGURE 27 - Analytically Predicted Dynamic Taxi Load Factors, Airplane B-1

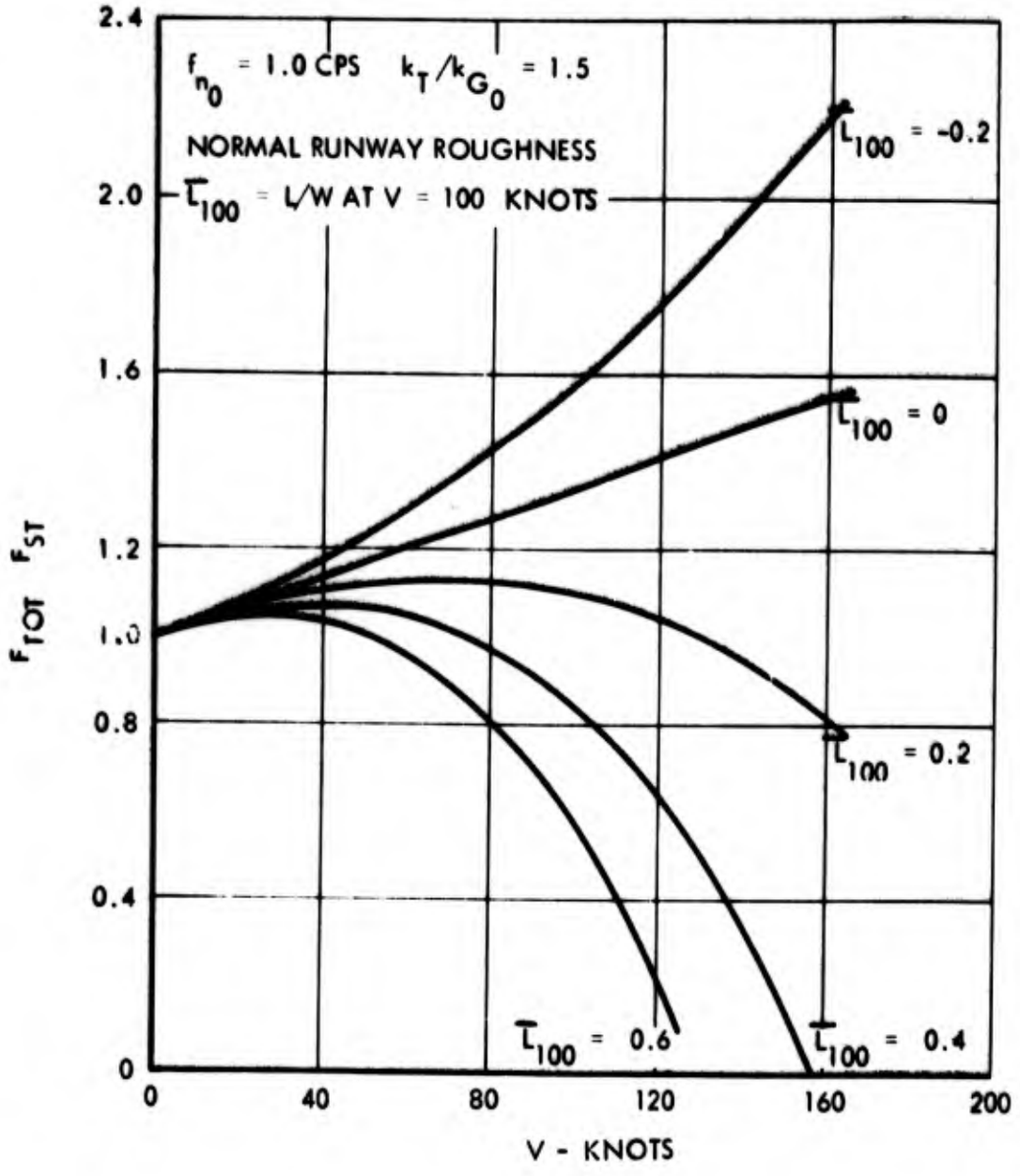

FIGURE 28 - Variation of Dynamic Taxi Load Factors with Aerodynamic Lift

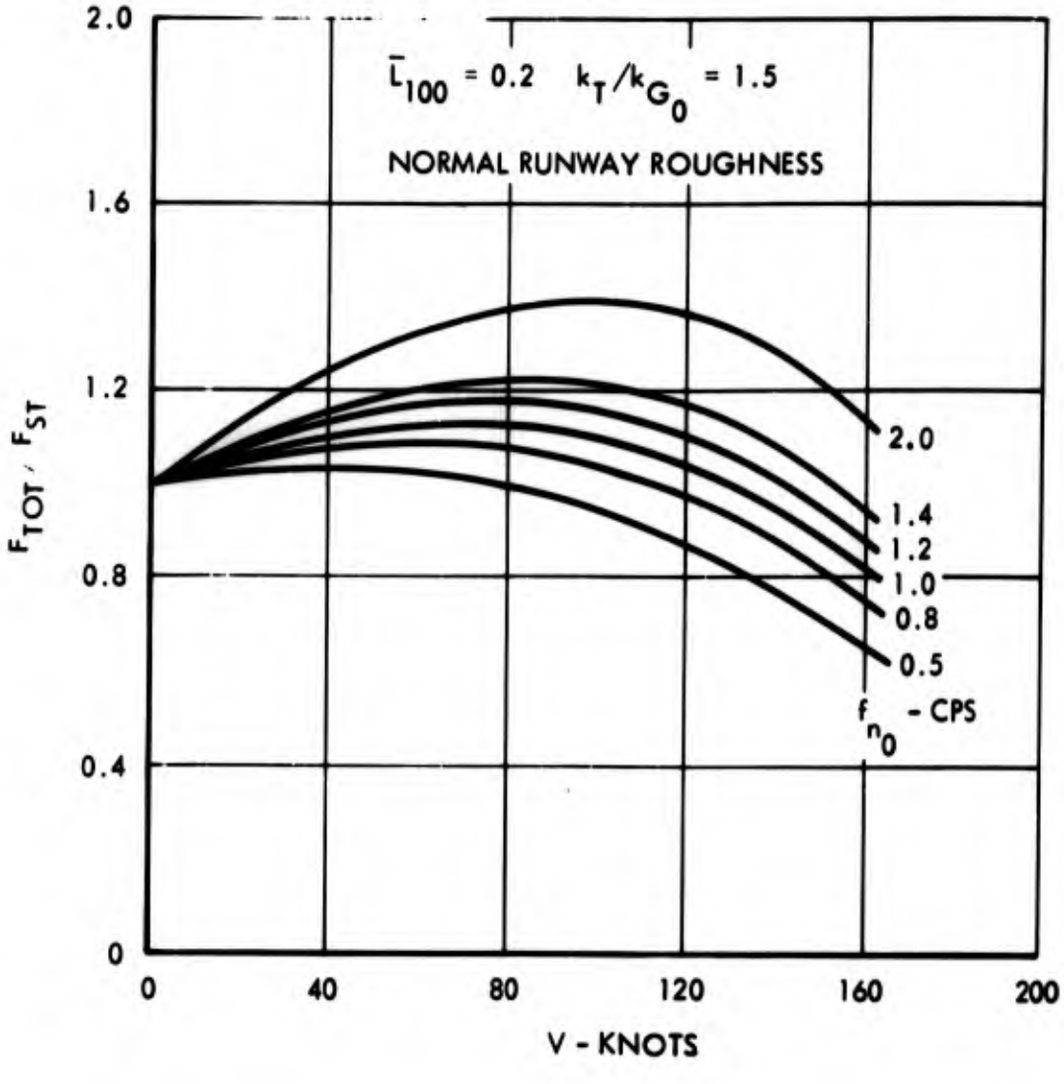

FIGURE 29 - Variation of Dynamic Taxi Load Factors with Plunge Mode Natural Frequency

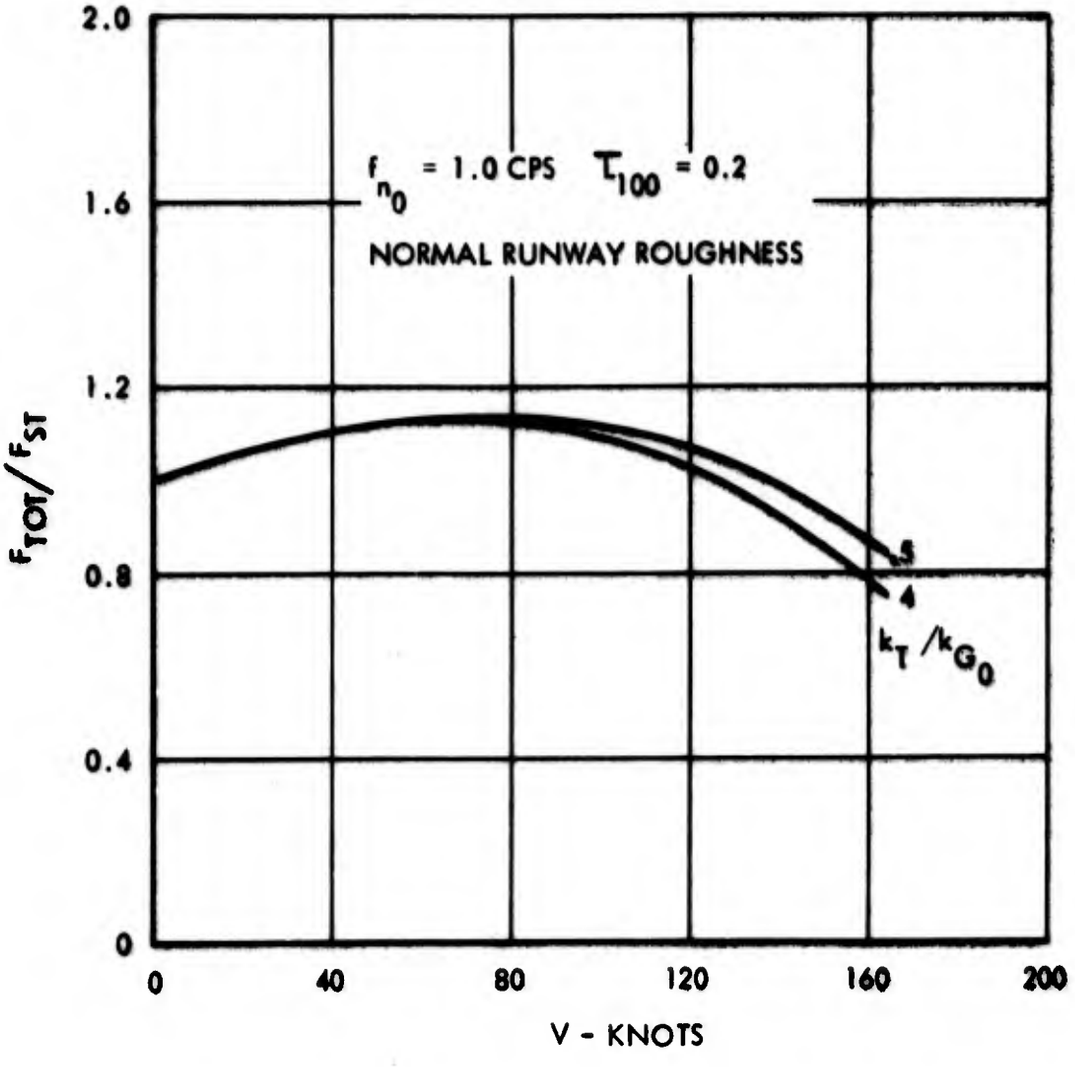

FIGURE 30 - Variation of Dynamic Taxi Load Factors with Ratio of Tire to Gear Stiffness

use a C" value of 0.00344, corresponding to normal runway roughness level. Clearly from Figure 28 the effect of lift is predominant. For zero lift, the load factor varies linearly with velocity. This is the result of assuming the runway power spectral density varies with the square of the wavelength. With negative lift, the load factors become quite severe. With positive lift, the load factors reach a peak value and then drop off. The less the lift, the higher the peak load factor and its corresponding velocity.

In Figure 29, the effect of f_{n_o}, the plunge mode natural frequency can be seen. The range of frequencies for the airplanes considered in this study is shown in Table 11.

TABLE 11—AIRPLANE DYNAMIC TAXI PARAMETERS

Airplane	f_{n_o}	K_T/K_{G_o}	$\bar{L}_{100}$
A-1	1.234	1.132	0.22
A-2	1.156	1.553	0.22
B-1	1.030	1.805	0.16
B-2	0.940	2.359	
B-3	0.924		
C-1	1.243	1.246	0.24
C-2	0.930	2.581	
D-1	0.927	2.021	−0.11

The peak values of F/F_{ST} are replotted from Figure 29 against natural frequency, f_{n_o}. This is shown in Figure 31. The peak F/F_{ST} is virtually linear with frequency over a rather broad range. Also shown in Figure 31 is the range of natural frequencies of the airplanes studied, from Table 11. Clearly the range is rather narrow, and the peak F/F_{ST} varies only from 1.1 to 1.2, or about ±5 percent from the middle value. Therefore, it can be concluded that for the current and near future jet transports studied, the plunge natural frequency does not have a strong influence on the total gear load transmitted to the pavement due to runway roughness.

Figure 31 shows a range of 0.1 to 0.2 in dynamic increment, or ± 33 percent of the middle value. The dynamic increment may be of importance in pavement fatigue considerations, in which case the plunge natural frequency would be a significant parameter.

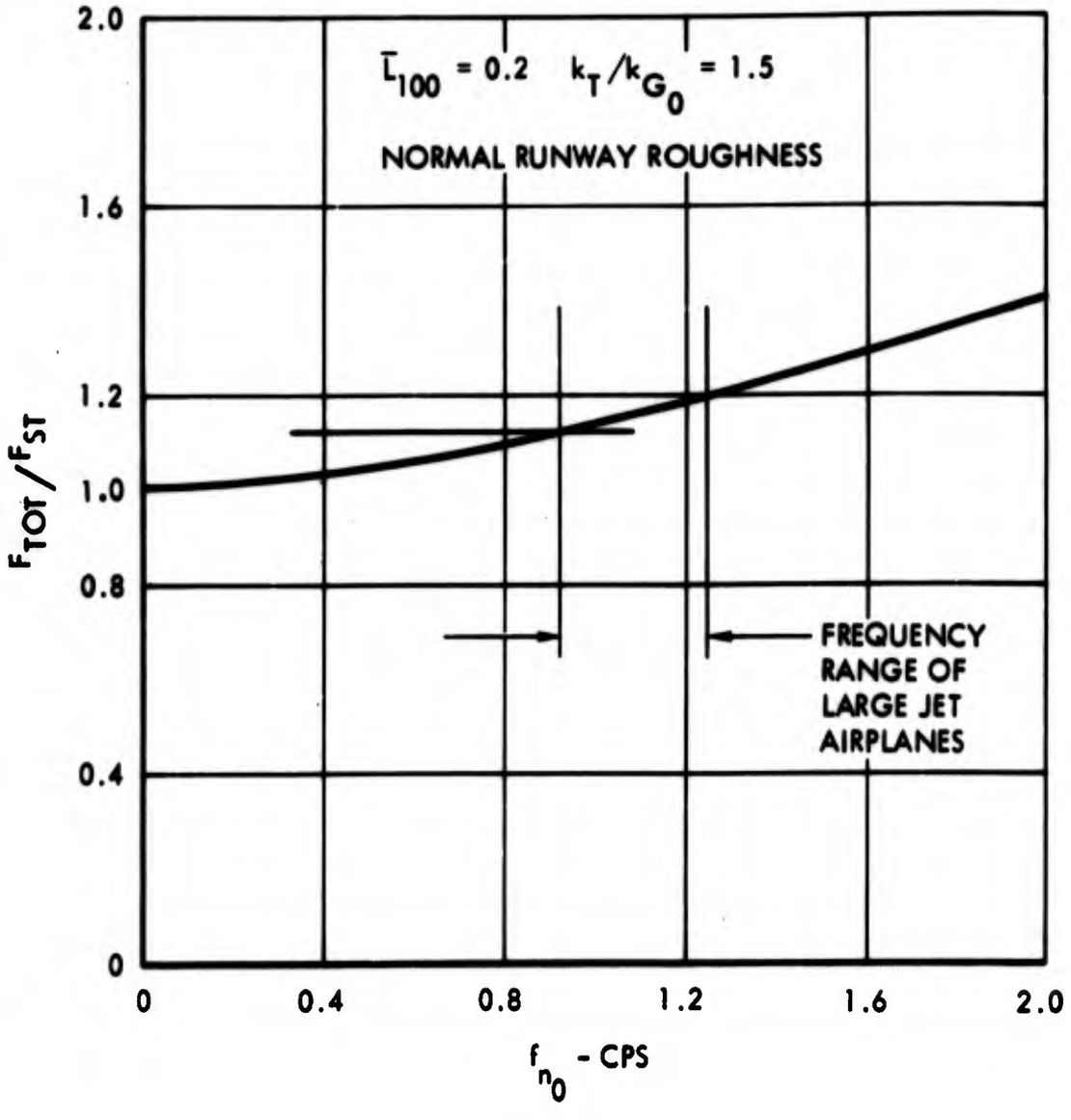

FIGURE 31 - Variation of Peak Dynamic Taxi Load Factors with Plunge Mode Natural Frequency

Figure 30 shows the variation in gear load factor with the ratio of tire to gear stiffness. Table 11 shows the range of values for this parameter for the airplanes studied. As can be seen from Figure 30 this parameter for the range of interest has a very moderate effect(< ± 2 percent)on the gear load factor, as might be expected.

In summary, it seems apparent that by far the most significant parameter in determining dynamic taxi loads is the aerodynamic lift. Unfortunately, this is also by far the weakest area of available information regarding the airplanes studied, as can be seen in Table 11 where the values of $\bar{L}_{100}$ (lift/weight at V = 100 knots) that are available are shown. From Figure 28, however, it can be clearly seen that there is a great deal of difference between a moderate amount of lift ($\bar{L}_{100} \approx 0.2$) and no lift at all or negative lift. Airplanes with the latter characteristics can obviously impose severe loading on airport pavements during the takeoff roll.

(f) Aborted Takeoff - High Speed Braking - An aborted takeoff is a maneuver which is rarely performed, but one which can yield very high pavement loading, particularly for the nose gear. All or any partial combination of the following actions are utilized to retard the airplane's forward velocity:

Spoiler deployment

Reverse thrust

Wheel braking

In addition, the pilot may change the elevator setting to alter the vertical loading on the main and nose gears. In particular, he may elect to use tail up elevator to increase the vertical load on the main gears, which would increase the effectiveness of wheel braking. Since the aborted takeoff is often associated with engine malfunction or failure, the pilot may not have full reverse thrust available. He may go with partial reverse thrust, symmetrically applied, or with all available reverse thrust, which may be unsymmetrically applied.

The latter case is very rare, since it results in a yawing moment being applied to the airplane, requiring nose gear steering to maintain a reasonably straight path.

All of the above actions alter the vertical loads applied to the main and nose gears. Spoiler deployment, in addition to increasing drag, reduces lift and gives a nose up pitching moment. Both of these tend to increase main gear vertical loads, while for nose gear vertical loads, the lift reduction tends to increase the load and the nose up pitching moment tends to decrease the load. Reverse thrust generally tends to give a nose down pitching moment, increasing the nose gear vertical load and decreasing the main gear load. The possible exception to this is when center engine reverse thrust only is used on three engine transports, which would probably be the case if a wing engine malfunction necessitated the aborted takeoff. Since the center engine (rear mounted) is normally above the airplane c.g., reverse thrust would

yield a nose up pitching moment. Wheel braking always produces a nose down pitching moment, increasing the nose gear vertical load and decreasing the main gear vertical load. In addition, the pilot may alter the elevator setting, as mentioned above, which would change the main and nose gear vertical loads. The situation is summarized in Table 12 which indicates whether an action has a postive or negative effect on vertical gear load (increasing or decreasing).

TABLE 12 - EFFECT OF VARIOUS ACTIONS DURING ABORTED TAKEOFF ON GEAR LOADS

Action	Main Gear	Nose Gear
Spoiler Deployment	+	±
Elevator Adjustment	±	∓
Reverse Thrust	∓	±
Wheel Braking	-	+

+ = increases vertical gear load

- = decreases vertical gear load

Where two signs are shown in Table 12, the more probable is shown on top. We see from the above table that the main and nose gear vertical loads during an aborted takeoff depend strongly on pilot technique and upon individual airplane aerodynamic characteristics. Since the necessary aerodynamic details were not available for the airplanes studied, time history analyses of aborted takeoffs were not performed.

However, dynamic braking time history runs were made. For a given rate of deceleration, wheel braking will always produce a greater nose down pitching moment than reverse thrust, since the line of action of the retarding force is at the ground plane. Hence, if it is assumed that a given deceleration rate is achieved solely by wheel braking, when in reality both wheel braking and reverse thrust are used, the nose gear vertical loads will be conservative (high).

Figure 32 shows the results of dynamic braking time history runs for three airplanes. A typical nose gear vertical load time history sketch is also shown in Figure 32. F_o is the initial gear force, different from F_{ST} (Static) due to aerodynamic and thrust effects. F_p is the peak dynamic nose gear load. The curves are normalized to the maximum static nose gear load, obtained at maximum ramp weight, forward c.g., zero velocity. This is denoted F_{ST_M}. The final steady braking load achieved is denoted F_g. The braking was ramped in

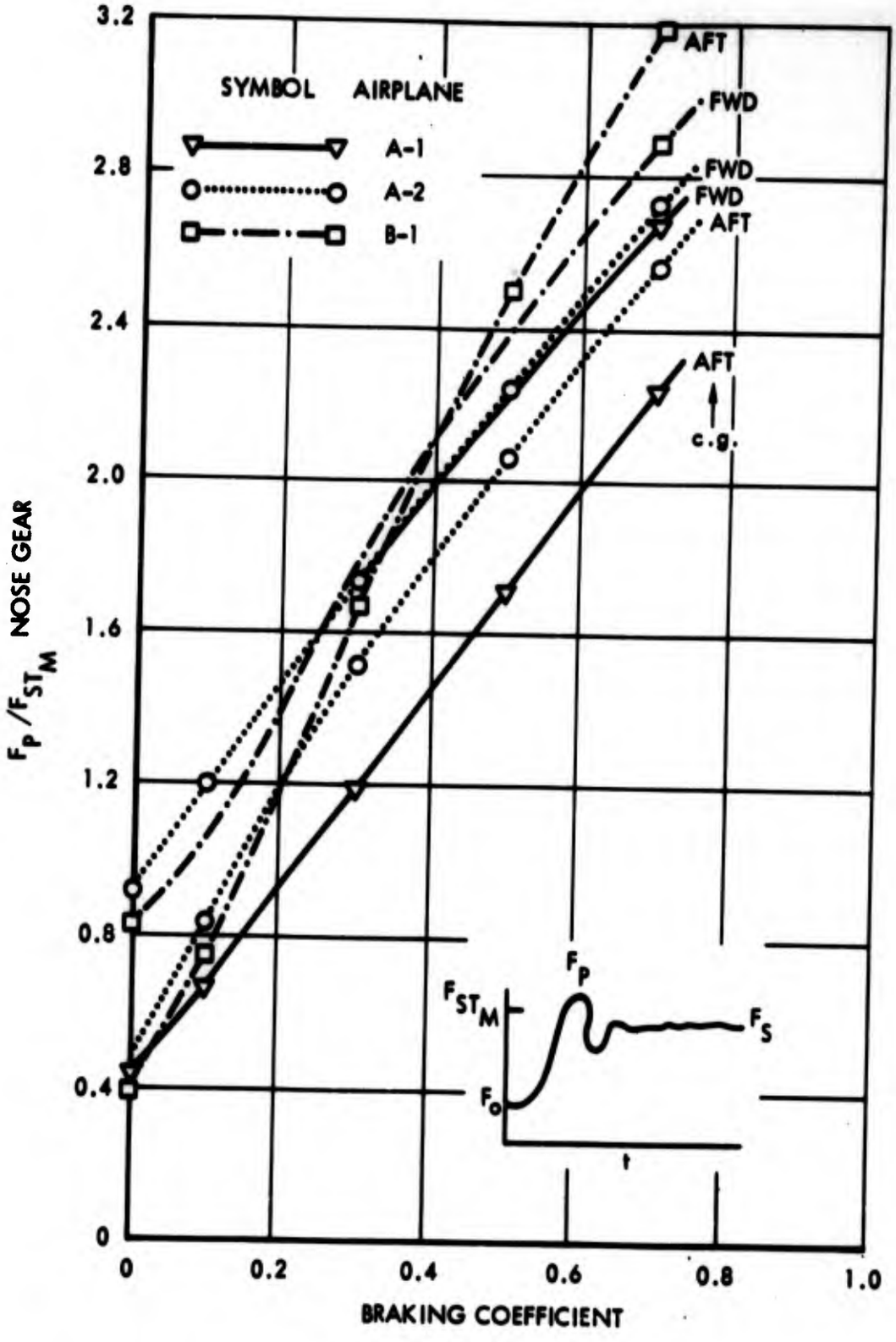

FIGURE 32 - Nose Gear Dynamic Braking Load Factors

from zero to the indicated braking coefficient in 0.3 second, and then held constant. The initial airplane velocity was 60 knots in each case.

For airplanes A-1 and A-2, the forward c.g. position is more critical than the aft c.g., while for airplane B-1 the aft c.g. is more critical at high braking coefficients. This is due to a high dynamic load amplification factor with an aft c.g., probably the result of the nose gear air curve, metering pin detail design.

It was shown earlier in the section on static loads that the main gear static loads are more critical than the nose gear loads. However, since during dynamic braking very large multiples of the maximum nose gear static load can be achieved (> 3 times max. static), it is pertinent to re-examine the relationship between main and nose gear loads. Using the data from Table 6, the following Table 13 shows the load per tire for main and nose gears, under maximum static load conditions. Also shown is the ratio of main gear load/tire to nose gear load/tire.

TABLE 13- MAXIMUM STATIC LOADS PER TIRE, MAIN AND NOSE GEARS

Airplane	Max. Main Gear Load/Tire	Max. Nose Gear Load/Tire	$\frac{\text{Main Gear Load/Tire}}{\text{Nose Gear Load/Tire}}$
A-1	36,700	16,420	2.235
A-2	36,400	17,180	2.119
B-1	48,900	19,950	2.451
B-2	48,300	23,020	2.098
C-1	41,600	35,650	1.167
C-2	50,500	23,280	2.169
D-1	45,600	29,550	1.543

From the above table we can see that the main gear load/tire is normally about 2 times the nose gear load/tire, with the notable exception of airplane C-1. Therefore, dynamic braking yielding $F_p/F_{ST_M} > 2$ gives nose gear loads which may be more critical than static main gear loads. This is rather approximate since it assumes equal tire pressures for main and nose gear tires, and ignores interaction effects between closely spaced tires. Nevertheless, from Figure 32 we see that braking coefficients in the order of 0.35 to 0.60 are sufficient to yield $F_p/F_{ST_M} > 2$.

Dynamic nose gear braking loads can be estimated from the following equation (see Appendix D):

$$\frac{F_p}{F_{ST_M}} = \frac{D}{\bar{r}_m}\left[\frac{(1-\bar{L}_A-\bar{L}_T)(\bar{r}+\mu\bar{h}) - \bar{c}'\frac{C_M}{C_L}\bar{L}_A - \bar{m}\,\bar{T}}{1+\mu\bar{h}}\right]$$

$$-\frac{(D-1)}{\bar{r}_m}\left[\frac{(1-\bar{L}_A-\bar{L}_T)\,\bar{r} - \bar{c}'\,\frac{C_M}{C_L}\bar{L}_A - \bar{m}\,\bar{T}}{1}\right] \qquad (7)$$

where

$$D \triangleq \frac{F_p - F_o}{F_s - F_o}$$

$$\bar{T} = \frac{\text{Thrust}}{\text{Weight}} = \frac{T}{W}$$

C_M = pitching moment aerodynamic coefficient

C_L = lift aerodynamic coefficient

$$\bar{L}_T = \frac{\text{"lift" due to thrust}}{\text{airplane weight}}$$

$$\bar{L}_A = \bar{L}_{100}\left(\frac{V}{100}\right)^2 \frac{\text{aerodynamic lift}}{\text{airplane weight}}$$

M_T = pitching moment due to thrust

$\bar{c}$ = mean aerodynamic chord

$m = M_{T/T}$

r = distance from c.g. to main gear

r_{max} = maximum "r"

$\bar{r}_m = r_{max}/\ell$

$\bar{h} = h/\ell$

$\bar{c}' = \bar{c}/\ell$

$\bar{m} = m/\ell$

u = braking coefficient = $\frac{\text{drag force at braked wheel}}{\text{vertical force at braked wheel}}$

The geometric parameters are shown in the following sketch:

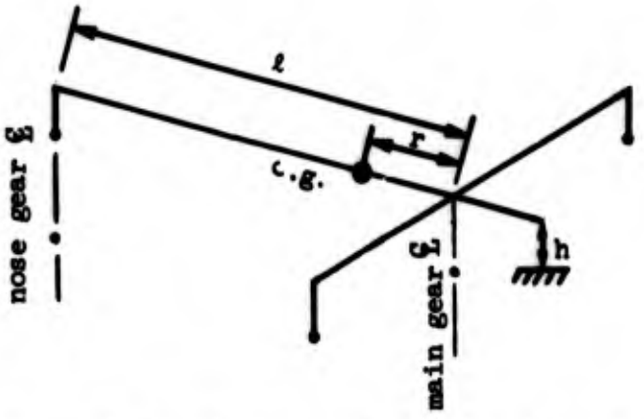

Equation (7) is derived by obtaining expressions for F_S and F_o (Figure 32) from equilibrium considerations, and by defining the dynamic load amplification factor as above. The aerodynamic effects of spoilers and elevator settings are included in C_M/C_L and $\bar{L}_{100}$. The effect of reverse thrust, if any, is included in $\bar{m}$ and $\bar{L}_T$.

Figures 33 through 38 show plots of Equation (7), for airplanes A-1, A-2 and B-1, aft and forward c.g. The plots are shown for various values of dynamic load amplification factor D. The D = 1 values correspond to the final steady braking load F_S. Also shown on each plot are the corresponding time history analysis results. From these figures we see the D value that gives the best fit of the time history results. This value is shown in Table 14.

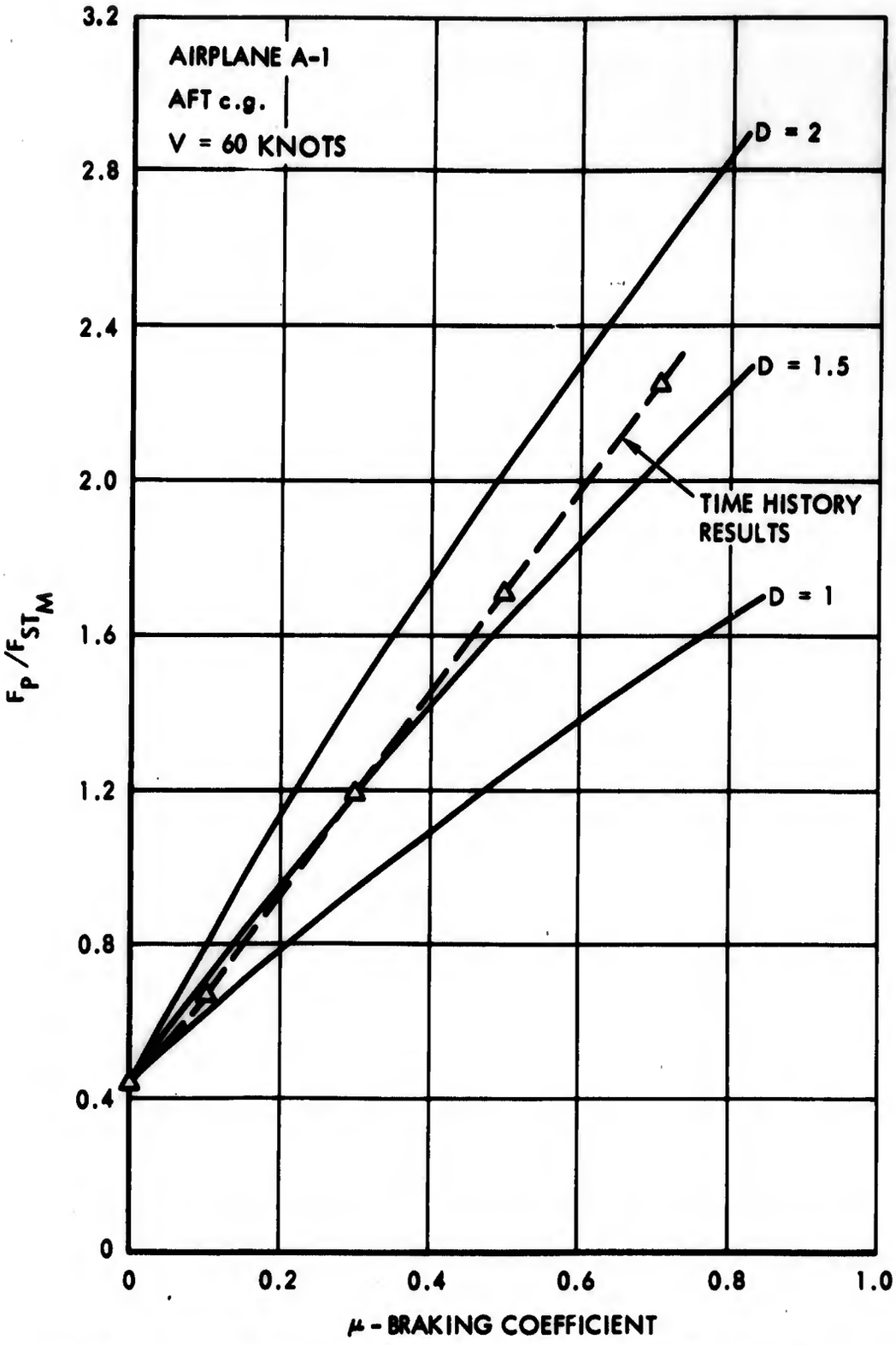

FIGURE 33 - Comparison of Time History and Simplified Dynamic Braking Analyses, Airplane A-1, Aft c.g.

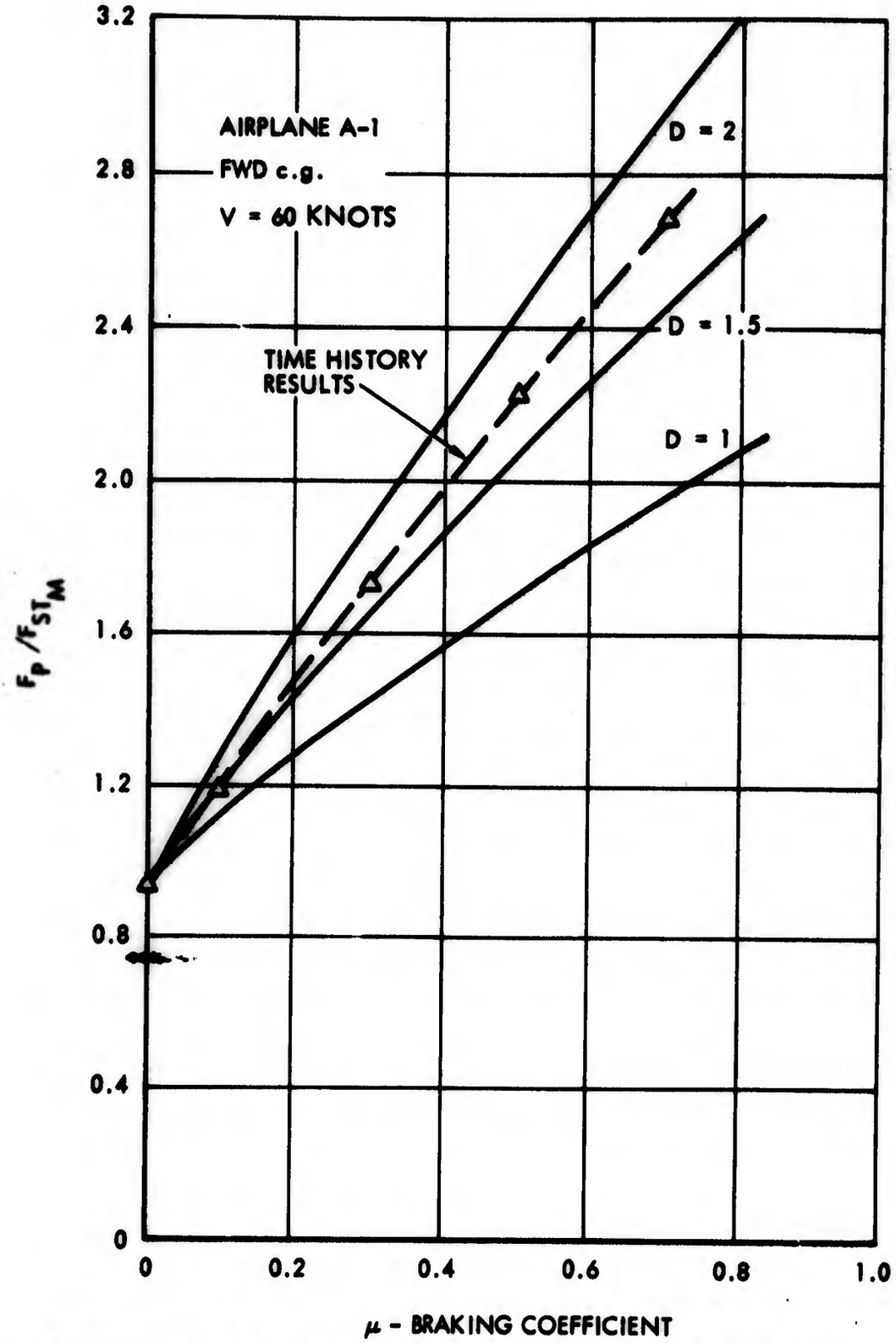

FIGURE 34 - Comparison of Time History and Simplified Dynamic Braking Analyses, Airplane A-1, Forward c.g.

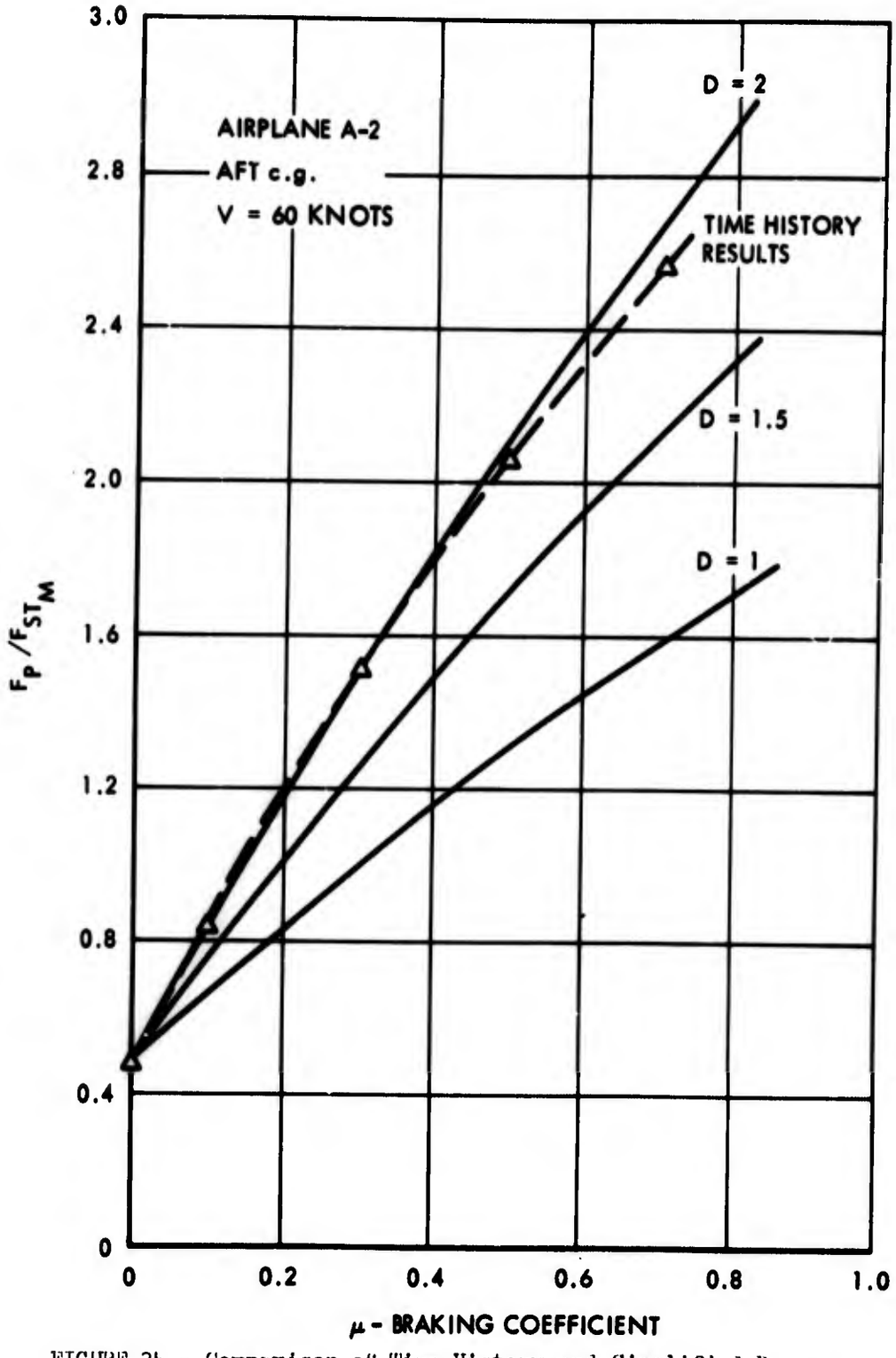

FIGURE 35 - Comparison of Time History and Simplified Dynamic Braking Analyses, Airplane A-2, Aft c.g.

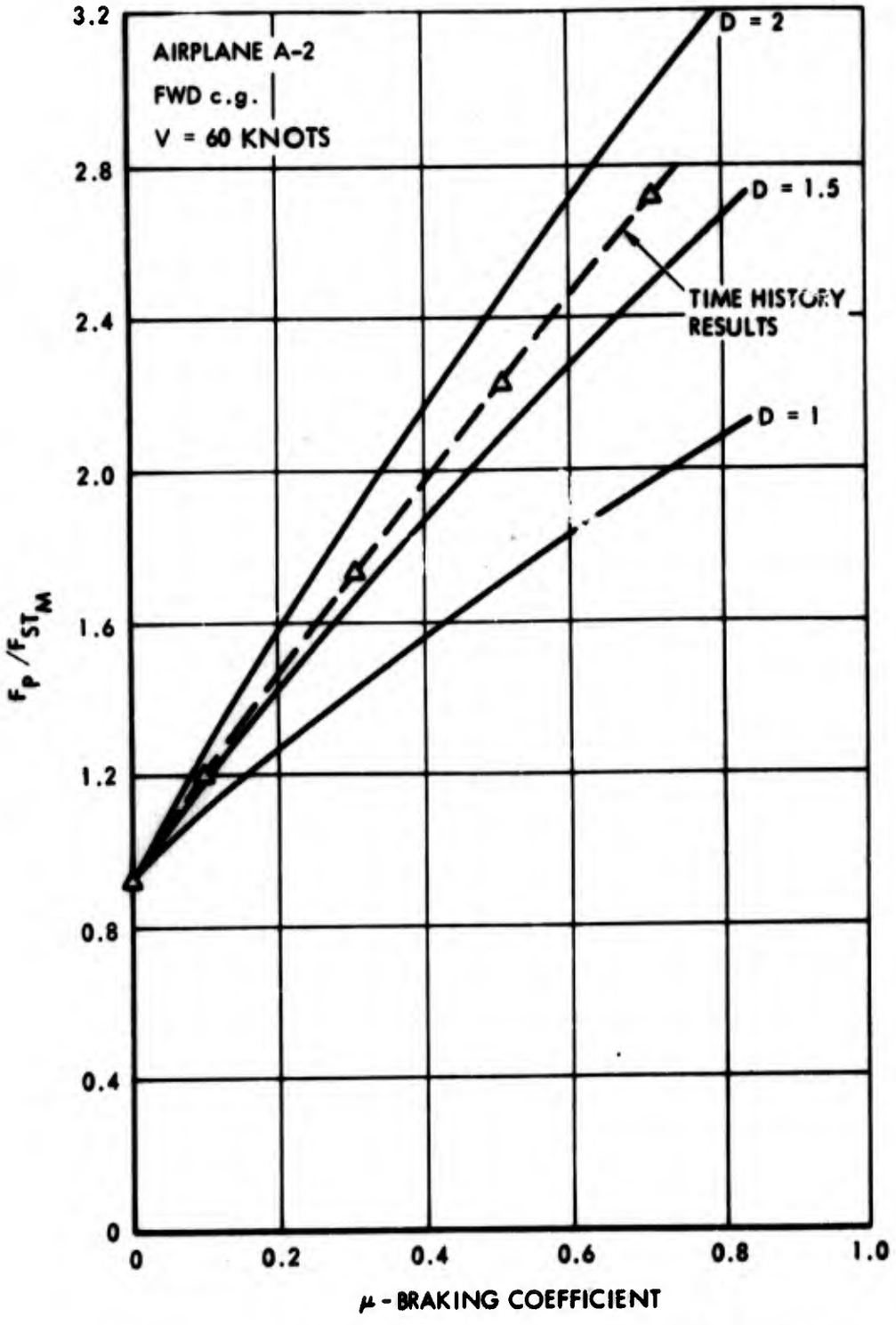

FIGURE 36 - Comparison of Time History and Simplified Dynamic Braking Analyses, Airplane A-2, Forward c.g.

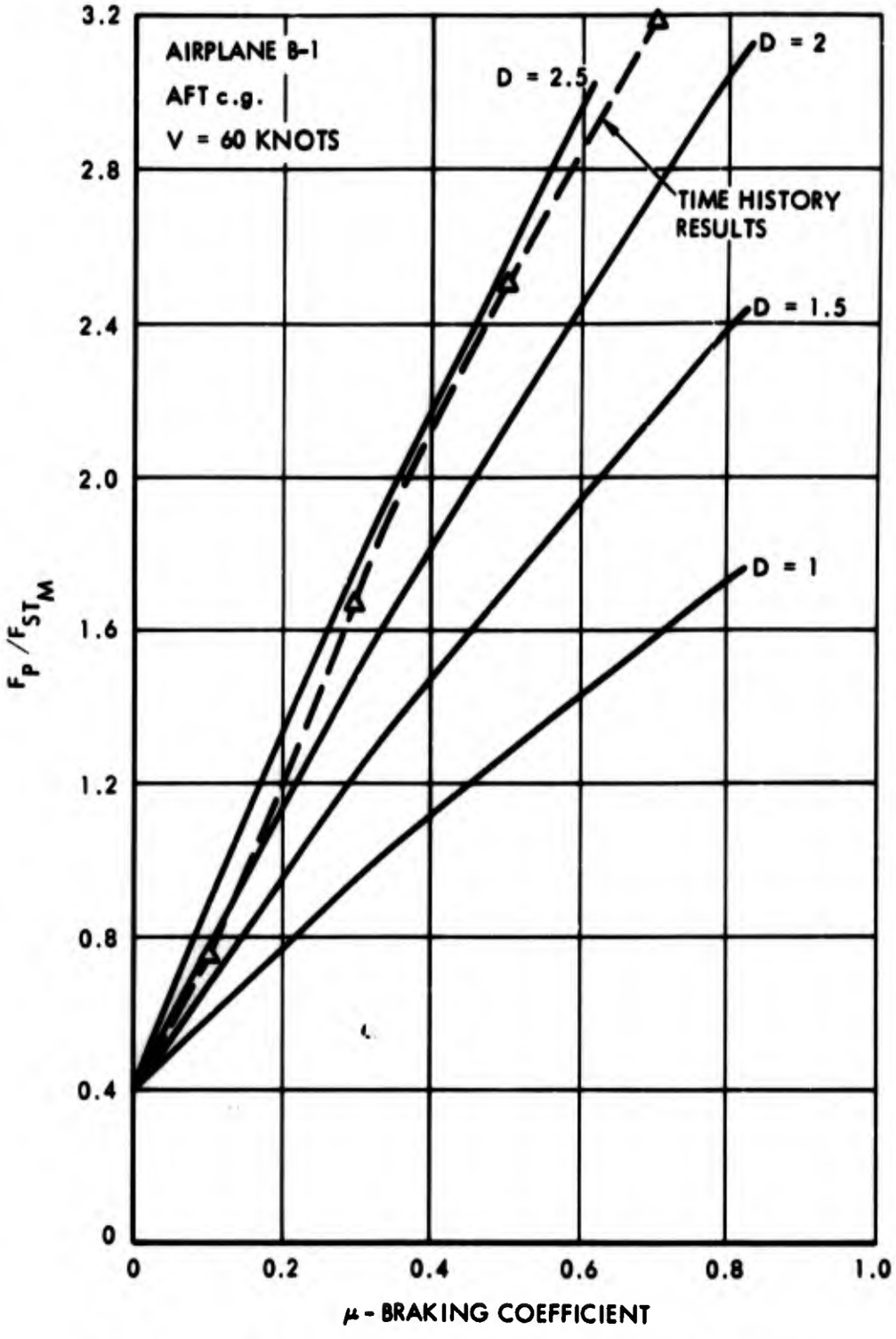

FIGURE 37 - Comparison of Time History and Simplified Dynamic Braking Analyses, Airplane B-1, Aft c.g.

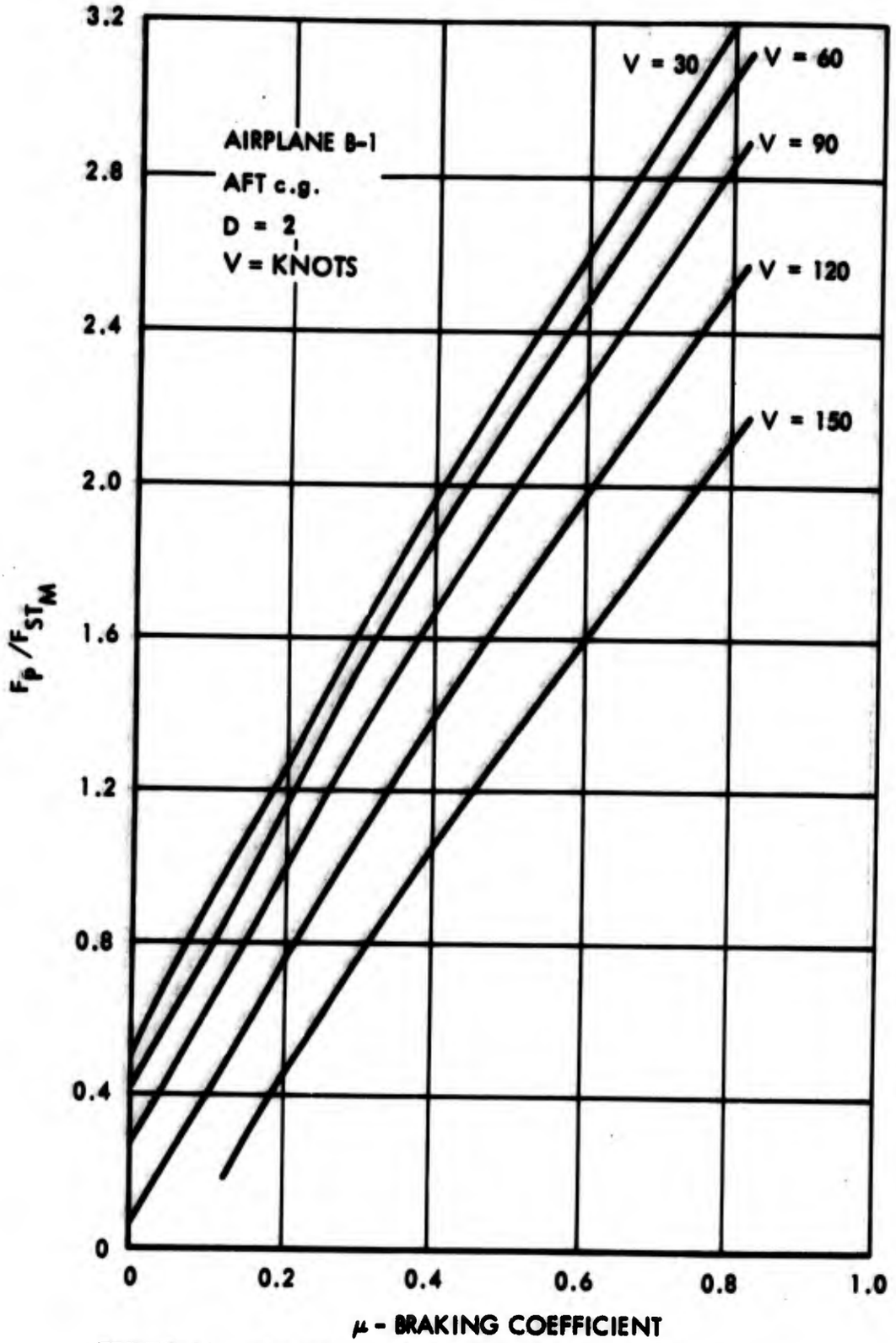

FIGURE 39 - Variation of Dynamic Braking Loads with Velocity, Airplane B-1, Aft c.g.

(g) Takeoff Rotation - Takeoff rotation occurs after the pilot has reached rotation velocity and is committed to a lift-off, i.e., decided not to abort the takeoff. At this time he alters the elevator setting in a tail-up direction, inducing a downward aerodynamic force at the tail which produces a nose-up pitching moment on the airplane. This pitching moment rotates the airplane nose-up until the attitude gives sufficient lift for lift-off. In the process, the downward force at the tail increases the main gear vertical forces above the value at the initiation of rotation.

A typical main gear vertical load time history is shown in the following sketch:

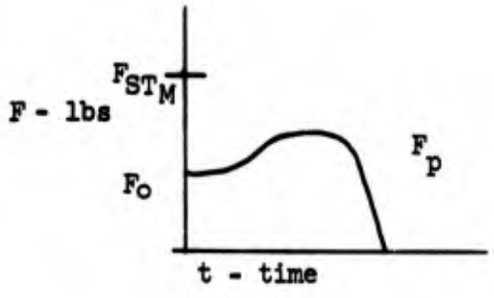

where

F_o = Initial force at the start of rotation

F_{ST_M} = Maximum static load due to aerodynamics

F_p = Peak load obtained during rotation

Time history analyses of rotation have been performed for various airplanes and the resulting F_p/F_o values are shown in Table 15 below.

TABLE 15 - TAKEOFF ROTATION MAIN GEAR LOAD RATIOS F_p/F_o

Airplane	Center of Gravity	
	Aft	Fwd
A-1	1.080	1.152
A-2	1.084	1.172
B-1	1.162	1.233
C-1	1.096	1.178
C-2	2.05, 1.053 (1)	2.08, 1.104 (1)
D-1	1.44	(2)

(1) Higher value applies to aft main gear, lower value to forward main gear

(2) Insufficient data

For all the runs shown in Table 15, the elevator input was ramped in 1.5 seconds. The peak load, relative to maximum static, can be expressed as

$$\frac{F_p}{F_{ST_M}} = \frac{F_p}{F_o} \left(\frac{F_o}{F_{ST_M}} \right)_{VR}$$

where $(F_o/F_{ST_M})_{VR}$ is the aerodynamic reduction (or increase) in main gear vertical load, relative to maximum static, at rotation velocity. The following table computes F_p/F_{ST_M} for the various airplanes, using the values from Table 15.

FIGURE 16 - TAKEOFF ROTATION LOAD FACTORS

Airplane	F_p/F_o	$(F_o/F_{ST_M})_{VR}$	F_p/F_{ST_M}
A-1	1.152	0.627	0.722
A-2	1.172	0.639	0.749
B-1	1.233	0.631	0.779
C-1	1.178	0.687	0.809
C-2	2.05	0.455	0.934 ⚠
D-1	1.44	1.25	1.80 ⚠

⚠ Aft c.g.

Note in the above table that airplane D-1 develops 25 percent negative lift at rotation velocity, giving $(F_o/F_{ST_M})_{VR} = 1.25$. This coupled with the high dynamic response F_p/F_o of 1.44, yields a peak rotation load of 1.8 times the maximum static load. This clearly indicates the seriousness of negative lift in increasing runway loading.

The effects of rotation on loads imposed on pavements can be influenced by main gear configurations especially those four strut arrangements which are longitudinally displaced from each other. The selection of a four strut main gear arrangement is normally the result of optimization studies which include such trade-off parameters as wing lift of the airplane in the three point attitude, response to pavement unevenness, elevator power and airplane pitching inertia. Therefore, while one airplane may exhibit a greater increase in strut load, due to rotation, the net effect of all parameters may be that the load will not exceed static.

Airplanes C-1 and C-2 have four main gears. However, airplane C-1 has a hydraulic interconnection between the forward and aft main gears on each side of the airplane. This interconnection is incorporated for the purpose

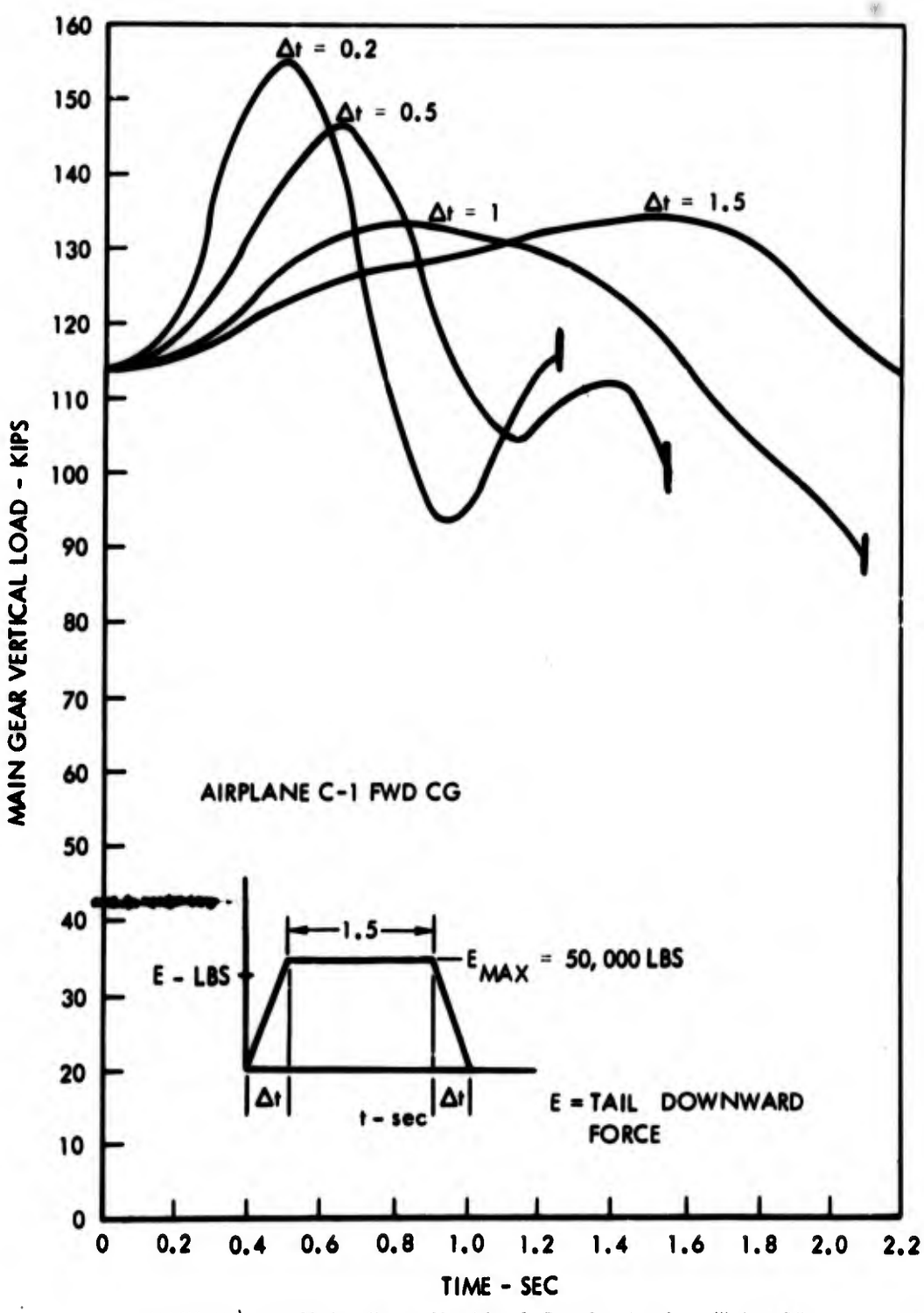

FIGURE 40 - Main Gear Vertical Loads during Takeoff Rotation, Airplane C-1, Forward c.g.

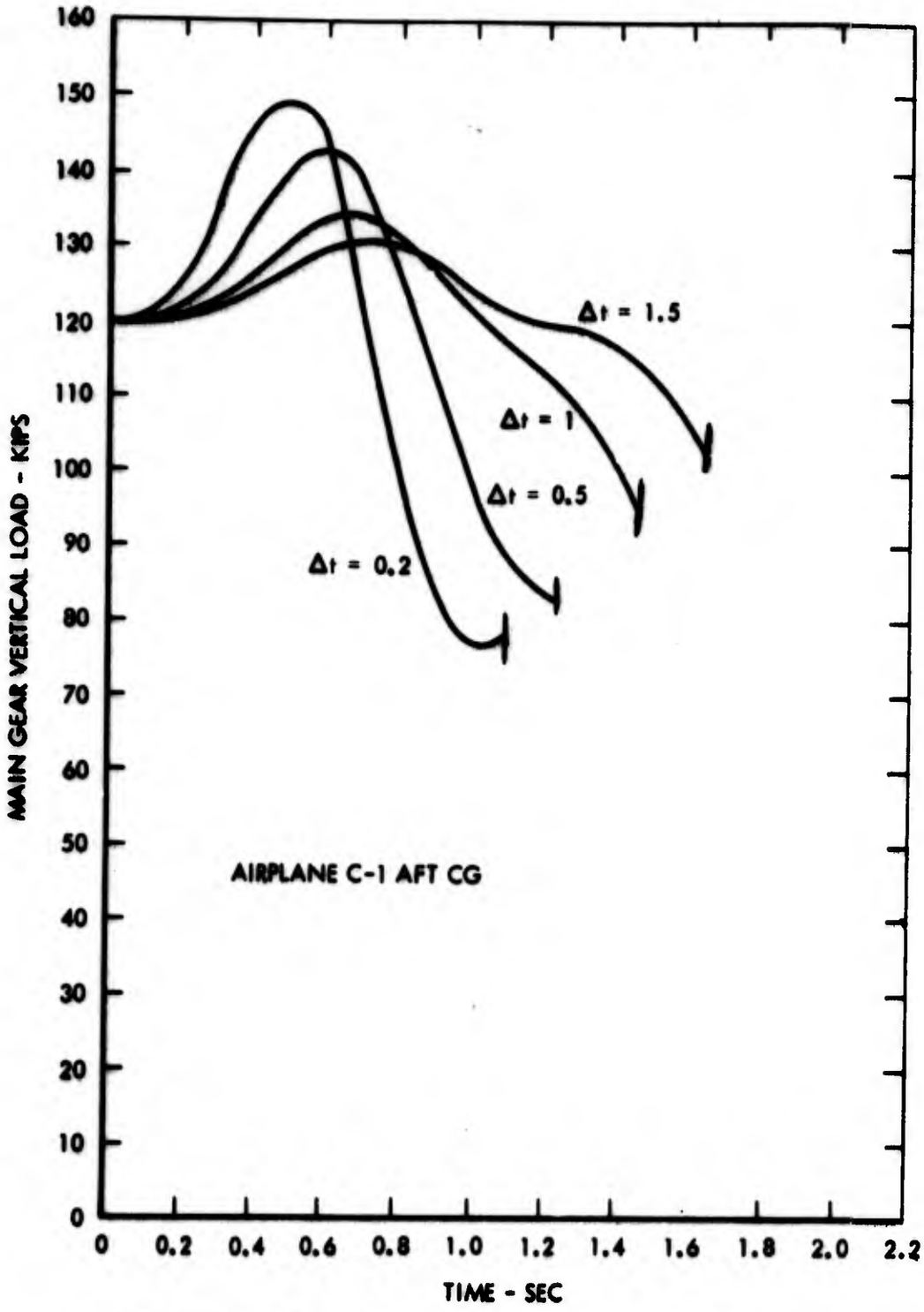

FIGURE 41 - Main Gear Vertical Loads during Takeoff Rotation, Airplane C-1, Aft c.g.

of providing a means of equalizing the loads between these two gears. The main gears on airplane C-2 are independent of each other. Figures 40 and 41 show main gear vertical load time histories for airplane C-1 during rotation. Also shown in figure 40 is a typical time history of elevator input force, E. These results were obtained with a simplified airplane model described in Appendix D. This model does not account for the bottoming of the equalizer piston, so that the results are not valid once the piston has bottomed. However, the load will amplify once metal to metal contact is made. Also, a linear gear is assumed to simplify the analysis, whereas actual gears are highly non-linear. Therefore, the magnitudes of the peak loads obtained are quite approximate.

In Figures 40 and 41 an ideal equalizer is assumed, i.e., one which has no pressure losses in the approximately 27 foot long interconnecting lines. Hence, with the airplane model assumed, the forward and aft main gear loads are equal. In actual practice, the aft main gear loads will be higher than those shown and the forward main gear loads less, due to the pressure differential from the fluid flow from aft to forward gear. The vertical hash marks on each curve represent the time when the aft gear equalizer piston bottoms, for a piston having a maximum displacement from neutral of 4 inches. After the piston bottoms, the aft main gear loads will increase above those shown.

Also shown in these figures is the effect of varying the elevator input time Δt. More rapid input naturally results in higher loads. For the forward c.g. case, the F_p/F_o value increases from 1.178 at $\Delta t = 1.5$ to 1.35 at $\Delta t = 0.2$. (All values shown in Tables 15 and 16 are based on $\Delta t = 1.5$). However, even the higher value gives a peak load less than maximum static, 1.35 X (0.687) = .927 for F_p/F_{ST_M}.

The rotation loads for airplane C-2, with independent main gears, are shown in Figures 42 and 43, for $\Delta t = 1.5$. In each figure, the highest and lowest curves represent the aft and forward main gears, respectively. The middle curve represents the loading that would result for each gear if an "ideal" load equalizer were used. Again, this curve is valid only up to the vertical hash marks, when the equalizer piston would bottom out (assuming a 4 inch piston displacement). Beyond this point the aft main gear loads would increase, although probably not to as high a value as shown for the aft gear with independent gears.

Table 16 shows the severest case for airplane C-2, where $F_p/F_o = 2.05$, significantly higher than for the other airplanes shown. However, airplane C-2 also develops a large amount of lift at rotation velocity, $(F_o/F_{ST_M})_{VR} = 0.455$, so that the resultant total load is still less than static. This indicates the importance of looking at the total airplane system when weighing the advantages and disadvantages of a load equalizer as a means of reducing the loads imposed on the pavement. For airplane C-2, a load equalizer would probably slightly reduce the take-off rotation loads, but these loads are already less than static and, hence, not critical without the equalizer.

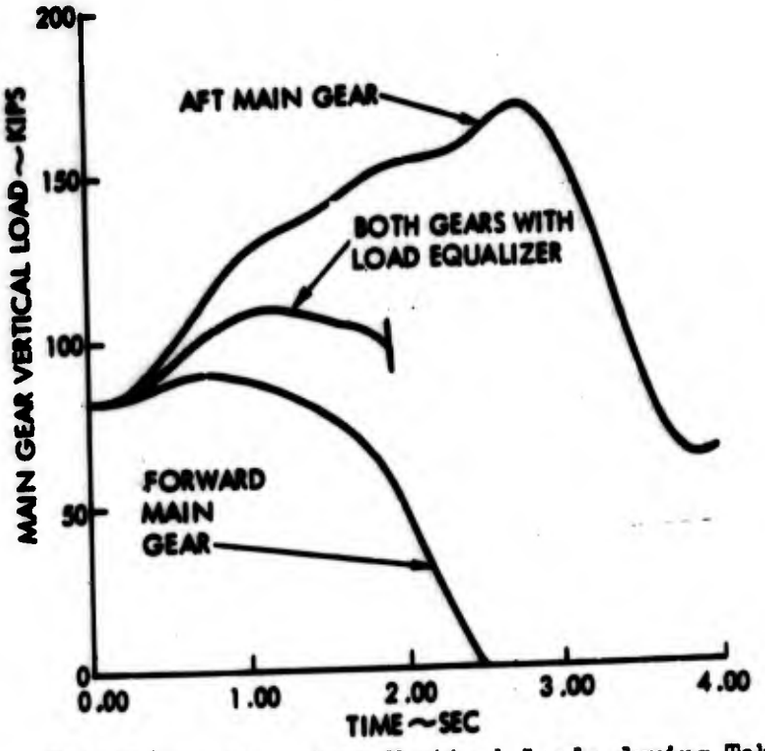

FIGURE 42 - Main Gear Vertical Loads during Takeoff Rotation, Airplane C-2, Forward c.g.

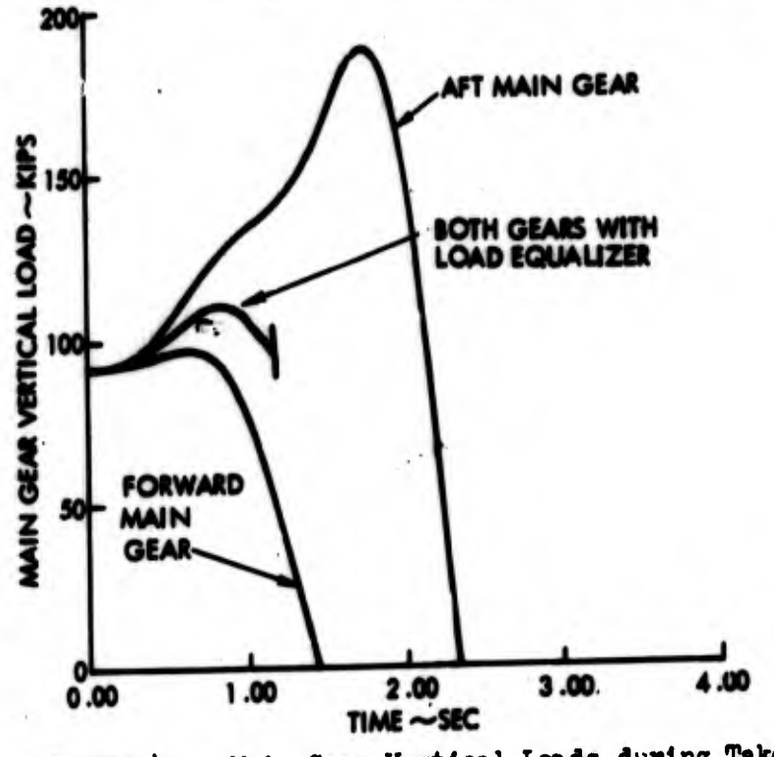

FIGURE 43 - Main Gear Vertical Loads during Takeoff Rotation, Airplane C-2, Aft c.g.

(h) Landing Impact - Landing impact loads, as well as loads during landing rollout and taxiing, are generally less severe than their counterparts during takeoff, since the airplane is at a lower gross weight. Table 17 lists the maximum takeoff and landing weights for the airplanes studied, and their ratios.

TABLE 17 - MAXIMUM TAKEOFF AND LANDING WEIGHTS

Airplane	Takeoff Gross Wt.	Landing Gross Wt.	Takeoff Gross Wt. / Landing Gross Wt.
A-1	310,000	207,000	1.498
A-2	310,000	199,500	1.554
B-1	411,000	348,000	1.181
B-2	413,000	347,000	1.188
B-3	510,000	375,000	1.360
C-1	713,000	564,000	1.264
C-2	861,000	699,000	1.233
D-1	595,000	350,000	1.700

For class A airplanes, the ratio is about 1.5, for class B from 1.2 to 1.4, for class C about 1.25, and 1.7 for class D. The higher ratios are indicative of longer range airplanes which have a higher percentage of take-off weight due to large fuel loads. The higher the ratio the more critical are the "departure" loads in comparison to the "arrival" loads. "Arrival" operations, (operations 9 to 14, Table 5) yield less critical loads than the corresponding "departure" operations (6 to 1 from Table 5), which occur at higher gross weight. The only potentially significant "arrival" operation is landing impact.

The main gear loads obtained during landing impact are primarily a function of sink speed and lift. Figure 44 shows the maximum main gear load, divided by maximum static load at maximum take-off gross weight, obtained from time history analyses of landing impacts for airplanes A-1, A-2 and B-1. All runs are at the maximum landing weight, 100 percent lift and an aft c.g. With the exception of airplane A-2, the main gear loads barely reach the static level at a sink speed of 10 feet/second. At more typical sink speeds of around 3 feet/second, the maximum main gear loads are less than 0.6 times the maximum static value.

Figure 45 shows the variation with lift in peak main gear loads during landing impact. These runs were performed at a sink speed of 10 feet/second,

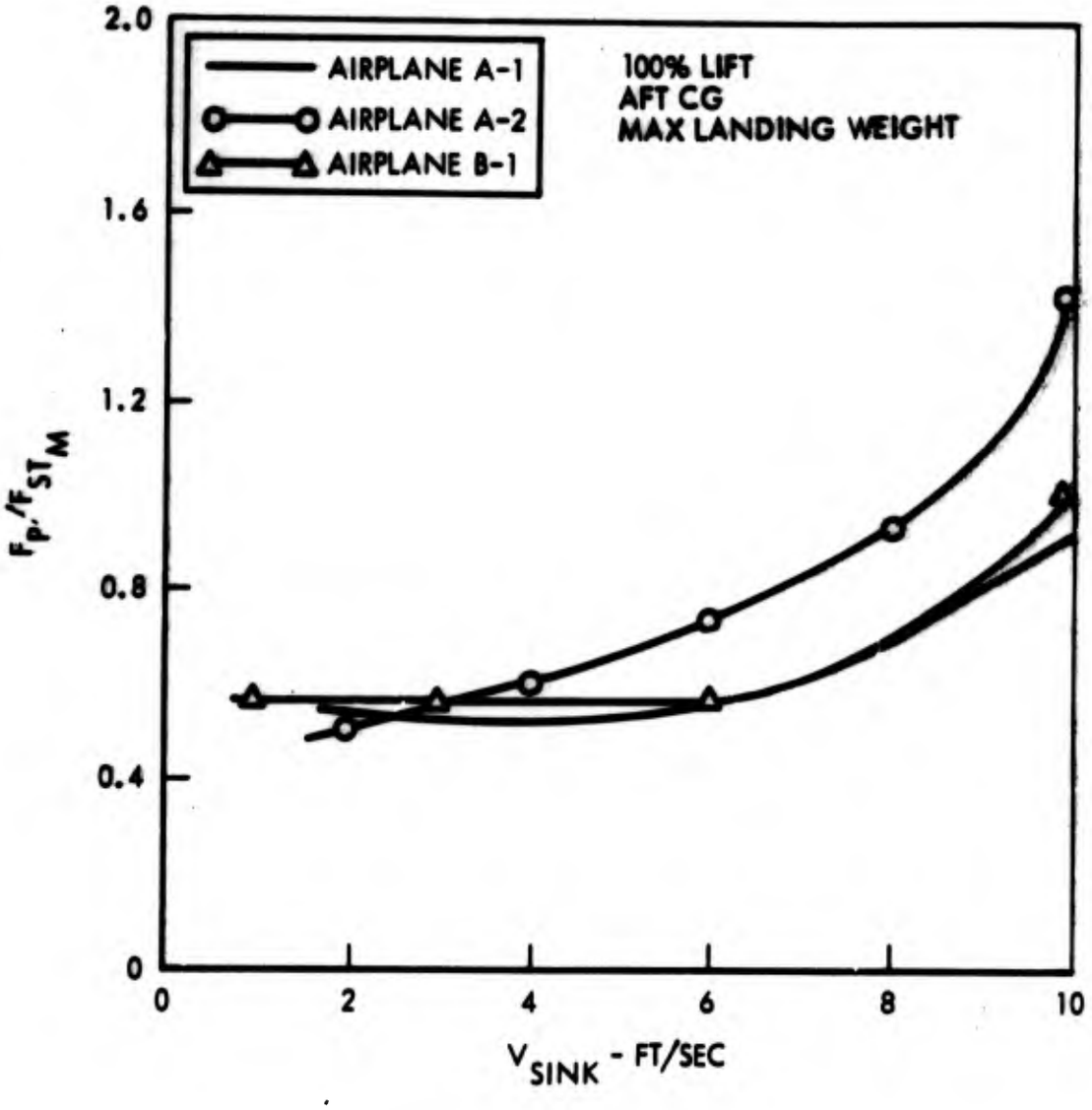

FIGURE 44 - Variation of Maximum Main Gear Loads during Landing Impact with Sink Speed

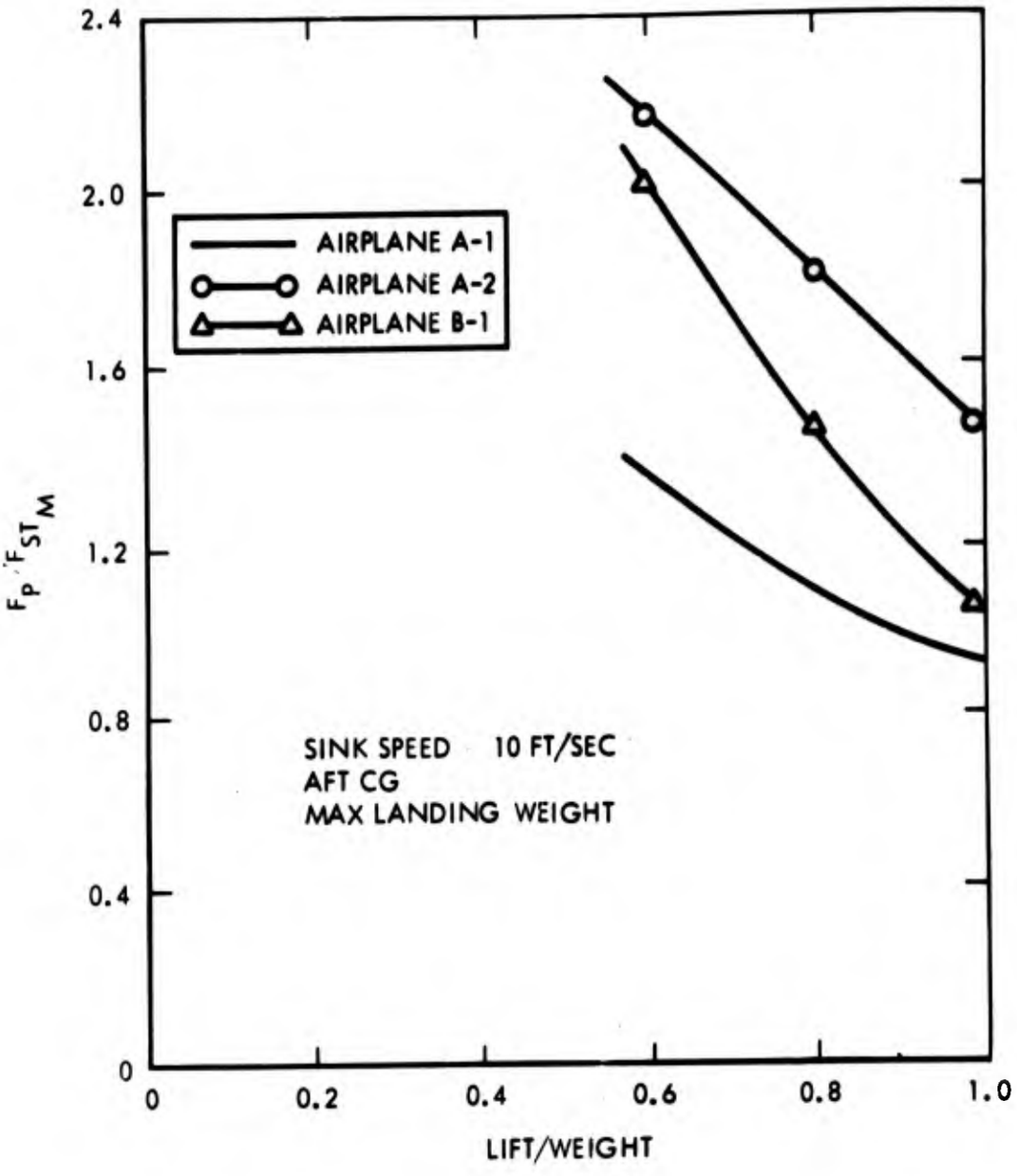

FIGURE 45 - Variation of Maximum Main Gear Loads during Landing Impact with Lift

aft c.g., and maximum landing weight. As before, the loads are normalized to the maximum static value at maximum take-off gross weight. The results clearly show the drastic effect of reduced lift. While these results show loads as high as twice maximum static, such reduced lift landings combined with the high sink speed are never encountered in normal operations.

Runs at a forward c.g. show, as expected, less critical main gear loads. The nose gear loads are typically higher with a forward c.g. position and maximum nose gear loads are sensitive to two other factors in addition to sink speed and lift. These factors are: (1) the airplane pitch attitude at touchdown, and (2) the manner in which the pilot "untrims" the airplane to let the nose gear down. Rapid untrimming,combined with a high nose up initial attitude, can result in very high theoretical nose gear loads. However, these loads are readily sensed and controlled by the pilot, so that the maximum theoretically predicted nose gear loads will not be achieved. The situation is analogous to low speed taxi in that pilot techniques will keep the loads down to an acceptable level. It is expected that the actual nose gear loads experienced would normally be less than twice the maximum static loads.

(i) High Speed Braking....., Static - The "arrival" operations are the same as the departure operations, except that the "arrival" operations are performed at a landing weight which is less than the take-off weight. The "arrival" aerodynamics are generally different than for "departure", normally involving a more tail down flap setting for landing with correspondingly greater lift. However, this greater lift is generally not present during the landing rollout because of spoiler deployment. For airplane B-1, the lift/landing weight with landing flaps and spoilers is about equal to the lift/take-off weight with take-off flaps and no spoilers. This is the only airplane studied for which detailed spoiler aerodynamics are available.

Regardless of the aerodynamic characteristics, however, it is clear that aborted take-off, with spoilers deployed and at take-off gross weight, will always be more critical than landing rollout. Similarly "arrival" operations, eleven through fourteen, will be less critical than their "departure" counterparts, four through one (see Table 5 on page 75).

A summary of the results of the complete loads analysis study is presented in the Section, Results of the Program, starting on page 161.

(2) Airport Pavement Response

(a) The Nature of Pavement Response.- Pavement response is the reaction of the pavement structure to the loading imposed on it. There are three basic types of response: (1) deflection (the local displacement of a segment of the pavement; also referred to as deformation or motion), (2) strain (the local rate of change of deflection; also called curvature), and (3) stress (the local force per unit area or force traction; also referred to as the pressure). The essence of pavement design is to keep these response variables less than certain prescribed limits which depend on the strength of the pavement construction materials. Generally, the most important response variables on airport pavements are the deflection of the top surface, w, the fiber stresses and strains in the top surface, σ and ϵ, the vertical normal pressure in the foundation, p_z, and the shearing stresses at the interface of surface layer and foundation, τ. The following sketch below shows these critical response variables at the location where they are generally a maximum.

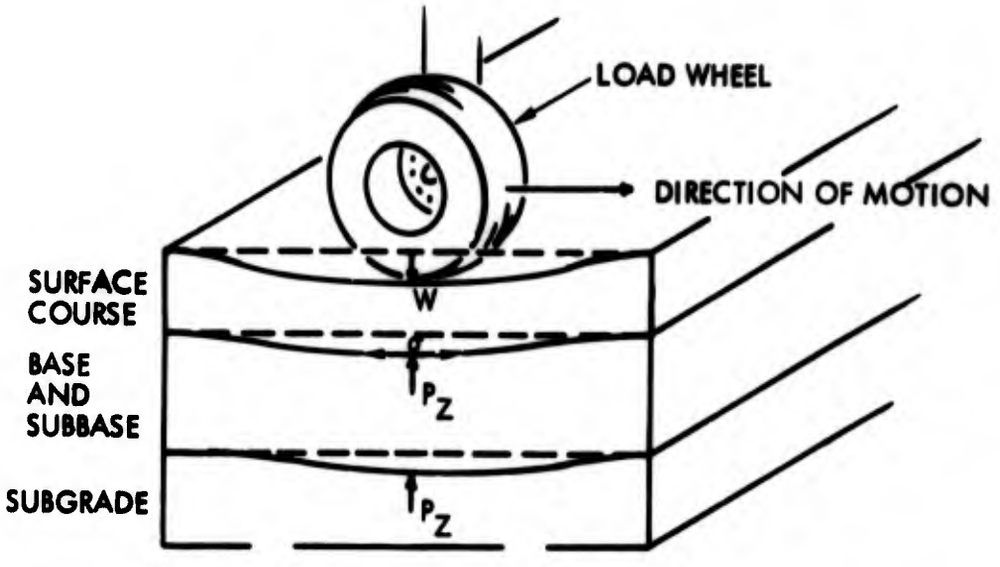

The magnitude and character of the critical response variables result from two things: (1) the nature of the applied loads and (2) the nature of the pavement structure. The loading experienced by airport pavements has been previously discussed and can be summarized as a vertical load P(t) and a horizontal load Q(t). Analysis of the response of pavement structures condenses down to the analysis of the response to P(t) and Q(t). Differing assumptions about the nature of the pavement structure is required in each case, as the effects of material type, layering, viscoelasticity, etc. have differing affects in each case.

(b) Pavement Response to a Vertical Moving Load.- The pavement and loading model used to compute pavement response to a moving load is shown in Figure 46. Actually, two models are used, one as a rigid pavement model and one as a flexible pavement model, but they differ only in the material characterization of the top layer. Briefly stated, the model is a two-layer

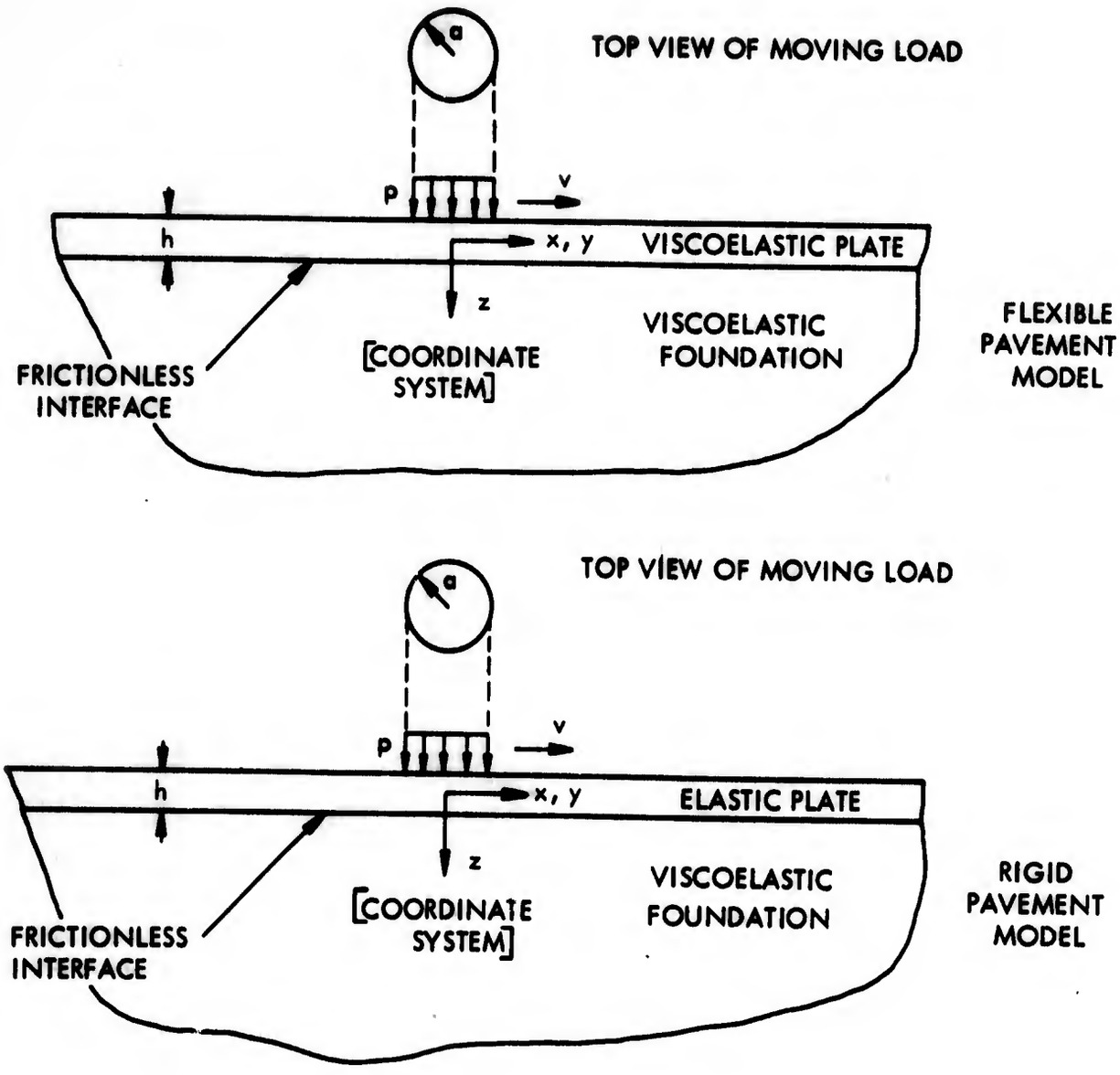

FIGURE 46 - Pavement and Loading Model: Moving Load Problem

system consisting of a thin plate resting on a three-dimensional elastic solid acted on by uniform pressure distributed over a circular area and moving at constant velocity. This type of model is known as "slab theory" and the background to it is discussed in Reference (5).

The analysis of this model is an extension of the analysis presented in Reference (6) using Laplace transform techniques and the superposition principle for loaded linear systems. Linear viscoelastic models were used to describe the materials for the plate and foundation. The specific models used are shown below. The essential feature of these models is that they are composed of linear springs and dashpots, and hence, there is a linear (albeit time-dependent) relationship between stress and strain. The effect of this linearity assumption (as well as the effects of the other assumptions) is discussed in paragraph (8) of this section. Suffice it to say that the three-element model was considered adequate to account for the basic effects of instantaneous elastic deformation, delayed viscoelastic deformation, and asymptotic deformation state which are present in pavement construction materials.

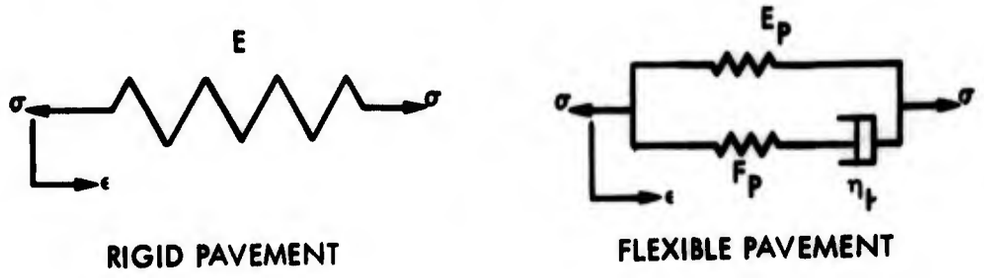

Diagram 1: Surface course model

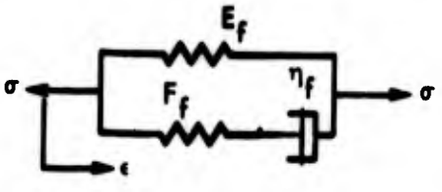

Diagram 2: Foundation Model - Rigid and Flexible Pavements Material Characterization

Mathematical analysis of the two-layer pavement system subjected to a moving load is presented in Appendix E. The solution to the problem consists of expressions for six different response variables:

w - plate deflection

p_z - foundation vertical normal pressure

σ_x - plate longitudinal fiber stress

σ_y - plate lateral fiber stress

ϵ_x - plate longitudinal fiber strain

ϵ_y - plate lateral fiber strain

These expressions involve double integrals, requiring computer evaluation, a description of which is found in paragraph (6) beginning on p. 144.

Simplifications to the response equations result if only values at the interface $z = h/2$ are considered. Table 18 summarizes these final expressions, and only the maximum lateral or longitudinal stresses and strains are taken.

TABLE 18 FINAL PAVEMENT RESPONSE EXPRESSIONS

Response	Symbol	Expression*
Plate Deflection	w	$C_w \frac{P\ell^2}{D}$ inches
Foundation Pressure	p_z	$C_p \frac{P}{\ell^2}$ psi
Plate Strain	ϵ	$C_\epsilon \frac{hP}{D}$ in/in
Plate Stress	σ	$C_\sigma \frac{(1+\nu_p)P}{h^2}$ psi

* P = total applied load

h = plate thickness

ℓ = system characteristic length = $\sqrt[3]{\frac{D}{E_f}}$

$$D = \frac{E_p h^3}{12\,(1-\nu_p^2)}$$

E_p = Static stiffness of plate

E_f = Static stiffness of foundation

ν_p = Poisson's ratio of plate

and

C_w, C_p, C_ε, C_σ are nondimensional correction factors which are functions the nondimensional variables in the problem:

X, Y, Z = nondimensional location of response $\left[X = \frac{x}{\ell}\,,\ Y = \frac{y}{\ell}\,,\ Z = \frac{z}{\ell}\right]$

V = nondimensional load velocity = $\begin{cases} \left(V\tau/\ell\right) & \text{flexible} \\ \left(V\tau_\sigma/\ell\right) & \text{rigid} \end{cases}$

ζ = damping-stiffness ratio = $\frac{\eta_\rho}{\eta_f}\,\frac{F_f}{F_p}$

μ_p = ratio of dynamic to static stiffness of plate = $(E_p + F_p)/E_p$

μ_f = ratio of dynamic to static stiffness of foundation = $(E_f + F_f)/F$

r = nondimensional load radius = a/ℓ

The response of the pavement system is generally a maximum directly under the load. In this case, X = Y = 0 and the response coefficients (C_i's) become functions of only five nondimensional variables:

V, - the nondimensional velocity

μ_p, μ_f, - the stiffness ratios

ζ, - the damping parameter

r - the nondimensional load radius

When the velocity is equal to zero (V = 0), the static case is recovered and nondimensional correction factors become functions solely of the nondimensional radius, r, as shown in Figure 47.

When the velocity is large (V>>0), the dynamic case is obtained and the nondimensional correction factors are functions of the stiffness ratios, μ_p and μ_f, as well as the nondimensional radius, r, and shown in Figures 48 and 49 The ordinates show the ratio of dynamic to static stress and pressure, respectively, which serve as dynamic correction factors. Both plate fiber stress (figure 48) and foundation pressure (figure 49) depend on the particular ratio μ_p/μ_f. This ratio can be rewritten as:

$$\xi = \frac{\mu_p}{\mu_f} = \left(\frac{E_{dyn.}}{E_{stat}}\right)_{plate} \left(\frac{E_{static}}{E_{dynamic}}\right)_{foundation}$$

$$\xi = \left(\frac{E_{plate}}{E_{foundation}}\right)_{dynamic} \left(\frac{E_{foundation}}{E_{plate}}\right)_{static} = \frac{K_{dynamic}}{K_{static}}$$

where: $K = \frac{E_{plate}}{E_{foundation}}$ = ratio of plate to foundation stiffness

Thus, K is a measure of the stiffness difference between top and bottom layers, and ξ is a measure of the change in this difference as the speed of travel of the load goes from static to the high speed. ξ is called the ratio of relative stiffnesses. Alternatively, ξ can be considered in its μ_p/μ_f form as the ratio of the stiffening properties of the top to the bottom layers. In other words, when ξ is less than 1, the foundation stiffens relative to the surface, and when ξ is greater than 1, the foundation weakens relative to the surface course. Actual values of ξ must be found by measuring the stiffnesses of the pavement materials under high and low rates of strain. This gives the μ values (measures of the viscoelastic stiffening of the material (an elastic material has a μ value of 1)), and these can then be used to find ξ . Although experimentation must ultimately determine the viscoelastic constant ξ , approximate values for typical pavements are given in Table 19. The non dimensional radius, r, shown in figures 47 - 49 is estimated to range from 1 to 5 for the more common asphaltic concrete (flexible) pavement systems for the classification of airplanes studied. Similarly, for concrete (rigid) pavement, r is estimated to be between .1 and 1.0. Based on r and ξ values discussed above, the approximate applicable range for the flexible and rigid pavement systems are depicted in figures 48 and 49.

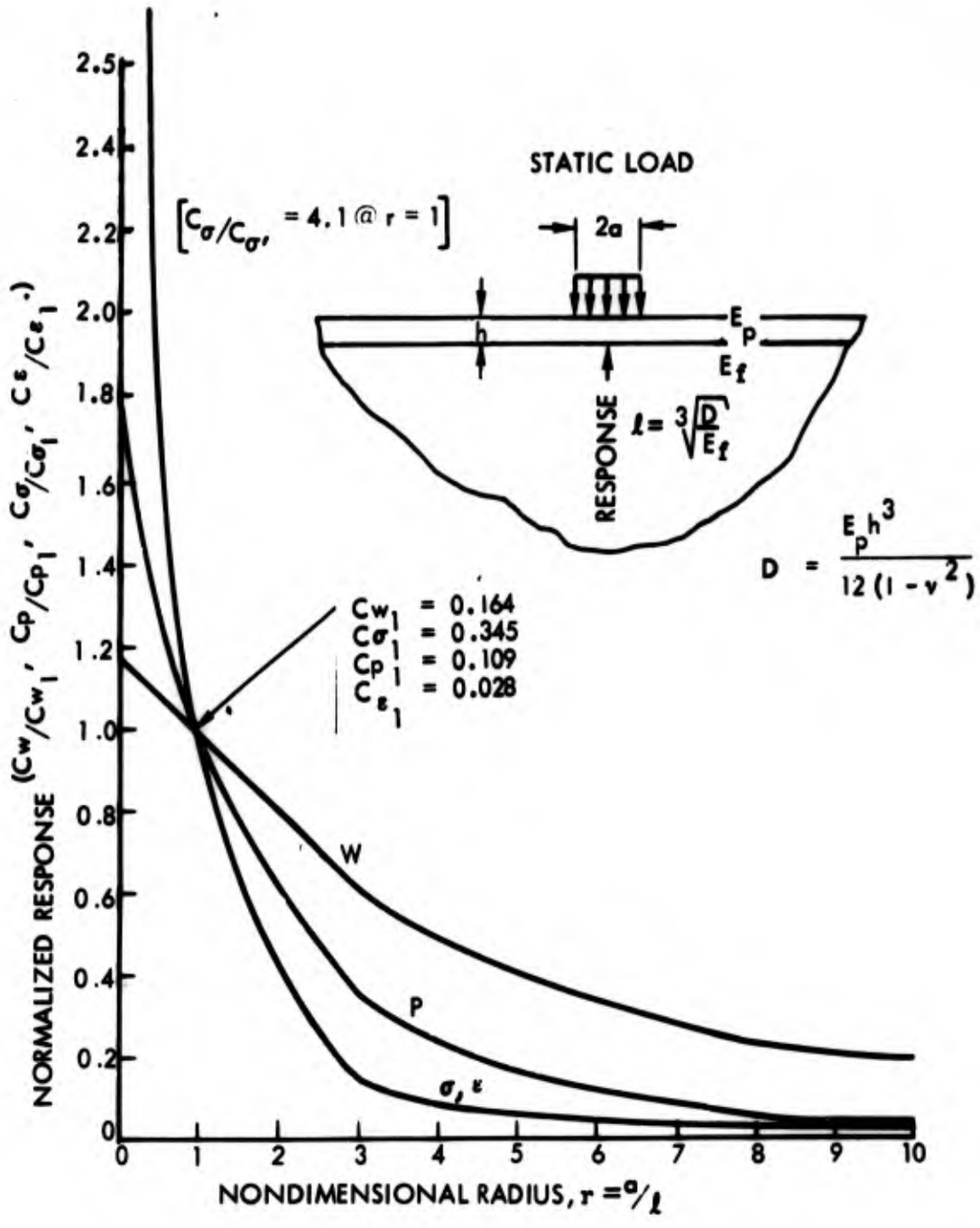

FIGURE 47 - Static Response

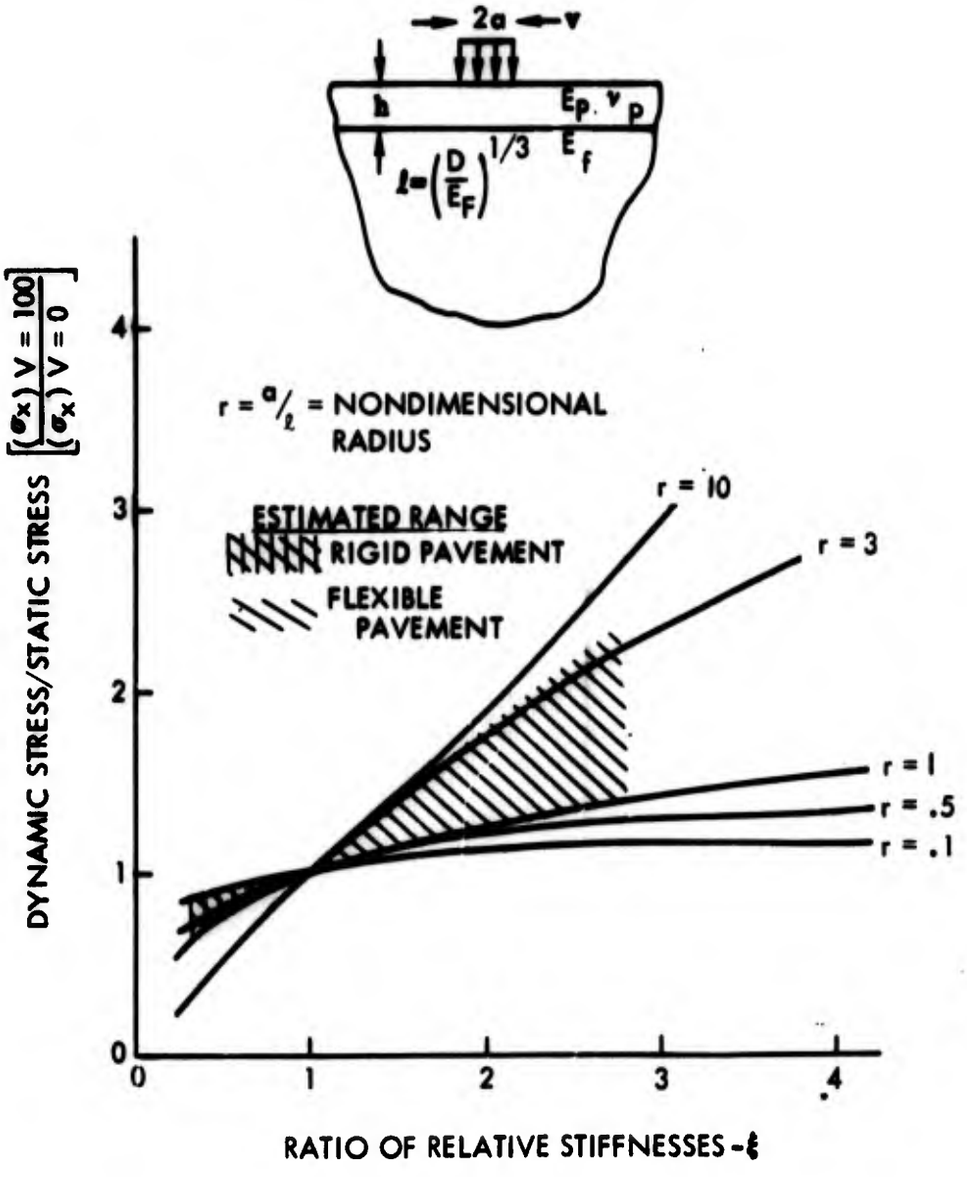

FIGURE 48 - Dynamic Stress Correction Factor

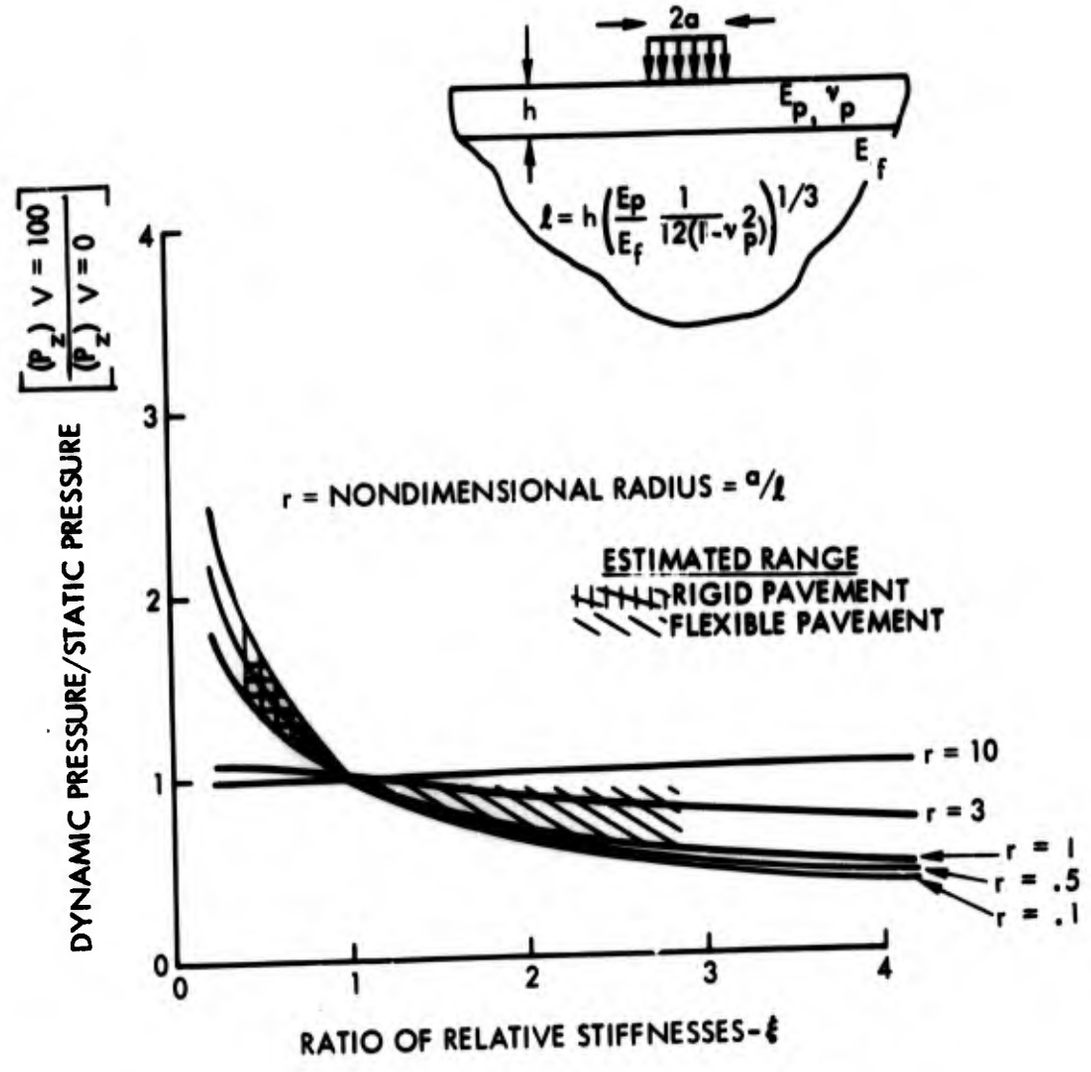

FIGURE 49 - Dynamic Pressure Correction Factor

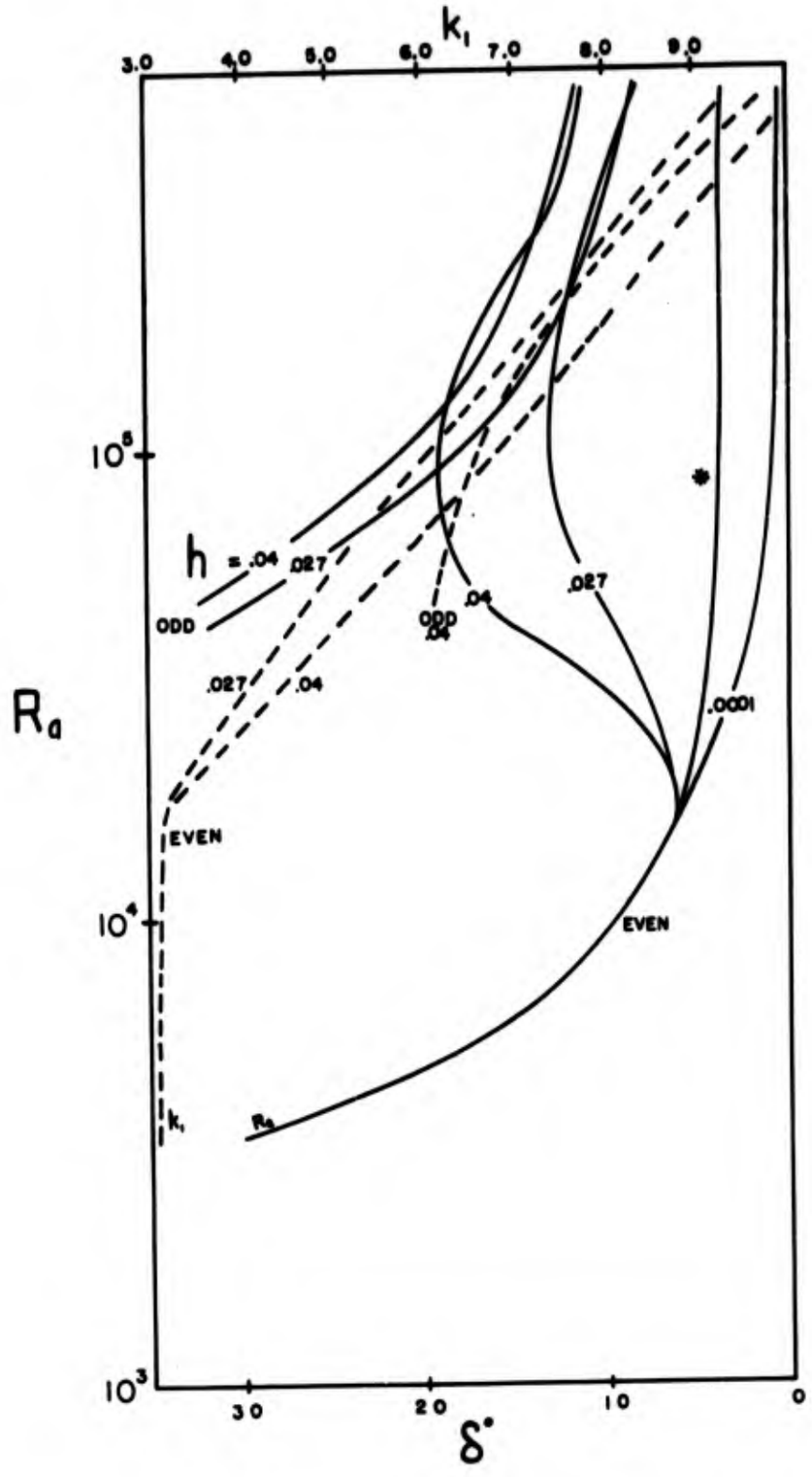

Figure 4.13 Neutral curves for R_a and k_1 for $\delta > 0$, $P_r = 6.7$.

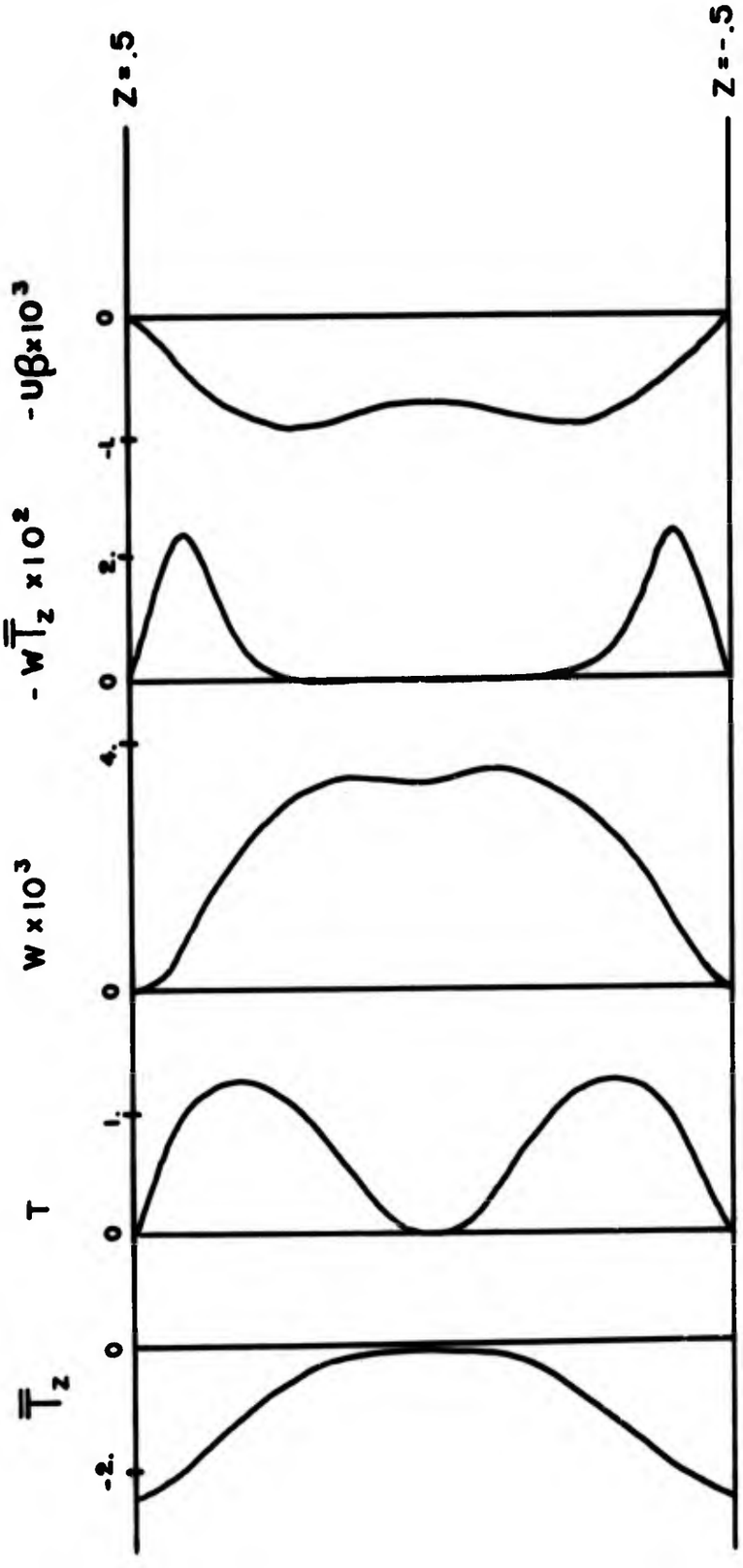

Figure 4.14 Solutions for P_r=6.7, h=.04, R_a=7370, δ=18°.

temperature field relative to the unstable cross-stream gradients. The picture becomes clearer when we consider the modal structure, especially the distributions of T, w and u since these most clearly reflect how the vortices are generated. Figure 4.14 shows profiles of these variables along with the mean fields for $R_a = 7.37 \times 10^4$, $\delta = 18°$. All the variables u, w, and T are cyclic in $\cos k_c y$ so the phase relationships shown hold for all y. The mean cross-stream field $\overline{T}$ is everywhere unstable but more so at the boundaries. The perturbation buoyancy is largest near the walls, and is positive throughout. This temperature excess comes out of the unstable $\overline{T}$. Evidently u is positive. The positive T generates it through the action of the upstream buoyancy force. As a result of advection of the upstream gradient by u the excess temperature is reduced.

Figure 4.15 shows the stability curves for $P_r = 6.7$, h = .04 and $\delta < 0$. Curve (b) is for $\beta = 0$ in (4.7.2), curve (a) is the complete solution. The critical Rayleigh numbers behave in a similar way but the wavenumber curves are entirely different. For case (b) instability is possible as a negative temperature gradient develops in $\overline{T}_z$. This is necessarily a small fraction of the gap so one would expect the associated wavenumbers to be large, as they are. For the complete problem the wave numbers decrease markedly as δ decreases. This suggests that the direct convective instability may exist near $\delta = 0$, but that the shear coupled modes, which tend to have smaller wavenumbers, may exist as the tilt tends

towards horizontal. This is suggested also by the energy distributions in Table 4.6. At low angles e_I is small but at large angles there is a large transfer of kinetic energy from the mean to the upstream velocity. Again the modal structure shows the mechanisms more clearly. Figure 4.16 shows this. As opposed to the example at $\delta = +18°$ vorticity is generated only at the center of the tank. The thermal excess that exists there for $\delta = -17°$ comes out of the advection of the cross-stream component of the basic stratification. The upstream velocity which is positive where T is positive (via buoyancy) tends to decrease the central excess temperature by advection. For $\delta = -60°$, the mean temperature gradient $\overline{T}_z$ is nowhere negative, the cross-stream temperature field is everywhere stabilizing. However, at these angles the effectiveness of the upstream buoyancy is reduced and via the shear advection term in (4.7.3) it is possible to have u negative where T is positive. This means that the thermal excess required for the generation of vorticity can be supplied by advection from the upstream gradient. Hence for these large negative angles the shear coupled mode predominates.

The strength of the shear interaction is roughly inversely proportional to the Prandtl number at fixed R_a. One would suspect that at low P_r the advective instability with its low wavenumbers would prevail but at high P_r the shear would not be important and instability would only involve the reverse gradient in

$\bar{T}(z)$ and would have larger wavenumbers. This is shown in figure 4.17 where we have displayed the results of calculations for four Prandtl numbers at $\delta = -45°$. In air ($P_r = .71$) instability occurs at a low Rayleigh number with a long wavelength. At large P_r the instability may approach a condition which is essentially independent of P_r as it would if it became purely convective. We actually have some experimental evidence which supports this P_r dependence, obtained from overhead streak photos in silicone oil.

TABLE 4.7

Some experimental data for $\delta < 0$

Pr	δ	Ra_c	k
6.7	-45	1.31x10	3.72
24	-45	1.52x10	5.28

Table 4.7 shows this data. The $P_r = 24$ experiment was rather crude and the onset point is probably not too accurate. However, the wavenumber dependence agrees rather well with that predicted by the theory.

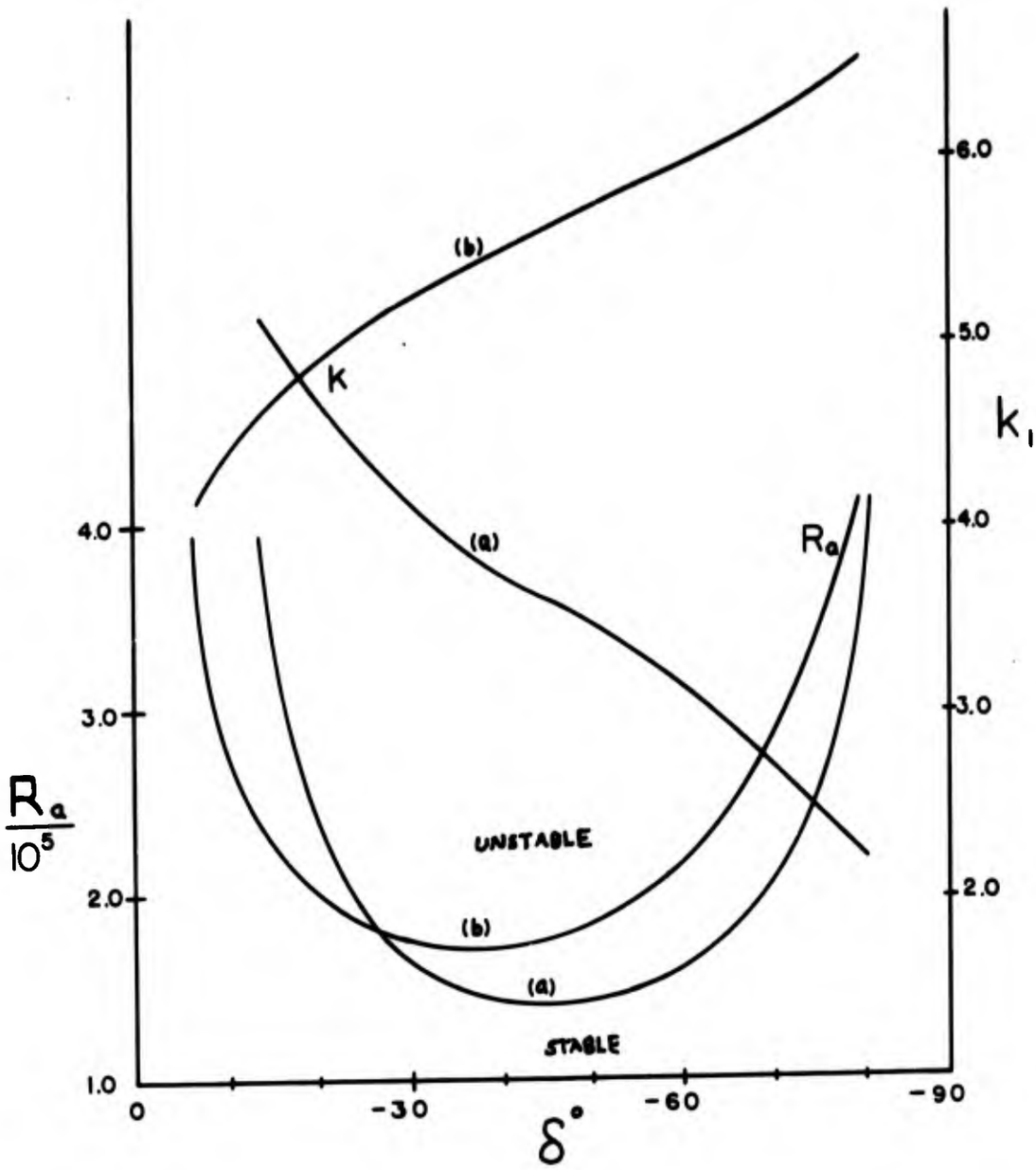

Figure 4.15 Neutral curves of R_a and k_1 for $\delta < 0$, $P_r = 6.7$.

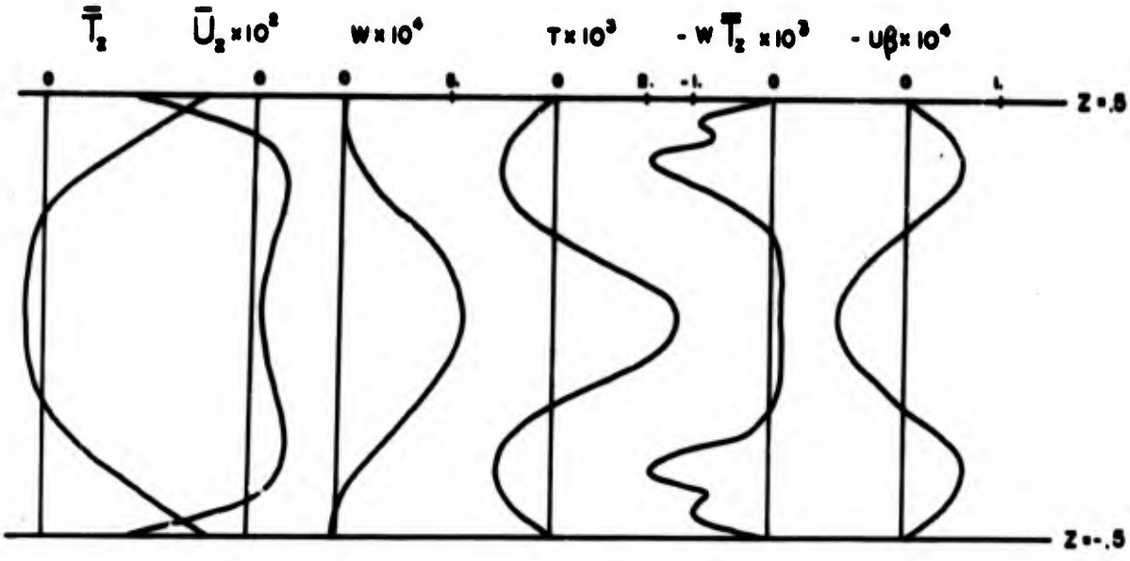

(a)

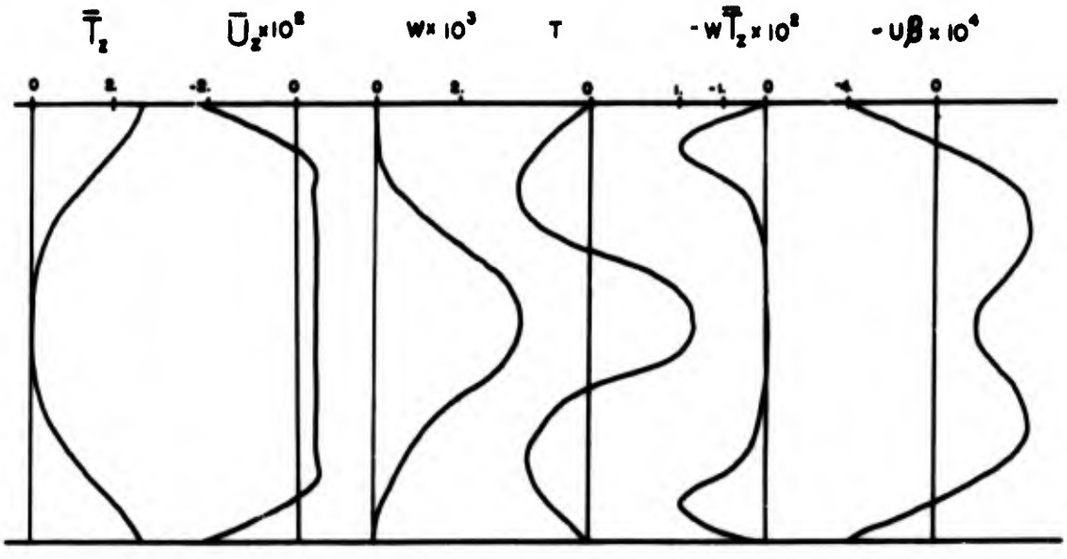

(b)

Figure 4.16 Solutions for P_r=6.7, h=.04, with (a): $\delta = -17^\circ$, and (b): $\delta = -60^\circ$.

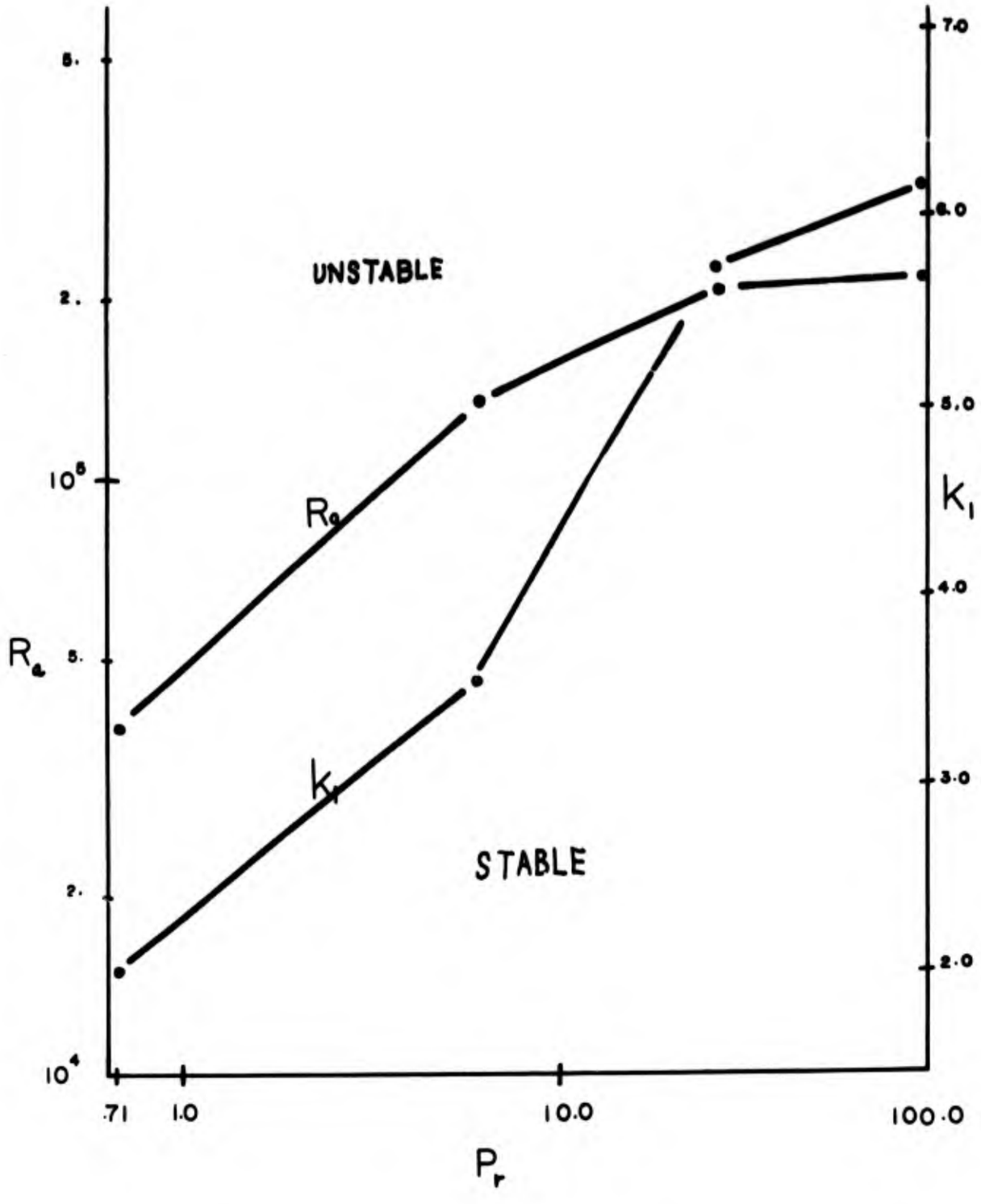

Figure 4.17 Neutral curves of R_a and k_1 as functions of the Prandtl number at $\delta = -45^\circ$.

4.8 Comparison with the experimental results.

Figures 4.18 - 4.22 contain the critical Rayleigh number, wavenumber and frequency data obtained using the experimental techniques discussed in chapter 3. Each plot also contains a solid curve which represents the results of the theory. First of all it should be noted that the theory successfully predicts the absence of any stationary transverse modes for $\delta < 90^\circ$. Outside of this, I think that the general agreement is rather good, especially when the complexity of the profiles and the approximations used to get a reasonable baseflow model are considered.

Figures 4.18 and 4.19 show the critical Rayleigh numbers for $\delta > 0$. The points for the longitudinal part of the h = .027 case lie right on the line, but I suspect this is a bit fortuitous, at least for the vertical part of the data which was determined by varying δ in small increments. The error is of order .5° and there always remains the possibility that the infinitesimal disturbances might have onset points which are slightly more into the stable (unicell only) region than the ones shown.

Figure 4.21 contains the critical data for $\delta < 0$. Generally the theory overestimates the onset of the longitudinal modes, but the shape of the critical curve is reproduced with cutoffs near the horizontal and vertical positions. Considering that these modes are especially sensitive to the x-dependent part of the temperature field (that part which perhaps contains the most dangerous approximation

we have made in the theory), it would have been rather surprising if the agreement had been better.

The theory underestimates the onset of the transverse travelling modes by as much as 80%. Part of this may be due to the difficulty associated with detecting these very weak fluctuations. I would be surprised if the actual onset points for infinitesimal disturbances were that much below the values from our measurements. More sensitive detection might be effected by putting a sharp narrow band-pass filter at the output of the thermocouple amplifier, using the frequencies observed here as a guide. It is also likely that the use of the parallel flow assumption and the neglect of sidewall effects are not entirely valid for these modes. It is encouraging, however, that the general stabilizing effect of negative tilt is reproduced. Figure 4.20 shows that critical wavenumbers and frequencies are in good agreement, even though they may have been measured at supercritical R_a . The wavenumbers may not change much in the range of R_a from theoretical to experimental onset. Since the frequency data is made non-dimensional by dividing by $g\gamma\Delta T D/\nu$, increases in f due to the raising of R_a by ΔT may be cancelled out.

Figures 4.22 and 4.23 contain the wavenumber data for the $h=.04$ longitudinal modes. The error bars here reflect variations in individual roll wavelengths across the tank, which may be due to slight non-uniformities or to the presence of sidewalls. They give the

maximum excursions from the average (represented by the point) of 6 or 7 measurements. The theory predicts wavenumbers which are quite consistent with the data.

We originally conducted the linear stability analysis in order to understand the physical basis for the rather peculiar behavior of the experimentally observed instabilities. To this end our effort, especially for the longitudinal modes, was very successful. To improve on this analysis would be very difficult because one needs to consider a basically non-parallel flow problem. Perhaps higher order corrections could be added to the present solutions, incorporating a more realistic base flow $T_o(x,z)$, $U_o(x,z)$, but this looks as if it would be a very complicated endeavour. If one wished to pursue the question of these types of instabilities further, it would probably be easier to design an experiment for which the present base flow model is exact, namely by constructing a tank with a very small h and with walls maintained at $T_o = \beta x \pm 1/2$.

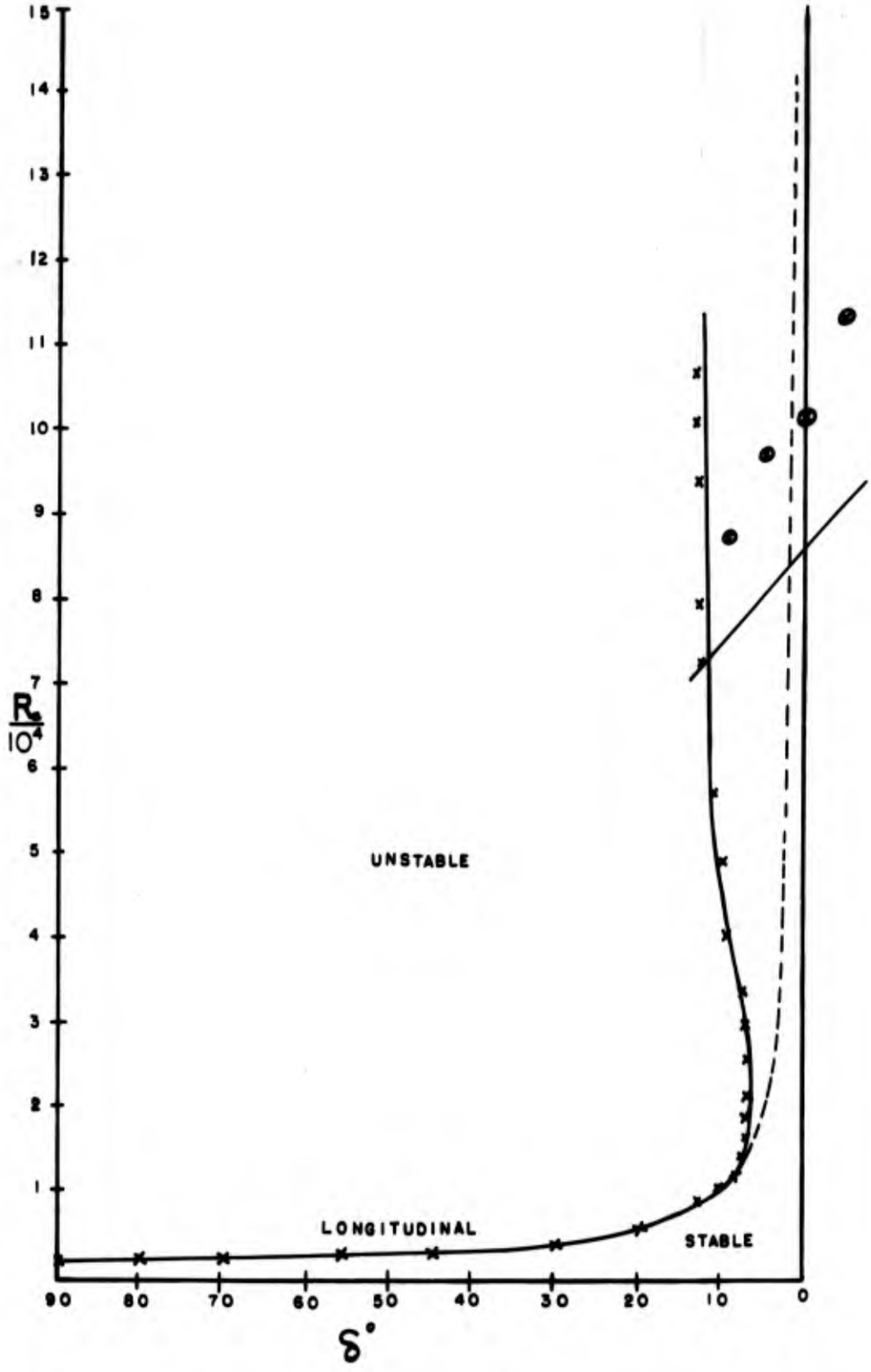

Figure 4.18 Theory and experimental points for transition to longitudinal (x) and to transverse (●) modes for h=.027. The dashed curve is from the simple Benard problem with reduced gravity $g\sin\delta$.

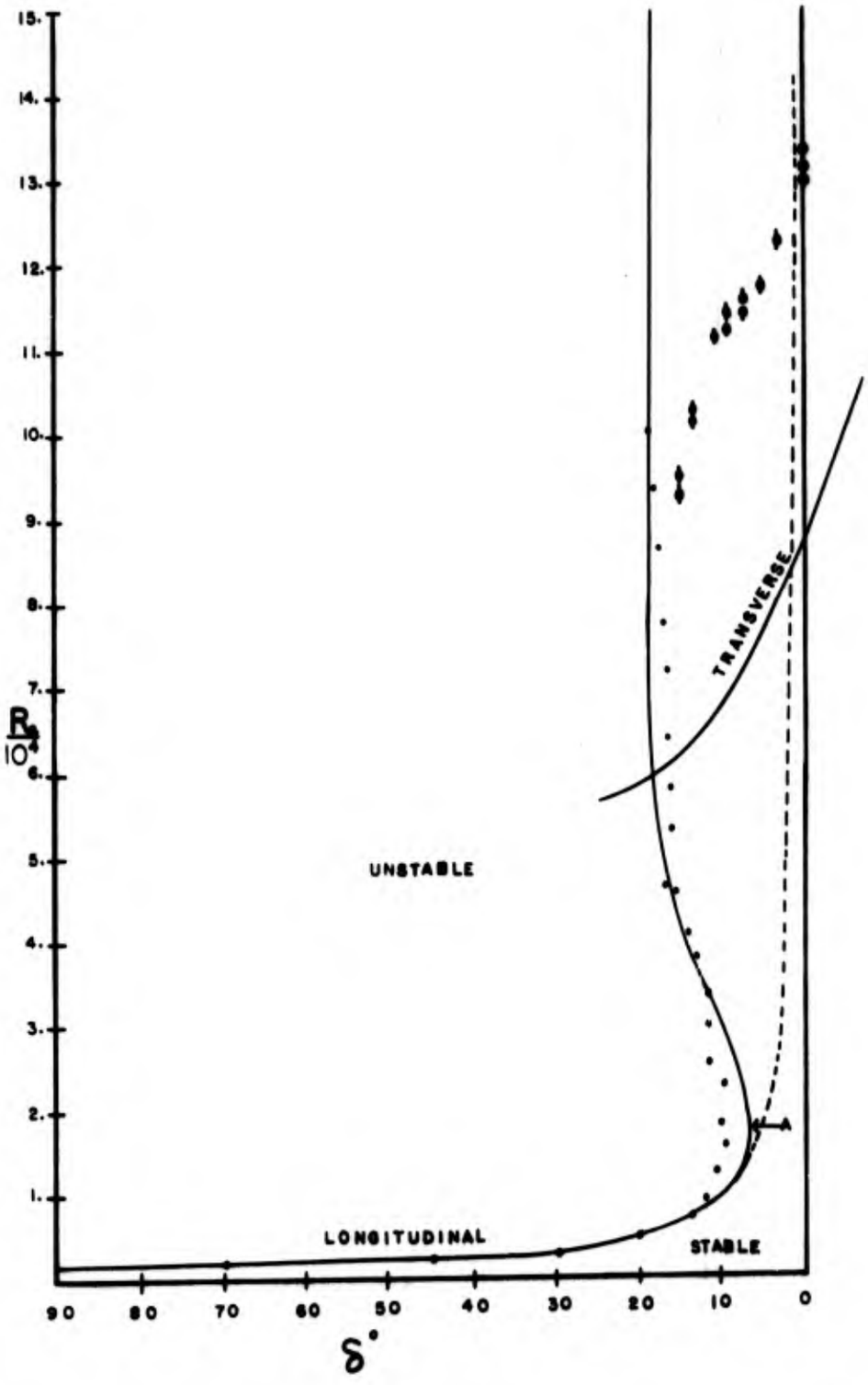

Figure 4.19 Theory and experimental points for transition to longitudinal (•) and to transverse (ϕ) modes for h=.04.

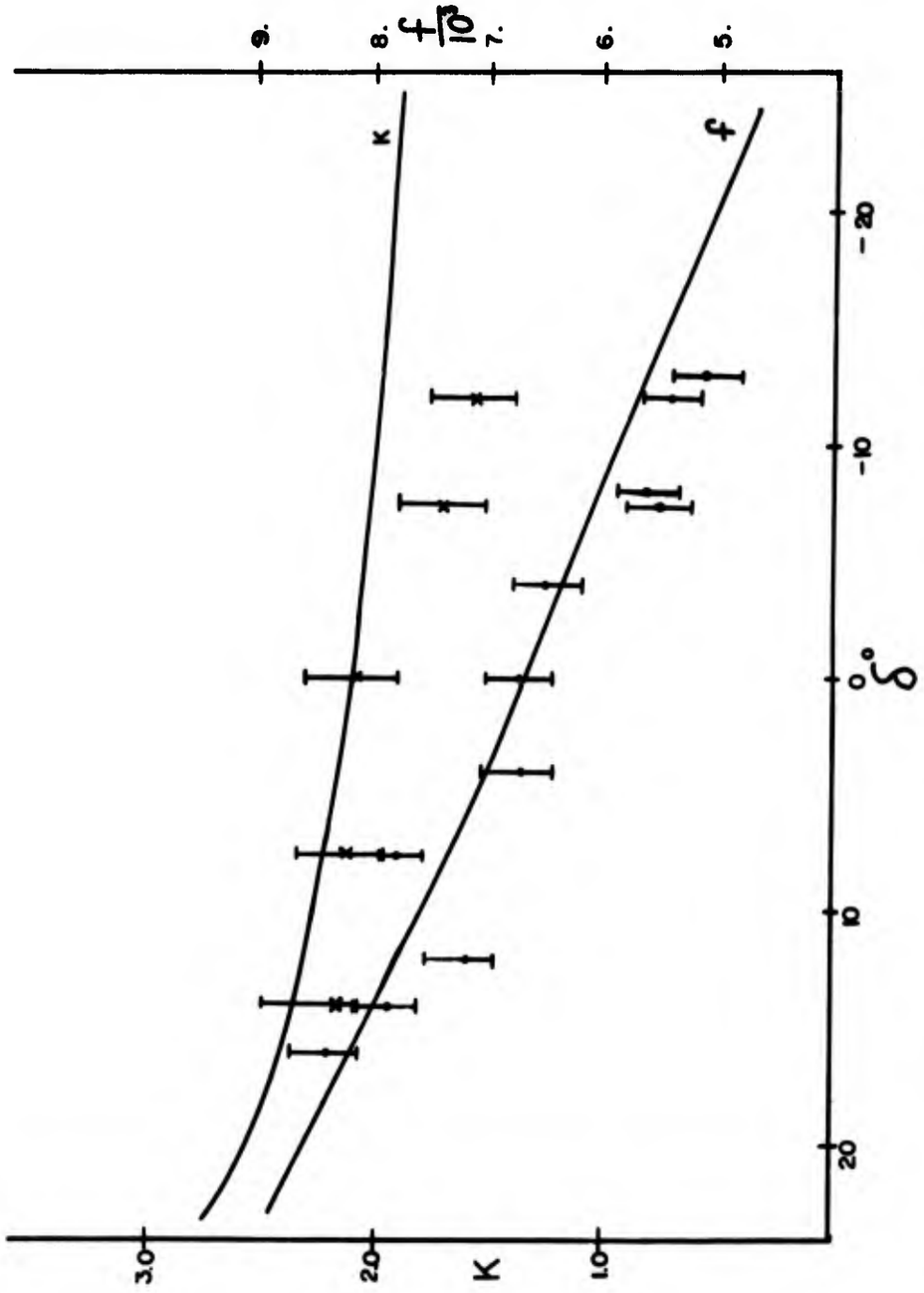

Figure 4.20 Wavenumbers (X) and frequencies (•) for the transverse modes. The solid curves are from the theory. h=.04.

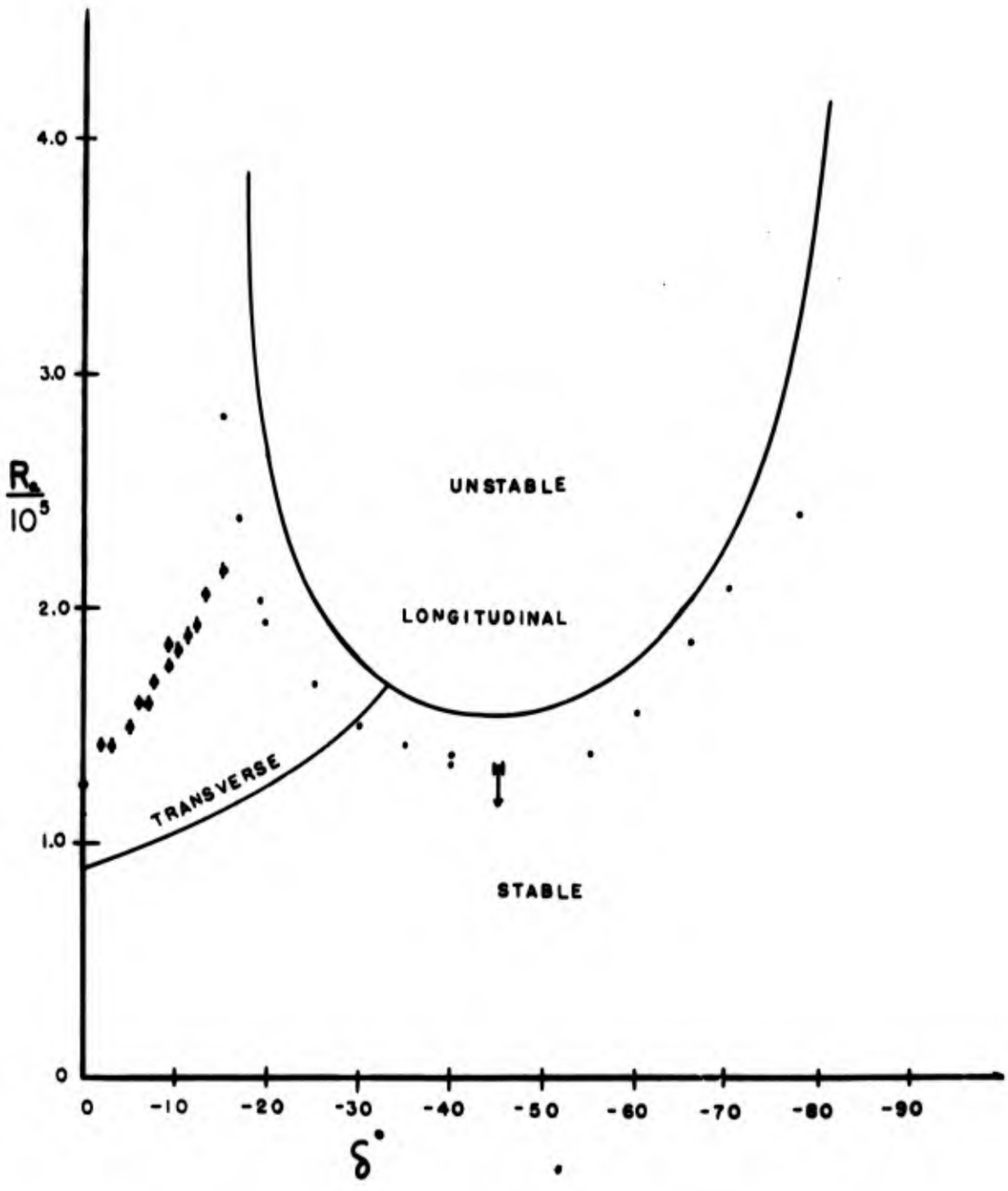

Figure 4.21 Theory and experimental points for transition to longitudinal (●) and to transverse (◆) modes for h= .04.

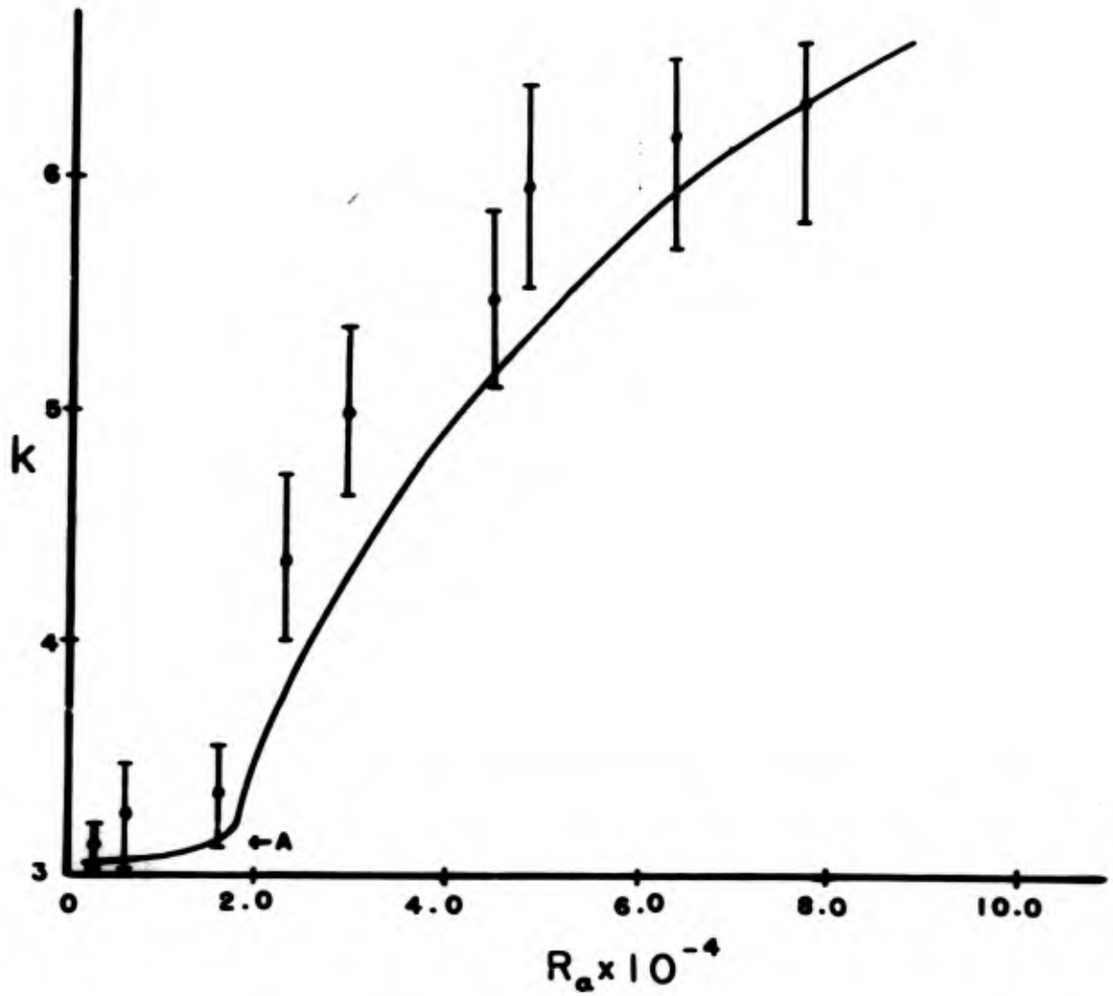

Figure 4.22 Critical wavenumbers for the longitudinal instabilities, $\delta > 0$.

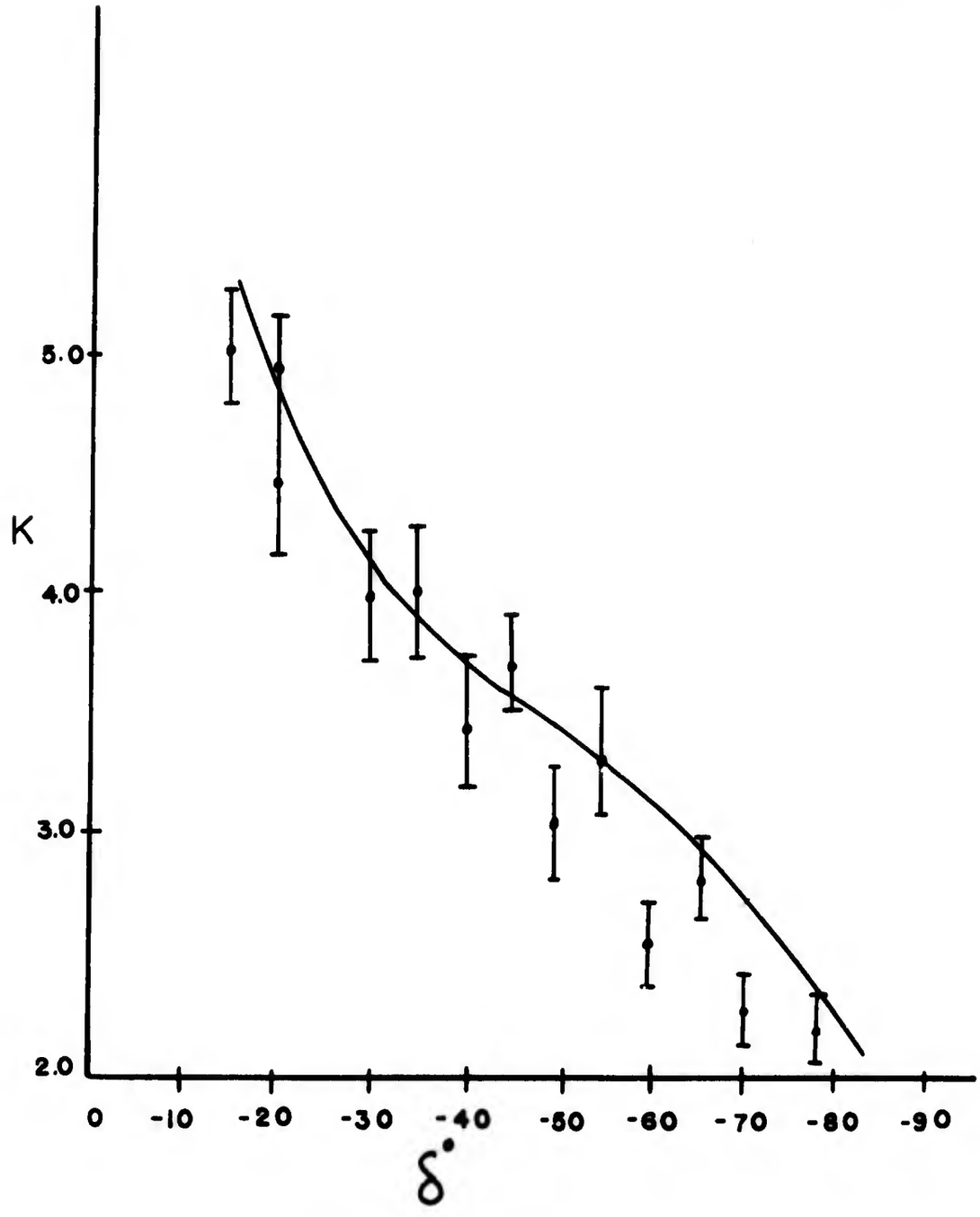

Figure 4.23 Critical wavenumbers for longitudinal instabilities.

CHAPTER V

Supercritical Behavior of the Secondary Instabilities

Before presenting results for the higher order instabilities and turbulence, I should like to briefly discuss how the infinitesimal perturbations observed in the experiments behave at supercritical conditions. It is convenient to discuss the longitudinal rolls and transverse waves separately.

5.1 Results for non-linear convective instabilities.

The onset of convective instabilities between horizontal, parallel, differentially heated plates was essentially described in 1916 by Rayleigh. Only recently have we obtained an understanding of the non-linear development of the secondary motions. Linear perturbations grow exponentially but as the instability eats away at the mean profile it is often possible for a steady equilibrium finite-amplitude motion to be set up. Various investigations have looked at this problem theoretically. Malkus and Veronis (1958) used a perturbation expansion in the secondary amplitude to obtain higher corrections to the linear modes. They also adopted Stuart's (1958) particularly simple energy equilibrium method in calculating the amplitudes for the secondary motions. Further developments of the non-linear problem include numerical solutions for 2-dimensional rolls by Kuo (1961), Deardorf (1964) and Foster (1969) among others.

Most of the non-linear theories involve the simplifying assumptions of 2-dimensional axisymmetric disturbances. Experimentally, the observed motions take plan forms which are strongly influenced by the geometry of the boundaries, variation of fluid properties, internal heating, etc. These plan-forms rarely are simple rolls. Mori and Uchida (1966) recently produced secondary motions of this type by setting up a Poiseulle flow between two differentially heated plates. As we have seen the velocity field will stabilize transverse modes and convective instabilities will tend to align with the mean velocity. Ogura and Yagihashi (1969) have had some success with numerical models of this situation. Since the Reynolds numbers of the forced flows were rather high ($R_e \sim 513$), this experiment is rather different from the ordinary convection problem. Since tilt very effectively damps all but the longitudinal rolls, it seemed that a nice way to get neatly aligned 2-dimensional instabilities would be to run experiments at very small α . The effect of tilt on the longitudinal modes would be small, but alignment would be guaranteed. For example at $\delta = 2°$ the Reynolds number at $R_a \sim 1.5\, R_{acrit.}$ is less than .1. The motions due to the convective rolls themselves are rather larger than the mean shear velocities so that to a first approximation the idealized situation of 2-dimensional parallel rolls is obtained.

Unfortunately we were not set up for detailed measurements of velocity and temperature fields within the rolls. I should think

that convection experiments in air (a fluid for which adequate probing techniques exist) done at a small tilt might come close to the idealized situation. Since we wanted to obtain some idea of the amplitudes of the secondary motions and perhaps say something about the flow structure, we ran a series of experiments at $\alpha = 1.5°$. Velocity profiles of the rolls were obtained by observing a dye wire stretched across the tank at $X = Z = 0$. There are several difficulties with this method. This gap D is small so that we can only make observations of dye lines over lengths only a few times greater than the minimum line width. If we take a longer time interval between dye emmission and picture, the dye will reach the turning regions near the plate. Even so I think it is possible to measure velocities to 10 or 20% in this way.

We were primarily interested in the amplitude of the longitudinal modes as a function of R_a. Malkus and Veronis' calculations for free boundaries imply that the amplitude a is given to 0 (a^2) by

$$a = \frac{(R_a - 657)^{1/2}}{R_{a2}} .$$

R_{a2} is a constant determined by the solvability condition applied to the higher order equations. For rigid boundaries the perturbation solutions become rather complex and it is simpler, although not necessarily better, to employ the energy method of Stuart to estimate the non-linear equilibrium amplitudes. In this calculation the non-linear solution is assumed to have the same <u>shape</u> as the linear modes,

and an amplitude consistent with energy requirements.

The thermal energy balance requires

$$\frac{\partial}{\partial t}\int_\Omega T^2/2 + R_a \int_\Omega \frac{\partial \overline{T}}{\partial z} wT = -\int_\Omega (\nabla T)^2 . \qquad (5.1.1)$$

Ω is the total enclosed volume with insulating sidewalls and conductive top and bottom boundaries, $\overline{T}(z)$ the mean field, and w and T the secondary motion variables. In a steady state the thermal balance equation gives us

$$R_a \frac{\partial}{\partial z} \iint wT \, dx\, dy = \frac{\partial^2}{\partial z^2} \iint T \, dx\, dy ,$$

or denoting these integrals with an overbar, and integrating,

$$\frac{\partial}{\partial z}\overline{T} = R_a \overline{wT} - 1 . \qquad (5.1.2)$$

Combining this relation with (5.1.1) we obtain for steady state,

$$R_a^2 \int_{-1/2}^{1/2} (\overline{wT})^2 dz - R_a \int_{-1/2}^{1/2} (\overline{wT}) dz = -\int_{-1/2}^{1/2} \overline{(\nabla T)^2} dz . \qquad (5.1.3)$$

To complete the formulation we only have to specify w and T. In the energy method this is done by neglecting harmonic generation and assuming that w and T have the same shape as the linear infinitesimal modes, but with arbitrary amplitude a.

In our case it is sufficiently accurate to take

$$w = a \sin \delta \, E_1(z) \cos k_1 y , \qquad (5.1.4)$$

$$T = 122.6\, a \cos \pi z \cos k_1 y \,, \tag{5.1.5}$$

with $k_1 = 3.05$. When these are substituted into equation (5.1.3) we obtain a quadratic expression for the amplitude, which can be reduced to

$$a = \frac{.103}{\sin \delta} \frac{(R_a \sin \delta - 1708)^{1/2}}{R_a} \,. \tag{5.1.6}$$

It is of particular interest to see to what extent relation (5.1.6) holds experimentally and how reasonable the assumptions it is based on are. Namely, at what R_a do harmonics become important, and to what extent does the "shape" of the rolls follow (5.1.4) and (5.1.5).

Figure 5.1 shows typical dye streaks for the experiment at $\alpha = 1.5°$, $P_r = 6.7$, $h = .027$. The straight horizontal line represents the dye wire, and the curve the leading edge of the trace 9 seconds after pulsation. Vertical velocities can be measured approximately by dividing vertical displacements by the time interval. It is noted that at the low Rayleigh numbers the motion remains sinusoidal, but at R_a about 4 times critical the profiles begin to become strongly jetlike with a predominance of the third spatial harmonic forcing the updrafts and downdrafts into thin columns (case (d)). This observation fits in very nicely with Kuo's nonlinear spectral solutions for 2-dimensional rolls with free boundaries. He represented the stream function as a series with terms

$$\Psi(\ell, n) \sim \sin(\ell k_1 x) \sin(n\pi z),$$

where k_1 is the critical wavenumber for onset. With a similar series for T he solves the non-linear equations for steady solutions for various R_a and P_r. As Kuo states, for $P_r = 10$, "Even though Ψ_{31} is a fifth order quantity, it becomes the largest higher mode of the Ψ field for $R_a > 3R_{acrit.}$". The temperature behaves in the same way. Unfortunately he does not display any velocity profiles, but I think our observation of the dominance of the third harmonic has a sound basis in theory.

Figure 5.2 shows experimental data of the amplitude a of the rolls (taken as the peak dye displacement) as a function of R_a. For convenience we have plotted $R_a \cdot a$ vs. $R_a - 1708$ so that a direct comparison can be made with the prediction based on Stuart's method. Thus, the solid line represents eqn. (5.1.6). Agreement is quite good up to Rayleigh numbers 2 or 3 times critical. This is consistent with the development of higher harmonics and the resultant distortion of the fundamental which Stuart's method does not account for. Because we measure the peak amplitudes, our measurements necessarily reflect the additional modes. The energy equilibrium method works rather better for predicting average quantities like the heat flux, or in cylindrical Couette flow the torque, where it is good to perhaps 10 times the critical onset parameter. For this latter problem Davey (1962) has shown by using a more exact

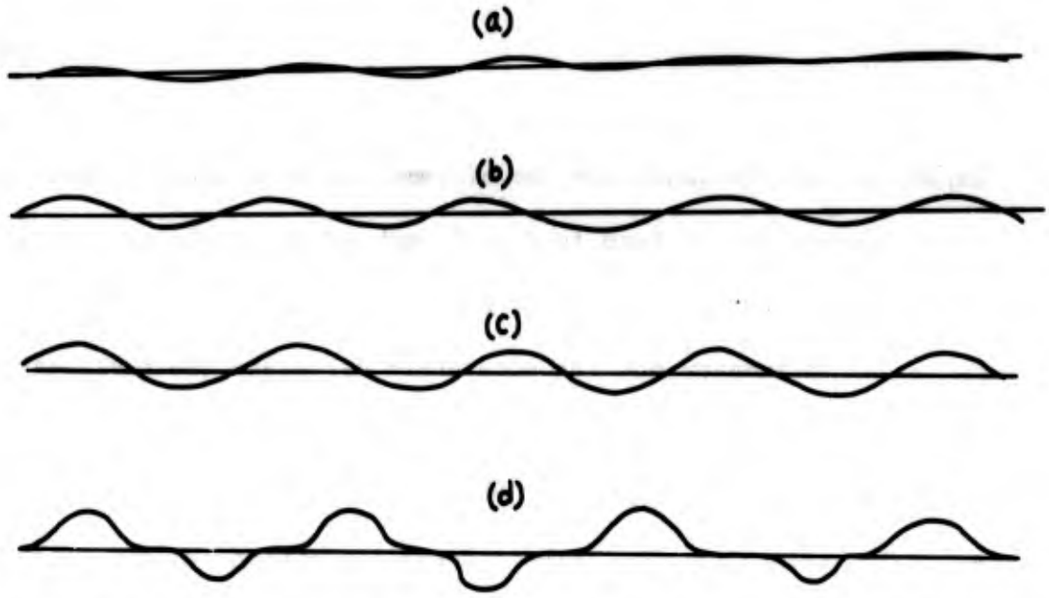

Figure 5.1 Tracings from dye streaks. $\alpha = 1.5°$, $h = .027$. Starting from the top R_a = 2436, 4547, 7145, and 8445. The last trace has a peak velocity of .02 cm/sec.

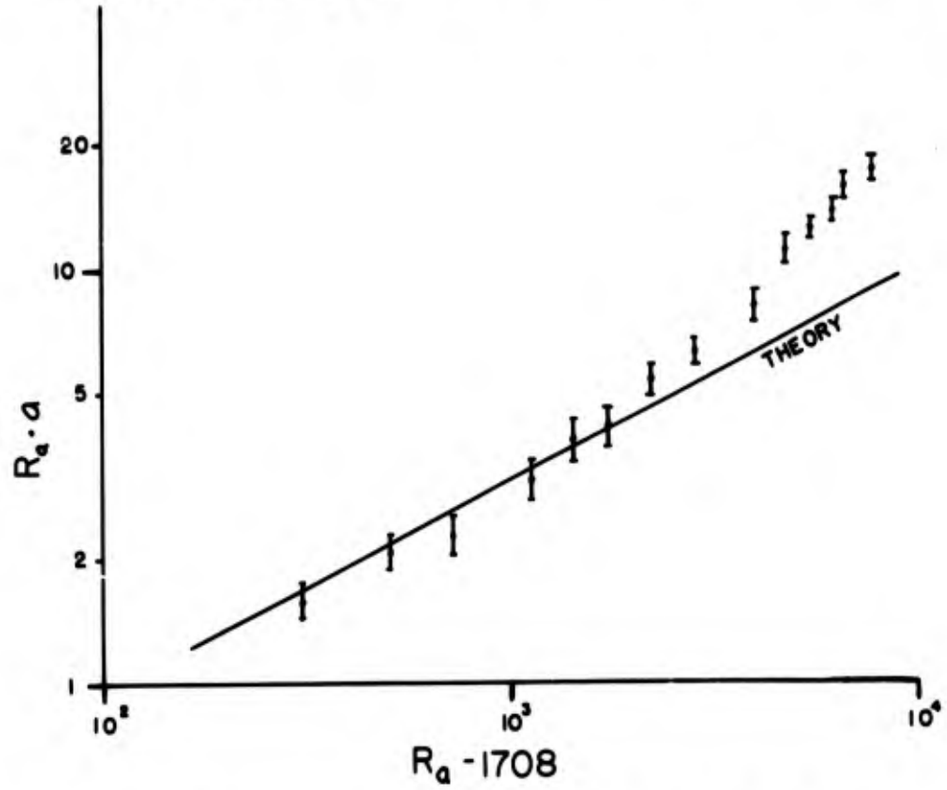

Figure 5.2 Amplitude a in terms of R_a. Solid line is the theoretical relation (5.1.3).

expansion that, because the two aforementioned processes left out in the energy method tend to cancel each other out in the required averages, it appears to work up to quite supercritical conditions.

In summary one can accurately calculate the nonlinear equilibrium state for two dimensional rolls using the particularly simple energy formulation for $R_a < 4500$. Beyond this the 3rd spatial harmonic becomes large and the assumptions of the method break down.

5.2 Development of the travelling waves.

Near $\delta = 0$ transverse disturbances were the first instability of the primary unicell. For $R_a > R_{acrit.}$ new modes with higher frequency seem to appear. The initial periodic wave form from a fixed point temperature measurements does not change its shape but rather becomes modulated. This is evident in figure 5.3(a) which gives the autocorrelation function of temperature at $x = y = 0$, $z = -.4$, in the hot boundary layer. There is some loss of correlation with τ because the two periodic signals do not have sharp frequency distributions. Along the hot plate the wave packet appears to move at about 4.2cm/sec., or in nondimensional terms .003, which is greater than the peak velocity of the mean stream.

If one looks at the power spectra of the temperature fluctuations it is seen that the modulation is accompanied by the onset of a higher frequency oscillation. In figure 5.4 we show four such spectra at increasing Rayleigh number. We have not calibrated the magnitudes here but it is the growth of the secondary peak relative to the primary which is important. At low R_a it is almost insignificant but at $R_a = 4.6 \times 10^5$ it is even larger than the primary. For this case the frequency spectrum is quite broad. Large amplitude response is observed primarily where temperature fluctuations in the two boundary layers are exactly out of phase. With a wider frequency band phase relationships will become more complex and the resultant

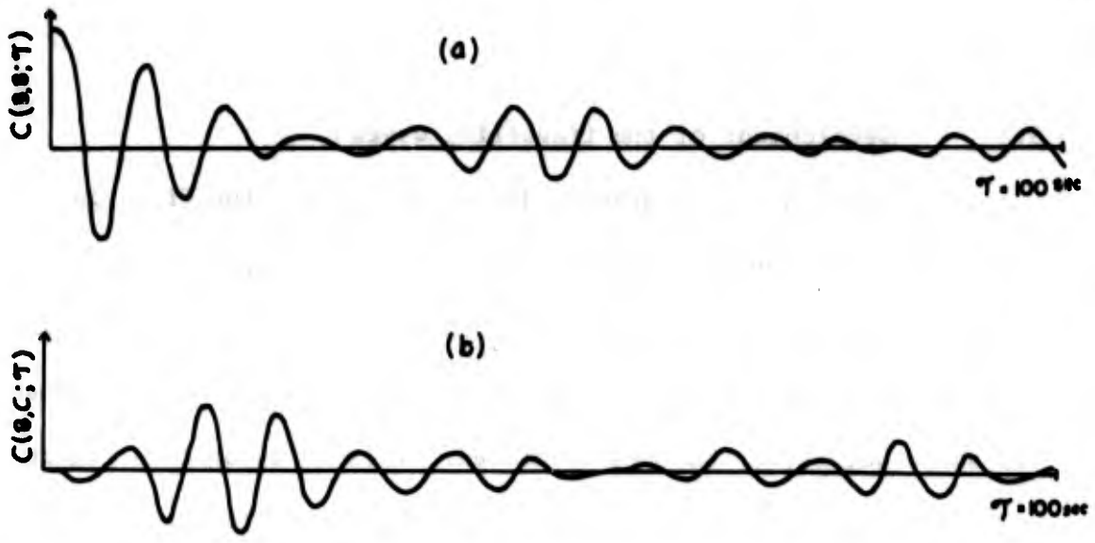

Figure 5.3 Correlograms of the temperature fluctuations for $\S = 10^{\circ}$, $R_a = 156000$. (a) is an auto- and (b) is a cross-correlation.

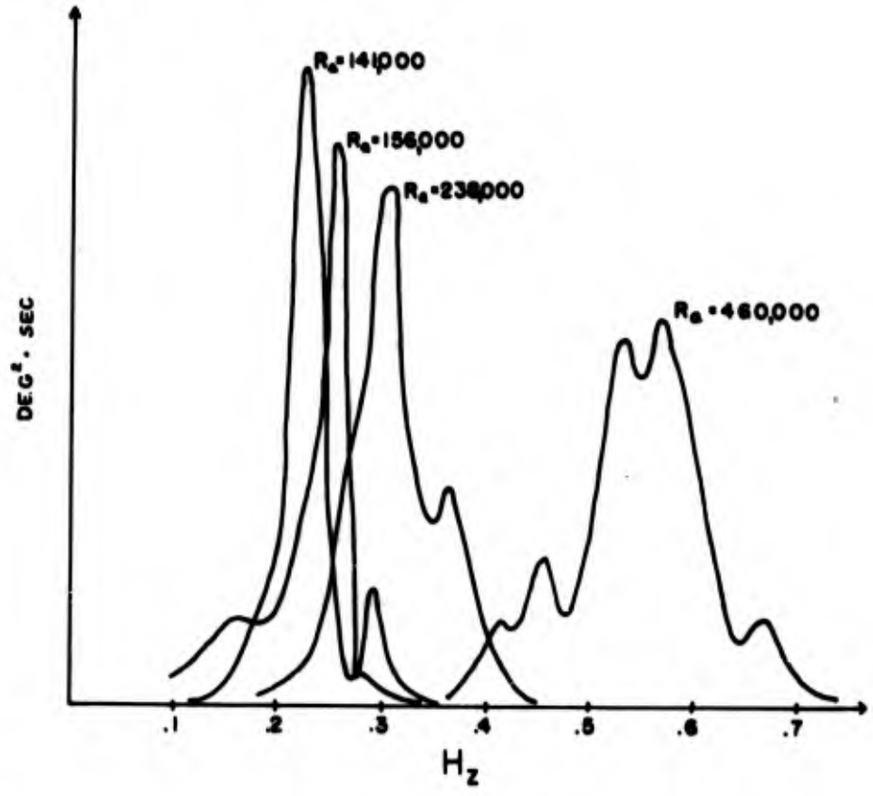

Figure 5.4 Examples of the spectral developement of the temperature fluctuations at 10°.

fluctuations will be more intermittent. This is indeed observed in the records: at large R_a , large amplitude bursts become more irregularly spaced with relatively long periods of inactivity in between.

I do not have a rigorous explanation for the higher frequency modes. The linear theory for completely transverse modes with $k_1 = 0$ has no higher order solutions with ω_r greater than the first most unstable mode. Perhaps the higher frequency peaks are due to slightly oblique waves with $k_2 >> k_1$. Some of these were observed in the plan view streak photographs at rather high R_a . The stability of these modes should be investigated.

CHAPTER VI

Meandering

6.1 Experimental determination of transition.

The visual study with particle suspensions indicated that for positive tilt angles and with sufficiently high Rayleigh numbers, waves or meanders could develop on the longitudinal convective rolls. This meandering seemed to be triggered by some sort of instability which was dependent on the tilt angle. Near the horizontal and vertical positions rolls remain straight and parallel to Rayleigh numbers five or six times that required for onset. At 45°, however, the meandering appears to set in at a Rayleigh number about 70% supercritical. Obviously the breaking and subsequent unsteady motion is highly nonlinear with rather strong interactions but since the unsteady states attained by the fluid seem to be closely connected with the meandering we would like to understand the mechanism by which wavy vortices are generated.

As a first attempt at this we have tried to measure onset more carefully. This was done by stimulating a longitudinal dye line running along $y=z=0$. Since the only cross-stream velocity in the roll + unicell regime (away from the end of the tank) is due to the rolls alone, the dye serves to indicate the orientation or alignment of the rolls. If they are purely longitudinal, the dye line will be advected either up or down uniformly along its length. If the vortices bend or become wavy relative to the wire, the dye line will become sheared. This

method is actually rather sensitive for detecting meanders. For each δ the Rayleigh number was increased slowly through the onset of the longitudinal rolls and pictures were taken for the supercritical regime at one minute intervals with the temperature difference coded on the photographs as discussed in section 3.1. Onset was characterized by the appearance of waves on the dye line. This was required to be a steady thing. Occasionally rolls would adjust themselves and transient dye waves would appear, but this was not taken as an onset point for the meanders which, once formed, persist and eventually break.

Figure 6.1 shows a typical case. One can clearly see the onset and the following breaking of the waves as the meanders attain large amplitude. The data indicate that at onset the meanders are stationary. Figure 6.2 summarizes the measurements of the critical Rayleigh numbers and critical wavenumbers obtained by this method. The observed wavenumbers are essentially constant with δ although there is a rather large range associated with these measurements due to variations in the wavelengths along the wires. We find that the wavenumber for the meanders , k_m , is related to the wavenumber of the longitudinal rolls, k_r , by

$$k_m \sim .57\, k_r . \qquad (6.1.1)$$

Meanders have also been observed in the longitudinal modes for $\delta < 0$. Recall that these had a wide range of wavelengths. However, it was

found that relation (6.1.1) is also valid for these angles. The critical curve shows that the meandering mechanism is most efficient when the cross-stream and up-stream buoyancy forces are equal, namely at 45°.

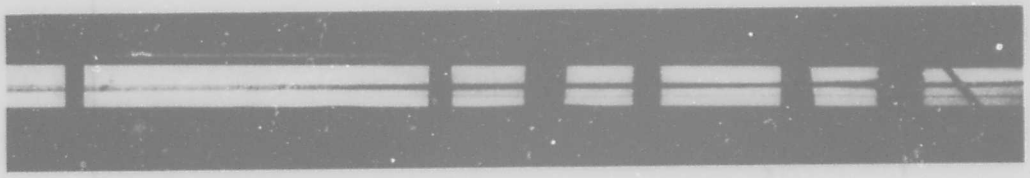

$R_a = 4510$

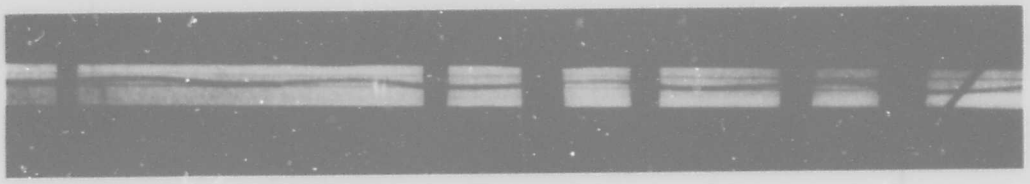

$R_a = 5160$

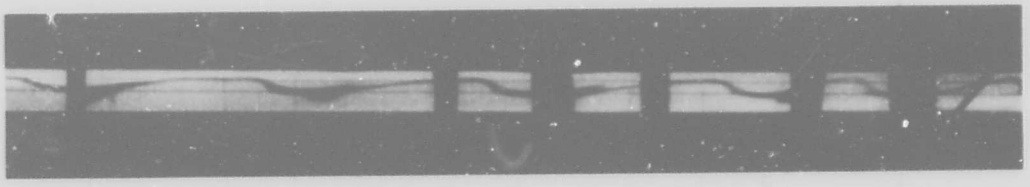

$R_a = 5780$

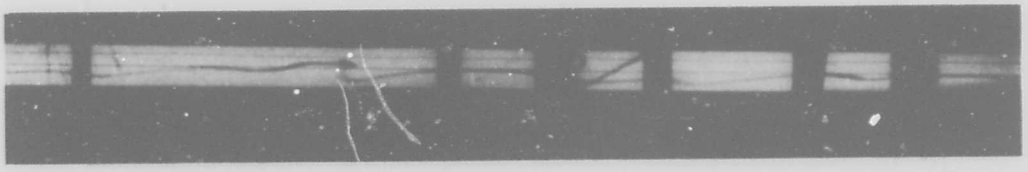

$R_a = 7570$

Figure 6.1 Visualization of the onset of meandering.
$P_r = 6.7$, $h = .027$, $\delta = 30^\circ$.

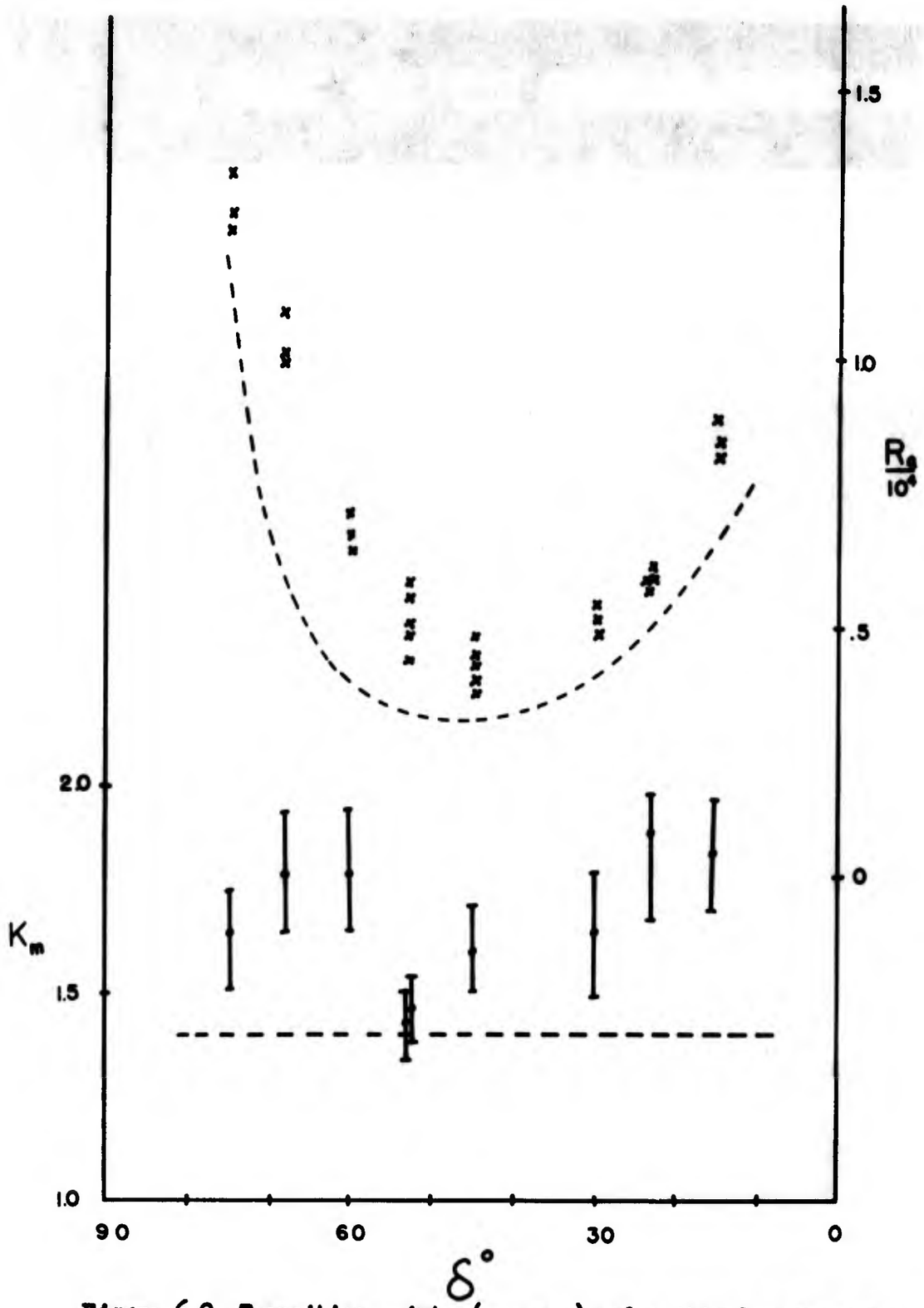

Figure 6.2 Transition points (crosses) and critical wavenumbers for the meanders. Dashed lines are from the results of section 6.2 .

6.2 Discussion.

The growth of the meanders is obviously a 3-dimensional non-linear problem. There are mathematical techniques for looking at such effects as developed by Watson, Stuart, and their co-workers. The non-linear equations are usually expanded in terms of the small time-varying amplitudes of a set of interacting modes. By separately solving for the spatial behavior of the modes one can obtain a set of non-linear equations in the amplitude functions, which can be analysed for possible stable equilibria. The method is nice because it can be made formally rigorous. In actual practice the determination of the coefficients in the amplitude equations is very complicated because the spatial structure of the modes must be determined. In horizontal convection with constant fluid properties and a constant applied temperature difference the spatial behavior of the linear modes is particularly simple and independent of orientation. This is perhaps why much of non-linear theory has centered on this problem and why it has been rather successful.

In our problem what we would like to do is interact the unicell (u_o , T_o) and the longitudinal rolls with various transverse or oblique convective modes which might lead to stable wavy vortices. In the slant convective case it is very difficult to carry this out because the structure of the oblique modes is so radically different from the longitudinal modes and generally can only be determined numerically. It is also seen that the meandering does not generally

occur in the weakly non-linear region so that the usual 3rd order series may not be sufficient for this problem.

Rather than get involved in complicated mathematics which would be quite beyond the scope of this paper, we look at two ways which the combined unicell-roll flow can become unstable to infinitesimal perturbations. The particular form which is thought to be relevant for the meanders is steady $\hat{z}$ -vorticity which for simplicity is taken independent of z.

The mean fields which are thought to be important are the equilibrium y-dependent temperature field from eqns. (5.1.5) and (5.1.6);

$$T_r = \frac{12.\,(R_a \sin\delta - 1708)^{1/2}}{R_a \sin\delta} \cos\pi z \cos k_r y \qquad (6.2.1)$$

and the y-dependent upstream velocity field driven by the above temperature field;

$$u_r \doteq .6 \cos\delta \frac{(R_a \sin\delta - 1708)^{1/2}}{R_a \sin\delta} \cos\pi z \cos k_r y \,. \qquad (6.2.2)$$

In this section the subscript r refers to the roll component of the mean fields. We now look for ways perturbation vorticity

$$\omega_m = \nabla^2 \eta \,,$$

with

$$u_m = -\eta_y \,, \quad v_m = \eta_x \,,$$

can be generated in a manner consistent with the observations.

The first possibility is through shear forces creating stationary disturbances on the velocity field (6.2.2). These are governed by the Orr-Sommerfeld equation, which for the z averaged u_r, and periodic fluctuations ($\eta \sim e^{ik_m x}$), is

$$\left(\frac{d^2}{dy^2} - k_m^2\right)^2 \eta - i k_m R_e \left[\cos k_r y \left(\frac{d^2\eta}{dy^2} - (k_m^2 - k_r^2)\eta\right)\right] = 0. \quad (6.2.3)$$

The lateral Reynolds number is

$$R_e \equiv \frac{g\gamma \Delta T D^2}{\nu} \cdot \frac{D}{\nu} \cdot |u_r|_{av.} = .06 \cot\delta (R_a \sin\delta - 1708)^{1/2}, \quad (6.2.4)$$

for water. Since the mean field is periodic in k_r it is reasonable to look for solutions to eqn. (6.2.3) which are also periodic with wavenumbers which are k_r or integral multiples of k_r. It is easy to see that solutions which are singly periodic in k_r do not exist. We have not tried numerical solutions of this problem but one can look at the magnitudes of the source and dissipation terms by plugging in the observed values of $k_m \doteq 1.7$, $k_r \doteq 3$, and estimating derivatives $\eta' \sim k_r \eta$. Then

$$R_e \sim \frac{(k_m^2 + k_r^2)^2}{k_m^3} \sim O(25). \quad (6.2.5)$$

The values of R_e for which the meanders are observed are typically O(1). Shear forces may be too weak to initiate instability.

There is, alternatively, the generation of $\hat{z}$-vorticity by the buoyancy torque T_y. This exists here only because of the

tilted geometry. If we neglect the mean velocity field entirely we obtain,

$$\nabla^4 \eta - \cos\delta \, T_y = 0 \tag{6.2.6}$$

and

$$\nabla^2 T + R_a \eta_x T_{ry} = 0 \tag{6.2.7}$$

Suppose we replace the sinusoidal mean field T_{ry} by a square wave field constructed from the average gradient from eqn. (6.2.9). Then one gets

$$\nabla^6 \eta + Q \eta_{xy} = 0 \tag{6.2.8}$$

where

$$Q = \pm 5.0 \, k_r \cot\delta \, (R_a \sin\delta - 1708)^{1/2} . \tag{6.2.9}$$

Periodic solutions in k_r and k_m exist as $\eta \sim e^{ik_r y} e^{\mp i k_m x}$, for which

$$Q = \frac{(k_r^2 + k_m^2)^3}{k_r k_m} . \tag{6.2.10}$$

Not only are the observational values of k_m and R_a consistent with this but one can solve for the minimum critical R_a. Here this occurs at

$$k_m = \frac{k_r}{\sqrt{15}} , \tag{6.2.11}$$

which, with $k_r = 3.0$ gives,

$$R_a \sim \frac{580 \sin\delta}{\cos^2\delta} + \frac{1708}{\sin\delta} . \qquad (6.2.12)$$

The dashed curves of figure 6.2 are from these two equations and it is seen that the theory is fairly consistent with the observations. However, this apparent agreement is a bit fortuitous. First of all we have made no attempt to satisfy lateral boundary conditions. If buoyancy acted alone in generating the meanders, the onset Rayleigh numbers would be independent of P_r . This independence is not found. Yet the smallness of the Reynolds numbers indicates that buoyancy probably plays some role in generating the vorticity, perhaps in the manner outlined above. Clearly more work is needed on this problem. For example it will be important to determine the z - dependence and the effects of the walls. In its simplest formulation one might obtain a 2-dimensional linear boundary value problem that could be solved numerically.

CHAPTER VII

Flow Structure At High Rayleigh Number

In this chapter I will briefly discuss some observations of the turbulent flows observed at high R_a. We originally took a set of 3 - point temperature fluctuation records in order to get some idea of the effect of slope on turbulent convection. The analysis of this data proved to be more complicated than I had originally anticipated. Time limitations prohibited digital processing of the data, so that the results presented here are rather preliminary. We shall try, however, to indicate how the turbulence is related to the linear instability properties and to the meandering discussed in the previous chapters.

Figure 7.1 shows some time average statistics from temperature time series taken by a single probe at $X = y = 0$, $Z = -.4$. The R.M.S. fluctuation amplitude gives an indication of the intensity of the time dependent motion while the correlation time σ_T yields an estimate of the characteristic time scale for the fluctuations. The curves presented here show that the behavior at $\zeta = 30°$ is rather different from that for the horizontal case. The shorter time scale and larger R.M.S. amplitude appear to be caused primarily by the lateral ($\hat{y}$) motions of quasi-longitudinal vortices. Elongated plumes are released on a relatively long time scale, but are swept sideways past the probe at a rather high frequency. This process

is evident in the plan-view photographs and appears to be a highly developed meandering.

The one most obvious characteristic of the tilt convective tubulence was the anisotropic behavior. This would be expected since for $\delta > \sim 10^\circ$ the linear instabilities were oriented in the upstream direction. It was seen how this motion became x dependent as meanders developed. Yet for $10^\circ < \delta < 90^\circ$, the typical wavelengths in the x direction, λ_x, appear to be larger than the lateral wavelengths λ_y. Figure 7.2 shows the relative anisotropy for various tilt angles as a function of Rayleigh number. The wavelengths were obtained from over-head streak photographs with silicone oil, $P_r = 25$, and with h = .027. At low Rayleigh numbers, where longitudinal rolls are predominant, the average ratio of λ_x to λ_y is very large. It drops off as meandering develops or, in the case of $\delta = 90^\circ$, as the effects of sidewalls diminish. At high Rayleigh numbers the horizontal convection becomes isotropic, but for tilt convection the "average" plume has an x/y aspect ratio significantly greater than one. There are some data which indicate that at very large R_a the influence of slope in elongating the plumes is reduced. What effect does this anisotropy have on the transfer properties of the system? It would be very interesting to measure the spatially averaged heat flux for the slanted system exhibiting convective turbulence, provided the effect of the primary flow alone could be ascertained, perhaps by running calibration

experiments at negative angles. Because of the turning regions the present problem may not be the most straightforward for studying slant convective turbulence. The measurements do suggest that the eddies can be considerably changed from their counterparts at $\delta = 90°$ and one might reasonably anticipate a significant change in the convective heat flux in more general systems.

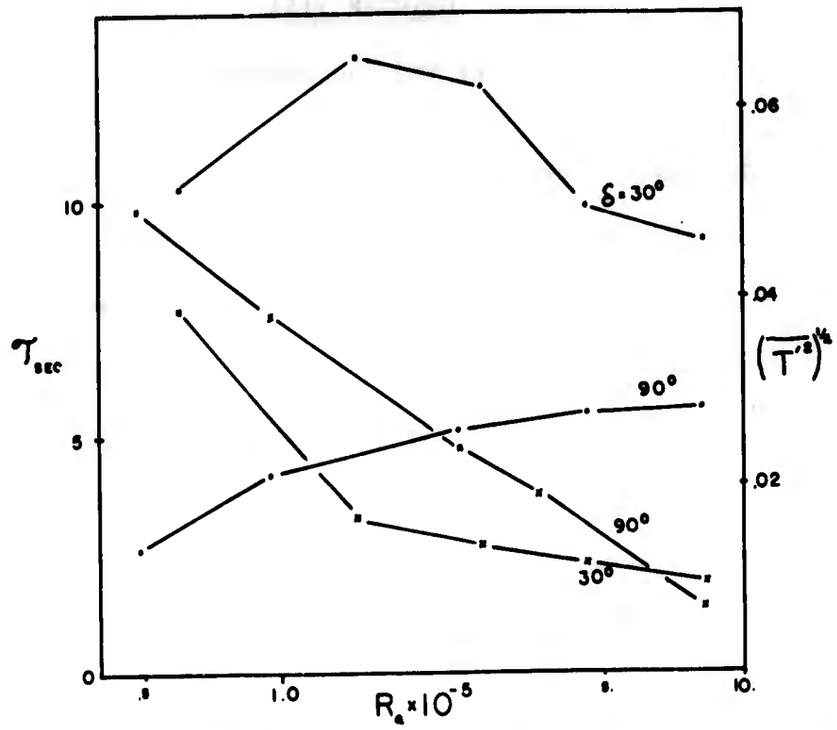

Figure 7.1 RMS temperature fluctuation (dots), and correlation time for various tilt angles and Rayleigh numbers.

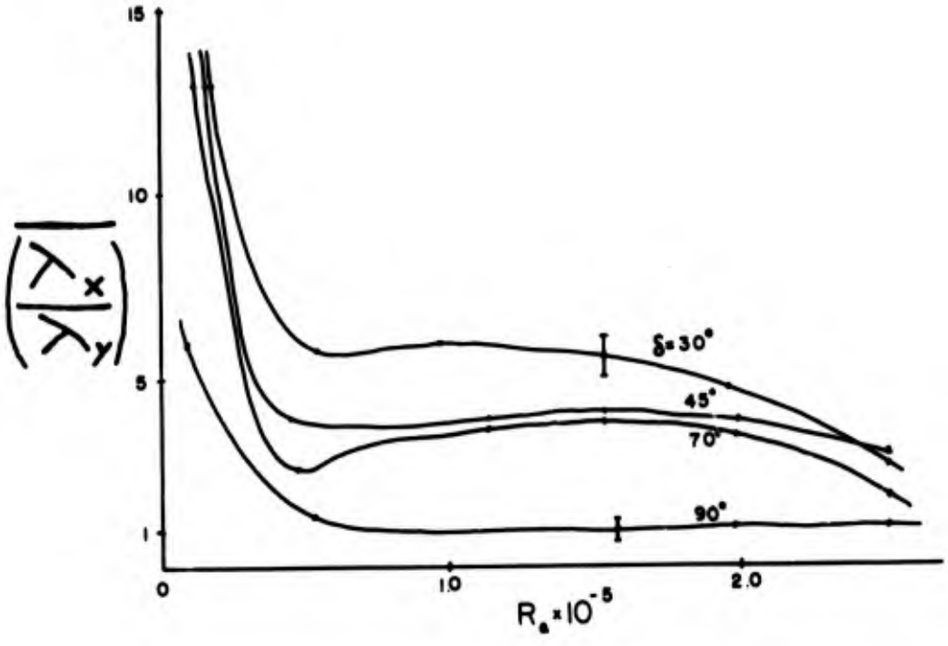

Figure 7.2 The average ratio of upstream to lateral wavelength.

CHAPTER VIII

Summary and Conclusions

8.1 The basic flow.

Experiments were done in the differentially heated, inclined, rectangular box. Temperature and velocity profiles were taken in the steady laminar two-dimensional flow regime. At fixed P_r and with a small aspect ratio h the form of the single cell circulation was a function of $R_a \cdot \cos\delta$ alone. Away from the turning regions the flow could be approximately represented by

$$T_o = \beta(R_a \cos\delta, h) \cdot x + \overline{T}(z, M) , \qquad (8.1.1)$$

$$u_o = \overline{u}(z, M) , \qquad (8.1.2)$$

with $M = 1.09 \, (R_a \cos\delta \, \beta/4)^{1/4}$.

For $|\delta| > 70°$, blocking regions formed in the corners and the above mathematical description ceased to apply.

8.2 Instabilities.

The simple unicellular circulation did not persist for all R_a, δ, P_r and h. Our measurements of transition points and the general agreement with the stability theory applied to (8.1.1) - (8.1.2) suggest that there are 5 possible types of instability, 3 of which are observed for our particular P_r =6.7, h =.04 or .027. Stationary transverse modes which obtain energy from either unstable gradients of $\overline{T}$ or from the mean velocity $\overline{u}$ are predicted to occur at Rayleigh numbers considerably higher than stationary longitudinal or travelling transverse modes. Longitudinal vorticity is maintained by buoyancy. The thermal excess required to maintain the perturbations against diffusion can be advected out of $\overline{T}(z, M)$ or out of the βx part of T_o. In the latter case the mechanism is then independent of cross-stream variations of the basic temperature field and can occur even if these are entirely stable. The observation of rolls at negative tilt angles support this interpretation. In a geophysical context, longitudinal instabilities may be possible whenever there is a variation of density in the direction of a vertically sheared velocity (e.g. air flow over a boundary with a thermal step).

For δ near zero the component of buoyancy in the cross-stream direction is reduced so that longitudinal instabilities are replaced by transverse travelling waves which receive their energy from working on the upstream buoyancy force.

One should note that the stability analysis of the approximate profiles can either underestimate or overestimate the experimental results. Since the profiles are quite complicated (e.g. inflection points at variable distances from the wall) the use of an approximate form can have different effects on different modes.

8.3 Supercritical Motions

Before the onset of meandering the growth of the longitudinal rolls is shape preserving up to Rayleigh numbers about 4 times supercritical where the third spatial harmonic becomes evident. For $\delta > 10°$ a second instability in which the longitudinal vortices become wavy was observed. The form of the stability curve suggests that it developes from a non-linear interaction in which the lateral buoyancy torque is important. The meandering is closely connected to the development of full turbulence, which was only observed for positive tilt angles. The meanders break and an unsteadiness develops in which plumes are elongated in the upstream direction. The results suggest that slant convective systems may have considerably different heat and mass transfer properties than the horizontal or vertical counterparts.

The growth of transverse waves near $\delta = 0$ seems to involve higher order, perhaps oblique, modes. There is a sort of meandering involved at these angles also. It seems that the development of wavy vortices is a rather common occurence in a wide number of supercritical flows (see next section), and should be studied more closely.

8.4 Cylindrical Couette flow

The particularly detailed account of Coles (1965) describes how longitudinal Taylor vortices form in cylindrical Couette flow, how they become wavy (meander), break, and form turbulence. This process resembles closely the sequence of events in the tilt convective tank (see figure 1.7). The similar behavior is not too surprising since it is well known that general two-dimensional rotating flow (Veronis, 1967) are similar to two-dimensional convective motions, or in particular that infinitesimal narrow-gap Taylor vortices and convective rolls are governed by the same equations and boundary conditions (Chandrasekhar, 1961, or Debler, 1966). One then is lead to ask whether the meanders have an analogous basis.

The theories of Davey, Diprima and Stuart (1968) and Meyer (1966) suggest that the Taylor vortex meanders with azimuthal wavenumber ~ 1 may be a result of shear instability involving axial gradients of mean azimuthal velocity. The long wavelength meanders have been observed by Donnelly and Schwarz (1965), but more prominant in the literature are wavy modes with meander wavenumbers one third or so the roll wavenumber. In the tilt convection experiment shear forces were though to be too weak to account for meanders with $k_m \sim k_r/2$ There, periodic $\hat{z}$-vorticity could be generated by the lateral buoyancy torque T_y at applied conditions consistent with the observations. There is an analogous way of generating the necessary $\hat{r}$ vorticity in the rotating case. If we think in terms of a rotating

reference system (Ω rad/sec) the meander vorticity can be generated by the Coriolis torque

$$2\Omega u_z$$

and the radial velocity (now analogous to the temperature) can be re-inforced by Coriolis turning and by advection of the mean azimuthal + Taylor vortex velocity fields.

I do not wish to pursue the question further here. There is again considerable difficulty in arriving at a tractable mathematical problem. It is, I think, interesting that one can find a physical process, analogous to the buoyancy mechanism, which may be capable of generating periodic radial vorticity with wavenumbers near those observed. Of course this mechanism is not a shear instability in the usual sense.

8.5 Thermohaline convection with shear.

As a second example we consider another buoyancy driven system which is not commonly found in nature in the theretical form which it was first postulated. Salt fingering was originally studied theretically in terms of constant gradient temperature fields (stable), salinity fields (unstable) and density field (stable). Motion was possible because the low diffusity of salt, relative to that of temperature, allows parcels to retain excess accelerating buoyancy (see Stern, 1960). In nature such gradients are rarely set up. They are usually time dependent, or accompanied by a large scale sheared velocity field. In fact gradients are usually set up by advection of one type water mass over another. Such situations must involve shear. One then asks whether or not diffusively organized convective instability is still possible. For the more interesting turbulent state this is a question which will be more easily answered experimentally. In slant convection, where transverse modes are strongly inhibited, turbulence is still possible. Plumes are longitudinal, elongated in the upslope direction (figure 1.7d). This suggests that in a shear flow, general convective turbulence (which includes salt fingers) will exist and transfer consituents (heat, salt, momentum).

It is interesting to note that shear and tilt tend to inhibit transverse infintesimal perturbations. One suspects that shear will have the same effect on salt fingers, allowing a longitudinal type turbulence at high Rayleigh numbers. In fact the

stability analysis of sections 4.2, 4.3 and 4.4 is easily adapted to treat linearly sheared salt fingers. We ask what types of infinitesimal instabilities are possible on the following basic fields:

$$T_o = \alpha z, \tag{8.5.1}$$

$$S_o = \beta z, \tag{8.5.2}$$

$$U_o = \frac{R_e}{G_r} z, \quad \alpha, \beta, R_e = \text{const.}, \tag{8.5.3}$$

with rigid conducting boundaries at $z = \pm 1/2$. The geometry of this situation is shown in figure 8.1. The stability problem is handled exactly as in section 4.3. The matrix equation is

$$\begin{bmatrix} \mathbf{B}^{-1}\mathbf{A} - \lambda \mathbf{I} & -\mathbf{B}^{-1}\mathbf{F} & \frac{\beta\Delta S}{\alpha\Delta T}\mathbf{B}^{-1}\mathbf{F} \\ \mathbf{D}^{-1}\mathbf{E} & \mathbf{D}^{-1}\mathbf{C} - \lambda\mathbf{I} & 0 \\ \mathbf{D}^{-1}\mathbf{E} & 0 & \mathbf{D}^{-1}\mathbf{C}^{*} - \lambda\mathbf{I} \end{bmatrix} \begin{bmatrix} \underset{\sim}{a} \\ \underset{\sim}{b} \\ \underset{\sim}{c} \end{bmatrix} = 0 \tag{8.5.4}$$

where,

$$\mathbf{C}^{*} = P_S \mathbf{C}_1 + \mathbf{Q}\mathbf{C}_2,$$

and where we take

$$P_S = \frac{k_{SALT}}{k_{HEAT}} = .01, \quad \frac{\beta\Delta S}{\alpha\Delta T} = .5, \quad P_r = 6.7 .$$

The results from numerical caculations are shown in figure 8.2. Again transverse instabilities are drastically damped by the shear but longitudinal modes are independent of it.

Naturally full turbulence involves transverse variations, so that shear may lower the heat (or salt) flux. Nonetheless one

should not think that shear, or slope, will inhibit turbulence, and turbulent transfer of energy. The turbulence may be anisotropic, and perhaps less efficient, but it still will exist, and will probably be quite significant for the transfer of properties important in geophysical phenomenae.

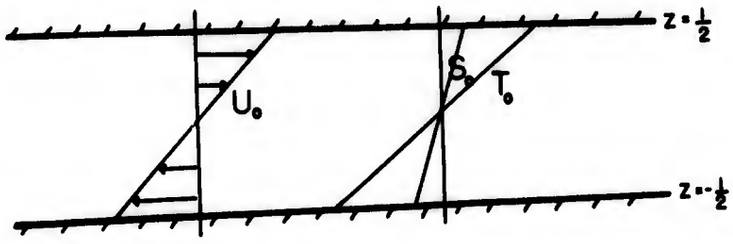

Figure 8.1 Geometry and mean fields for the sheared thermohaline convection problem.

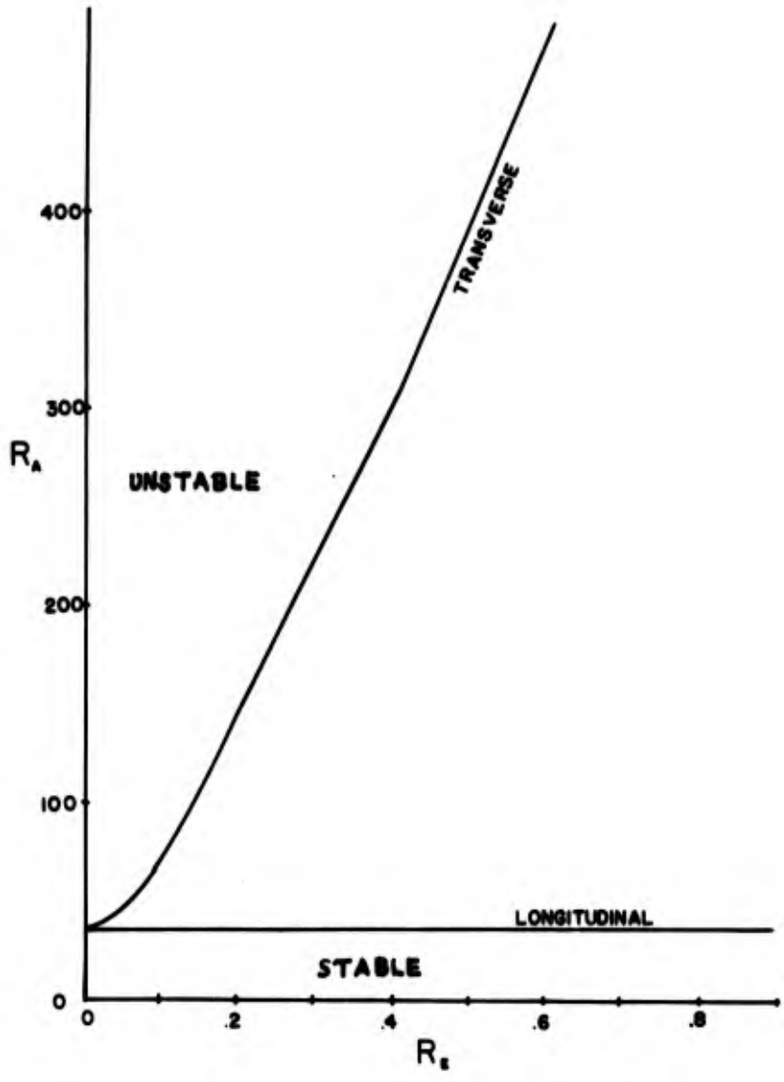

Figure 8.2 Neutral stability curves for two orientations. In these calculations $P_T = 6.7$, $P_S = .01$, and $\beta\Delta S/\alpha\Delta T = .5$.

Appendix I - Energy equations

We derive the appropriate perturbation energy equations for the various modes. We had the kinetic energy equation,

$$\frac{\partial}{\partial t}\frac{1}{2}\langle u'^2+v'^2+w'^2\rangle = \cos\delta\,\langle u'T'\rangle + \sin\delta\,\langle w'T'\rangle - G_r\langle u'w'\bar{U}_z\rangle - \langle \sigma u'^2+\sigma v'^2+\sigma w'^2\rangle . \tag{4.1.12}$$

For the transverse modes we had

$$w' = w(z)\, e^{-i(\omega t - k_x x)},$$

where $$w(z) = w_r(z) + i w_i(z) = \sum_1^N (a_{n_r} + i a_{n_i}) Y_n(z). \tag{A.1.1}$$

Also,

$$v = 0,$$

$$u = \frac{i}{k_x} w_z .$$

The energy equation can be written entirely in terms of w and T. Since $T = \sum_1^N (b_{n_r} + i b_{n_i}) S_n$, the coefficients being determined from the eigenanalysis, the energy balance can be easily found. If the brackets average process is defined as

$$\langle\ \rangle = \int_{-1/2}^{1/2} dz \int_0^{2\pi/k} dx ,$$

we obtain, with primes now denoting derivations,

$$G_r\,\omega_i\,E_k = e_c + e_u + e_T + e_v \tag{A.1.2}$$

where:

$$e_u = \cos\delta\, k_2 \int_{-1/2}^{1/2} dz \left[T_i w_r' - T_r w_i' \right],$$

$$e_c = \sin\delta\, k_2^2 \int \left[w_r T_r + w_i T_i \right],$$

$$e_v = - \int \left[(w_r'' - k^2 w_r)^2 + (w_i'' - k^2 w_i)^2 \right],$$

$$E_k = \int \left[|w'|^2 + k^2 |w|^2 \right],$$

$$e_I = - G_r k_2 \int \left[w_i w_r' - w_r w_i' \right] \bar{u}_z .$$

For the longitudinal modes (A.1.2) continues to hold. However since u is governed by a more complicated differential equation which must be solved explicitly, we must alter the formulation to include

$$u = \sum_1^N (C_{n_r} + i C_{n_i}) S_n(z) .$$

The various conversion terms for the longitudinal modes are now:

$$e_u = \cos\delta \int_{-1/2}^{1/2} dz \left[u_r T_r + u_i T_i \right],$$

$$e_I = G_r \int \left[u_r w_r + u_i w_i \right] \bar{u}_z ,$$

$$e_c = \sin\delta \int \left[w_r T_r + w_i T_i \right],$$

$$E_k = k^{-2} \int \left[|w'|^2 + k^2 |w|^2 \right] + \int |u|^2 ,$$

$$e_v = - k^{-2} \int \left[(w_r'' - k^2 w_r)^2 + (w_i'' - k^2 w_i)^2 \right]$$

$$- \int \left[|u'|^2 + k^2 |u|^2 \right] .$$

The above integrals involve the coefficients a_n, b_n and C_n of the eigenfunction expansion of $w, T,$ and u . The integrations

then are just integrals over various combinations of Y_n and S_n. Most of these were calculated for the stability analysis itself and the additional computation needed to find the energy balance is rather minimal.

Appendix II - Solutions near $\delta = 90°$.

As stated in section 4.2 we look for solutions to the stability equations near $\alpha = 0$ which have

1. free boundaries
2. $k_1 = 0$
3. $\omega = 0$

For this purpose we prefer to use the $\hat{y}$ vorticity equation formed from (4.1.1) and (4.1.3) instead of the complex forms (4.1.7) ff. The equations governing the perturbations are then with $\frac{\partial}{\partial y} = \frac{\partial}{\partial t} = 0$,

$$\sin\alpha \frac{R_a}{P_r} \left[\bar{u} \nabla^2 \Psi_x - \Psi_x \nabla^2 \bar{u} \right] = \cos\alpha T_x - \sin\alpha T_z + \nabla^4 \Psi \,, \qquad \text{(A.2.1)}$$

$$\sin\alpha R_a \left[\bar{u} T_x \right] = \nabla^2 T + R_a \Psi_x \,, \qquad \text{(A.2.2)}$$

where we have written

$$w = \Psi_x \,, \qquad \text{(A.2.3)}$$

$$u = -\Psi_z \,, \qquad \text{(A.2.4)}$$

$$\bar{u} = \sin\alpha \, u \,, \qquad \text{(A.2.5)}$$

with $$u = Az + Bz^3 \,, \qquad \text{(A.2.6)}$$

and $$\nabla^2 = \frac{\partial^2}{\partial x^2} + \frac{\partial^2}{\partial z^2} \,. \qquad \text{(A.2.7)}$$

Near $\alpha = 0$ we expand solutions in power series of α,

$$\psi = \psi_0 + \alpha \psi_1 \cdots ,$$

$$T = T_0 + \alpha T_1 \cdots ,$$

$$R_a = R_{a_0} + \alpha R_{a_1} + \cdots ,$$

$$\cos\alpha = 1 - \alpha^2/2 + \cdots ,$$

$$\sin\alpha = \alpha - \alpha^3/6 + \cdots .$$

At 0 (1) we have

$$\nabla^4 \psi_0 + T_{0x} = 0 , \tag{A.2.8}$$

$$\nabla^2 T_0 + R_{a_0} \psi_{0x} = 0 , \tag{A.2.9}$$

or $$\nabla^6 \psi_0 - R_{a_0} \psi_{0xxx} = \mathcal{L}(\psi_0) = 0 , \tag{A.2.10}$$

subject to $\psi_0 = \nabla^2 \psi_0 = \nabla^4 \psi_0 = 0$ at $z = \pm 1/2$.

The most unstable mode is easily found (this is just the classical Rayleigh problem):

$$\psi_0 = \cos kx \cos \pi z , \tag{A.2.11}$$

$$T_0 = - \frac{(k^2+\pi^2)^2}{k} \cos \pi z \sin kx , \tag{A.2.12}$$

with $$R_{a0} = \frac{(k^2+\pi^2)^3}{k^2} = 657 \quad \text{at} \quad k^2 = \pi^2/2 .$$

At 0 (α):

$$\nabla^4 \psi_1 + T_{1x} = T_{0z} + \frac{R_{a0}}{P_r} \left[\bar{u} \nabla^2 \psi_{0x} - u_{zz} \psi_{0x} \right] , \tag{A.2.13}$$

$$\nabla^2 T_1 + R_{a_0} \Psi_{1x} = R_{a_0} u T_{0x} - R_{a_1} \Psi_{0x} \quad . \qquad \text{(A.2.14)}$$

Since $u_{zzzz} = 0$ and $\nabla^4 \psi_0 = -T_{0x}$ these combine into

$$\mathcal{L}(\Psi_1) = \nabla^2 T_{0z} + R_{a_1} \Psi_{0xx} - R_a \left(1 + 1/P_r\right) u T_{0xx} \quad . \qquad \text{(A.2.15)}$$

It can be shown that a necessary and sufficient condition for the existence of a non-trivial solution to this inhomogeneous differential equation is that

$$\int_\Omega \Psi_0 \cdot \Psi_1 \, d\Omega = 0 \, , \qquad \text{(A.2.16)}$$

and $$\int_\Omega \Psi_0 \cdot f \, d\Omega = 0 \, , \qquad \text{(A.2.17)}$$

where f is the forcing term, and Ω is across the gap in z and over one cycle in x. Applying these conditions to (A.2.15) we obtain:

$$R_{a_1} \int_{-1/2}^{1/2} dz \int_0^{\lambda = \frac{2\pi}{k}} dx \, \Psi_0 \Psi_{0xx} = \iint dx dz \, \Psi_0 \left\{ R_{a_0} \left(1 + \frac{1}{P_r}\right) u T_{0xx} - \nabla^2 T_{0z} \right\} . \qquad \text{(A.2.18)}$$

Ψ_0 and T_0 are given in (A.2.11) and (A.2.12). The right hand side of (A.2.18) is zero because Ψ_0 is even, u odd, and T_0 even in z. Thus,

$$R_{a_1} = 0 \, . \qquad \text{(A.2.19)}$$

At $0(\alpha^2)$:

$$\nabla^4 \Psi_2 - T_{2x} = T_{1z} + \frac{T_{0x}}{2} + \frac{R_{a_0}}{P_r} \left[u \nabla^2 \Psi_{1x} - u_{zz} \Psi_{1x} \right] , \qquad \text{(A.2.20)}$$

$$\nabla^2 T_2 + R_{a_0} \Psi_{2x} = R_{a_0} u T_{1x} - R_{a_2} \Psi_{0x} \,, \tag{A.2.21}$$

or,

$$\mathcal{L}(\Psi_2) = \nabla^2 T_{12} + \frac{\nabla^2 T_{0x}}{2} + \frac{R_{a_0}}{P_r} u \nabla^4 \Psi_{1x} - R_{a_0} u T_{1xx} + R_{a_2} \Psi_{0xx} \,. \tag{A.2.22}$$

The solvability condition specifies R_{a_2} :

$$R_{a_2} \int_{-\pi/k}^{\pi/k} dz \int_0^{2\pi/k} dx \, \Psi_0 \Psi_{0xx} = R_{a_0} \iint u \Psi_0 T_{1xx} - \iint \Psi_0 \nabla^2 \left(T_{12} + \frac{T_{0x}}{2} \right) - \frac{R_{a_0}}{P_r} \iint \Psi_0 u \nabla^4 \Psi_{1x} \,. \tag{A.2.23}$$

Unfortunately in order to calculate R_{a_2} we need to know Ψ_1 and T_1. These are determined by solving (A.2.15) which may be written

$$\nabla^6 \Psi_1 - R_{a_0} \Psi_{1xx} = -(bz + cz^3) \cos \pi z \sin kx - a \sin \pi z \sin kx \,, \tag{A.2.24}$$

where $a = \dfrac{\pi (k^2+\pi^2)^3}{k}$, slope effect

$b = R_{a_0} (1 + P_r^{-1}) k (k^2+\pi^2) A$, } advection of vorticity and temperature by the mean field

$c = \dfrac{bB}{A}$. }

The forced solution to (A.2.24) is found in terms of a Fourier series. After some tedious manipulation we obtain

$$\Psi_1 = -\frac{2}{\pi} \sum_{p_{even}=2}^{\infty} \frac{\sin p\pi z \sin kx \sin (p-1)\pi/2}{k} \left\{ \right\}_* , \qquad (A.2.25)$$

$$T_1 = -\frac{2}{\pi} \sum_{p\ even}^{\infty} \frac{\sin p\pi z \cos kx \sin (p-1)\pi/2}{p^2\pi^2 + k^2} \left[\left\{ \right\}_* - R_{a_0} (k^2+\pi^2) b_p \right] , \qquad (A.2.26)$$

Here we have defined

$$\left\{ \right\} = \frac{(k^2+\pi^2)^3 a_p + R_{a_0} k^2 (k^2+\pi^2)^2 (1+P_r^{-1}) b_p}{\left[R_{a_0} k^2 - (p^2\pi^2+k^2)^3 \right]} ,$$

$$a_p = \frac{2p}{p-1} ,$$

$$b_p = \frac{p}{\pi^2 (p^2-1)^2} \left(4A + 3B - \frac{48B(p^2+1)}{\pi^2 (p^2-1)^2} \right) .$$

By condition (A.2.16) there is no free solution to (A.2.24). To find R_{a_2} we put (A.2.25) and (A.2.26) into the integral expression (A.2.23) and perform the required operations. It turns out that only the first terms in the p series are significant for the correction to the Rayleigh number. We arrive at

$$\frac{R_a}{657} - 1 = \alpha^2 \left[.445 - \left(5.46 - \frac{.58}{P_r} \right) Y + \left(2.15 + \frac{.22}{P_r} + \frac{.22}{P_r^2} \right) Y^2 \right] . \qquad (A.2.27)$$

Y defines the effect of the mean shear flow and is found from the

expression for b_p with $p = 2$:

$$Y = 4A + .38 .$$

In (A.2.27) we have set $R_{a_0} = 657$ and $k^2 = \pi^2/2$. One expects that there may be a change in k associated with the correctin to the critical Rayleigh number. We have not calculated this since it involves the quite complicated derivative of R_a with respect to k . Another point is that one can estimate the range of validity of (A.2.27) by looking at the magnitudes of

$$\frac{\alpha \iint \Psi_1^2 \, dx\,dz}{\iint \Psi_0^2 \, dx\,dz} \quad \text{or} \quad \frac{\alpha \iint T_1^2 \, dx\,dz}{\iint T_0^2 \, dx\,dz} .$$

These are small if $\alpha < \sim 5^\circ$, $P_r \sim O(1)$.

Appendix III - Some preliminaries for the Galerkin method.

The Galerkin method rests on the use of expansion functions which satisfy all the boundary conditions and which are complete and orthogonal. We use Y_n and S_n defined as solutions of

$$\frac{d^4 Y_n}{dz^4} - \lambda_n Y_n = 0 \qquad \text{(A.3.1)}$$

and

$$\frac{d^2 S_n}{dz^2} + \Sigma_n S_n = 0 \qquad \text{(A.3.2)}$$

subject to

$$Y_n = \frac{dY_n}{dz} = S_n = 0 \quad \text{at} \quad z = \pm 1/2 .$$

These functions are orthogonal as is easily seen by multiplying and integrating. It is convenient to use solutions which are separately even or odd. We find

$$Y_n = \begin{cases} E_n = \dfrac{\cosh \rho_n z}{\cosh \rho_n/2} - \dfrac{\cos \rho_n z}{\cos \rho_n/2} & \text{for n odd} \\ O_n = \dfrac{\sinh \mu_n z}{\sinh \mu_n/2} - \dfrac{\sin \mu_n z}{\sin \mu_n/2} & \text{for n even,} \end{cases}$$

$$S_n = \begin{cases} \cos \; n\pi z & \text{for n odd} \\ \sin \; n\pi z & \text{for n even.} \end{cases}$$

The eigenvalues ρ_n and μ_n are given by

$$\tanh \rho_n/2 + \tan \rho_n/2 = 0 , \qquad \text{(A.3.3)}$$

$$\coth \mu_n/2 - \cot \mu_n/2 = 0 . \qquad \text{(A.3.4)}$$

The Y_n are essentially made up of the functions of Reid and Harris (1958). If λ_n is defined to be ρ_n or μ_n as n is odd or even respectively, it can be seen that the eigenvalues λ_n (and of course $\Sigma_n = n\pi$ also) form an infinite ordered sequence with distinct eigenfunctions. I now state a theorem which is a slight variation of one proved in Mikhlin (1964) para. 31. The proof of the present statement is an obvious modification of the proof given there.

Theorem: If $\mathcal{L}$ is a linear operator positive bounded below which has an infinite ordered sequence of eigenvalues and eigenfunctions, the set formed from these eigenfunctions is complete in the sense of convergence in the mean.

We have only to show that the operators in (A.3.1) and (A.3.2) are positive bounded below which means that if

$$\mathcal{L}u - \lambda u = 0 ,$$

$$(\mathcal{L}u, u) \geq 0 .$$

Quite simply,

$$\int_{-1/2}^{1/2} dz \frac{d^4 Y_n}{dz^4} Y_n = \int_{-1/2}^{1/2} dz \left(\frac{d^2 Y_n}{dz}\right)^2 \geq 0 ,$$

and $$-\int_{-1/2}^{1/2} \frac{d^2 S_n}{dz^2} S_n \, dz = \int_{-1/2}^{1/2} \left(\frac{dS_n}{dz}\right)^2 \geq 0 \quad .$$

The theorem then assures us that the coordinate functions will be complete.

It is considerably more difficult to show that the application of the Galerkin method with truncated N term expansion yields a convergent process for finding the eigenvalues. Mikhlin has given a quite general proof for single linear differential operators with the form

$$T u + \lambda u = f \tag{A.3.5}$$

The operator T is supposed to be factorable into two parts A_0 and K such that $T = A_0^{-1} K$. If K is bounded in a Hilbert space $H \geq H_0$ (e.g. $(k\phi, \phi) < \text{const}\,(\phi, \phi)$) and if A_0^{-1} is completely continuous (almost degenerated), Mikhlin shows that T is completely continuous in H_0 and that the use of the Bubnov-Galerkin method in finding the eigenvalues of (A.3.5) with $f = 0$ is convergent in the sense that if λ and u are the true solutions then $|\lambda_n - \lambda|$ and $\|u_n - u\|$ tend to zero as n goes to infinity (not necessarily at the same rate). If we had reduced our stability equations to a single differential equation in w the above mentioned proofs would apply. This was not at all convenient and we dealt with systems of linear differential equations with the form:

$$\underset{\sim}{V} - \mathbf{T}\underset{\sim}{V} = 0 \qquad \text{(A.3.6)}$$

We wrote the solution vector $\underset{\sim}{V} = V_j$ in terms of a sum of function vectors $\underset{\sim}{\phi}_k = \phi_{j,k}$ defined over a region Ω such that

$$V_j = \begin{pmatrix} v_1 \\ v_2 \\ \vdots \end{pmatrix} = \sum_{k=1}^{\infty} \begin{pmatrix} a_{11} & 0 \\ 0 & a_{22} \\ & \ddots \end{pmatrix}_k \begin{pmatrix} \phi_1 \\ \phi_2 \\ \vdots \end{pmatrix}_k ,$$

which can be written more simply as

$$\underset{\sim}{V} = \sum_{k=1}^{\infty} \mathbf{A}_k \underset{\sim}{\phi}_k$$

The diagonal coefficient matrix is found by applying the Galerkin orthogonality relation to (A.3.6).

If the vector $\underset{\sim}{V}$ is of rank P, this equation results in a PN x PN system of linear equations for the coefficients. One can now work through the general proofs of Mikhlin with a vector instead of a scalar function space. This technique almost works. The trouble is that in our problem the elements of the operator $\mathbf{T}$ have different fields of definition, namely various combinations of twice differentiable and four time differentiable continuous functions. One may indeed be able to prove that the Galerkin method must converge when applied in this manner to systems of equations but at this time I have no completely rigorous proof, nor do I know of any. Hence we must rely on our heuristic tests of convergence, some intuitive faith,

and on the experiences of other inveatigators in successfully applying the method to similar problems.

We conclude this appendix with a short list of integrals necessary in the computation of the matrix elements. These were obtained by hand analysis, but have been checked by numerical integration.

$$\int_{-1/2}^{1/2} Y_m Y_n \, dz = \begin{cases} 0 & m \neq n \\ 1 & m = n \end{cases} \qquad \text{(A.3.7)}$$

$$\int_{-1/2}^{1/2} \frac{d^4 Y_m}{dz} Y_n \, dz = \begin{cases} \rho_n^4 & m=n, \ n \text{ odd} \\ \mu_n^4 & m=n, \ n \text{ even} \\ 0 & \text{otherwise} \end{cases} \qquad \text{(A.3.8)}$$

$$\int_{-1/2}^{1/2} \frac{d^2 Y_m}{dz^2} Y_n \, dz = \begin{cases} 0 & (n+m) \text{ odd} \\ \frac{1}{2}\rho_m^{-4} E_m''(\tfrac{1}{2}) E_m'''(\tfrac{1}{2}) - \left(\rho_m \tanh \frac{\rho_m}{2}\right)^2 & n=m, \ m \text{ odd} \\ \frac{1}{2}\mu_m^{-4} O_m''(\tfrac{1}{2}) O_m'''(\tfrac{1}{2}) - \left(\mu_m \coth \frac{\mu_m}{2}\right)^2 & n=m, \ m \text{ even} \\ (\rho_m^4 - \rho_n^4)^{-1}\left(2E_m'''(\tfrac{1}{2})E_n''(\tfrac{1}{2}) - 2E_m''(\tfrac{1}{2})E_n'''(\tfrac{1}{2})\right) & n \neq m, \ m \text{ odd} \\ (\mu_m^4 - \mu_n^4)^{-1}\left(2O_m'''(\tfrac{1}{2})O_n''(\tfrac{1}{2}) - 2O_m''(\tfrac{1}{2})O_n'''(\tfrac{1}{2})\right) & n \neq m, \ m \text{ even} \end{cases} \qquad \text{(A.3.9)}$$

$$\int_{-1/2}^{1/2} Y_m S_n \, dz = \begin{cases} 0 & (m+n) \text{ odd} \\ 2n\pi \left(\rho_m^4 - n^4\pi^4\right)^{-1} E_m''\left(\tfrac{1}{2}\right) \sin\frac{n\pi}{2} & m \text{ even} \\ -2n\pi \left(\mu_m^4 - n^4\pi^4\right)^{-1} O_m''\left(\tfrac{1}{2}\right) \cos\frac{n\pi}{2} & m \text{ odd} \end{cases} \tag{A.3.10}$$

$$\int_{-1/2}^{1/2} S_m S_n \, dz = \begin{cases} 0 & m \neq n \\ .5 & m = n \end{cases} \tag{A.3.11}$$

$$\int_{-1/2}^{1/2} \frac{d^2 S_m}{dz^2} S_n \, dz = \begin{cases} 0 & m \neq n \\ -\frac{n^2\pi^2}{2} & m = n \end{cases} \tag{A.3.12}$$

$$\int_{-1/2}^{1/2} \frac{dS_m}{dz} Y_n \, dz = \begin{cases} 0 & (n+m) \text{ even} \\ 2n\pi \left(m^4\pi^4 - \mu_n^4\right)^{-1} O_n'''\left(\tfrac{1}{2}\right) \sin\left(\frac{m\pi}{2}\right) & n \text{ odd} \\ -2n\pi \left(m^4\pi^4 - \rho_n^4\right)^{-1} E_n'''\left(\tfrac{1}{2}\right) \cos\left(\frac{m\pi}{2}\right) & n \text{ even} \end{cases} \tag{A.3.13}$$

BIBLIOGRAPHY

Avsec, D., 1939, Science and Technical Publication of Air Ministry, No. 155, Paris

Baker, D.J., 1966, A technique for the precise measurement of small fluid velocities, J. Fluid Mech., 26.

Batchelor, G.K., 1954, Heat transfer by free convection across a closed cavity between vertical boundaries at different temperatures, Q. Applied Math., 12, 209-233.

Chandrasekhar, S., 1961, Adjoint differential systems in the theory of hydrodynamic stability, J. Math. Mech., 10, 683.

Davey, A., 1962, The growth of Taylor vortices in flow between rotating cylinders, J. Fluid Mech., 14, 336-368.

Davey, A., Diprima, R.C., and Stuart, J.T., 1968, On the stability of Taylor vortices, J. Fluid Mech., 31, 17-52.

Davis, S.H., 1967, Convection in a box: Linear theory, J. Fluid Mech., 30, 465-478.

Deardorf, J.W., 1964, A numerical study of 2-dimensional parallel plate convection, J. Atmos. Sci., 21, 419-438.

Deardorf, J.W., 1965, Gravitational instability between horizontal planes with shear, Phys. of Fluids, 8, 1027-1030.

Debler, W.R., 1966, On the analogy between thermal and rotational hydrodynamic stability, Q. Appl. Math., 13, 55-62.

Donelly, R.J., and Schwarz, K.W., 1965, Experiments on the stability of viscous flow between rotating cylinders, Proc. Roy. Soc., A283, 531-549.

Eckert, E.R.G., and Carlson, W.O.,
1961, Natural convection in an air layer enclosed between two vertical plates with different temperatures,
Int. J. Heat, Mass Transfer, 2, 106-120.

Elder, J.W., 1965a, Laminar free convection in a vertical slot,
J. Fluid Mech., 23, 77-98.

Elder, J.W., 1965b, Turbulent free convection in a vertical slot,
J. Fluid Mech., 23, 99-111.

Elder, J.W., 1966, Numerical experiments with free convection in a vertical slot,
J. Fluid Mech., 24, 823-843.

Foster, T.D., 1969, The effect of initial conditions and lateral boundaries on convection,
J. Fluid Mech., 37, 81-94.

Gallagher, A., and McD. Mercer, A.,
1965, On the behavior of small disturbances in plane Couette flow with a temperature gradient,
Proc. Roy. Soc., (London), A 286, 117-128.

Gershuni, G.Z., 1955, On the question of stability of plane convective motion of a liquid,
Zhurnal Teknischeskoi Fiziki, 25, 351-357.

Gill, A.E., 1966, The boundary layer regime for convection in a rectangular cavity,
J. Fluid Mech., 26, 515-536.

Gill, A.E., and Davey, A.,
1969, Instabilities of a buoyancy driven system,
J. Fluid Mech., 35, 775-793.

Harris, D.L., and Reid, W.H.,
1958, On orthogonal functions which satisfy four boundary conditions,
Astrophys. J. Suppl., 3, 429-447.

Howard, L.N., 1966, Convection at high Rayleigh number, Proc. 11'th Int. Congress. Appl. Mech., Munich, 1109-1115.

Ingersol, A.P., 1966, Convective instabilities in plane Couette flow, Phys. of Fluids, 9, 682-689.

Koshmeider, E., 1966, On convection on a uniformly heated plane, Beitr. Phys. Atmos., 39, 1-11.

Krishnamurti, R., 1968, Finite amplitude convection with changing mean temperature. Part 1, Theory. Part 2, Experimental test of the theory, J. Fluid Mech., 33, 445-463.

Kuo, H.L., 1961, Solution of the non-linear equations of cellular convection and heat transport, J. Fluid Mech., 10, 611-634.

Malkus, W.V.R., and Veronis, G., 1958, Finite amplitude convection, J. Fluid Mech., 14, 225-260.

Mikhlin, S.G., 1964, Variational Methods in Mathematical Physics, Pergammon Press, New York.

Mori, Y., and Uchida, Y., 1966, Forced convective heat transfer between horizontal flat plates, Int. J. Heat Mass Transfer., 9, 803-817.

Ogura, Y., and Yagihasi, A., 1969, A numerical study of convective rolls in a flow between horizontal parallel plates, J. Meteor. Soc. Japan., 47, 205-217.

Pellew, A., and Southwell, R.V., 1940, On maintained convective motion in a fluid heated from below, Proc. Roy. Soc., A 176, 312-343.

Rayleigh, L., 1916, On convection currents in a horizontal layer of fluid, when the higher temperature is on the underside, Philosophical Magazine, Series 6, 32.

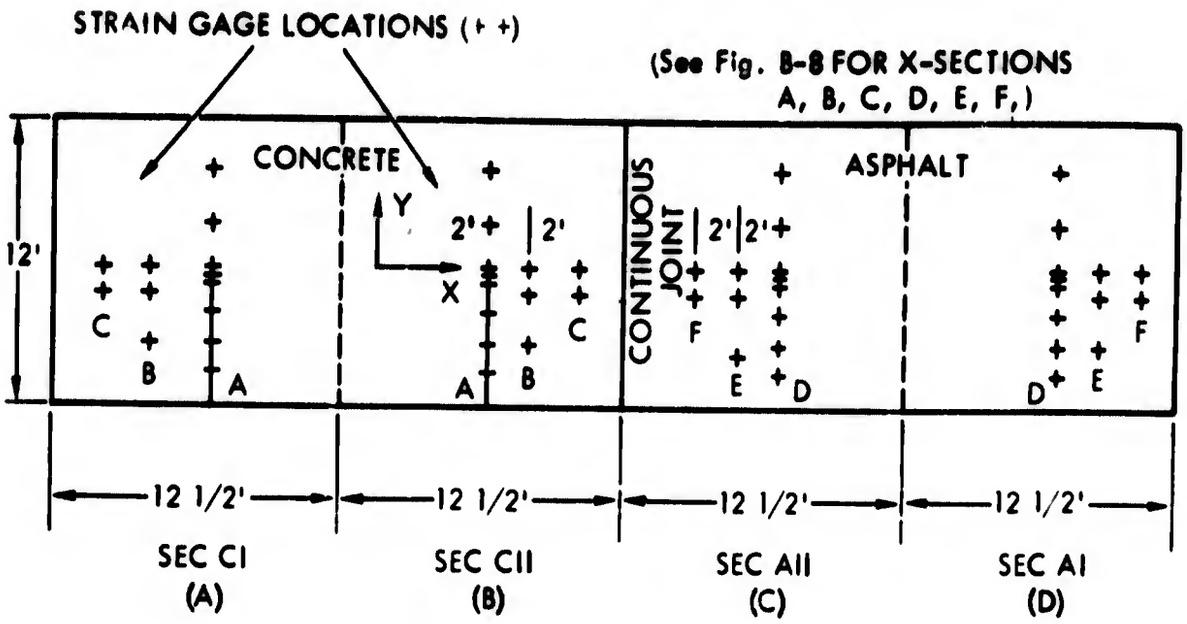

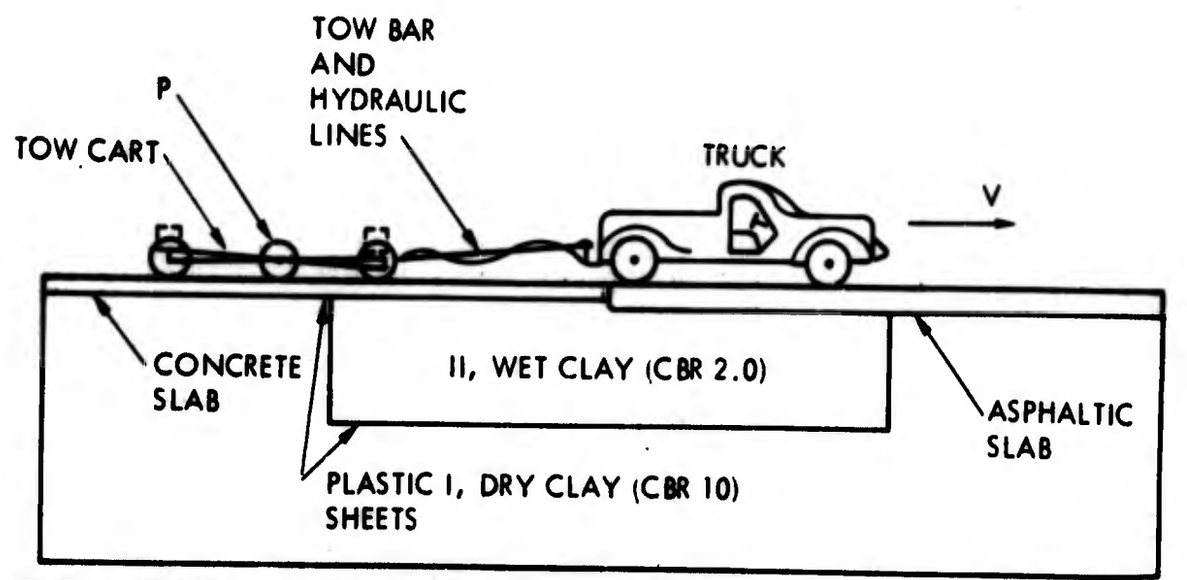

TWO CART SPECS: FORD XL CHASSIS, LOAD P APPLIED BY COIL SPRING AT CENTER LOADED BY A BAR - HYDRAULIC CYLINDER ARRANGEMENT ACTIVATED AT TRUCK.

FIGURE B-7 - Scaled Runway Test Arrangement

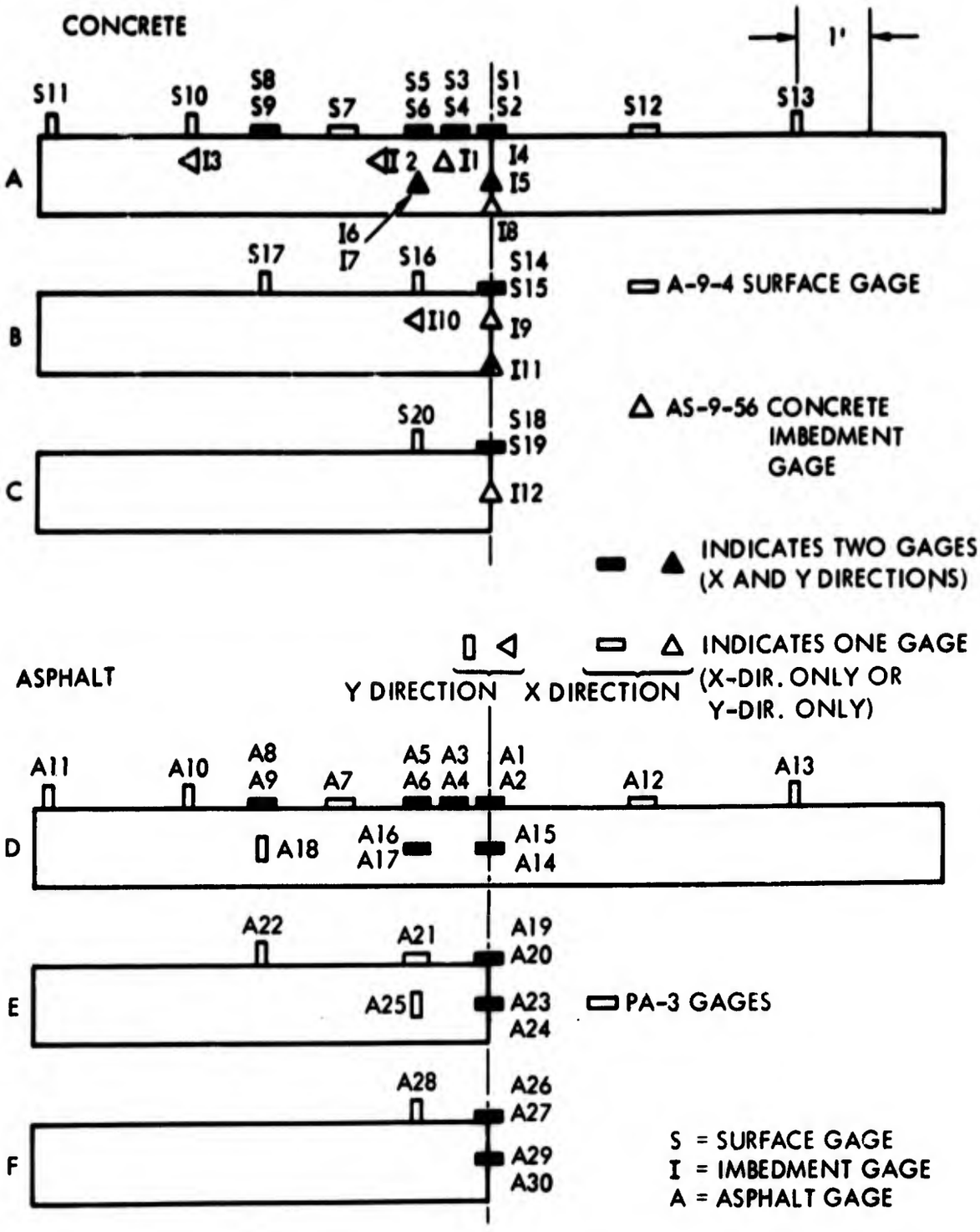

FIGURE B-8 - Strain Gage Location

TWENTY GAGES DISTRIBUTED AT FOUR LOCATIONS (X - SECTIONS A AND D IN FIG. B-8) AS FOLLOWS:

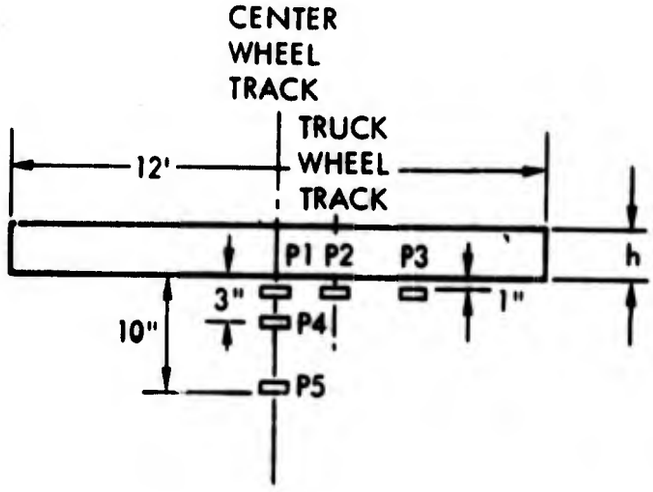

FIGURE B-9 - Pressure Gage Locations

(F) Data to be Recorded

Speed: Magnetic pulse counter reading on gear wheel

Strain: Oscillograph time histories of voltage drop across strain gages

Deflection: Film of Moire pattern

Pressure: Time histories of pressure in each pressure cell

Load: Dynamometer time history of gear load

NOTE: All readings should be synchronized.

(G) Data to be Delivered to Lockheed-California Company - (Data must be reduced to this form for each test)

Velocity (in./sec)

Strain time histories (in./in. vs. seconds)

Gear load time history (pounds vs. seconds)

Pressure time histories (psi vs. seconds)

Deflection time histories (inches vs. seconds), various locations.

All time histories should start at the same time, and any error sources in measuring this starting time should be noted.

(H) Peripheral Data to be Furnished by Lockheed-Georgia Company

(1) Pavement properties

Concrete modulus (psi) at start of test sequence

Concrete modulus (psi) at end of test sequence

Asphaltic concrete bending strength (psi), start and end

(2) Soil properties

CBR of dry soil at start and end

CBR of wet soil at start and end

Measurement of the damping characteristics of wet and dry soil

3. TEST INSTALLATION

(A) Construction of Loading Device - Discussions of required wheel loads and speeds indicated that some added means of minimizing the low-frequency, vertical-load oscillations would be required if the desired objective were to be met. The original trailer was a three-wheel device with no springs or shocks other than the tires. Several alternatives were examined, and the following were among them:

- Shock isolation of the trailing wheel
- Shock isolation of all three wheels
- Mounting the wheel on a simplified oleo shock strut
- Mounting the wheel inside a four-wheel carriage frame free in pitch and yaw

The last approach was chosen as resulting in the least cost and shortest time effort. The most obvious source of a ready-made, four-wheel frame was an automobile chassis. An undamaged chassis was located, and the aft half of the existing trailer was attached to the frame at the location of the aft motor mounts. In order to reduce the inertial mass on the test wheel, lead weights were bolted to the chassis over the front and rear wheels. This load is transferred to the test wheel through a spring which is loaded by a hydraulic cylinder.

To isolate the towed wheel and its carriage from the towing vehicle, a 10-foot towing bar was used. This carriage showed good stability and handling. The frequency response of the test wheel appeared to be quite high compared to the previous configuration.

(B) Hydraulic System Design - A hydraulic loading cylinder was at first envisioned as a device to be loaded by hand to the desired load level and left loaded at all times. It was then realized that the test carriage weight should be transferred back to the four-wheel chassis for braking effectiveness on the towed vehicle.

A hydraulic system was designed using a pump, accumulator and reservoir with a directional control valve to apply load to the wheel and then release it for braking. Pressure limitation to set the load level is by use of one-half of a C-130 brake control valve. Brakes on the towed test vehicle are controlled from the towing vehicle through an automobile brake master cylinder mounted adjacent to the test wheel hydraulic control system.

Checkout of the system showed satisfactory operation of the hydraulic and brake systems except for the unloading rate of the test wheel. The wheel load should be released in a few tenths of a second because of the rapid brake application needed for high-speed tests. A manual-control bypass valve was installed which connects both sides of the hydraulic cylinder through a large-diameter hose to speed up the load transfer.

(C) Soil Bed Installation - Initial plans were for installation of one 25-foot test bed at a time at one moisture content. Later clarifications indicated a need for two 25-foot test beds with two moisture contents under each type of surface. This resulted in the requirement of moisture control and compaction of approximately 45 cubic yards of material. It was thought that in-place processing of at least 1 foot of material could be done; however, when the surface layer was removed in the test area, it was found that there was a considerable amount of gravel mixed in the soil, making it unsuitable for processing. New soil was then removed from an embankment approximately 100 yards from the test site. All soil to a depth of 2 feet was replaced in the test area. It was desired to construct the hard-soil sections to CBR 10. Fortunately, the soil as found had a moisture content of around 20 percent and compacted to the desired value without the addition of water. The soft soil desired CBR was 2.0, or a moisture content of around 30 percent. Approximately 1000 gallons of water had to be hauled to the test site and mixed with the material to reach the desired CBR. Material was placed in the test pits with a front-end loader and compacted with a Thor gasoline-driven, vibratory compactor. The results of the installation indicated that the control was good for the soil properties.

Subsequent compaction and drying of the hard soils and increasing moisture due to added water in the soft-soil sections resulted in some loss of control between installation of the trial soil bed (discussed below) and the final test beds.

(D) Trial Concrete Test Sections - There were some questions as to the proper thickness of the concrete test section to transmit measurable pressures to the subsoil and yet not crack under the applied wheel loads. The Ohio River Division of the U.S. Army Corps of Engineers was contacted, and they recommended a thickness of about 2 inches as suitable for the wheel loads being tested. Other calculations indicated that a thicker slab might be necessary.

It was decided to make a trial installation to see what pressures would be seen and if cracking would occur. The 25-foot slabs of concrete were poured, one 2 inches thick and one 3 inches thick. A very dry mix was used to obtain high strengths; however, the concrete hardened before adequate spreading and finishing could be made. Consequently, poor thickness control was obtained; some sections were less than 2 inches and some sections were greater than 3 inches. The next day a finishing coat of sand cement was applied to smooth out bumps to allow high speed-vehicle passage.

A few tests were run to determine the pressure gages output; it was found to be only 2 millivolts, and little difference could be seen between the two concrete thicknesses. The differences that were seen were attributed to wheel load variation rather than to the effects of concrete thickness.

It was determined that the pressure measurements would have to be amplified to obtain meaningful results. Twenty-five direct-current amplifiers were wired into the circuits.

In order to meet schedules the trial test beds could remain installed only a short time. The concrete over the pressure gages was removed by sawing through the pavement on either side of the gage station.

(E) Final Test Section Installation - The final test sections chosen were 2 inches of concrete and 5 inches of asphalt, based on preliminary concrete testing and analytical calculations by the California Company (see Figure B-7 for sketch of test configuration). The concrete test section was poured in a manner similar to the initial test slab but with a greater slump to provide better workability. The concrete was ordered with a 3-inch slump, but tests on site showed a 4-inch slump. This was probably because of water added during a rather long wait by the delivery truck at the gate. The section over the hard-soil surface was poured and imbedded gages were placed without difficulty. As the gage forms were removed from the soft-soil surface, a large curing crack was found beneath the form 6.25 feet from the end of the bed. However, several strain gages were installed in the cracked concrete section (since pressure gages were already installed) to note any differences in response.

(F) Instrumentation - Considerably more work than anticipated was involved in setting up the instrumentation system. An initial 20 channels for pressure gages and 20 channels for strain gages were allowed. The stress gages were considered to be four-arm Wheatstone bridge gages on a bar to be imbedded in the pavement to measure bending stresses.

The gage configuration evolved into considerably more than 20 channels of strain measurements. To obtain adequate readings, a four-arm Wheatstone bridge circuit was made for each channel. These can be plugged into the cables going to the instrumentation trailer (up to 20 circuits at one time).

The pressures underneath the trial concrete sections were so small that amplification of the signals before recording was considered necessary. Twenty-four direct-current amplifiers were wired for a gain of 200 to be plugged into the circuits needing amplification.

(G) Transducers - All of the pressure gages installed underneath the pavement were in working condition. All of the imbedded gages in the asphalt were working just before the second 2-1/2 inches of material was applied. Only two of the 20 gages installed had to be replaced due to open-gage wiring. The imbedded gages in the concrete sections over the hard-soil base were in good condition except one gage, buried 2/3 inch below the surface, which became dislodged.

4. SCALED RUNWAY TEST SUMMARY DATA

(A) Slab Designation

Material	Subbase	Designation
Concrete	CBR 10	A
Concrete	CBR 2	B
Asphalt	CBR 2	C
Asphalt	CBR 10	D

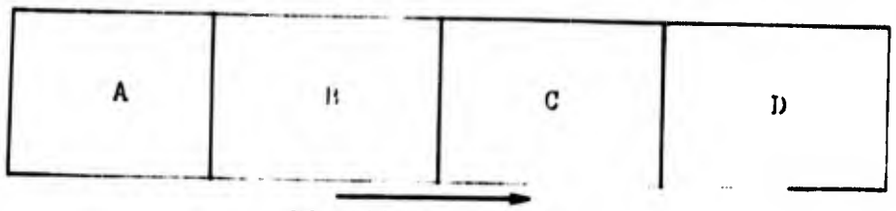

(B) Calibration Factors

Load:

V_1 1780 lbs/in

V_2 1795 lbs/in

Pressure Gages: Psi/in

P1A	1.80	
P2A	1.87	
P3A	1.815	
P1B	1.85	
P2B	–	(Didn't Balance)
P3B	1.735	
P1C	1.73	
P2C	1.80	
P3C	0.92	
P1D	0.93	
P2D	1.27	
P3D	1.63	
P4A	1.96	
P5A	1.89	
P4C	1.85	
P5C	1.68	
P4D	1.71	

Strain Gages:

Concrete "A"	μin./in	Asphalt "C"	μin./in	Asphalt "D"	μin./in
S2	364	A1C	385	A7D	3060
S3	364	A2C	385	A10D	384
S6	364	A3C	384	A17D	3090
				A19D	384
S7	362	A4C	383	A20D	384
		A5C	383		
S11	363	A6C	381	A21D	386
				A25D	389
S13	364	A8C	384	A26D	379
S15	365	A9C	385	A28D	383
I1	912	A13C	382	A29D	383
		A14C	383		
I3	910	A19C	384	A30D	382
I4	912	A28C	384		
I6	909				
I8	912				
I9	909				
I10	909				
I11	912				

(C) Initial Combinations

COMBINATION A (Maximum Priority Gages)

P1, P2, P3

S1, S2, S5, S6, S8, S9, I4

A1, A2, A5, A6, A8, A9, A14

COMBINATION B

P4, P5

S3, S4, S7, S11, I1, I3, I5, I8

A3, A4, A7, A11, A15, A16, A17, A18

COMBINATION C

S10, S12, S13, S14, S15, I2, I6, I7, I11

A10, A12, A13, A19, A20, A21, A22, A23, A24, A25

COMBINATION D (Lowest Priority Gages)

S16, S17, I9, I10, S18, S19, S20, I12

A26, A27, A28, A29, A30

(D) Test Sequence

(1) Static Tests: 1-4, Date 7/19/69

(2) Moving Load Tests

Date	Trailer Trace	Truck Number Trace	Combination	Speed (MPH)
7/19	9	6	A (weak asphalt)	3
	10	7	A	6
	11	8	A	10
	12	9	A	20
	13	10	A	30
	14	12	A	40
7/22	18	1	A	3
	20	2	A	10
	21	3	A	6
	22	4	A	20
	23	-	A	30
	24	-	A	40
	25	-	B (Concrete)	3
	27	55556	B	3
	28	55556	B	6
	29	55556	B	10
7/23	1	1	B	10
	2	2	B	20
	3	3	B	20
	5	4	B	30
	6	5	B	40
	7	Truck Only	B	45
	8	Truck Only	B	50
	10	Truck Only	B	55
	11	Sports Car	B	65
	13	Sports Car	B	60

Date	Trailer Trace	Truck Trace	Combination	Speed (MPH)
7/24	7	14	B (weak asphalt)	3
	8	16	B	6
	9	17	B	10
	10	18	B	20
	11	19	B	30
	12	20	B	40
7/25	13	21	C (strong asphalt)	3
	14	22	C	6
	15	23	C	10
	16	24	C	20
	17	25	C	30
7/26	18	26	C	40
	19	27	D (strong asphalt)	3
	20	28	D	6
	21	29	D	10
	22	31	D	20
	23	32	D	30
	24	33	D	40
	35	-	D	3
	36	-	D	6
	37	-	D	10
	38	-	D	20
	39	-	D	30
	40	-	D	40
	41	-	D	30

(3) Impact Tests: 1-9, Date 7/28/69

SCALED RUNWAY TEST DATA

Strain Gages - Moving Load
R = Right L = Left

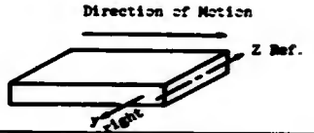

Data Point Number	Test Data		Load Data				Location			Air Temp °F	Response gin/in	Comments
	Trace Numbers	Date	Speed	Mean Load	Variation From Mean %	Tracking Error	Y	Z	Pavement Section			
A19D	27	7/26	4.34	2525	8.3	0	0	-2.5	D	82	286	Trace indicates possible gage slippage
A19D	28	7/26	6.3	2595	10.8	2.5 R	0	-2.5	D	82	134	
A19D	29	7/26	8.3	2480	12.1	2 R	0	-2.5	D	82	128	
A19D	31	7/26	16.0	2695	28.0	2.5 R	0	-2.5	D	82	125	
A19D	32	7/26	22.5	2665	26.8	2 R	0	-2.5	D	84	98	
A19D	33	7/26	37	2665	41.0	2.5 R	0	-2.5	D	84	116	
A20D	27	7/26	4.34	2525	8.3	0	0	-2.5	D	82	163	
A20D	28	7/26	6.3	2595	10.8	2.5 R	0	-2.5	D	82	58	Possible track error
A20D	29	7/26	8.3	2480	12.1	2 R	0	-2.5	D	82	48	Possible track error
A20D	31	7/26	16.0	2695	28.0	2.5 R	0	-2.5	D	82	134	
A20D	32	7/26	22.5	2665	26.8	2 R	0	-2.5	D	84	131	
A20D	33	7/26	37	2665	41.0	2.5 R	0	-2.5	D	84	98	
A21D	27	7/26	4.34	2525	8.3	0	12	-2.5	D	82	47	
A21D	28	7/26	6.3	2595	10.8	2.5 R	12	-2.5	D	82	28	
A21D	29	7/26	8.3	2480	12.1	2 R	12	-2.5	D	82	38	
A21D	31	7/26	16.0	2695	28.0	2.5 R	12	-2.5	D	82	28	
A21D	32	7/26	22.5	2665	26.8	2 R	12	-2.5	D	84	19	
A21D	33	7/26	37	2665	41.0	2.5 R	12	-2.5	D	84	19	

SCALED RUNWAY TEST DATA

Data Point Number	Test Data		Load Data				Location			Air Temp °F	Response	Comments
	Trace Numbers	Date	Speed	Mean Load	Variation From Mean %	Tracking Error	Y	Z	Pavement Section			
A1C	18	7/22	4.9	2480	10.2	Unknown	0	-2.5	C	83	364 270	Estimated load range
A1C	20	7/22	8.7	2505	13.1	Unknown	0	-2.5	C	85	465 415	Estimated load range
A1C	21	7/22	6.5	2500	12.4	Unknown	0	-2.5	C	85	557 476	Estimated load range
A1C	22	7/22	16.4	2530	32.6	Unknown	0	-2.5	C	88	810 699	Estimated load range
A1C	23	7/22	22.2	2455	28.8	Unknown	0	-2.5	C	86	679 578	Estimated load range
A1C	24	7/22	32.6	2480	20.4	Unknown	0	-2.5	C	87	719 699	Estimated load range
A2C	9	7/19	3	1145	29%	0	0	-2.5	C		504	ECF
A2C	10	7/19	5.8	2110	14.5%	0	0	-2.5	C		645	ECF
A2C	11	7/19	7	2245	7%	0	0	-2.5	C		635	ECF
A2C	12	7/19	17.5	2080	28%	0	0	-2.5	C		617	ECF
A2C	13	7/19	25.1	1985	77%	-	0	-2.5	C		180	ECF
A2C	14	7/19	33.7	2450	57%	0	0	-2.5	C		504	ECF
A3C	6	7/24	4.6	2900	12	Unknown	6	-2.5	C	72	213	Too high response - tracking error
A3C	7	7/24	5.9	3015	12	Unknown	6	-2.5	C	72	281	Too high response - tracking error
A3C	8	7/24	8.0	3110	13	Unknown	6	-2.5	C	72	226	Too high response - tracking error
A3C	9	7/24	14.9	3145	27	Unknown	6	-2.5	C	72	192	Too high response - tracking error
A3C	10	7/24	21.7	3170	25	Unknown	6	-2.5	C	72	185	Too high response - tracking error
A3C	11	7/25	19.6	3120	30	Unknown	6	-2.5	C	72	247	Too high response - tracking error

SCALED RUNWAY TEST DATA

Data Point Number	Test Data		Load Data				Location			Air Temp °F	Response	Comments
	Trace Numbers	Date	Speed	Mean Load	Variation From Mean %	Tracking Error	Y	Z	Pavement Section			
A4C	6	7/24	4.6	2900	12	Unknown	6	-2.5	C	72	182	Estimated tracking
A4C	7	7/24	5.9	3015	12	Unknown	6	-2.5	C	72	247	Estimated tracking
A4C	8	7/24	8.0	3110	13	Unknown	6	-2.5	C	72	198	Estimated tracking
A4C	9	7/24	14.9	3145	27	Unknown	6	-2.5	C	72	136	Estimated tracking
A4C	10	7/24	21.7	3170	25	Unknown	6	-2.5	C	72	156	Estimated tracking
A4C	11	7/25	19.6	3120	30	Unknown	6	-2.5	C	72	191	Estimated tracking
A5C	9	7/19	3	1145	25 -	0	12	-2.5	C		115	Estimated calibration
A5C	10	7/19	5.8	2110	14.5	0	12	-2.5	C		121	
A5C	11	7/19	7	2245	7	0	12	-2.5	C		85	
A5C	12	7/19	17.5	2080	28	0	12	-2.5	C		115	
A5C	13	7/19	25.1	1985	77	-	12	-2.5	C		45	
A5C	14	7/19	33.7	2450	57	0	12	-2.5	C		58	

SCALED RUNWAY TEST DATA

Data Point Number	Test Data		Load Data				Location			Air Temp °F	Response	Comment
	Trace Numbers	Date	Speed	Mean Load	Variation From Mean %	Tracking Error	Y	X	Pavement Section			
A6C	9	7/19	5	11k5	25	0	12	-2.5	C		120	Estimated Calibration
A6C	18	7/22	4.9	2480			12	-2.5	C	85	10	
A6C	10	7/19	5.8	2110	14	0	12	-2.5	C		108	
A6C	11	7/19	7	2245	7	0	12	-2.5	C		160	
A6C	12	7/19	17.5	2080	28	0	12	-2.5	C		120	
A6C	13	7/19	25.1	19.85	77	-	12	-2.5	C		52	
A6C	14	7/19	33.7	2490	57	0	12	-2.5	C		68	
A6C	20	7/22	8.7	2505	13.1	Unknown	12	-2.5	C	85	10	
A6C	21	7/22	6.5	2500	12.4	Unknown	12	-2.5	C	85	10	
A8C	9	7/19	5	11k5	25	0	36	-2.5	C		9.6	ECF
A8C	12	7/19	17.5	2080	28	0	36	-2.5	C		10	ECF
A8C	11	7/19	7	2245	7	0	36	-2.5	C		10	ECF
A8C	14	7/19	33.7	2490	57	0	36	-2.5	C		10	ACF
A10D	27	7/26	4.34	2525	8.5	0	48	-2.5	D	82	16	
A10D	28	7/26	6.3	2595	10.8	2.5 R	48	-2.5	D	82	11	
A10D	32	7/26	22.5	2665	26.8	2 R	48	-2.5	D	84	11	
A10D	33	7/26	37	2665	41	2.5 R	48	-2.5	D	84	11	
A13C	22	7/26	5.9	2635	9.4	2.5 R	48	-2.5	C	74	402	Gage Identity in Error

SCALED RUNWAY TEST DATA

Data Point Number	Test Data		Load Data				Location			Air Temp °F	Response	Comments
	Trace Numbers	Date	Speed	Mean Load	Variation From Mean %	Tracking Error	Y	Z	Pavement Section			
A14C	10	7/19	5.8	2110	14.0	0	0	0	C		42	Estimated gage conversion factor (ECF)
A14C	11	7/19	7.0	2245	7.0	0	0	0	C		46	ECF
A14C	12	7/19	17.5	2080	28.0	0	0	0	C		50	ECF
A14C	13	7/19	25.1	1985	77.0	-	0	0	C		20	ECF
A14C	14	7/19	33.7	2450	57.0	0	0	0	C		20	ECF
A19C	21	7/26	5.5	2195	10.3	0	0	-2.5	C	86	1200	
A19C	22	7/26	5.9	2635	9.4	2.5 R	0	-2.5	C	74	1360	
A19C	23	7/26	8.4	2700	9.7	0	0	-2.5	C	74	1075	
A19C	24	7/26	17.1	2544	23.6	2 R	0	-2.5	C	75	1090	
A19C	25	7/26	22.5	2628	21.1	4 R	0	-2.5	C	75	920	
A19C	26	7/26	35.0	2604	23.0	0	0	-2.5	C	75	737	

SCALED RUNWAY TEST DATA

Data Point Number	Test Data		Load Data				Location			Air Temp °F	Response	Comments
	Trace Numbers	Date	Speed	Mean Load	Variation From Mean %	Tracking Error	Y	Z	Pavement Section			
A25D	27	7/26	4.34	2525	8.3	0	12	0	D	82	63	
A25D	28	7/26	6.3	2595	10.8	2.5 R	12	0	D	82	44	
A25D	29	7/26	8.3	2480	12.1	2 R	12	0	D	82	38	
A25D	31	7/26	16.0	2695	28	2.5 R	12	0	D	82	31	
A25D	32	7/26	22.5	2665	26.8	2 R	12	0	D	84	25	
A25D	33	7/26	37	2665	41	2.5 R	12	0	D	84	31	
A26D	35	7/26	4.43			2 R	0	-2.5	D		227	Questionable load trace
A26D	36	7/26	6			3 R	0	-2.5	D		227	Questionable load trace
A26D	37	7/26	7.64			4 R	0	-2.5	D		218	Questionable load trace
A26D	38	7/26	16.8			4 R	0	-2.5	D		246	Questionable load trace
A26D	39	7/26	26			5.5 R	0	-2.5	D		190	Questionable load trace
A26D	40	7/26	35			-	0	-2.5	D		250	Questionable load trace
A26D	41	7/26	26.3			3 R	0	-2.5	D		161	Questionable load trace

SCALED RUNWAY TEST DATA

Data Point Number	Test Data		Load Data				Location			Air Temp °F	Response	Comments
	Trace Numbers	Date	Speed	Mean Load	Variation From Mean	Tracking Error	Y	Z	Pavement Section			
A26C	35	7/26	4.43			2 R	12	-2.5	C		351	
A26C	36	7/26	6			3 R	12	-2.5	C		162	Questionable response trace
A26C	37	7/26	7.64			4 R	12	-2.5	C		175	Questionable response trace
A26C	38	7/26	16.8			4 R	12	-2.5	C		303	
A26C	39	7/26	26			5.5 R	12	-2.5	C		276	
A26C	40	7/26	35			-	12	-2.5	C		323	
A26C	41	7/26	26.3			3 R	12	-2.5	C		275	
A26D	35	7/26	4.43			2 R	12	-2.5	D		172	Questionable response trace
A26D	36	7/26	6			3 R	12	-2.5	D		114	
A26D	37	7/26	7.64			4 R	12	-2.5	D		148	
A26D	38	7/26	16.8			4 R	12	-2.5	D		146	
A26D	39	7/26	26			5.5 R	12	-2.5	D		67	Possible tracking error
A26D	40	7/26	35			-	12	-2.5	D		148	Questionable response trace
A26D	41	7/26	26.3			3 R	12	-2.5	D		87	

SCALED RUNWAY TEST DATA

Data Point Number	Test Data		Load Data				Location			Air Temp °F	Response	Comments
	Trace Numbers	Date	Speed	Mean Load	Variation From Mean	Tracking Error	Y	Z	Pavement Section			
A29D	35	7/26	4.43			2 R	0	0	D		115	
A29D	36	7/26	6			3 R	0	0	D		77	
A29D	37	7/26	7.64			4 R	0	0	D		96	
A29D	38	7/26	16.8			4 R	0	0	D		86	
A29D	39	7/26	26			5.5 R	0	0	D		38	
A29D	40	7/26	35			-	0	0	D		96	
A29D	41	7/26	26.3			3 R	0	0	D		49	
A30D	35	7/26	4.43			2 R	0	0	D		253	
A30D	36	7/26	6			3 R	0	0	D		214	
A30D	37	7/26	7.64			4 R	0	0	D		224	
A30D	38	7/26	16.8			4 R	0	0	D		224	
A30D	39	7/26	26			5.5 R	0	0	D		95	
A30D	40	7/26	35			-	0	0	D		214	
A30D	41	7/26	26.3			3 R	0	0	D		121	

SCALED RUNWAY TEST DATA

Data Point Number	Test Data		Load Data				Location			Temp °F	Response	Comments
	Trace Numbers	Date	Speed	Mean Load	Variation From Mean %	Tracking Error	Y	Z	Pavement Section			
83	25	7/22	5.2	2450	42	Unknown	6	-1	A	92	32	
83	27	7/22	6	2475	8.3	Unknown	6	-1	A	93	70	
83	28	7/22	5.2	2500	11.3	6 R	6	-1	A	96	38	
83	29	7/22	7.5	2500	13.4	1.5 R	6	-1	A	98	32	
87	1	7/23	7.6	2210	16.6	2 R	24	-1	A	75	37	Wrong gage identification
87	2	7/23	14.6	2185	30.1	2.5 R	24	-1	A	77	32	Wrong gage identification
87	3	7/23	17.5	2070	30.2	2 R	24	-1	A	78	37	Wrong gage identification
87	5	7/23	25.3	1395	45.9	3 R	24	-1	A	76	21	Wrong gage identification
87	6	7/23	36	1850	37.8	6 R	24	-1	A	71	27	Wrong gage identification
13	1	7/23	7.6	2210	16.6	2 R	48	-1/2	A	75	24	Wrong gage identification
13	2	7/23	14.6	2185	30.1	2.5 R	48	-1/2	A	77	18	Wrong gage identification
13	3	7/23	17.5	2070	30.2	2 R	48	-1/2	A	78	12	Wrong gage identification
13	5	7/23	25.3	1395	45.9	3 R	48	-1/2	A	76	12	Wrong gage identification
13	6	7/23	36	1850	37.8	6 R	48	-1/2	A	71	12	Wrong gage identification

SCALED RUNWAY TEST DATA

Pressure Gages - Moving Load

Data Point Number	Test Data		Load Data				Location			Air Temp °F	Response (psi)	Comments
	Trace Numbers	Date	Speed	Mean Load	Variation From Mean $	Tracking Error	Y	Z	Pavement Section			
P4A	25	7/22	5.2	2450	4.2	Uneven	0	4	A	92	.30	Possible PSA gage
P4A	27	7/22	6	2475	8.3	6 R	0	4	A	93	.24	Possible PSA gage
P4A	28	7/22	5.2	2500	11.3	6 R	0	4	A	96	.36	Possible PSA gage
P4A	29	7/22	7.5	2500	13.4	1.5 R	0	4	A	98	.32	Possible PSA gage
P4A	1	7/23	7.6	2210	16.6	2 R	0	4	A	75	.43	
P4A	2	7/23	14.6	2185	30.1	2.5 R	0	4	A	77	.43	
P4A	3	7/23	17.5	2070	38.2	2 R	0	4	A	78	.52	
P4A	5	7/23	25.3	1395	45.9	3 R	0	4	A	76	.21	
P4A	6	7/23	36	1880	37.8	6 R	0	4	A	71	.49	
P4C	21	7/26	5.5	2195	18.3	0	0	5.5	C	86	6.1	
P4C	22	7/26	5.9	2695	9.4	2.5 R	0	5.5	C	74	3.47	
P4C	23	7/26	8.4	2700	9.7	0	0	5.5	C	74	2.86	
P4C	24	7/26	17.1	2564	23.6	2 R	0	5.5	C	75	3.33	
P4C	25	7/26	22.5	2628	21.1	4 R	0	5.5	C	75	2.27	
P4C	26	7/26	35	2604	25	4 R	0	5.5	C	75	2.62	

SCALED RUNWAY TEST DATA

Data Point Number	Test Data		Load Data				Location			Temp °F	Response (psi)	Comments
	Trace Numbers	Date	Speed	Mean Load	Variation From Mean %	Tracking Error	Y	Z	Pavement Section			
P4D	6	7/24	4.6	2900	12	Unknown	0	5.5	D	72	2.96	Questionable response
P4D	7	7/24	5.9	3015	12	Unknown	0	5.5	D	72	1.80	
P4D	9	7/24	14.9	3145	27	Unknown	0	5.5	D	72	1.95	
P4D	10	7/24	21.7	3170	25	Unknown	0	5.5	D	72	1.80	
P4D	11	7/25	19.6	3120	30	Unknown	0	5.5	D	72	2.91	
P4D	35	7/26	4.43	Unknown		2 R	0	5.5	D		5.85	
P4D	36	7/26	6.0	Unknown		3 R	0	5.5	D		2.24	
P4D	37	7/26	7.64	Unknown		4 R	0	5.5	D		2.44	
P4D	38	7/26	16.8	Unknown		4 R	0	5.5	D		3.16	
P4D	39	7/26	26	Unknown		5.5 R	0	5.5	D		1.15	Questionable response
P4D	40	7/26	35	Unknown		-	0	5.5	D		2.54	
P4D	41	7/26	26.3	Unknown		3 R	0	5.5	D		.90	Questionable response
P4D	27	7/25	4.3	2525	8.3	0	0	5.5	D	82	4.81	
P4D	28	7/26	6.3	2595	10.8	2.5 R	0	5.5	D	82	3.38	
P4D	29	7/26	8.3	2480	12.1	2 R	0	5.5	D	82	3.54	
P4D	31	7/26	16.0	2695	28	2.5 R	0	5.5	D	82	1.43	
P4D	32	7/26	22.5	2665	28.6	2 R	0	5.5	D	84	1.65	Questionable speed
P4D	33	7/26	37	2665	42	2.5 R	0	5.5	D	84	3.36	Questionable speed

SCALED RUNWAY TEST DATA

Data Point Number	Test Data		Load Data				Location			Temp °F	Response (mil)	Comments
	Trace Numbers	Date	Speed	Mean Load	Variation From Mean $	Tracking Error	Y	Z	Pavement Section			
P5A	25	7/22	5.2	2490	42	Unknown	0	11	A	92	1.05	Possibly P4A
P5A	27	7/22	6	2475	8.3	6 R	0	11	A	95	.91	Possibly P4A
P5A	28	7/22	5.2	2580	11.3	6 R	0	11	A	96	1.06	Possibly P4A
P5A	29	7/22	7.5	2580	13.4	1.5 R	0	11	A	98	1.14	Possibly P4A
P5A	1	7/23	7.6	2210	16.6	2 R	0	11	A	75	1.28	
P5A	2	7/23	14.6	2185	30.1	2.5 R	0	11	A	77	1.33	
P5A	3	7/23	17.5	2070	30.2	2 R	0	11	A	78	.78	
P5A	5	7/23	25.3	1395	45.9	3 R	0	11	A	76	1.50	
P5A	6	7/23	36	1850	37.8	6 R	0	11	A	71	.43	
P5C	6	7/24	4.6	2980	12	Unknown	0	12.5	C	72	2.85	
P5C	7	7/24	5.9	3015	12	Unknown	0	12.5	C	72	3.80	
P5C	8	7/24	8.0	3130	13	Unknown	0	12.5	C	72	3.19	
P5C	9	7/24	14.9	3145	27	Unknown	0	12.5	C	72	2.66	
P5C	10	7/24	21.7	3170	25	Unknown	0	12.5	C	72	2.83	
P5C	11	7/25	19.6	3120	30	Unknown	0	12.5	C	72	3.41	

SCALED RUNWAY TEST DATA

Data Point Number	Test Data		Load Data				Location			Air Temp °F	Response (psi)	Comments
	Trace Numbers	Date	Speed	Mean Load	Variation From Mean %	Tracking Error	Y	Z	Pavement Section			
P2A	12	7/19	17.5	2080	28	4 L	31	2	A		.17	
P2A	10	7/19	5.8	2110	14	4 L	31	2	A		.14	
P2A	11	7/19	7	2245	7	0	31	2	A		.07	
P2A	13	7/19	25.1	1985	77	4 L	31	2	A		.07	

SCALED RUNWAY TEST DATA

Static Tests

Data Point Number	Test Data		Load Data				Location			Air Temp °F	Response	Comments
	Trace Numbers	Date	Speed	Mean Load	Variation From Mean %	Tracking Error	Y	Z	Pavement Section			
A1C	5	7/19	Static Test	1560 2610	9.6 11.8		0	-2.5	C		48	
A2C	5	7/19	Static Test	1560 2610	9.6 11.8		0	-2.5	C		48	ECF
A5C	5	7/19	Static Test	1560 2610	9.6 11.8		12	-2.5	C		48	ECF
A1D	6	7/19	Static Test	1550 2600	-		0	-2.5	D		297 670	ECF Estimated Load
A2D	6	7/19	Static Test	1550 2600	-		0	-2.5	D		395 498	ECF Estimated Load
A5D	6	7/19	Static Test	1550 2600	-		12	-2.5	D		128 177	ECF Estimated Load
F1A	2	7/19	Static Test	1440 2450	10.9 12.5		0	5.5	A		-	Load trace questionable
S1	2	7/19	Static Test	1440 2450	10.9 12.5		0	-1	A		1.3 56	ECF
S2	2	7/19	Stat.c Test	1440 2450	10.9 12.5		0	-1	A		103 55 56	
A2C	8	7/19	Static Test	-	-		0	-2.5	C		- 121	No load trace Response patterns questionable

5. IMPACT TEST EQUATIONS

The drop test rig is a weight W and a spring k released from a given height h

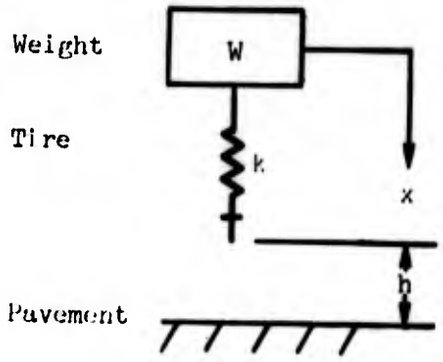

where

$W = mg$

x = weight displacement

The equation for this system is

$$m\ddot{x} + kx = mg \qquad (5\text{-}1)$$

Its solution (and derivatives) are

$$x = A \sin \omega t + B \cos \omega t + \frac{mg}{k} \qquad (5\text{-}2)$$

$$\dot{x} = A\omega \cos \omega t - B\omega \sin \omega t \qquad (5\text{-}3)$$

$$\ddot{x} = A\omega^2 \sin \omega t - B\omega^2 \cos \omega t \qquad (5\text{-}4)$$

where

ω = natural frequency $= \sqrt{\frac{k}{m}}$

The initial conditions for the test (taken at the point of impact) are

$$x_o = 0 \; ; \; \dot{x}_o = \sqrt{2gh} \quad @ \; t = 0 \tag{5-5}$$

which imply

$$B = -\frac{mg}{k} = -\frac{W}{k} \tag{5-6}$$

$$A = \sqrt{2gh}\sqrt{\frac{m}{k}} = \sqrt{\frac{2Wh}{k}} \tag{5-7}$$

So complete solution is

$$x = \sqrt{\frac{2Wh}{k}} \sin \omega t - \frac{W}{k} \cos \omega t + \frac{W}{k} \tag{5-8}$$

and force delivered to pavement is

$$F = kx = \sqrt{2Whk} \sin \omega t - W \cos \omega t + W \tag{5-9}$$

or

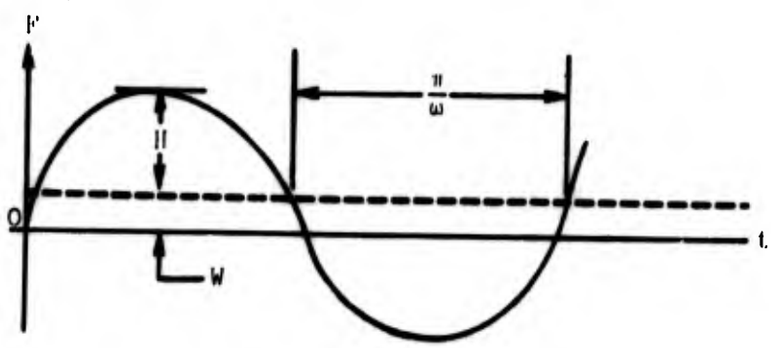

where

$$H^2 = 2\,Whk + W^2 \text{ and } \frac{\pi}{\omega} = \text{half period} \tag{5-10}$$

Now H and W are not arbitrary but are constrained by three equations:

$H > W$ (The larger H is greater than W the closer the force time history is approximately a sine wave.) (5-11)

and

$H + W < B$ (where B = bottoming load of tire since tire cannot bottom) (5-12)

$W > W\ min$ (where W_{min} = min possible drop weight) (5-13)

and the drop height is found from Equation (5-10)

$$H^2 = 2Whk + W^2 \tag{5-14}$$

with

$$H = nW; \quad n > 1$$

$$h = \frac{(n^2 - 1)\ W}{2k} \tag{5-15}$$

6. MOVING LOAD TEST VELOCITY - IMPACT TEST LOAD PULSE FREQUENCY RELATIONSHIP

A concentrated load moving at velocity V has an influence on a stationary point which can be approximated by a sinusoidal load acting at the stationary point.

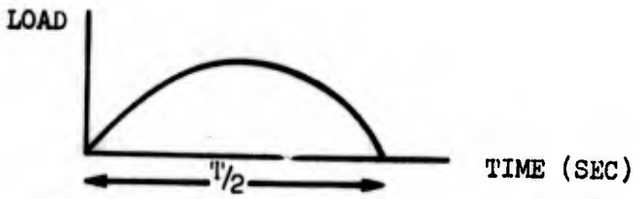

where T is the period of the sinusoidal load and is equal to

$$T = \frac{L}{V} \frac{1}{\pi} \left(\frac{\text{sec}}{\text{rad}}\right)$$

where L/2 is the distance from the stationary point at which the moving load begins to influence the point, and it depends on the characteristics of the particular pavement system

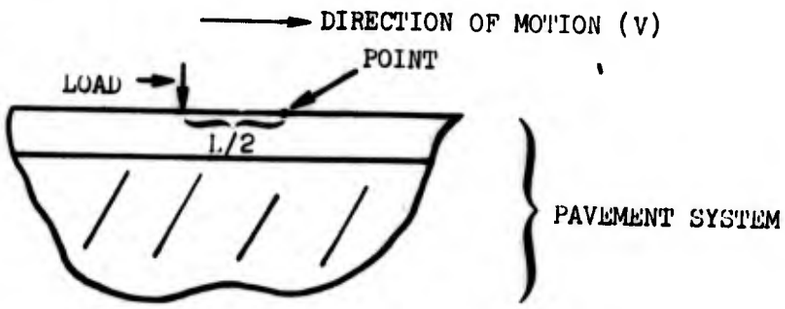

Since $T = \frac{1}{2\pi f}$ where f is the frequency of the sinusoidal load in cycles per second, the relation between f and V is

$$v = 2\,Lf\ (\text{in/sec})$$

If v is in miles/hour, in/sec x .057 = mi/hr.

$$v = 0.11\tfrac{1}{4}\,fL$$

For the scaled runway test L ≅ 72 inches, so an impact test frequency of about 4.3 Hz corresponds to a velocity of

$$v \cong 37 \text{ mph}$$

APPENDIX C

LABORATORY TESTS

TABLE OF CONTENTS

LIST OF ILLUSTRATIONS

LIST OF TABLES

1. TEST PROGRAM

Sample 1 (Moisture content 20%, Dry Density 107.9 lbs/ft^3)

Repeated load test for the determination of M_R at three stress levels (σ_d = 6, 8 and 10 psi) and three frequencies (1,3,5 cps). After the repeated load test had been conducted, the sample was subjected to a conventional unconfined compression test with loading and unloading to determine the 'static' stress-strain curve and the area of the hysteresis loop.

Sample 2 (Moisture content 30%, Dry Density 91.2 lbs/ft^3)

Repeated load test for M_R at one stress level (σ_d = 3 psi) and three frequencies (1,3,5 cps). After the repeated load tests had been conducted, the sample was subjected to a conventional unconfined test with loading and unloading to determine the static stress-strain curve and the area of the hysteresis loop. It was originally planned to test this sample at higher stress levels, but the response of the sample indicated that failure might be induced at the higher stress levels.

2. COMMENTS ON TEST PROGRAM

Because of time and budget limitations it was necessary to conduct the tests on one sample at each moisture content and dry density. To obtain reliable results, it is advisable to conduct more than one test for each soil condition to eliminate possible errors intests and inconsistencies in the sample. Furthermore it would have been desirable to conduct the unconfined tests on untested specimens.

3. COMMENTS ON TEST RESULTS

The test results are presented in Table C-1 and Figures C-1 to C-7. In general the test results appear reasonable. There are some minor inconsistencies which may be a result of peculiarities in the particular sample tested. Certain significant aspects of the test results are summarized below.

1. The M_R values for Sample 2 are approximately 50% of Sample 1. This is consistent with the difference in CBR values.

2. For Sample 1 there is no significant change in M_R with stress level between 6 and 8 psi but the M_R decreases with an increase in stress level to 10 psi. The decrease in M_R is consistent with published data.

3. For Sample 1 the effects of frequency on M_R do not agree entirely with published data. The effect of frequency for a change from 3 to 5 cps causes an increase in M_R. This is consistent with available information. However the decrease in M_R with a frequency change from 1 to 3 cps is at variance with published experimental data.

4. The effects of frequency on M_R for Sample 2 are consistent with published information.

5. The 'modulus' as determined from the static tests is approximately 25% of the M_R value.

6. Hysteresis loops from dynamic and static tests can be used to determine equivalent viscous damping. For a method to compute damping see the paper by L. S. Jacobsen "Damping in Composite Structures" Proc. Second World Conference on Earthquake Engineering, 1960.

TABLE C-1 Results of Repeated Load Tests

SAMPLE 1 Moisture Content 20%, Dry Density = 107.9, corresponds to a CBR-10.0

Modulus of Resilience (psi)	σ_d(psi)	Frequency (cps)
10,260	6	1
10,400	8	1
8,600	10	1
8,219	6	3
8,600	8	3
8,000	10	3
9,092	6	5
9,302	8	5
8,000	10	5

SAMPLE 2 Moisture Content 30%, Dry Denisty = 91.2, corresponds to a CBR = 2.0

Modulus of Resilience (psi)	σ_d(psi)	Frequency (cps)
3,614	3	1
4,228	3	3
5,130	3	5

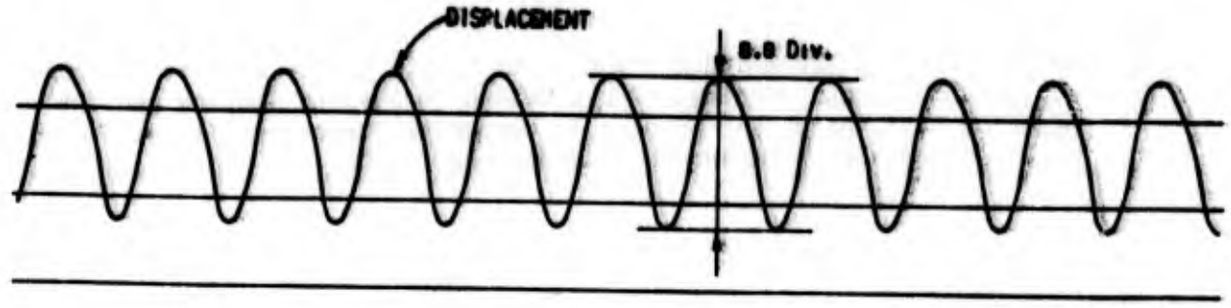

1 Div. = .0003"

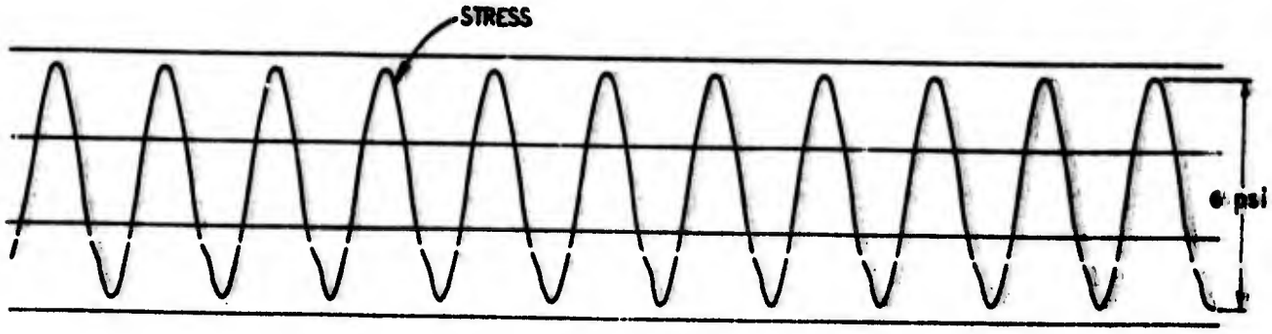

$\sigma_d = \sigma_1 - \sigma_3 = 6$ psi, FREQUENCY = 3 cps

MOISTURE CONTENT = 20%
DRY DENSITY = 107.9 LBS/CU. FT. } ← CORRESPONDS TO A CBR = 10.0
HEIGHT OF SAMPLE = 6.00"

Figure C-1 Stress and Strain Output from Dynamic Tests

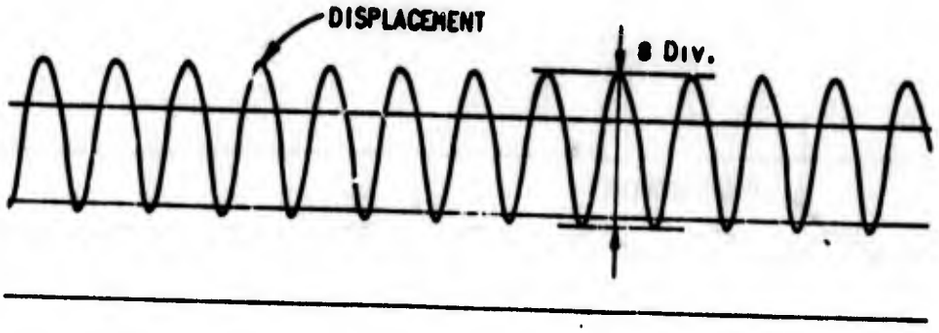

1 Div. = .0005"

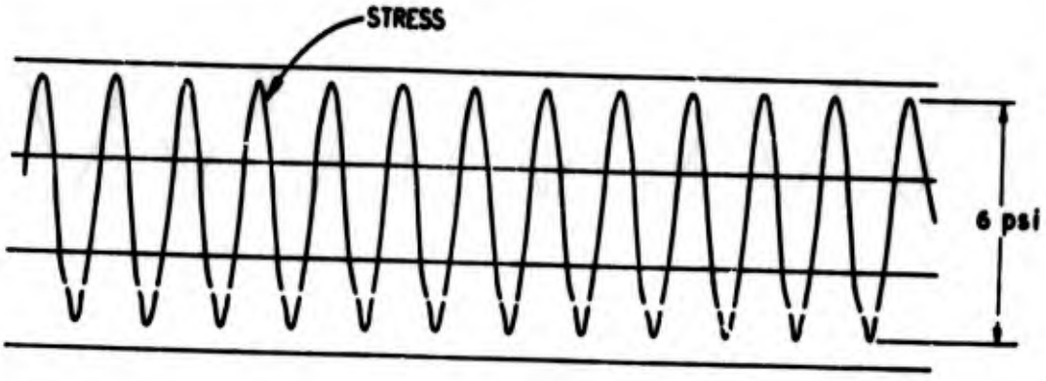

$\sigma_d = \sigma_1 - \sigma_3 = 6$ psi, FREQUENCY = 5 cps

MOISTURE CONTENT = 20%
DRY DENSITY = 107.9 LBS/CU. FT. } ← CORRESPONDS TO A CBR = 10.0
HEIGHT OF SAMPLE = 6.00"

Figure C-2 Stress and Strain Output from Dynamic Tests

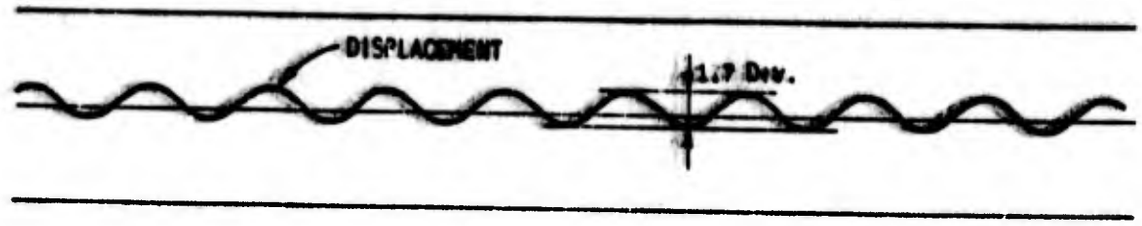

1 Div. = .0025"

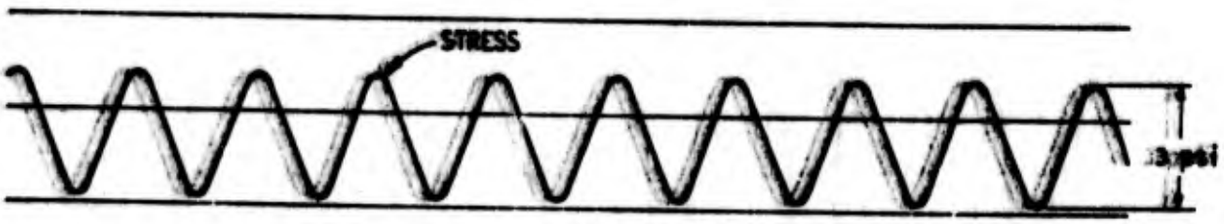

$\sigma_d = \sigma_1 - \sigma_3$ = 3 psi, FREQUENCY = 3 cps

MOISTURE CONTENT = 10%
DRY DENSITY = 91.2 lbs/cu. ft. } ← CORRESPONDS TO A CBR = 2.0
HEIGHT OF SAMPLE = 6.00"

Figure C-3 Stress and Strain Output from Dynamic Tests

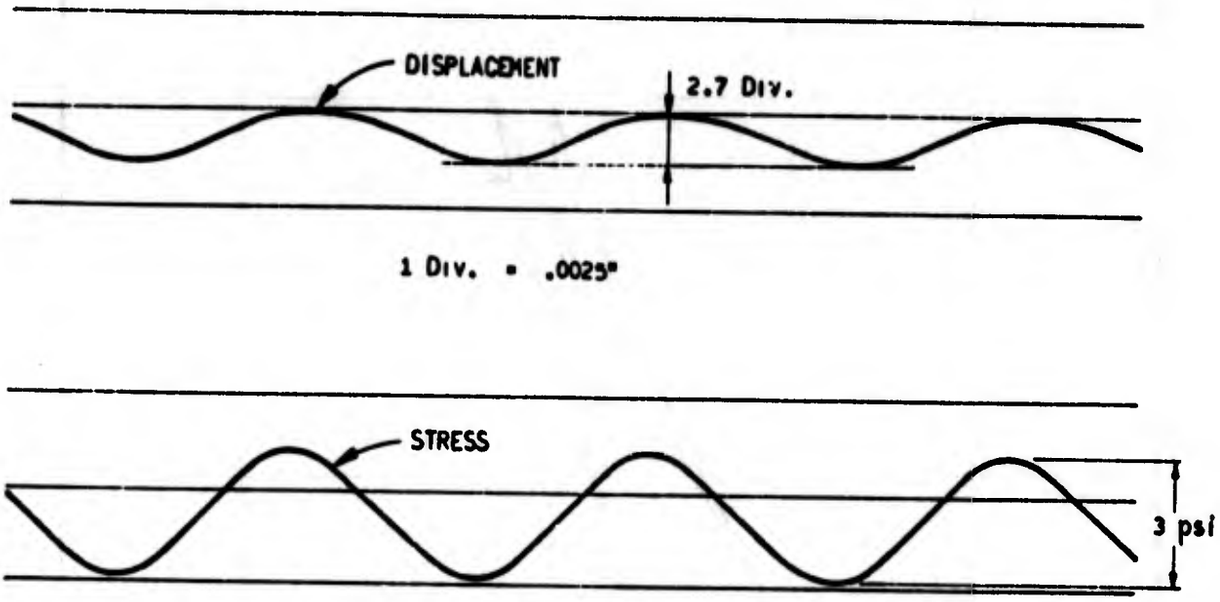

$\sigma_d = \sigma_1 - \sigma_3 = 3$ psi, FREQUENCY = 1 cps

MOISTURE CONTENT = 30%
DRY DENSITY = 91.2 LBS/CU. FT. } ← CORRESPONDS TO A CBR = 2.0
HEIGHT OF SAMPLE = 6.00"

Figure C-4 Stress and Strain Output from Dynamic Tests

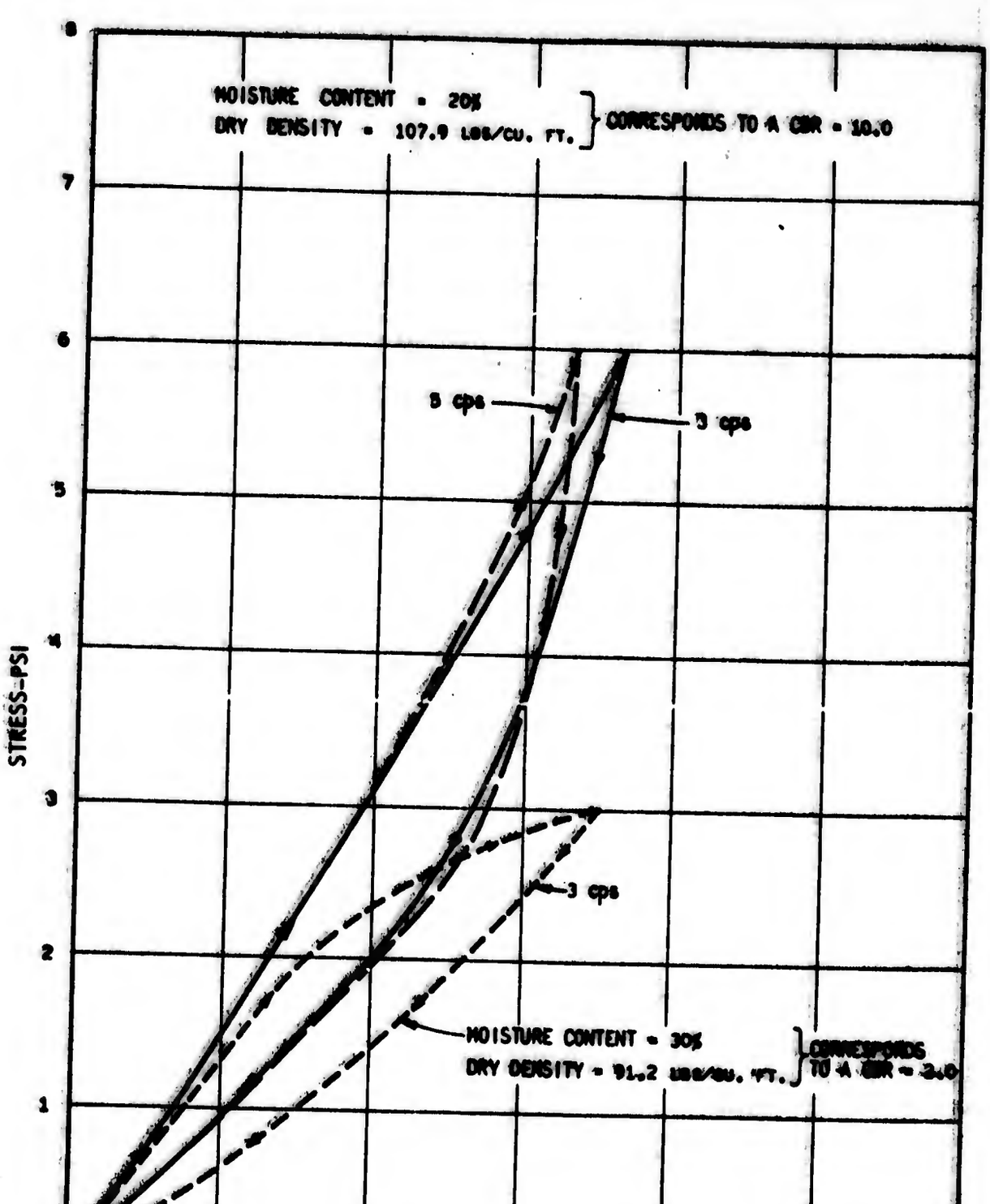

Figure C-5 Loading and Unloading Curve for Resilient Strain Repeated Load Test

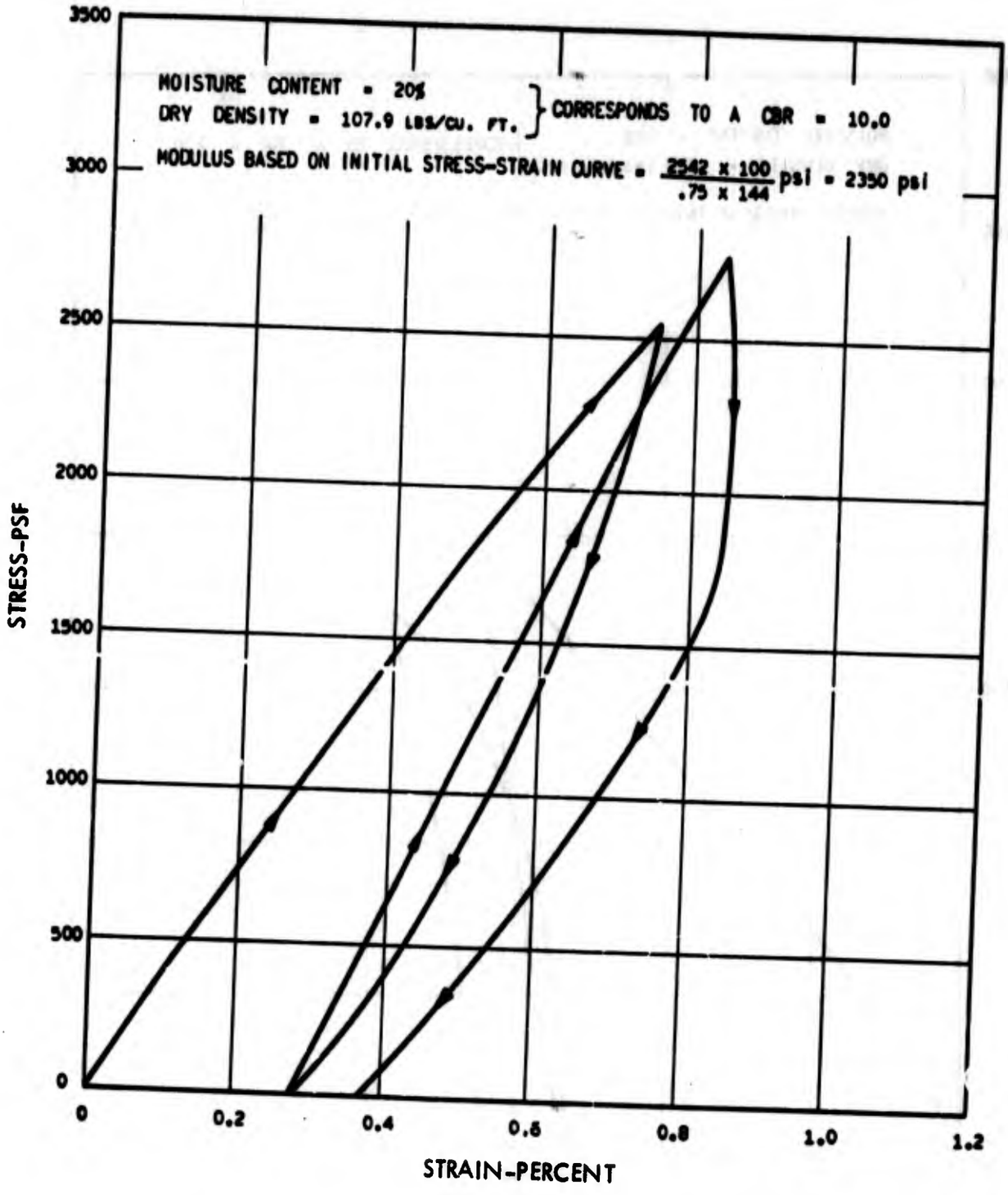

Figure C-6 Unconfined Compression Test

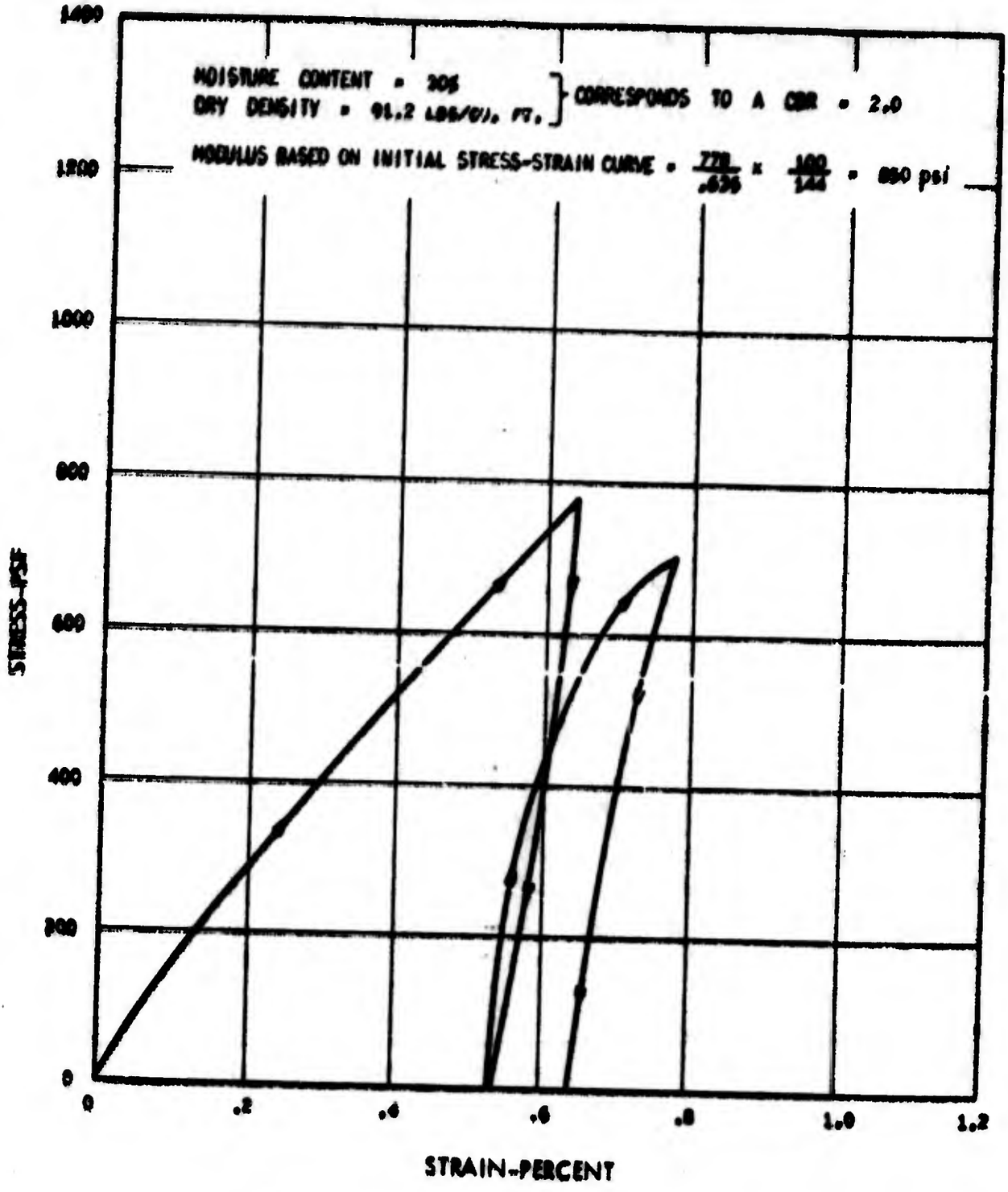

Figure C-7 Unconfined Compression Test

APPENDIX D

METHODS USED IN AIRPLANE ANALYSIS

TABLE OF CONTENTS

1. DERIVATION OF EXPRESSION FOR GEAR INCREMENTAL LOAD FACTOR DUE TO RUNWAY ROUGHNESS

For a given runway bump, the incremental gear load factor due to runway roughness can be assumed to vary linearly with the ratio of effective gear stiffness to airplane weight. This reflects the fact that the incremental gear load will vary approximately linearly with effective gear stiffness, and that dividing by airplane gross weight converts to an incremental load factor form. Therefore, $\Delta n_{g\ \text{roughness}}(V)$ can be expressed in the form

$$\Delta n_{g\ \text{roughness}}(V) = C\,\frac{K_e(V)}{W} \qquad (1\text{-}1)$$

where

$K_e(V)$ = effective main gear stiffness, tires and oleo in series @ V

W = maximum airplane takeoff gross weight

C = constant proportional to bump height or runway roughness.

$K_e(V)$ is a function of velocity due to the effects of aerodynamics on strut position and hence oleo stiffness. It can also be shown that the steady-state acceleration response of a single degree-of-freedom oscillator at resonance is proportional to the square of the natural frequency, in agreement with the above equation.

However, the airplane does not experience constant bump amplitude at all velocities. The airplane will tend to respond to the roughness components at wavelengths corresponding to the airplane's natural plunge frequency. At high velocities, the airplane will "see" the longer wavelength roughness, and respond at resonance to this roughness. The runway roughness increases with wavelength, as may readily be seen from any runway power spectral density plot such as Figure 23. Therefore, the airplane will respond to rougher bumps at high speeds than at low speeds. This indicates that C in Equation (1-1) should not be a constant but a function of wavelength. If it is further assumed that the power spectral density of runway roughness varies inversely with the square of the reduced frequency Ω ($\Omega = \frac{2\pi}{L}$, L = wavelength), a reasonable approximation for most runway PSD's, then

$$\phi \propto \frac{1}{\Omega^2} \propto L^2$$

$$\sqrt{\phi} \propto L$$

Since the power spectral density ϕ is proportional to the runway roughness squared, $\sqrt{\phi}$ is proportional to the runway roughness. Therefore, C in Equation (1-1)could be replaced with

$$C = C'L \tag{1-2}$$

where C' is a direct measure of the runway roughness and Equation (1-2)shows its variation with wavelength.

Furthermore, the velocity, plunge natural frequency, and resonant bump wavelength are related by

$$V = f_n L \tag{1-3}$$

Combining (1-1), (1-2) and (1-3) we have

$$\Delta n_{g\ \text{roughness}}(V) = C' \frac{V}{f_n(v)} \cdot \frac{K_e(V)}{W} \tag{1-4}$$

But $f_n(v)^2 \alpha K_e(V)/W$, ignoring the nose gear's contribution to the plunge mode natural frequency, so that the above equation finally becomes

$$\Delta n_{g\ \text{roughness}}(V) = C'' V f_n(V) \tag{1-5}$$

where

C'' = constant proportional to level of runway roughness

V = airplane velocity (knots)

$f_n(V)$ = airplane plunge natural frequency (cps), ignoring contribution of nose gear stiffness

$f_n(V)$ is a function of velocity for the same reason that Ke(V) is.

The total load factor is given by

$$F_{TOT}(V)/F_{ST} = 1 + \Delta n_{g_a}(V) + C''Vf_n(V) \qquad (1\text{-}6)$$

where $\Delta n_{g_a}(V)$ is the incremental load factor due to aerodynamic lift on a smooth runway.

The natural frequency as a function of velocity can be expressed as

$$f_n(V) = f_{n_o}\sqrt{\frac{K_e(V)}{K_{e_o}}} \qquad (1\text{-}7)$$

where

f_{n_o} = natural frequency at V = 0

K_{e_o} = effective main gear stiffness at V = 0

It can also be shown that the ratio of effective gear stiffnesses is given by

$$\frac{K_e(V)}{K_{e_o}} = \left(\frac{F(V)}{F_{ST}}\right)^2 \frac{1 + K_T/K_{G_o}}{\left(\frac{F(V)}{F_{ST}}\right)^2 + \frac{K_T}{K_{G_o}}} \qquad (1\text{-}8)$$

where

F(V) = total gear force at velocity V, smooth runway

K_T = linear tire stiffness, combining all tires on one gear in parallel

K_{G_o} = linear gear stiffness at V = 0, slope of air load stroke curve at static position

By definition we have

$$\frac{F(V)}{F_{ST}} = 1 + \Delta n_{g_a} \qquad (1\text{-}9)$$

Combining Equations (1-6) through (1-9), we obtain

$$\frac{F_{TOT}}{F_{ST}} = \left[1 + \Delta n_{g_a}\right] \left\{ 1 + C'' V f_{n_o} \left[\frac{1 + K_T/K_{G_o}}{(1 + \Delta n_{g_a})^2 + K_T/K_{G_o}} \right]^{1/2} \right\} \qquad (1\text{-}10)$$

Furthermore, if the effect of thrust is negligible, and if the airplane pitch attitude is nearly constant during the takeoff roll, then Δn_{g_A} is given approximately by

$$\Delta n_{g_A} = - \bar{L}_{100} \left(\frac{V}{100}\right)^2 \qquad (1\text{-}11)$$

where

$$\bar{L}_{100} = \frac{\text{(total airplane aerodynamic lift at V = 100 knots)}}{\text{Maximum takeoff gross weight}}$$

V = airplane velocity in knots

$\bar{L}_{100}$ is positive for airplanes developing positive lift. Combining (1-10) and (1-11), we finally obtain

$$\frac{F_{TOT}}{F_{ST}} = \left[1 - \bar{L}_{100}\left(\frac{V}{100}\right)^2\right] \left\{ 1 + C''V f_{n_o} \left[\frac{1 + K_T/K_{G_o}}{\left(1 - \bar{L}_{100}\left(\frac{V}{100}\right)^2\right)^2 + K_T/K_{G_o}} \right]^{1/2} \right\} \qquad (1\text{-}12)$$

This is given as Equation (6) on page 91 .

2. DERIVATION OF EXPRESSION FOR NOSE GEAR LOAD FACTOR FROM DYNAMIC BRAKING

Assume the airplane is initially in a steady-state balance under the influence of aerodynamic lift and pitching moment, and lift and pitching moment due to thrust (forward or reverse). Then assume the brakes are suddenly applied giving the following nose gear vertical force time history:

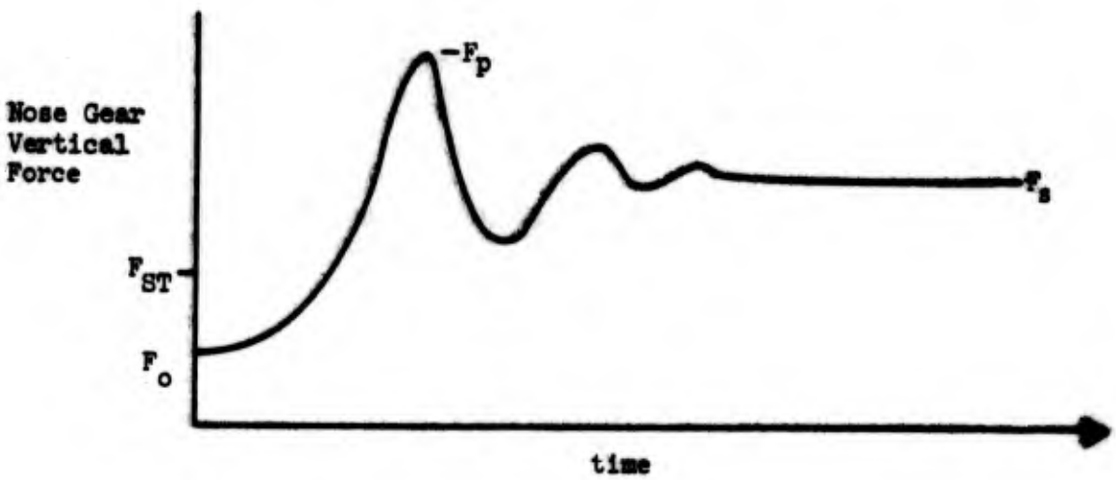

F_{ST} is the static, zero thrust, nose gear load at the given c.g.

F_o is different from F_{ST} due to the influence of aerodynamics and thrust.

F_p is the peak dynamic value reached, due to dynamic wheel braking.

F_S is the final steady-state value reached including steady braking.

Assume the braking time history looks like:

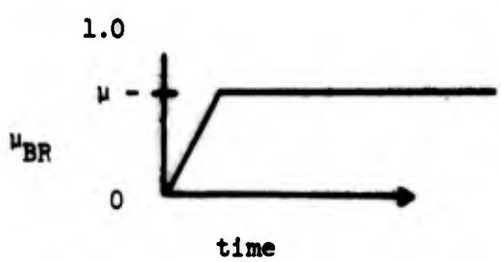

It is assumed that any spoilers, elevator, or reverse thrust application yields a static response, i.e., no overshoot due to rapid application such as exists for wheel braking. What is desired are expressions for F_p and F_S as a function of μ (braking coefficient) and V (airplane velocity). These are to be normalized to the maximum nose gear static load, zero thrust, at the same gross weight, maximum forward c.g. This is denoted F_{ST_M}.

Assume that the dynamic amplification due to braking is accounted for by a dynamic overshoot factor, D, defined as

$$D \triangleq \frac{F_p - F_o}{F_S - F_o} \geq 1.0 \qquad (2\text{-}1)$$

so that

$$F_p = D(F_S - F_o) + F_o = DF_S - (D-1)\,F_o$$

and

$$\frac{F_p}{F_{ST_M}} = D\frac{F_s}{F_{ST_M}} - (D-1)\frac{F_o}{F_{ST_M}} \qquad (2\text{-}2)$$

F_s is merely the nose gear load under the influence of steady braking, aero, and thrust. F_o is the same thing with 0 braking.

The following sketch shows the forces and moments acting on the airplane:

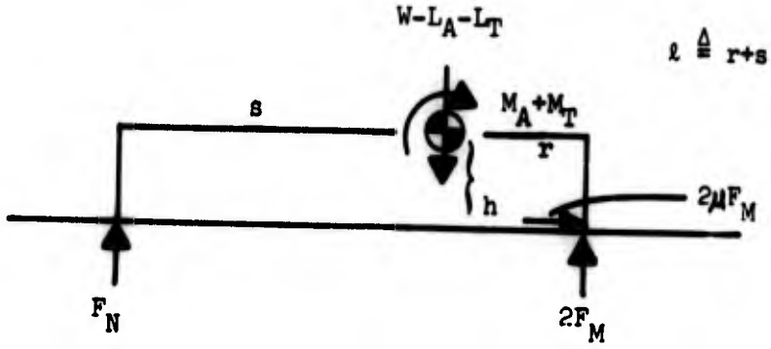

where

L_A = aero lift L_T = thrust lift + 1

M_A = aero moment M_T = thrust moment + C

function of velocity constant

Summation of vertical forces yields

$$F_N + 2F_M = W - L_A - L_T \qquad \text{or} \qquad F_M = \frac{W - L_A - L_T - F_N}{2}$$

Summation of moments yields

$$sF_N - 2rF_M - 2h\mu F_M = -M_A - M_T$$

so

$$sF_N - 2(r+\mu h)\frac{(W - L_A - L_T - F_N)}{2} = -M_A - M_T$$

$$F_N (s + r + \mu h) = -M_A - M_T + (r + \mu h)(W - L_A - L_T)$$

$$F_N = \frac{(W - L_A - L_T)(r + \mu h) - M_A - M_T}{\ell + \mu h} \qquad (2\text{-}3)$$

This is equal to the desired F_s. F_o is the same at $\mu = 0$ F_{ST_M} is the same with $L_A = L_T = M_A = M_T = \mu = 0$ and $r = r_{MAX}$. So

$$F_o = \frac{(W - L_A - L_T)\, r - M_A - M_T}{\ell} \qquad (2\text{-}4)$$

$$F_{ST_M} = \frac{W r_{MAX}}{\ell}$$

Combining (2-2), (2-3) and 2-4) we get

$$\frac{F_p}{F_{ST_M}} = \frac{D\ell}{Wr_{MAX}}\left[\frac{(W-L_A-L_T)\ (r+\mu h) - M_A-M_T}{\ell+\mu h}\right] - \frac{(D-1)\ \ell}{Wr_{MAX}}\left[\frac{(W-L_A-L_T)\ r - M_A-M_T}{\ell}\right]$$

Defining

$$\bar{L}_A \triangleq \frac{L_A}{W};\quad \bar{M}_A = \frac{M_A}{W};\quad \bar{L}_T = \frac{L_T}{W};\quad \bar{M}_T = \frac{M_T}{W}$$

we get

$$\frac{F_p}{F_{ST_M}} = \frac{D\ell}{r_{MAX}}\left[\frac{(1-\bar{L}_A-\bar{L}_T)\ (r+\mu h) - \bar{M}_A-\bar{M}_T}{\ell+\mu h}\right] - \frac{(D-1)\ \ell}{r_{MAX}}\left[\frac{(1-\bar{L}_A-\bar{L}_T)\ r-\bar{M}_A-\bar{M}_T}{\ell}\right]$$

and

$$\frac{F_p}{F_{ST_M}} = \frac{D}{\bar{r}_M}\left[\frac{(1-\bar{L}_A-\bar{L}_T)\ (\bar{r}+\mu\bar{h}) - \bar{M}_A/\ell - \bar{M}_T/\ell}{1+\mu\bar{h}}\right]$$

$$-\frac{(D-1)}{\bar{r}_M}\left[\frac{(1-\bar{L}_A-\bar{L}_T)\ \bar{r} - \bar{M}_A/\ell - \bar{M}_T/\ell}{1}\right]$$

where

$$\bar{r} \triangleq r/\ell\ ;\quad \bar{r}_M \triangleq r_{MAX}/\ell;\quad \bar{h} \triangleq h/\ell\ ;\quad \bar{L}_A(V) = \bar{L}_{A_{100}}\left(\frac{V}{100}\right)^2$$

and $\bar{M}_A(V) = \bar{M}_{A_{100}}\left(\frac{V}{100}\right)^2$

Furthermore, assume

$$\bar{M}_A = \bar{L}_A \bar{c} \frac{C_M}{C_L} \text{ and } \bar{M}_T = \frac{M_T}{W} = m\left(\frac{T}{W}\right) = \bar{m}\bar{T}$$

Defining

$$\frac{\bar{c}}{\ell} \triangleq \bar{c}' \text{ and } \frac{m}{\ell} \triangleq \bar{m},$$

we finally have

$$\frac{F_p}{F_{ST_M}} = \frac{D}{\bar{r}_M}\left[\frac{(1-\bar{L}_A-\bar{L}_T)(\bar{r}+\mu\bar{h}) - \bar{c}'\frac{C_M}{C_L}\bar{L}_A - \bar{m}\bar{T}}{1+\mu\bar{h}}\right] \tag{2-5}$$

$$-\frac{(D-1)}{\bar{r}_M}\left[\frac{(1-\bar{L}_A-\bar{L}_T)\bar{r} - \bar{c}'\frac{C_M}{C_L}\bar{L}_A - \bar{m}\bar{T}}{1}\right]$$

where

$\bar{r}_M = r_{MAX}/\ell$ constant

$\bar{r} = r/\ell = \frac{r}{r_{MAX}} \cdot \bar{r}_M$ function of c.g. position

$\bar{h} = h/\ell$ constant

$\bar{c}' = \bar{c}/\ell$ constant

$\bar{m} = m/\ell$ constant where $M_T = mT$

$\bar{L}_A = \bar{L}_{A_{100}} \left(\frac{V}{100}\right)^2$ function of V $\bar{L}_A = \frac{\text{Lift}}{W}$

$\bar{L}_T$ = $\frac{\text{thrust "lift"}}{W}$ = $\gamma \bar{T}$ where $L_T = \gamma T$

$\frac{C_M}{C_L}$ = function of α, δ_e, spoilers - constant for given case

$\bar{T}$ = $\frac{\text{thrust}}{W}$

D = dynamic amplification factor $\triangleq \frac{F_p - F_o}{F_S - F_o}$

μ = braking coefficient

This is Equation 7 on page 103.

3. SIMPLIFIED MODEL OF FIVE-GEAR AIRPLANE USED FOR TAKEOFF ROTATION ANALYSES

Takeoff rotation analyses of airplanes C-1 and C-2 were performed with a relatively simple digital computer program. This program models the airplane with three degrees of freedom; pitch, plunge and main gear load equalizer motion. The model is shown below:

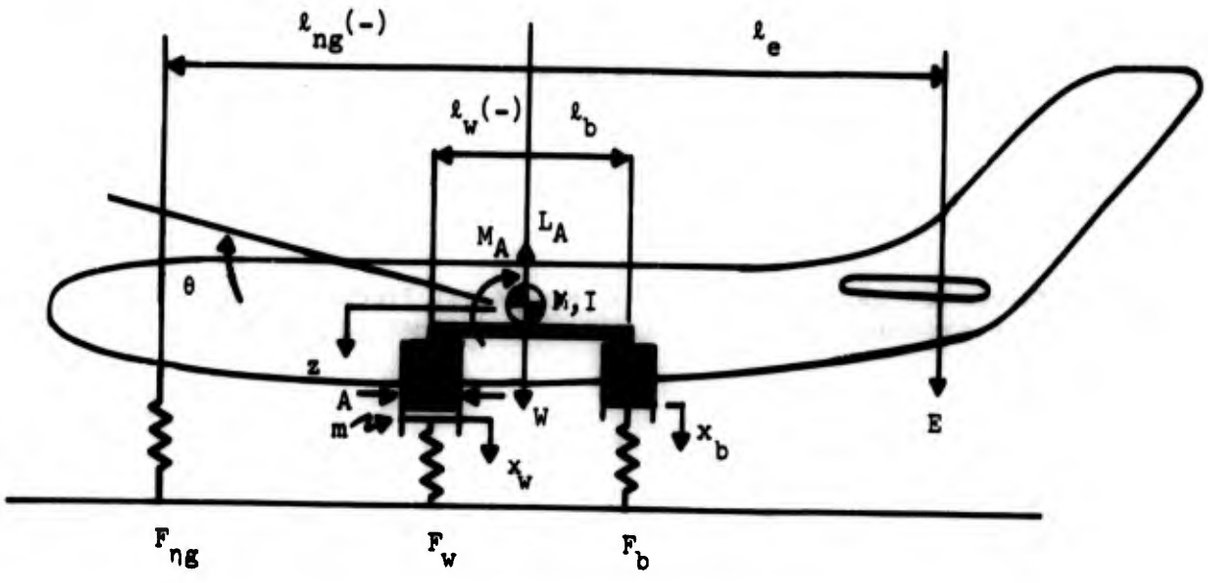

The three degrees of freedom are θ, z and x_b. The airplane plunge and pitch mode equations of motion are

$$\frac{W}{g}\ddot{z} = W + E - L_A - F_{ng} - Ap_w - Ap_b \qquad (3\text{-}1)$$

and

$$I\ddot{\theta} = M_A + E\,\ell_e - F_{ng}\,\ell_{ng} - Ap_w\,\ell_w - Ap_b\,\ell_b \qquad (3\text{-}2)$$

The equalizer equations of motion are

$$m\ddot{x}_w = Ap_w - F_w \qquad (3\text{-}3)$$

$$m\ddot{x}_b = Ap_b - F_b \qquad (3\text{-}4)$$

The displacements at the gears, positive downward, are given by

$$y_{ng} = z + \ell_{ng}\,\theta \qquad (3\text{-}5)$$

$$y_w = z + \ell_w\,\theta \qquad (3\text{-}6)$$

$$y_b = z + \ell_b\,\theta \qquad (3\text{-}7)$$

The gear forces are calculated using an equivalent linear spring representing the combined linearized air curve and tires in series

$$F_{ng} = k_{ng}\,y_{ng} \qquad (3\text{-}8)$$

$$F_w = k_m\,x_w \qquad (3\text{-}9)$$

$$F_b = k_m\,x_b \qquad (3\text{-}10)$$

The aerodynamic lift and pitching movement are given by

$$L_A = qS\,(C_{L_\alpha}\,\alpha + C_{L_o}) \tag{3-11}$$

$$M_A = qS\bar{c}\,(C_{m_\alpha}\,\alpha + C_{m_o}) \tag{3-12}$$

where

$$\alpha = \theta + \alpha_c$$

α_c is an input constant

It is assumed that the oil in the load equalizer is incompressible, in giving the following relation

$$y_w - x_w = -(y_b - x_b) \tag{3-13}$$

The pressure loss in the equalizer tube is assumed to be proportional to the flow velocity squared

$$p_w - p_b \triangleq \Delta p = k\,V|V| \tag{3-14}$$

where the flow velocity V is given by

$$V = \frac{4A}{\pi D^2}(\dot{y}_w - \dot{x}_w) \tag{3-15}$$

A is the cross-sectional area of the equalizer piston, and D is the diameter of the interconnecting line.

Subtracting (3-4) from (3-3) yields

$$\ddot{x}_w - \ddot{x}_b = \frac{1}{m}(A\,\Delta p - (F_w - F_b)) \tag{3-16}$$

Differentiating (3-13) twice gives

$$\ddot{x}_w + \ddot{x}_b = \ddot{y}_w + \ddot{y}_b \tag{3-17}$$

Adding (3-16) to (3-17) gives

$$\ddot{x}_w = \frac{1}{2}\left(\ddot{y}_w + \ddot{y}_b + \frac{A}{m}\Delta p - \frac{(F_w - F_b)}{m}\right) \tag{3-18}$$

Differentiating (3-6) and (3-7) twice and substituting into (3-18) gives

$$\ddot{x}_w = \ddot{z} + \frac{1}{2}(\ell_w + \ell_b)\ddot{\theta} + \frac{1}{2m}\left(A\Delta p - (F_w - F_b)\right) \tag{3-19}$$

Substituting in equations of motion (3-1) and (3-2) for $\ddot{x}$ and $\ddot{\theta}$, we get

$$\ddot{x}_w = \frac{g}{W}\left(W - L + E - F_{ng} - Ap_w - Ap_b\right) + \tag{3-20}$$

$$\frac{(\ell_w+\ell_b)}{2I}\left(M + Ei_e - F_{ng}\ell_{ng} - A_{pw}\ell_w - A_{pb}\ell_b\right) + \frac{1}{2m}\left(A\Delta p - (F_w - F_b)\right)$$

From (3-3), (3-4) and (3-16) we have

$$P_w = \frac{1}{A}(m\ddot{x}_w + F_w) \tag{3-21}$$

$$P_b = \frac{1}{A}\left[m\ddot{x}_w - \left(A\Delta p - (F_w - F_b)\right) + F_b\right] \tag{3-22}$$

$$P_b = \frac{1}{A}\left(m\ddot{x}_w - A\Delta p + F_w\right) = p_w - \Delta p \tag{3-23}$$

Substituting back into (3-20) finally yields the following equation of motion for X_w:

$$\ddot{X}_w = \frac{1}{1 + m\left(2\frac{g}{W} + \frac{(\ell_w + \ell_b)^2}{2I}\right)} \left[\frac{g}{W}\left(W + E - L - F_{ng} + A\Delta p - 2F_w\right)\right.$$

$$+ \frac{\ell_w + \ell_b}{2I}\left(M + E\ell_e - F_{ng}\ell_{ng} - F_w\left(\ell_w + \ell_b\right) + A\Delta p\ell_b\right) \qquad (3\text{-}24)$$

$$\left. + \frac{1}{2m}\left(A\Delta p - (F_w - F_b)\right)\right]$$

Equations (3-24), (3-1), and (3-2) are numerically integrated to yield the system response to an input elevator force time history E (t) . k in Equation (3-14) is chosen as zero to represent a full load equalizing system. For non-zero values of k the aft main gear attains a higher load level than the forward main gear. Above k of about 20, the results are constant and representative of independent non-interconnected main gears.

APPENDIX E

PAVEMENT RESPONSE TO MOVING LOAD

TABLE OF CONTENTS

PAVEMENT RESPONSE TO MOVING LOAD

1. FUNDAMENTAL EQUATIONS

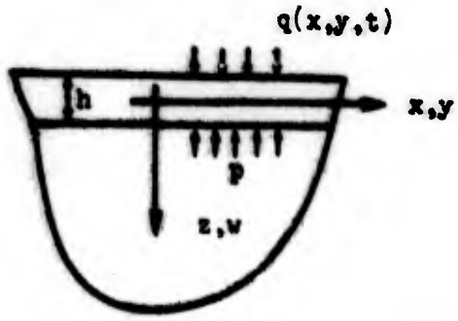

Consider a plate of thickness h under a general normal load q(x,y,t) resting on a half-space. Assume that interface to be incapable of transmitting horizontal shears. If the materials are viscoelastic, the equations describing the system are (from *)

$$D_t \nabla^4 w = p - q \qquad \nabla^2 \phi = 0 \tag{1-1}$$

Where p and q denote the normal surface tractions on the positive and negative plate faces ($z = \pm h/2$) respectively. The quantity D_t is a general time dependent plate bending stiffness operator and ϕ is the harmonic stress function. The symbols ∇^4 and ∇^2 denote, respectively the plane biharmonic and the space harmonic operators.

The general solution to these equations is (from *)

$$w(x,y,t) = \frac{1}{4\pi^2} \iint_{-\infty}^{\infty} I_1 e^{-i(\alpha x+\beta y)} d\alpha d\beta \tag{1-2}$$

$$\phi(x,y,z,t) = \frac{1}{4\pi^2} \mathcal{L}^{-1} \left[\iint_{-\infty}^{\infty} J_1 e^{-(\alpha^2+\beta^2)^{1/2}(z-\frac{h}{2})} e^{-i(\alpha x+\beta y)} d\alpha d\beta \right] \tag{1-3}$$

where

$$I_1 = \mathcal{L}^{-1} \left[\frac{\ell^{*3}(s)\, \bar{q}^*(\alpha,\beta,s)}{D^*(s)\{(\alpha^2+\beta^2)^2 \ell^{*3}(s) + (\alpha^2+\beta^2)^{1/2}\}} \right] \tag{1-4}$$

$$J_1 = \frac{\bar{q}^*(\alpha,\beta,s)}{2G^*(s)\,(\alpha^2+\beta^2)\{1+(\alpha^2+\beta^2)^{3/2}\ell^{*3}(s)\}} \tag{1-5}$$

---

* Item (26) in Appendix A

Here, * indicates the Laplace transform and ⁻ indicates a double Fourier transform. D^*, G^*, ν^* are respectively plate stiffness, foundation shear modulus and Poisson's ratio after Laplace operation,

and

$$\ell^* = \frac{D^*(1-\nu^*)}{G^*} \tag{1-5a}$$

Making a variable change $\alpha = (\rho/\ell)\cos\theta$, $\beta = (\rho/\ell)\sin\theta$ and introducing non-dimensional variables $X = x/\ell$, $Y = y/\ell$, $Z = z/\ell$ (ℓ= characteristic length)

$$w(X,Y,t) = \frac{1}{4\pi^2}\int_0^\infty\int_0^{2\pi} I_2 e^{-i\lambda}\, d\theta\, d\rho \tag{1-6}$$

$$\phi(X,Y,Z,t) = \frac{1}{4\pi^2}\,\mathcal{L}^{-1}\left[\int_0^\infty\int_0^{2\pi} J_2 e^{-\rho Z'} e^{-i\lambda}\, d\theta\, d\rho\right] \tag{1-7}$$

where

$$I_2 = \mathcal{L}^{-1}\left[\frac{1}{\ell}\,\bar{}\,\left|\frac{\bar{q}^*\,\ell^{*3}}{D^*\left\{\rho^3\frac{\ell^{*3}}{\ell^3}+1\right\}}\right|\right] \tag{1-8}$$

$$J_2 = \frac{\bar{q}^*}{2G^*\rho\left\{\rho^3\frac{\ell^{*3}}{\ell^3}+1\right\}} \tag{1-9}$$

$$\lambda = \rho(X\cos\theta + Y\sin\theta) \tag{1-10}$$

$$X = \frac{x}{\ell}\,, \qquad Y = \frac{y}{\ell} \tag{1-10a}$$

$$Z' = \frac{1}{\ell}\left(z - \frac{h}{2}\right) \tag{1-11}$$

If the load P is concentrated and moves at a constant velocity v, it can be represented as

$$q = P\delta(x-vt)\,\delta(y), \qquad \delta(\ ) = \text{Dirac delta function} \tag{1-12}$$

so that

$$\bar{q}^*(\alpha,\beta,s) = \frac{P}{s-i\alpha v} \tag{1-13}$$

and

$$w(X,Y,t) = \frac{1}{4\pi^2}\frac{P}{\ell}\int_0^{\infty}\int_0^{2\pi} Ie^{-i\lambda}\,d\theta\,d\rho \tag{1-14}$$

$$\phi(X,Y,Z,t) = \frac{P}{4\pi^2}\,\mathcal{L}^{-1}\left[\int_0^{\infty}\int_0^{2\pi} Je^{-\rho Z'}e^{-i\lambda}\,d\theta\,d\rho\right] \tag{1-15}$$

where

$$I = \mathcal{L}^{-1}\left[\frac{1}{s-i\frac{V\rho}{\ell}\cos\theta}\,\frac{\rho^3}{D^*\left\{1+\rho^3\frac{\rho^3}{\ell^3}\right\}}\right] \tag{1-16}$$

$$J = \frac{1}{s-i\frac{V\rho}{\ell}\cos\theta}\,\frac{1}{2G^*\rho\left\{1+\rho^3\frac{\rho^3}{\ell^3}\right\}} \tag{1-17}$$

2. FOUNDATION VERTICAL PRESSURE

The vertical foundation stress p_z is defined in terms of the harmonic stress function as [26],

$$p_z = \mathcal{L}^{-1}\left[2G^*(s)\left\{z'\frac{\partial^3\phi^*(s)}{\partial z'^3} - \frac{\partial^2\phi^*(s)}{\partial z'^2}\right\}\right] \qquad (2\text{-}1)$$

From Equation (1-15)

$$\phi^*(s) = \frac{P}{4\pi^2}\int_0^\infty\int_0^{2\pi} J e^{-\rho z'} e^{-i\lambda}\, d\theta\, d\rho \qquad (2\text{-}2)$$

Differentiating equation (2-2)

$$\frac{\partial\phi^*}{\partial z'} = \frac{P}{4\pi^2}\iint\left(-\frac{\rho}{\ell}\right)e^{-\rho z'}e^{-i\lambda}\, d\theta\, d\rho \qquad (2\text{-}3)$$

$$\frac{\partial^2\phi^*}{\partial z'^2} = \frac{P}{4\pi^2}\iint -\frac{\rho^2}{\ell}e^{-\rho z'}e^{-i\lambda}\, d\theta\, d\rho \qquad (2\text{-}4)$$

$$\frac{\partial^3\phi^*}{\partial z'^3} = \frac{P}{4\pi^2}\iint\left(-\frac{\rho}{\ell}\right)^3 e^{-\rho z'}e^{-i\lambda}\, d\theta\, d\rho \qquad (2\text{-}5)$$

Therefore,

$$p_z = -\frac{P}{4\pi^2\ell^2}\int_0^\infty\int_0^{2\pi}\mathcal{L}^{-1}\left[J_p\right]\rho(1+\rho z')e^{-\rho z'}e^{-i\lambda}\, d\theta\, d\rho \qquad (2\text{-}6)$$

where

$$J_p = \frac{1}{s - i\frac{v\rho}{\ell}\cos\theta}\,\frac{1}{1+\rho^3\frac{\ell^{*3}}{\ell^3}} \qquad (2\text{-}7)$$

3. PLATE STRAINS

The longitudinal and lateral strains are defined by (from *)

$$\epsilon_x = - z \frac{\partial^2 w}{\partial x^2} \quad , \quad \epsilon_y = - z \frac{\partial^2 w}{\partial y^2} \tag{3-1}$$

Now, from Equation (1-14)

$$\frac{\partial^2 w}{\partial x_1^2} = \frac{1}{4\pi^2} \frac{P}{\ell} \int_0^\infty \int_0^{2\pi} I \frac{\partial^2}{\partial x_1^2} (e^{-i\lambda}) d\theta d\rho \tag{3-2}$$

Since,

$$\frac{\partial^2}{\partial x^2}(e^{-i\lambda}) = (-i\frac{\rho}{\ell}\cos\theta)^2 e^{-i\lambda} = -\frac{1}{\ell^2}(\rho\cos\theta)^2 e^{-i\lambda} \tag{3-3}$$

and

$$\frac{\partial^2}{\partial y^2}(e^{-i\lambda}) = -\frac{1}{\ell^2}(\rho\sin\theta)^2 e^{-i\lambda} \tag{3-4}$$

it follows that

$$\epsilon_x = \frac{z}{4\pi^2} \frac{P}{\ell^3} \int_0^\infty \int_0^{2\pi} I(\rho\cos\theta)^2 e^{-i\lambda} d\theta d\rho \tag{3-5}$$

$$\epsilon_y = \frac{z}{4\pi^2} \frac{P}{\ell^3} \int_0^\infty \int_0^{2\pi} I(\rho\sin\theta)^2 e^{-i\lambda} d\theta d\rho \tag{3-6}$$

---

* Item (20) from Appendix A

4. PLATE STRESSES

The longitudinal and lateral stresses are defined by (from *)

$$\sigma_x = \frac{12z}{h^3} M_x \quad , \quad \sigma_y = \frac{12z}{h^3} M_y \tag{4-1}$$

and the bending moments by (from *)

$$M_x = - D_t \left(\frac{\partial^2 w}{\partial x^2} + \nu_p \frac{\partial^2 w}{\partial y^2} \right) \tag{4-2}$$

$$M_y = - D_t \left(\frac{\partial^2 w}{\partial y^2} + \nu_p \frac{\partial^2 w}{\partial x^2} \right) \tag{4-3}$$

Taking Laplace transform and then inverting

$$M_x = \mathcal{L}^{-1} \left[-D_t^* \left(\frac{\partial^2 w^*}{\partial x^2} + \nu_p \frac{\partial^2 w^*}{\partial y^2} \right) \right] \tag{4-4}$$

$$M_y = \mathcal{L}^{-1} \left[-D_t^* \left(\frac{\partial^2 w^*}{\partial y^2} + \nu_p \frac{\partial^2 w^*}{\partial x^2} \right) \right] \tag{4-5}$$

Taking the Laplace transform of Equation (3-2)

$$\frac{\partial^2 w^*}{\partial x^2} = - \frac{1}{4\pi^2} \frac{P}{\ell^3} \int_0^\infty \int_0^{2\pi} I'(\rho \cos\theta)^2 e^{-i\lambda} d\theta d\rho \tag{4-6}$$

$$\frac{\partial^2 w^*}{\partial y^2} = - \frac{1}{4\pi^2} \frac{P}{\ell^3} \int_0^\infty \int_0^{2\pi} I'(\rho \sin\theta)^2 e^{-i\lambda} d\theta d\rho \tag{4-7}$$

---

* Item (20) in Appendix A

Substituting into Equations (4-4) and (4-5)

$$M_x = -\frac{1}{4\pi^2}\frac{P}{\ell^3}\int_0^\infty\int_0^{2\pi} \mathcal{L}^{-1}\left[D_c^* I'\right] \rho^2(\cos^2\theta+\nu_p\sin^2\theta)e^{-i\lambda}\,d\theta d\rho \qquad (4-8)$$

$$M_y = -\frac{1}{4\pi^2}\frac{P}{\ell^3}\int_0^\infty\int_0^{2\pi} \mathcal{L}^{-1}\left[D_c^* I'\right] \rho^2(\sin^2\theta+\nu_p\cos^2\theta)e^{-i\lambda}\,d\theta d\rho \qquad (4-9)$$

where

$$I' = \frac{1}{s-i\frac{V\rho}{\ell}\cos\theta}\,\frac{\rho^3}{D_c^*\left[1+\rho^3\frac{\rho^3}{\ell^3}\right]} \qquad (4-10)$$

And the final stress expressions are

$$\sigma_x = \frac{3z}{\pi^2 h^3}\frac{P}{\ell^3}\int_0^\infty\int_0^{2\pi} I_\sigma \rho^2(\cos^2\theta+\nu_p\sin^2\theta)e^{-i\lambda}\,d\theta d\rho \qquad (4-11)$$

$$\sigma_y = \frac{3z}{\pi^2 h^3}\frac{P}{\ell^3}\int_0^\infty\int_0^{2\pi} I_\sigma \rho^2(\sin^2\theta+\nu_p\cos^2\theta)e^{-i\lambda}\,d\theta d\rho \qquad (4-12)$$

where

$$I_\sigma = \mathcal{L}^{-1}\left[\frac{1}{s-i\frac{V\rho}{\ell}\cos\theta}\,\frac{\rho^3}{1+\rho^3\frac{\rho^3}{\ell^3}}\right] \qquad (4-13)$$

5. MATERIAL CHARACTERIZATION, FLEXIBLE PAVEMENTS

The plate is represented by the following rheological model:

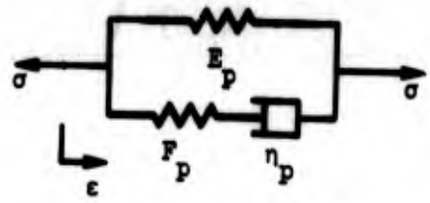

(5-1)

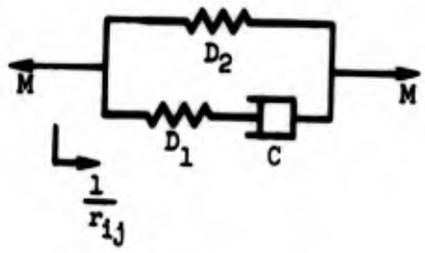

where

σ = stress

ε = strain

M = plate bending moment

r_{ij} = radius of curvature

$$\frac{1}{r_{ij}} = \frac{1}{r_i} + \nu_p \frac{1}{r_j}$$

ν_p = plate Poisson's ratio

E_p, F_p, η_p = plate material stiffnesses, damping

$$D_1 = \frac{F_p h^3}{12(1-\nu_p^2)}, \quad D_2 = \frac{E_p h^3}{12(1-\nu_p^2)}, \quad C = \frac{\eta_p h^3}{12(1-\nu_p^2)} \qquad (5\text{-}2)$$

This rheological model is represented by the following equation.

$$\boxed{\left(\frac{d}{dt}+\frac{1}{\tau}\right) M_1 = (D_1 + D_2)\left(\frac{d}{dt}+\frac{1}{\mu_p \tau}\right)\frac{1}{r_{ij}}} \qquad (5\text{-}3)$$

where

$$\mu_p = 1 + \frac{D_1}{D_2} = 1 + \frac{F_p}{E_p} = \frac{E_p + F_p}{E_p} = \left(\frac{E_{dyn}}{E_{static}}\right)_{plate} \qquad (5\text{-}4)$$

and

$$\tau = \frac{C}{D_1} = \frac{\eta_p}{F_p} = \text{plate material relaxation time} \qquad (5\text{-}5)$$

The foundation half-space is represented by the following rheological model and corresponding constitutive equations (from *)

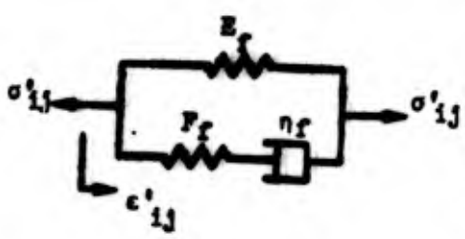

$$\boxed{\begin{aligned}\left(1+\tau_\sigma \frac{d}{dt}\right)\sigma'_{ij} &= E_f\left(1+\tau_\varepsilon \frac{d}{dt}\right)\varepsilon'_{ij} \\ \sigma_{aa} &= 3k\varepsilon_{aa}\end{aligned}} \qquad (5\text{-}6)$$

where

$$\tau_\sigma = \frac{\eta_f}{F_f}, \quad \tau_\varepsilon = \eta_f\left(\frac{1}{E_f}+\frac{1}{F_f}\right)$$

k = bulk modulus of foundation material

* Item (20) in Appendix A

$\sigma'_{ij} = \sigma_{ij} - \frac{1}{3}\sigma_{\alpha\alpha}\delta_{ij}$, $\varepsilon'_{ij} = \varepsilon_{ij} - \frac{1}{3}\varepsilon_{\alpha\alpha}\delta_{ij}$

E_f, F_f = foundation stiffnesses, n_f = foundation damping, and

τ_o, τ_ε = foundation material relaxation times

where

δ_{ij} = Kronecker delta, σ'_{ij} = stress deviation, (5-7)

ε'_{ij} = strain deviation, $\sigma_{\alpha\alpha} = \sigma_{11} + \sigma_{22} + \sigma_{33}$ = mean stress, and

$\varepsilon_{\alpha\alpha} = \varepsilon_{11} + \varepsilon_{22} + \varepsilon_{33}$ = mean strain

After taking the Laplace transform, the parameterized material constants become (from *)

$$D^*(s) = M^* r^* = \frac{D_1 + D_2}{\mu_p} \frac{1 + \mu_p \tau s}{1 + \tau s} = D_2 \frac{1 + \mu_p \tau s}{1 + \tau s} \qquad (5\text{-}8)$$

$$G^*(s) = \frac{E_f}{2} \frac{1 + \tau_\varepsilon s}{1 + \tau_\sigma s} \quad , \quad \nu^*(s) = \frac{3k(1+\tau_\sigma s) - E_f(1+\tau_\varepsilon s)}{6k(1+\tau_\sigma s) + E_f(1+\tau_\varepsilon s)} \qquad (5\text{-}9)$$

For simplicity, assume $\nu^* = \frac{1}{2}$, which is equivalent to the assumption that

$$k >> E_f \quad \text{and} \quad k\tau_\sigma >> E_f\tau_\varepsilon \qquad (5\text{-}10)$$

---

* Item (19) in Appendix A

Then

$$\ell^{*3}(s) = \frac{D^*(s)\left[1-\nu^*(s)\right]}{G^*(s)} = \frac{D^*(s)}{2G^*(s)} = \ell^3 \frac{1+\mu_p \tau s}{1+\tau s} \frac{1+\tau_\sigma s}{1+\tau_c s} \qquad (5\text{-}11)$$

where

$$\ell^3 = \frac{D_1+D_2}{\mu_p E_f} = \frac{D_2}{E_f} = \frac{h^3}{12(1-\nu_p^2)}\left(\frac{E_p}{E_f}\right) \qquad (5\text{-}12)$$

and

$$\frac{\ell^*(s)}{D^*(s)} = \frac{\ell^3}{D_2} \frac{1+\tau_\sigma s}{1+\tau_c s} \qquad (5\text{-}13)$$

6. MATERIAL CHARACTERIZATION, RIGID PAVEMENT

The rheological model for the plate is simply elastic. As shown,

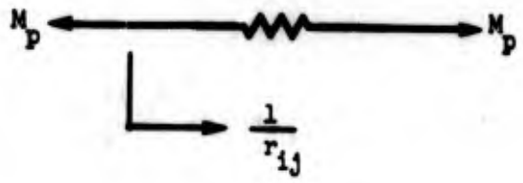

The constitutive relation for this model is,

$$M_p = \frac{D}{r_{ij}} \tag{6-1}$$

where

$$D = \frac{Eh^3}{12(1-\nu_p^2)}$$

and

E = plate Young's modulus, and

ν_p = plate Poisson's ratio

r_{ij} = radius of curvature (as before)

The foundation rheology is standard viscoelastic which has a mathematical representation identical to that for the flexible pavement.

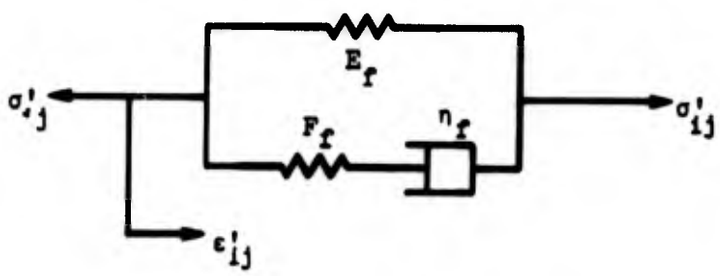

(6-2)

The parametrized material constants associated with these constitutive relations, assuming foundation Poisson's ratio = $\frac{1}{2}$, are (from *)

$$D^*(s) = D, \quad G^*(s) = \frac{E_f}{2}\frac{1+\tau_\sigma s}{1+\tau_\varepsilon s} \tag{6-3}$$

$$t^{*3}(s) = t^3\frac{1+\tau_\sigma s}{1+\tau_\varepsilon s}, \quad t^3 = \frac{D}{E_f}, \text{ and} \tag{6-4}$$

$$\frac{t^{*3}(s)}{D^*(s)} = \frac{t^3}{D}\frac{1+\tau_\sigma s}{1+\tau_\varepsilon s} \tag{6-5}$$

* Item (19) in Appendix A

7. FLEXIBLE PAVEMENT EQUATIONS, CONCENTRATED LOAD

Substitution of Equations (5-11) and (5-12) into Equation (5-13) yields flexible pavement deflection

$$I = \mathcal{L}^{-1}\left[\frac{1}{s-i\frac{V\rho}{\ell}\cos\theta}\,\frac{\ell^3}{D_2}\,\frac{1+\tau_\sigma s}{1+\tau_\epsilon s}\,\frac{1}{1+\rho^3\,\frac{1+\mu_p\tau s}{1+\tau s}\,\frac{1+\tau_\sigma s}{1+\tau_\epsilon s}}\right] \tag{7-1}$$

This reduces to

$$I = \frac{\ell^3}{D_2}\frac{1}{\delta}Q_F,\quad Q_F = \mathcal{L}^{-1}\left[\frac{s^2+\frac{a_1}{\tau}s+\frac{a_o}{\tau^2}}{(s-i\frac{\Omega}{\tau})(s+\frac{\Gamma_1}{\tau})(s+\frac{\Gamma_2}{\tau})}\right] \tag{7-2}$$

where

$$\delta = \rho^3\mu_p+\mu_f\,,\quad \Omega = V\rho\cos\theta\,,\quad V = \frac{V\tau}{\ell}$$

$$a_1 = \zeta+1\,,\quad a_o = \zeta\,,\quad \zeta = \frac{\tau}{\tau_\sigma}\,,\quad \mu_f = 1+\frac{F_f}{E_f} \tag{7-3}$$

$$\Gamma_1 = \frac{1}{2}\left(G-\sqrt{G^2-4F}\right),\quad \Gamma_2 = \frac{1}{2}\left(G+\sqrt{G^2-4F}\right)$$

$$G = \frac{1}{\delta}\left[\zeta(\rho^3\mu_\rho+1)+(\rho^3+\mu_f)\right]\,,\quad F = \frac{\zeta}{\delta}(\rho^3+1)$$

Hence, the deflection is

$$w = \frac{1}{4\pi^2}\frac{P\ell^2}{D_2}\int_0^{\infty}\int_0^{2}\frac{Q_F}{\delta}e^{-i\lambda}\,d\theta d\rho \tag{7-4}$$

Transform inversion and manipulation (8 Rigid Pavement Equations- Concentrated Load) gives the steady state part of Q_R as,

where
$$Q_R = Q_{\text{steady state}} = N\, e^{i(\Omega T+\Psi)} \tag{7-5}$$

$$N = \sqrt{\frac{a_1^2\Omega^2+(a_o-\Omega^2)^2}{(\Gamma_1^2+\Omega^2)(\Gamma_2^2+\Omega^2)}}\,, \quad T = \frac{t}{\tau} \tag{7-6}$$

$$\Psi = \tan^{-1}\frac{a_1\Omega}{a_o-\Omega^2} - \tan^{-1}\frac{\Omega}{\Gamma_1} - \tan^{-1}\frac{\Omega}{\Gamma_2} \tag{7-7}$$

The final expression for the steady state deflection is then

$$W = k_w \int_0^{\infty}\int_0^{2\pi} I_w\, d\theta\, d\rho \tag{7-8}$$

where

$$I_w = \frac{N}{\rho}\cos(\lambda-\Psi) \tag{7-9}$$

$$k_w = \frac{1}{4\pi^2}\frac{P\ell^2}{D_2}$$

$$\lambda = \rho(X\cos\theta + Y\sin\theta) \tag{7-10}$$

in a coordinate system that moves with the load (X, Y).

$$X_{\text{moving}} = X_{\text{stationary}} - VT \tag{7-10a}$$

Transform inversion and manipulation (8. Rigid Pavement Equations - Concentrated Load) gives the steady state part of Q_R as,

where $$Q_R = Q_{\text{steady state}} = N\, e^{i(\Omega T+\Psi)} \tag{7-5}$$

$$N = \sqrt{\frac{a_1^2\Omega^2+(a_o-\Omega^2)^2}{(\Gamma_1^2+\Omega^2)(\Gamma_2^2+\Omega^2)}}\,, \quad T = \frac{t}{\tau} \tag{7-6}$$

$$\Psi = \tan^{-1}\frac{a_1\Omega}{a_o-\Omega^2} - \tan^{-1}\frac{\Omega}{\Gamma_1} - \tan^{-1}\frac{\Omega}{\Gamma_2} \tag{7-7}$$

The final expression for the steady state deflection is then

$$W = k_w \int_0^{\infty}\int_0^{2\pi} I_w\, d\theta\, d\rho \tag{7-8}$$

where

$$I_w = \frac{N}{\delta}\cos(\lambda-\Psi) \tag{7-9}$$

$$k_w = \frac{1}{4\pi^2}\frac{P\ell^2}{D_2}$$

$$\lambda = \rho(X\cos\theta + Y\sin\theta) \tag{7-10}$$

in a coordinate system that moves with the load (X, Y).

$$X_{\text{moving}} = X_{\text{stationary}} - VT \tag{7-10a}$$

To determine flexible pavement vertical foundation pressures, we use Equation (2-7)

$$J_p = \frac{1}{s-i\frac{V\rho}{L}\cos\theta} \; \frac{1}{1+\rho^3 \frac{1+\mu_\rho \tau s}{1+\tau s} \frac{1+\tau_\sigma s}{1+\tau_\varepsilon s}} \tag{7-11}$$

This becomes

$$\mathcal{L}^{-1}\left[J_p\right] = \frac{\mu_f}{\delta} Q \tag{7-12}$$

where

$$Q = \mathcal{L}^{-1}\left[\frac{s^2 + \frac{a_1'}{\tau} s + \frac{a_o'}{\tau^2}}{(s-i\frac{\omega}{\tau})(s+\frac{\Gamma_1}{\tau})(s+\frac{\Gamma_2}{\tau})}\right] \tag{7-13}$$

with

$$a_1' = \frac{\zeta}{\mu_f} + 1, \quad a_o' = \frac{\zeta}{\mu_f} \tag{7-14}$$

Reduces as for the deflection, yields the steady state vertical pressure

$$P_z = k_p \int_0^\infty \int_0^{2\pi} I_p e^{i\theta} d\rho \tag{7-15}$$

with

$$I_p = \frac{N'}{\delta} \cos(\lambda-\psi) \left[1+\rho Z'\right] \rho e^{-\rho Z'}$$

$$N' = \sqrt{\frac{a_1'^2\Omega^2-(a_o'-\Omega^2)}{(\Gamma_1^2+\Omega^2)(\Gamma_2^2+\Omega^2)}} \qquad (7\text{-}16)$$

$$k_p = -\frac{1}{4\pi^2}\frac{P}{\ell^2} \text{ "f}$$

$$\Psi' = \tan^{-1}\frac{a_1'\Omega}{a_o-\Omega} - \tan^{-1}\frac{\Omega}{\Gamma_1} - \tan^{-1}\frac{\Omega}{\Gamma_2}$$

The expression for strain comes from Equations (3-5) and (3-6) and the integrand reduces in a manner identical to that for the deflection, so the steady state strain is

$$\varepsilon_x = k_\varepsilon \int_0^\infty \int_0^{2\pi} I_{\varepsilon_x}\, d\theta d\rho \qquad (7\text{-}17)$$

$$\varepsilon_y = k_\varepsilon \int_0^\infty \int_0^{2\pi} I_{\varepsilon_y}\, d\theta d\rho \qquad (7\text{-}18)$$

with

$$I_{\varepsilon_x} = I_w(\rho\cos\theta)^2 \;,\; I_{\varepsilon_y} = I_w(\rho\sin\theta)^2 \qquad (7\text{-}19)$$

$$k_\varepsilon = \frac{z}{4\pi^2}\frac{P}{D_2}$$

The expressions for plate stress are obtained by substituting Equation (5-11) into Equation (4-13)

$$I_\sigma = \mathcal{L}^{-1}\left(\frac{1}{s-i\frac{v\rho}{\ell}\cos\theta}\right)\left(\ell^3\,\frac{1+\mu_p\tau s}{1+\tau s}\,\frac{1+\tau_\sigma s}{1+\tau_\varepsilon s}\right)\left(\frac{1}{1+\rho^3\,\frac{1+\mu_p\tau s}{1+\tau s}\,\frac{1+\tau_\sigma s}{1+\tau_\varepsilon s}}\right) \tag{7-20}$$

This becomes

$$I_\sigma = \frac{\mu_p}{\delta}\ell^3 Q\ ,\ Q = \mathcal{L}^{-1}\left[\frac{s^2+\frac{a_1''}{\tau}s+\frac{a_0''}{\tau^2}}{(s-i\frac{\Omega}{\tau})(s+\frac{\Gamma_1}{\tau})(s+\frac{\Gamma_2}{\tau})}\right] \tag{7-21}$$

where

$$a_1'' = \zeta+\frac{1}{\mu_p}\ ,\ a_0'' = \frac{\zeta}{\mu_p} \tag{7-22}$$

Hence, (see 8. Rigid Pavement Equation - Concentrated Load)

$$\sigma_x = k_\sigma \int_0^\infty \int_0^{2\pi} I_{\sigma_x}\, d\theta d\rho \tag{7-23}$$

$$\sigma_y = k_\sigma \int_0^\infty \int_0^{2\pi} I_{\sigma_y}\, d\theta d\rho \tag{7-24}$$

where

$$I_{\sigma_x} = \frac{N''}{\delta} \cos(\lambda - \psi'')\rho^2(\cos^2\theta + \nu_p \sin^2\theta)$$

$$I_{\sigma_y} = \frac{N''}{\delta} \cos(\lambda - \psi'')\rho^2(\sin^2\theta + \nu_p \cos^2\theta)$$

$$N'' = \sqrt{\frac{a_1''^2\,\Omega^2 + (a_o'' - \Omega^2)^2}{(\Gamma_1^2 + \Omega^2)(\Gamma_2^2 + \Omega^2)}} \qquad (7\text{-}25)$$

$$\psi'' = \tan^{-1}\frac{a_1''\,\Omega}{a_o'' - \Omega^2} - \tan^{-1}\frac{\Omega}{\Gamma_1} - \tan^{-1}\frac{\Omega}{\Gamma_2}$$

$$k_\sigma = \frac{3\pi}{\pi h^3} P \mu_p$$

8. RIGID PAVEMENT EQUATIONS, CONCENTRATED LOAD

Substituting Equations (6-4) and (6-5) into Equation (1-16) gives the deflection expression:

$$I = \mathcal{L}^{-1}\left[\frac{1}{s-i\frac{V}{\ell}\cos\theta}\,\frac{\ell^3}{D}\,\frac{1+\tau_\sigma s}{1+\tau_\varepsilon s}\,\frac{1}{1+\rho^3\,\frac{1+\tau_\sigma s}{1+\tau_\varepsilon s}}\right] \tag{8-1}$$

$$= \mathcal{L}^{-1}\left[\frac{\ell^3}{D}\,\frac{1}{s-i\frac{V\rho}{\ell}\cos\theta}\,\frac{1}{\frac{1+\tau_\varepsilon s}{1+\tau_\sigma s}+\rho^3}\right] \tag{8-2}$$

This becomes

$$I = \frac{1}{\delta}\,\frac{\ell^3}{D}\,Q_R,\quad Q_R = \mathcal{L}^{-1}\left[\frac{s+\frac{1}{\tau_\sigma}}{(s-i\frac{\Omega}{\tau_\sigma})(s+\frac{F}{\tau_\sigma})}\right] \tag{8-3}$$

Inverting and manipulating, the steady state term (Section 9) becomes

$$I_s = \frac{\ell^3}{D}\,\frac{N}{\delta}\,e^{+i(\Omega T+\Psi)} \qquad \Omega T = \frac{V\tau_\sigma}{\ell}\rho\cos\theta\,(\frac{t}{\tau_\sigma}) \tag{8-4}$$

And hence the real part of the steady state deflection term is

$$w = \frac{1}{4\pi^2}\,\frac{P\ell^2}{D}\int_0^\infty\int_0^{2\pi}\frac{N}{\delta}\cos(\phi-\Psi)\;d\theta d\rho \tag{8-5}$$

where

$$N = \sqrt{\frac{1+\Omega^2}{F^2+\Omega^2}}$$

$$\Psi = \tan^{-1}\frac{F}{\Omega} - \tan^{-1}\frac{1}{\Omega} \qquad (8\text{-}6)$$

$$\delta = \rho^3+\mu_f$$

$$F = \frac{1}{\delta}(\rho^3+1)$$

Using Equation (2-7) to get the foundation pressure expression

$$J_p = \frac{1}{s-i\frac{V\rho}{\ell}\cos()}\ \frac{1}{1+\rho^3\frac{\ell^{*3}}{\ell^3}} \qquad (2\text{-}7)$$

$$= \frac{1}{s-i\frac{\Omega}{\tau_\sigma}}\ \frac{1}{1+\rho^3\frac{1+\tau_\sigma s}{1+\tau_\varepsilon s}} \qquad (8\text{-}7)$$

$$= \frac{1}{s-i\frac{\Omega}{\tau_\sigma}}\ \frac{1+\tau_\varepsilon s}{1+\tau_\varepsilon s+\rho^3+\rho^3\tau_\sigma s} \qquad (8\text{-}8)$$

$$= \left(\tau_\varepsilon\ \frac{1}{s-i\frac{\Omega}{\tau_\sigma}}\right)\left[\frac{s+\frac{1}{\tau_\varepsilon}}{s+\frac{1+\rho^3}{\tau_\varepsilon+\tau_\sigma\rho^3}}\right] \qquad (8\text{-}9)$$

$$= \frac{\mu_f}{\delta} \frac{1}{s-i\frac{\Omega}{\tau_\sigma}} \frac{s+\frac{1}{\tau_c}}{s+\frac{F}{\tau_\sigma}} \tag{8-10}$$

$$\mathcal{L}^{-1}\left[\bar{J}_p\right] = \frac{\mu_f}{\delta} Q'_R \,, \quad Q'_R = \mathcal{L}^{-1}\left[\frac{s+a'_o}{(s-i\frac{\Omega}{\tau_\sigma})(s+\frac{F}{\tau_\sigma})}\right] \tag{8-11}$$

Reduces to (steady state)

$$Q'_R = N' e^{i(\Omega T+\Psi')} \tag{8-12}$$

where

$$N' = \sqrt{\frac{\frac{1}{\mu_f^2}+\Omega^2}{F^2+\Omega^2}} = \frac{1}{\mu_f}\sqrt{\frac{1+(\mu_f\Omega)^2}{F^2+\Omega^2}} \tag{8-13}$$

$$\Psi' = \tan^{-1}\frac{F}{\Omega} - \tan^{-1}\frac{1}{\mu_f\Omega} \tag{8-14}$$

So that from Equation (4-10) the steady state pressure is

$$p_z = -\frac{P}{4\pi^2\ell^2}\int_o^\infty\int_o^{2\pi} \frac{N'}{\delta}\cos(\phi-\Psi')\rho(1+\rho Z')e^{-\rho Z'}\,d\theta d\rho \tag{8-15}$$

Following the derivation for deflection, the expressions for rigid pavement stain is

$$\epsilon_x = k_\varepsilon \int_0^\infty \int_0^{2\pi} \frac{N}{\delta} \cos(\phi-\Psi)\,(\rho\cos\theta)^2 \, d\theta d\rho \tag{8-16}$$

$$\epsilon_y = k_\varepsilon \int_0^\infty \int_0^{2\pi} \frac{N}{\delta} \cos(\phi-\Psi)\,(\rho\sin\theta)^2 \, d\theta d\rho \tag{8-17}$$

where

$$k_\varepsilon = \frac{z}{4\pi^2} \frac{P}{D} \tag{8-18}$$

From Equation (4-13) comes the expression for pavement stresses

$$I_\sigma = \mathcal{L}^{-1}\left[\frac{1}{s-i\frac{\Omega}{\tau_\sigma}}\, \ell^3 \frac{1+\tau_\sigma s}{1+\tau_\varepsilon s} \frac{1}{1+\rho^3 \frac{1+\tau_\sigma s}{1+\tau_\varepsilon s}}\right] \tag{8-19}$$

Same as deflection expression, so

$$I_\sigma = \ell^3 \frac{N}{\delta}\, e^{i(\Omega T+\Psi)} \tag{8-20}$$

and

$$\sigma_x = k_\sigma \int_0^\infty \int_0^{2\pi} \frac{N}{\delta} \cos(\phi-\psi)\, \rho^2(\cos^2\theta+\nu_p \sin^2\theta)\, d\theta d\rho \qquad (8\text{-}21)$$

$$\sigma_y = k_\sigma \int_0^\infty \int_0^{2\pi} \frac{N}{\delta} \cos(\phi-\psi)\, \rho^2(\cos^2\theta+\nu_p \cos^2\theta)\, d\theta d\rho \qquad (8\text{-}22)$$

where

$$k_\sigma = \frac{3zP}{\pi^2 h^3} \qquad (8\text{-}23)$$

9. TRANSFORM INVERSION

For flexible pavement equation

$$Q_F = \mathcal{L}^{-1}\left[\frac{s^2+\frac{a_1}{\tau}s+\frac{a_0}{\tau^2}}{(s-i\frac{\Omega}{\tau})(s+\frac{\Gamma_1}{\tau})(s+\frac{\Gamma_2}{\tau})}\right] \tag{9-1}$$

$$= \mathcal{L}^{-1}\left[\frac{(s^2+\frac{a_1}{\tau}s+\frac{a_0}{\tau^2})(s+i\frac{\Omega}{\tau})}{(s^2+\frac{\Omega^2}{\tau^2})(s+\frac{\Gamma_1}{\tau})(s+\frac{\Gamma_2}{\tau})}\right] \tag{9-2}$$

$$= \mathcal{L}^{-1}\left[\frac{(s^2+\frac{a_1}{\tau}s+\frac{a_0}{\tau^2})s}{(s^2+\frac{\Omega^2}{\tau^2})(s+\frac{\Gamma_1}{\tau})(s+\frac{\Gamma_2}{\tau})}\right. \tag{9-3}$$

$$\left. + \frac{(s^2+\frac{a_1}{\tau}s+\frac{a_0}{\tau^2})i\frac{\Omega}{\tau}}{(s^2+\frac{\Omega^2}{\tau^2})(s+\frac{\Gamma_1}{\tau})(s+\frac{\Gamma_2}{\tau})}\right]$$

$$= \left[\frac{\partial}{\partial\tau}+i\frac{\Omega}{\tau}\right]\mathcal{L}^{-1}\left[B\right] \tag{9-4}$$

where

$$\mathcal{L}^{-1}\left[B\right] = \frac{s^2+\frac{a_1}{\tau}s+\frac{a_0}{\tau^2}}{(s^2+\frac{\Omega^2}{\tau^2})(s+\frac{\Gamma_1}{\tau})(s+\frac{\Gamma_2}{\tau})} \tag{9-5}$$

Inverting by tables

$$\mathcal{L}^{-1}\left[B\right] = \tau\left\{\left(\frac{\Gamma_1^2-a_1\Gamma_1+a_o}{(\Gamma_2-\Gamma_1)(\Gamma_1^2+\Omega^2)}\right)e^{-\Gamma_1 T}+\left(\frac{\Gamma_2^2-a_1\Gamma_2+a_o}{(\Gamma_1-\Gamma_2)(\Gamma_2^2+\Omega^2)}\right)e^{-\Gamma_2 T}\right.$$

$$\left.+\frac{1}{\Omega}\sqrt{\frac{a_1^2\Omega^2+(a_o-\Omega^2)^2}{(\Gamma_1^2+\Omega^2)(\Gamma_2^2+\Omega^2)}}\sin(\Omega T+\Psi)\right\} \tag{9-6}$$

where

$$\Psi = \tan^{-1}\left(\frac{a_1\Omega}{a_o-\Omega^2}\right)-\tan^{-1}\left(\frac{\Omega}{\Gamma_1}\right)-\tan^{-1}\left(\frac{\Omega}{\Gamma_2}\right) \tag{9-7}$$

$$T = \frac{t}{\tau} = \text{nondimensional time} \tag{9-8}$$

Look at the steady state case (T>>0)

$$\mathcal{L}^{-1}\left[B\right] = \frac{\tau}{\Omega}N\sin\left(\Omega T+\psi\right) \tag{9-9}$$

where

$$N = \sqrt{\frac{a_1^2\Omega^2+(a_o-\Omega^2)^2}{(\Gamma_1^2+\Omega^2)\,(\Gamma_2^2+\Omega^2)}} \tag{9-10}$$

$$\therefore \quad Q_F = N\cos(\Omega T+\psi)+iN\sin(\Omega T+\psi) \tag{9-11}$$

$$\boxed{Q_F = Ne^{i(\Omega T+\psi)}}$$

For rigid pavement equations

$$Q_R = \mathcal{L}^{-1}\left[\frac{s+a_o}{(s-i\frac{\Omega}{\tau_\sigma})(s+\frac{F}{\tau_\sigma})}\right] \tag{9-12}$$

$$\mathcal{L}^{-1}\left[\frac{(s+a_o)(s+i\frac{\Omega}{\tau_\sigma})}{(s^2-\frac{\Omega^2}{\tau_\sigma^2})(s+\frac{F}{\tau_\sigma})}\right] \tag{9-13}$$

$$= \left(\frac{\partial}{\partial t}+i\frac{\Omega}{\tau_\sigma}\right)\mathcal{L}^{-1}[B] = \left(\frac{\partial}{\partial \tau}+i\frac{\Omega}{\tau_\sigma}\right)\mathcal{L}^{-1}\left[\frac{(s+a_o)}{\left(s^2+\frac{\Omega^2}{\tau_\sigma^2}\right)\left(s+\frac{F}{\tau_\sigma}\right)}\right] \tag{9-14}$$

Inverting by tables

$$\mathcal{L}^{-1}[B] = \frac{\tau_\sigma(1+F)}{F^2+\Omega^2}e^{-FT} + \frac{\tau_\sigma}{\Omega}\sqrt{\frac{1+\Omega^2}{F^2+\Omega^2}}\sin(\Omega T+\psi) \tag{9-15}$$

where

$$\psi = \tan^{-1}\frac{F}{\Omega}-\tan^{-1}\frac{1}{\Omega} \qquad T = \frac{t}{\tau_\sigma} \tag{9-16}$$

The steady state case (T>>0) (9-17)

$$\mathcal{L}^{-1}[B] = \frac{\tau_\sigma}{\Omega}N\sin(\Omega T+\psi) \tag{9-18}$$

where $N = \sqrt{\frac{1+\Omega^2}{F^2+\Omega^2}}$

$$\therefore \quad Q_R = N e^{i(\Omega T+\psi)} \tag{9-19}$$

10. EXTENSION TO DISTRIBUTED LOAD

As an approximation to an actual tire footprint (a rectangle with semi-circular ends), let load be distributed over a circular area equal to the footprint area:

$$P = p\pi a^2 \tag{10-1}$$

where

p = tire pressure

a = effective footprint radius

P = total load

Choose a coordinate system (X, Y) which moves with the load and let A be the point at which the deflection is to be calculated and B be a point at which an element of the load ($p\rho_1 d\rho_1 d\alpha_1$) adds:

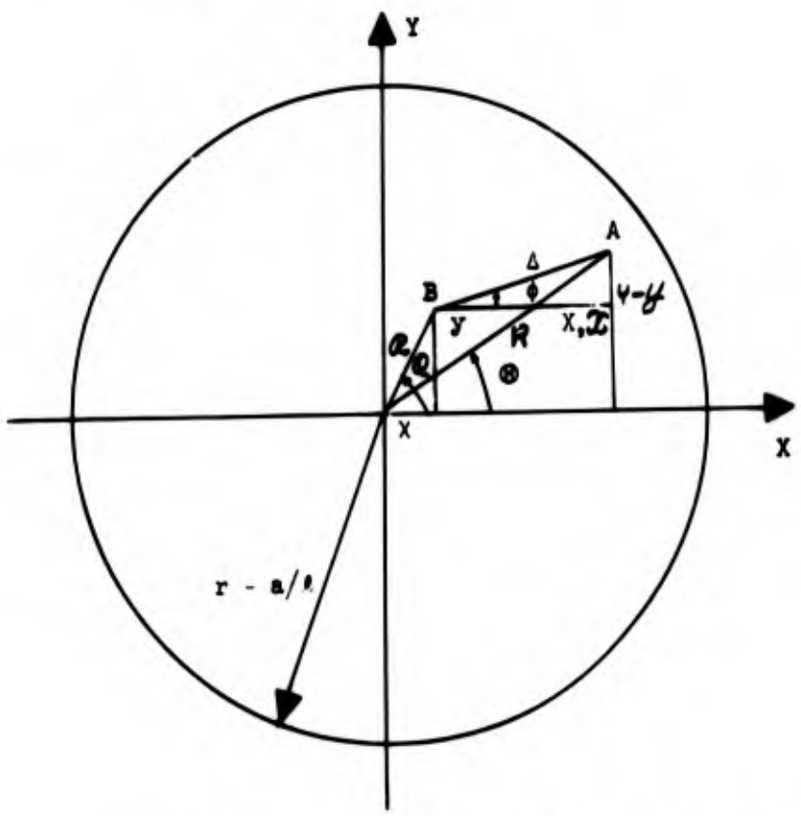

$$X = \rho\cos\alpha\,, \quad = \rho\sin\alpha\,, \quad X = R\cos\theta\,, \quad Y = R\sin\theta \tag{10-2}$$

$$X - X = \Delta\cos\phi\,, \quad Y - y = \Delta\sin\phi \tag{10-3}$$

$$R\cos\theta - \rho\cos\alpha = \Delta\cos\phi\,, \quad R\sin\theta - \rho\sin\alpha = \Delta\sin\phi \tag{10-4}$$

The infinitesimal deflection due to the pressure acting on the small area

$$dw = \ell^2 \frac{p}{P} w(\Delta, \phi) \mathcal{R} d\mathcal{R} d\mathcal{Q} \tag{10-5}$$

where w is the steady state deflection caused by a moving concentrated load acting on the pavement system.

So the total deflection is

$$w(R,\Theta) = \int_0^r \int_0^{2\pi} \ell^2 \frac{p}{P} w(\Delta, \phi) \mathcal{R} d\mathcal{Q} d\mathcal{R} \tag{10-6}$$

Now, for a viscoelastic plate on a viscoelastic half-space Equation (6-8)

$$w(\Delta\ \phi) = \frac{1}{4\pi^2} \frac{P\ell^2}{D_2} \int_0^\infty \int_0^{2\pi} I_w(\Delta, \phi) d\theta d\rho \tag{10-7}$$

where

$$I_w = A_1(\rho,\theta)\cos(\rho\Delta\cos(\phi-\theta)) + A_2(\rho,\theta)\sin(\rho\Delta\cos(\phi-\theta)) \tag{10-8}$$

$$= A_1\cos(\rho(\Delta\cos\phi\cos\theta + \Delta\sin\phi\sin\theta)) \tag{10-9}$$

$$+ A_2\sin(\rho(\Delta\cos\phi\cos\theta + \Delta\sin\phi\sin\theta))$$

$$= A_1\cos(\rho(R\cos\Theta - \mathcal{R}\cos\mathcal{Q})\cos\theta + \rho(R\sin\Theta - \mathcal{R}\sin\mathcal{Q})\sin\theta) \tag{10-10}$$

$$+ A_2\sin(\rho(R\cos\Theta - \mathcal{R}\cos\mathcal{Q})\cos\theta + \rho(R\sin\Theta - \mathcal{R}\sin\mathcal{Q})\sin\theta)$$

$$= A_1\cos(\rho(R\cos(\Theta-\theta) - \mathcal{R}\cos(\mathcal{Q}-\theta))) \tag{10-11}$$

$$+ A_2\sin(\rho(R\cos(\Theta-\theta) - \mathcal{R}\cos(\mathcal{Q}-\theta)))$$

$$= A_1 \left[\cos(\rho R\cos(\Theta-\theta))\cos(\rho\ell\cos(\alpha-\theta)) \right. \tag{10-12}$$

$$\left. + \sin(\rho R\cos(\Theta-\theta))\sin(\rho\ell\cos(\alpha-\theta)) \right]$$

$$+A2 \left| \sin(\rho R\cos(\Theta-\theta))\cos(\rho\ell\cos(\alpha-\theta)) - \cos(\rho R\cos(\Theta-\theta))\sin(\rho\ell\cos(\alpha-\theta)) \right|$$

$$= \cos(\rho\ell\cos(\alpha-\theta)) \left[A_1\cos(\rho R\cos(\Theta-\theta)) + A_2\sin(\rho R\cos(\Theta-\theta)) \right] \tag{10-13}$$

$$+ \sin(\rho\ell\cos(\alpha-\theta)) \left[A_1\sin(\rho R\cos(\Theta-\theta)) - A_2\cos(\rho R(\Theta-\theta)) \right]$$

Then

$$I_w(\Lambda,\phi) = K_1\cos(\rho\ell\cos(\alpha-\theta)) + K_2\sin(\rho\ell\cos(\alpha-\theta)) \tag{10-14}$$

$$= I_w(R,\Theta,\ell,\alpha)$$

where

$$K_1(R,\Theta,\rho,\theta) = A_1\cos(\rho R\cos(\Theta-\theta)) + A_2\sin(\rho R\cos(\Theta-\theta)) \tag{10-15}$$

$$K_2(R,\Theta,\rho,\theta) = A_1\sin(\rho R\cos(\Theta-\theta)) - A_2\cos(\rho R\cos(\Theta-\theta)) \tag{10-16}$$

Now, the deflection becomes

$$w = \int_0^r \int_0^{2\pi} \left[\frac{1}{4\pi^2} \frac{P\ell^4}{D_2} \int_0^\infty \int_0^{2\pi} I_w \, d\theta d\rho \right] \ell d\alpha d\ell \tag{10-17}$$

Interchanging the order of integration

$$w = \frac{1}{4\pi^2} \frac{P\ell^4}{D_2} \int_0^\infty \int_0^{2\pi} (K_1 I_1 + K_2 I_2) d\theta d\rho \tag{10-18}$$

where

$$I_1 = \int_0^r \int_0^{2\pi} \cos(\rho\mathcal{R}\cos(\alpha-\theta))\mathcal{R}\,d\alpha\,d\mathcal{R} \tag{10-19}$$

$$I_2 = \int_0^r \int_0^{2\pi} \sin(\rho\mathcal{R}\cos(\alpha-\theta))\mathcal{R}\,d\alpha\,d\mathcal{R} \tag{10-20}$$

Integrate first over θ, then θ can be neglected at each value it assumes, since the integrand is cyclic in 2π.

So

$$I_1 = \int_0^r \int_0^{2\pi} \cos(\rho\mathcal{R}\cos\alpha)\mathcal{R}\,d\alpha\,d\mathcal{R} = 2\pi \int_0^r J_0(\rho\mathcal{R})\mathcal{R}\,d\mathcal{R} \tag{10-21}$$

$$= \frac{2\pi}{\rho^2}\int_0^{\rho r} J_0(x)x\,dx = \frac{2\pi}{\rho^2}xJ_1(x)\Big|_0^{\rho r} = \frac{2\pi}{\rho^2}\rho r J_1(\rho r)$$

$$= \pi r^2\left(\frac{2}{\rho r}J_1(\rho r)\right) \tag{10-22}$$

$$I_2 = \int_0^r \int_0^{2\pi} \sin(\rho\mathcal{R}\cos\alpha)\mathcal{R}\,d\alpha\,d\mathcal{R} = 0 \tag{10-23}$$

Therefore, by substituting $(r=\frac{a}{\ell})$, it follows that

$$w(R,\Theta) = \frac{1}{4\pi^2}\frac{(\pi a^2 p)\ell^2}{D_2}\int_0^{\infty}\int_0^{2\pi} \frac{2}{\rho r}J_1(\rho r)K_1(R,\Theta)\,d\theta\,d\rho \tag{10-24}$$

which can be written, as follows, since $P = \pi a^2 p$

$$w = \frac{1}{4\pi^2}\frac{P\ell^2}{D_2}\int_0^{\infty}\int_0^{2\pi} C_r I_w(R,\Theta)\,d\theta\,d\rho \qquad (10\text{-}25)$$

where

$$\boxed{C_r = \frac{2}{\rho r}J_1(\rho r)} \qquad (10\text{-}26)$$

Comparing Equation (10-25) with Equation (10-7), it can be seen that they differ only by the factor C_r. Therefore, the deflection due to a circularly distributed load can be obtained from the deflection due to a concentrated load by application of a correction factor dependent on the radius.

This correction factor is also applicable to the expressions for pressure, strain, and stress Equations (7-15), (7-17), (7-18), (7-23), (7-24), since the deflection expression can be differentiated and manipulated without altering the correction factor C_r. Note that the expression for pressure has an analogous form to the deflection expression and the above argument can be directly applied to it.

In addition, the correction factor can be applied to the rigid pavement response Equations (8-5, 8-15, 8-16, 8-17, 8-21, 8-22) since the spatial dependence of these equations is the same as for the flexible pavement.

11. COMPLETE PAVEMENT RESPONSE, DISTRIBUTED LOAD

Combining the flexible and rigid pavement response Equations (7-8, 7-15, 7-17, 7-18, 7-23, 7-24, 8-5, 8-15, 8-16, 8-17, 8-21, 8-22) with the correction factor for distributed load (10-26) gives the complete steady state pavement response due to a moving distributed load. This response can be put in a particularly simple form:

$$\boxed{\text{RESPONSE} = \Lambda_{i_j} = k_{i_j}\, c_{i_j}} \qquad (11\text{-}1)$$

where

$i = w, p, \sigma,$ or ε (response type) (11-2)

$j = x, y,$ or z (response direction) (11-3)

k_{i_j} = dimensional constant (11-4)

c_{i_j} = nondimensional correction factor (11-5)

Expanding this notation gives the response equation in more conventional notation:

Plate deflection	$w = k_w\, c_w$	(11-6)
Plate longitudinal strain	$\varepsilon_x = k_\varepsilon\, c_{\varepsilon_x}$	(11-7)
Plate lateral strain	$\varepsilon_y = k_\varepsilon\, c_{\varepsilon_y}$	(11-8)
Plate longitudinal stress	$\sigma_x = k_\sigma\, c_{\sigma_x}$	(11-9)
Plate lateral stress	$\sigma_y = k_\sigma\, c_{\sigma_y}$	(11-10)
Foundation vertical pressure	$p_z = k_p\, c_p$	(11-11)

The dimensional terms and the correction factors are

$$k_w = \frac{P\ell^2}{D_2} \qquad C_w = \frac{1}{4\pi^2}\int_0^{\infty}\int_0^{2\pi} I_w\, C_r\, d\theta d\rho \tag{11-12}$$

$$k_\varepsilon = \frac{hP}{D_2} \qquad C_{\varepsilon_x} = \frac{z}{4\pi^2 h}\int_0^{\infty}\int_0^{2\pi} I_{\varepsilon_x}\, C_r d\theta d\rho \tag{11-13}$$

$$C_{\varepsilon_y} = \frac{z}{4\pi^2 h}\int_0^{\infty}\int_0^{2\pi} I_{\varepsilon_y}\, C_r d\theta d\rho \tag{11-14}$$

$$k_\sigma = \frac{P(1+\nu_p)}{h^2} \qquad C_{\sigma_x} = \frac{3z\mu_p}{\pi h(1+\nu_p)}\int_0^{\infty}\int_0^{2\pi} I_{\sigma_x}\, C_r d\theta d\rho \tag{11-15}$$

$$C_{\sigma_y} = \frac{3z\mu_p}{\pi h(1+\nu_p)}\int_0^{\infty}\int_0^{2\pi} I_{\sigma_y}\, C_r d\theta d\rho \tag{11-16}$$

$$k_p = \frac{P}{\ell^2} \qquad C_p = -\frac{\mu_f}{4\pi^2}\int_0^{\infty}\int_0^{2\pi} I_p\, C_r d\theta d\rho \tag{11-17}$$

In which

$$C_r = \frac{2}{\rho r} J_1(\rho r) \tag{11-18}$$

$$r = \frac{a}{\ell} = \text{nondimensional footprint radius} \tag{11-19}$$

and the integrands are

$$I_w = \frac{N}{\delta} \cos (\lambda - \psi) \tag{11-20}$$

$$I_{\epsilon_x} = I_w (\rho \cos \theta)^2 \tag{11-21}$$

$$I_{\epsilon_y} = I_w (\rho \sin \theta)^2 \tag{11-22}$$

$$I_{\sigma_x} = \frac{N''}{\delta} \cos (\lambda - \psi'') \rho^2 (\sin^2\theta + \nu_p \cos^2\theta) \tag{11-23}$$

$$I_{\sigma_y} = \frac{N''}{\delta} \cos (\lambda - \psi'') \rho^2 (\cos^2\theta + \nu_p \sin^2\theta) \tag{11-24}$$

$$I_p = \frac{N'}{\delta} \cos (\lambda - \psi') \rho (1 + \rho Z') \rho e^{-\rho Z'} \tag{11-25}$$

The spatially associated terms are

$$\lambda = (X \cos \theta + Y \sin \theta) \tag{11-26}$$

$$X = \frac{x}{\ell}, \quad Y = \frac{y}{\ell}, \quad Z = \frac{z}{\ell}, \quad H = \frac{h}{\ell} \tag{11-27}$$

$$Z' = Z - \frac{H}{2} \tag{11-28}$$

x, y, z is a coordinate system moving at a velocity v (11-29)

For flexible pavements

$$N = f_F(a_1, a_0) \tag{11-30}$$

$$N' = f_F(a_1', a_0') \tag{11-31}$$

$$N'' = f_F(a_1'', a_0'') \tag{11-32}$$

$$f_F(a_1, a_0) = \sqrt{\frac{a_1^2\Omega^2 + (a_0 - \Omega^2)^2}{(\Gamma_1^2 + \Omega^2)(\Gamma_2^2 + \Omega^2)}} \tag{11-34}$$

$$\psi = g_F(a_1, a_0) \tag{11-35}$$

$$\psi' = g_F(a_1', a_0') \tag{11-36}$$

$$\psi'' = g_F(a_1'', a_0'') \tag{11-37}$$

$$g_F(a_1, a_0) = \tan^{-1}\frac{a_1\Omega}{a_0 - \Omega^2} - \tan^{-1}\frac{\Omega}{\Gamma_1} - \tan^{-1}\frac{\Omega}{\Gamma_2} \tag{11-38}$$

$$\delta = \mu_p\rho^3 + \mu_f \tag{11-38a}$$

For rigid pavements

$$N = \sqrt{\frac{1 + \Omega^2}{F^2 + \Omega^2}} \tag{11-39}$$

$$N' = \frac{1}{\mu_f}\sqrt{\frac{1 + (\mu_f\Omega)^2}{F^2 + \Omega^2}} \tag{11-40}$$

$$N'' = N \tag{11-41}$$

$$\psi = \tan^{-1}\frac{F}{\Omega} - \tan^{-1}\frac{1}{\Omega} \tag{11-42}$$

$$\psi' = \tan^{-1}\frac{F}{\Omega} - \tan^{-1}\frac{1}{\mu_f\Omega} \tag{11-43}$$

$$\psi'' = \psi \tag{11-44}$$

Specific terms for flexible pavements are

$$a_1 = \zeta + 1 \qquad a_0 = \zeta \tag{11-45}$$

$$a_1' = \frac{\zeta}{\mu_f} + 1 \qquad a_0' = \frac{\zeta}{\mu_f} \tag{11-46}$$

$$a_1'' = \zeta + \frac{1}{\mu_p} \qquad a_0'' = \frac{\zeta}{\mu_p} \tag{11-47}$$

$$\Gamma_1 = \frac{1}{2}\left(G - \sqrt{G^2 - 4F}\right),\ \Gamma_2 = \frac{1}{2}\left(G + \sqrt{G^2 - 4F}\right) \tag{11-48}$$

$$G = \frac{1}{\delta}\left[\zeta\left(\rho^3\mu_p + 1\right) + \left(\rho^3 + \mu_f\right)\right],\quad F = \frac{\zeta}{\delta}\left(\rho^3 + 1\right) \tag{11-49}$$

$\zeta = \frac{\tau}{\tau_\sigma}$ = damping-stiffness ratio (11-50)

$\tau = \frac{\eta_p}{F_\rho}$ = plate material relaxation time (11-51)

$\tau_\sigma = \frac{\eta_f}{F_f}$ = foundation material relaxation time (11-52)

$\mu_p = 1 + \frac{F_p}{E_p}$ = ratio of dynamic to static stiffness of plate (11-53)

$$\mu_f = 1 + \frac{F_f}{E_f} = \text{ratio of dynamic to static stiffness of foundation} \quad (11\text{-}54)$$

$$E_p = \text{plate primary stiffness} \quad (11\text{-}55)$$

$$F_p = \text{plate secondary stiffness} \quad (11\text{-}56)$$

$$\eta_p = \text{plate damping} \quad (11\text{-}57)$$

$$E_f = \text{foundation primary stiffness} \quad (11\text{-}58)$$

$$F_f = \text{foundation secondary stiffness} \quad (11\text{-}59)$$

$$\eta_f = \text{foundation damping} \quad (11\text{-}60)$$

Specific terms for the rigid pavement are

$$F = \frac{1}{\delta}(\rho^3 + 1) \quad (11\text{-}61)$$

$$\mu_f = 1 + \frac{F_f}{E_f} = \text{ratio of dynamic to static stiffness} \quad (11\text{-}62)$$

$$\tau_\sigma = \frac{\eta_f}{F_f} = \text{foundation relaxation time} \quad (11\text{-}63)$$

$$E_p = \text{stiffness of plate} \quad (11\text{-}64)$$

$$E_f = \text{primary stiffness of foundation} \quad (11\text{-}65)$$

$$F_f = \text{secondary stiffness of foundation} \quad (11\text{-}66)$$

$$\eta_f = \text{foundation damping} \quad (11\text{-}67)$$

In general

$$\Omega = V\rho \cos\theta \tag{11-68}$$

$$V = \text{nondimensional velocity} \tag{11-69}$$

The nondimensional velocities are different for the two pavement types

$$V_{flexible} = \frac{V\tau}{\ell} \tag{11-70}$$

$$V_{rigid} = \frac{V\tau_\sigma}{\ell} \tag{11-71}$$

$$\tau = \frac{\eta_p}{F_p} \quad , \tau_\sigma = \frac{\eta_f}{F_f} \tag{11-72}$$

$$\ell = \left(\frac{D}{E_f}\right)^{1/3}, \quad D = \frac{E_p h^3}{12(1 - \nu_p^2)} \tag{11-73}$$

$$\nu_p = \text{plate Poisson's ratio} \tag{11-74}$$

$$h = \text{plate thickness} \tag{11-75}$$

12. PROGRAM INPUT REQUIREMENTS

FLEXIBLE PAVEMENT RESPONSE - ID No. 3634 FR
RIGID PAVEMENT - ID No. 3634 RR
NONDIMENSIONAL CORRECTION FACTORS - ID No. 3634 CF

Card 001

Same for all three programs
$\Delta\rho$ = Increment in ρ (size of a section) $1 \leq \rho \leq 5$
ERR = Allowable error due to change in $\rho \approx .001$

ERRI = Allowable error due to change in number of $\approx .01$ integration strips

Limit = Sets a limit to the number of times that ρ is incremented. This is an integer and must be right - adjusted in the fourth field. ≤ 100

ERR and ERRl affect the integration time which increases as these functions are decreased and vice versa.

Card 002

This card is input once per run

Card 003

This card is repeated for each case

All fields contain nine columns and all input valves, with the exception of LIMIT, are real variables.

Symbols 3634 FR

E_p = Plate primary stiffness - psi
F_p = Plate secondary stiffness - psi
E_f = Foundation primary stiffness - psi
F_f = Foundation secondary stiffness - psi
p = Tire pressure - psi
h = Plate thickness - in

P = Load magnitude - lbs

V = Velocity of load - mph

X, Y, Z = Spatial coordinates

η_p = Plate damping - lb

η_f = Foundation damping - lb

ν_p = Poisson's ratio

Symbols 3634 RR

E = Plate stiffness
All other symbols the same as in 3634 FR

Symbols 3634 CF

ζ = Damping-stiffness ratio

μ_f = Ratio of static to dynamic stiffness of foundation

μ_p = Ratio of static to dynamic stiffness of plate

r = Non dimensional radius

V = Non dimensional velocity

See p. 127

H_{dim} = Non dimensional thickness = h/l

Z_{dim} = Non dimensional depth = z/l

All other symbols the same as in 3634 FR

12. PROGRAM LISTINGS

ID 3634 FR

```
      COMMON/DTA/UP,UF,S,ZETA,A1,A0,AP1,AP0,CAPX,CAPY,G,AOW,A1W,VP,CAPZP36340001
      DIMENSION ANSW(6),ANSW1(6),IRR(13),ANSW2(6)                       36340002
      DATA IRR/2,4,6,8,10,12,16,20,24,28,32,36,40/                      36340003
      WRITE (6,2)                                                       36340004
      WRITE (6,3)                                                       36340005
      PI=3.141593                                                       36340006
      READ(5,95) DELI,ERR,ERR1,LIM                                      36340007
55    READ(5,100)EP,EF,FE,FF,SP,H                                       36340008
1     READ (5,100,END=999) CP,V,X,Y,Z,ETAP,ETAF,VP                      36340009
      IF (CP.EQ.0.0) GO TO 55                                           36340010
      D2=EP*H**3/(12.*(1.-VP**2))                                       36340041
      SL=    (D2/EF)**(1./3.)                                           36340012
      TS=ETAF/ELI                                                       36340013
      TE=ETAF*(1./EF+1./FF)                                             36340014
      TAU=ETAP/EP                                                       36340015
      UP=(EP+EP)/EP                                                     36340016
      UF=(EF+EF)/EF                                                     36340017
      ZETA=ETAP*FF/(ETAF*EP)                                            36340018
      CAPX=X/SL                                                         36340019
      CAPY=Y/SL                                                         36340020
      R=SQRT(CP/(PI*SP))                                                36340021
      G=R/SL                                                            36340022
      AKW=CP*SL/(4.*PI**2*D2) *SL                                       36340023
      AKP=    -CP*UF/(4.*PI**2*SL**2)                                   36340024
      A1=ZETA+1.                                                        36340025
      A0=ZETA                                                           36340026
      AP1=ZETA/UF+1.                                                    36340027
      AP0=ZETA/UF                                                       36340028
      AOW= ZETA/UP                                                      36340029
      A1W= ZETA+1./UP                                                   36340030
      ZP=Z-(H/2.)                                                       36340031
      CAPZ=Z/SL                                                         36340032
      CAPZP=ZP/SL                                                       36340033
      AKI=+7*AKW/SL**2                                                  36340034
      AKSIG= +3.*CP*Z/PI**2/H**3*UP                                     36340035
      S=17.6*V*TAU/SL                                                   36340036
      I=1                                                               36340037
      ICOUNT = 1                                                        36340038
      TLI = DELI                                                        36340039
      BLI = 0.0                                                         36340040
      DO 20 J=1,6                                                       36340041
20    ANSW2(J)=0.                                                       36340042
30    DO 4 J=1,6                                                        36340043
4     ANSW1(J)=0.                                                       36340044
1000  CALL SQII(IRR(I),6,2.*PI,0.,TLI,BLI,ANSW)                         36340045
      DO 41 J=1,6                                                       36340046
41    IF(ABS (ANSW1(J)-ANSW(J))          .GT.ERR1) GO TO 42             36340047
      GO TO 43                                                          36340048
42    IF(I.EQ.13) GO TO 43                                              36340049
      I=I+1                                                             36340050
      DO 421 J=1,6                                                      36340051
421   ANSW1(J)=ANSW(J)                                                  36340052
      GO TO 1000                                                        36340053
43    DO 44 J=1,6                                                       36340054
44    ANSW2(J) = ANSW2(J) + ANSW(J)                                     36340055
      IF(ICOUNT.EQ.1) GO TO 46                                          36340056
      DO 45 J=1,6                                                       36340057
45    IF(ABS(ANSW(J) )/ABS(ANSW2(J)).GT. ERR) GO TO 46                  36340058
      GO TO 48                                                          36340059
46    IF(ICOUNT .GE. LIM) GO TO 96                                      36340060
```

```
 47   ICOUNT = ICOUNT + 1                                                    36340061
      TLI = TLI + DELL                                                       36340062
      BLI = BLI + DELL                                                       36340063
      I=1                                                                    36340064
      GO TO 30                                                               36340065
  98  WRITE(6,99) I,N,J                                                      36340066
 48   W=AKW*ANSW2(1)                                                         36340067
      PZ=AKP*ANSW2(2)                                                        36340068
      EX=AKE*ANSW2(3)                                                        36340069
      EY=AKE*ANSW2(4)                                                        36340070
      SIGX=AKSIG*ANSW2(5)                                                    36340071
      SIGY=AKSIG*ANSW2(6)                                                    36340072
                          WRITE(6,200)                                       36340073
      WRITE(6,220) VP,X        ,FP,Y        ,FP,Z        ,ETAP,FF,FF,ETAF,36340074
     1 CP,H,SP,V                                                             36340075
      WRITE(6,225) UP,TAU,UF,D2,ZETA,SL,CAPZ,AKW,CAPZP,AKP,CAPX,AKE,        36340076
     1 CAPY,AKSIG,S,P,TS,TF                                                  36340077
      WRITE (6,230)AG,A1,APO,AP1,AOW,A1W                                     36340078
      WRITE (6,400) W,PZ,EX,EY,SIGX,SIGY                                     36340079
      GO TO 1                                                                36340080
 2    FORMAT('1',T55,'FLEXIBLE PAVEMENT RESPONSE'//                          36340081
     A'       ABSTRACT-  THIS PROGRAM COMPUTES THE RESPONSE OF A FLEXIBLE36340082
     B PAVEMENT SYSTEM TO MOVING TIRE LOADS.  ANALYTICALLY, THE       '//36340083
     C' FLEXIBLE PAVEMENT SYSTEM IS AN INFINITE VISCOELASTIC PLATE RESTI36340084
     DING ON A VISCOELASTIC HALF-SPACE WITH NO HORIZONTAL SHEARING    '//36340085
     E' STRESSES TRANSMITTED AT THE INTERFACE.  THE VISCOELASTICITY OF 36340086
     BOTH THE PLATE AND THE HALF-SPACE IS DESCRIBED BY A THREE-ELEMENT'//36340087
     G/' MODEL CONSISTING OF A LINEAR SPRING (E) IN PARALLEL WITH A LINE36340088
     HAR SPRING (E) AND LINEAR DASH POT (ETA) IN SERIES.              '//36340089
     I'       ANALYTICALLY, THE MOVING TIRE LOAD IS MODELED AS A LOAD OF'36340090
     J,' MAGNITUDE (UPPER CASE P)',                                          36340091
     K' DISTRIBUTED SO THAT THERE IS A UNIFORM'//' PRESSURE, P,36340092
     L, OVER A CIRCULAR AREA.  THE ENTIRE LOAD SYSTEM MOVES LONGITUDINAL36340093
     LLY (X - DIRECTION) AT A VELOCITY V.')                                  36340094
 3    FORMAT(/                                                               36340095
     A'       THE INPUTS TO THE PROGRAM ARE THE VISCOELASTIC MATERIAL CON36340096
     BSTANTS (E(P), E(P), ETA(P), NU(P), E(E), E(E), ETA(E)), THE      '//36340097
     C' PAVEMENT THICKNESS (H), THE SPACE VARIABLES (IN A COORD. SYSTEM 36340098
     DTHAT MOVES WITH THE LOAD) (X,Y,Z), AND THE LOAD VARIABLES       '//36340099
     E' (UPPER CASE P, P, V).  STANDARD ENGINEERING UNITS ARE USED, EXCE36340100
     EPT FOR THE VELOCITY WHICH IS IN MILES PER HOUR.                 '//36340101
     G'       THE OUTPUT OF THE PROGRAM IS PAVEMENT DEFLECTION (W), PAVEM36340102
     HENT LONGITUDINAL STRAIN (E(X)), PAVEMENT LATERAL STRAIN (E(Y)),'//36340103
     I' PAVEMENT LONGITUDINAL STRESS (SIG(X)), PAVEMENT LATERAL STRESS (36340104
     JSIG(Y)), AND FOUNDATION VERTICAL PRESSURE (P(Z)).')                    36340105
 95  FORMAT(3F9.0,I2)                                                       36340106
 99  FORMAT(' NO CONVERGENCE IN ',I4,' STEPS FOR FUNCTION ',I1)             36340107
100  FORMAT(8F9.0)                                                          36340108
200  FORMAT('1')                                                            36340109
220  FORMAT(' INPUT'//' MATERIAL CONSTANTS-', T23,'PAVEMENT POISSONS RA36340110
     ATIO, NU(P) =',T62,E13.5,T79,'RESPONSE LOCATION-',T100,'LONGITUDINA36340111
     AL, X =',T118, E13.5/T23,'PAVEMENT PRIMARY STIFFNESS, E(P) =',T62, 36340112
     CE13.5,T100,'LATERAL, Y =',T118,E13.5/T23,'PAVEMENT SECONDARY STIF36340113
     DNESS, E(P) =',T62,E13.5,T100,'VERTICAL, Z =',T118,E13.5          36340114
     C/ T23,'PAVEMENT DAMPING, ETA(P) =',T62,E13.5/ T23,'SOIL PRIMARY S136340115
     DIFFNESS, E(E) =',T62,E13.5/ T23,'SOIL SECONDARY STIFFNESS, E(E) ='36340116
     E,T62,E13.5/T23,'SOIL DAMPING, ETA(E) =',T62,E13.5//' LOAD VARIABL36340117
     ES-',T23,'TOTAL LOAD, CAP P =',T62,E13.5,T79,'PAVEMENT THICKNESS-',36340118
     GT100,'H =', T118,E13.5/T23,'TIRE PRESSURE, P ='                   36340119
     G,T62,E13.5/ T23,'LOAD VELOCITY, V =',T62,E13.5)                   36340120
```

```
225  FORMAT(/'0OUTPUT'/                                                    36340121
     0/' PAVEMENT STIFFNESS RATIO, MU(P) =',T42,F13.5,T65,'PAVEMENT RELA36340122
     IXATION TIME, TAU =',T108,E13.5/' SOIL STIFFNESS RATIO, MU(F) =',T436340123
     J2,E13.5,T65,'PAVEMENT PRIMARY BENDING STIFFNESS, D(2) =',T108,E13.36340124
     K5/' DAMPING RATIO X STIFFNESS RATIO, ZETA =',T42,E13.5,T65,'CHARAC36340125
     LTERISTIC LENGTH, L =',T108,E13.5/' NONDIMENSIONAL COORDINATE, Z =36340126
     M,T42,E13.5,T65,'DEFLECTION COEFFICIENT, K(W)=  ',T108,E13.5/' NON36340127
     NDIMENSIONAL COORDINATE, Z'' =',T42,E13.5,T65,'PRESSURE COEFFICIENT36340128
     0, K(P) =',T108,E13.5/' NONDIMENSIONAL COORDINATE, X =',T42,E13.5,T36340129
     P65,'STRAIN COEFFICIENT, K(E) =',T108,E13.5/' NONDIMENSIONAL COORDI36340130
     ONATE, Y =',T42,E13.5,T65,'STRESS COEFFICIENT, K(S) =',T108,E13.5/'36340131
     P NONDIMENSIONAL VELOCITY V =',T42,E13.5,T65,'EFFECTIVE FOOTPRINT R36340132
     SADIUS, P =',T108,E13.5/' SOIL RELAXATION TIME, TAU(SIGMA) = ',T42,36340133
     TE13.5,T65,'SOIL RELAXATION TIME, TAU(E) =',T108,E13.5)            36340134
230  FORMAT('0DEFLECTION TERMS A(0) =',T42,E13.5,T65,'A(1) =',T108,E13.36340135
     A5/' PRESSURE TERMS, A(0)'' =',T42,E13.5,T65,'A(1)'' =',T108,E13.5/36340136
     B' STRESS TERMS, A(0)'''' =',T42,E13.5,T65,'A(1)'''' =',T108,E13.5)36340137
400  FORMAT(                                                               36340138
     N/' DEFLECTION, W = ',T42,E13.5,T65,'PRESSURE, P(Z) = ',T108,E13.5 36340139
     0/' PAVEMENT LONG. STRAIN, E(X) = ',T42,E13.5,T65,'PAVEMENT LATERAL36340140
     P STRAIN, E(Y) = ',T108,E13.5                                      36340141
     Q/' PAVEMENT LONG. STRESS, SIG X= ',T42,E13.5,T65,'PAVEMENT LATERAL36340142
     P STRESS, SIG Y= ',T108,E13.5)                                     36340143
999  STOP                                                                36340144
     END                                                                 36340145
```

ID 3634 CF

```
      COMMON/DTA/UP,UF,V,ZETA,A1,A0,AP1,AP0,X,Y,R,AOW,AIW,VP,ZP          36340001
      DIMENSION ANSW(6),ANSW1(6),IRR(13),ANSW2(6)                        36340002
      DATA IRR/2,4,6,8,10,12,16,20,24,28,32,36,40/                       36340003
      PI=3.14159                                                         36340004
      PI2=PI**2                                                          36340005
      READ(5,95) DELL,EPN,FRR1,LIM                                       36340006
      READ(5,100) ZETA,VP,H,DH,X,Y,Z,DZ                                  36340007
1     READ(5,100,END=999) V,UF,UP,R                                      36340008
      NAT=0                                                              36340009
      DUM=1./(4.*PI2)                                                    36340010
      DUM1=DUM*DZ/DH                                                     36340011
      DUM2=3.*DZ*UP/(PI2*DH*(1.+VP))                                     36340012
      DUM3=-DUM*UF                                                       36340013
      A0=ZETA                                                            36340014
      A1=ZETA+1                                                          36340015
      AP0=ZETA/UF                                                        36340016
      AP1=ZETA/UF+1.                                                     36340017
      AOW=ZETA/UP                                                        36340018
      AIW=ZETA+1./UP                                                     36340019
      ZP=Z-(H/2.)                                                        36340020
      I=1                                                                36340021
      ICOUNT = 1                                                         36340022
      TLL = DELL                                                         36340023
      BLL = 0.0                                                          36340024
      DO 2 J=1,6                                                         36340025
2     ANSW2(J)=0.                                                        36340026
3     DO 4 J=1,6                                                         36340027
4     ANSW1(J)=0.                                                        36340028
1000  CALL SQI(IRR(I),6,2.*PI,0.,TLL,BLL,ANSW)                          36340029
      DO 41 J=1,6                                                        36340030
41    IF(ABS (ANSW1(J)-ANSW(J))          .GT.FRR1) GO TO 42              36340031
      GO TO 43                                                           36340032
42    IF(I.EQ.13) GO TO 43                                               36340033
      I=I+1                                                              36340034
      DO 421 J=1,6                                                       36340035
421   ANSW1(J)=ANSW(J)                                                   36340036
      GO TO 1000                                                         36340037
43    DO 44 J=1,6                                                        36340038
44    ANSW2(J) = ANSW2(J) + ANSW(J)                                      36340039
      IF(ICOUNT.EQ.1) GO TO 46                                           36340040
      DO 45 J=1,6                                                        36340041
45    IF(ABS(ANSW(J) )/ABS(ANSW2(J)).GT. FRR) GO TO 46                   36340042
      GO TO 48                                                           36340043
46    IF(ICOUNT .GE. LIM) GO TO 96                                       36340044
47    ICOUNT = ICOUNT + 1                                                36340045
      TLL = TLL + DELL                                                   36340046
      BLL = BLL + DELL                                                   36340047
      I=1                                                                36340048
      GO TO 3                                                            36340049
  96  WRITE(6,99) LIM,J                                                  36340050
48    IF(MOD(NAT,4).EQ.0) WRITE(6,200)                                   36340051
      NAT=NAT+1                                                          36340052
      WRITE(6,220) UP,X,UF,Y,ZETA,Z,VP,DZ,R,H,V,DH                       36340053
      ANSW2(1)=ANSW2(1)*DUM                                              36340054
      ANSW2(2)=ANSW2(2)*DUM3                                             36340055
      ANSW2(3)=ANSW2(3)*DUM1                                             36340056
      ANSW2(4)=ANSW2(4)*DUM1                                             36340057
      ANSW2(5)=ANSW2(5)*DUM2                                             36340058
      ANSW2(6)=ANSW2(6)*DUM2                                             36340059
      WRITE(6,400)  ANSW2(1),(ANSW2(J),J=3,6),ANSW2(2)                   36340060
```

```
      GO TO 1                                                           36340061
   95 FORMAT(8F9.0,I9)                                                  36340062
   99 FORMAT(' NO CONVERGENCE IN ',I4,' STEPS FOR FUNCTION ',I1)        36340063
  100 FORMAT(8F9.0)                                                     36340064
  200 FORMAT('1')                                                       36340065
  220 FORMAT(' PAVEMENT STIFFNESS RATIO, MU(P) =',T42,F13.5,T65,'NONDIME36340066
     1NSIONAL COORDINATE X=',T108,F13.5/                                36340067
     A' SOIL STIFFNESS RATIO, MU(S) =',                                 36340068
     2T42,F13.5,T65,'NONDIMENSIONAL COORDINATE Y =',T108,F13.5/' DAMPING36340069
     3 RATIO X STIFFNESS RATIO, ZETA =',T42,F13.5,T65,'NONDIMENSIONAL CO36340070
     4ORDINATE Z =',T108,F13.5/' PAVEMENT POISSONS RATIO, NU(P) =',T42, 36340071
     5F13.5,T65,'COORDINATE Z =',T108,F13.5/' NONDIMENSIONAL FOOTPRINT R36340072
     6ADIUS, R =',T42,F13.5,T65,'NONDIMENSIONAL PAVEMENT THICKNESS H =',36340073
     7T108,F13.5/' NONDIMENSIONAL VELOCITY V =',T42,F13.5,T65,          36340074
     8 'PAVEMENT THICKNESS H =',T108,F13.5)                             36340075
  400 FORMAT(///' NONDIMENSIONAL CORRECTION FACTORS',                   36340076
     A       /' C(W) =',T20,F13.5,T40,'C(EPSILON X) =',T60,F13.5,T80,   36340077
     1 'C(EPSILON Y) =',T100,F13.5/' C(SIGMA X) =',T20,F13.5,T40,       36340078
     2 'C(SIGMA Y) =',T60,F13.5,T80,'C(P) =',T100,F13.5///)             36340079
  999 STOP                                                              36340080
      END                                                               36340081
```

ID 3634 RR

```
      COMMON /DTA/ UF,S,G,VP,CAPX,CAPY,CAPZP                            36340001
      DIMENSION ANSW(6),ANSW1(6),IRR(13),ANSW2(6)                       36340002
      DATA IRP/2,4,6,8,10,12,16,20,24,28,32,36,40/                      36340003
      WRITE(6,2)                                                        36340004
      WRITE(6,3)                                                        36340005
      NAT=1                                                             36340006
      PI=4.141593                                                       36340007
      READ(5,95) DELL,ERR,ERR1,LIM                                      36340008
      READ(5,100) E,VP,H,SP                                             36340009
1     READ(5,100,END=999) FF,EE,ETAF,V,CP,X,Y,Z                         36340010
      D=E*H**3/(12.-12.*VP**2)                                          36340011
      SL=(D/FF)**(1./3.)                                                36340012
      CAPX=X/SL                                                         36340013
      CAPY=Y/SL                                                         36340014
      ZP=Z-(H/2.)                                                       36340015
      CAPZ=Z/SL                                                         36340016
      CAPZP=ZP/SL                                                       36340017
      R=SQRT(CP/(PI*SP))                                                36340018
      G=R/SL                                                            36340019
      UF=1.+EE/FF                                                       36340020
      TS=ETAF/FF                                                        36340021
      TT=ETAF*(1./EE+1./FF)                                             36340022
      AKW=CP*SL**2/(4.*PI**2*D)                                         36340023
      AKP=-CP/(4.*PI**2*SL**2)                                          36340024
      AKT=2*CP/(4.*PI**2*D)                                             36340025
      AKSIG=4.*Z*CP/(PI**2*H**3)                                        36340026
      NAT=NAT+1                                                         36340027
      S=V      *TS/SL                                                   36340028
      I=1                                                               36340029
      ICOUNT=1                                                          36340030
      TL1 = DELL                                                        36340031
      BL1 = 0.0                                                         36340032
      DO 20 J=1,6                                                       36340033
20    ANSW2(J)=0.                                                       36340034
30    DO 4 J=1,6                                                        36340035
4     ANSW1(J)=0.                                                       36340036
1000  CALL SOLEIRP(I,6,2.*PI,0.,TL1,BL1,ANSW)                           36340037
      DO 41 J=1,6                                                       36340038
41    IF(ABS(ANSW1(J)-ANSW(J))          .GT.ERR1) GO TO 42              36340039
      GO TO 43                                                          36340040
42    IF(I.EQ.13) GO TO 43                                              36340041
      I=I+1                                                             36340042
      DO 421 J=1,6                                                      36340043
421   ANSW1(J)=ANSW(J)                                                  36340044
      GO TO 1000                                                        36340045
43    DO 44 J=1,6                                                       36340046
44    ANSW2(J) = ANSW2(J) + ANSW(J)                                     36340047
      IF(ICOUNT.EQ.1) GO TO 48                                          36340048
      DO 45 J=1,6                                                       36340049
45    IF(ABS(ANSW(J) )/ABS(ANSW2(J)).GT. ERR) GO TO 46                  36340050
      GO TO 48                                                          36340051
46    IF(ICOUNT .GE. LIM) GO TO 96                                      36340052
47    ICOUNT = ICOUNT + 1                                               36340053
      TL1 = TL1 + DELL                                                  36340054
      BL1 = BL1 + DELL                                                  36340055
      I=1                                                               36340056
      GO TO 30                                                          36340057
  96  WRITE(6,99) LIM,J                                                 36340058
48    W=AKW*ANSW2(1)                                                    36340059
      PZ=AKP*ANSW2(2)                                                   36340060
```

```
      EX=AKE*ANSW2(3)                                                    36340061
      EY=AKE*ANSW2(4)                                                    36340062
      SIGX=AKSIG*ANSW2(5)                                                36340063
      SIGY=AKSIG*ANSW2(6)                                                36340064
      IF (MOD(NAT,2).EQ.0) WRITE(6,200)                                  36340065
      IF (MOD(NAT,2).NE.0) WRITE(6,250)                                  36340066
      WRITE(6,300) E,X,VP,Y,EF,Z,FF,ETAF,CP,H,SP,V                       36340067
      WRITE(6,350) DF,TS,CAPZ,TE,CAPZP,D,CAPX,SL,CAPY,AKW,S,AKE,R,AKP,   36340068
     1 AKSIG                                                             36340069
      WRITE (6,400) W,PZ,EX,EY,SIGX,SIGY                                 36340070
      GO TO 1                                                            36340071
    2 FORMAT('1',T53,'RIGID PAVEMENT RESPONSE'//                         36340072
     1'      ABSTRACT-  THIS PROGRAM COMPUTES THE RESPONSE OF A RIGID PA36340073
     2VEMENT SYSTEM TO MOVING TIRE LOADS.  THE ANALYTICAL MODEL OF     '//36340074
     3' THE PAVEMENT SYSTEM IS AN INFINITE ELASTIC PLATE RESTING ON A VI36340075
     4SCOELASTIC HALF-SPACE WITH NO HORIZONTAL SHEARING STRESSES       '//36340076
     5' TRANSMITTED AT THE INTERFACE.  THE VISCOELASTICITY OF THE HALF-S36340077
     6PACE IS REPRESENTED BY A THREE-ELEMENT MODEL CONSISTING OF A     '//36340078
     7' LINEAR SPRING (E(F)) IN PARALLEL WITH A LINEAR SPRING (F(F)) ANDO36340079
     8 A LINEAR DASH POT (ETA(F)) IN SERIES.                           '//36340080
     9'      THE MOVING TIRE LOAD IS MODELLED AS A LOAD OF MAGNITUDE (UP36340081
     APER CASE P) DISTRIBUTED SO THAT THERE IS A UNIFORM PRESSURE      '//36340082
     B' (P) OVER A CIRCULAR AREA.  THE ENTIRE LOAD SYSTEM MOVES LONGITUD36340083
     CINALLY (X - DIRECTION) AT A VELOCITY V.')                          36340084
    3 FORMAT(/                                                           36340085
     1'      INPUTS TO THE PROGRAM ARE THE MATERIAL CONSTANTS FOR THE PL36340086
     2ATE (E, MODULUS AND NU(P), POISSON'S RATIO), THE MATERIAL        '//36340087
     3' CONSTANTS OF THE HALF-SPACE (E(F), F(F), ETA(F)), THE PLATE-THIC36340088
     4KNESS (H), THE SPACE VARIABLES (IN A COORDINATE SYSTEM THAT      '//36340089
     5' MOVES WITH THE LOAD) (X,Y,Z), AND THE LOAD VARIABLES (UPPER CASE36340090
     6 P, P, V).  STANDARD ENGINEERING UNITS ARE USED, EXCEPT FOR      '//36340091
     7' THE VELOCITY WHICH IS IN MILES PER HOUR.                       '//36340092
     8'      THE OUTPUT OF THE PROGRAM IS THE STEADY-STATE RESPONSE OF T36340093
     9HE SYSTEM-  THE PLATE DEFLECTION (W), PAVEMENT LONGITUDINAL      '//36340094
     A' STRAIN (E(X)), PAVEMENT LATERAL STRAIN (E(Y)), PAVEMENT LONGITUD36340095
     BINAL STRESS (SIG(X)), PAVEMENT LATERAL STRESS (SIG(Y)), AND      '//36340096
     C' FOUNDATION VERTICAL PRESSURE (P(Z)).')                           36340097
   95 FORMAT(3E9.0,I9)                                                   36340098
   99 FORMAT(' NO CONVERGENCE IN 'I4,' STEPS FOR FUNCTION 'I1)           36340099
  100 FORMAT(8E9.0)                                                      36340100
  200 FORMAT('1')                                                        36340101
  250 FORMAT(///)                                                        36340102
  300 FORMAT(' INPUT'//' MATERIAL CONSTANTS-',T23,'PAVEMENT MODULUS, E =36340103
     1',T62,E13.5,T79,'RESPONSE LOCATION-',T100,'LONGITUDINAL, X =',T118336340104
     2,E13.5/T23,'PAVEMENT POISSON'S RATIO, NU(P) = ',T62,E13.5,T100,   36340105
     3'LATERAL, Y =',T118,E13.5/T23,'SOIL PRIMARY STIFFNESS, E(F) =',T6236340106
     4,E13.5,T100,'VERTICAL, Z =',T118,E13.5/T23,'SOIL SECONDARY STIFFNE36340107
     5SS, F(F) =',T62,E13.5/T23,'SOIL DAMPING, ETA(F) =',T62,E13.5//    36340108
     6' LOAD VARIABLES-',T23,'TOTAL LOAD, CAP P =',T62,E13.5,T79,'PAVEME36340109
     7NT THICKNESS-',T100,'H =',T118,E13.5/T23,'TIRE PRESSURE, P =',T62,36340110
     8E13.5/T23,'LOAD VELOCITY, V =',T62,F13.5)                          36340111
  350 FORMAT(/'OOUTPUT'//                                                36340112
     1' SOIL STIFFNESS RATIO, MU(F) =',T42,E13.5,T65,'SOIL RELAXATION TI36340113
     2ME, TAU(SIGMA) =',T108,E13.5/' NONDIMENSIONAL COORDINATE, Z =',T4236340114
     3,E13.5,T65,'SOIL RELAXATION TIME, TAU(E) =',T108,E13.5/           36340115
     4' NONDIMENSIONAL COORDINATE, Z'' =',T42,E13.5,T65,'PLATE BENDING S36340116
     5TIFFNESS, D =',T108,E13.5/' NONDIMENSIONAL COORDINATE, X =',T42,  36340117
     6E13.5,T65,'CHARACTERISTIC LENGTH, L =',T108,E13.5/' NONDIMENSIONAL36340118
     7 COORDINATE, Y =',T42,E13.5,T65,'DEFLECTION COEFFICIENT, K(W) =', 36340119
     8T108,E13.5/' NONDIMENSIONAL VELOCITY, V =',T42,E13.5,T65,'STRAIN C36340120
```

```
     OEFFICIENT, K(F) =',T108,E13.5/' EFFFCTIVE FOOTPRINT RADIUS, R =',36340121
     AT42,F13.5,T65,'PRESSURF COEFFICIENT, K(P) =',T108,E13.5/T65,      36340122
     B 'STRESS COEFFICIENT, K(S) =',T108,E13.5)                         36340123
400   FORMAT(                                                          36340124
     N/' DEFLECTION, W = ',T42,E13.5,T65,'PRESSURE, P(Z) = ',T108,E13.5 36340125
     O/' PAVEMENT LONG. STRAIN, E(X) = ',T42,E13.5,T65,'PAVEMENT LATERAL36340126
     P STRAIN, E(Y) = ',T108,E13.5                                      36340127
     Q/' PAVEMENT LONG. STRESS, SIG X= ',T42,E13.5,T65,'PAVEMENT LATERAL36340128
     R STRESS, SIG Y= ',T108,E13.5)                                     36340129
999   STOP                                                             36340130
      END                                                              36340131
```

Subroutines:

```
      SUBROUTINE PFXI(RHO,THT,PS)                (ID 3634 RR only)     36340132
      COMMON /DTA/ UF,V,R,VP,CAPX,CAPY,CAPZP                           36340133
      DIMENSION RS(6)                                                  36340134
      P3=RHO**3                                                        36340135
      DEL=P3+UF                                                        36340136
      F=(P3+1.)/DEL                                                    36340137
      OMF=V*RHO*COS(THT)                                               36340138
      PSI=ATAN2(F,OMF)-ATAN2(1.,OMF)                                   36340139
      PSIP=ATAN2(F,OMF)-ATAN2(1.,OMF*UF)                               36340140
      CAPN=SQRT((1.+OMF**2)/(F**2+OMF**2))                             36340141
      CAPNP=SQRT((1./UF**2+OMF**2)/(F**2+OMF**2))                      36340142
      PHI=RHO*(CAPX*COS(THT)+CAPY*SIN(THT))                            36340143
      RS(1)=CAPN*COS(PHI-PSI)/DEL                                      36340144
      RS(2)=CAPNP*COS(PHI-PSIP)  *RHO*(1.+RHO*CAPZP)*EXP(-RHO*CAPZP)/DEL36340145
      DUM1=CAPN*COS(PHI-PSI)/DEL                                       36340146
      RS(3)=DUM1*(RHO*COS(THT))**2                                     36340147
      RS(4)=DUM1*(RHO*SIN(THT))**2                                     36340148
      RS(5)=DUM1*RHO**2*(COS(THT)**2+VP*SIN(THT)**2)                   36340149
      RS(6)=DUM1*RHO**2*(SIN(THT)**2+VP*COS(THT)**2)                   36340150
      CALL HFSJ(R*RHO,1,CR,1.E-4,IER)                                  36340151
      DO 1 I=1,6                                                       36340152
1     RS(I)=RS(I)*CR**2./(R*RHO)                                       36340153
      RETURN                                                           36340154
      END                                                              36340155
```

```
      SUBROUTINE SQI (N,NP,TL,BL,TL1,BL1,STORE3)                       SQI 0000
C        N - NUMBER OF STRIPS                                          SQI 0001
C N CAN =2,4,6,8,10,12,16,20,24,28,32,36,40 ONLY                       SQI 0002
C        NP - NUMBER OF FUNCTIONS COMPUTED AT ONE INTRY TO SPAN-F(Y)    SQI 0003
C        TL - TOP LIMIT                                                SQI 0004
C        BL - BOTTOM LIMIT                                             SQI 0005
C        STORE3 - Y(NP)   ANSWERS STORED IN ONE DIMENSION ARRAY        SQI 0006
C        SUBROUTINE CHWI(THETA,STORE,NP)                               SQI 0007
C             THETA - VALUE AT WHICH TO EVALUATE FUNCTION              SQI 0008
C             STORE - EVALUATED FUNCTION                               SQI 0009
      DIMENSION CON(322),STORE1(200),STORE2(200),STORE3(200)           SQI 0010
     A,CAN(104),CBN(114),CCN(104)                                      SQI 0011
```

```
     8,ISH(21)                                                                  SQI 0012
       EQUIVALENCE  (CON(1),CAN(1)),(CON(109),CBN(1)),(CON(219),CCN(1))         SQI 0013
      DATA ISH/104,0,4,8,14,20,28,36,46,106,118,130,144,158,56,174,194,         SQI 0014
     A 218,72,246,282/                                                          SQI 0015
      DATA CAN                  /0.0,.88888889,.774596669,.555555556,           SQI 0016
     1.339981044,..652145155,..861136312,..347854845,0.0,..568888889,           SQI 0017
     2.53846931,..47862867,..906179846,..238926885,..238619186,..467913935,     SQI 0018
     3.661209386,..360761573,..932469514,..171324492,0.0,..417959184,           SQI 0019
     4.405845151,..38183005,..741531186,..279705391,..949107912,..129484966,    SQI 0020
     5.183434642,..362683783,..52553241,..313706646,..796666477,..222381034,    SQI 0021
     6.960289856,..101228536,0.0,..350239355,..324253423,..312347077,           SQI 0022
     7.613371433,..260610696,..836031107,..180648161,..96816024,..081274388,    SQI 0023
     8.148874339,..295524225,..433395394,..269266719,..679409568,..219086363,SQI 0024
     9.865063367,..149451349,..973906529,..066671344,..09501251,..18945061,     SQI 0025
     A.281603551,..182603415,..458016778,..169156519,..617876244,..149595989,SQI 0026
     B.755404408,..124628971,..865631202,..095158512,..944575023,..062253524,SQI 0027
     C.989400935,..027152459,..048307666,..096540089,..144471962,..09563872,   SQI 0028
     D.239287362,..093844400,..331868602,..091173879,..421351276,..087652093,SQI 0029
     E.506899909,..083311924,..587715757,..078193896,..663044267,..072345794,SQI 0030
     F.732182119,..065822223,..794483796,..058684093,..849367614,..050998059,SQI 0031
     G.896321156,..042835898,..934906076,..034273863,..964762256,..025392065,SQI 0032
     H.985611512,..016274395,..997263862,..00701861/                            SQI 0033
      DATA CBN                  /.577350269,1.0,0.0,..272925087,..269543156,    SQI 0034
     1.262804544,..519096129,..233193765,..730152006,..186290211,..8870626,     SQI 0035
     2.12558037,..978228658,..055668567,..125333408,..249147046,..367831499,    SQI 0036
     3.233492536,..587317954,..203167427,..769902674,..160078328,..904117256,SQI 0037
     4.106939326,..981560634,..047175336,0.0,..232551553,..230458316,           SQI 0038
     5.226283180,..448492751,..207816048,..642349339,..178145981,..801578091,SQI 0039
     6.138873510,..917568399,..0921215,..984183055,..040484005,..108054949,     SQI 0040
     7.215263854,..319112369,..205198464,..515248636,..185538398,..687292905,SQI 0041
     8.157203167,..827201315,..121518571,..928434884,..080158087,..986283809,SQI 0042
     9.03511946,0.0,..202578242,..201194094,..198431485,..394151347,            SQI 0043
     A.186161,..570572173,..166269206,..724417731,..139570678,..848206583,     SQI 0044
     B.10715922,..937273392,..070366048,..987992518,..030753242,..076526521,    SQI 0045
     C.152753387,..227785851,..149172986,..373706089,..142096109,..510867002,SQI 0046
     D.131688638,..636053681,..118194532,..746331906,..10193012,..839116972,    SQI 0047
     E.083276742,..912234428,..062672048,..963971927,..04060143,..993128599,    SQI 0048
     F.017614007,..064056893,..127938195,..191118867,..125837456,..31504268,    SQI 0049
     G.121670473,..433793508,..115505668,..545421471,..10744427,..648093652,    SQI 0050
     H.097618652,..740124192,..086190162,..820001986,..073346481,..886415527,SQI 0051
     I.059298585,..938274552,..044277439,..974728556,..028531389,..99518722,    SQI 0052
     J.012341237/                                                               SQI 0053
      DATA  CCN                 /.05507929,..110047013,..164569282,             SQI 0054
     1.108711192,..272061628,..106055766,..376251516,..102112968,..475874225,SQI 0055
     2.096930658,..569720472,..090571744,..656651094,..083113417,..735610878,SQI 0056
     3.074646214,..805641371,..065272924,..865892523,..055107346,..915633026,SQI 0057
     4.044272935,..954259281,..032901428,..981303165,..021132113,..996442498,SQI 0058
     5.009124283,..043018198,..085983276,..128736104,..085346686,..213500892,SQI 0059
     6.084078219,..296684995,..082187267,..377672547,..079687829,..455863944,SQI 0060
     7.076598411,..530680286,..072941885,..601567658,..068745324,..668001237,SQI 0061
     8.064039797,..729489172,..058860144,..78557623,..053244714,..835847167,    SQI 0062
     9.047235083,..879929801,..040875751,..917497775,..034213811,..948272984,SQI 0063
     A.027298621,..972027691,..020181515,..988586479,..012915947,..997830462,SQI 0064
     B.00556572,..038772418,..077505948,..116084071,..077039818,..192697581,    SQI 0065
     C.076110362,..268152185,..074723169,..341994091,..072886582,..413779204,SQI 0066
     D.070611647,..483075802,..067912046,..549467125,..064804013,..61255389,    SQI 0067
     E.061306242,..671956685,..057439769,..727318255,..053227847,..778305651,SQI 0068
     F.048695809,..824612231,..043870908,..865959503,..038782168,..902098807,SQI 0069
     G.033460195,..932812808,..027937007,..957916819,..022245849,..97725995,    SQI 0070
     H.016421058,..990726239,..010498285,..99823771,..004521277/                SQI 0071
15    JT = N - 1                                                                SQI 0072
      IF (JT.LT.16)  GO TO 16                                                   SQI 0073
      JT = (N - 16)/4 + 15                                                      SQI 0074
16    K=ISH(JT)                                                                 SQI 0075
325   DO 330 IP=1,NP                                                            SQI 0076
      STORE3(IP) = 0.0                                                          SQI 0077
```

```
  330  CONTINUE                                                          SQI 0078
       PLUS = (TL+BL)/2.0                                                SQI 0079
       PMUS = (TL-BL)/2.0                                                SQI 0080
       DO 400 I=1,N,2                                                    SQI 0081
       IC = K+I                                                          SQI 0082
       I1 = IC+1                                                         SQI 0083
       PHI = PLUS-PMUS*CON(IC)                                           SQI 0084
       CALL GQI(N ,NP,TL1,BL1,PHI,STORE1)                                SQI 0085
       IF (CON(IC)) 345,335,345                                          SQI 0086
  335  DO 340 IX=1,NP                                                    SQI 0087
       STORE2(IX) = 0.0                                                  SQI 0088
  340  CONTINUE                                                          SQI 0089
       GO TO 347                                                         SQI 0090
  345  PHI = PLUS+PMUS*CON(IC)                                           SQI 0091
       CALL GQI(N ,NP,TL1,BL1,PHI,STORE2)                                SQI 0092
  347  DO 350 J=1,NP                                                     SQI 0093
       STORE3(J) = (STORE1(J)+STORE2(J))*CON(I1)+STORE3(J)               SQI 0094
  350  CONTINUE                                                          SQI 0095
  400  CONTINUE                                                          SQI 0096
       DO 450 IP=1,NP                                                    SQI 0097
       STORE3(IP) = STORE3(IP)*PMUS                                      SQI 0098
  450  CONTINUE                                                          SQI 0099
       RETURN                                                            SQI 0100
       END                                                               SQI 0101

       SUBROUTINE GQI (N,NP,TL ,BL ,FVAL2,STORE3)
C         N - NUMBER OF STRIPS                                           GQI 0000
C N CAN =2,4,6,8,10,12,16,20,24,28,32,36,40 ONLY                         GQI 0001
C         NP - NUMBER OF FUNCTIONS COMPUTED AT ONE INTRY TO SPAN-F(Y)     GQI 0002
C         TL - TOP LIMIT                                                 GQI 0003
C         BL - BOTTOM LIMIT                                              GQI 0004
C         STORE3 - Y(NP)   ANSWERS STORED IN ONE DIMENSION ARRAY         GQI 0005
C         SUBROUTINE SPAN(PHI,STORE,NP)                                  GQI 0006
C              PHI -  VALUE AT WHICH TO EVALUATE FUNCTION                GQI 0007
C              STORE -  EVALUATED FUNCTION                               GQI 0008
       DIMENSION CON(322),STORE1(200),STORE2(200),STORE3(200)            GQI 0009
      A,CAN(104),CBN(114),CCN(104)                                       GQI 0010
      B,ISH(21)                                                          GQI 0011
        EQUIVALENCE  (CON(1),CAN(1)),(CON(105),CBN(1)),(CON(219),CCN(1)) GQI 0012
       DATA ISH/104,0,4,8,14,20,28,36,46,106,118,130,144,158,56,174,194, GQI 0013
      A 218,72,246,282/                                                  GQI 0014
       DATA CAN              /0.0,.88888889,.774596669,.555555556,        GQI 0015
      1.339981044,.652145155,.861136312,.347854845,0.0,.568888889,       GQI 0016
      2.53846931,.47862967,.906179846,.236926885,.238619186,.467913935,  GQI 0017
      3.661209386,.360761573,.932469514,.171324492,0.0,.417959184,       GQI 0018
      4.405845151,.38183005,.741531186,.279705391,.949107912,.129484966, GQI 0019
      5.183434642,.362683783,.52553241,.313706646,.796666477,.222381034,  GQI 0020
      6.960289856,.101228536,0.0,.330239355,.324253423,.312347077,        GQI 0021
      7.813371433,.260610696,.836C31107,.180648161,.96816024,.081274388,  GQI 0022
      8.148874338,.295524225,.433395394,.269266719,.679409568,.219086363,GQI 0024
      9.865063367,.149451349,.973906529,.066671344,.09501251,.18945061,   GQI 0025
      A.281603551,.182603415,.458016778,.169156519,.617876244,.149595989,GQI 0026
      B.755404408,.124628971,.965631202,.095158512,.944575023,.062253524,GQI 0027
      C.989400935,.027152459,.048307666,.096540089,.144471962,.09563872, GQI 0028
      D.238287362,.093844400,.331868602,.091173879,.421351276,.087652093,GQI 0029
      E.506899909,.083311924,.587715757,.078193896,.663044267,.072345794,GQI 0030
      F.732182119,.065822223,.794483796,.058684093,.849367614,.050998059,GQI 0031
      G.896321156,.042835898,.934906076,.034273863,.964762256,.025392065,GQI 0032
      H.985611512,.016274395,.997263862,.00701861/                       GQI 0033
       DATA CBN              /.577350269,1.0,0.0,.272925087,.269543156,   GQI 0034
      1.262804544,.519096129,.239193765,.730152006,.186290211,.8870626,   GQI 0035
      2.125580837,.97822865A,.055668567,.125333408,.249147046,.367831499, GQI 0036
      3.233452536,.587317954,.203167427,.769902674,.160078328,.904117256,GQI 0037
      4.106939326,.981560634,.047175336,0.0,.232551553,.230458316,        GQI 0038
      5.226283180,.448492751,.207816048,.642349339,.178145981,.801578091,GQI 0039
      6.138873510,.917598399,.0921215,.984183055,.040484005,.108054949,   GQI 0040
```

```
     7.215263854,.319112369,.205198464,.515248636,.185538398,.687292905,GQI 0041
     8.157203167,.827201315,.121518571,.928434884,.080158087,.986283809,GQI 0042
     9.03511946,0.0,.202578242,.201194094,.198431485,.394151347,        GQI 0043
     A.186161,.570972173,.166269206,.724417731,.139570678,.848206583,   GQI 0044
     B.10715922,.937274392,.070366048,.987992518,.030753242,.076526521, GQI 0045
     C.152753387,.227785851,.149172986,.373706089,.142096109,.510867002,GQI 0046
     D.131688638,.636053681,.118194532,.746331906,.10193012,.839116972, GQI 0047
     E.083276742,.912234428,.062672048,.963971927,.04060143,.993128599, GQI 0048
     F.017614007,.064056893,.127938195,.191118867,.125837456,.31504268, GQI 0049
     G.121670472,.433793508,.115505668,.545421471,.10744427,.648093652, GQI 0050
     H.097618652,.740124192,.086190162,.820001986,.073346481,.886415527,GQI 0051
     I.059288585,.938274552,.044277439,.974728556,.028531389,.99518722, GQI 0052
     J.012341237
      DATA  CCN                                                         GQI 0053
     1/.055C7929,.110047013,.164569282,                                 GQI 0054
     1.108711192,.27206162B,.106055766,.376251516,.102112968,.475874225,GQI 0055
     2.096930658,.569720472,.090571744,.656651094,.083113417,.735610878,GQI 0056
     3.074646214,.805641371,.065272924,.865892523,.055107346,.915633026,GQI 0057
     4.044272935,.954259281,.03290142B,.981303165,.021132113,.996442498,GQI 0058
     5.009124283,.C43018198,.085983276,.128736104,.085346686,.213500892,GCI 0059
     6.084078219,.296684995,.082187267,.377672547,.079687829,.455843944,GQI 0060
     7.076598411,.530680286,.072941885,.601567658,.068745324,.668001237,GQI 0061
     8.064039797,.729499172,.058860144,.78557623,.053244714,.838847167, GQI 0062
     9.047235083,.879929801,.040875751,.917497775,.034213811,.948272984,GQI 0063
     A.027298621,.972027691,.020181515,.988586479,.012915947,.997830462,GQI 0064
     B.00556572,.038772418,.077505948,.116084071,.077039818,.192697581, GQI 0065
     C.076110362,.268152185,.074723169,.341994091,.072886582,.413779204,GQI 0066
     D.070611647,.483075802,.067912046,.549467125,.064804013,.61255389, GQI 0067
     E.061306242,.671956685,.057439769,.727318255,.053227847,.778305651,GQI 0068
     F.048695808,.824612231,.04387090B,.865959503,.038782168,.902098807,GCI 0069
     G.033460195,.932812808,.027937007,.957916819,.022245849,.97725995, GQI 0070
     H.016421058,.990726239,.010498285,.99823771,.0045212777/           GQI 0071
15   JT = N - 1                                                         GQI 0072
     IF (JT.LT.16)  GO TO 16                                            GCI 0073
     JT = (N - 16)/4 + 15                                               GQI 0074
16   K=ISH(JT)                                                          GQI 0075
325  DO 330 IP=1,NP                                                     GCI 0076
     STORE3(IP) = 0.0                                                   GQI 0077
330  CONTINUE                                                           GQI 0078
     PLUS = (TL+AL)/2.0                                                 GQI 0079
     PMUS = (TL-AL)/2.0                                                 GQI 0080
     DO 400 I=1,N,2                                                     GQI 0081
     IC = K+I                                                           GQI 0082
     I1 = IC+1                                                          GQI 0083
     PHI = PLUS-PMUS*CON(IC)                                            GQI 0084
     CALL PEXI (PHI,EVAL2,STORE1)                                       GQI 0085
     IF (CON(IC)) 345,335,345                                           GQI 0086
335  DO 340 IX=1,NP                                                     GQI 0087
     STORE2(IX) = 0.0                                                   GQI 0088
340  CONTINUE                                                           GQI 0089
     GO TO 347                                                          GQI 0090
345  PHI = PLUS+PMUS*CON(IC)                                            GQI 0091
     CALL PEXI (PHI,EVAL2,STORE2)                                       GQI 0092
347  DO 350 J=1,NP                                                      GQI 0093
     STORE3(J) = (STORE1(J)+STORE2(J))*CON(I1)+STORE3(J)                GQI 0094
350  CONTINUE                                                           GQI 0095
400  CONTINUE                                                           GQI 0096
     DO 450 IP=1,NP                                                     GQI 0097
     STORE3(IP) = STORE3(IP)*PMUS                                       GQI 0098
450  CONTINUE                                                           GQI 0099
     RETURN                                                             GQI 0100
     END                                                                GQI 0101
```

```
      SUBROUTINE PFXI(RHO,THT,RS)          (3634 FR & 3634 CF)                PFXI0000
      COMMON/DTA/UP,UF,V,ZETA,A1,A0,AP1,APO,CAPX,CAPY,R,AOW,A1W,VP,CAPZPPFXI0001
      DIMENSION RS(6)                                                         PFXI0002
      P3=RHO**3                                                               PFXI0003
      DEL=UP*P3+UF                                                            PFXI0004
      OME=V*RHO*COS(THT)                                                      PFXI0005
      G=(ZETA*(P3*UP+1.)+P3+UF)/DEL                                           PFXI0006
      F=ZETA*(P3+1.)/DEL                                                      PFXI0007
      DUM1=SQRT(G**2-4.*F)                                                    PFXI0008
      R1=.5*(G-DUM1)                                                          PFXI0009
      R2=.5*(G+DUM1)                                                          PFXI0010
      DUM1=-ATAN2(OME,R1)-ATAN2(OME,R2)                                       PFXI0011
      PSI=ATAN2(A1*OME,A0-OME**2) +DUM1                                       PFXI0012
      PSIP=ATAN2(AP1*OME,APO-OME**2 )+DUM1                                    PFXI0013
      PSIW=ATAN2(A1W*OME,AOW-OME**2)+DUM1                                     PFXI0014
      DUM1=(R1**2+OME**2)*(R2**2+OME**2)                                      PFXI0015
      CAPN=SQRT((A1**2*OME**2+(A0-OME**2)**2)/DUM1)                           PFXI0016
      CAPNP=SQRT((AP1**2*OME**2+(APO-OME**2)**2)/DUM1)                        PFXI0017
      CAPNW=SQRT((A1W**2*OME**2+(AOW-OME **2)**2)/DUM1)                       PFXI0018
      PHI=RHO*(CAPX*COS(THT)+CAPY*SIN(THT))                                   PFXI0019
      RS(1)=CAPN*BOS(PHI-PSI,1)/DEL                                           PFXI0020
      RS(2)=CAPNP*BOS(PHI-PSIP,1)/DEL*(1.+RHO*CAPZP)*RHO*EXP(-RHO*CAPZP)PFXI0021
      RS(3)=RS(1)*(RHO*COS(THT))**2                                           PFXI0022
      RS(4)=RS(1)*(RHO*SIN(THT))**2                                           PFXI0023
      AIWP = CAPNW     *BOS(PHI-PSIW,1)/DEL*RHO**2                            PFXI0024
      RS(5)=  AIWP*(COS(THT)**2+VP*SIN(THT)**2)                               PFXI0025
      RS(6)=  AIWP*(SIN(THT)**2+VP*COS(THT)**2)                               PFXI0026
      CALL BESJ(R*RHO,1,CR,1.E-4,IER)                                         PFXI0027
      DO 1 I=1,6                                                              PFXI0028
    1 RS(I)=RS(I)*CR*2./(R*RHO)                                               PFXI0029
      RETURN                                                                  PFXI0030
      END                                                                     PFXI0031
C     ..................................................................BESJ0001
C                                                                             BESJ0002
C        SUBROUTINE BESJ                                                      BESJ0003
C                                                                             BESJ0004
C        PURPOSE                                                              BESJ0005
C           COMPUTE THE J BESSEL FUNCTION FOR A GIVEN ARGUMENT AND ORDER      BESJ0006
C                                                                             BESJ0007
C        USAGE                                                                BESJ0008
C           CALL BESJ(X,N,BJ,D,IER)                                           BESJ0009
C                                                                             BESJ0010
C        DESCRIPTION OF PARAMETERS                                            BESJ0011
C           X  -THE ARGUMENT OF THE J BESSEL FUNCTION DESIRED                 BESJ0012
C           N  -THE ORDER OF THE J BESSEL FUNCTION DESIRED                    BESJ0013
C           BJ -THE RESULTANT J BESSEL FUNCTION                               BESJ0014
C           D  -REQUIRED ACCURACY                                             BESJ0015
C           IER-RESULTANT ERROR CODE WHERE                                    BESJ0016
C              IER=0  NO ERROR                                                BESJ0017
C              IER=1  N IS NEGATIVE                                           BESJ0018
C              IER=2  X IS NEGATIVE OR ZERO                                   BESJ0019
C              IER=3  REQUIRED ACCURACY NOT OBTAINED                          BESJ0020
C              IER=4  RANGE OF N COMPARED TO X NOT CORRECT (SEE REMARKS)      BESJ0021
C                                                                             BESJ0022
C        REMARKS                                                              BESJ0023
C           N MUST BE GREATER THAN OR EQUAL TO ZERO, BUT IT MUST BE           BESJ0024
C           LESS THAN                                                         BESJ0025
C              20+10*X-X** 2/3   FOR X LESS THAN OR EQUAL TO 15               BESJ0026
C              90+X/2            FOR X GREATER THAN 15                       BESJ0027
C                                                                             BESJ0028
C        SUBROUTINES AND FUNCTION SUBPROGRAMS REQUIRED                        BESJ0029
C           NONE                                                              BESJ0030
C                                                                             BESJ0031
C        METHOD                                                               BESJ0032
C           RECURRENCE RELATION TECHNIQUE DESCRIBED BY H. GOLDSTEIN AND       BESJ0033
C           R.M. THALER, 'RECURRENCE TECHNIQUES FOR THE CALCULATION OF        BESJ0034
```

```
C           BESSEL FUNCTIONS',M.T.A.C.,V.13,PP.102-108 AND I.A. STEGUN  BESJ0035
C           AND M. ABRAMOWITZ,'GENERATION OF BESSEL FUNCTIONS ON HIGH   BESJ0036
C           SPEED COMPUTERS',M.T.A.C.,V.11,1957,PP.255-257              BESJ0037
C                                                                       BESJ0038
C     ..................................................................BESJ0039
      SUBROUTINE BESJ(X,N,BJ,D,IER)                                     BESJ0040
C                                                                       BESJ0041
      BJ=.0                                                             BESJ0042
      IF(N)10,20,20                                                     BESJ0043
   10 IER=1                                                             BESJ0044
      RETURN                                                            BESJ0045
   20 IF(X)30,30,31                                                     BESJ0046
   30 IER=2                                                             BESJ0047
      RETURN                                                            BESJ0048
   31 IF(X-15.)32,32,34                                                 BESJ0049
   32 NTEST=20.+10.*X-X** 2/3                                           BESJ0050
      GO TO 36                                                          BESJ0051
   34 NTEST=90.+X/2.                                                    BESJ0052
   36 IF(N-NTEST)40,38,38                                               BESJ0053
   38 IER=4                                                             BESJ0054
      RETURN                                                            BESJ0055
   40 IER=0                                                             BESJ0056
      N1=N+1                                                            BESJ0057
      BPREV=.0                                                          BESJ0058
C                                                                       BESJ0059
C     COMPUTE STARTING VALUE OF M                                       BESJ0060
C                                                                       BESJ0061
      IF(X-5.)50,60,60                                                  BESJ0062
   50 MA=X+6.                                                           BESJ0063
      GO TO 70                                                          BESJ0064
   60 MA=1.4*X+60./X                                                    BESJ0065
   70 MB=N+IFIX(X)/4+2                                                  BESJ0066
      MZERO=MAXO(MA,MB)                                                 BESJ0067
C                                                                       BESJ0068
C     SET UPPER LIMIT OF M                                              BESJ0069
C                                                                       BESJ0070
      MMAX=NTEST                                                        BESJ0071
  100 DO 190 M=MZERO,MMAX,3                                             BESJ0072
C                                                                       BESJ0073
C     SET F(M),F(M-1)                                                   BESJ0074
C                                                                       BESJ0075
      FM1=1.0E-28                                                       BESJ0076
      FM=.0                                                             BESJ0077
      ALPHA=.0                                                          BESJ0078
      IF(M-(M/2)*2)120,110,120                                          BESJ0079
  110 JT=-1                                                             BESJ0080
      GO TO 130                                                         BESJ0081
  120 JT=1                                                              BESJ0082
  130 M2=M-2                                                            BESJ0083
      DO 160 K=1,M2                                                     BESJ0084
      MK=M-K                                                            BESJ0085
      BMK=2.*FLOAT(MK)*FM1/X-FM                                         BESJ0086
      FM=FM1                                                            BESJ0087
      FM1=BMK                                                           BESJ0088
      IF(MK-N-1)150,140,150                                             BESJ0089
  140 BJ=BMK                                                            BESJ0090
  150 JT=-JT                                                            BESJ0091
      S=1+JT                                                            BESJ0092
  160 ALPHA=ALPHA+BMK*S                                                 BESJ0093
      BMK=2.*FM1/X-FM                                                   BESJ0094
      IF(N)180,170,180                                                  BESJ0095
  170 BJ=BMK                                                            BESJ0096
  180 ALPHA=ALPHA+BMK                                                   BESJ0097
      BJ=BJ/ALPHA                                                       BESJ0098
      IF(ABS(BJ-BPREV)-ABS(D*BJ))200,200,190                            BESJ0099
                                                                        BESJ0100
```

```
  190 APREV=BJ                                                    BESJ0101
      IER=3                                                       BESJ0102
  200 RETURN                                                      BESJ0103
      END                                                         BESJ0104
      FUNCTION BOS(C,K)                                           BOS 0000
      B=SIGN(1.,C)                                                BOS 0001
      A=ABS(C)                                                    BOS 0002
      PI=3.141593                                                 BOS 0003
   10 IF (A.LT.PI*2.**18) GO TO 11                                BOS 0004
      A=A-PI*2.**18                                               BOS 0005
      GO TO 10                                                    BOS 0006
   11 IF (K) 12,13,12                                             BOS 0007
   12 BOS=COS(A*B)                                                BOS 0008
      GO TO 14                                                    BOS 0009
   13 BOS=SIN(A*B)                                                BOS 0010
   14 RETURN                                                      BOS 0011
      END                                                         BOS 0012
```

FORM 8104 14_ℓ SAMPLE INPUT/OUTPUT

3634 FR FLEXIBLE PAVEMENT RESPONSE SAMPLE RUN

SEQ.								
001	$\Delta\rho$	ERR	ERRI	LIMIT				
002	E_p	F_p	E_f	R_f	b	h		
003	P	V	X	Y	Z	N_p	η_f	ν_p

SEQ.								
001	1.	.001	.01	100				
002	.1	E06.1	E06.1	E05.1	E05200.	10.		
003	.42	E050.0	0.0	0.0	5.0	.6	E04.2	E04.4
003	.42	E050.0	1.0	0.0	5.0	.6	E04.2	E04.4
003	.42	E050.0	3.0	0.0	5.0	.6	E04.2	E04.4

SAMPLE CASES; VARY X COORDINATE 0, 1.0, 3.0
EVERYTHING ELSE CONSTANT

PROGRAM OUTPUT - (3634 FR)

PROGRAM OUTPUT:

FLEXIBLE PAVEMENT RESPONSE (3634 FR)

ABSTRACT- THIS PROGRAM COMPUTES THE RESPONSE OF A FLEXIBLE PAVEMENT SYSTEM TO MOVING TIRE LOADS. ANALYTICALLY, THE FLEXIBLE PAVEMENT SYSTEM IS AN INFINITE VISCOELASTIC PLATE RESTING ON A VISCOELASTIC HALF-SPACE WITH NO HORIZONTAL SHEARING STRESSES TRANSMITTED AT THE INTERFACE. THE VISCOELASTICITY OF BOTH THE PLATE AND THE HALF-SPACE IS DESCRIBED BY A THREE-ELEMENT MODEL CONSISTING OF A LINEAR SPRING (E) IN PARALLEL WITH A LINEAR SPRING (F) AND LINEAR DASH POT (ETA) IN SERIES.

ANALYTICALLY, THE MOVING TIRE LOAD IS MODELED AS A LOAD OF MAGNITUDE (UPPER CASE P) DISTRIBUTED SO THAT THERE IS A UNIFORM PRESSURE, P, OVER A CIRCULAR AREA. THE ENTIRE LOAD SYSTEM MOVES LONGITUDINALLY (X - DIRECTION) AT A VELOCITY V.

THE INPUTS TO THE PROGRAM ARE THE VISCOELASTIC MATERIAL CONSTANTS (E(P), F(P), ETA(P), NU(P), E(F), F(F), ETA(F)), THE PAVEMENT THICKNESS (H), THE SPACE VARIABLES (IN A COORD. SYSTEM THAT MOVES WITH THE LOAD) (X,Y,Z), AND THE LOAD VARIABLES (UPPER CASE P, P, V). STANDARD ENGINEERING UNITS ARE USED, EXCEPT FOR THE VELOCITY WHICH IS IN MILES PER HOUR.

THE OUTPUT OF THE PROGRAM IS PAVEMENT DEFLECTION (W), PAVEMENT LONGITUDINAL STRAIN (E(X)), PAVEMENT LATERAL STRAIN (E(Y)), PAVEMENT LONGITUDINAL STRESS (SIG(X)), PAVEMENT LATERAL STRESS (SIG(Y)), AND FOUNDATION VERTICAL PRESSURE (P(Z)).

INPUT

MATERIAL CONSTANTS-	PAVEMENT POISSONS RATIO, MU(P) =	0.40000E 00	RESPONSE LOCATION-	LONGITUDINAL, X =	0.0
	PAVEMENT PRIMARY STIFFNESS, E(P) =	0.10000E 08		LATERAL, Y =	0.0
	PAVEMENT SECONDARY STIFFNESS, E(P) =	0.10000E 05		VERTICAL, Z =	0.50000E 01
	PAVEMENT DAMPING, ETA(P) =	0.60000E 04			
	SOIL PRIMARY STIFFNESS, E(F) =	0.13000E 05			
	SOIL SECONDARY STIFFNESS, E(F) =	0.10000E 05			
	SOIL DAMPING, ETA(F) =	0.20000E 04			
LOAD VARIABLES-	TOTAL LOAD, CAP P =	0.42000E 05	PAVEMENT THICKNESS-	H =	0.10000E 02
	TIRE PRESSURE, P =	0.20000E 03			
	LOAD VELOCITY, V =	0.0			

OUTPUT

PAVEMENT STIFFNESS RATIO, MU(P) =	0.20000E 01	PAVEMENT RELAXATION TIME, TAU =	0.60000E-01
SOIL STIFFNESS RATIO, MU(F) =	0.20000E 01	PAVEMENT PRIMARY BENDING STIFFNESS, D(2) =	0.99206E 07
DAMPING RATIO X STIFFNESS RATIO, ZETA =	0.30000E 00	CHARACTERISTIC LENGTH, L =	0.99735E 01
NONDIMENSIONAL COORDINATE, Z =	0.50133E 00	DEFLECTION COEFFICIENT, K(W)=	0.10667E-01
NONDIMENSIONAL COORDINATE, Z' =	0.0	PRESSURE COEFFICIENT, K(P) =	-0.21391E 02
NONDIMENSIONAL COORDINATE, X =	0.0	STRAIN COEFFICIENT, K(E) =	0.53619E-03
NONDIMENSIONAL COORDINATE, Y =	0.0	STRESS COEFFICIENT, K(S) =	0.12764E 03
NONDIMENSIONAL VELOCITY V =	0.0	EFFECTIVE FOOTPRINT RADIUS, P =	0.81759E 01
SOIL RELAXATION TIME, TAU(SIGMA) =	0.20000E 00	SOIL RELAXATION TIME, TAU(F) =	0.40000E 00
DEFLECTION TERMS A(0) =	0.30000E 00	A(1) =	0.13000E 01
PRESSURE TERMS, A(0)' =	0.15000E 00	A(1)' =	0.11500E 01
STRESS TERMS, A(0)'' =	0.15000E 00	A(1)'' =	0.80000E 00
DEFLECTION, W =	0.72073E-01	PRESSURE, P(Z) =	-0.51048E 02
PAVEMENT LONG. STRAIN, E(X) =	0.15092E-02	PAVEMENT LATERAL STRAIN, E(Y) =	0.15092E-02
PAVEMENT LONG. STRESS, SIG X=	0.25153E 03	PAVEMENT LATERAL STRESS, SIG Y=	0.25153E 03

INPUT

MATERIAL CONSTANTS-	PAVEMENT POISSONS RATIO, MU(P) =	0.40000E 00	RESPONSE LOCATION-	LONGITUDINAL, X =	0.10000E 01
	PAVEMENT PRIMARY STIFFNESS, E(P) =	0.16000E 06		LATERAL, Y =	0.0
	PAVEMENT SECONDARY STIFFNESS, E(P) =	0.10000E 06		VERTICAL, Z =	0.50000E 01
	PAVEMENT DAMPING, ETA(P) =	0.60000E 04			
	SOIL PRIMARY STIFFNESS, E(F) =	0.10000E 05			
	SOIL SECONDARY STIFFNESS, E(F) =	0.10000E 05			
	SOIL DAMPING, ETA(F) =	0.20000E 04			
LOAD VARIABLES-	TOTAL LOAD, CAP P =	0.42000E 05	PAVEMENT THICKNESS-	H =	0.10000E 02
	TIRE PRESSURE, P =	0.20000E 03			
	LOAD VELOCITY, V =	0.0			

OUTPUT

PAVEMENT STIFFNESS RATIO, MU(P) =	0.20000E 01	PAVEMENT RELAXATION TIME, TAU =	0.60000E-01
SOIL STIFFNESS RATIO, MU(F) =	0.20000E 01	PAVEMENT PRIMARY BENDING STIFFNESS, D(2) =	0.99284E 07
DAMPING RATIO X STIFFNESS RATIO, ZETA =	0.30000E 00	CHARACTERISTIC LENGTH, L =	0.99735E 01
NONDIMENSIONAL COORDINATE, Z =	0.50133E 00	DEFLECTION COEFFICIENT, K(W)=	0.10647E-01
NONDIMENSIONAL COORDINATE, Z* =	0.0	PRESSURE COEFFICIENT, K(P) =	-0.21391E 02
NONDIMENSIONAL COORDINATE, X =	0.10027E 00	STRAIN COEFFICIENT, K(E) =	0.53619E-03
NONDIMENSIONAL COORDINATE, Y =	0.0	STRESS COEFFICIENT, K(S) =	0.12764E 03
NONDIMENSIONAL VELOCITY V =	0.0	EFFECTIVE FOOTPRINT RADIUS, A =	0.91759E 01
SOIL RELAXATION TIME, TAU(SIGMA) =	0.20000E 00	SOIL RELAXATION TIME, TAU(E) =	0.40000E 00
DEFLECTION TERMS A(0) =	0.30000E 00	A(1) =	0.13000E 01
PRESSURE TERMS, A(0)* =	0.15000E 00	A(1)* =	0.11000E 01
STRESS TERMS, A(0)** =	0.15000E 00	A(1)** =	0.00000E 00
DEFLECTION, W =	0.71922E-01	PRESSURE, P(Z) =	-0.50814E 02
PAVEMENT LONG. STRAIN, E(X) =	0.14923E-02	PAVEMENT LATERAL STRAIN, E(Y) =	0.15035E-02
PAVEMENT LONG. STRESS, SIG X=	0.24925E 03	PAVEMENT LATERAL STRESS, SIG Y=	0.25087E 03

INPUT

MATERIAL CONSTANTS-	PAVEMENT POISSONS RATIO, MU(P) =	0.40000E 00	RESPONSE LOCATION-	LONGITUDINAL, X =	0.30000E 01
	PAVEMENT PRIMARY STIFFNESS, E(P) =	0.10000E 06		LATERAL, Y =	0.0
	PAVEMENT SECONDARY STIFFNESS, E(P) =	0.10000E 06		VERTICAL, Z =	0.50000E 01
	PAVEMENT DAMPING, ETA(P) =	0.60000E 04			
	SOIL PRIMARY STIFFNESS, E(F) =	0.10000E 05			
	SOIL SECONDARY STIFFNESS, E(F) =	0.10000E 05			
	SOIL DAMPING, ETA(F) =	0.20000E 04			
LOAD VARIABLES-	TOTAL LOAD, CAP P =	0.42000E 05	PAVEMENT THICKNESS-	H =	0.10000E 02
	TIRE PRESSURE, P =	0.20000E 03			
	LOAD VELOCITY, V =	0.0			

OUTPUT

PAVEMENT STIFFNESS RATIO, MU(P) =	0.20000E 01	PAVEMENT RELAXATION TIME, TAU =	0.60000E-01
SOIL STIFFNESS RATIO, MU(F) =	0.20000E 01	PAVEMENT PRIMARY BENDING STIFFNESS, D(2) =	0.99206E 07
DAMPING RATIO X STIFFNESS RATIO, ZETA =	0.30000E 00	CHARACTERISTIC LENGTH, L =	0.99739E 01
NONDIMENSIONAL COORDINATE, Z =	0.50133E 00	DEFLECTION COEFFICIENT, K(W)=	0.10667E-01
NONDIMENSIONAL COORDINATE, Z' =	0.0	PRESSURE COEFFICIENT, K(P) =	-0.21391E 02
NONDIMENSIONAL COORDINATE, X =	0.30080E 00	STRAIN COEFFICIENT, K(E) =	0.53619E-03
NONDIMENSIONAL COORDINATE, Y =	0.0	STRESS COEFFICIENT, K(S) =	0.12764E 03
NONDIMENSIONAL VELOCITY V =	0.0	EFFECTIVE FOOTPRINT RADIUS, R =	0.91759E 01
SOIL RELAXATION TIME, TAU(SIGMA) =	0.20000E 00	SOIL RELAXATION TIME, TAU(E) =	0.40000E 00
DEFLECTION TERMS A(0) =	0.30000E 00	A(1) =	0.13000E 01
PRESSURE TERMS, A(0)' =	0.15000E 00	A(1)' =	0.11500E 01
STRESS TERMS, A(0)'' =	0.15000E 00	A(1)'' =	0.00000E 00
DEFLECTION, W =	0.70736E-01	PRESSURE, P(Z) =	-0.48995E 02
PAVEMENT LONG. STRAIN, E(X) =	0.13809E-02	PAVEMENT LATERAL STRAIN, E(Y) =	0.14643E-02
PAVEMENT LONG. STRESS, SIG X=	0.23412E 03	PAVEMENT LATERAL STRESS, SIG Y=	0.24000E 03

FORM 8104

SEQ.

3634 RR - RIGID PAVEMENT RESPONSE SAMPLE RUN

	1	5	10	15	20	25	30	35	40	45	50	55	60	65	70
001		$\Delta\rho$		ERR		ERRI		LIMIT							
002		E		$\upsilon\rho$		h		μ							
003		E_f		F_f		η_f		V		P		x		y		z

	1	5	10	15	20	25	30	35	40	45	50	55	60	65	70
001	1.			.001		.01			100						
002	.2		E07	.15		10.		200.							
003	.2		E06	.1		E04	.1		E0400		.42		E0500		0.		0.
003	.2		E06	.1		E04	.1		E0400		.42		E0503		0.		0.
003	.2		E06	.1		E04	.1		E0400		.42		E0515		0.		0.

SAMPLE CASES; VARY X COORDINATE 0, 3, 15

EVERYTHING ELSE CONSTANT

PROGRAM OUTPUT:

RIGID PAVEMENT RESPONSE (3634 RR)

ABSTRACT- THIS PROGRAM COMPUTES THE RESPONSE OF A RIGID PAVEMENT SYSTEM TO MOVING TIRE LOADS. THE ANALYTICAL MODEL OF THE PAVEMENT SYSTEM IS AN INFINITE ELASTIC PLATE RESTING ON A VISCOELASTIC HALF-SPACE WITH NO HORIZONTAL SHEARING STRESSES TRANSMITTED AT THE INTERFACE. THE VISCOELASTICITY OF THE HALF-SPACE IS REPRESENTED BY A THREE-ELEMENT MODEL CONSISTING OF A LINEAR SPRING (E(F)) IN PARALLEL WITH A LINEAR SPRING (F(F)) AND A LINEAR DASH POT (ETA(F)) IN SERIES.

THE MOVING TIRE LOAD IS MODELLED AS A LOAD OF MAGNITUDE (UPPER CASE P) DISTRIBUTED SO THAT THERE IS A UNIFORM PRESSURE (P) OVER A CIRCULAR AREA. THE ENTIRE LOAD SYSTEM MOVES LONGITUDINALLY (- DIRECTION) AT A VELOCITY V.

INPUTS TO THE PROGRAM ARE THE MATERIAL CONSTANTS FOR THE PLATE (E, MODULUS AND MU(P), POISSON'S RATIO), THE MATERIAL CONSTANTS OF THE HALF-SPACE (E(F), F(F), ETA(F)), THE PLATE THICKNESS (H), THE SPACE VARIABLES (IN A COORDINATE SYSTEM THAT MOVES WITH THE LOAD) (X,Y,Z), AND THE LOAD VARIABLES (UPPER CASE P, R, V). STANDARD ENGINEERING UNITS ARE USED, EXCEPT FOR THE VELOCITY WHICH IS IN MILES PER HOUR.

THE OUTPUT OF THE PROGRAM IS THE STEADY-STATE RESPONSE OF THE SYSTEM- THE PLATE DEFLECTION (W), PAVEMENT LONGITUDINAL STRAIN (E(X)), PAVEMENT LATERAL STRAIN (E(Y)), PAVEMENT LONGITUDINAL STRESS (SIG(X)), PAVEMENT LATERAL STRESS (SIG(Y)), AND FOUNDATION VERTICAL PRESSURE (P(Z)).

INPUT

MATERIAL CONSTANTS-	PAVEMENT MODULUS, E =	0.20000E 07	RESPONSE LOCATION-	LONGITUDINAL, X =	0.0
	PAVEMENT POISSON'S RATIO, NU(P) =	0.15000E 00		LATERAL, Y =	0.0
	SOIL PRIMARY STIFFNESS, E(F) =	0.20000E 06		VERTICAL, Z =	0.50000E 01
	SOIL SECONDARY STIFFNESS, E(F) =	0.10000E 06			
	SOIL DAMPING, ETA(F) =	0.10000E 04			
LOAD VARIABLES-	TOTAL LOAD, CAP P =	0.42000E 05	PAVEMENT THICKNESS-	H =	0.10000E 02
	TIRE PRESSURE, P =	0.20000E 03			
	LOAD VELOCITY, V =	0.0			

OUTPUT

SOIL STIFFNESS RATIO, MU(F) =	0.10050E 01	SOIL RELAXATION TIME, TAU(SIGMA) =	0.10000E 01
NONDIMENSIONAL COORDINATE, Z =	0.52731E 00	SOIL RELAXATION TIME, TAU(E) =	0.10050E 01
NONDIMENSIONAL COORDINATE, Z' =	0.0	PLATE BENDING STIFFNESS, D =	0.17050E C9
NONDIMENSIONAL COORDINATE, X =	0.0	CHARACTERISTIC LENGTH, L =	0.94820E 01
NONDIMENSIONAL COORDINATE, Y =	0.0	DEFLECTION COEFFICIENT, K(W) =	0.56099E-03
NONDIMENSIONAL VELOCITY, V =	0.0	STRAIN COEFFICIENT, K(E) =	0.31198E-04
EFFECTIVE FOOTPRINT RADIUS, R =	0.81750E 01	PRESSURE COEFFICIENT, K(P) =	-0.11833E 02
		STRESS COEFFICIENT, K(S) =	0.63832E 02
DEFLECTION, W =	0.37559E-02	PRESSURE, P(Z) =	-0.54831E C2
PAVEMENT LONG. STRAIN, E(X) =	0.83548E-04	PAVEMENT LATERAL STRAIN, E(Y) =	0.83548E-04
PAVEMENT LONG. STRESS, SIG X=	0.19658E 03	PAVEMENT LATERAL STRESS, SIG Y=	0.19658E C3

INPUT

MATERIAL CONSTANTS-	PAVEMENT MODULUS, E =	0.20000E 07	RESPONSE LOCATION-	LONGITUDINAL, X =	0.10000E 01
	PAVEMENT POISSON'S RATIO, NU(P) =	0.15000E 00		LATERAL, Y =	0.0
	SOIL PRIMARY STIFFNESS, E(F) =	0.20000E 06		VERTICAL, Z =	0.50000E 01
	SOIL SECONDARY STIFFNESS, E(F) =	0.10000E 06			
	SOIL DAMPING, ETA(F) =	0.10000E 04			
LOAD VARIABLES-	TOTAL LOAD, CAP P =	0.42000E 05	PAVEMENT THICKNESS-	H =	0.10000E 02
	TIRE PRESSURE, P =	0.20000E 03			
	LOAD VELOCITY, V =	0.0			

OUTPUT

SOIL STIFFNESS RATIO, MU(F) =	0.10050E 01	SOIL RELAXATION TIME, TAU(SIGMA) =	0.10000E 01
NONDIMENSIONAL COORDINATE, Z =	0.52731E 00	SOIL RELAXATION TIME, TAU(E) =	0.10050E 01
NONDIMENSIONAL COORDINATE, Z' =	0.0	PLATE BENDING STIFFNESS, D =	0.17050E C9
NONDIMENSIONAL COORDINATE, X =	0.10546E 00	CHARACTERISTIC LENGTH, L =	0.94820E 01
NONDIMENSIONAL COORDINATE, Y =	0.0	DEFLECTION COEFFICIENT, K(W) =	0.56099E-03
NONDIMENSIONAL VELOCITY, V =	0.0	STRAIN COEFFICIENT, K(E) =	0.31198E-04
EFFECTIVE FOOTPRINT RADIUS, R =	0.81750E 01	PRESSURE COEFFICIENT, K(P) =	-0.11833E C2
		STRESS COEFFICIENT, K(S) =	0.63832E C2
DEFLECTION, W =	0.37475E-02	PRESSURE, P(Z) =	-0.54571E C2
PAVEMENT LONG. STRAIN, E(X) =	0.82634E-04	PAVEMENT LATERAL STRAIN, E(Y) =	0.83238E-04
PAVEMENT LONG. STRESS, SIG X=	0.19462E 03	PAVEMENT LATERAL STRESS, SIG Y=	0.19567E 03

INPUT

MATERIAL CONSTANTS-	PAVEMENT MODULUS, E =	0.20000E 07	RESPONSE LOCATION-	LONGITUDINAL, X =	0.30000E 01
	PAVEMENT POISSON'S RATIO, NU(P) =	0.15000E 00		LATERAL, Y =	0.0
	SOIL PRIMARY STIFFNESS, E(F) =	0.20000E 06		VERTICAL, Z =	0.50000E 01
	SOIL SECONDARY STIFFNESS, E(F) =	0.10000E 04			
	SOIL DAMPING, ETA(F) =	0.10000E 04			
LOAD VARIABLES-	TOTAL LOAD, CAP P =	0.42000E 05	PAVEMENT THICKNESS-	H =	0.10000E 02
	TIRE PRESSURE, P =	0.20000E 03			
	LOAD VELOCITY, V =	0.0			

OUTPUT

SOIL STIFFNESS RATIO, MU(F) =	0.10050E 01	SOIL RELAXATION TIME, TAU(SIGMA) =	0.10000E 01
NONDIMENSIONAL COORDINATE, Z =	0.52731E 00	SOIL RELAXATION TIME, TAU(E) =	0.10050E 01
NONDIMENSIONAL COORDINATE, Z* =	0.0	PLATE BENDING STIFFNESS, D =	0.17050E C9
NONDIMENSIONAL COORDINATE, X =	0.31639E 00	CHARACTERISTIC LENGTH, L =	0.94820E 01
NONDIMENSIONAL COORDINATE, Y =	0.0	DEFLECTION COEFFICIENT, K(W) =	0.56099E-03
NONDIMENSIONAL VELOCITY, V =	0.0	STRAIN COEFFICIENT, K(E) =	0.31198E-04
EFFECTIVE FOOTPRINT RADIUS, R =	0.81759E 01	PRESSURE COEFFICIENT, K(P) =	-0.11833E 02
		STRESS COEFFICIENT, K(S) =	0.63832E 02
DEFLECTION, W =	0.36818E-02	PRESSURE, P(Z) =	-0.52536E 02
PAVEMENT LONG. STRAIN, E(X) =	0.76300E-04	PAVEMENT LATERAL STRAIN, E(Y) =	0.81042E-04
PAVEMENT LONG. STRESS, SIG X=	0.18098E 03	PAVEMENT LATERAL STRESS, SIG Y=	0.18923E 03

INPUT

MATERIAL CONSTANTS-	PAVEMENT MODULUS, E =	0.20000E 07	RESPONSE LOCATION-	LONGITUDINAL, X =	0.80000E 01
	PAVEMENT POISSON'S RATIO, NU(P) =	0.15000E 00		LATERAL, Y =	0.0
	SOIL PRIMARY STIFFNESS, E(F) =	0.20000E 06		VERTICAL, Z =	0.50000E 01
	SOIL SECONDARY STIFFNESS, E(F) =	0.10000E 04			
	SOIL DAMPING, ETA(F) =	0.10000E 04			
LOAD VARIABLES-	TOTAL LOAD, CAP P =	0.42000E 05	PAVEMENT THICKNESS-	H =	0.10000E 02
	TIRE PRESSURE, P =	0.20000E 03			
	LOAD VELOCITY, V =	0.0			

OUTPUT

SOIL STIFFNESS RATIO, MU(F) =	0.10050E 01	SOIL RELAXATION TIME, TAU(SIGMA) =	0.10000E 01
NONDIMENSIONAL COORDINATE, Z =	0.52731E 00	SOIL RELAXATION TIME, TAU(E) =	0.10050E 01
NONDIMENSIONAL COORDINATE, Z* =	0.0	PLATE BENDING STIFFNESS, D =	0.17050E C9
NONDIMENSIONAL COORDINATE, X =	0.84370E 00	CHARACTERISTIC LENGTH, L =	0.94820E 01
NONDIMENSIONAL COORDINATE, Y =	0.0	DEFLECTION COEFFICIENT, K(W) =	0.56099E-03
NONDIMENSIONAL VELOCITY, V =	0.0	STRAIN COEFFICIENT, K(E) =	0.31198E-04
EFFECTIVE FOOTPRINT RADIUS, R =	0.81759E 01	PRESSURE COEFFICIENT, K(P) =	-0.11833E 02
		STRESS COEFFICIENT, K(S) =	0.63832E 02
DEFLECTION, W =	0.32769E-02	PRESSURE, P(Z) =	-0.39860E 02
PAVEMENT LONG. STRAIN, E(X) =	0.30785E-04	PAVEMENT LATERAL STRAIN, E(Y) =	0.66128E-04
PAVEMENT LONG. STRESS, SIG X=	0.83283E 02	PAVEMENT LATERAL STRESS, SIG Y=	0.14475E 03

INPUT

MATERIAL CONSTANTS-	PAVEMENT MODULUS, E =	0.20000E 07	RESPONSE LOCATION-	LONGITUDINAL, X =	0.15000E 02
	PAVEMENT POISSON'S RATIO, MU(P) =	0.15000E 00		LATERAL, Y =	0.0
	SOIL PRIMARY STIFFNESS, E(F) =	0.20000E 06		VERTICAL, Z =	0.50000E 01
	SOIL SECONDARY STIFFNESS, E(F) =	0.10000E 04			
	SOIL DAMPING, ETA(F) =	0.10000E 04			
LOAD VARIABLES-	TOTAL LOAD, CAP P =	0.42000E 05	PAVEMENT THICKNESS-	H =	0.10000E 02
	TIRE PRESSURE, P =	0.20000E 03			
	LOAD VELOCITY, V =	0.0			

OUTPUT

SOIL STIFFNESS RATIO, MU(F) =	0.10050E 01	SOIL RELAXATION TIME, TAU(SIGMA) =	0.10000E 01
NONDIMENSIONAL COORDINATE, Z =	0.52731E 00	SOIL RELAXATION TIME, TAU(E) =	0.10050E 01
NONDIMENSIONAL COORDINATE, Z* =	0.0	PLATE BENDING STIFFNESS, D =	0.17050E 09
NONDIMENSIONAL COORDINATE, X =	0.15819E 01	CHARACTERISTIC LENGTH, L =	0.94820E 01
NONDIMENSIONAL COORDINATE, Y =	0.0	DEFLECTION COEFFICIENT, K(W) =	0.56099E-03
NONDIMENSIONAL VELOCITY, V =	0.0	STRAIN COEFFICIENT, K(E) =	0.31198E-04
EFFECTIVE FOOTPRINT RADIUS, B =	0.81759E 01	PRESSURE COEFFICIENT, K(P) =	-0.11833E 02
		STRESS COEFFICIENT, K(S) =	0.63832E 02
DEFLECTION, W =	0.24940E-02	PRESSURE, P(Z) =	-0.20050E 02
PAVEMENT LONG. STRAIN, E(X) =	-0.14977E-04	PAVEMENT LATERAL STRAIN, E(Y) =	0.35918E-04
PAVEMENT LONG. STRESS, SIG X=	-0.19620E 02	PAVEMENT LATERAL STRESS, SIG Y=	0.69893E 02

INPUT

MATERIAL CONSTANTS-	PAVEMENT MODULUS, E =	0.20000E 07	RESPONSE LOCATION-	LONGITUDINAL, X =	0.25000E 02
	PAVEMENT POISSON'S RATIO, MU(P) =	0.15000E 00		LATERAL, Y =	0.0
	SOIL PRIMARY STIFFNESS, E(F) =	0.20000E 06		VERTICAL, Z =	0.50000E 01
	SOIL SECONDARY STIFFNESS, E(F) =	0.10000E 04			
	SOIL DAMPING, ETA(F) =	0.10000E 04			
LOAD VARIABLES-	TOTAL LOAD, CAP P =	0.42000E 05	PAVEMENT THICKNESS-	H =	0.10000E 02
	TIRE PRESSURE, P =	0.20000E 03			
	LOAD VELOCITY, V =	0.0			

OUTPUT

SOIL STIFFNESS RATIO, MU(F) =	0.10050E 01	SOIL RELAXATION TIME, TAU(SIGMA) =	0.10000E 01
NONDIMENSIONAL COORDINATE, Z =	0.52731E 00	SOIL RELAXATION TIME, TAU(E) =	0.10050E 01
NONDIMENSIONAL COORDINATE, Z* =	0.0	PLATE BENDING STIFFNESS, D =	0.17050E 09
NONDIMENSIONAL COORDINATE, X =	0.26366E 01	CHARACTERISTIC LENGTH, L =	0.94820E 01
NONDIMENSIONAL COORDINATE, Y =	0.0	DEFLECTION COEFFICIENT, K(W) =	0.56099E-03
NONDIMENSIONAL VELOCITY, V =	0.0	STRAIN COEFFICIENT, K(E) =	0.31198E-04
EFFECTIVE FOOTPRINT RADIUS, B =	0.81759E 01	PRESSURE COEFFICIENT, K(P) =	-0.11833E 02
		STRESS COEFFICIENT, K(S) =	0.63832E 02
DEFLECTION, W =	0.16033E-02	PRESSURE, P(Z) =	-0.50598E 01
PAVEMENT LONG. STRAIN, E(X) =	-0.18779E-04	PAVEMENT LATERAL STRAIN, E(Y) =	0.13938E-04
PAVEMENT LONG. STRESS, SIG X=	-0.94165E 02	PAVEMENT LATERAL STRESS, SIG Y=	0.22754E 02

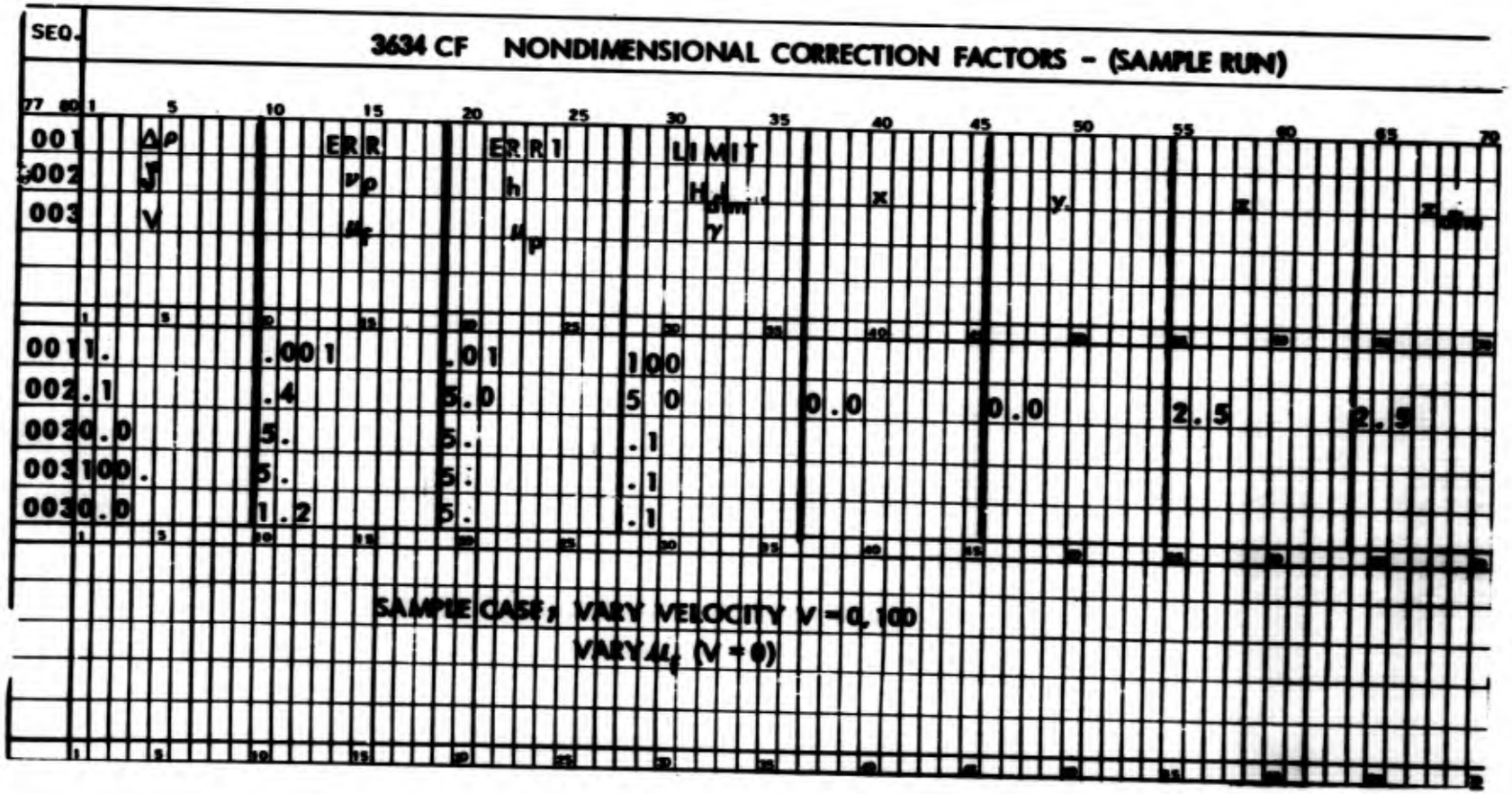
SEQ.
3634 CF NONDIMENSIONAL CORRECTION FACTORS - (SAMPLE RUN)
77 80
001
002
003
ERR
ERR1
LIMIT
001 1.
002 .1
0030.0
003100.
0030.0
.001
.4
5.
5.
1.2
.01
5.0
5.
5.
5.
100
50
.1
.1
.1
0.0
0.0
2.5
2.5
SAMPLE CASE; VARY VELOCITY V = 0, 100
VARY μ_f (V = 0)

NONDIMENSIONAL OUTPUT

PAVEMENT STIFFNESS RATIO, MU(P) =	0.50000E 01	NONDIMENSIONAL COORDINATE X=	0.0
SOIL STIFFNESS RATIO, MU(F) =	0.12000E 01	NONDIMENSIONAL COORDINATE Y =	0.0
DAMPING RATIO X STIFFNESS RATIO, ZETA =	0.10000E 00	NONDIMENSIONAL COORDINATE Z =	2.5
PAVEMENT POISSONS RATIO, NU(P) =	0.40000E 00	COORDINATE Z =	2.5
NONDIMENSIONAL FOOTPRINT RADIUS, R =	0.10000E 00	NONDIMENSIONAL PAVEMENT THICKNESS H =	5.0
NONDIMENSIONAL VELOCITY V =	0.0	PAVEMENT THICKNESS H =	5.0

NONDIMENSIONAL CORRECTION FACTORS

C(W) =	0.19172E 00	C(EPSILON X) =	0.11765E 00	C(EPSILON Y) =	0.11765
C(SIGMA X) =	0.14118E 01	C(SIGMA Y) =	0.14118E 01	C(P) =	-0.18220

PAVEMENT STIFFNESS RATIO, MU(P) =	0.50000E 01	NONDIMENSIONAL COORDINATE X=	0.0
SOIL STIFFNESS RATIO, MU(F) =	0.50000E 01	NONDIMENSIONAL COORDINATE Y =	0.0
DAMPING RATIO X STIFFNESS RATIO, ZETA =	0.10000E 00	NONDIMENSIONAL COORDINATE Z =	2.5
PAVEMENT POISSONS RATIO, NU(P) =	0.40000E 00	COORDINATE Z =	2.5
NONDIMENSIONAL FOOTPRINT RADIUS, R =	0.10000E 00	NONDIMENSIONAL PAVEMENT THICKNESS H =	5.0
NONDIMENSIONAL VELOCITY V =	0.0	PAVEMENT THICKNESS H =	5.0

NONDIMENSIONAL CORRECTION FACTORS

C(W) =	0.19172E 00	C(EPSILON X) =	0.11765E 00	C(EPSILON Y) =	0.23530
C(SIGMA X) =	0.14118E 01	C(SIGMA Y) =	0.14118E 01	C(P) =	-0.18225

PAVEMENT STIFFNESS RATIO, MU(P) =	0.50000E 01	NONDIMENSIONAL COORDINATE X=	0.0
SOIL STIFFNESS RATIO, MU(F) =	0.50000E 01	NONDIMENSIONAL COORDINATE Y =	0.0
DAMPING RATIO X STIFFNESS RATIO, ZETA =	0.10000E 00	NONDIMENSIONAL COORDINATE Z =	2.5
PAVEMENT POISSONS RATIO, NU(P) =	0.40000E 00	COORDINATE Z =	2.5
NONDIMENSIONAL FOOTPRINT RADIUS, R =	0.10000E 00	NONDIMENSIONAL PAVEMENT THICKNESS H =	5.0
NONDIMENSIONAL VELOCITY V =	0.10000E 03	PAVEMENT THICKNESS H =	5.0

NONDIMENSIONAL CORRECTION FACTORS

C(W) =	0.38368E-01	C(EPSILON X) =	0.23529E-01	C(EPSILON Y) =	0.11765
C(SIGMA X) =	0.14116E 01	C(SIGMA Y) =	0.14116E 01	C(P) =	-0.18220

APPENDIX F

SUPPLEMENTARY STUDIES

TABLE OF CONTENTS

LIST OF ILLUSTRATIONS

LIST OF TABLES

SUPPLEMENTARY STUDIES

1. PAVEMENT RESPONSE TO A HORIZONTAL LOAD

Let the pavement be represented by a two-layer system (both layers being three-dimensional elastic solids) bonded at the interface and acted on by a circularly distributed shearing traction.

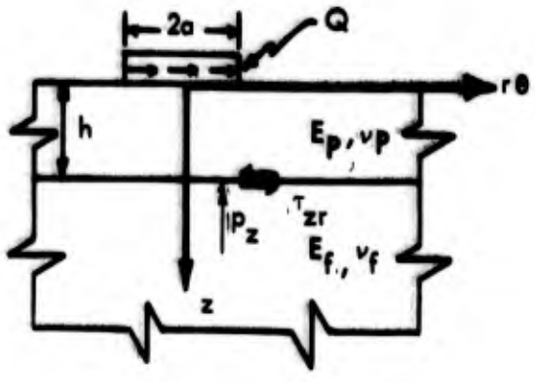

The solution to this problem is described in (1) and the results can be simply presented.

$$\text{Interface Normal Stress} = P_z = I_p \frac{Q}{a^2} \cos\theta \qquad (1\text{-}1)$$

$$\text{Interface Shear Stress} = \tau_{zr} = I_{\tau_{zr}} \frac{Q}{a^2} \cos\theta \qquad (1\text{-}2)$$

$$\text{Interface Shear Stress} = \tau_{z\theta} = I_{\tau_{z\theta}} \frac{Q}{a^2} \sin\theta \qquad (1\text{-}3)$$

where

Q = total shear load (lbs.)

a = radius of distribution (footprint radius) - in.

z, r, θ = polar coordinates (1-4)

E_p = top layer stiffness (psi)

E_f = bottom layer stiffness (psi)

ν_p, ν_f = top and bottom layer Poisson's ratio

and I_p, $I_{\tau_{zr}}$, $I_{\tau_{zo}}$ are correction factors which depend on h/a, E_f/E_p and r/a, as shown in Figures F-1 through F-6.

The interface normal stress can also be calculated by use of the Boussinesq expression

$$P_z = \frac{3Q\ x\ z^2}{2\pi(x^2 + y^2 + z^2)^{5/2}} \qquad (1\text{-}5)$$

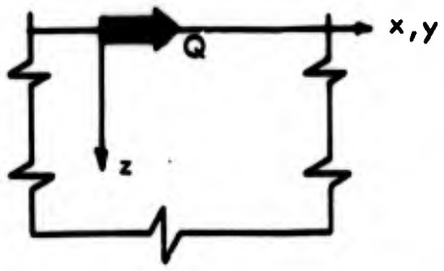

$$(r^2 = x^2 + y^2)$$

In either method the shear load Q is related to the normal load P by

$$Q = \mu P \qquad (1\text{-}6)$$

and the total load can be related to the tire pressure by

$$\pi a^2 p = P \qquad (1\text{-}7)$$

Using Equations (1-6) and (1-7), the pavement response to a shear load can be written

$$P_z = I_p \quad (\pi p \mu \cos \theta) \qquad (1\text{-}8)$$

$$\tau_{z\theta} = I_{\tau_{z\theta}} \quad (\pi p \mu \cos \theta) \qquad (1\text{-}9)$$

$$\tau_{zr} = I_{\tau_{zr}} \quad (\pi p \mu \sin \theta) \qquad (1\text{-}10)$$

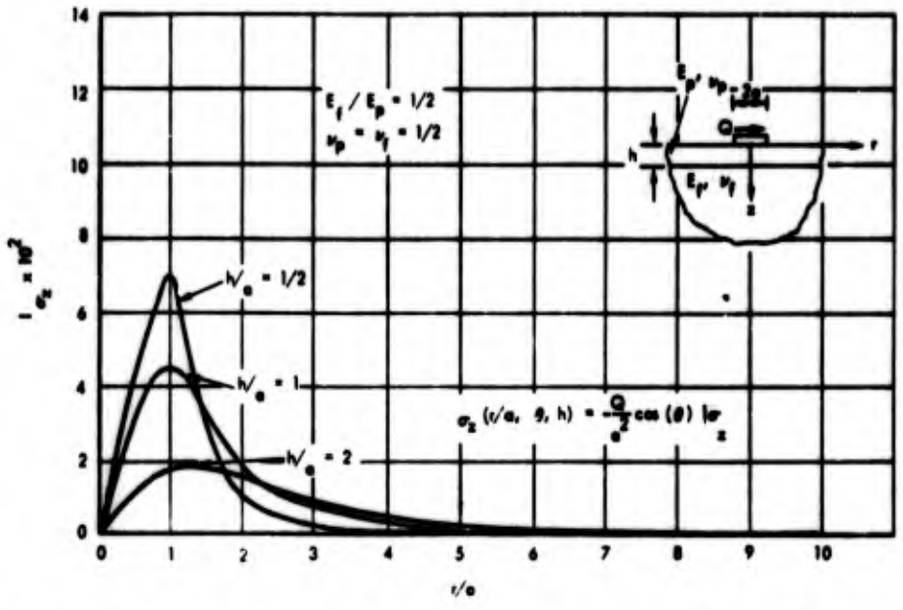

FIGURE F-1 - Interface Normal Stress Corrector Factors $E_f/E_p = 1/2$

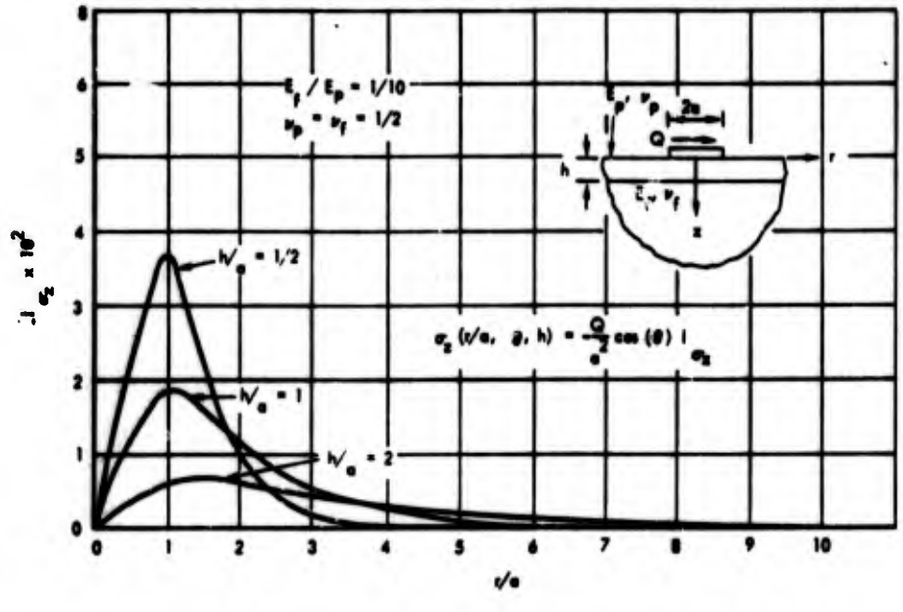

FIGURE F-2 - Interface Normal Stress Corrector Factors $E_f/E_p = 1/10$

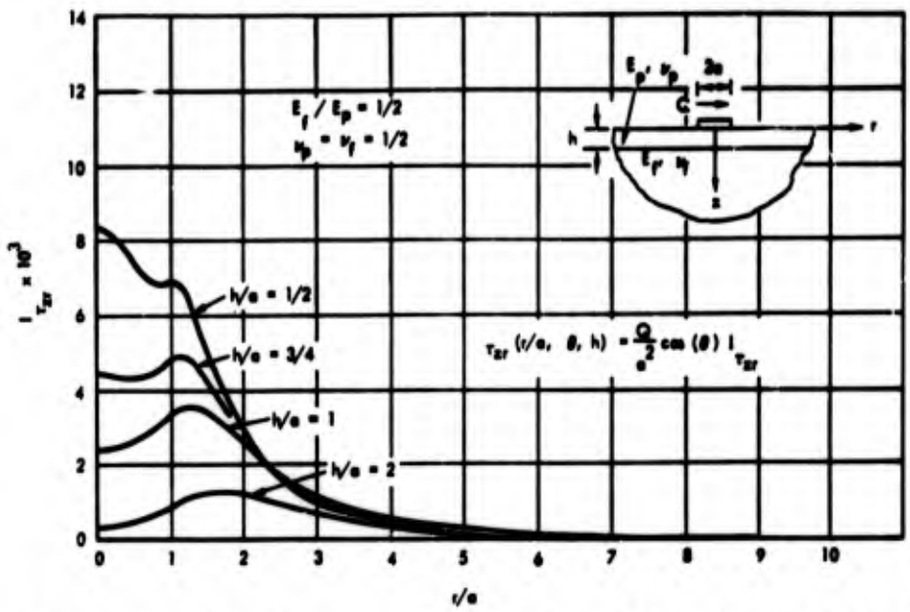

FIGURE F-3 - Interface Shear Stress Correction Factors $E_f/E_p = 1/2$

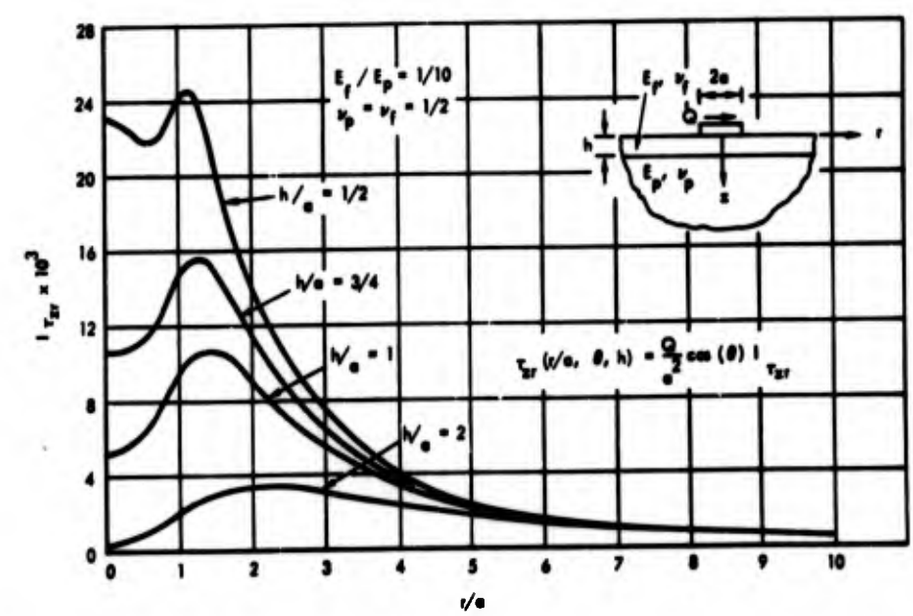

FIGURE F-4 - Interface Shear Stress Correction Factors $E_f/E_p = 1/10$

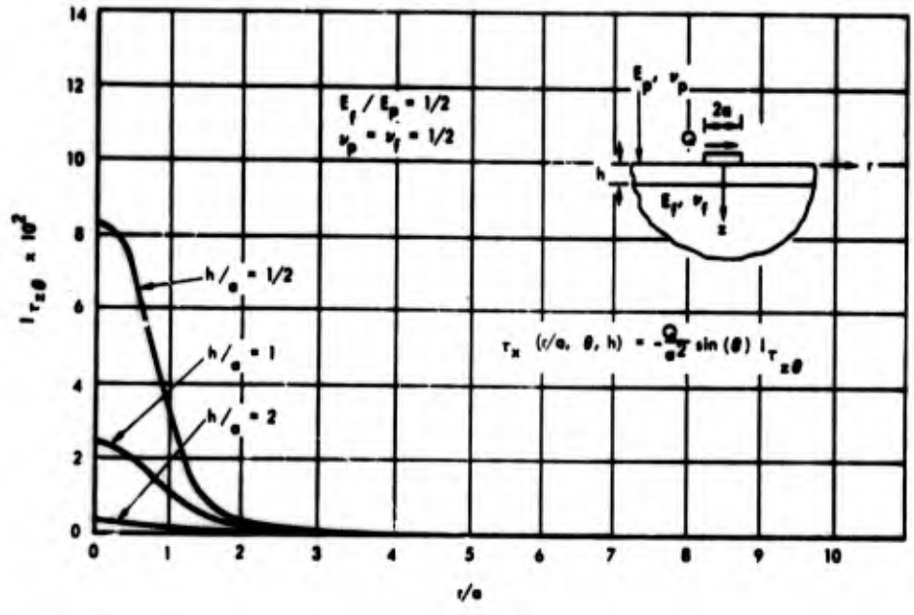

FIGURE F-5 - Interface Shear Stress Correction Factors $E_f/E_p = 1/2$

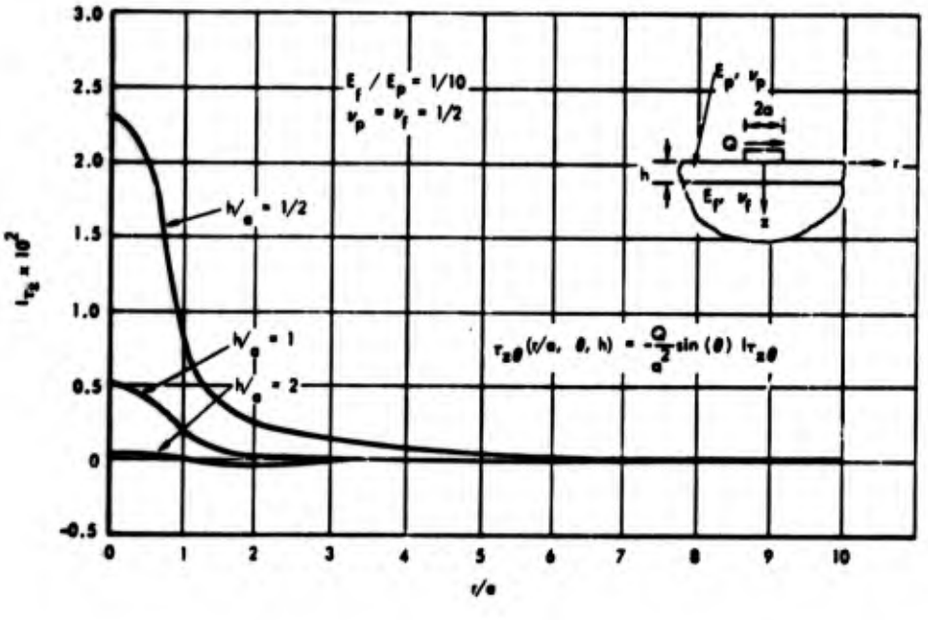

FIGURE F-6 - Interface Shear Stress Correction Factors $E_f/E_p = 1/10$

2. INERTIA EFFECTS

The following analysis was performed to determine the magnitude of the inertia force relative to the subgrade pressure force at the pavement subgrade interface and to ascertain the consequences of neglecting inertia effects.

The pavement vertical deflection versus time looks like:

The maximum pavement vertical acceleration occurs at the peak deflection point, and is related to the longitudinal strain at all points as follows:

$$\frac{dw}{dt} = \frac{\partial w}{\partial x}\frac{dx}{dt} \tag{2-1}$$

$$\frac{d^2w}{dt^2} = \frac{d}{dt}\left[\frac{\partial w}{\partial x}\frac{dx}{dt}\right] = \frac{\partial w}{\partial x}\frac{d^2x}{dt^2} + \frac{dx}{dt}\left[\frac{d}{dt}\frac{\partial w}{\partial x}\right]$$

where

$$\frac{dx}{dt}\left[\frac{d}{dt}\frac{\partial w}{\partial x}\right] = \frac{dx}{dt}\left[\frac{\partial}{\partial x}\frac{\partial w}{\partial x}\frac{dx}{dt}\right] = \left(\frac{dx}{dt}\right)^2\frac{\partial^2 w}{\partial x^2}$$

$$\frac{d^2w}{dt^2} = \frac{\partial w}{\partial x}\frac{d^2x}{dt^2} + \left(\frac{dx}{dt}\right)^2\frac{\partial^2 w}{\partial x^2} \tag{2-2}$$

For a non-accelerating airplane,

$$\frac{d^2x}{dt^2} = 0 \tag{2-3}$$

so

$$\frac{d^2w}{dt^2} = V^2\frac{\partial^2 w}{\partial x^2} \tag{2-4}$$

V = airplane velocity

But

$$\epsilon_x = z \frac{\partial^2 w}{\partial x^2} \quad \text{- longitudinal strain at} \tag{2-5}$$

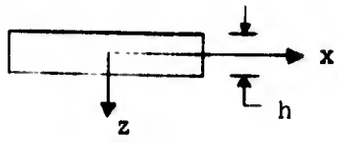

So that

$$\frac{\partial^2 w}{\partial x^2} = -\frac{\epsilon_x}{z} \tag{2-6}$$

$$\frac{d^2 w}{dt^2} = V^2 \frac{\epsilon_x}{z} \quad \text{or, evaluating } \epsilon_x \text{ at } z = \frac{h}{2}\text{, we have}$$

$$\frac{d^2 w}{dt^2} = -\frac{2V^2}{h} \epsilon_x \left(\frac{h}{2}\right) \tag{2-7}$$

Assume that a small finite cylindrical portion of the pavement located at $x = 0$, $y = 0$ attains the acceleration given by (2-7). The mass of this section is

$$m = \rho A h \tag{2-8}$$

where

ρ = pavement mass density

A = area of circular segment

h = pavement thickness

The inertia force on this section is given by

$$F_I = -m \frac{d^2 w}{dt^2}$$

$$F_I = \rho A h \frac{2V^2}{h} \epsilon_x \left(\frac{h}{2}\right) \qquad \text{from (2-7) and (2-8)}$$

$$F_I = 2 \rho A V^2 \epsilon_x \left(\frac{h}{2}\right) \tag{2-9}$$

To determine the significance of this inertia force, we compare it to the force from the subgrade pressure acting on the circular segment at the subgrade-pavement interface. This force is given by

$$F_p = \iint_A p(x,y)\, dxdy \qquad (2\text{-}10)$$

If the area of the circular segment of pavement is chosen sufficiently small, we can assume that the average pressure acting over the area is equal to the maximum pressure at x = 0, y = 0, since the pressure (x,y) curve is similar to the deflection curve shown above, i.e., its maximum is at x = 0, y = 0. (This is strictly true only for V = 0 and V = ∞.) With this assumption, the pressure force becomes

$$F_p = p_{max} A \qquad (2\text{-}11)$$

Combining (2-9) and (2-10) we have

$$\frac{F_I}{F_p} \frac{\Delta}{} = R = 2\rho \frac{V^2 \epsilon_x (\frac{h}{2})}{p_{max}} \qquad (2\text{-}12)$$

where both ϵ_x and p_{max} are evaluated at x = 0, y = 0. From p. 126,

$$\epsilon_x (\tfrac{h}{2}) = C_\epsilon \frac{hP}{D}$$

and

$$p_{max} = C_p \frac{P}{\ell^2}$$

Equation (2-12) becomes

$$R = 2\rho V^2 \frac{C_\epsilon}{C_p} \frac{h\ell^2}{D}$$

but

$$\frac{h\ell^2}{D} = \frac{hD^{2/3}}{E_f^{2/3} D} = \frac{h}{D^{1/3} E_f^{2/3}} = \frac{h\, 12^{1/3} (1-\upsilon_p^2)^{1/3}}{E_p^{1/3} h E_f^{2/3}}$$

so

$$R = 2\rho V^2 \frac{C_\epsilon}{C_p} \frac{12^{1/3} (1-\upsilon_p^2)^{1/3}}{E_p^{1/3} E_f^{2/3}}$$

$$R = [2 (12^{1/3})(1-\upsilon_p^2)^{1/3} \rho] \frac{1}{E_p^{1/3} E_f^{2/3}} \frac{C_\epsilon(V)}{C_p(V)} V^2$$

Define $K \triangleq 2 \times 12^{1/3} (1-\nu_p^2)^{1/3}$ $\sigma \approx$ constant for concrete or asphalt

$$R = \frac{K}{E_p^{1/3} E_f^{2/3}} \frac{C_\epsilon(V)}{C_p(V)} V^2 \qquad (2\text{-}13)$$

$$\frac{C_\epsilon(V)}{C_p(V)} \quad \frac{C_{\epsilon_1}}{C_{p_1}} \times \frac{C_\epsilon(V,r,\xi)}{C_p(V,r,\xi)} \qquad \text{at } V = 0,\ r = 1 \text{ and } \xi = 1$$

From page 129, $C_{\epsilon_1} = .028$ $\quad C_{p_1} = .109$ so

$$\frac{C_\epsilon(V)}{C_p(V)} = \frac{.028}{.109} \frac{C_\epsilon}{C_p}(V,r,\xi)$$

For asphalt, $\sigma_{max} = 1.59 \times 10^{-4}$, $\nu_p = .4$

concrete, $\sigma_{max} = 2.25 \times 10^{-4}$, $\nu_p = .15$

$K_a = 2 \times 12^{1/3} (1 - .16)^{1/3}\ 1.59 \times 10^{-4} = 6.87 \times 10^{-4}$

$K_c = 2 \times 12^{1/3} (1 - .0225)^{1/3}\ 1.59 \times 10^{-4} = 10.22 \times 10^{-4}$

Subst. into (2-13)

$$R_{asphalt} = \frac{724}{E_p^{1/3} E_f^{2/3}} \times \frac{C_\epsilon}{C_p}(V,r,\xi) \left(\frac{V_{Kts}}{100}\right)^2$$

$$R_{concrete} = \frac{1078}{E_p^{1/3} E_s^{2/3}} \times \frac{C_\epsilon}{C_p}(V,r,\xi) \left(\frac{V_{Kts}}{100}\right)^2 \qquad (2\text{-}14)$$

From page 134, for $r = 1$, $\xi = 4.5$

$$\frac{C_\epsilon(V=\infty)}{C_p(V=\infty)} = \frac{.32}{.48} = .667$$

$$R = \begin{bmatrix} 483 \text{ asphalt} \\ 719 \text{ concrete} \end{bmatrix} \times \frac{1}{E_p^{1/3} E_f^{2/3}} \left(\frac{V_{Kts}}{100}\right)^2$$

Asphalt: $E_p = 200{,}000$ psi $\qquad E_f = 30{,}000$ psi

Concrete: $E_p = 4 \times 10^6$ psi $\qquad E_f = 30{,}000$ psi

Asphalt

$$E_p^{1/3} = (.2)^{1/3} (10^6)^{1/3} = .45 \times 10^2 = 45$$

$$E_f^{2/3} = (30)^{2/3} (10^3)^{2/3} = 961$$

$$R = \frac{483}{(45)(961)} \left(\frac{V}{100}\right)^2$$

$$\Rightarrow R_{200\ kts} = .0447$$

Concrete

$$E_p^{1/3} = 4^{1/3} \times 10^2 = 159$$

$$E_f^{2/3} = 961$$

$$R_{200} = \frac{4\ (719)}{(159)\ 961} = .0188$$

The inertia forces during taxi are shown to be very small ($< 5\%$) compared to subgrade pressure forces acting at the interface of the pavement and subgrade.

3. WAVE PROPAGATION VELICITIES FOR PAVING MATERIALS

Wave propagation velocities for paving materials have been determined in the laboratory and in the field. Field testing has been conducted through the application of a vibratory load to the surface of the pavement. Details of this procedure have been discussed by Jones (2, 3 and 4). The primary purpose for determining wave velocities in paving materials has been to measure the elastic properties of the materials in-situ.

Wave velocities as measured in various paving materials are summarized briefly in the following pages.

(A) Portland Cement Concrete

Jones (2) developed a vibration method for measuring the thickness of concrete road slabs in-situ. He reported that the type of wave measured in concrete road slabs was dependent on the frequency of vibration. In the frequency range from 1,000 c/s to 4,000 c/s, the vibrations were identified as flexural waves, the velocity was dependent on the frequency, the thickness and the elastic constants of the slab. At frequencies above 50 kc/s, the velocity was constant, and the propagation became independent of the frequency and the thickness of the slab, i.e., it is then the Rayleigh wave velocity of surface waves in the concrete. The frequency at which the Rayleigh wave velocity may be measured depends on the thickness of the slab.

Jones (2, 3 and 4) reported that the Rayleigh wave velocity was approximately 8,350 ft/sec., for concrete.

(B) Asphaltic Concrete

Because properties of an asphaltic concrete change with temperature and duration of loading, flexural wave velocity for asphaltic concrete would also vary with temperature, duration of loading as well as frequency. Very little information concerning wave velocity in asphaltic concrete slabs was reported in the literatures. Nijboer(5) in his paper reported that the flexural waves in an asphaltic layer were measured at the various frequencies ranging from 200 to 3,000 cps depending on temperature and the thickness of the asphaltic layer. The measured velocities of the flexural waves varied from 4,200 ft/sec to 800 ft/sec depending on frequency, temperature and the thickness of the asphaltic layer. The Rayleigh waves were not measured in his study. It is expected that higher frequencies are required in order that the Rayleigh waves may be measured.

(C) Granular Materials

It should be noted that the dynamic behavior of granular materials depend on a number of factors such as confining pressure, density and degree of saturation.

Selig and Vey (6) reported that the wave velocity in Ottawa sands varied from 930 ft/sec to 1,330 ft/sec for specimen densities ranging from 100 to 112 pcf and confining pressures ranging from 5 to 12.5 psi.

The shear wave velocity in Ottawa sands as reported by Hardin and Richart (7) varied from 500 to 1,300 ft/sec for void ratios ranging from 0.3 to 0.8 and confining pressures ranging from 500 to 6,000 psf.

Shock wave velocities as reported by Zaccor (8) for various sands ranged from 450 to 1,200 ft/sec for various incident axial overpressures ranging from 10 to 400 psi.

Heukelom and Foster (9) performed dynamic testing on pavements and measured velocities of the Rayleight waves. They observed that the wave velocity for sands varies from 390 to 590 ft/sec/, the wave velocity for clay gravels varies from 620 to 1,300 ft/sec.

(D) Subgrade Soils

Jones (10) reported in his paper that velocities of the Rayleigh wave in subgrade soils were measured by vibration methods to be in the range of 440 to 700 ft/sec. Heukelom and Foster (9) reported that velocities of the Rayleigh wave in clays are in the range of 300 to 490 ft/sec and in sandy clays are in the range of 490 to 650 ft/sec. Nijboer and Metcalf (11) reported that the wave velocity in silty clay was measured to be 500 ft/sec.

TABLE F-1 Summary of Wave Velocity Data

MATERIAL	REFERENCE	TYPE OF TEST	TYPE OF WAVE	VELOCITY FT/SEC
Portland cement concrete	Jones (2) Jones (3) Jones and Mayhew (4)	Vibration on concrete road slab	Love Wave	16,000
			Rayleigh Wave	8,350
Asphaltic concrete	Nijboer (5)	Vibration on pavements	Flexural Wave (assumption of free plate)	4,590 (3,000 c/s thickness of AC layer = 6.3 in. 43°F) 2,310 (700 c/s thickness of AC layer = 6.3 in. 43°F) 2,950 (3,000 c/s thickness of AC layer = 2.7 in. 72°F) 760 (200 c/s thickness of AC layer = 2.7 in 72°F)
Granular Materials				
Ottawas Sand	Selig and Vey (6)	Shock pulse	Shock induced stress wave compression	930 to 1,330 (for σ_3 = 5 to 12.5 psi)*
	Hardin and	Shock pulse		500 to 1,300 (for σ_3 = 3.5 to 41.7 psi)
Sand	Zaccor (8)	Square-wave pulse	"	450 to 1,200 (for incident axial over-pressure = 10 to 400 psi)
Sand	Heukelom and Foster (9)	Vibratory testing of pavements	Rayleigh wave	390 to 590
Clayey gravel	" (9)	"	"	620 to 1,050
Moraine	Heukelom and Foster (9)	Vibratory testing of pavements	Rayleigh wave	820 to 1,300
Subgrade soils	Jones (10)	Vibratory testing of pavements	Rayleigh wave	440 to 700
Clays	Heukelom and Foster (9)	Vibratory testing of pavements	Rayleigh wave	300 to 490
sandy clay	"	"	"	490 to 650
Subgrade soils (silty clay)	Nijboer and Metcalf (11)	"	"	520

*σ_3 = confining pressure

4. LIST OF REFERENCES

1. Yang, Nai C, "Interaction of a Vehicle and Pavement and its Application to Pavement Design Construction, Maintenance and Safety Evaluation," PNYA, April 1969.

2. Jones, R., "A Vibration Method for Measuring the Thickness of Concrete Road Slabs in-situ," Magazine of Concrete Research, Vol. 7 No. 20; 1955, pp. 97, 1955.

3. Jones, R., "Measurement and Interpretation of Surface Vibration on Soil and Roads," Highway Research Board, Bull. 277, 1960.

4. Jones, R. and Mayhew, J. C., "Thickness and Quality of Cemented Surfacings and Bases - Measuring by a Non-Destructive Surface Wave Method," Civil Engineering and P. W. Rev. 1965, 60, 705, pp. 523-529, 1965.

5. Nijboer, L. W., "New Development in Vibration Techniques," 2nd Int. Conf. on the Structural Design of Asphalt Pavements pp. 422, 1967.

6. Selig, E. T. and Vey, E., "Shock Induced Stress Wave Propagation in Sand," ASCE, J. of SMFD. May 1965, pp. 19-49 Proc. 4332, 1965.

7. Hardin, B. O. and Richart, F. E., Jr., "Elastic Wave Velocities in Granular Soils," ASCE, J. of SMFD, Feb. 1963, pp. 33-65, 1963.

8. Zaccor, James V., "Dynamic Behavior of Granular Media," Proc. Symposium on Soil Structure Interaction, New Mexico, pp. 62-72, 1964.

9. Heukelom, W. and Foster, C. R., "Dynamic Testing of Pavements," ASCE, J. of SMFD, Feb. 1960.

10. Jones, R. (1958), "In-situ Measurement of the Dynamic Properties of Soil by Vibration Methods," Geotechnique, vol. Viii, March 1958.

11. Nijboer, L. W. and Metcalf, C. T., (1962), "Dynamic Testing at the AASHO Road Test," Proc. 1st Int. Conf. on the Structural Design of Asphalt Pavements, Ann Arbor, Michigan, pp. 713-721, 1962.

BLANK PAGE

APPENDIX G

PROPOSED FULL SCALE TEST PLANS

TABLE OF CONTENTS

LIST OF ILLUSTRATIONS

PROPOSED FULL SCALE TEST PLANS

Two plans are presented for performing moving load tests: (1) Operational Statistical Tests and (2) Moving Load Track Tests. The differences in concept are that (1) employs airport pavements and operational airplanes to provide statistical data, while (2) uses specially prepared pavements and a controlled load cart to provide point-by-point data for correlation with analyses. The following discussion sets forth the detailed test programs for each of the methods.

1. OPERATIONAL STATISTICAL TESTS

(A) Introduction - The Operational Statistical Tests, as the name implies, depends largely on obtaining an adequate statistical sample of airline takeoff, landing and taxi operations for support of correlation studies and the development of design criteria. Since the loads imposed by the airplane on the pavement, will be estimated from photographic coverage, the size of the samples will be quite large. Because of the dependence of the program on the adequacy of the sample data, reduction and correlation studies will be performed at each of the airports used in the survey.

(B) Test Organization - Figure G-1 sets forth an organization for the test program which consists of various participating airlines, airports and airframe manufacturers in addition to the test leader and operations safety officer. The responsibilities of the various participants are as follows:

(1) Airlines - They will supply the following airplane configuration data for each flight:

- Nose and Main Gears
  - Tire pressures
  - Strut air pressures and corresponding static strut position
- Takeoff and Landing
  - Gross weight
  - Center-of-gravity position
- Representative airplanes to do static tests

(2) Airports - Supply the following data and services:

- Construction details on selected runway and taxiway pavements
- Provide Operations Safety Man along with necessary communication system

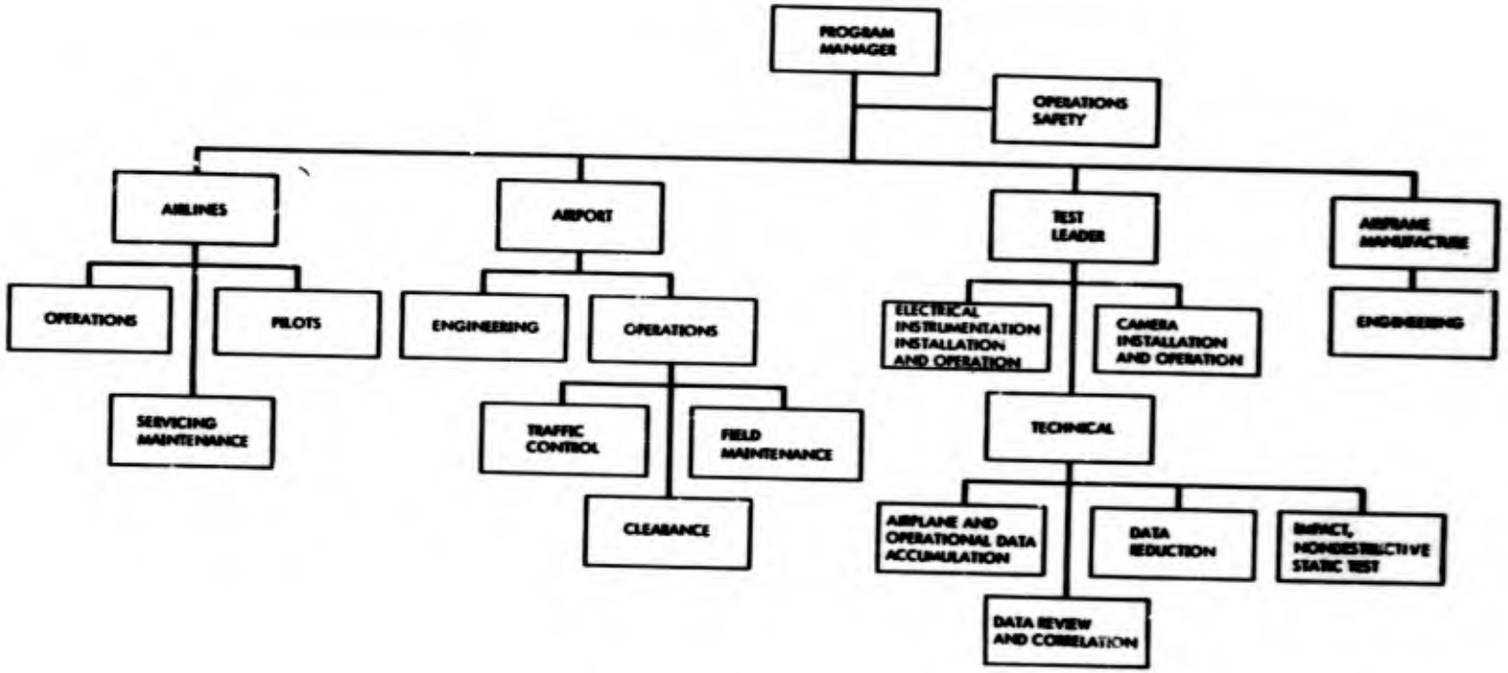

FIGURE G-1 - Organizational Chart for Operational Statistical Tests

- Provide work time during periods of low traffic for electrical instrumentation installation

- Provide necessary electrical power at the test sites for operating instrumentation installation equipment, instrumentation, cameras and lights

- Provide office space, telephones and necessary furniture for test planning, data gathering, data reduction and performing data analysis

- Provide historical data regarding the amount of heavy gross weight traffic on the pavement to be tested

(3) Airframe Manufacturers - Supply the following technical information concerning the airplanes participating in the tests:

- Airplane basic geometry including gear positions, wing area, tail area, leading edge mean aerodynamic chord position, wheel geometries, and engines' reverse thrust and their line of action

- Vertical center-of-gravity position and pitch moment of inertia and corresponding gross weight and loading configuration

- Lift and pitch aerodynamic data for both the takeoff and landing configurations

- Main and nose landing gear air pressure and tire pressure curves

(4) Test Leader - The test leader is responsible for the following aspects of the testing portion of the program:

- Selection of the points on the runways and taxiways for performing tests

- Installation and operation of all instrumentation and cameras

- Development of the test plan including the sequence and the number of tests to be performed

- Coordination with the Operations Safety Man in the proper and safe conduct of all tests concerned with runways and taxiways

- Setting-up the data reduction systems and the data review methods to provide timely support of the testing

- Correlating measured and analytical data

- Preparation of all reports including the final report

(C) Test Schedule - Figure G-2 is the Test Schedule for the 12-month duration Operational Statistical Tests program. The tasks that will be performed will include the following:

(1) Preparation for Tests - This activity will include:

- Selection of the six airports to be used in the program. Four to be extremes in asphaltic-concrete and Portland cement constructed pavements and two will be representative of the average of both types of runways.

- Prepare support requirements and coordinate with each of the airports.

- Obtain necessary airplane support data from the airframe manufacturers of the 727, 707, DC-8 and the 747 airplanes.

- Prepare airplane configuration data sheets to be filled out by the cognizant airline personnel.

- Prepare test plan to serve as an advance briefing document for the participating airlines and airports.

- Purchase the necessary surface strain gages (approximately 180 per airport), the necessary taxi path switches (approximately 70 per airport), and the material for wiring and installing the instrumentation (It is assumed that the recorders are or can be made available).

- Develop methods for reducing data obtained from the cameras including: airplane velocity, airplane net lift and loads imposed by the airplane on the pavement using calculated strut and tire data.

- Develop statistical sample size criterion.

- Develop methods for determining maximum strains under the gear.

- Set up data reduction techniques for the nondestructive and impact tests.

- Acquire equipment needed to perform nondestructive impact tests.

(2) Field Tests - It is expected that the tests at airport A will require extra time for training personnel and solving problems related to instrumentation installation and efficient operations. By about the third airport the time required for the tests would be about five weeks. The crew for the tests will be divided into two parts as follows:

TEST SCHEDULE

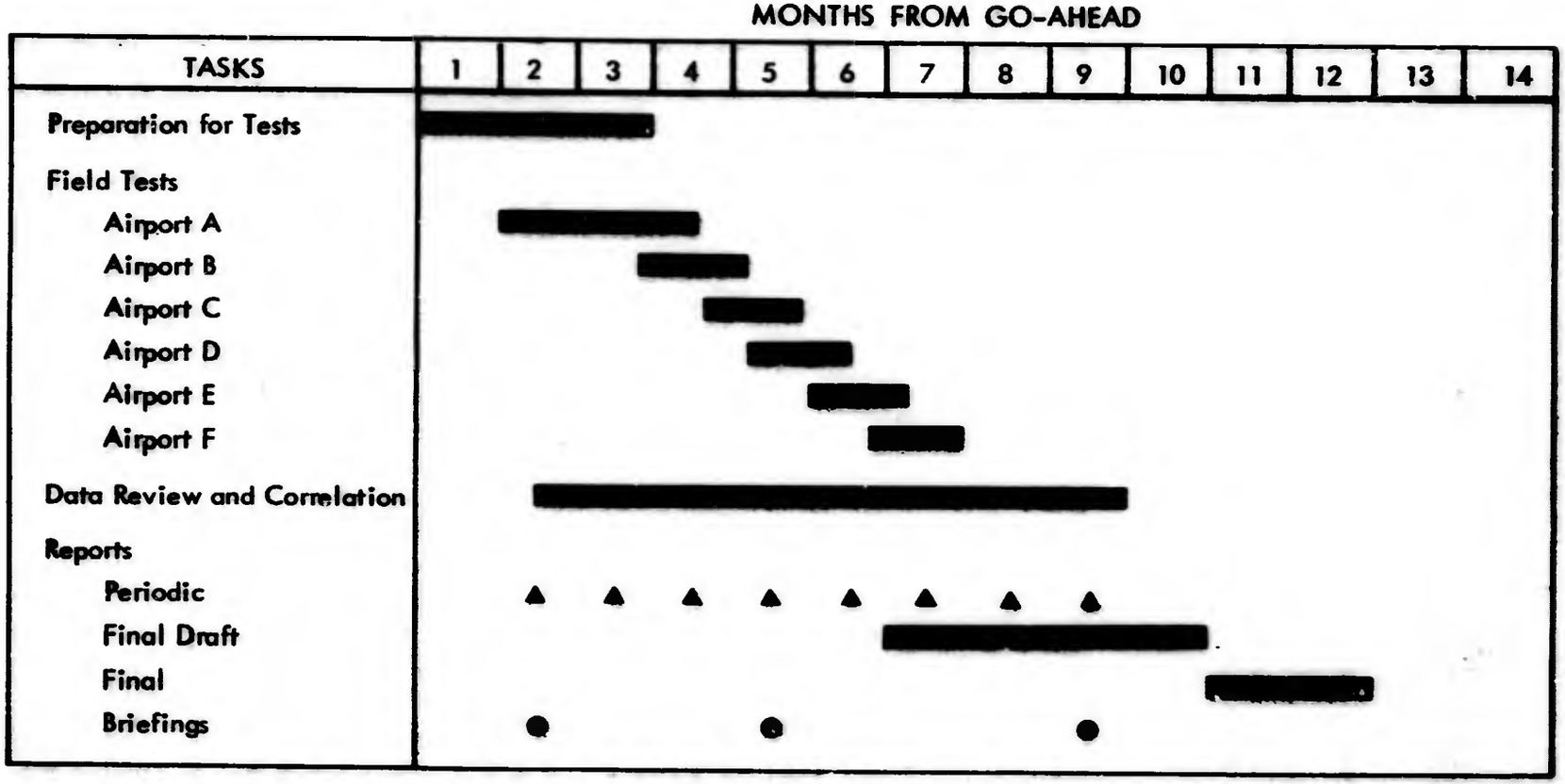

FIGURE G-2 - Test Schedule for The Operational Statistical Tests

- The first section of the crew will make all the initial on-site preparations such as: briefing the participants from the airports and airlines, selection of test sites, installation of strain gages and contact switches, arrangements for power sources and setting up the data gathering and reduction center.

- The second section will perform the tests which will include: completing the instrumentation, installation of cameras, calibration, performance of all tests, repair of instrumentation, data reduction and removal of instrumentation.

Dividing the test crew into two sections permits work at each of the airports to overlap as is shown in Figure G-2. The manner in which the work will flow at a typical field test airport is depicted in Figure G-3.

(3) Data Review and Correlation - This effort requires close coordination with Field Tests in order to make decisions as to the need for further testing at a particular site in a timely manner. The work to be performed in this task will also include:

- The development of methods for correlating the measured data with analyses

- Performance of correlation studies

- The development of the methods employed in establishing pavement design criteria for moving loads and the performance of the work incident thereto

(D) Equipment Required for Test Programs - The following equipment will be required in support of the test program:

- Nondestructive test equipment such as the Shell machine

- Impact test device such as available at the Lockheed-Georgia Company but with a greater load capacity

- Pavement grinder for providing a slight recess for installation of strain gages

- A viewer to be used in obtaining data from the photographic film

- Desk type computer to support data reduction and on the spot check of correlation

- Desk calculator as back-up to the desk computer

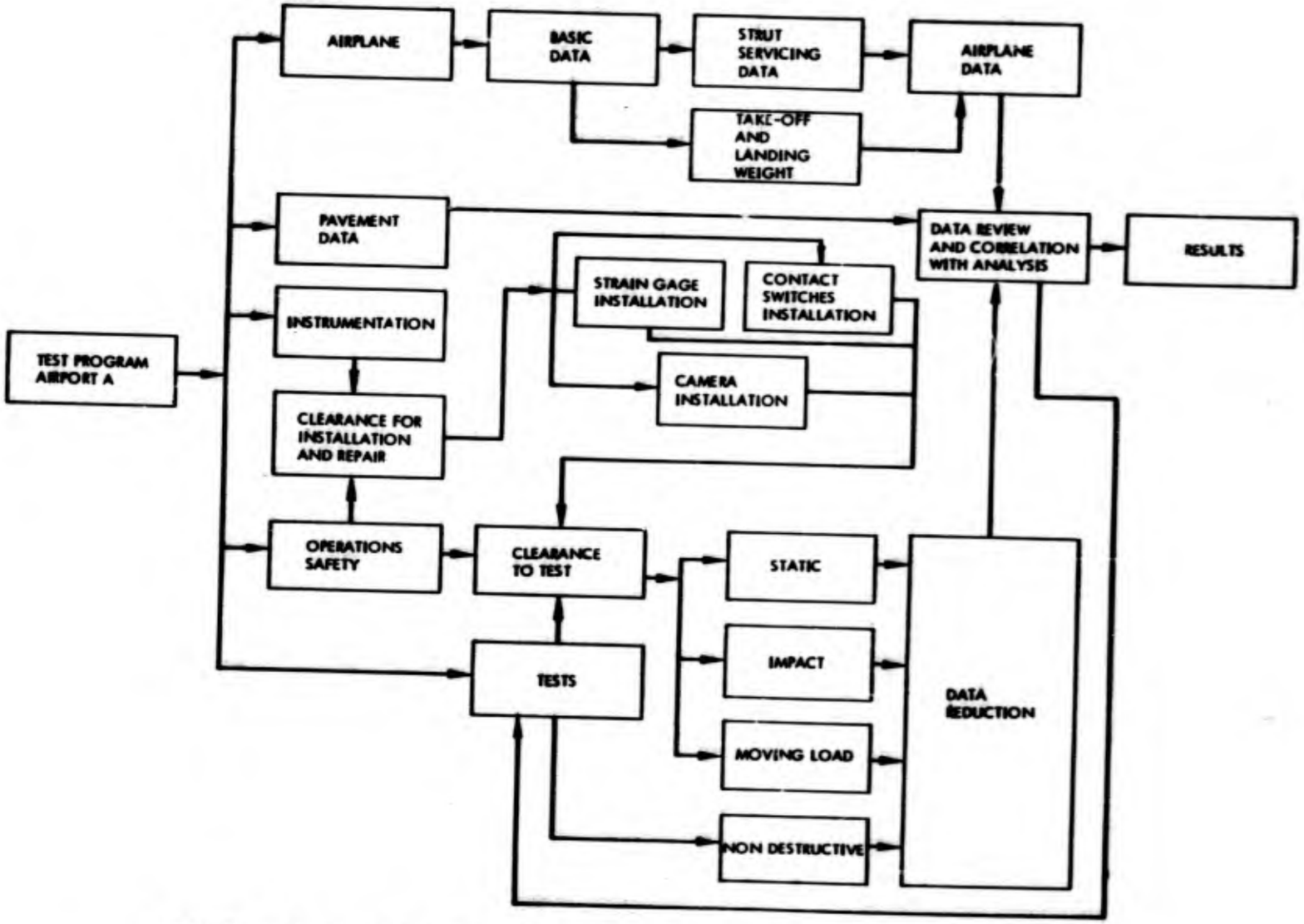

FIGURE G-3 - Work Flow Chart for Operational Statistical Tests at a Typical Airport

(E) Instrumentation Location - The location of the instrumentation consisting of strain gages and contact switches will be at four cross runway and two cross taxiway locations at each of the airports. The selection of the runway sites will be such that the loads imposed on the pavement are steady and not transient as can be encountered from pavement uneveness and rotation during takeoff. In addition the instrumentation sites will be located such that four different ranges of takeoff roll or landing roll velocities are obtained. The two taxiway sites will be selected on the basis of being representative of low speed taxi (10 to 25 knots).

The strain gages at the sites will be arranged to measure strains parallel and normal to the flight path. The spacing between the strain gages and the contact switches will be stratigically located such as to capture as much maximum strain data as is practical when considering main gear tread and distances between wheels.

Because of the number of recording channels needed it is anticipated that only one site will be operated at a time.

One camera equipped with timing and framing devices will be located such that it will provide data for airplane velocity, pitch attitude and flight control position with the least amount of triangulation involved. The other camera will be equipped with a telephoto lens such that tire and strut deflection can be readily measured. Both cameras will be collated with the strain gage data recording by means of lights activated by the contact switches.

(F) Data to be Acquired During Tests - The following data will be acquired during the tests in addition to that listed under the prior paragraph (B) Test Organization, for the airlines, airports and airframe manufacturers:

- Photography - Airplane pitch attitude and velocity relative to the ground, airplane pitch flight control surface position, tire deflection and strut extension

- Electrically Recorded - Either tape or oscillograph equipment will be used to record strain gage (normal and parallel to airplane path) and contact switch output.

(G) Tests to be Performed - The following four types of tests are to be performed at each of the sites:

(1) Nondestructive - These tests will provide data regarding the characteristics of the pavement to various depths. The results will be compared to the historical data on construction and pavement traffic.

(2) Static - These tests will provide basic data for comparison with the moving load data and for correlation with analytically obtained data.

(3) Impact - The impact test provides a simple means by which the moving load effect can be simply checked on other runways. Therefore the data obtained will be used to support development of this technique.

(4) Moving Load - These tests will provide the data for correlation with analyses and will form the basis for the development of pavement design criteria for moving loads. Because these tests are not well suited for point-by-point comparison with analyses, statistical methods of data analysis will be employed.

(H) Summary - The success of the Operational Statistical Tests will rely greatly on the cooperation of several different activities. The coordination will have to be developed at six airports. Most likely, each will have sufficiently different needs which in turn will require a great deal of flexibility on the part of the test crew.

Since the vertical load imposed by the gear on the runway is to be obtained by calculations from photographic data, the quality of the data will be degraded. Therefore, particular attention has to be paid to assuring that an adequate sample of data is obtained and that the test sites selected will hold airplane transient load effects to a minimum.

2. MOVING LOAD TRACK TESTS

(A) Introduction - The Moving Load Track Tests are designed to produce collated data of a high degree of accuracy under controlled conditions. The program requires a track from which precise control of the moving load on the pavement can be achieved. Velocities of the load can be preselected and transient loads from pavement uneveness and aerodynamic effects can be held to a minimum. In addition, the load imposed on the pavement can be obtained from strain gage information and accurately collated with the response of the pavement. Since the pavements are to be constructed at the site, additional instrumentation can be installed to measure soil pressures and pavement deflection. The data collected can be correlated on a point-by-point basis.

(B) Test Organization - Figure G-4 sets forth an organization for the test program consisting of four principal well coordinated groups. Once pavement installation and load cart development are complete, the group number is reduced to two. The responsibilities of the participants are as follows:

(1) Controlled Test Track Facility - This activity will supply the following equipment and services:

- Provide Track Safety Officer along with the necessary communication system
- Provide the test track including arresting gear and the pusher carts and all attendent modifications and maintenance. Once the load cart has been fabricated, its maintenance requirements will also be assumed.

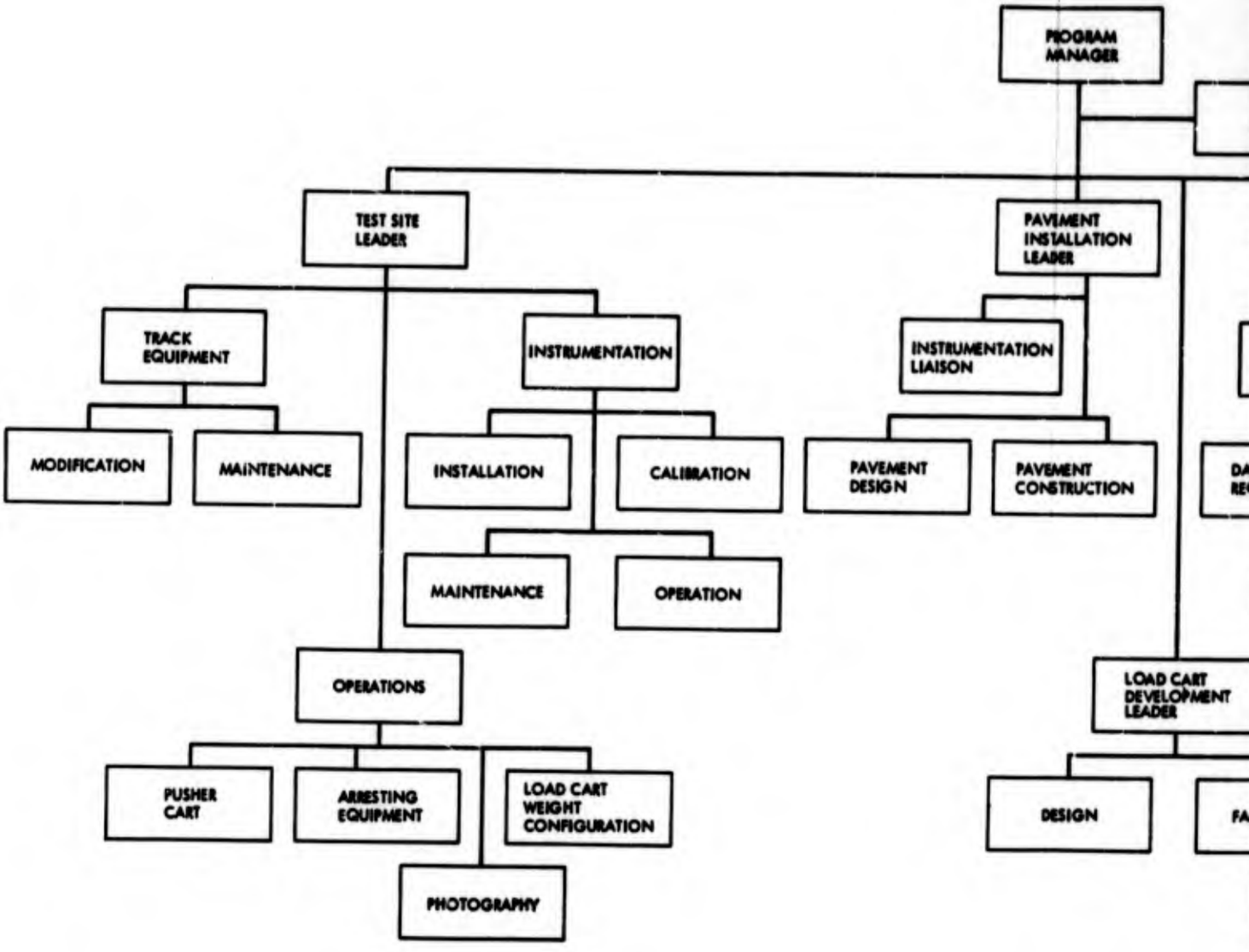
PROGRAM MANAGER
TEST SITE LEADER
PAVEMENT INSTALLATION LEADER
TRACK EQUIPMENT
INSTRUMENTATION
INSTRUMENTATION LIAISON
MODIFICATION
MAINTENANCE
INSTALLATION
CALIBRATION
PAVEMENT DESIGN
PAVEMENT CONSTRUCTION
MAINTENANCE
OPERATION
OPERATIONS
LOAD CART DEVELOPMENT LEADER
PUSHER CART
ARRESTING EQUIPMENT
LOAD CART WEIGHT CONFIGURATION
DESIGN
PHOTOGRAPHY

A

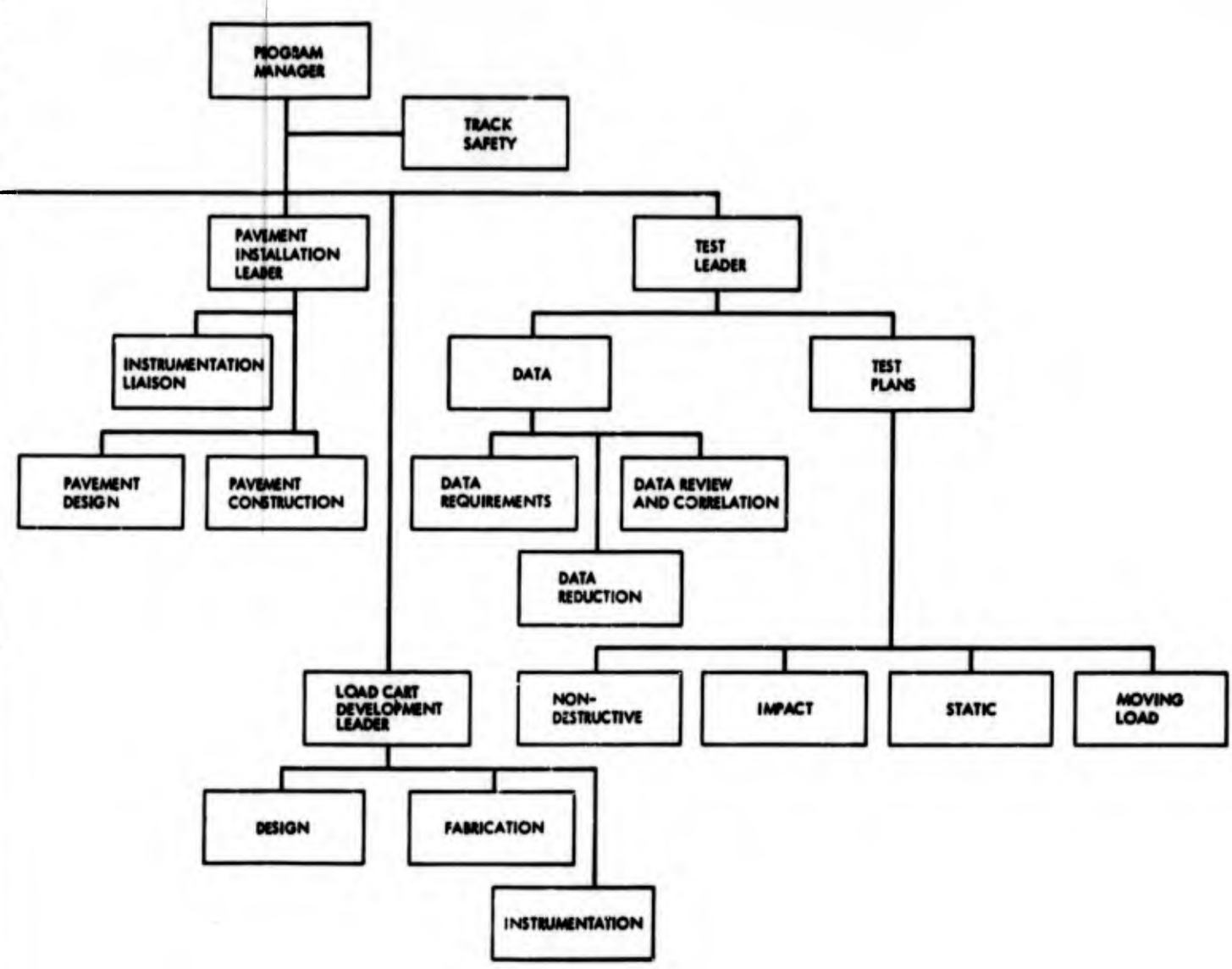

FIGURE G-4 - Organizational Chart for Moving Load Track Tests

- Provide instrumentation recording system for both the moving and stationary instrumentation installations including a quick look capability system. The maintenance required for instrumentation system is also to be provided.

- An Operations Officer will be supplied who will coordinate the load cart weight with the arresting gear settings and the pusher cart thrust duration requirements. Also, he will assure that historical motion picture coverage is obtained.

(2) Pavement Installation Contractor - This activity will perform the following services and supply the material incident to installation of the pavement:

- Provide an instrumentation liaison man to assure proper coordination between the installers of the instrumentation and the pavement builders

- Design the pavements including the proper incorporation of all pavement instrumentation

- Remove old pavement in the test area

- Install the test pavements to the design specifications. Particular attention is to be paid to instrumentation installation and assuring that pavement surface uneveness is held to a minimum.

(3) Load Cart Developer - This activity will be responsible for the design, fabrication and instrumentation of the load cart. Once the load cart has been fabricated and instrumented this activity will be complete. Maintenance requirements will be the responsibility of the operating activities.

(4) Test Leader - The test leader is responsible for the following aspects of the testing portion of the program:

- Set forth the test plan including the sequence and number of runs and any alterations required thereto

- Setting-up the data requirements, the data reduction system and the data review system

- Coordination with the Track Safety and Operations Officers to assure that tests to be performed are within the capabilities of the equipment

- Correlating measured and analytical data

- Preparation of all reports including the final report

(C) Test Schedule - Figure G-5 is the Test Schedule for the 12 month duration Moving Load Track Tests. The tasks that will be performed will include the following:

(1) Preparation for Tests - This activity will include:

- Selection of the construction techniques and materials to be employed in the six test pavements. The pavement to be asphalt concrete (4) and Portland cement (2).
- Purchase the necessary strain gages (120), pressure gages (36), deflection gages (18) and the material for wiring and installing the instrumentation.
- Set forth requirements for the design of the load cart.
- Develop preliminary test plan indicating general requirements to aid in preparation of test track. Such information as load cart weight, range, velocity requirements, approximate number of tests, test pavement location, instrumentation requirements and approximate amount of data reduction needed will be included.
- Prepare detail test plans for nondestructive, static, impact and moving load tests.
- Prepare detail instrumentation requirements for the pavements and the load cart.
- Prepare data test sheets
- Establish data reduction techniques for the nondestructive and impact tests.
- Develop methods and criteria to be employed in the data review.
- Acquire equipment needed to perform nondestructive and impact tests.

(2) Load Cart Development - The load cart will be designed to have the following features:

- The gross weight can be varied from 110,000 to 175,000 pounds.
- Ninety percent of the weight will be carried on the main struts.
- Auxiliary struts and wheels will be provided to stabilize the cart during track acceleration and speed retardation in the arresting gear.

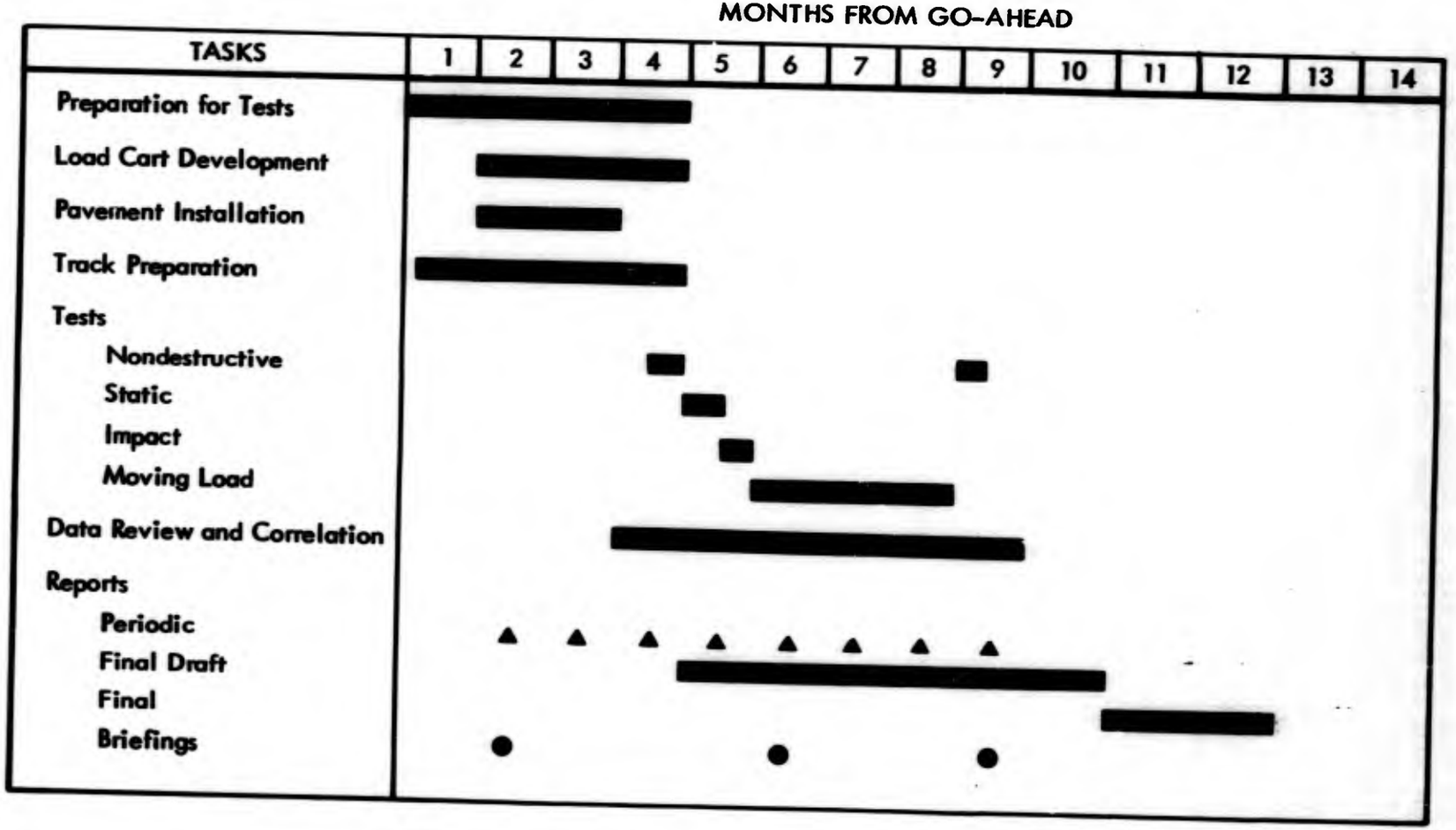

FIGURE G-5 - Test Schedule for The Moving Load Track Tests

- The main struts will be obtained from an obsolete 707 or DC-8 and will be modified to have interchangeable wheel configurations (single, dual and tandem). The strut on the test pavement side of the cart will be instrumented to measure vertical load

- The wheels will be located from the centerline of the cart such that they will pass over the center of the test pavement

- Provide the necessary fixtures for mating the pusher cart with the load cart

- Guide wheels or slippers will be installed to mate with the track directional guide rails and so located longitudinally that a 3,000 pound side force on the rail will not be exceeded

- The cart will be capable of velocities up to 150 knots

(3) Pavement Installation - Six test pavements will be installed in series with materials and construction techniques being selected during the Preparation for Tests task. In addition, the pavements will have the following features:

- Be a square, each side 25 feet in length

- Pinned together to take vertical shear

- Instrumentation such as pressure and strain gages to be located in and on the pavement

- The surface shall be as smooth as possible, including joints, so as to reduce transient loads to a minimum as a result of cart response to surface uneveness

- Reasonably fast cure materials will be used

(4) Track Preparation - The following work will be performed in preparing the track and its equipment for the test program in addition to normal maintenance activity:

- Provide office space, telephones and necessary furniture for test planning, data gathering, data reduction and performing data analysis

- Remove present pavement from the area for installation of test pavements and excavate the area in preparation for pavement construction

- Install the necessary instrumentation wiring

- Develop operation plan for conduct of the tests

- Provide cart load and velocity charts.
- Establish maintenance activities for support of instrumentation, the carts and track equipment.

(5) Tests - Figure G-6 illustrates the manner in which the work will flow for the entire program. The relationship of the actual performance of the test, including changes in the test plan, is also shown. Tests will include both field and laboratory tests prior to and after the conclusion of the program. Among the tests will be on site soil measurements to determine significant compactive characteristics such as moisture content, grain size, distribution, California Bearing Ratio and dry density. Sample specimens will be laboratory tested under steady and repeated cyclic loads to determine static and dynamic moduli and damping properties. The tests will be used to ascertain the limiting responses for the various materials and to determine the effect combined layers, versus individual layers, have on pavement response.

(6) Data Review and Correlation - The work to be performed in this task includes:

- The development of methods for correlating the measured data with analyses
- Performance of correlation studies
- The development of the methods employed in establishing pavement design criteria for moving loads and the performance of the work incident thereto

(D) Equipment Required for Test Program - The following equipment will be required in support of the test program:

- Nondestructive test equipment such as the Shell machine
- Impact test device such as available at the Lockheed-Georgia Company but with a greater load capacity
- Desk type computer to support data reduction and on the spot check of correlation
- Desk calculator as back-up to the desk computer

(E) Instrumentation - The location of the pavement instrumentation consisting of strain pressure and deflection gages will be across each test section about in the middle in the longitudinal direction. The strain gages at the sites will be arranged to measure strains parallel and normal to the flight path. The pressure gages will be located directly under some of the strain gages and will be 1, 3 and 8 feet below the under surface of the pavement.

(F) Tests to be Performed - The following four types of tests are to be performed on each of the test pavements:

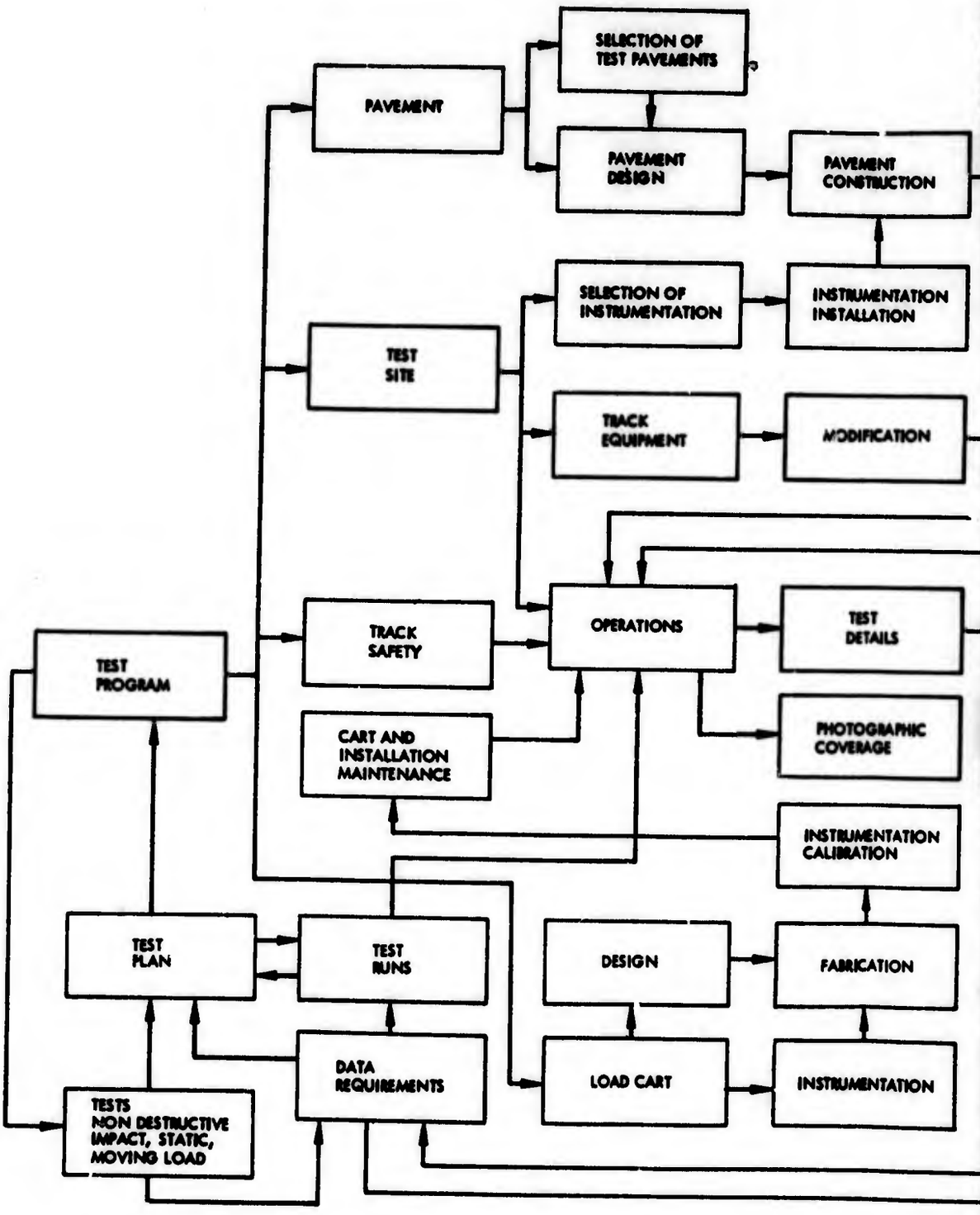
SELECTION OF TEST PAVEMENTS
PAVEMENT
PAVEMENT DESIGN
PAVEMENT CONSTRUCTION
SELECTION OF INSTRUMENTATION
INSTRUMENTATION INSTALLATION
TEST SITE
TRACK EQUIPMENT
MODIFICATION
TRACK SAFETY
OPERATIONS
TEST DETAILS
TEST PROGRAM
CART AND INSTALLATION MAINTENANCE
PHOTOGRAPHIC COVERAGE
INSTRUMENTATION CALIBRATION
TEST PLAN
TEST RUNS
DESIGN
FABRICATION
DATA REQUIREMENTS
LOAD CART
INSTRUMENTATION
TESTS NON DESTRUCTIVE IMPACT, STATIC, MOVING LOAD

FI

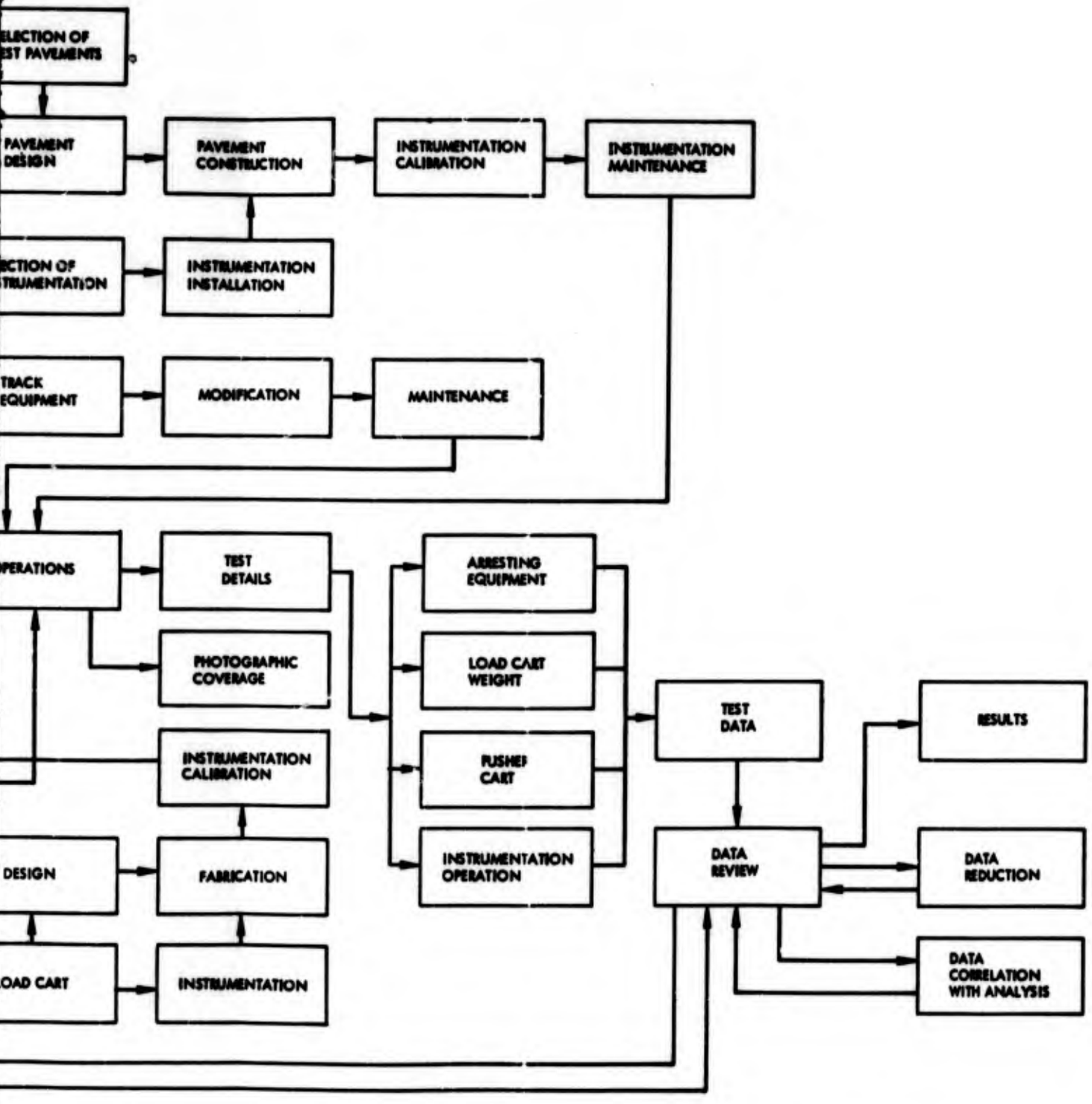

FIGURE G-6 - Work Flow Chart for Moving Load Track Tests

B

(1) Nondestructive - These tests will provide data regarding the characteristics of the pavement to various depths before and after the moving load tests. The results will be compared.

(2) Static - These tests will provide basic data for comparison with the moving load data and for correlation with analytically obtained data.

(3) Impact - The impact test provides a simple means by which the moving load effect can be simply checked on other runways. Therefore, the data obtained will be used to support development of this technique.

(4) Moving Load - These tests will provide the data for correlation with analyses and form the basis for the development of pavement design criteria for moving loads. Because these tests are not well suited for point-by-point comparison with analyses, statistical methods of data analysis will be employed.

(G) Summary - The moving load tests will provide precise data under controlled conditions. Because of this, interpolations of the data to fit other types of runway constructions can be accomplished with a much greater degree of confidence than can be placed in using data collected in the Operational Statistical Tests.

APPENDIX H

CRITIQUE OF MATERIALS CHARACTERIZATION AND DESIGN TECHNIQUES FOR AIRPORT PAVEMENTS

TABLE OF CONTENTS

LIST OF FIGURES

1. BACKGROUND

Pavements are complex physical systems which involve the interaction of a number of interrelated factors. In order to develop a rational design procedure, it is necessary to develop a systematic and logical approach to the design of pavements. In deciding on the suitability of a design, in addition to structural considerations, economics, safety, reliability and other user controlled factors play an important part. This review does not consider all these factors. It deals only with the structural design variables. Figure H-1 indicates the many variables and some of the interaction that should be accounted for in the complete design of a pavement system. This was developed for a highway pavement system by Materials Research and Development (1968), but is applicable to the airport pavement problem.

The structural design aspect of the pavement problem consists of determining and evaluating the primary response. A review of this aspect is the major objective of this report. This phase of the design is indicated in Figure H-1 and detailed in Figure H-2. In Figure H-2 the process of checking the computed primary response against observed behavior and modifying the idealizations as necessary is also indicated. The primary response is defined by the mechanical state (stress, strain and deflection) that is induced in a pavement system. The evaluation of the primary response is based primarily on material failure theories. It is appropriate to comment briefly on the steps, as shown in Figure H-1, that are involved in the structural design of pavements and indicate how both empirical methods and methods founded on sound theoretical principles fall within this general frame work.

Step 1: Appropriate input and output (response) variables must be defined. Inputs to the system include a variety of load, environmental, construction, and maintenance variables. The load variables are stochastic in nature and are difficult to specify accurately.

Pavement response refers to the behavior of the physical system when subjected to inputs such as load or temperature. This response in the context of structural design is defined by the mechanical state, i.e., deflection, stress, and strain*. When the primary response reaches some limiting value, distress, in the form of rupture, distortion, or disintegration can occur in the pavement.

Step 2: The pavement structure must be defined geometrically and the materials and construction techniques identified. This may be considered a description of the pavement system.

Step 3: The response of the pavement system to all classes of input expected to occur in-service must be determined.

*It should be recognized that the chemical state in the pavement could be a significant factor in its performance.

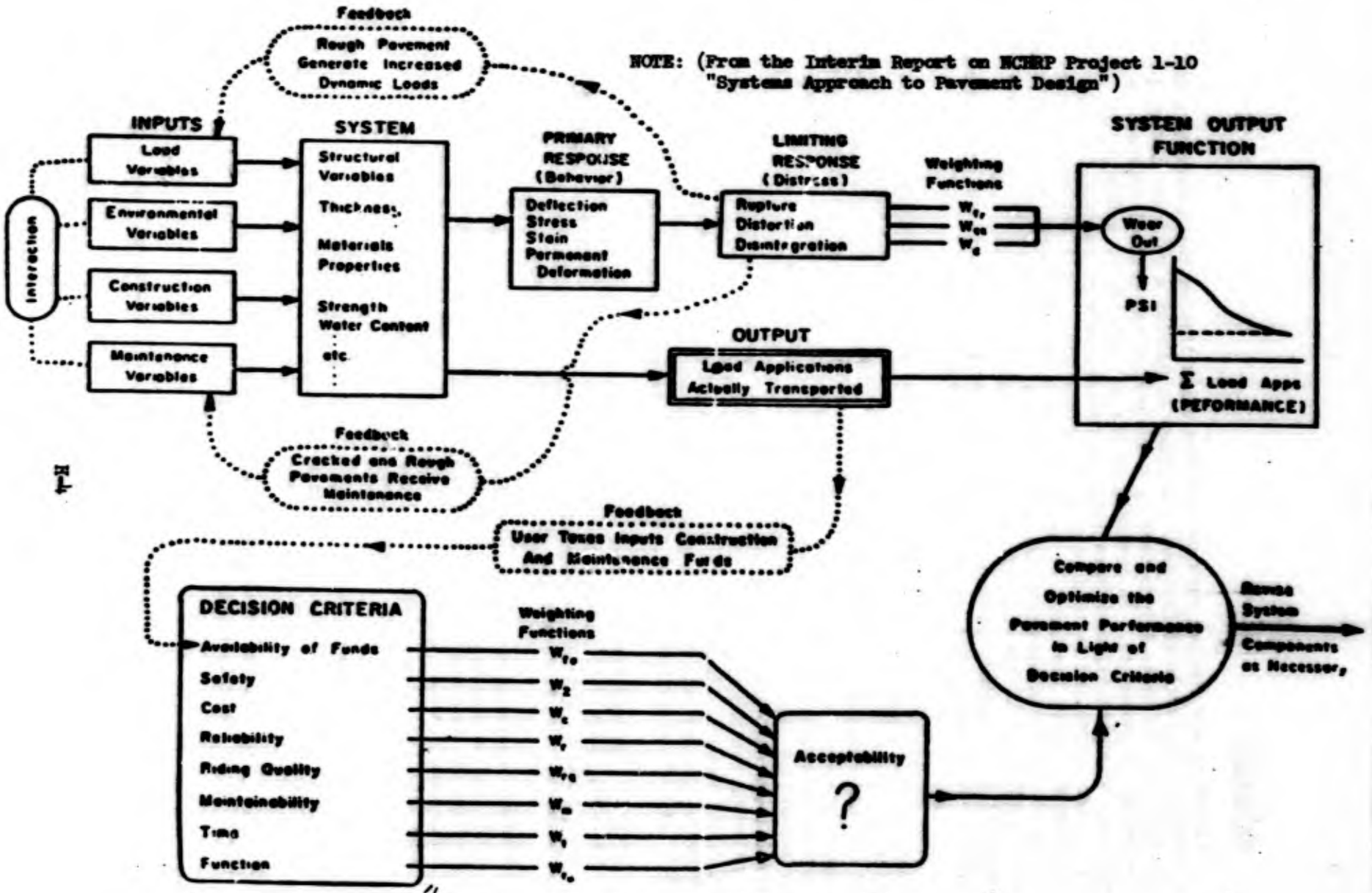

Figure H-1 Block Diagram of the Pavement System

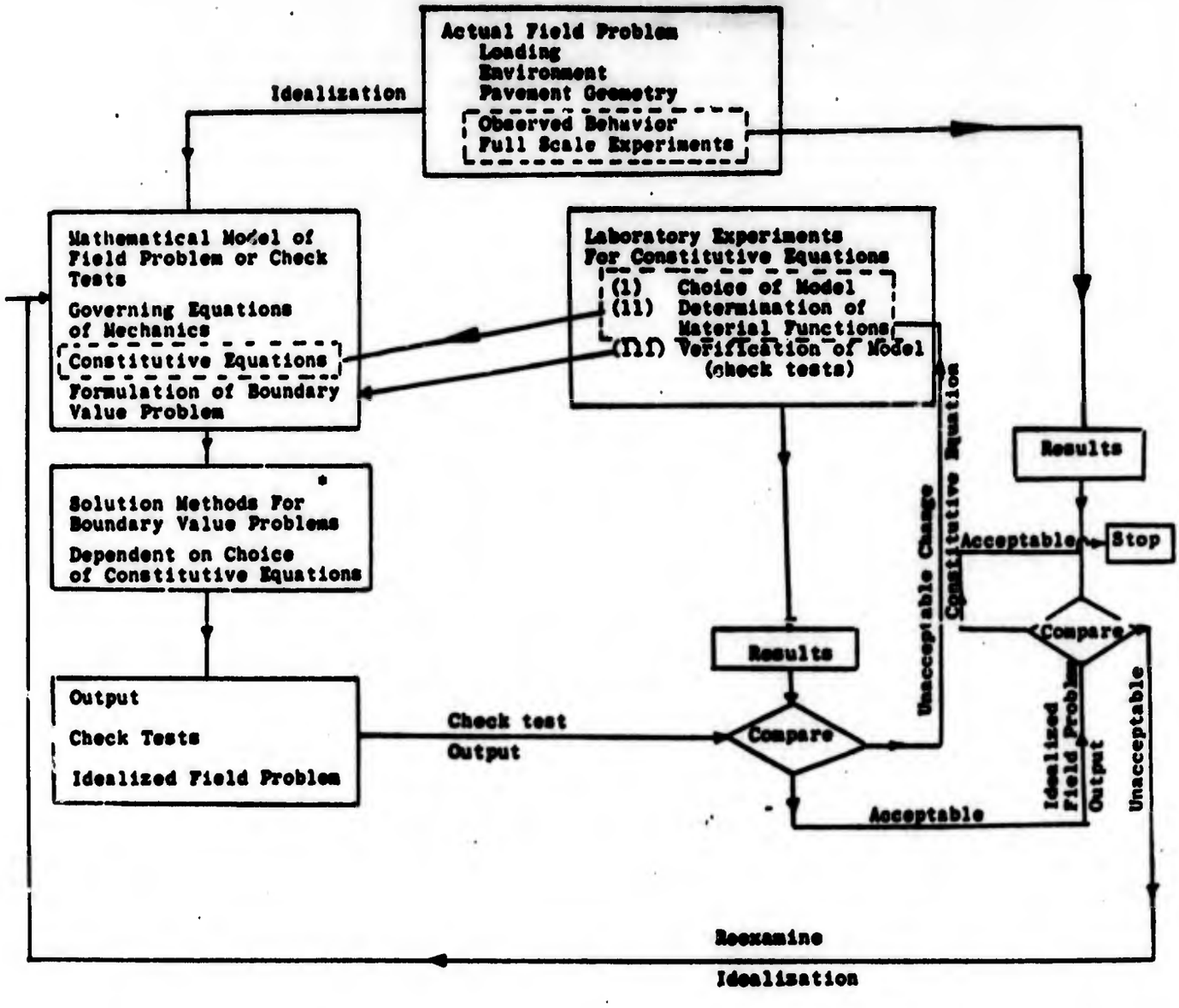

• The Solution Methods involve Iterative Techniques for Nonlinear Constitutive Equations

Figure H-2 Development of a Model for Determining Primary Response

This involves determination of the system function. There are two* general engineering approaches for determining the system function:

(a) Testing Approach - This requires testing under service conditions (full scale and model) and results in various empirical design procedures. This approach to pavement design would require carrying out a series of experiments in which typical pavement sections were subject to expected traffic and environmental inputs fed into the system and the response measured. It will be necessary that a measure of the performance of the system be set up. Performance is, in some sense, a measure of the response, e.g., whether or not breakdown (i.e., distress) of the system results during the response or whether excessive permanent deformation occurs and, furthermore, whether or not good performance is attained for reasonable cost, both initial and maintenance. Evidently, an objective measure of performance will involve concepts of mechanical and economical life of the system. In order to obtain an optimum design, it is necessary to alter the structure of the system until a maximum mechanical-economic life is achieved for a given range of inputs. (Existing methods of design fall in this category).

The principal disadvantage of the type of approach described above is that it is not predictive; that is, changes of input variables or changes in the systems function falling outside of the range covered in the experiment must be examined by extrapolation rather than interpolation. This is especially true for airfield pavements where the rapid changes in the load inputs have made it difficult to apply empirical design procedures. Furthermore, the large number of variables involved in the system (input, response, and materials) magnifies the experimental task enormously. Consequently, it is highly desirable to place the design process on a rational basis.

(b) Macroanalytical Approach - This forms much of the theoretical basis of most of the work in applied science and engineering. Continuum (solid) mechanics is the main discipline in this method, and the object may be considered to be the formulation and solution of an appropriate boundary value problem is an important phase of the investigation. The major advantage of this approach is that it is predictive and places the design process in a rational framework.

Step 4: Appropriate criteria have to be formulated to judge the response of the system from the performance standpoint.

These criteria involve the limiting values of stress and strain and other factors such as funding, cost, reliability, and riding quality. These must be combined in an appropriate way to select the proper level of acceptability for a particular purpose. This level of acceptability then provides a basis for comparing and optimizing the system output or

*A third approach, the micromechanistic approach, which deals with behavior at the atomic or molecular level, is not considered here.

pavement performance. For the structure design, limiting values of the primary response (stress, strain, and deflection) form the basis of performance criteria.

Step 5: Modification of the pavement system must be permitted in order to attain as near an optimum condition as possible.

These are the basic steps in the development of a rational method for the design of airfield pavements. A critique of the available methods of accounting for the various factors that are involved in the structural design of airfield pavements will involve the evaluation of research conducted for the design of highway pavements. A great deal of this research is directly applicable to airfield pavements. It is therefore appropriate to comment on the similarities and differences between airfield and highway pavements. In addition it is considered desirable to provide the reader with some general comments on the choice of materials and techniques of construction for pavements.

Airfield Vs. Highway Pavements - Modern pavements for both airfields and highways are quite similar to the extent that they are essentially layered systems placed on the ground surface and designed to support imposed traffic and to withstand the detrimental effects of environmental factors without distorting, cracking or disintegrating beyond acceptable limits.

Although the general principles of pavement structural design and analysis are common to both airfield and highway pavements, there are significant differences in loading characteristics and geometrical configurations which preclude free interchange of experience and research results obtained on one type of facility to the other. However, it is a fact that the preponderance of research and experience, information and data on pavement structures is in the highway field; thus, it is only logical to take all possible advantage of this large fund of knowledge. This can be done by recognizing what the principal differences are and how they may influence pavement behavior and performance.

Loading Characteristics - The characteristics of the applied loadings to airfield and highway pavements are quite different. Heavy duty highway loadings are characterized by axle loadings limited by statute, (e.g. 18,000 lb. single axle, 32,000 lb. tandom axle), tire pressures less than 100 psi, and channelized traffic in high volumes (e.g. over 1 million equivalent 18,000 lb. wheel loads per year) running at speeds generally less than 70 mph. A modern highway is, in effect, fairly uniformly traversed by traffic of low stress intensity but of high numbers of repetitions at moderate speeds.

Heavy duty airfield loadings, on the other hand, are characterized by high strut loadings (approaching 200,000 lbs.) with wheel loadings, depending on wheel configuration (as high as 50,000 lbs.) tire pressures of 200 psi and higher, and traffic patterns depending on the function of the pavement. Semi-channelized traffic is found on portions of runways and aprons and

highly channelized traffic on taxiways, with numbers of movements seldom exceeding 100,000 movements a year, at speeds ranging from high speed (up to 140 mph) on runways to creep speeds on taxiways and aprons. A modern airfield pavement is, in effect, non-uniformly traversed by traffic of high stress intensity but of relatively low numbers of repetitions at both creep and high speeds, with most of the pavement area never touched by a wheel load during the life of the pavement.

The significance of differences in airport and highway loading characteristics may be summarized as follows:

- The fewer load repetitions, by an order of magnitude, per year on airfield pavements means higher pavement deflections can be tolerated than on highway pavement, based on fatigue considerations.

- The higher stresses induced by airport type loadings, particularly stationary loads and those travelling at creep speed, will cause larger deformations in airfield pavement components as compared to highway pavements.

- The combination of high loads and high speed on runways introduces dynamic effects on airport pavements not experienced on highways, which make the grade and smoothness tolerances of runways quite important.

- The performance of the extensive unloaded areas of airport pavements cannot be tied in to observations on highway pavements, where such a condition does not exist.

Geometrical Configurations - The geometrical configurations in both plan and structural cross-section of airfield pavements are quite different from highway pavements. Only the central portions of runways and taxiways which are generally constructed of widths and lengths with ample space for aircraft maneuvers, are subjected to traffic, a whereas for highway pavements the traffic lanes are relatively narrow. In cross-section, modern airfield pavements are considerably thicker than highway pavements because of the heavier total load to be supported during a single movement of load. It is not uncommon to have airfield pavement thicknesses exceeding twice the thickness of a highway pavement for equivalent soil conditions.

In view of the differences in geometrical conditions, certain significant influences may be expected as follows:

- Edge loadings conditions of airfield pavements are essentially non-existent compared to highway pavements.

- Drainage problems, both surface and subsurface, are much greater with airfield pavements which cover vast expanses and must dispose of larger

volumes of water at relatively flat gradients as compared to highway pavements which can have high gradients both laterally and longitudinally.

- Environmental factors influencing pavement thickness (e.g. freezing and frost heaving) are not as large a problem with airfield pavements as they are with the thinner highway sections.

- Environmental factors affecting surface deterioration of both asphalt and portland cement concrete are more active on the relatively unused areas of airfield pavements which calls for more durable materials and mixed designs for airfield pavements.

Classes and Properties of Materials - In general, the predominant physical feature of materials utilized in pavement structures is granularity. Crushed stone and gravels, natural gravels and cohesionless sands make up, by far the majority of the structural cross-section. Admixtures, such as portland cement and asphalt cement, are utilized to bind the aggregate particles to the degree necessary for the bound materials either to serve as wearing surfaces or to increase the stiffness of the pavement component layers.

It has been found that the most practical way to construct a pavement structure with acceptable levels of performance is by forming layers of granular materials of gradually increasing strength and durability characteristics on the subgrade soil. Figure H-3 illustrates typical pavement cross-sections and indicates the types of materials used as components of each layer.

Techniques of Construction - The significant aspects of construction techniques as they influence the behavior characteristics of airfield pavements are quite varied and much too complex to discuss here in any detail. Several of the more important construction techniques, however, are listed below with comments on the role each plays in making the pavement system function:

Compaction - Of all construction techniques, compaction is the most important because granular materials develop and maintain the desired behavior characteristics as pavement components only when adequately compacted. Both under and over compaction can cause problems associated with such undesirable manifestations of distress as rutting, instability and aggregate degradation.

Uniformity - Although the use of highest quality materials is generally desired and specified, it is of great significance in pavement construction to utilize construction techniques which will produce a material of uniform composition and good quality. Uniformity makes the design simpler. Methods of construction which produce and place material of high variability will result in highly erratic pavement behavior characteristics.

a) Asphalt Concrete Pavement

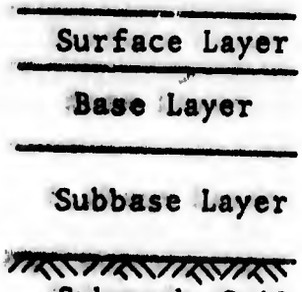

b) Portland Cement Concrete Pavement

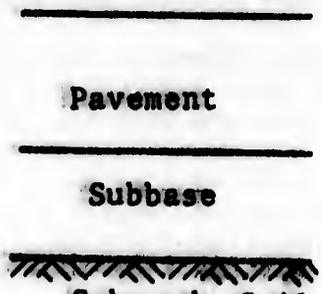

Typical Airfield Pavement Cross-sections

Pavement Component	Materials Used
	Type
Surface Layer	Portland Cement Concrete
	Asphalt Concrete
Base Layer	Crushed Rock or Crushed Gravel
	Cement Treated Gravel
	Asphalt Treated Gravel
Subbase Layer	Gravel
	Sand

Classes and Properties of Materials Used as Pavement Components

Figure H-3 Typical Pavement Sections and Materials

Bonding - During construction it is necessary to insure that adequate bond is developed between layers of pavement components, or the possibility of slippage type failures will exist. This is particularly true for airfield pavements because of the high horizontal thrust exerted to a pavement surface by the braking and turning actions of heavy aircraft. This problem is particularly critical on asphalt concrete pavements.

Load Transfer at Joints - In the construction of portland cement concrete pavements, it is imperative that techniques of placing load transfer devices at longitudinal and transverse joints be such that vertical movement be restrained without constraining the lateral working of the joint. Dowels and key joints should be skillfully placed or formed to accomplish the above. Failure to do so generally results in cracks developing in the interior of the slab, which do not have provisions for load transfer, and in serious problems of spalling and even pumping.

Workmanship - This term covers the entire range of construction techniques and is aimed at the use of precision and care in whatever construction method utilized. Its main significance is that the final dimensions and tolerances are greatly affected and, thus, the riding quality and effectiveness of drainage facilities. Rough or uneven pavements result in the ponding of water in "bird baths" and the "porpoising" of aircraft traveling at high speeds on runways during take-offs and landing operation. Both are objectionable features on airfield pavements for safety reasons.

2. STRUCTURAL DESIGN

Having established a background, the rest of this report will consist of a critique of the existing methods of accounting for the various factors that are involved in the structural design of airfield pavements. The critique will consider four of the five basic steps outlined earlier as essential to the development of a rational design process. The fifth design step, optimization through the monitoring and evaluation of performance is outside the scope of this report.

(a) INPUT VARIABLES

Loads - Static and dynamic loads are applied to airfield pavements. The nature and magnitude of these loads depends on the type of aircraft, the function it is performing i.e., taxiing, taking off, braking or turning, and the characteristics of the pavement. Furthermore, the loads are not applied at regular intervals and it is not possible to predict the frequency or magnitude of load applications. Therefore, consideration should be given to treating the loads stochastically.

At the present time, the stresses, strains, and deflection that occur in a pavement are computed on the basis of treating the applied loads as static. The rationale behind this is that if under the most severe static

load the stresses, strains and deflections are below certain limiting values the pavement is structurally sound. Obviously this is not a very sound argument as repeated loads, each of which result in stresses and strains below a limiting value can cause failure due to fatigue. In order to consider the repeated nature of the loads, material properties and failure concepts should include testing under dynamic loads.

The primary reason for treating the load as static is the difficulty in analyzing the dynamic problem. A plate or a beam on a Winkler foundation can be analyzed for a moving load as can a halfspace consisting of linear elastic and/or various special viscoelastic material properties, Pister and Westmann (1961), Moavenzadeh (1968). However, all these analyses are based on a great many assumptions regarding the material properties. Therefore, it has been the practice to simplify the load and permit greater flexibility in modelling the material behavior. Recently developed computational techniques indicate that it would be possible to incorporate a time dependent load with non linear material properties, Wilson (1965), Zienkiewicz (1967).

Because of the unavailability of a general three dimensional analysis, the loads have to be reduced to an axisymmetric configuration. The contact area underneath a tire is generally close to elliptical; however, an equivalent circular area is used. For purposes of analysis, loads are considered as acting normal to the surface. In reality, shear stresses are also applied to the surface especially during braking and turning.

Aircraft loads are transmitted through multiwheel landing gears. If the pavement system is linear then the effects due to the various loads can be superimposed. However, most materials comprising a pavement system are significantly nonlinear. Hence superposition is not valid. Consequently an "equivalent single wheel load" has to be used. This equivalent single wheel load can be determined on the basis of a linear analysis by examining the influence of adjacent wheel loads on the stresses beneath a single wheel.

In summary, there are two general approaches to the problem:

1. Treat the load as a moving axisymmetric load and simplify the description of the system from a standpoint of material response and structural behavior.

2. Treat the load as a static axisymmetric load. Under such an assumption representations which are more realistic than possible under (1) can be made with regard to material response and structural behavior.

Currently used methods of pavement design use the approach outlined in (2) above.

Environmental Factors - Current pavement design methods treat environmental effects by designing the pavement for the most severe considerations which are appropriate to the distress mode under consideration. A familiar example is the determination of the CBR for a soaked condition. It should be recognized that assuming that all the components of a pavement system are subject to their most unfavorable conditions at one time will in general lead to an overly conservative design.

The two most important environmental factors are moisture and temperature. Moisture exerts a great deal of influence on the soil layers in the pavement system, i.e., the base, subbase and subgrade, while the temperature exerts a significant influence on the response of asphalt concrete.

It is generally assumed that the effects of temperature, and moisture can be considered separately (decoupled). The distribution of stress due to load and the distribution of temperature and moisture can be obtained from the solution of independent boundary value problems.

The effects of temperature and moisture can be grouped into two categories:

1. Thermal and hygrostresses which may be introduced in the pavement system due to the existence of temperature or moisture differential in the system. This requires the use of mathematical models to represent the material and is therefore an iterative process.

2. The temperature and moisture in the system may affect the material properties. The range of temperature and moisture used in testing the materials must reflect the values likely to occur in-service.

Other environmental factors that are important are the effects of frost and time (aging) on the asphalt. Existing airfield pavement design procedures do not treat the problem in a satisfactory manner. Recently developed procedures for use in the design of highway pavements can be used in the design of airfield pavements. Some of these concepts with regards to moisture and temperature are discussed in subsequent paragraphs.

Moisture - The variation of material properties as a function of moisture is discussed later under material characterization. In this section, the determination of the moisture conditions that are likely to exist in a pavement system is discussed.

The majority of studies, Atchison (1965), Atchison and Richards (1965), Redus (1957), and Kersten (1944), indicate that the moisture conditions in the subgrade and subbase reach a stable value approximately

two years after construction and that further fluctuations are minor except near the edges where rainfall caused substantial changes. The variations near the edges were found to decrease in a few days.

In order to consider moisture effects in design, it is necessary to develop a procedure for determining the moisture state in the subgrade. The most significant work in this direction has been by Atchison and Richards and their co-workers, who have utilized concepts of soil moisture suction. These studies have been confined primarily to no-frost areas, though research at the Norwegian Geotechnical Institute has shown the concept to be useful in the study of frost action, Williams (1967). Atchison (1965) has proposed a method for determining the equilibrium soil moisture suction. This is based on climate, depth to the water table and soil type. Sauer and Monismith (1968) have applied soil suction concepts in the determination of material properties for use in pavement design.

Based on the information available it would be reasonable to conclude that soil suction concepts offer a means for determining the equilibrium moisture state that is likely to develop in an airfield pavement system. Future studies should be directed in this direction.

Temperature - The importance of temperature as a factor in the design of pavements has been recognized for some time. The incorporation of temperature stresses in the design of portland cement concrete pavements has been in practice for some time. In asphalt concrete pavements, in addition to the introduction of thermal stresses, the effect of temperature on the properties of the asphalt concrete is of major importance.

In order to incorporate the effects of temperature, the temperature profile over the expected life of the pavement has to be determined. When designing against rutting for stationary and slow moving loads, the practice has been to consider the highest temperature. This has been done through the design of asphalt concrete mixtures for stability at 140° F. While the stability problem is severest at the high temperatures, the stresses are most likely to be highest at the lowest temperature.

A number of experimental studies have been undertaken which have recorded the temperature in pavements over an extended period of time, Kallas (1966), Straub et al (1968), Dunstan (1967). A major conclusion of these studies is that the actual variation in temperature is extremely complicated and a detailed analysis would be impractical for any design purpose. Furthermore, experimental information is only valid for conditions under which the information was obtained. A predictive method for obtaining the temperature profile is necessary for design. The method used in the highway field is due to Barber (1957). This method is based on the solution of the heat conduction equation for a semi-infinite mass subject to a surface temperature which has a sinusoidal variation. Solar radiation and irradiation from the surface are accounted

for by approximate techniques. Since the atmospheric temperature is a readily available quantity, Barber's solution can be utilized for design purposes. Comparison with available temperature measurements indicate that this method provides a reasonable estimate of the temperature profile in the pavement and therefore can be used in the design stage. The effect of the temperature on the material properties and it influence in introducing thermal stresses will be discussed in later sections.

It should be recognized that some of the concepts outlined above have been developed for use in highway pavement design and have not been applied to airfield pavements.

Construction Effects - The influence of construction on the structural design of airfield pavements consists primarily in its effect on the properties of the materials comprising the pavement system. Other important considerations are the influence of joints and reinforcement of the performance of concrete pavements.

Construction techniques might cause the material to be nonhomogeneous and anisotropic. The use of field samples for laboratory testing is an attempt to include construction effects into the characterization of materials. Extensive research on the influence of compaction techniques on the properties of cohesive subgrade soils has been summarized by Seed et al (1967). These studies indicate that if appropriate laboratory sample preparation and conditioning techniques are used, field conditions can be duplicated in the laboratory with satisfactory accuracy.

In addition to the influence on the formation of the various materials, various methods of construction might result in significant residual stresses existing in the pavement system. It will be necessary to incorporate these stresses into the determination of the stress state in the pavement system. At the present time there are no satisfactory methods for determining the existing residual stresses.

(b) DESCRIPTION OF PAVEMENT SYSTEM

Geometrical Description - The geometrical description consists of establishing the thickness and horizontal extent of the various layers. Defining the thicknesses of the various layers presents no difficulties. There are two approaches in defining the horizontal extent of the various layers.

The first is to treat the pavement surface layer as a plate of finite extent resting on an elastic foundation (Winkler assumption). This is the approach commonly used to design portland cement concrete pavements. Its main advantage is that it can account for corner and edge loadings. However, the assumptions of plate theory and the treatment of the supporting material as a Winkler foundation are far from realistic.

The second approach is to treat the pavement structural system as a layered half space. The resulting boundary value problems are more complex to solve though the representation is more realistic. The half-space assumption is not suitable for considering problems where the load is near the edge.

Material Description - This is an essential step in the development of any rational design procedure and is emphasized in this review. There are two basic approaches in describing a material for inclusion in analysis and design. The first is through various empirical properties which are determined by certain standard testing procedures. Examples of such properties are the CBR and the Cone penetration resistance. The use of such properties in design can only be done through empirical correlation. Such descriptions of material properties and the resulting design procedures have played an extremely important role in the development of airfield pavement design. However, the thrust of this study is the development of a rational method and the empirical properties do not assist in the development.

The second approach consists of describing the material through the use of appropriate constitutive equations. At the present time, general constitutive equations to cover all aspects of material response are not available. The approach utilized at present is to use constitutive equations which are really simplified forms of general equations and only include (for the particular problem or aspect of a problem) those phenomena which are of importance. For example, such a simplified model is the theory of elasticity; further simplifications for various special problems result in the separate theories of shells, plates, and beams. It should be emphasized that a simple model containing the important physical aspects of a problem is superior to a model of considerable generality which is deficient in it's representation of the physical behavior of the particular material for the problem under considerationn.

Research workers in the field of mechanics have devised various mathematical models and the advent of the digital computer has greatly increased the capability of obtaining solutions to boundary value problems incorporating these models. It is, therefore, necessary to correctly characterize the materials which comprise a pavement system in order to derive the full benefits of the advances in these areas.

The decision as to whether a particular model is suitable for use in a specific problem rests with those who understand the physical nature of the particular problem. If the models now available are not satisfactory in representing essential aspects of material behavior, then the material response must be described to the research worker in mechanics so that an appropriate mathematical model may be developed. It is the blending of theory and physical reality that is the key to the development of improved methods of material characterization and progress in the development of methods in the structural design of pavements.

Steps in Selecting a Mathematical Model - Selecting a mathematical model to represent material behavior requires the reduction of experimental observations, which are always limited in scope, into a mathematical law. This should be done in a logical manner and in accordance with the general principles of solid mechanics. The process of choosing a mathematical model to represent a material and determining the necessary material constants can be subdivided into a number of steps, these are illustrated in Figure H-4. This is an amplification of certain steps in Figure H-2. This approach, recently developed by MR&D, Inc., has been used in the development of a design procedure for highway pavement analysis. It should be recognized that material characterization is in general an iterative process in which continued experimentation, field verification, and development of constitutive equations lead to improved modeling of material response.

In the subsequent paragraphs brief summaries of the significant mechanical response* based on available experimental information for various materials commonly used in the pavement system are presented.

Asphalt Concrete: The experimental information on asphalt is reviewed under the various categories that are considered significant to the selection of constitutive equations. Some typical experimental data is included to illustrate various observed effects.

Linear and Non-Linear Behavior - There is a considerable evidence on non-linear behavior as indicated by the influence of stress level on the material response and the difference in behavior under tensile and compressive loads. At higher temperatures non-linear behavior is more pronounced. Non-linear behavior exists over extended time intervals. (Figures H-5, H-6, and H-7). Under uniaxial stress conditions, for small strains (less than 1%), linear behavior appears to form a satisfactory first approximation.

Time Dependent Behavior - The response of asphalt concrete has both time dependent and instantaneous components. The relative importance of these components depend on the nature of the applied load. For loads of long duration, the time dependent response is the most significant, for short duration dynamic loads the resilient deformation (elastic response) is the most significant, (Figures H-5, H-8, and H-9). The nature of time dependent response has not been clearly established.

*It should be recognized that there are many material properties which are important in the overall design, such as durability and aging of asphalt, frost susceptibility of soils, which are not included in this discussion.

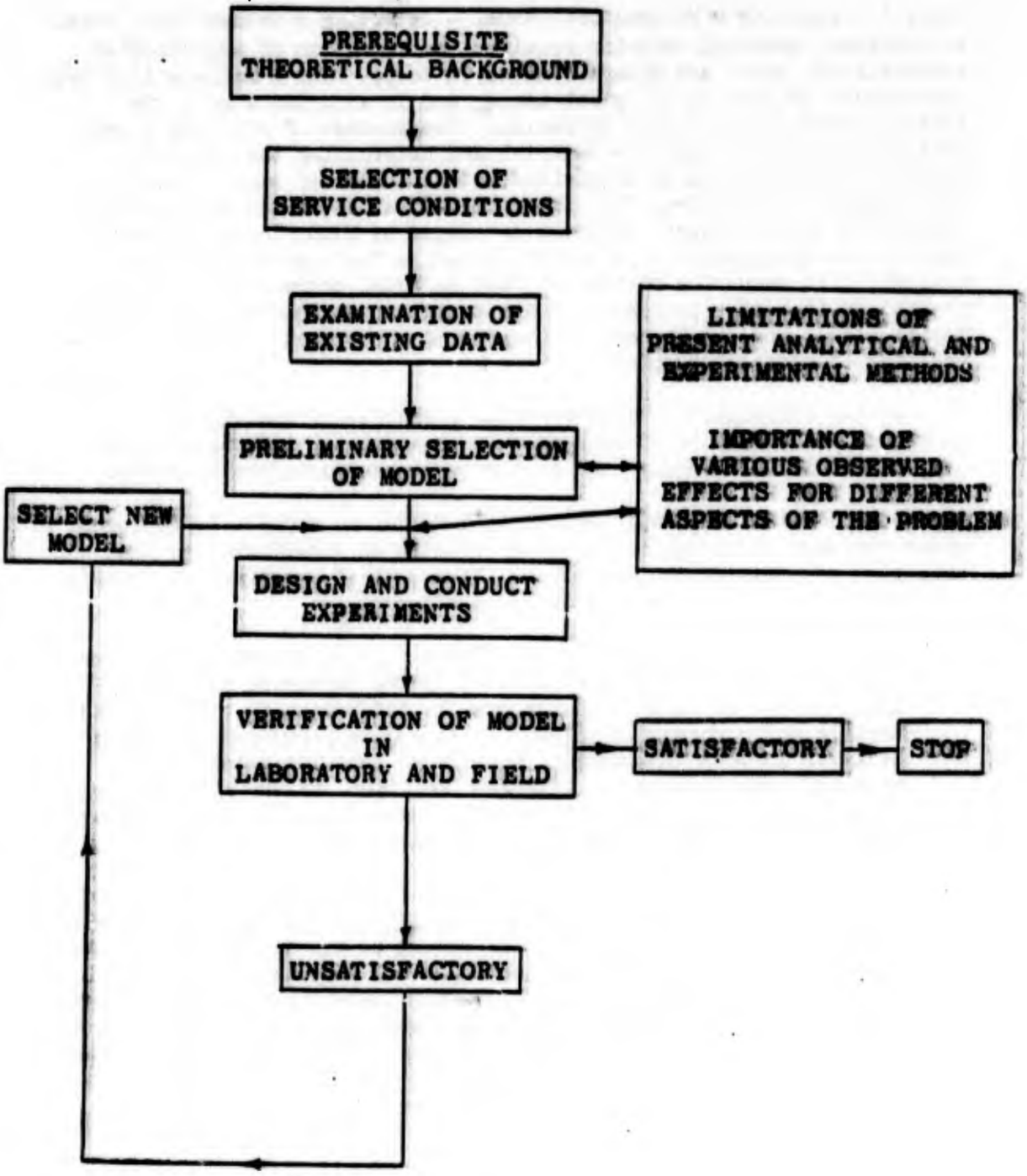

Figure H-4 Steps in Material Characterization

(After Monismith Alexander & Secor 1966)

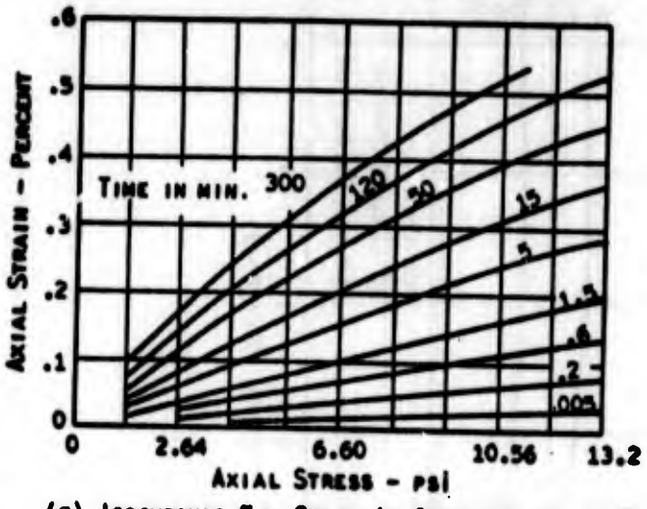

(a) Isochrones For Creep In Compression (75°F)

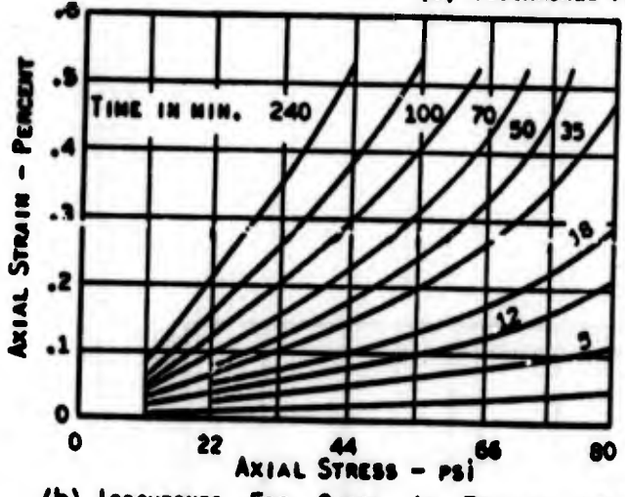

(b) Isochrones For Creep In Tension (40°F)

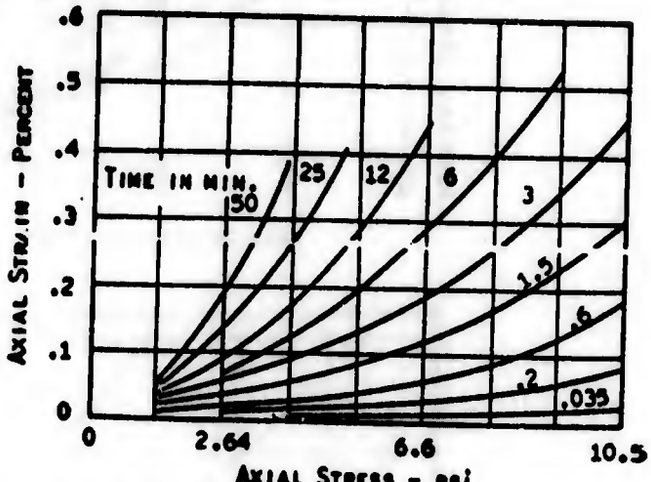

(c) Isochrones For Creep In Tension (75°F)

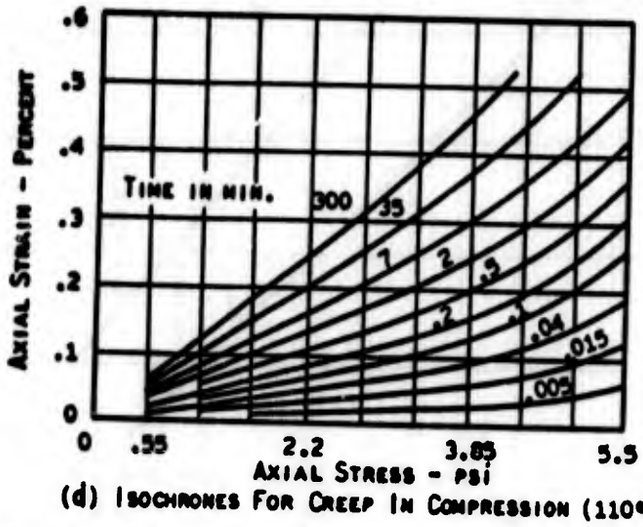

(d) Isochrones For Creep In Compression (110°F)

Figure H-5 Data from Creep Tests on Asphalt Concrete

(After Shaub & Goetz 1961)

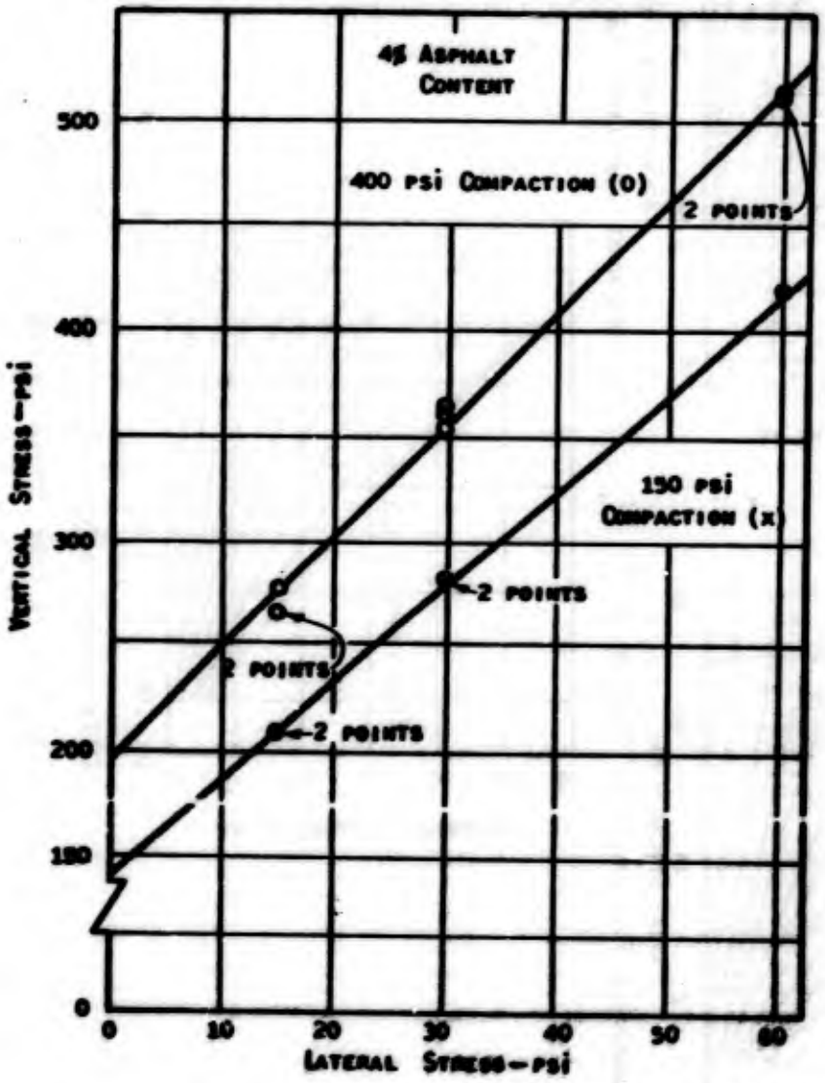

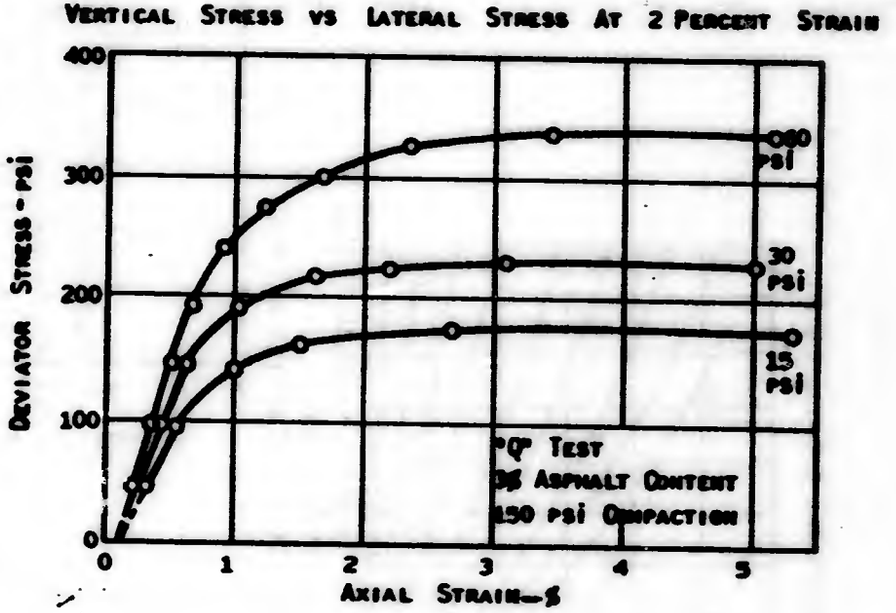

Figure H-6 Data from Triaxial Tests

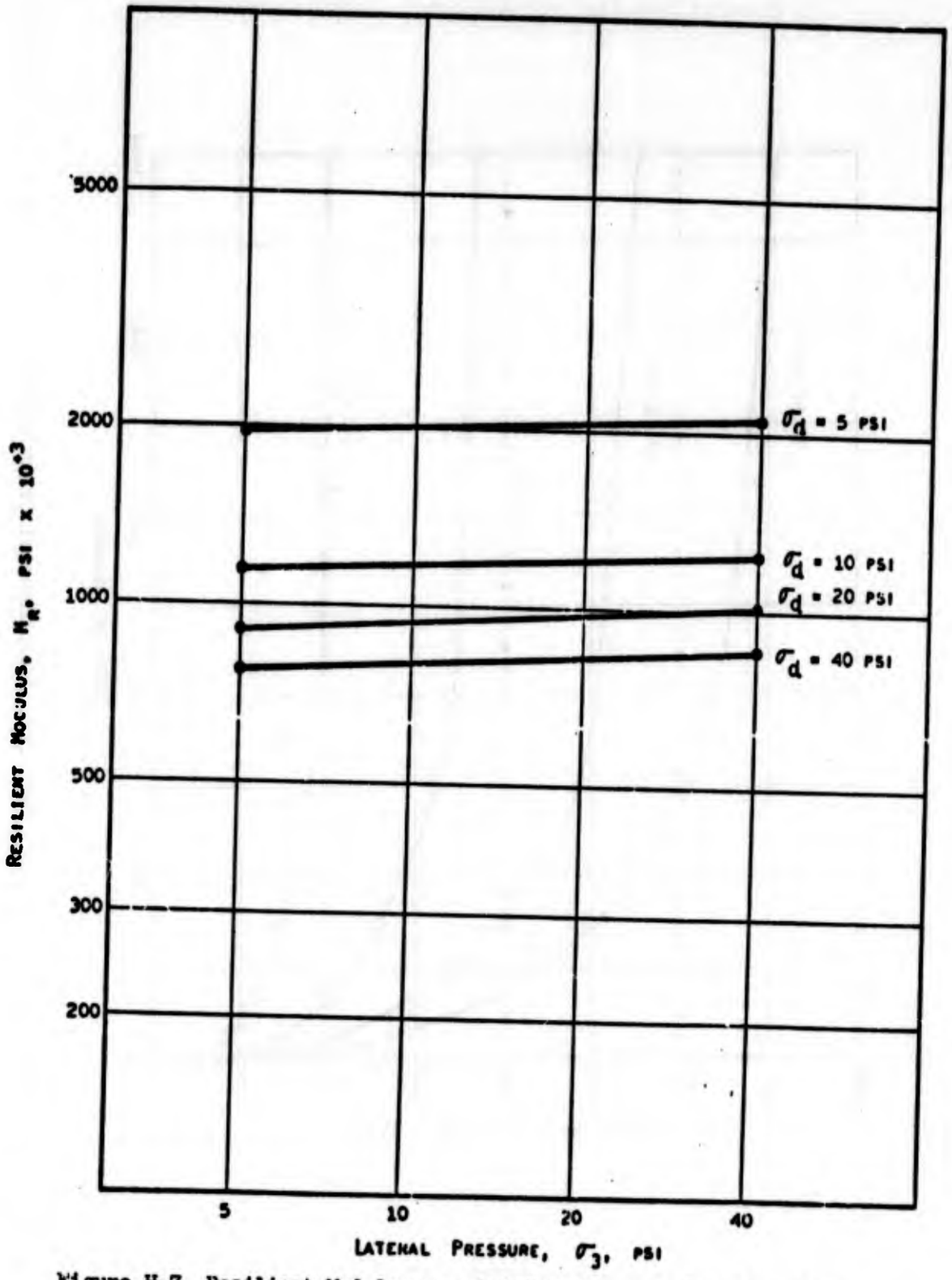

Figure H-7 Resilient Modulus vs. Lateral Pressure for Laboratory Prepared Specimens of Asphalt Concrete Base Tested at 68°F (After Terrel 1967)

(After Pagen 1953)

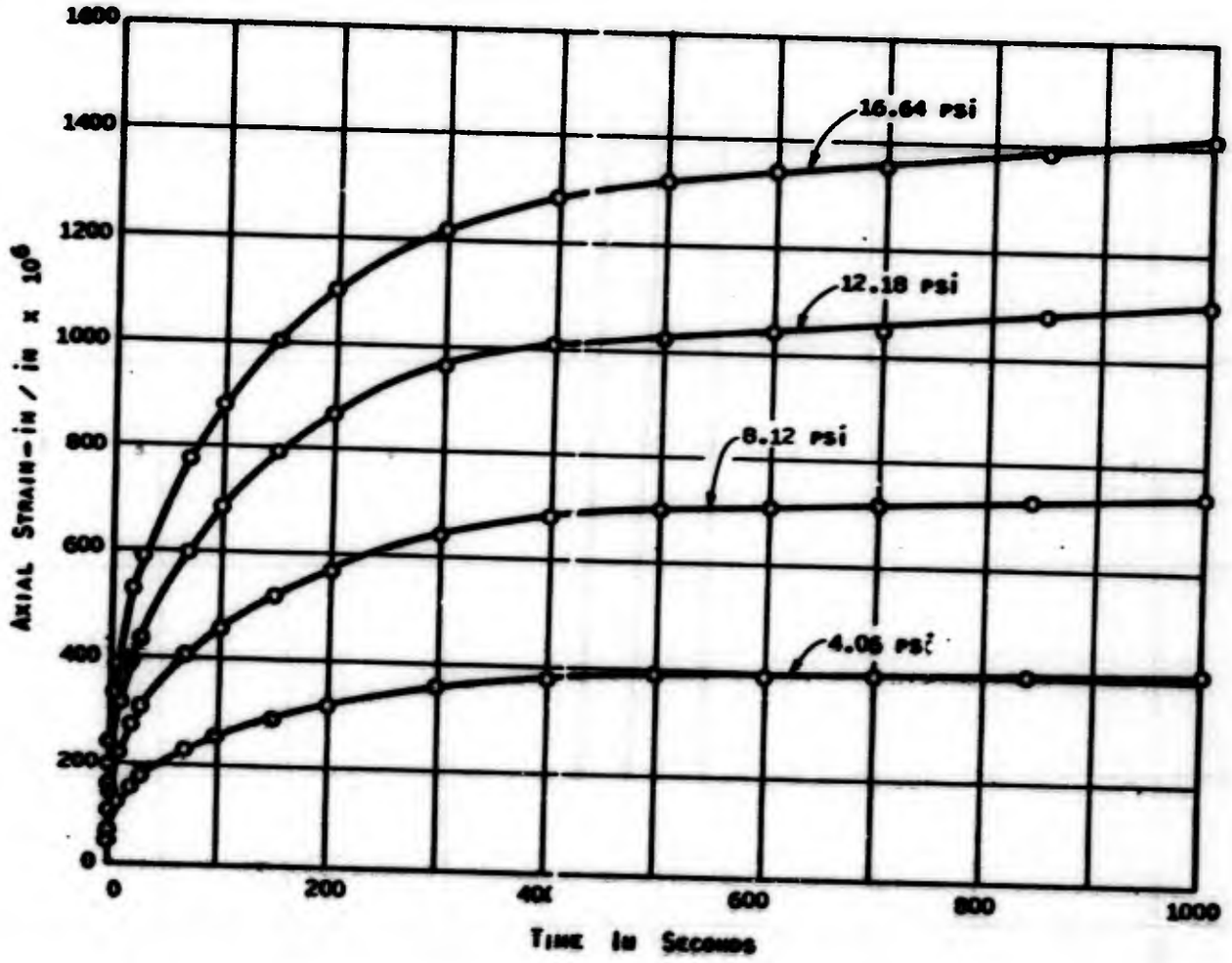

Figure H-8 Data from Uniaxial Creep Tests

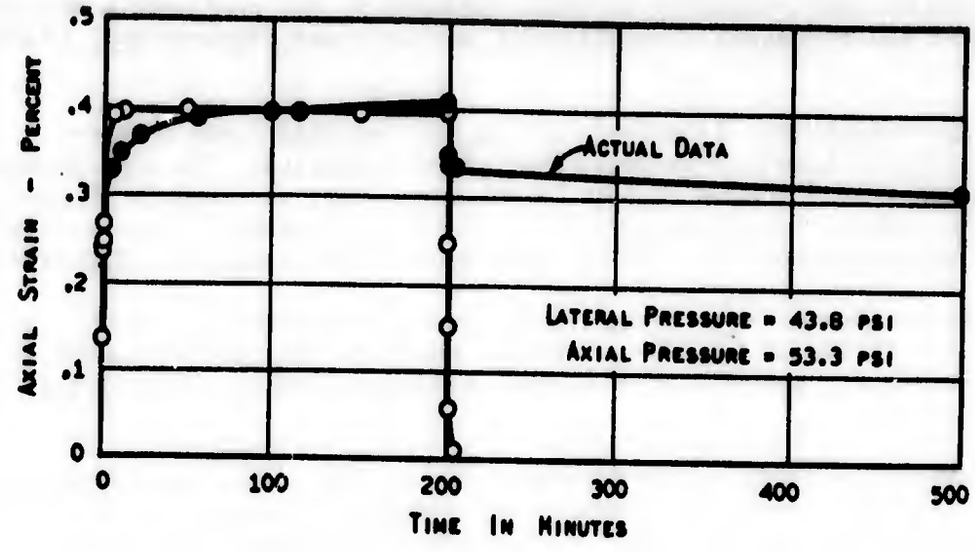

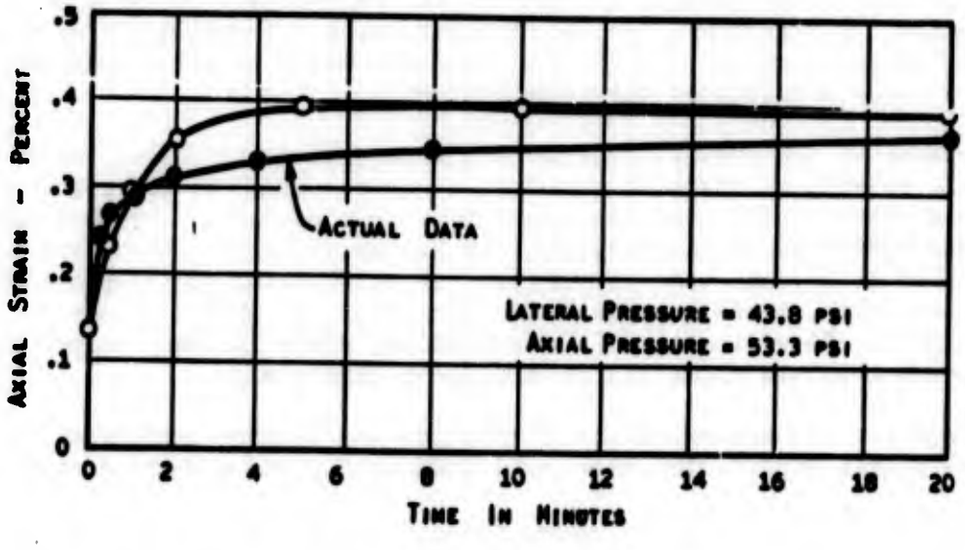

Figure H-9 Uniaxial Tests on Asphalt Concrete

Permanent Deformation - The permanent deformation that occurs has both time dependent and independent components. Under repeated loading conditions after an initial conditioning period, the amount of permanent deformation that occurs under each application of a load of short duration is small compared to the recoverable deformation and decreases with number of applications, Figures H-9, 10 and 11.

Time Independent Behavior - For rapidly applied loads of short duration, time independent behavior predominates. The time dependent component of the deflection is not completely recoverable (Figure H-9) The number of applications of the load has a minor influence on the time independent (resilient) component of the response, (Figure H-12)

Temperature Effects - Temperature has a considerable influence on the response of asphalt concrete. Based on the data available, a preliminary assumption of thermo rheological simplicity appears justified

Stress History and Rate Effects - The nature of the time dependence of asphalt concrete indicates that stress history and rate of load application have an effect on response of asphalt concrete. These effects are not necessarily linear. No significant investigations of stress history have been reported.

To incorporate all these effects into a single mathematical model is not possible at the present time. The combination of non-linear and time dependent behavior suggests the possibility of non-linear visco-elasticity. However, such a model cannot account for non-recoverable instantaneous deformation. Furthermore, the use of a non-linear visco-elastic constitutive law does not appear to afford a practical means of solving appropriate boundary value problems at the present time.

Because of the inability to develop a general constitutive law to model all aspects of observed behavior, it is necessary to subdivide the problem of determining the mechanical state in a pavement. By considering these subdivisions individually, the number of effects that have to be modelled at any one time is reduced. In considering the response of asphalt concrete, there appears to be three distinct phases of the problem of the determination of the mechanical state (primary response) in a pavement system which can be considered separately:

Phase I. The determination of stresses and strains introduced by the single application of a wheel load acting for a short duration.

For this phase, it would appear that non-linear and rate effects are important for loads for short duration and that as a first approximation the residual deformation in any one application can be neglected. Hence linear and non-linear elasticity and linear viscoelasticity have

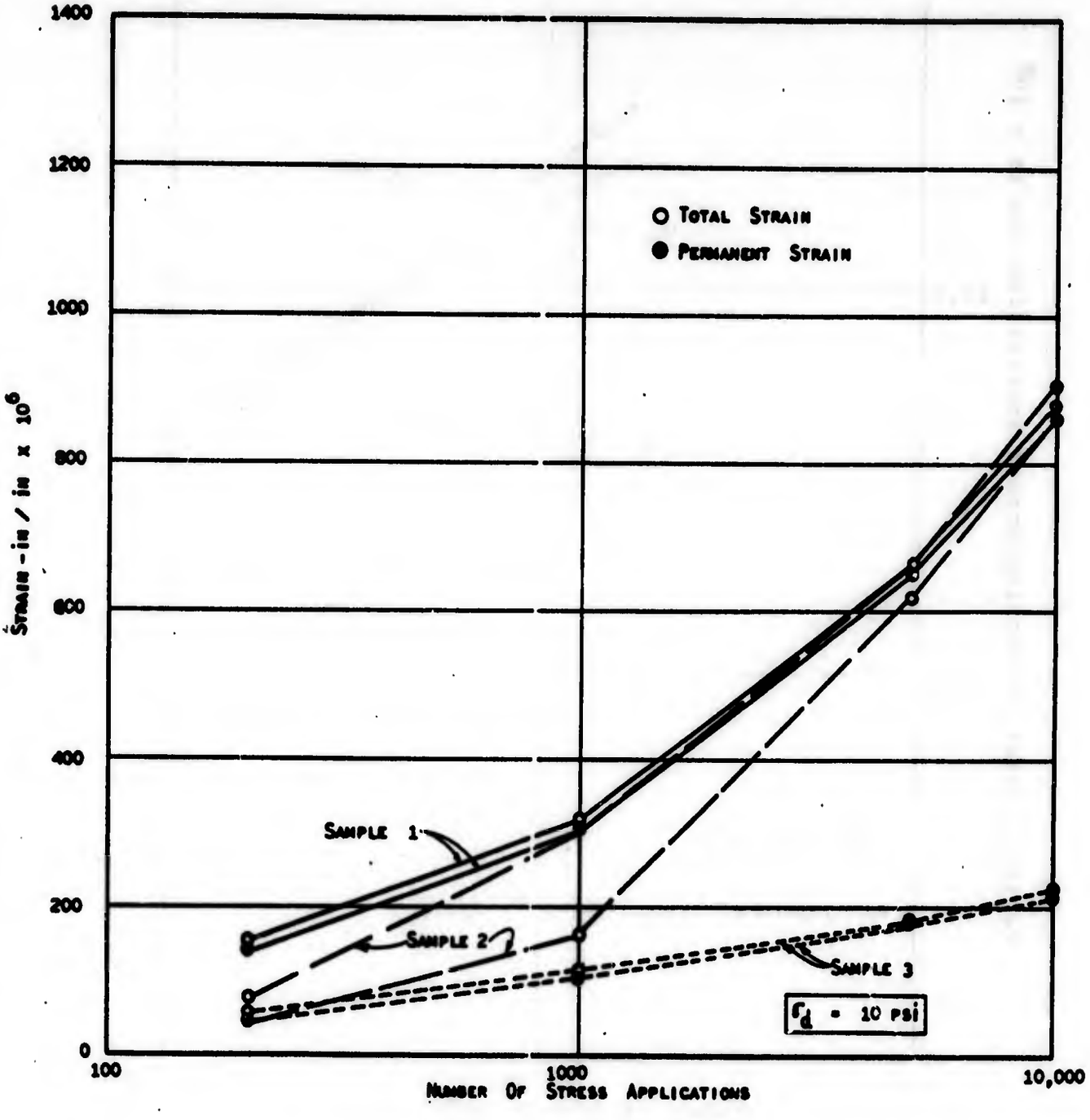

Figure H-10 Total Residual and Resilient Axial Strain as a Function of Number of Stress Applications in a Repeated Load Test

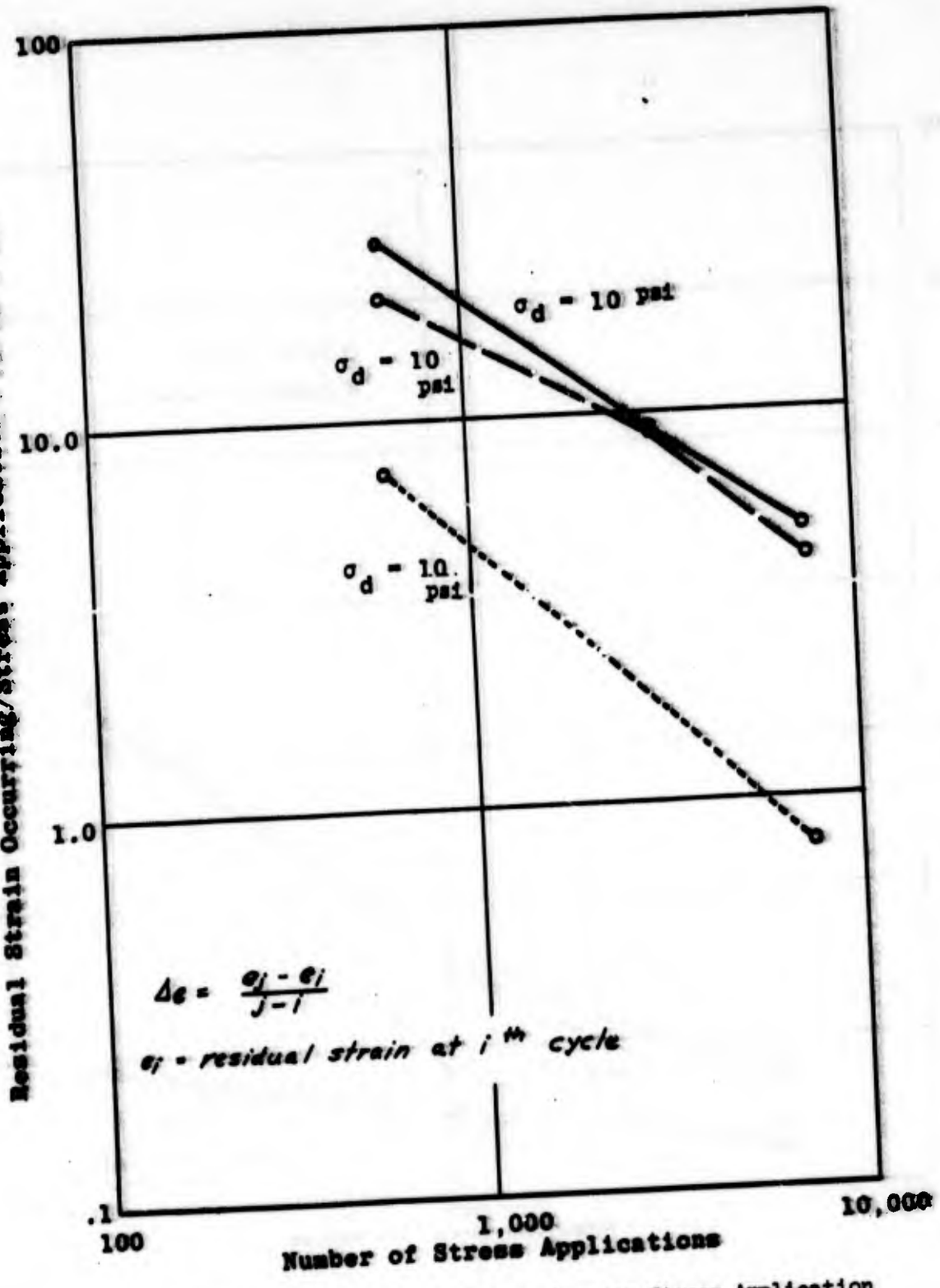

Figure H-11 Residual Strain Occurring per Stress Application as a Function of Number of Stress Applications

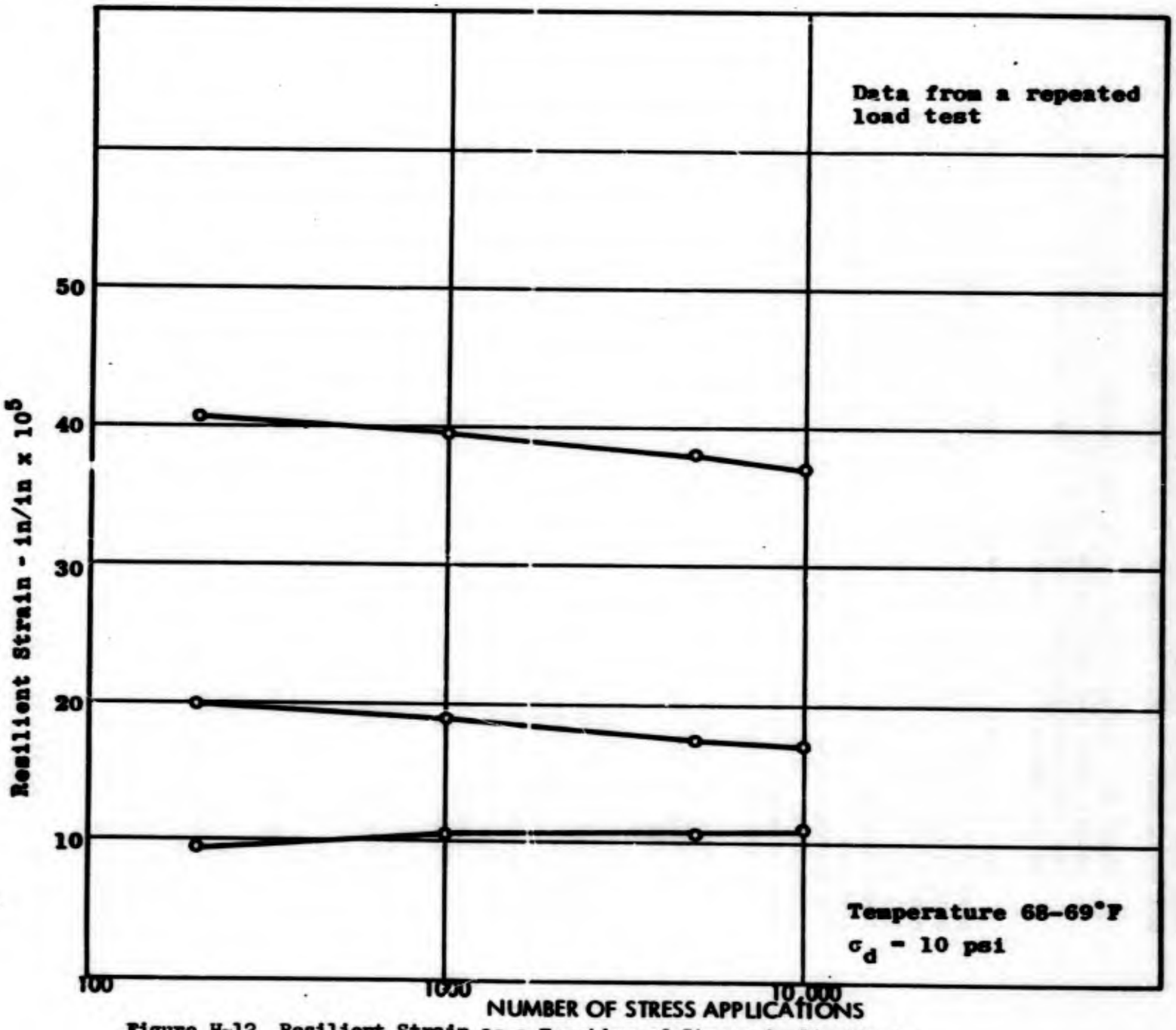

Figure H-12 Resilient Strain as a Function of Stress Applications

been used to model asphalt concrete behavior, e.g., Materials Research and Development (1968), Monismith, et al (1966) and Pagen (1965).

Phase II. The determination of the permanent deformation that occurs under each application of a load of short duration so that the cumulative permanent deformation that might occur over the life of the pavement can be computed.

For this aspect of the problem there appear to be three practical possibilities for modelling material response: (i) Linear elasticity with creep, (ii) Non-linear elasticity with creep, (iii) Linear visco-elasticity using a constitutive law which permits permanent deformation. (i) and (ii) are often used in the analysis of metals at elevated temperatures. Based on the available experimental data, it would be possible to formulate an appropriate creep law to use in the analysis. The approach used in such an analysis would be similar to that used in incremental plasticity, the creep strain being calculated over small time intervals. Linear visco-elasticity has the soundest theoretical basis and has been widely used in pavement analysis.

Phase III. The determination of the time dependent deformation under a load which is maintained for a long time, i.e., a standing load.

For this aspect of the problem it appears that the three models suggested for Phase II, would also be appropriate for this phase of the problem. A preliminary selection of the linear visco-elastic models which can account for permanent deformation would appear to be a satisfactory first approximation. However, because of the large variation of stress levels in the asphalt concrete, non-linear effects are likely to be important. Linear elasticity with a non-linear creep law might be considered as an alternative to linear visco-elasticity.

Cohesive Soils: The experimental data on cohesive soils is fairly extensive. For purposes of this discussion only compacted cohesive soils are considered. It is in the compacted state that cohesive soils most often enter into the structural design of a pavement system. Furthermore, the data reviewed will primarily consist of results obtained from experimental procedures that simulate service conditions.

In recent years, the majority of testing of subgrade soils for pavement studies has been under repeated loads. Some creep testing has also been reported. Until recently the emphasis in testing soils for pavement studies was to determine the shear strength of the material. At the present time, because of the well designed pavements, shear strength failure in the soil has almost been eliminated.

The observed behavior in compacted cohesive soils is reviewed briefly under various aspects of material response which are of significance in selecting a suitable constitutive equation.

Linear and Non-linear behavior of the material to repreated loads (Figure H-13) - This non-linear behavior is most apparent at the stress levels likely to exist in a subgrade. Difference in behavior in tension and compression is another expression of non-linear behavior. It has been found that under uniaxial conditions and in a limited stress range, linear behavior may be a satisfactory first approximation. For a particular problem the validity of this approximation will have to be established.

Time Dependent Behavior - Relaxation and creep tests (loads of long duration) indicate that the response of the material has a significant time dependent component, e.g., (Figure H-14). The nature of the time dependent component, e.g., viscous or non-viscous has not been clearly established. As pointed out under (1), there is evidence of non-linear time dependent behavior.

Permanent Deformation - The permanent deformation that occurs has a time dependent and time independent component. (Figures H-14 and H-15). For repeated applications of a load or short duration, it has been found that after an 'initial conditioning' the amount of permanent deformation that occurs under a single application decreases with the number of applications and is very small when compared to the recoverable deformation, Figures H-15 and H-16.

Time Independent Behavior - For rapidly applied loads of short duration, after an 'initial conditioning' the time independent effects predominate. The time independent deformation that occurs on the application of a load is not completely recoverable on removal of the load. As pointed out under (1), the time independent behavior is significantly influenced by the stress level.

Moisture Effects - The moisture content has a considerable influence on the response of the material to load. At higher moisture contents there is greater deformation and the non-linear effects are more significant, Figure H-14. Moisture effects may be incorporated into the behavior by testing at different moisture contents.

Stress History and Rate of Loading Effects - As pointed out in (2), the response of the material is time dependent. Both stress history and rate of loading have an effect on the response. There is very significant information on these subjects.

Temperature Effects - For the range of temperatures considered, temperature effects are not considered significant in the response of cohesive subgrade soils.

It is not possible at the present time to incorporate all of these effects into a general mathematical model. Because of this inability it is necessary, as was the case for asphalt concrete, that the problem of

(After Seed et al, 1967)

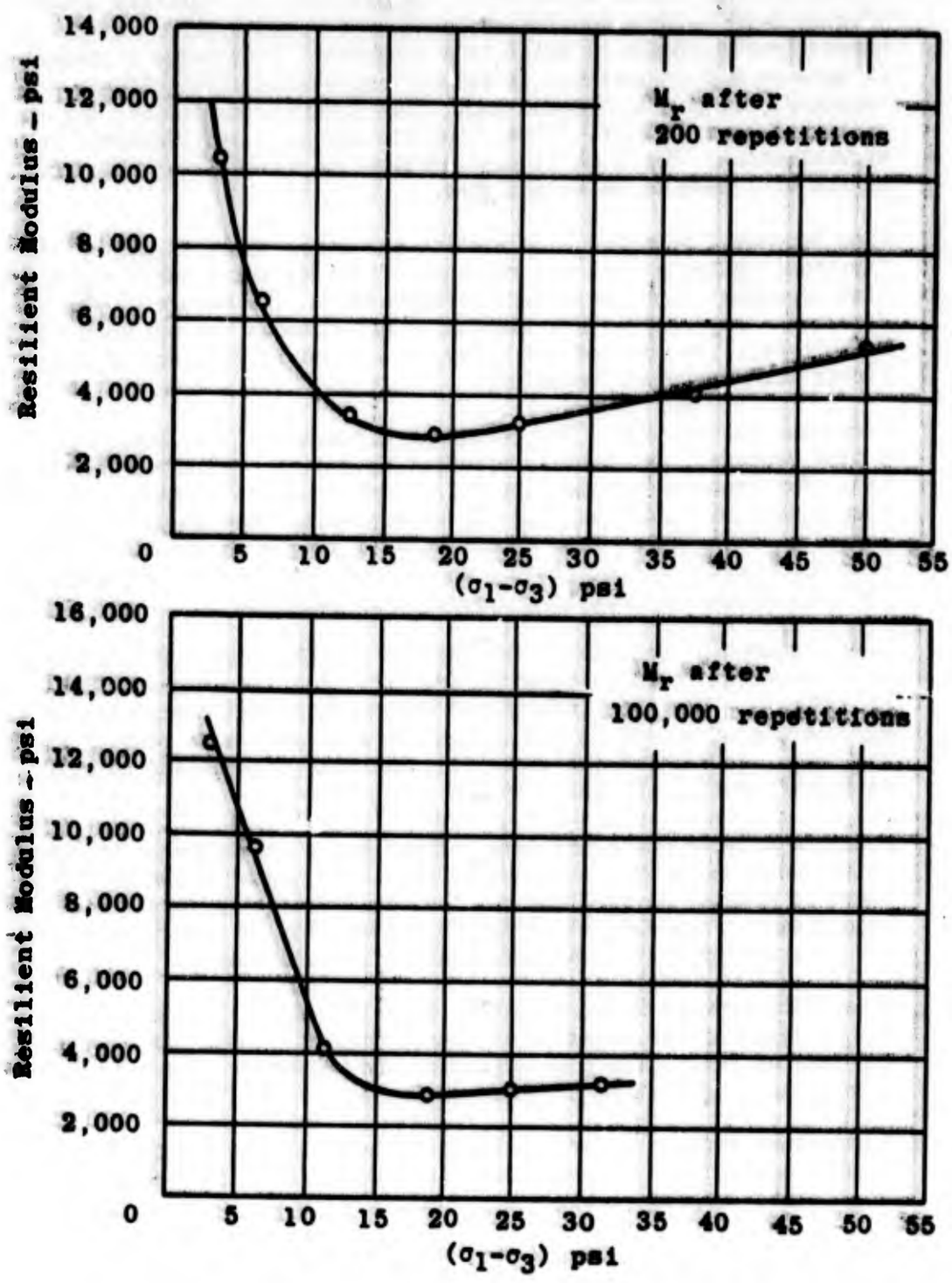

Figure H-13 Modulus of Resilience as a Function of $(\sigma_1 - \sigma_3)$

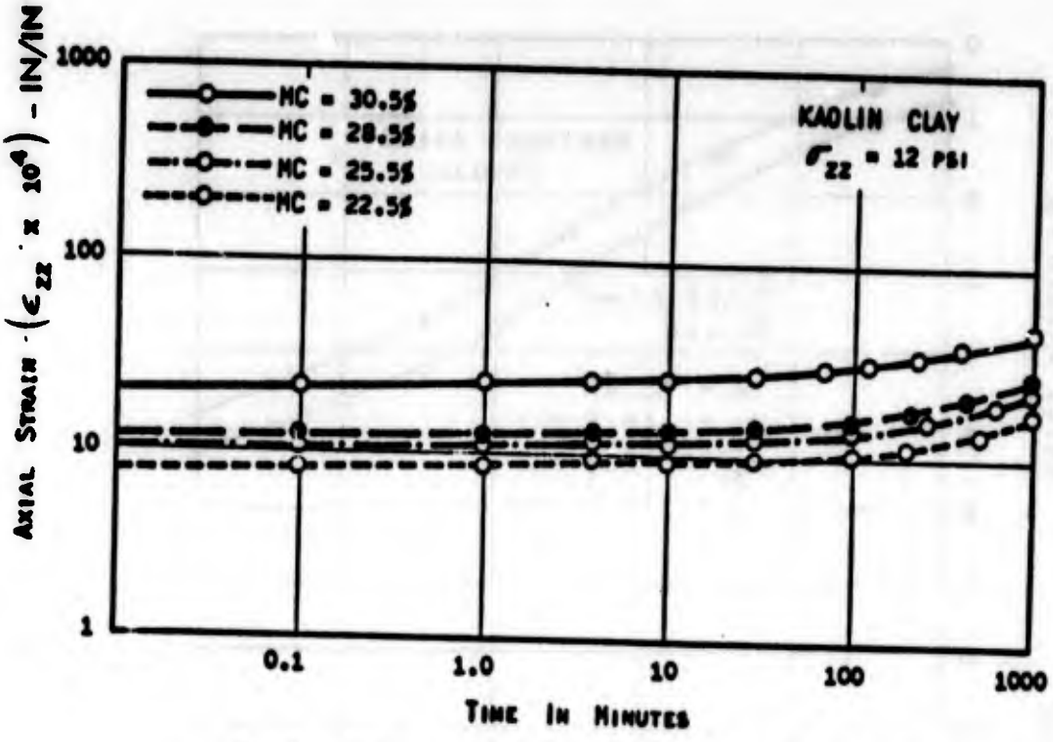

(a) AXIAL STRAIN VS TIME IN A CREEP TEST

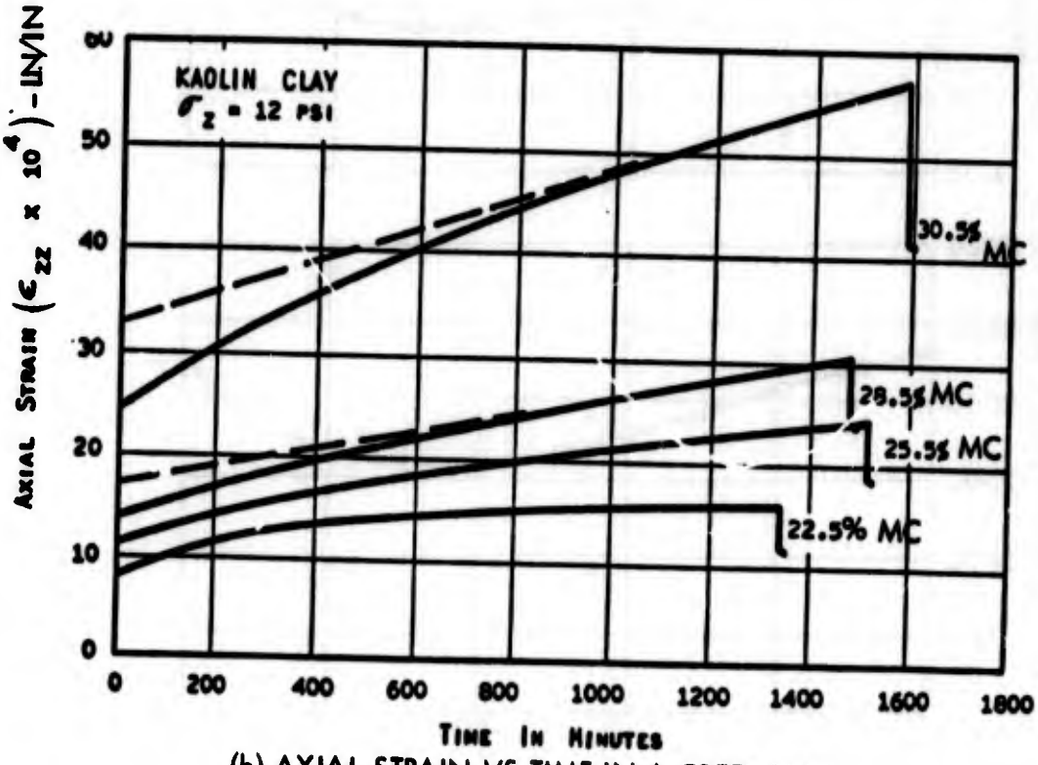

(b) AXIAL STRAIN VS TIME IN A CREEP TEST

Figure H-14 Uniaxial Creep Test on Clay

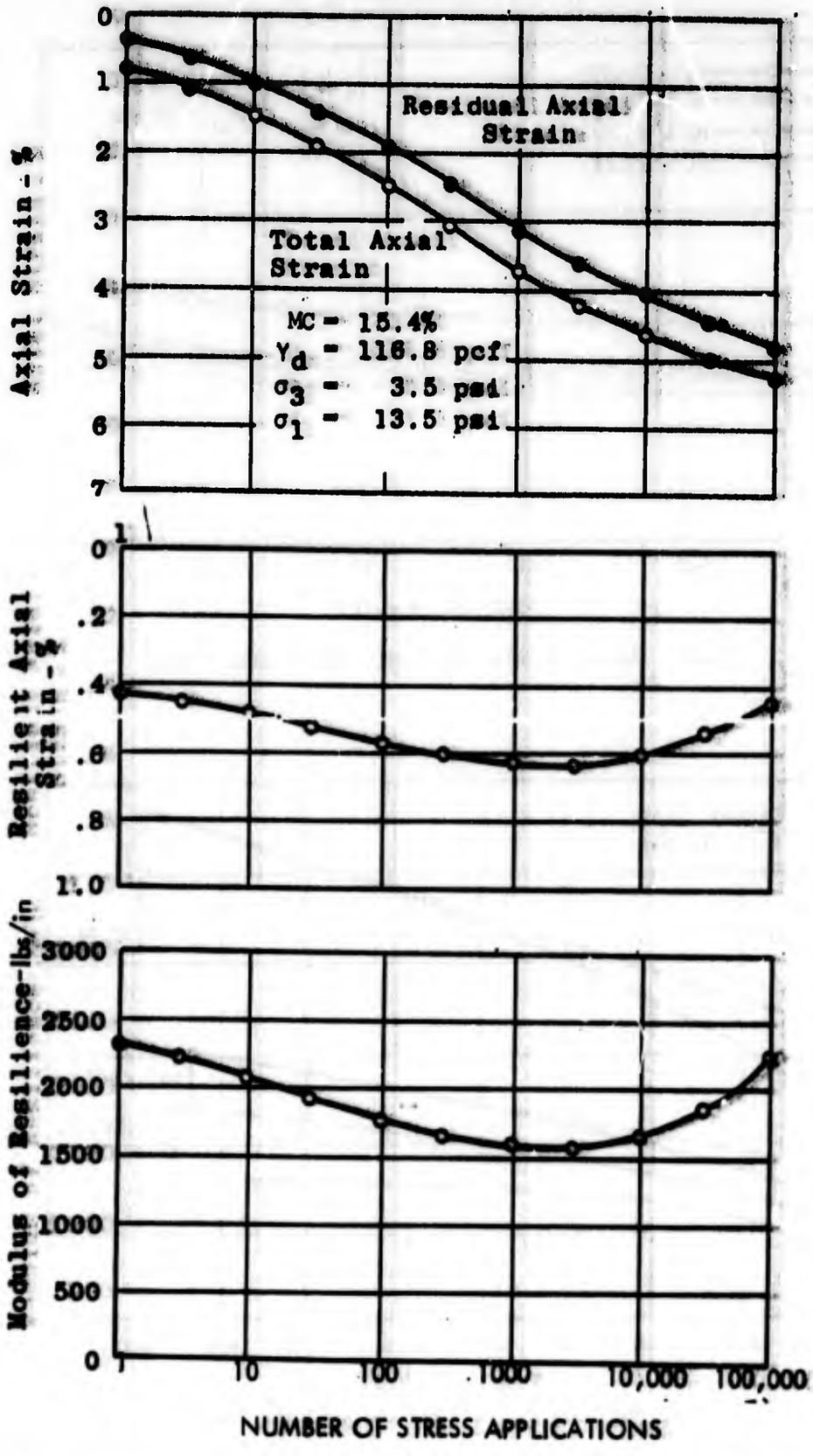

Figure H-15 Typical Results of Repeated Loading Triaxial Compression Test, Aasho Subgrade Soil, Frequency of Stress Applications = 20/Min.

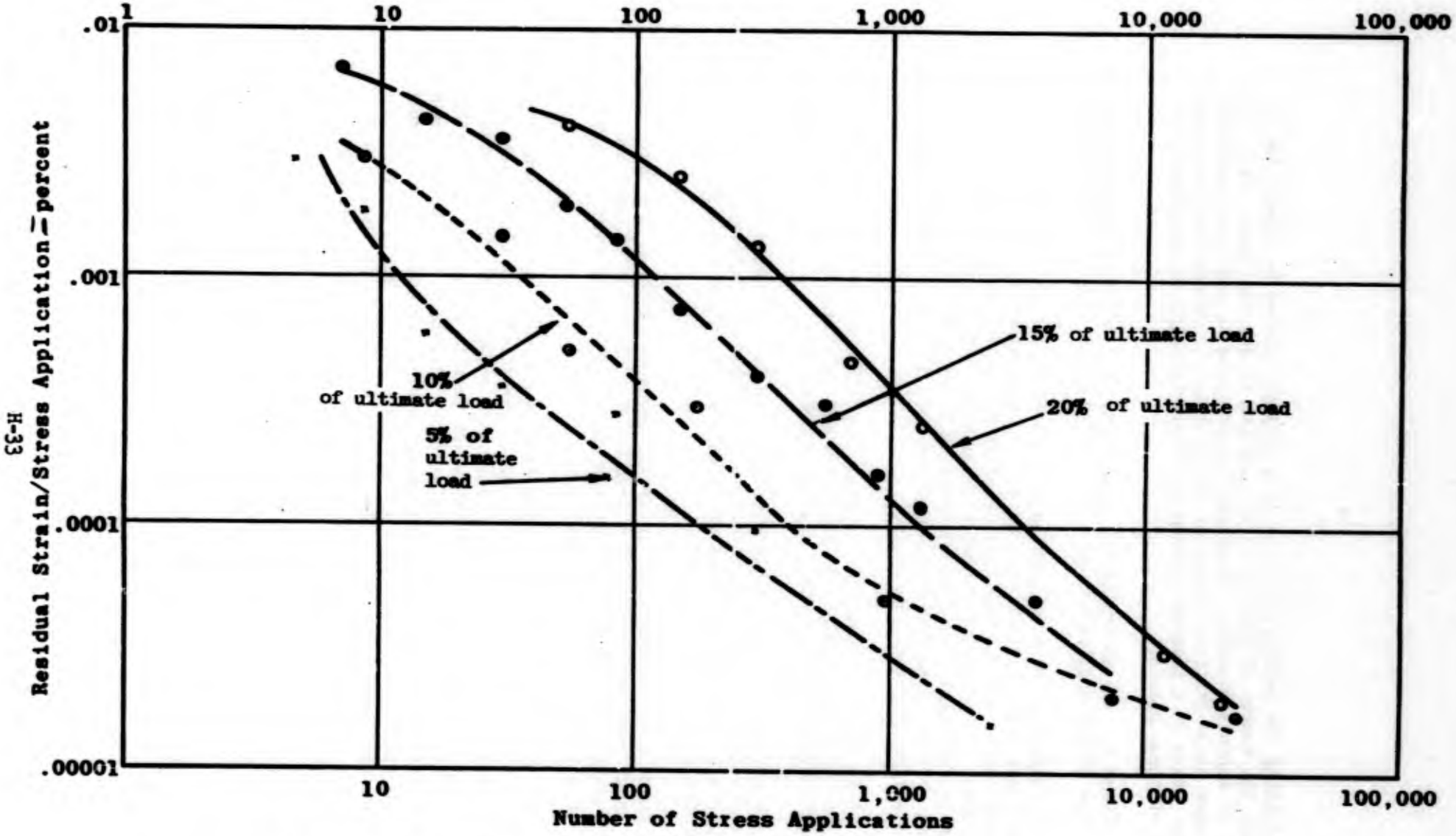

Figure H-16 Residual Strain as a Function of Number of Stress Applications

determining the mechanical state in a pavement system be subdivided to reduce the number of effects to be modelled at any one time. As in the case of asphalt concrete, it appears appropriate to consider separately the same three distinct phases of the problem for determining the mechanical state in a pavement system and characterizing the material for each of these phases.

Phase I - The determination of stresses and strains introduced by the single application of a wheel load acting for a short duration.

Considering the available data, it would appear that non-linear effects are important and that as a first approximation the residual deformation in any one application after an initial conditioning can be neglected. To account for frequency effects it is suggested that suitable frequencies of load application be selected and tests be conducted at these frequencies recognizing that different material functions be determined for each frequency.

It is possible that under certain conditions, the stress distribution in the subgrade might be predominately uniaxial. In such a case a linear elastic representation may be satisfactory.

To account for the moisture effects, it will be necessary to test the subgrade soil at different moisture contents and determine the appropriate material functions which will be valid for the equilibrium or other design moisture contents.

Phase II - The determination of the permanent deformation that occurs under each application of a load of short duration so that the cumulative permanent deformation which might occur over the life of the pavement can be computed.

For this aspect of the problem there appears to be three practical possibilities for modelling the material response: (i) Linear elasticity with creep, (ii) Non-linear elasticity with creep, (iii) Linear viscoelasticity using a constitutive law which permits permanent deformation. (i) and (ii) are often used in the analysis of metals at elevated temperatures. Based on the experimental data, it would be possible to formulate an appropriate creep law to use in the analysis. It would be possible to use a non-linear creep law. It should be pointed out that none of the models mentioned above account for any instantaneous permanent deformation.

Phase III- The determination of the time dependent deformation under load which is maintained for a long time, i.e., a standing load. As for Phase I the effects of the moisture would have to be considered.

It appears that the three models suggested for Phase II would also be appropriate for this phase of the problem. Because of the large

variation of stress levels in the asphalt concrete, non-linear effects are likely to be important; however, there is little quantitative information about these effects. Linear elasticity with a non-linear creep law might be considered as an alternative to linear visco-elasticity.

Granular Materials: Granular materials have been subjected to fairly intensive experimental study. The majority of the recent work with application to pavement design has been concerned with the response of granular materials to repeated load tests. The major differences between granular and cohesive soils is that the former exhibits no significant time dependent effects. The most significant aspect of the behavior of granular material is its non-linear response to load, time dependent and permanent deformation aspects after an initial conditioning do not appear to be significant.

The modulus of resilience as determined in a triaxial test has been found to be dependent on the confining pressure. Biarez (1962), Trollope et al (1962) and Morgan (1966) have all reported a significant increase in the modulus of resilience for sand as a consequence of increasing the confining pressure. Typical results presented by Seed et al (1967) are shown in Figure H-17 and indicate the effect of confining pressure on the response of sand in a repeated load triaxial test. The expression for M_r (Modulus of Resilience) given on Figure H-17 was found to apply to gravel with a change in the exponent. Similar data has been obtained by Kallas and Riley (1967) and Shifley (1967). Brown and Pell (1967) observed similar effects from plate load tests on a pavement test section. Fundamental work by Ko and Scott (1967) have indicated that the effect of the first stress invarient on the stress-strain behavior of granular material is very significant. Another significant non-linear aspect of the response of granular material is its inability to carry any tensile load.

In accounting for these factors in the analysis of pavement system, it would appear that a non-linear elastic constitutive law which would admit the possibility of different behavior in tension and compression would be the most representative of the response of granular material. Presently various iterative techniques are used in which the modulus is adjusted on the basis of the computed stresses, Duncan et al (1968).

Lime and Cement Treated Materials: In considering treated materials it is important to recognize the variability in the end product because of variations in the method of treatment, the soil type, the density moisture content and the time of curing factors. The majority of experimental information relevant to the pavement problem in treated materials is obtained from repeated load tests in triaxial compression and flexure, Mitchell (1966), Mitchell and Shen (1967), and Mitchell et al (1965).

(Seed et al., 1967)

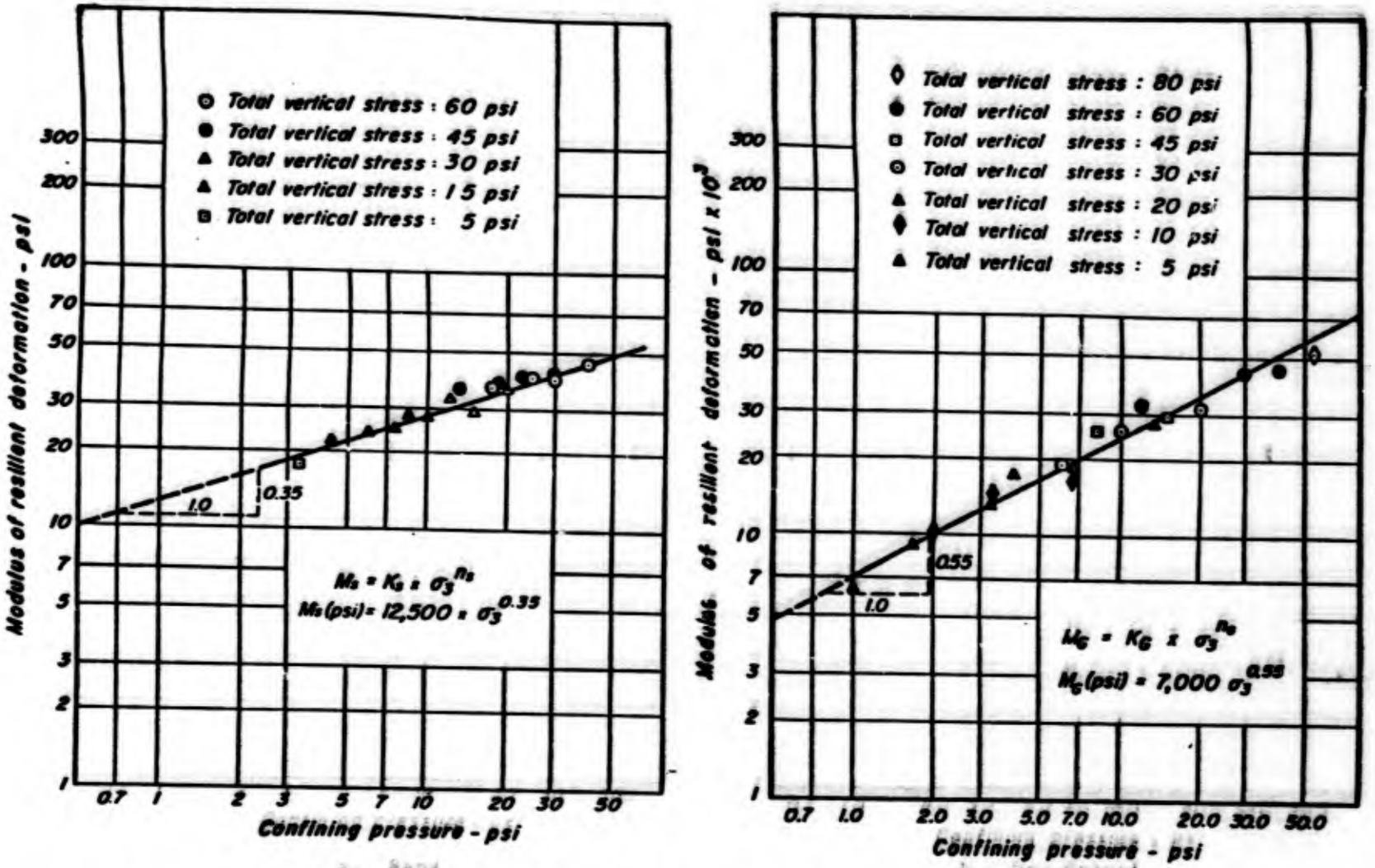

a. Sand

b. Dry Gravel

Figure H-17 Effect of Confining Pressures on the Resilient Moduli of Sand and Gravel Measured in Repetitive Load Triaxial Tests

Stabilized cohesive materials exhibit many of the same characteristics as cohesive soils. Fossberg (1969) found that the modulus of resilience was influenced by the confining pressure and the axial stress. From tests on treated silty clay Mitchell found that modulus of resilience was effected by the stress difference ($\sigma_1 - \sigma_3$)*. Wang (1965) has reported on a cement treated silty clay and has found that the modulus of resilience increased with an increase in confining pressure and decreased with an increase in ($\sigma_1 - \sigma_3$) while non linear behavior is evident in repeated triaxial tests, flexural tests do not show any influence of stress level.

At the present time most methods of analysis consider the treated soil as a linear elastic material. Additional studies are needed in characterizing cement treated bases.

(c) SOLUTION OF BOUNDARY VALUE PROBLEMS (Determination of Primary Response)

Having defined the input variables, the geometry of the system and the material characteristics the next step in the determination of the primary response is the formulation and solution of pertinent boundary value problems. Based on the discussion of the geometry of the system there are two general categories of boundary value problems, (i) the thin elastic plate on the Winkler foundation** and (ii) the layered half space. In both these cases the external load is a static load.

Until recently the methods that were used in solving these boundary value problems attempted to obtain closed form analytical solution. Recently the development of numerical techniques has permitted the analysis of more complicated and realistic problems using the elastic plate on the Winkler foundation. Hudson and Matlock (1967), Zienkiewicz and Cheung (1967). It is now possible to analyze discontinuities and cracks in the slab and variation in support over the area of the slab including local loss of support.

The fundamental solution applied to the layered half-space used in pavement design was due to Burmister who analyzed the problem of the circular load on a two and later three layered half-space. Computations for more than three layers becomes extremely tedious without the use of a digital computer. The Burmister method of solution has been programmed for a digital computer and existing programs can treat a 15 layer system.

*σ_1 is axial stress, σ_3 is the radial or confining stress. ($\sigma_1 - \sigma_3$) is often referred to as the deviator stress.

**The characterization of the supporting subgrade as a Winkler model were not discussed earlier. A complete discussion may be found in Terzaghi (1955).

More recently the finite element method has been applied to the analysis of pavement systems, Duncan et al (1967). The finite element technique permits the inclusion of orthotropic and non-homogeneous material properties and can through the use of various approximate techniques incorporate non linear, time and temperature effects. Recent developments will permit the analysis of the effect of dynamic loads to a layered half space. This is a significant advance over available techniques of solution. However, the general three dimensional problem remains to be solved.

It can be concluded that the majority of future significant progress in the solution of appropriate boundary value problems will come from the further development of numerical techniques.

(d) LIMITING RESPONSE

The limiting response in the overall pavement design shown in Figure G-1 is divided into three basic distress modes. There are various distress mechanisms which can result in these distress modes. These distress mechanisms and the corresponding distress modes are shown in Figure H-18.

It can be seen that the disintegration mode is influenced primarily by factors which are not dependent on the mechanical state. The fracture (or rupture) mode and the distortion mode are dependent primarily on the mechanical state induced in the pavement.

In recent years the major emphasis in research in this area has been concerned with the fracture (or rupture) mode of distress. The permanent deformation (rutting) that occurs due to excessive loading has been significantly reduced for most major pavement structures subjected to conventional traffic loads. This was done primarily on the basis of keeping the shear stress in the pavement system below specified limiting values which were based on the Mohr-Coulomb criteria.

For concrete pavements the rupture strength of the concrete is used as limiting criteria and is compared with the stresses that are induced in the pavement.

In many cases empirical correlations between deflection and strains under a specified load and observed performance are used as a criteria for determining if a pavement section will perform satisfactorily. In such procedures limiting deflection (or strain) criteria are used to determine if the computer deflection or strain are within acceptable limits. While such an approach is admittedly empirical, it is still essential to the design of pavements. At the present time there is insufficient theoretical work to enable a designer to predict the initiation and propogation of failure for all modes of distress.

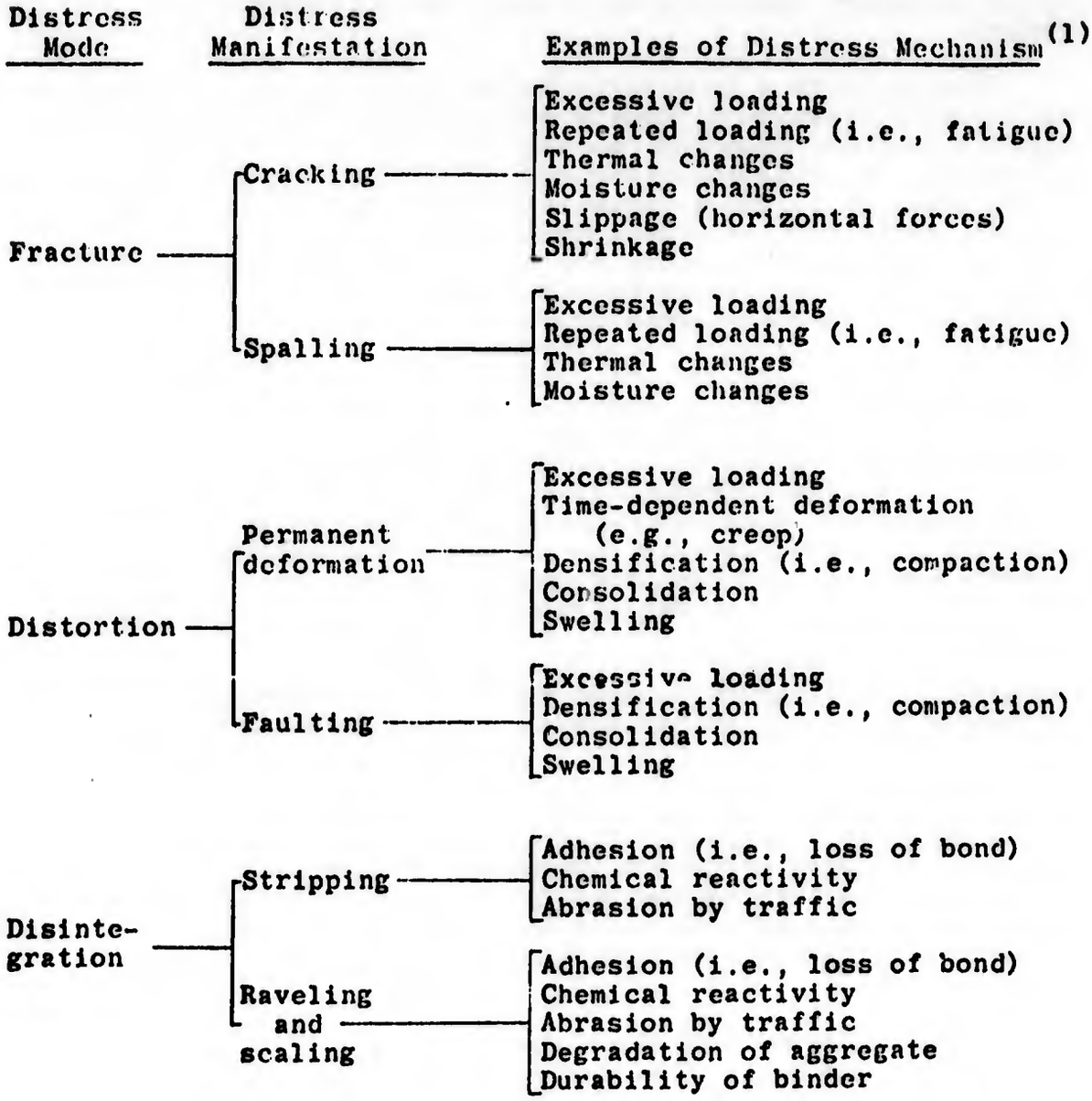

(1) Not intended to be a complete listing of all possible distress mechanisms.

Figure H-18 Categories of Pavement Distress

The most significant work that has been done recently in determining limiting criteria for the design of pavements has been with respect to cumulative damage concepts (fatigue) which results in cracking and rupture.

There appear to be three test procedures that have been used recently for the study of fatigue problems in pavement design. These are: (a) Repeated Flexure of beams using controlled stresses or strain loading developed at the University of California by Monismith and his associates (1966, 1966, 1967), (b) A uniform sinusoidal bending moment (stress control) applied to a necked down specimen and oscillating torsional strains (strain control) applied over the length of a similar specimen; these tests have been reported by Pell (1962, 1967, 1969), (c) Repeated loading of a uniformly supported circular clamped slab, Jimenez and Gallaway (1962).

The great majority of the fatigue testing results reported in the literature have been obtained from beam tests. The method utilized by Pell is similar in principle to that developed by Monismith and his associates. The major difference is with the method of load application. The results of beam tests have indicated that under repeated loading and under the conditions of testing, fatigue failure does occur in asphalt concrete specimens. The results are presented in the form of curves which relate stress (or strain) to cycles of load application to failure.

The present method of testing beam specimens cannot directly include the effect of variations in subgrade support. At this time, this is done indirectly by adjusting the stress and strain level under which testing is to be performed.

The slab test as utilized by Jimenez and Gallaway (1962) suffers from a number of disadvantages. The required complete fixity along the edges of the slab is difficult to obtain and the dimensions of the slab are such that the end conditions appear to exert a significant influence on the stresses and deflections over the entire slab. Therefore, uncertainty in the edge conditions complicates the stress analysis of the slab.

The simplicity and ease of analysis of beam testing is an advantage; the representative nature of the test conditions in relation to stresses in a pavement have to be evaluated. The slab test does attempt to introduce a more realistic stress condition but suffers from several other disadvantages.

In spite of extensive data obtained from beam tests, there are some fundamental questions which have not been resolved. Can the accumulated damage that occurs in a pavement be predicted on the basis of fatigue tests on laboratory beam specimens? Work by Kasiunchuk (1968) has indicated that this might be possible. However, it should be recognized

that the occurrence of fatigue in a structural member is dependent on the geometry of the member and the mode of loading. An important concept in the occurrence of distress in an actual pavement is the process of crack propagation after crack initiation. The time lag between failure due to extensive cracking and crack initiation can be quite large. In a beam test, because of the geometry of the specimen, there is very little time for crack propagation. Complete failure and crack initiation occur in rapid succession. Therefore, it is important to establish if it is possible to predict the cumulative damage that will lead to distress under multiaxial states of stress in pavement slabs from results based on simple beam fatigue tests.

The synthesis of the results of a test procedure with stress analyses and a failure hypothesis is an attempt to complete a subsystem for predicting the possible occurrence of distress in a pavement. An attempt to do this for the fatigue mode of distress has been made by Kasiunchuk (1968) for highway pavements. It seems reasonable to extend this work to airfield pavements.

It should be recognized that material failure in itself does not constitute a failure in the pavement system. Failure in the pavement system means that the system is not acceptable to the user. A cracked pavement may be acceptable to the user as long as it provides a satisfactory riding surface. However, from the standpoint of structural design, material failure is the only controlling factor. Admittedly this is a limited framework and may be overly conservative. However, until a complete analysis, which includes user acceptability criteria, is devised, structural design will continue to be governed exclusively by limiting response criteria.

In discussing the various factors involved in the structural design of pavements, emphasis has been placed on those factors that are significant in developing a design approach which is based on sound theoretical principles.

The ability to consider the input variables has been limited by existing computational techniques to solve pertinent boundary value problems. The development of powerful numerical techniques will probably allow a better representation of the input variables than has been heretofore possible. Improvements should be made in accounting for environmental factors in design. The major emphasis in past research has been toward the externally applied loads. Environmental and construction effects have not been studied in detail except with respect to material characteristics.

In material characterization the trend is to develop constitutive equations which are more realistic of the actual response of the materials in their service conditions rather than empirical material properties. Improved testing techniques and the development of more

powerful computational techniques to include more complex constitutive equations than heretofore possible in the solution of boundary value problems has contributed significantly to increased research in materials characterization.

In the fatigue mode of failure considerable progress has been made. At the present time it would be possible to use a fatigue failure as a limiting criteria in airfield pavement analysis and design. Still further work needs to be done on the initiation and propagation of failure. There has been a lack of significant work in other areas of limiting response criteria. Present design methods rely almost exclusively on limiting deflection, strain and stress on the basis of correlations with performance.

Having indicated the direction of some of the recent work in pavement research it is appropriate to provide a critique of the more commonly used pavement design procedures.

3. EXISTING PAVEMENT DESIGN PROCEDURES

All currently used pavement design methods can be classified under the two general categories (1) empirical and (2) analytical. An empirical procedure relies on the correlation of past performance with experimental data, e.g., CBR, soil classification, etc. The major disadvantage is that new experiments have to be performed when conditions, not included in the original set of experiments, have to be accounted for. This disadvantage is of great significance in the design of airfield pavements where the loading conditions have changed radically in the last decade.

The analytical methods attempt to set up a physical and mathematical model to predict pavement response to a prescribed input. The major advantage of such a method is that it is predictive. However, it must be recognized that any physical and mathematical model is an idealization of the real field problem. These idealizations should be evaluated with regard to their ability to represent the field problem. Analytical methods can treat 'rigid' and 'flexible' pavements in the same general framework. It is felt that pavement design procedures should be developed on the basis of sound theoretical principles and that there be a minimal use of empirical procedure in the design of airfield pavements.

The discussion presented in previous sections of this report do not differentiate between 'rigid' and 'flexible' pavements and it is felt that the development of a rational method of pavement design should not make such a distinction. The term rigid and flexible only imply different material properties and it should be possible to account for this in a design method based on sound theoretical principles. However, design methods currently in use for airport pavements differentiate between rigid and flexible pavements and in reviewing these methods it is necessary to maintain this distinction.

(a) FLEXIBLE PAVEMENTS

An outline of the essential steps in four representative procedures for design is presented below. These only illustrate the basic concepts in these design procedures; detailed descriptions of the various methods are not included. References to publications where such descriptions may be found are provided. The methods discussed are (i) The U. S. Navy Method, (ii) Corps of Engineers (CBR) method, (iii) The McLeod Method (Canadian Airports) and, (iv) The FAA method. All these methods are empirical in the context of the discussion above. Therefore, the major disadvantage of these methods is that they are non predictive and hence cannot be used without extrapolation to new conditions.

U. S. Navy Method - This method uses the plate bearing test as means for evaluating the properties of the subgrade and base course, Palmer and Thompson (1947), U. S. Navy (1953). The pavement section is designed on the basis of a limiting deflection. The essential steps in the method are listed below.

1. Determine the modulus of elasticity of the subgrade. This is done by a plate load test (30" dia. plate) where the deflection is measured under a known applied stress. The modulus of elasticity can be determined using the formula*.

$$\Delta = 1.18 \frac{p\,a}{E_2}$$

where: Δ = deflection
p = applied pressure
a = radius of plate
E_2 = modulus of elasticity of the subgrade

2. Determine the modulus of elasticity of the base course by conducting a plate load test on a 6" layer (or some other known thickness) of base resting on the subgrade. By measuring the deflection of the surface, the modulus of the base can be determined as follows: First determine F_2 from the following formula:

$$\Delta = \frac{1.18\,pa}{E_2} F_2$$

where: F_2 = a factor which includes the influence of the base course

The factor F_2 is based on Burmister's analysis of a circular load on a two layer system. From the results of this analysis if F_2 and $\frac{h}{a}$ are known, the ratio between E_2 and E_1 can be determined. Having

*This formula is from the analysis of a rigid plate resting on a linear homogeneous isotropic elastic solid.

determined E_2 in step 1, the modulus of elasticity of the base course can be calculated.

3. Substitute in formula 2 the tire pressure based on the design wheel load and the assumed radius of the circular area which this pressure is supposed to act. Using a limiting deflection of 0.2 inches, F_2 is determined. Using Burmister's analysis with known values of F_2 and the ratio of E_1/E_2, the ratio $\frac{h}{a}$ is determined. Knowing the radius of the loaded area, a, the thickness of the required pavement is computed.

4. Modifications to calculated thickness. The Navy procedures recommend that the computed thickness be modified to account for various factors that have not been included in the calculation. These include corrections for saturated conditions, multiple wheel loads and the influence of surface course materials. It has also been recommended that trial sections be built to refine the design thickness.

Corps of Engineers (CBR) Method - This method used the California Bearing Ratio (CBR) as a measure of material properties. The CBR is determined from what may be considered basically a penetration test. The CBR compares the penetration resistance of the material under test to that of a standard value for crushed stone. Based on comprehensive test programs the Corps of Engineers has developed design curves for various wheel loads, tire pressure and wheel configurations, Corps of Engineers, (1969). These curves relate the thickness required above a layer to the CBR of that layer. In addition to determining the thickness of the layers, the Corps of Engineers design procedure also includes certain methods for protection against frost action.

The design steps in the Corps of Engineers method can be summarized as follows:

1. Determine the CBR of the subgrade. This is done by molding laboratory test specimens at a range of moisture and density conditions developed in the field. The specimens are then surcharged and soaked in water to represent the most unfavorable situation, prior to determining the CBR value.

2. Based on the CBR value, the applied load and the location of the pavement section in the airport (e.g. taxiways, runways, etc.) the total thickness of pavement required can be determined from the appropriate empirically determined curve, relating CBR value to required total pavement thickness.

3. To achieve the total thickness required various combinations of base and subbase materials can be utilized. For each such material the CBR is evaluated to establish the thickness of the various

components of the pavement. There is usually a specified minimum thickness for the asphalt concrete surface layer.

If the pavement is to be built in a frost susceptible area then the following two concepts are used in designing an adequate pavement section

(i) Use of a reduced subgrade CBR during the thaw cycle or

(ii) Provide a sufficient thickness of pavement to limit frost penetration.

The Corps of Engineers uses a relation between the freezing index and the depth of frost penetration and then determines a base thickness to provide a limited subgrade frost penetration on the basis of curves determined through experimental and field investigation.

On the basis of the extensive experimental data that has been collected by the Corps of Engineers, they have imposed a method for extrapolating the available curves for higher loading conditions, Ahlvin (1962).

The McLeod Method - This method is based on a study of the performance of Canadian airports, McLeod (1947, 1953, 1956). It utilizes a plate loading test to obtain information for the design of flexible pavements. A repeated plate load test using the following procedure is conducted. A load which gives a deflection of about .05 inches is first applied and maintained until the rate of increase of deflection is below .001 in/min for 3 mins. The load is then removed and kept off until the rate of rebound is below .001 in/min for 3 minutes. The load is applied and released in this manner six times. The load is then increased to give a deflection of approximately .2 inches and applied and released six times and finally the load is increased to give a deflection of about .4 inches and applied and released six times.

Based on such a test procedure, deflection versus the log of the number of repetitions of a load is plotted for each of the loads applied. Straight lines were drawn through the six points for each load and extrapolated to 10, 100, 100, etc., repetitions of load. Based on the traffic and the performance of various airports the following criteria have been proposed. A limiting deflection of .5 inches for ten applications of load for runway design and .35 inches for ten applications for taxiways, apron and turn around areas. An outline of the steps in design are as follows:

1. Conduct a plate test on the subgrade in the manner described above and determine the deflection after 10 repetitions for a given pressure.

2. Compute the area of contact of the tire and the perimeter over area ratio.

3. From the results of the plate load test the pressure to obtain a 0.2 in deflection for 30 in. dia. plate is known. With this information the pressure (unit support) for other areas (tire contact area) and other deflections (limiting deflection) can be determined.

4. From the unit support determine the total support by multiplying the unit support by the tire contact area.

5. Use the formula* $T=K \log \frac{P}{S}$ to determine the total thickness of pavement.

where T = thickness of pavement
K = base - course constant
P = load
S = total support

(This is determined from a chart and depends on plate diameter). For multiple wheel loads an equivalent single wheel load is determined by using elastic solutions to examine the influence of an adjacent wheel on the stress directly under a wheel.

FAA Design Method - This method is based on a soil classification system, Federal Aviation Administration (1967). The design soil classifications are influenced by the drainage and frost conditions. These conditions are dependent to a certain extent on the judgement of the engineer in the field. Once the classification has been made, design charts are used to determine the total pavement thickness and the thicknesses of the various component layers.

To account for non-uniform subgrade conditions along the length of the pavement the FAA utilizes a method for modifying the thickness of the pavement layers. The pavement thickness requirement is greater in the critical areas such as aprons, taxiways and ends of runways than in noncritical areas where the loading conditions are less adverse.

Discussion of Flexible Pavement Design Procedures - In discussing the empirical design procedures outlined above, it is convenient to subdivide the problem into three aspects: the input variables, material properties and, limiting criteria.

Input Variables - The input variables can be divided into three categories. (a) externally applied loads, (b) environmental effects which include moisture and temperature and, (c) construction effects. It is appropriate to consider how each of the variables is accounted for by the various design methods.

*The basis of this formula has been discussed by McLeod (1956).

External Loads - The FAA design method presents separate pavement design curves for single dual and dual tandem gear aircraft. Based on aircraft gross weight and the soil classification, the required based thickness and total pavement thickness are determined for the respective gear configuration. The other design methods, which treat the applied load as static and distributed over a circular area account for multiple wheel loads by determining an "equivalent" single wheel load. Since the applied loads are dynamic, all of these methods are approximate. Furthermore, the repeated nature of the load is not directly considered in any design procedure. The Corps of Engineers and the FAA procedure account for load repetitions by providing a means of converting aircraft operations to coverages. A coverage occurs when each point of the pavement surface has been subjected to one maximum stress by the operating aircraft. The McLeod method accounts for repetitious loading by conducting a plate loading test using a repetitive loading procedure up to six repetitions which is extrapolated to a larger number of loads.

Environmental Effects - All the design methods provide some means to account for frost action. The FAA design methods use frost susceptibility as a factor in classifying subgrade soils. The other methods compute a thickness of pavement sufficient to prevent frost penetration. Temperature effects, which are known to be important, are not directly included in the design of flexible pavements. Seasonal variations in temperature, which have been shown to significantly change the properties of asphalt concrete, are also not included in the design procedures. Moisture effects are not included on a rational basis. The CBR method uses a soaked condition, whereas the plate bearing test procedures (Navy and McLeod) conduct tests on the in-place subgrade. Neither of these procedures consider what the equilibrium moisture condition will be under the constructed pavement.

Construction Effects - Construction effects are not included in the design procedures except that in some cases an attempt is made to test the materials in the state in which they will be placed in the field. The plate bearing test procedures do this by testing the subgrade and other pavement layers in the field. The Corps of Engineers method uses the CBR test to evaluate the materials and relies on the construction specifications for the various materials to meet certain minimum standards. An attempt is made to duplicate the compactive effort in preparing the sample for the CBR test. The FAA procedure requires several soil tests in order to correctly analyze the conditions on the

site. Included are mechanical analysis, liquid and plastic limit tests, maximum density and optimum moisture content determination.

Material Properties - In empirical design procedures a material property or a set of material properties determined in a standard manner are used to determine the required pavement thickness. In general these material properties are not of a fundamental engineering character.

The Corps of Engineers method is based on an empirical correlation using the CBR which is a soil property that is determined from a standard test. The CBR test does not represent the loading or the soil response conditions as they occur in the field. Furthermore, the CBR is of little value in granular materials. The major reason for the wide use of the procedure is the extensive correlative data that has been obtained by the Corps of Engineers.

The FAA method is based on soil classification tests. Soil classification tests can, at best, be considered to be broad indicators of those properties which may be significant in pavement response. They do not measure quantitatively any soil property which can be directly related to soil behavior in its response to traffic type loads.

The plate bearing load tests used by the Navy and McLeod measure the deflection of the soil under a load. The computations used by the Navy to convert this measured information to pavement design thicknesses is questionable. The Burmister analysis that is used is based on a uniformly loaded flexible area whereas the expression used to compute the initial deflection is based on the deflection under a rigid plate. The McLeod method makes an attempt at determining the response under repeated loads but the number of repetitions used are extremely small. The Navy method does not measure the soil response under representative loading conditions.

Design Criteria (Limiting Response) - Both the Navy method and the McLeod method use deflection criteria as the governing factor in pavement design. The McLeod procedure uses a different number of load repetitions and limiting deflection for taxiways and runways. The Navy method does not differentiate between taxiways and runways in its deflection criteria. The Corps of Engineer procedures do not have any direct design criteria. The Corps of Engineers does differentiate between highly and heavily trafficked areas on the basis of correlations, i.e., they have different curves for these areas. The FAA procedures are based on working stress allowables. None of the design methods differentiate between various modes of failure that might occur in a pavement. The accumulation of damage

through repeated loads is not accounted for in any direct manner. No limiting material failure criteria are utilized. All the design criteria are based solely on correlative information and therefore their value for new and different loading conditions is very questionable.

(b) RIGID PAVEMENTS

The design of rigid pavements is almost exclusively based on the analysis of elastic slabs resting on the Winkler foundation with certain modifications and appropriate factors of safety. A notable exception is the FAA method which utilizes a soil classification system. However, for unusual conditions or where economics dictate a detailed analysis the FAA does recommend using a design based on the analysis of elastic slabs.

Design Methods Based on an Analysis of Elastic Slabs - The problem is formulated as a thin elastic plate resting on a Winkler foundation, Westergaard (1948), Pickett and Ray (1950). Various modifications have been incorporated into the analyses to account for edge effects, temperature stresses and cracking. The results of various analyses have been reduced to the form of design charts, where the stress in psi is related to the wheel load, the modulus of subgrade reaction, and the required thickness.

The steps in the design process may be summarized as follows:

1. Determine the modulus of subgrade reaction for the subgrade soil.

2. Determine the modulus of rupture for the concrete.

3. Establish a factor of safety against rupture in the concrete.

4. Having determined the items in steps 1 to 3 the required pavement thickness can be determined from the design charts.

The Corps of Engineers procedures include modifications to account for temperature effects, fatigue in the concrete and frost action, Corps of Engineers (1958C, 1958D). The Navy, and the Portland Cement Association have also put out design manuals which describe in detail the various design procedures, U. S. Navy (1962), Portland Cement Association (1966). The FAA (1967) recommends the use of the elastic slab analyses for the design of rigid pavements in those situations where a detailed analysis is deemed necessary. For routine design, the FAA uses a soil classification system combined with an evaluation of the drainage and frost conditions to determine the necessary pavement thickness. Design curves have also been developed for determining the subbase and surface thickness for different soils to withstand various magnitude of single, dual, or dual tandem gear loads. FAA design curves are based on the gross weight of the airplane.

Discussion of Rigid Pavement Design Procedures - As for flexible pavements, it is appropriate to divide the discussion into three areas: input variables, material properties and, limiting criteria.

Input Variables

External Loads - All design methods treat the applied load as static and distributed over a circular area. For multiple wheel loads, an "equivalent" single wheel load is used. The FAA is an exception in that its method is based on aircraft gross weight and not "equivalent" single wheel load. Repeated load effects are not directly included in the design procedure. However, the FAA does provide a means of converting airplane operations to coverages which account for cumulative pavement stress.

Environmental Effects - Frost action is provided for in all the design methods. Temperature effects are included in the design of rigid pavements in the computation of temperature stresses. There is no significant change in properties with temperature. Moisture effects are not included in a satisfactory manner in any of the design procedures.

Construction Effects - These effects are not included directly into the design procedures. The elastic slab analysis or the design methods based on soil classification do not consider the moisture density and other significant compactive characteristics of the subgrade or subbase soil.

Material Properties

There are two major limitations in the design methods based on the Westergaard elastic slab analysis.

(1) The representation of the concrete pavement as a thin plate composed of an elastic material. It is felt that a thin plate analysis overestimates the bending moments in the slab. It is difficult to justify the use of the plate bending theory in the case of concrete pavement when a layered system analysis is necessary to analyze flexible pavements.

(2) The representation of the pavement support (subbase and subgrade) as a Winkler Model. It is well known that the Winkler model does not satisfactorily represent certain soil types. It is also not possible to evaluate the stresses in the supporting soils under this assumption.

For those noncritical areas where soil classification tests are used as the basis for design, engineering properties of the soil are not directly included in the analysis.

Design Criteria (Limiting Response)

When the structural section is based on design curves relating airplane gross weight to thickness which depend on soil classification then no direct design criteria is used. Design criteria is implicit in the presentation of the curves. The FAA design procedure uses a limiting stress criteria based on the rupture strength of the concrete.

4. OUTLINE OF PROPOSED DESIGN PROCEDURE

It is evident from the above discussions that existing pavement design procedures have not taken advantage of the recent research that has been performed into performance and analysis of pavement systems.

The outline of a design procedure proposed below indicates what is desirable and what is possible within the present state of the art. The most pressing research needs in various areas are discussed later. The procedure is limited to the determination of the primary response and comparing it with some limiting criteria.

A complete design procedure should follow the steps indicated in Figure H-1. Though this might be the ultimate goal, at present a simplified approach which does take advantage of recent research and which is still within the general framework is considered to be the most practical procedure. Such a procedure, divided into three steps, is outlined below*:

Step 1. Data Collection.

(1) Estimate the traffic and loads that are to be applied to the pavement. Projections as to increase in load magnitudes and repetitions should be included in this estimate.

(2) Perform a topographic and soil survey of the area. Conduct routine soil identification tests.

(3) Locate sources of materials to be used in construction.

(4) For the available meteorological data determine the environmental conditions likely to exist at the pavement site.

(5) Based on past experience and empirical design procedures prepare a preliminary structural section design. This design

*A similar procedure has been outlined for highway pavement by Kasiunchuk (1968).

is used as a preliminary estimate for analysis later in the procedure.

Step 2. Materials Characterization

(1) The asphalt concrete, portland cement concrete, subgrade soil and other materials should be tested to determine appropriate material properties. Triaxial tests with repeated loads are used to determine elastic properties. Creep and relaxation tests are used to determine viscoelastic and time dependent properties. These tests should be conducted under representative moisture and temperature conditions.

(2) Field verification of laboratory properties. If the problem consists of redesigning an existing pavement, then by measuring the response of the pavement section in the field to a known load, it is possible to determine the properties of the pavement components in place.

(3) Test materials to determine (limiting response) failure criteria. At the present time there is incomplete information on the three distress mechanisms listed in Figure H-17. For asphalt concrete the fatigue mode of failure can be considered. For portland cement concrete a rupture criteria is utilized.

a) The asphalt concrete should be tested in fatigue.

b) The rupture strength of the concrete should be evaluated.

Step 3. Analysis and Evaluation

(1) Formulate an appropriate boundary value problem for analysis. Present methods of analysis treat the problem as a layered system. Formulation of the problem requires the following steps:

a) Definition of Loads. Based on the studies in Step 1, the loads are selected. The definition of the loads is dependent on the analytical methods available to solve a boundary value problem. At present the loads must be treated as static loads. Design temperature variations should also be established.

b) Define Geometry of the Problem and Boundary Conditions. This includes identifying the thickness of the various layers and defining the stress and displacement conditions on the various boundaries. For numerical procedures it

is necessary to provide horizontal and vertical limits for the extent of the pavement. These limits are placed at a distance sufficient to have a negligible effect on the stresses in the vicinity of the load.

c) Selection of Constitutive Equations. Based on the tests conducted in Step 2 appropriate constitutive equations for the various materials will be selected. Existing computational techniques limit the choice of constitutive equations to linear elasticity, certain special cases of non linear elasticity and linear visco-elasticity. It should be recognized that more than one constitutive equation may be necessary to define the various materials. Furthermore, the material properties will vary with seasonal variations in moisture content and temperature. This should be included.

(2) Determine Stresses and Strains in the Pavement. Having formulated the boundary value problem the solution is obtained. Solutions for temperature and traffic load conditions should be obtained. This is generally done through the use of numerical techniques because they can account for general conditions. The finite element method has been found to be the most powerful of these numerical techniques. The solution of the BVP* provides the stresses and strains in the pavement structure. The analysis is performed for different material properties to determine the stress and strains in the pavement at various times.

(3) Compare Stresses and Strains Induced With Limiting Values. For fatigue considerations, cumulative effects will have to be considered based on the traffic volumes. For rupture failure the stresses determined can be compared with the rupture strength. Other failure modes are accounted for in the design of the structural section through the choice of materials and their composition. If the stresses are excessive it is necessary to select an alternate section and reanalyze.

The design procedure outlined above does not have to be changed as new loads or materials are introduced. This general methodology has been used in design of airfield pavements by Materials Research and Development**

**Fatigue concepts have not been applied to airfield pavements but have been used in the design of highway pavements.

* BVP - boundary value problem

5. RESEARCH AREAS FOR PAVEMENT DESIGN

The most important short term advance that could be made in the structural design of pavements would be taking the recent developments in the field and incorporating them into a design method. The method outlined above indicates a general framework for doing this.

While the design approach outlined is more rational than any of the procedures currently in use, there are certain areas where further research is required. Those areas where research would be of immediate benefit to the development of pavement research are discussed below.

Definition of Inputs - At present the externally applied loads are treated as static loads. This is largely due to present limitations in analyzing dynamic loads on layered systems. It is likely that the analytical difficulty will be overcome in the near future; therefore, it would be extremely desirable if accurate descriptions of the loading as functions of space and time could be developed.

Specific information on environmental conditions is difficult to obtain. This is especially true of moisture conditions. Definitive work needs to be conducted which will prove a means for establishing the equilibrium moisture conditions. Temperature variations within the pavement should be defined.

Consideration should be given to setting up a data-bank where load and environmental data is stored and can be readily retrieved for design purposes.

Selecting Constitutive Equations for Pavement Materials - The majority of the previous work in the analysis of pavement structures has been on the basis of linear elasticity. It is well known that asphalt concrete, granular materials and subgrade soils do not satisfy many of the criteria necessary for the application of linear elasticity. Research work is underway to determine realistic constitutive equations to represent paving materials that includes the development of new testing techniques. A great deal of additional work needs to be done in this area.

Development of Failure Criteria - The development of failure criteria and it incorporation into the structural design of pavements is perhaps the most urgent research problem in the area of pavement design. The various mechanisms of failure are not fully understood. Considerable progress has been made in applying fatigue concepts to failure in asphalt pavements. There has been very little work in crack formation and crack propagation as applied to pavements.

Methods of Analysis - The analytical techniques used to solve pertinent boundary value problems for pavement design are generally developed by workers in the field of solid and structural mechanics. There is a need to modify and apply these techniques to specific problems in pavement design.

These are the major areas of research which are likely to have the most significant impact on the structural design of pavements. There are other aspects of the total pavement design problem which are not covered here. These include the material composition, construction practices, economic factors and maintenance considerations.

6. LIST OF REFERENCES

1. Materials Research and Development Inc., (1968), "Systems Approach to Pavement Design". Final Report, NCHRP Project 1-10, Submitted to the Highway Research Board.

2. Pister, K.S., and R.A. Westmann (1962), "Analysis of Viscoelastic Pavements Subjected to Moving Loads", Proc. Int. Conf. on the Structural Design of Asphalt Pavements, Aug. 1962.

3. Moavenzadeh, F., and Elliet, J.F. (1968), "Moving Load on a Viscoelastic Layered System", R. 68-37, Dept. of Civil Eng. M.I.T. for U.S. Department of Transportation, F.H.A., Bureau of Public Roads.

4. Zienkiewicz, O.C., and Cheung, Y.K. (1967), "The Finite Element Method in Structural and Continuum Mechanics", McGraw-Hill Co.

5. Wilson, E.L. (1965), "Structural Analysis of Axisymmetric Solids". Jour. American Institute of Aeronautics and Astronautics.

6. Aitchison, G.D. (1965), "Statement of the Review Panel", in Moisture Equilibria and Moisture Changes in Soils Beneath Covered Areas, Butterworths, Inc., Australia.

7. Aitchison, G.D. (1965), "A Broad-Scale Study of Moisture Conditions in Pavement Subgrades Throughout Australia", in Moisture Equilibria and Moisture Changes in Soils Beneath Covered Areas, Butterworths, Inc., Australia.

8. Redus, J. F., (1957), "Moisture Conditions under Flexible Airfield Pavements", Proceedings, Soil Mechanics and Foundations Division, American Society of Civil Engineers, Vol. 83.

9. Kersten, M.S., (1944), "Survey of Subgrade Moisture Conditions", Proceedings, Highway Research Board, Vol. 24.

10. Williams, P.J., (1967), Properties and Behavior of Freezing Soils, Norwegian Geotechnical Institute Publication No. 72, Oslo.

11. Sauer, E.K., and Monismith, C.L., (1968), "Influence of Soil Suction on Behavior of a Glacial Till Subjected to Repeated Loading", in Moisture Responses, Under Clay Development and Frost Action, Highway Research Record No. 215, Highway Research Board, Washington, D.C.

12. Kallas, B.F., (1966), "Asphalt Pavement Temperatures", in Asphalt Pavements, Bases and Surface Treatments, Highway Research Record No. 150, Washington, D.C.

13. Straub, A.L., Schenk, H.N., Jr., and Przybycian, F.E., (1968), Bituminous Pavement Temperature Related to Climate, Paper presented at 47th Annual Meeting of the Highway Research Board, Washington, D.C.

14. Dunstan, D.G., (1967), "Temperature Variations in a Bituminous Concrete Surfacing at a Site Near Melbourne". Australian Road Research, Vol. 3, No. 3.

15. Barber, E.S., (1967), "Calculation of Maximum Pavement Temperatures from Weather Reports", in Fundamental and Practical Concepts of Soil Freezing, Bulletin No. 168, Highway Research Board, Washington.

16. Seed, H.B., Mitry, F.G., Monismith, C.L., and Chan, C.K., (1967), "Prediction of Flexible Pavement Deflections from Laboratory Repeated Load Tests". National Cooperative Highway Research Program, Report 35, HRB.

17. Monismith, C.L., Alexander, R.L., and Secor, K.E., (1966), "Rheologic Behavior of Asphalt Concrete", Proceedings, The Association of Asphalt Paving Technologits, Vol. 35.

18. Pagen, C.A., (1965), "Rheological Response of Bituminous Concrete". Highway Research Record 67, HRB, Washington.

19. Biarez, J., (1962), Contribution a l'Etude des Properietes Mechaniques des Sols et des Materiau Pulverulents. D. Sc. Thesis, University of Grenoble, France.

20. Trollope, D.H., Lee, I.K., and Morris, J., (1962), "Stresses and Deformations in Two-layer Pavement Structures Under Slow Repeated Loading". Proc. Australian Road Research Board.

21. Morgan, J.R., (1966), "The Response of Granular Materials to Repeated Loading", Proc. 3rd Conference, Australian Road Research Board, Part 2, p. 1178.

22. Kallas, B.F., and Riley, J.C., (1967), "Mechanical Properties of Asphalt Pavement Materials", Proc. 2nd International Conference on the Structural Design of Asphalt Pavements, Ann Arbor, Michigan.

23. Shifley, L.H., (1967), "The Influence of Subgrade Characteristics on the Transient Deflections of Asphalt Concrete Pavements", D. Eng. Thesis, University of California, Berkeley.

24. Brown, S.F., and Pell, P.S., (1967), "An Experimental Investigation of the Stresses, Strains and Deflections in a Layered Pavement Structure Subjected to Dynamic Loads", Proceedings, Second International Conference on the Structural Design of Asphalt Pavements, University of Michigan.

25. Ko, H.Y., and Scott, R.F., (1967), "Deformation of Sand in Hydrostatic Compression", Journal Soil Mechanics and Foundation Division ASCE, May.

26. Duncan, J.M., Monismith, C.L., and Wilson, E.L., (1968), "Finite Element Analysis of Pavements", Highway Research Record 228, HRB, Washington, D.C.

27. Mitchell, J.K., and Monismith, C.L., (1966), "Behavior of Stabilished Soils Under Repeated Loading. Report 2: Behavior in Repeated Flexure, Frequency and Duration Effects, Fatigue Failure Analyses", Corps of Engineers, Vicksburg, Contract Report.

28. Mitchell, J.K., and Shen, C.K., (1967), "Soil-cement Properties Determined by Repeated Loading in Relation to Bases for Flexible Pavements", Proc. 2nd International Conference on the Structural Design of Asphalt Pavements, Ann Arbor, Michigan.

29. Mitchell, J.K., Shen, C.K., and Monismith, C.L., (1965), "Behavior of Stabilized Soils Under Repeated Loading. Report 1: Background Equipment, Preliminary Investigations, Repeated Compression and Flexure Tests on Cement-Treated Silty Clay", Corps of Engineers, Vicksburg, Contract Report 3-145.

30. Fossberg, P.E., (1969), "Some Deformation Characteristics of a Lime-stabilized Clay", Highway Research Board, Annual Meeting, Washington, D.C.

31. Wang, M.C., (1968), "Stresses and Deflections in Cement Stabilized Soil Pavements", Ph. D Dissertation, University of California, Berkeley.

32. Terzaghi, K., (1955) "Evaluation of Coefficients of Subgrade Reaction". Geotechnique, Vol. 5, No. 4.

33. Zienkiezicz, O.C., and Cheung, Y.K., (1964), "The Finite Element Method of Analysis of Elastic Isotropic and Orthotropic Slabs", Proc. Inst. of Civil Eng., Vol. 28.

34. Hudson, W.R., and Hudson Matlock, (1966), "Discontinuous Orthotropic Plates and Pavement Slabs", Research Report No. 56-6. Center of Highway Research, University of Texas, Austin.

35. Monismith, C.L., (1966), Asphalt Mixture Behavior in Repeated Flexure, Report No. TE-66-6, University of California, Berkeley.

36. Monismith, C.L., (1966), Fatigue of Asphalt Paving Mixtures, A paper presented at the First Annual Street and Highway Conference, University of Nevada.

37. Monismith, C.L., and Deacon, J.A., (1967), Fatigue of Asphalt Paving Mixtures, A paper presented to the ASCE Meeting, Dallas, Texas.

38. Pell, P.S., (1963), "Fatigue Characteristics of Bitumen and Bituminous Mixes", Proceedings, International Conference on the Structural Design of Asphalt Pavements, University of Michigan.

39. Pell, P.S., "Fatigue of Asphalt Pavement Mixes", (1967), Proceedings, Second International Conference on Structural Design of Asphalt Pavements, University of Michigan.

40. Pell, P.S., and Taylor, I.F., (1969), "Ashpaltic Road Materials in Fatigue", Paper presented at the Annual Meeting, Association of Asphalt Paving Technologists, Los Angeles.

41. Jimenez, R.A., and Gallaway, B.M., (1962), "Preliminary Report of an Apparatus for the Testing of Asphaltic Concrete Diaphrams", Proceedings, Association of Asphalt Paving Technologists, Vol. 31.

42. Kasiunchuk, D.A., (1968), "Fatigue Considerations in the Design of Asphalt Concrete Pavements", Ph. D Thesis, University of California, Berkeley.

43. Palmer, L.A., and Thompson, J.B., (1947), "Pavement Evaluation by Loading Tests at Naval and Marine Corps Air Stations", Proceedings, Highway Research Board.

44. United States Navy, (1953), "Airfield Pavement", Department of the Navy, Bureau of Yards and Docks, Technical Publication, NAVDOCKS TP-PW-4.

45. Corps of Engineers, (1945), "The California Bearing Ratio Test as Applied to the Design of Flexible Pavements for Airports", Waterways Experiment Station Technical Memorandum 213-1.

46. Corps of Engineers, (1950), "Effects of Traffic With Small High Pressure Tires on Asphalt Pavements", Waterways Experiment Station Technical Memorandum 3-312.

47. Corps of Engineers, (1954), "The Computation of Stress and Strain in a Two-Layer System", Waterways Experiment Station Miscellaneous Papers 4-102.

48. Corps of Engineers, (1955), "Design of Flexible Airfield Pavements for Multiple Wheel Landing Gear Assemblies", Waterways Experiment Station Technical Memorandum 3-349.

49. Corps of Engineers, (1956), "Mathematical Expression of the CBR Relations", Waterways Experiment Station Technical Report 3-441.

50. Corps of Engineers, (1957), "Demonstration Test of the Performance of Heavy-Load Airfield Pavement, Kelley AFB, San Antonio, Texas", Water-Ways Experiment Station Technical Report 3-459.

51. Corps of Engineers, (1958), "Engineering and Design, Flexible Pavements", EM 1110-45-302, 1968. Waterways Experiment Station Technical Report 3-475.

52. Corps of Engineers, (1958), "Pavement Design for Frost Conditions", EM 1110-345-306.

53. McLeod, Norman W., (1947), "Runway Evaluation in Canada", Highway Research Board Report 4-B.

54. McLeod, Norman W., (1953), "Some Basic Problems in Flexible Pavement Design", Proceedings, Highway Research Board.

55. McLeod, Norman W., (1956), "Flexible Pavement Thickness Requirements", Proceedings, The Association of Asphalt Paving Technologists.

56. Federal Aviation Administration, (1967), "Airport Paving", U.S. Government Printing Office.

57. Westergaard, H. M., (1948), "New Formulas for Stresses in Concrete Pavements of Airfields", Transactions, ASCE.

58. Pickett, Gerald, and Ray, G.K., (1950), "Influence Charts for Concrete Pavements", Transactions, ASCE.

59. Corps of Engineers, (1958), "Engineering and Design, Rigid Airfield Pavements", EM 1110-45-303.

60. Ahlvin, R.G., (1962), "Flexible Pavement Design Criteria", Journal Aero. Space Transport Division Proc. ASCE Vol. 88 No. AT 1.

61. Corps of Engineers, (1958), "Engineering and Design, Frost Conditions", EM 1110-345-306.

62. Portland Cement Association, (1966), "Thickness Design for Concrete Pavements", Portland Cement Association, Chicago, Illinois.

63. United States Navy, (1962), "Airfield Pavement", Technical Publication, NAVDOCKS, Bureau of Yards and Docks, DM21.

APPENDIX I

APPROXIMATION OF DYNAMIC LOADS BY AN EQUIVALENT STATIC LOAD FOR THE DESIGN OF AIRPORT PAVEMENTS

TABLE OF CONTENTS

List of Illustrations

List of Tables

1. GENERAL

The objective of this task is to develop a method for determining a static load which can be used in the structural design of pavements in lieu of the dynamic loads that are actually applied to the pavement.

In order to place this objective within the general framework of pavement design it is appropriate to examine Figure I-1. As shown in Figure I-1 [a] the pavement system is subject to dynamic loads in the field. A great deal of previous work was performed with static loads and material properties determined under static loading conditions (Figure I-1 [b]). The static loads are determined from the wheel load based on the gross weight of the airplane contact area and the tire pressure. Typical material properties determined from static tests are the CBR and shear strength. Recognizing that payments are in reality subject to dynamic loads, and that material properties vary with the nature of the loading, there has been, in the last decade, considerable interest in the determination of paving material properties under representative dynamic loads. This situation is represented in Figure I-1 [c]. For methods of structural analysis currently in use it is necessary to represent the material properties by a 'modulus'. From the dynamic tests that are presently being utilized this modulus is termed the modulus of resilience (M_R). As discussed under "Critique of Materials Characterization and Design Techniques for Airport Pavements", Appendix H, modern methods in pavement design as recommended by Materials Research and Development Inc., utilize M_R or some other material property determined under repeated load tests. However in conducting the stress analysis for the system it is still the practice to use a static load based on the gross weight of the vehicle applied through the wheel to the pavement system.

The ideal situation would be when a 'complete' dynamic analysis can be conducted using the representative dynamic loads and material properties which are appropriate to the loading conditions (Figure I-1 [a]). It should be recognized that material properties enter into the structural design of pavements in two aspects (i) constitutive equations (stress strain characteristics) which are required to conduct a stress analysis and (ii) limiting stress or strain criteria which are used to evaluate failure.

At the present time the static load used in design is defined by (i) the pressure, which is taken equal to the tire pressure and (ii) the contact area which is obtained by proportioning the weight of the airplane over the various wheels and dividing the load on one wheel by the contact pressure. It is the purpose of this discussion to evaluate the static loads presently used in design and to determine a procedure for determining the static load which will be representative of the dynamic loads applied to the pavements. The basic criteria of determining an equivalent static load is (i) that the response (mechanical state) of the pavement under such a load satisfactorily approximates the response that would be generated under a dynamic load and (ii) the prediction of failure under the static load approximates the failure under representative dynamic loads.

2. DYNAMIC LOADS APPLIED TO AIRPORT PAVEMENTS

The first step is to evaluate the nature of dynamic loads that are applied to the pavement. This information, based on the results of the study described in the main report section entitled "Loadings Imposed on Airport Pavements", is grouped into the following four categories.

Taxiing - During taxiing the maximum load applied through the main gear may be as much as twice the maximum static load and the frequency range is from .8 to 1.4 cps. For the nose gear the frequency range is from .5 to 1.5 cps and the loads would be about 1.5 times the maximum static load applied to the nose gear.

Braking - During braking the load on the nose gear reaches about three times the maximum static load and the frequency range of interest is .5 to 1.5 cps. The increase in the loads on the main gear is of the order of 10% and the frequency range is from .5 to 1.5 cps.

Landing - During landing the load on the nose gear is about twice the maximum static value and the frequency of load application is about 1 cps. For the main gear the load is about .6 times maximum static.

Turning - During turning the main gear load may reach as high as 1.7 times the maximum static value, including runway roughness.

Based on experimental information it has been estimated that the rise time for the applied loads may vary from .02 to 1 second. An important consideration in evaluating dynamic effects is the velocity of the moving load. The magnitude of the velocity will determine if inertial effects will be important in dynamic analysis. Aircraft speeds can be as high as 200 to 250 fps.

3. RESPONSE OF PAVING MATERIALS TO DYNAMIC LOADS*

In examining the effect of dynamic loads on material behavior it is appropriate to divide the discussion into two areas (i) stress-strain relations and (ii) failure criteria.

Stress-Strain Relations:

In the development of modern methods for analyzing pavement systems** the stress-strain characteristics of the materials comprising the pavement are represented by 'modulus' values. This is because these methods rely primarily on an elastic analysis which requires some form of 'modulus.'***

* Only dynamic loads which represent those applied to pavements will be considered.

** The method for analyzing pavement systems considered here is that proposed by MR&D Inc., and reviewed in Appendix H.

*** For linear viscoelastic material the complex modulus is used.

As pointed out earlier, it is assumed that these modulus values are obtained by repeated load tests. Figure I-2 indicates the difference in 'modulus' as obtained from an unconfined compression test and a repeated load test* on a cohesive soil. It is likely that such effects would be less for portland cement concrete, asphalt concrete and granular materials.

In evaluating laboratory data on paving materials subject to dynamic loads it was found that the information was almost exclusively based on repeated load tests. For certain soil type, various other forms of dynamic loads, e.g., pulse loads, had been used. The important considerations are the effect of stress level, frequency and rate of load application.

Stress Level - With the exception of portland cement concrete, and asphalt concrete at temperatures below 65°F, all other paving materials are significantly influenced in their response to stress by the stress level. The influence of stress level on the stress-strain characteristics of various paving materials as determined from modulus of resilience values has been summarized in Appendix H.

Frequency - Investigations on the frequency of load applications have been limited (1, 2, 3). This has been primarily due to the assumption that the lower frequencies were critical in the design of pavements. Laboratory and field tests have verified this assumption. In general the modulus increases with an increase in frequency. Frequency effects are of importance in those materials which have a significant time dependent component in their response to load, e.g., asphalt concrete and cohesive soils. For granular materials and portland cement concrete, frequency effects can be considered negligible.

The experimental information indicates that the method of test influences the magnitude of the effect of frequency on the 'modulus' of the material. If the material is treated as linear viscoelastic the influence of frequency on the 'modulus' can be determined from a creep test. This influence is greater than that determined from a repeated load test conducted at different frequencies. Typical data on asphalt concrete and a silty clay subgrade which illustrate the effect of frequency on 'modulus' is shown in Figures I-3 and I-4. A comparison of frequency effects on 'modulus' for asphalt concrete, aggregate and a silty clay is shown in Figure I-5.

It would appear that for asphalt concrete and cohesive subgrades the frequency of the load is a significant factor in determining the stress-strain characteristics. However, the data obtained at low frequencies is conservative.

Rate of Loading Effects - The effects of rate of loading on the stress-strain characteristics and the strength characteristics of soils have been studied by various investigators (4 to 13). The results of these investigations lead to the conclusion that increased rates of loading increase the

---

* The rates of loading for a conventional unconfined compression can be determined by using the criteria that approximately 10 minutes are used for developing the failure load. In the repeated load test the rate of loading depends on the wave form. The rate of loading is highest for the square wave.

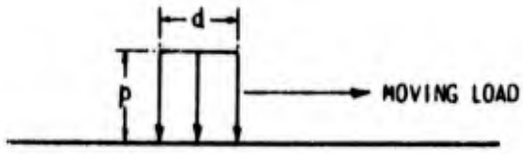

PAVEMENT SYSTEM
(MATERIAL CHARACTERISTIES SHOULD BE DETERMINED UNDER APPROXIMATE DYNAMIC LOADS)

1 (a)

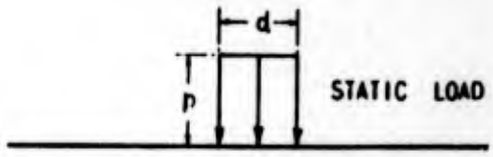

MATERIAL PROPERTIES BASED ON 'STATIC' LOAD TESTS

1 (b)

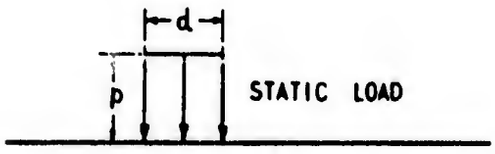

MATERIAL PROPERTIES BASED ON DYNAMIC TESTS

1 (c)

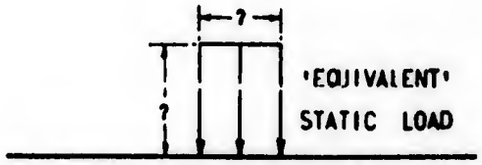

MATERIAL PROPERTIES BASED ON DYNAMIC TESTS

1 (d)

Figure I-1 Approximate Loads and Determination of Material Properties for the Structural Analysis of Pavements

(After Seed et al, 1965)

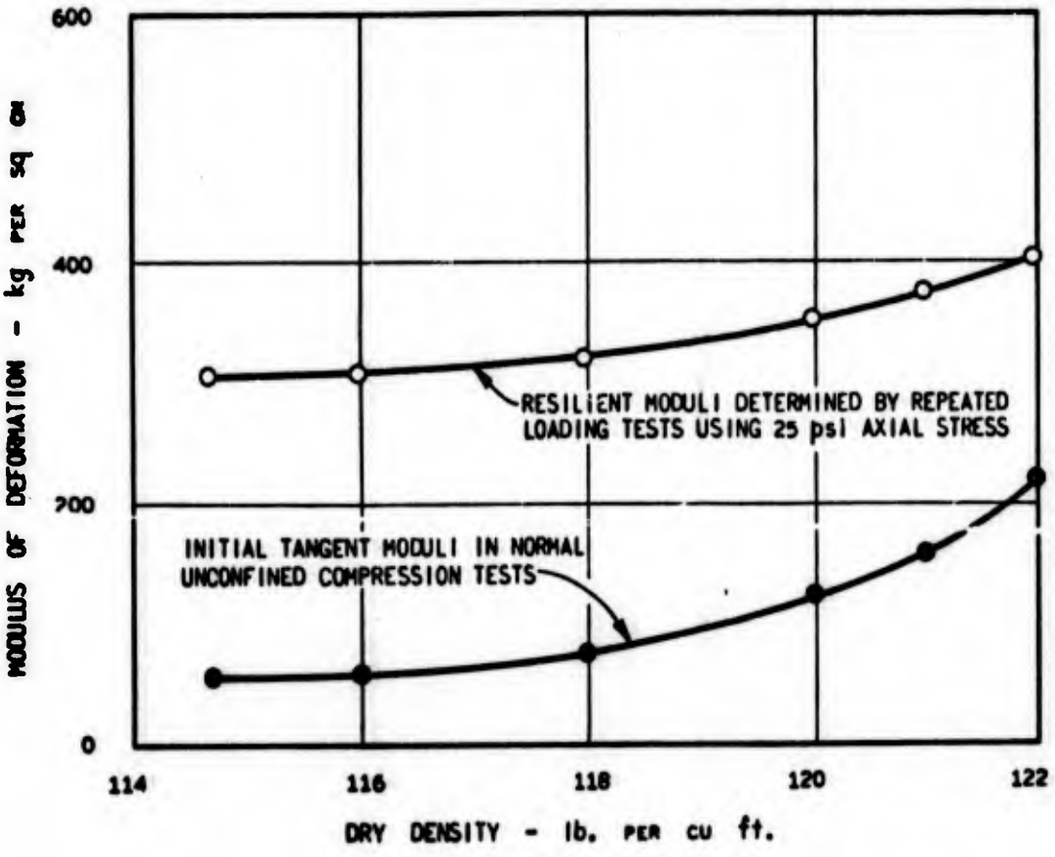

Figure I-2 Comparison of Modulus Values in Unconfined Compression Tests and in Repeated Load Tests for a Cohesive Subgrade Soil.

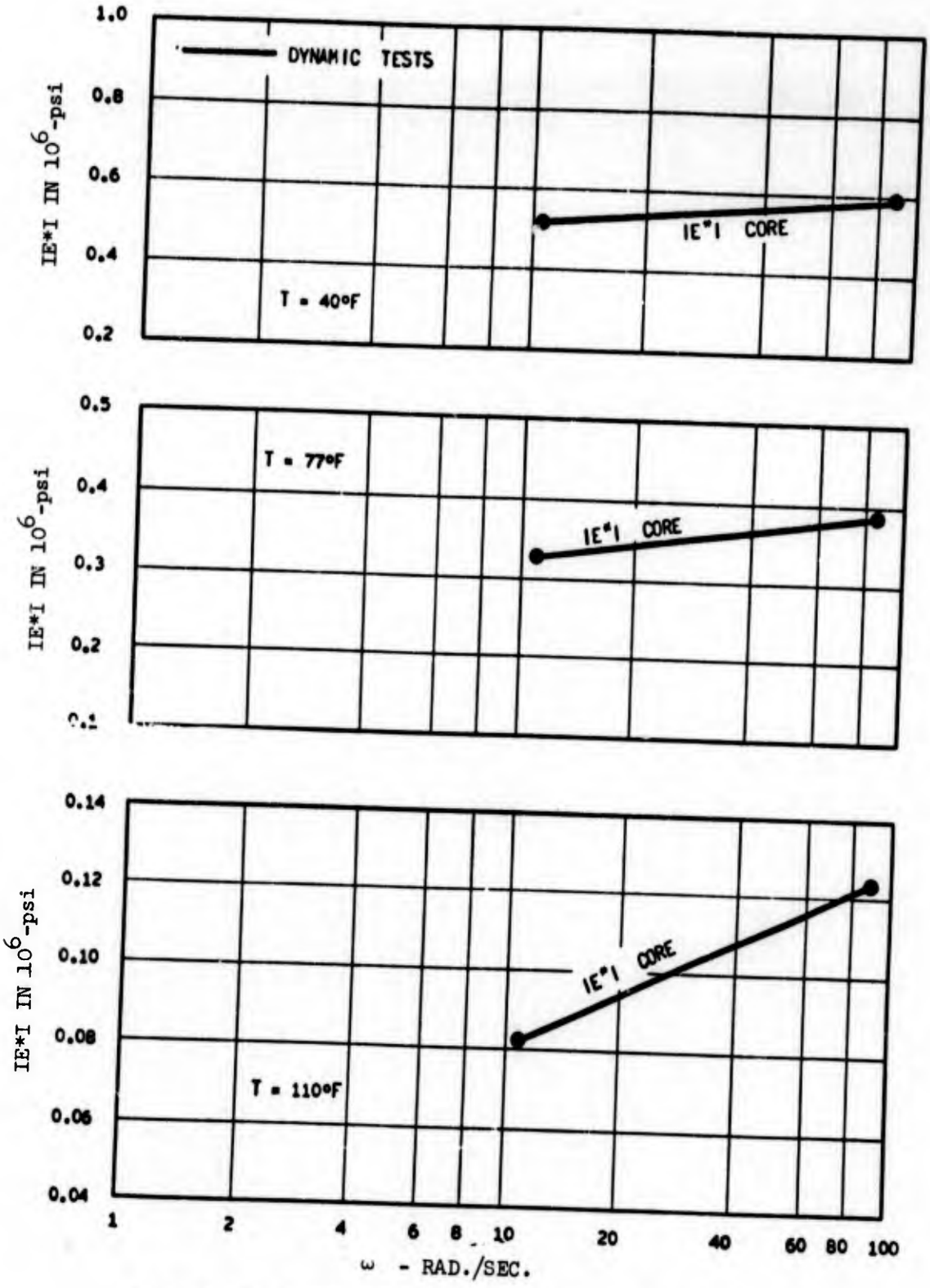

Figure I-3 Complex Modulus for Cored Samples of Asphalt Concrete as a Function of Frequency (After Coffman, 1967)

(After Coffman, 1967)

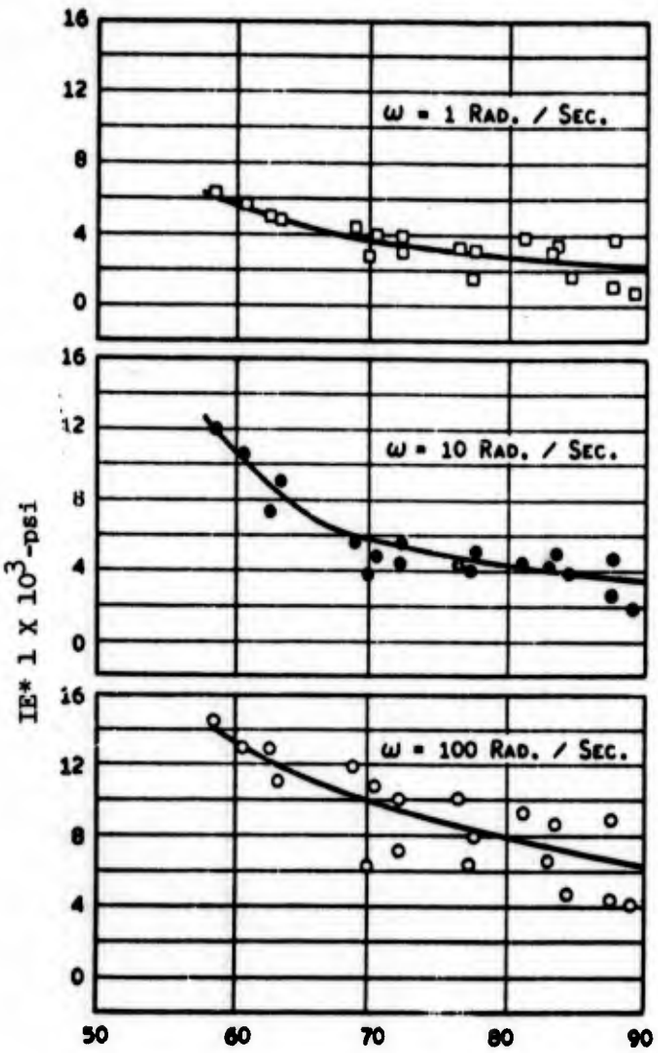

Figure I-4 Complex Modulus of a Subgrade as a Function of Frequency and Degree of Saturation.

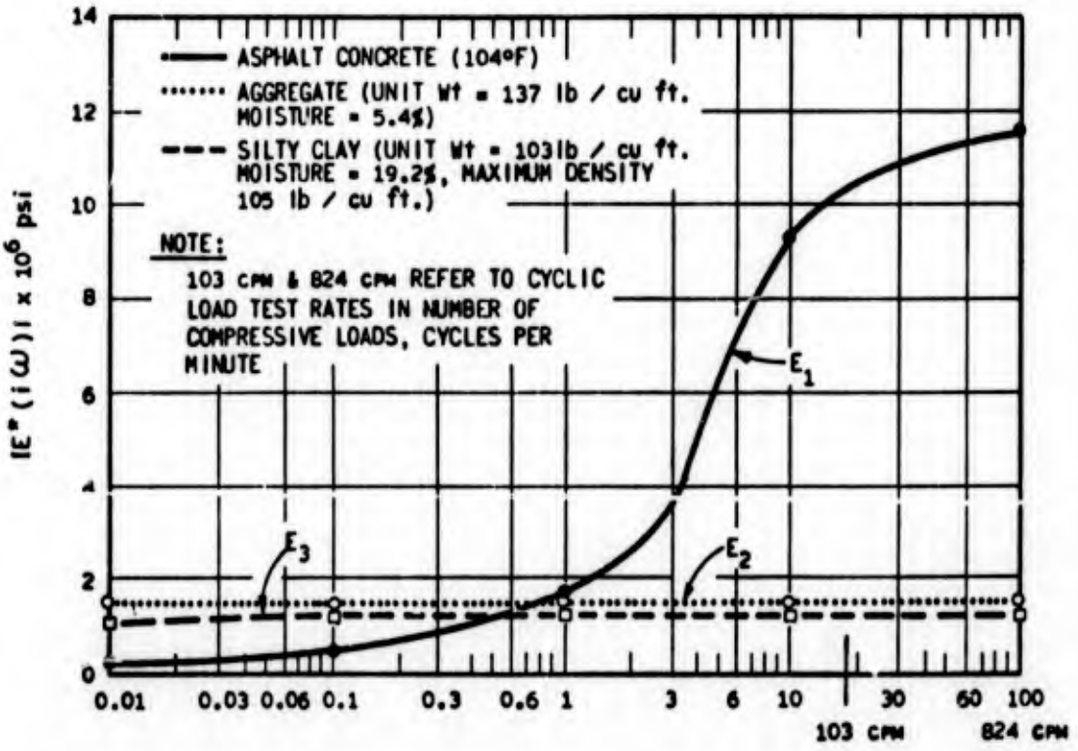

Angular Frequency, ω-Rad./Sec.

Figure I-5 Complex Modulus as a function of Frequency

'modulus' as determined from the slope of the stress-strain curve. When compared to 'static' tests this increase may be as large as 100% for cohesive soils. For cohesionless soils the increase is much smaller.* For asphalt concrete these effects are not significant under confining pressures of the of 30 psi. Based on the available data it can be concluded that if M_R values as determined from repeated load tests are used, it can be assumed that the effects of the rate of loading on the stress-strain characteristics have already been included.

Failure Criteria:

There are three basic distress modes which occur in pavements: (i) Fracture, (ii) Distortion and (iii) Disintegration. The various distress mechanisms and manifestations associated with these distress modes are listed in Figure 18 of Appendix H.

From the standpoint of structural design the major failure criteria currently in use are (i) failure due to excessive loads in a single or few (less than 100) applications and (ii) failure due to fatigue because of the repeated loads. For (i), the failure theories are based on a limiting value of the stress conditions. The most commonly used theory in this connection is the Mohr Coulomb theory which establishes the shear strength of the material. The rate of loading can have a significant influence on the shear strength of the material. Shear failure occurs primarily in the sub-grade and base materials. Typical values of the dynamic and static shear strengths for various soils are shown in Table I-1. It can be observed that the influence of the rate of loading is of most significance in the clays. In the sands and silty sands, with the exception of the loose saturated sand, the effects of the rate of loading are of the order of 10 to 20%.

Repeated loading of beam specimens is the current method for determining the fatigue strength of asphalt concrete, (15, 16). The loading is in the form of a square wave; hence, any benefits that might be the result of an increased rate of loading have already been included. At the present time there are no results which document the effects of rate of loading on the fatigue strength. In general the stress level controls the number of cycles to failure under a given set of environmental conditions.

If the information summarized above is examined from the standpoint of evaluating the influence of the dynamic character of the loads on material properties, the following conclusions can be drawn.

- The dynamic nature of the load has a significant influence on the stress-strain characteristics of the various materials comprising a pavement system. However, if stress-strain characteristics based on dynamic testing techniques currently in use are adopted, no rate of loading effects need be considered in evaluating stress-strain characteristics.

---

* The increase in modulus values is of the same order of magnitude as the increases in shear strength presented in Table I-1.

SUMMARY OF DYNAMIC TEST RESULTS: SAND

Date	Author	Test type	Confining pressures	Rise times (used to determine strain-rate effect)	Strain-Rate effect on compressive strength	Soil and condition
1948	Casagrande and Shannon	Vacuum Triaxial Compression	0.3 or 0.9 kilograms per square centimeter	0.03 to 2100 seconds	1.1	dense dry medium grained
1954	Seed and Lundgren	Undrained Triaxial Compression	2 kilograms per square centimeter	0.02 and 600-900 seconds	1.15 to 1.20	Saturated dense and loose; fine and coarse grained
1953 and 1954	Taylor, Whitman, and others	Vacuum Triaxial Undrained Triaxial	1/3 & 1 atm. $\bar{\sigma}_i$ = 30 pounds per square inch	.005 to 300 seconds .005 to 300 seconds 0.2 to 180 seconds	1.1 1.1 2.0	3 comprehensive soils Saturated dense coarse Saturated loose fine
1962	Whitman and Healy	Vacuum Triaxial Compression	$\bar{\sigma}_i$ = 10 pounds per square inch	0.025 to 5 seconds	1.4	Same as above and Saturated loose coarse
1962	Healy	Triaxial Compression	5, 10, 20, & 40 pounds per square inch	0.013 to 4 seconds	1.1 to 1.2	Fine silty sand

SUMMARY OF DYNAMIC TEST RESULTS: CLAY

Date	Author	Test type	Confining pressures	Rise times (used to determine strain-rate effect)	Strain-Rate effect on compressive strength
1948	Casagrande and Shannon	Unconfined and Triaxial Compression	3 or 6 kilograms per square centimeter	0.01 to 600 seconds	1.5 to 2.0
1953 and 1954	Taylor, Whitman and others	Unconfined and Triaxial Compression	30, 42 or 85 pounds per square inch	0.005 to 300 seconds	1.3 to 2.0
1962	Whitman, Richardson and Nasim	Triaxial Compression	normal consolidation at 60 pounds per square inch and OCR 3, 16	time to 1% strain 0.0015 to 300 seconds	1.57 to 1.71
1964	Kane, Davisson and others	Triaxial Compression	114 to 1010 pounds per square inch	0.003 to 100 seconds	1.5

Table I-1 Summary of Dynamic Test Results

- The stress-strain characteristics, as represented by a modulus, is dependent on the frequency of loading for asphalt concrete and cohesive soils. With an increase in frequency the modulus also increases. For granular materials and portland cement concrete the influence of frequency is not significant.

- The stress-strain characteristics of all paving materials with the exception of portland cement concrete are dependent on the level of stress to which they will be subjected.

- The rate of loading has a considerable influence on the shear strength characteristics of the various materials.

4. CRITERIA FOR SELECTION OF EQUIVALENT STATIC LOAD

The effects of dynamic loads in the design of pavements can be grouped into three categories. These are discussed in the following paragraphs.

A. Dynamic effects which can be accounted for through a change in material properties: In this category are the effects of frequency and rates of loading. The influence of these two factors in the structural analysis of pavement systems can be taken into account by testing the paving materials under the appropriate frequencies and rates of loading. 'Static' tests would give very conservative stress-strain characteristics. Since the effects of frequency and rate of loading can be adequately included in the choice of material properties they do not have to be considered in the selection of an equivalent static load.

B. Dynamic effects which influence the magnitude of the applied load and the material properties: In this category is the effect of stress level. The stress level that exists in a material influences the 'modulus' to be used in the current state of the art of 'ad hoc' nonlinear elastic analysis. The stress level is influenced by the magnitude of the load applied to the pavement. Because of the dynamic character of the load, e.g., during landing, passing over uneven pavements, etc., the loads applied can be much larger than those computed from static considerations. The magnitude of the dynamic load, in that it influences the stresses in the pavement directly and through its effect on the material properties, is a significant factor in the selection of the static load. It is also possible that during braking and turning shear stresses would be applied to the pavement surface.

C. Dynamic effects which, at present, cannot be accounted for by a change in material properties or applied load: The important considerations in this category are the inertia effects. All current methods of pavement design neglect them. Inertia effects have never been considered significant because the

basic theory for the structural analysis of pavements have been developed for highways (17, 18). The ratio of the speed of the moving load to the Rayleigh wave velocity of the subgrade has been used to evaluate the significance of inertia effects. For highway problems the ratio is small and the inertia effects can be assumed to be insignificant. The subgrade has in general the lowest Rayleigh wave velocity of all the materials comprising a pavement system. It is not clear whether the Rayleigh wave velocity of the subgrade can be used as the sole criteria in a layered system. However, the speeds at which aircraft might operate (circa 250 fps) are sufficiently close to the Rayleigh wave velocity of the subgrade to warrant an investigation of inertia effects. Because of a lack of theoretical analyses for this problem it is not possible at this time to consider the effects of inertia on the response of the pavement system.

In view of the above discussion it can be concluded that the critical factor in the selection of the equivalent static load is the magnitude and distribution of the applied loads. Stress level based on static analysis is controlled by two factors, the unit pressure and the size of the loaded area. The unit pressure applied to the surface of the pavement is controlled by the inflatable tire pressure. The loaded area is governed by the total load that is applied. The summary of dynamic loads applied to pavements indicates that the maximum load on the various wheels can be much greater than the static load.

5. METHOD FOR SELECTING EQUIVALENT STATIC LOAD

The method for selecting an equivalent static load is divided into a number of steps. Stress level is the critical factor in determining an equivalent static load.

- Determine the maximum dynamic loads for the main gear and nose gear. A summary of airplane operating loads is presented under the section "Dynamic Loads Applied to Airfield Pavements."
- Establish the tire pressure.
- Proportion the loads to the various wheels and determine the area of contact using the tire pressure from above. It should be recognized that these will be larger than if the gross weight of the aircraft was used.

In addition to these steps the following additional factors are essential to the complete design process.

- Stress-strain characteristics be determined at appropriate frequencies, rates of loading and stress levels.
- Fatigue as a mode of failure should be considered under the path of the nose and main gear.

- In using shear strength criteria, the rate of loading effect should be considered. Conventional 'slow' compression tests are likely to be too conservative.

It is important to recognize that inertia effects have not been considered. This might prove to be an important factor in the selection of a static load. Further work in this area would be desirable.

It is important to recognize that time effects can be significantly different for dynamic loads of short duration and for static loads which are applied to pavements for an extended period of time.

The response of paving materials to short linear dynamic loading is primarily elastic. In a repeated load test the majority of the permanent deformation occurs in the first 50 to 100 cycles. However, during each application there is a certain amount of permanent deformation. It is the accumulation of this deformation that can lead to rutting. Calculation of the permanent deformation can be made on the basis of linear viscoelasticity.

Materials, such as asphalt concrete in which the elastic response will dominate the behavior under short linear loads, can behave quite differently under static loads of long duration. Under such circumstances, where unloading does not occur to permit the sample to recover, the primary concern is then dependent deformation. Such effects are of significance at high temperatures for asphalt concrete and at high moisture contents for cohesive subgrades. For portland cement concrete and granular materials time-dependent behavior is not of great significance. Details regarding the choice of constitutive equations to represent these different aspects of material behavior have been discussed in Apendix H.

6. ILLUSTRATIVE EXAMPLE

As pointed out in the previous discussion, the present state of knowledge indicates that the only significant effect of the dynamic nature of the loads applied to airfield pavements is in the level of stress induced. If inertia effects are neglected the determination of the equivalent static load as outlined above is a simple procedure. It is important to recognize that dynamic effects have to be included in determining material properties.

Selection of Equivalent Static Load:

The example formulated is for illustrative purposes and does not represent any specific conditions.

- Assume a gross weight of airplane to be 200,000 lbs.

  Static main gear load = 90,000

  Static nose gear load = 20,000

- Maximum dynamic load on the pavement

  (i) Applied load through the nose gear for braking operation = dynamic load factor X static nose gear load

  = 3 X 20,000 = 60,000 lbs

  (ii) Applied load through the main gear for taxi operation = dynamic load factor X static main gear load

  = 2 X 90,000 = 180,000 lbs

  (See summary of dynamic loads, page I-3)

- No. of wheels in main gear = 4

  Load per wheel, main gear = 45,000 lbs

  Tire pressure, main gear = 200 psi

  Contact area per wheel,

  main gear = 225 sq. in.

- No. of wheels in nose gear = 2

  Load per wheel, nose gear = 30,000 lbs

  Tire pressure, nose gear = 200 psi

  Contact area per wheel,

  nose gear = 150 sq. in.

- Equivalent static load/wheel for main gear = pressure (200 psi times area 225 sq. in.)

  Equivalent static load/wheel for nose gear = pressure (200 psi times area 150 sq. in.)

The area of contact for the load and hence the total load, is greater than it would be for the simple static case. The load as defined above is

to be used in a static stress analysis. All methods of layered system analysis currently in use are confined to axisymmetric configurations. Therefore, the effect of all the wheel loads can be included by superimposing the effects of each load. This of course is only valid for a linear analysis.

In order to conduct a stress analysis it is necessary to define properties of the materials comprising the system under appropriate loading conditions. The effects of frequency and rate of loading on paving materials have been discussed.

Selection of Material Properties for Dynamic Loads:

As pointed out in Appendix H, limitations in the present state of knowledge make it necessary to subdivide the pavement analysis problem into three phases.

For Phases I and II the dynamic response was considered the most significant. It was recommended that material properties under repeated loading conditions be determined.

It is assumed that the Modulus of Resilience or some other 'equivalent' elastic modulus or the complex modulus has been determined from repeated load tests. In order to include the effects of frequency and rate of loading the following suggestions are made.*

Asphalt Concrete - Above a frequency of 1 cps to a maximum of 5 cps, an increase in modulus of 20% would be appropriate. From a value of .5 cps to 1 cps an increase of 50% is suggested. Temperature influences the effect of frequency on the modulus. The modulus values obtained at lower frequencies are conservative. Figures I-3 and I-5 can be used as a guide for estimating frequency effects.

Portland Cement Concrete - At the stress levels and frequencies under consideration it is not likely that frequency will affect the modulus of portland cement concrete.

Granular Material - From Figure I-5 it can be seen that frequency has a very minor effect on the modulus of granular materials.

Cohesive Subgrade Soil - From the values indicated in Figure I-4 it can be seen that an increase in frequency from 1 to 5 cps causes an increase in modulus of approximately 20%. The increase decreases with a decrease in the degree of saturation.

Table I-1 can be used as a basis for determining the rate of loading effects on material properties. If repeated load tests are used the loading rates currently in use are adequate to account for loading rate effects. There is no significant data on the effect of impact on paving materials.

---

* It should be recognized that the data on which these recommendations are made is very limited.

For Phase III of the problem different material representations are required. Phase III deals with long term effects under 'static' loads. In this phase of the problem the 'time' effects are due to the material behavior and not due to the nature of the loads.

If the materials comprising a pavement system were ideal the properties determined from the dynamic tests could be used directly in analyzing long term effects. However, this is not the case, and experimental evidence has indicated that it is necessary to determine material properties under simulated loading conditions. At the stress levels under consideration time effects are of major significance for asphalt concrete. In some cases, cohesive subgrade soils also exhibit time dependent response. If a linear viscoelastic representation for the material is used, creep or relaxation tests are required and the appropriate constants (E, ν, creep or relaxation functions) can be determined. Detailed discussion of the viscoelastic behavior of asphalt concrete including representative material constants is given in (19). For cohesive soils typical values are provided in (20 and 21). If an elastic analysis is to be performed then it is necessary to determine an 'equivalent elastic' modulus. This can be determined on the basis of the anticipated final deformation and can differ from a 'dynamic' modulus by a factor of 10 or more as can be observed from Figures H-10 and H-15 of Appendix H.

Having selected the loads, in terms of pressure and contact area, the next step is to conduct a stress analysis for the system. If it is desired to take into account the influence of the stress level on the modulus then it will be necessary to iterate using the computed stresses as a basis for determining the modulus for the next iteration. The analysis is repeated until no further change in modulus is required. Since the stress level in a material influences the modulus, the use of an equivalent load which is considerably greater than the static load is of significance.

7. LIST OF REFERENCES

1. Papzian, H. S., "The Response of Linear Viscoelastic Materials in the Frequency Domain." PhD Diss. Ohio State University, Eng. Expt. Sta. 1961.

2. Coffman, B. S., "Pavement Deflections from Laboratory Tests and Layer Theory." 2nd International Conference on the Structural Design of Asphalt Pavements, 1967.

3. Gardner, L. J. and Skok, E. L., "Use of Viscoelastic Concepts to Evaluate Laboratory Test Results and Field Performance of Some Minnesota Asphalt Mixtures." 2nd International Conference on the Structural Design of Asphalt Pavements, 1967.

4. Schimming, B. B., Haas, J. J. and Saxe, H. C., "Study of Dynamic and Static Failure Envelopes." Journal of the Soil Mechanics and Foundation Division, ASCE, March 1966.

5. Taylor, D. W., and Whitman, R. V., "The Behavior of Soils Under Dynamic Loadings, Report 2 Interim Report on Wave Propagation and Strain-Rate Effects," Armed Forces Special Weapons Project-117, for Office of the Chf. of Engrs., July, 1953.

6. Whitman, R. V., Cheatham, J. F., Jackson, J. A., Landale, T. D., Soteriades, M. D., and Wang, W. S., "The Behavior of Soils Under Dynamic Loadings, Report 3: Final Report on Laboratory Studies," Armed Forces Special Weapons Project-118, for Office of the Chf. of Engrs., August, 1954.

7. Whitman, R. V., and Healy, K. A., "The Response of Soils to Dynamic Loadings, Report 9: Shearing Resistance of Sands During Rapid Loadings," for U. S. Army Engrs., Waterways Experiment Sta., Vicksburg, Miss., May, 1962.

8. Whitman, R. V., Richardson, A. M., JR., and Nasim, N. W., "The Response of Soils to Dynamic Loadings, Report 10: Strength of Saturated Fat Clay," for U. S. Army Engrs., Waterways Experiment St., Vicksburg, Miss., June, 1962.

9. Healy, K. A., "The Response of Soils to Dynamic Loadings, Report of Triaxial Tests Upon Saturated Fine Silty Sand." for U. S. Army Engrs., Waterways Experiment Sta., Vicksburg, Miss., September, 1962.

10. Seed, H. B., and Lundgren, R., "Investigation of the Effects of Transient Loading on the Strength and Deformation Characteristics of Saturated Sands," Proceedings, ASTM, Vol. 54, 1954, pp. 1288-1306.

11. Kane, H., Davison, M. T., Oleson, R. E., and Sinnamon, G. K., "A Study of the Behavior of a Clay under Rapid and Dynamic Loading in the One-Dimensional and Triaxial Tests," Report No. RTD TDR-63-3116, Air Force Weapons Lab., June, 1964.

12. Whitman, R. V., "Testing Soils with Transient Loads, Mexico City Conference on Soils for Engineering Purposes, ASTM, Special Technical Publication STP No. 232, December, 1957, pp. 242-254.

13. Casagrande, A., and Shannon, W. L., "Strength of Soils Under Dynamic Loads," Proceedings, ASCE, Vol. 74, April, 1948, pp. 591-608.

14. Hewitt, W. L. and Slate, F. O., "The Effects of Rheological Properties of Asphalt on Strength Characteristics of Asphalt Concrete." Proc. 2nd International Conference on the Structural Design of Asphalt Pavements. Ann Arbor, 1967.

15. Pell, P. S., "Failure of Asphalt Pavement Mixes." Proc. 2nd International Conference on the Structural Design of Asphalt Pavements. Ann Arbor, 1967.

16. Monismith, C. L., "Asphaltic Mixture Behavior in Repeated Flexture." Report No. TE-65-9. Institute of Engineering Research. University of Calif., Berkeley Nov. 1965.

17. Avramesco, A., "Dynamic Phenomena in Pavements Considered as Elastic Layered Structures." Proc. 2nd International Conference on the Structural Design of Asphalt Pavements. Ann Arbor, 1967.

18. Pister, K. S. and Westmann, R. A., "Analysis of Viscoelastic Pavements Subjected to Moving Load." Proc. 1st International Conference on the Structural Design of Asphalt Pavements. Ann Arbor, 1962.

19. Finn, F. F., "Factors Involved in the Design of Asphaltic Pavement Surfaces." NCHRP Report 39.

20. Lara, Thomas M. "Time-Dependent Deformation of Clay Soils Under Shear Stress," International Conference on the Structural Design of Asphalt Pavements, Proceedings, 1962.

21. Pagen, C. A. and Jagannath, B. N., "Evaluation of Soil Compaction by Rheological Techniques," Highway Research Record No. 177, 1967.

GPO 894-220